



HAL
open science

Robust control of linear hyperbolic partial differential equations systems interconnected in a chain

Jeanne Redaud

► **To cite this version:**

Jeanne Redaud. Robust control of linear hyperbolic partial differential equations systems interconnected in a chain. Analysis of PDEs [math.AP]. Université Paris-Saclay, 2023. English. NNT : 2023UPAST153 . tel-04313615v2

HAL Id: tel-04313615

<https://hal.science/tel-04313615v2>

Submitted on 8 Feb 2024

HAL is a multi-disciplinary open access archive for the deposit and dissemination of scientific research documents, whether they are published or not. The documents may come from teaching and research institutions in France or abroad, or from public or private research centers.

L'archive ouverte pluridisciplinaire **HAL**, est destinée au dépôt et à la diffusion de documents scientifiques de niveau recherche, publiés ou non, émanant des établissements d'enseignement et de recherche français ou étrangers, des laboratoires publics ou privés.

Robust control of linear hyperbolic partial differential equations systems interconnected in a chain

*Contrôle robuste de systèmes linéaires d'EDP
hyperboliques interconnectés en réseaux de chaîne*

Thèse de doctorat de l'université Paris-Saclay

École doctorale n°580, Sciences et Technologies de l'Information et de la
Communication (STIC)

Spécialité de doctorat : Automatique

Graduate School : Sciences de l'Ingénierie et des Systèmes (SIS)

Référent : Faculté des Sciences d'Orsay

Thèse préparée dans l'unité de recherche **Laboratoire des signaux et systèmes**
(Université Paris-Saclay, CNRS, CentraleSupélec), sous la direction de **Jean AURIOL**,
Chargé de Recherche au CNRS

Thèse soutenue à Paris-Saclay, le 16 Novembre 2023, par

Jeanne REDAUD

Composition du jury

Membres du jury avec voix délibérative

Sabine MONDIE Professor titular, CINVESTAV-IPN	Présidente
Thomas MEURER Professor, Karlsruhe Institute of Technology	Rapporteur & Examineur
Christophe PRIEUR Directeur de recherche CNRS, Université Grenoble Alpes	Rapporteur & Examineur
Miroslav KRSTIC Full Professor, UC San Diego	Examineur
Yongxin WU Maître de conférence, Université de Franche-Comté	Examineur

Titre : Contrôle robuste de systèmes linéaires d'équations aux dérivées partielles hyperboliques interconnectés en réseaux de chaîne.

Mots clés : EDPs hyperboliques, systèmes à retard de type neutre, contrôle par backstepping, systèmes interconnectés, robustesse.

Résumé : Cette thèse porte sur la synthèse de contrôleurs robustes par retour de sortie pour des systèmes d'équations aux dérivées partielles (EDP) hyperboliques interconnectés en une structure de chaîne. Nous proposons des solutions innovantes basées sur la méthode de backstepping et exploitant les liens entre systèmes d'EDP hyperboliques et systèmes à retard de type neutre présentés en Partie I. Nous étudions ici deux configurations d'actionnement de structures en chaîne. Tout d'abord, nous examinons le cas où l'actionnement est disponible à une extrémité (Partie II) pour deux différents réseaux (ODE-EDP-ODE et N EDPs-ODE). Ces structures peuvent modéliser des systèmes de forage. Ensuite, nous considérons une chaîne simple où l'actionnement est disponible au niveau de la jonction (Partie III). Sa stabilisation nécessite une transformation intégrale plus générale. Enfin, nous explorons les aspects négligés des contrôleurs basés sur la méthode de backstepping (Partie IV), tels que le choix d'un système cible atteignable avec des propriétés de stabilité spécifiques, ou la réduction du temps de calcul par des techniques d'apprentissage automatique.

Title : Robust control of linear hyperbolic partial differential equations systems interconnected in a chain network.

Keywords : hyperbolic PDEs, neutral time-delay systems, backstepping-based control, interconnected systems, robustness.

Abstract : This thesis focuses on designing robust output-feedback backstepping-based controllers for hyperbolic partial differential equation (PDE) systems interconnected in a chain structure. We take advantage of connections between the class of hyperbolic PDE systems under consideration and time-delay systems of the neutral type presented in Part I. Then, we focus on two classes of chain structures. First, we consider the case where the actuation is available at one end (Part II) for two different networks (ODE-PDE-ODE and arbitrarily many N PDEs-ODE). Such chain structures can be found in drilling applications. Next, we consider a simple chain of two hyperbolic PDE subsystems where the actuation is available at the junction (Part III). A more general integral transform is necessary for its stabilization. Finally, we explore controller design tuning and implementation limitations of backstepping-based controllers (Part IV). We question the choice of a reachable target system with specific stability properties. Additionally, we examine the potential of machine learning techniques to improve computation time in distributed state and parameter estimation.

À Goustan. De notre amour sera né ce manuscrit, ce n'est finalement pas si mal.
過去5年間に私たちが見たすべてに感謝します。それは約束だった、博士になりました。

Remerciements - Acknowledgments

En tout premier lieu, je souhaite remercier mon encadrant de thèse, Jean Auriol. Sans sa sollicitation, je n'aurais jamais imaginé devenir un jour docteur. Ces trois années de thèse mirent mon abnégation à rude épreuve, mais je ressortirai grandie humainement des épreuves surmontées. Merci pour ton enthousiasme à partager tes connaissances. Tu m'as plusieurs fois rassuré lorsque je doutais de la qualité de mon travail, et cela m'a bien aidé à mener cette thèse à son terme.

Je tiens à remercier Thomas Meurer et Christophe Prieur, qui m'ont fait l'honneur d'accepter d'être rapporteurs de cette thèse. Merci également à Yongxi Wu, Sabine Mondié, et Miroslav Krstic d'avoir participé à mon jury de soutenance. Vos questions et précieux commentaires ont considérablement contribué à l'amélioration de ce manuscrit et m'ont fourni de nouvelles pistes de travail. *I thank Thomas Meurer and Christophe Prieur, who have done me the honor of agreeing to be rapporteurs for this thesis. Thanks also to Yongxi Wu, Sabine Mondié, and Miroslav Krstic for participating in my defense jury. Your questions and valuable comments have contributed considerably to the improvement of this manuscript and provided me with new avenues of work.*

Mes remerciements vont également à tous les membres du Laboratoire Signaux et Systèmes de CentraleSupélec, et notamment, Pascal Bondon, Audrey Bertinet et Stéphanie Douesnard et l'ensemble des personnels administratifs. Je remercie également les personnels de l'Université qui ont fait suite à ma demande de médiation. Je regrette que mon parcours ne puisse témoigner pour de futurs doctorants qu'il est possible de faire évoluer cette université à deux vitesses. Je remercie toutefois l'infirmière Aurore Gava qui a pris régulièrement de mes nouvelles et écouté avec bienveillance.

J'ai une pensée très chère pour mes camarades doctorants du L2S. Je remercie Fabien et Anas, qui m'ont accompagnée dans la parfois lourde mission de représentant des doctorants. Je remercie aussi Diego et Can-Kutlu, qui au-delà de partager un (ex-)directeur de thèse maltraitant ou absent¹, sont devenus au fil du temps des amis et confidents. *Como dice Luffy, "La vida es una lucha. Si no luchas, no puedes ganar". Tezden sonra sana her seyin en iyisini diliyorum!* Enfin Maël, avec qui j'ai eu le plaisir de partager mon bureau lors de notre retour en présentiel. Plus largement, j'ai une pensée pour tous les doctorants que j'ai pu rencontrer au sein de l'Université Paris Saclay, dans le cadre d'échanges scientifiques comme de rencontres informelles, et en particulier Lolita, Erick, Maxime, Sayan, Giann, David, Paul, Aliaume et Emmanuel.

Je souhaite également remercier les différentes équipes de recherche avec lesquelles j'ai pu collaborer au cours de ma thèse. Tout d'abord, Federico Bribiesca-Argomedo, du Laboratoire Ampère à Lyon, pour m'avoir introduit aux subtilités de l'analyse fréquentielle et aux méthodes de filtrages. Je remercie ensuite Yann le Gorrec, du laboratoire FEMTO-ST à Besançon, pour m'avoir fait découvrir le formalisme Hamiltonien à Port. J'ai apprécié ta bienveillance au cours de tous les échanges que nous avons pu avoir. *I thank Roman Shor, from the University of Calgary. Thanks to you, I discovered the potential of geothermal energy, and did one of the most memorable hikes of my life.* Je remercie Pablo Piantanida d'avoir organisé ma mobilité au Laboratoire ILLS, CNRS à Montréal. Ce séjour de deux mois fût riche de rencontres et d'approfondissements scientifiques. Je remercie également Sabine

1. Dacă întâmplător ai citit această teză într-o zi, să știi că nu am uitat promisiunea ta de șampanie...;-)

Mondié du CINVESTAV, à l'Université de Mexico, pour nos échanges très riches, ainsi que Fernando Mendez Barrios, de l'UASLP. Ta bienveillance et ton soutien indéfectible m'ont beaucoup touché. *Si no puedes ser miembro del jurado de mi tesis, estarás en mi corazón.* Finally, I would like to thank Professor Hideki Sano, from Kobe University, for his confidence and reliability. Working three months as a Postdoctoral fellow at Kobe University was an outstanding experience that reconciled me with research and confirmed my attraction to Japan. I would also like to thank the Japanese Society for Promotion of Science which supported this 3-months research program in Japan. *あなたのおかげで私の夢が叶いました。いつも感謝しています。*

Je remercie ensuite tous ceux qui ont été à mes côtés au cours de ces trois dernières années, et en particulier tous ceux qui m'ont dit un jour qu'ils étaient fiers de moi. La liste est longue, et j'oublierai sûrement des noms.

Mes parents d'abord, qui ont suivi avec patience mes états d'âme et m'ont toujours assisté dans les épreuves. Vos conseils ont toujours été, et seront toujours, précieux. Merci de m'avoir laissé cultiver mon jardin et désolée pour la C4. Merci à Emilie pour sa bienveillance et son accueil toujours ressourçant, et à Joseph qui me laisse finalement rester le seul docteur de la famille (ce qui ne réduit en rien mon estime de toi). Je remercie également ma tante Florence qui par sa force de caractère et son optimisme à toute épreuve a été un modèle de persévérance dans ces années difficiles.

Je remercie ensuite mes (nombreux) amis doctorants. Théodore, pour ses conseils, ses concerts privés et ses plateaux télé toujours réconfortants; Bruno, pour toutes nos riches discussions sur des chemins de randonnée ou autour de petits plats; Goustan, pour son accueil chaleureux et son sourire; Cyril, pour son rire communicatif et son amour partagé des ramens; Joël, pour ses conseils bienveillants, Mathieu, pour son soutien indéfectible et son écoute. Au plaisir de vous appeler docteur. Une pensée à ceux de mes amis, non thésards, qui n'ont pas échappé à mes atermoiements, en particulier, Hugues et Palmyre, Paul (x3), Eloi, Pierre, Côme, Nicolas, Kossi, Matthieu.

Enfin, je remercie Samson qui a grandi à mes côtés et m'a soutenu avec amour (et humour) pendant deux années, malgré mes absences et ma mauvaise humeur.

Table of contents

1	Introduction	5
I	Modelisation and preliminary results	11
2	Preliminary results on scalar linear hyperbolic PDE systems	15
3	Characterization of P/PI controllers for a simple chain structure	35
II	Chain structure with actuation at one end	51
4	Output regulation for linear ODE - hyperbolic PDE - ODE systems	55
5	Stabilizing a chain of N hyperbolic PDE systems interconnected with an ODE	77
6	Application to drilling systems for state estimation and trajectory tracking	97
III	Chain structure with actuation at the in-between boundary	121
7	Stabilizing two hyperbolic PDE systems with in-between boundary actuation	125
8	Application to the stabilization of a clamped string	149
IV	Exploring implementation aspects of backstepping controllers	171
9	Arbitrary target system for a general class of nonscalar hyperbolic PDE systems	175
10	On the use of the Port-Hamiltonian framework to determine adequate target systems	195
11	Machine learning techniques for distributed state and parameter estimation	213
	Conclusions	235
	Bibliography	239
A	A tutorial on numerical methods for solving kernel equations	255
B	Proof of Theorem 7.2.2	265
C	Comments on target systems and kernels dof for a Timoshenko beam observer design	273

Notations

For any $n, m, p \in \mathbb{N}$ strictly positive integers, and for any compact set \mathbb{K} , we use the following notations throughout the thesis.

General notations

1. For any multivariate function, we denote $\frac{\partial}{\partial x} f$ the derivative of a function f with respect to variable x . For any differentiable function f defined on $I \subset \mathbb{R}$, we denote $f'(x) = \frac{df(x)}{dx}$ its derivative.
2. For all $a, b, \nu \in \mathbb{R}$, $a < b$, define the *characteristic function* $\mathbb{1}_{[a,b]}(\nu)$, as the function equal to 1 if $\nu \in [a, b]$, and equal to 0 elsewhere.
3. We denote δ_n^m the Kronecker symbol ($\delta_n^m = 1$ if $n = m$, 0 else). We extend this definition with $\delta_{n \asymp m} \doteq 1$ if $n \asymp m$, 0, where \asymp denote any order relation (Chapter 10).
4. For any matrix $A \in \mathbb{R}^{n \times p}$, we denote $A^\top \in \mathbb{R}^{p \times n}$ its transpose and $\sigma(A) \subset \mathbb{R}$ its spectrum i.e. the set of its eigenvalues.
5. We denote D_n^+ , the set of diagonal matrices in $\mathbb{R}^{n \times n}$ with positive coefficients, extended to $D_n^+(I)$ for matrix-valued functions defined on interval I .
6. We denote I_n the $n \times n$ identity matrix, $0_n = 0_{\mathbb{R}^{n \times n}}$. The index may be omitted.

Compact sets

1. Denote $\mathcal{S} \in [0, 1]^2$ the unit square, $\mathcal{T}^- = \{(x, y) \in [0, 1]^2, x \geq y\}$ its lower triangular part and $\mathcal{T}^+ = \{(x, y) \in [0, 1]^2, x \leq y\}$ its upper triangular part.
2. For any $\lambda, \mu > 0$, we define the two triangular spaces
 - $\mathcal{T}_\lambda^+ = \{(x, y) \in [0, 1] \times [0, \frac{1}{\lambda}] \mid 0 \leq y \leq \frac{x}{\lambda}\} \subset \mathbb{R}^2$,
 - $\mathcal{T}_\mu^- = \{(x, y) \in [0, 1] \times [0, \frac{1}{\mu}] \mid 0 \leq y \leq \frac{1}{\mu}(1-x)\} \subset \mathbb{R}^2$,and for $a > 0$, the two parallelogram domains,
 - $\mathcal{P}_{a,\lambda}^+ = \{(x, y) \in [0, 1] \times [0, a + \frac{1}{\lambda}] \mid \frac{x}{\lambda} \leq y \leq a + \frac{x}{\lambda}\} \subset \mathbb{R}^2$,
 - $\mathcal{P}_{a,\mu}^- = \{(x, y) \in [0, 1] \times [0, a + \frac{1}{\mu}] \mid \frac{1-x}{\mu} \leq y \leq a + \frac{1-x}{\mu}\} \subset \mathbb{R}^2$ (Chapter 10).

Functional spaces

1. We denote $C^0(\mathbb{K}, \mathbb{R}^n)$ the space of continuous functions defined on \mathbb{K} with values in \mathbb{R}^n , and $C^1(\mathbb{K}, \mathbb{R}^n)$ the space of differentiable functions with a continuous derivative. We also denote $C^1(\mathbb{K}, \mathbb{R}^n)^+$ its subset of strictly positive functions (Chapter 10).

2. We denote $L^2([0, 1], \mathbb{R}^n)$ the Hilbert space of square integrable functions with values in \mathbb{R}^n , and $H^1([0, 1], \mathbb{R}^n)$ the Sobolev space of L^2 -functions whose derivative is in L^2 .
3. For any compact sets $\mathbb{K}_1, \mathbb{K}_2$, the space of piecewise continuous functions defined on \mathbb{K}_1 with values in \mathbb{K}_2 is denoted $C_{pw}^0(\mathbb{K}_1, \mathbb{K}_2)$. Similarly, we denote $C_{pw}^n(\mathbb{K}_1, \mathbb{K}_2)$ the space of differentiable functions with piecewise continuous n^{th} derivative.
4. For any fixed time-delay $\tau > 0$, $n \in \mathbb{N}$, we denote $D_\tau = H^1([0, \tau], \mathbb{R}^n)$ the Sobolev space of H^1 functions mapping the interval $[0, \tau]$ into \mathbb{R}^n . For a function $\phi : [0, \infty) \mapsto \mathbb{R}^n$, its partial trajectory $\phi_{[t]} \in D_\tau$ is defined by $\phi_{[t]}(\theta) = \phi(t - \theta)$, $0 \leq \theta \leq \tau$.
5. We denote $\Xi = L^2([0, 1], \mathbb{R}^n) \times \mathbb{R}^p$ (Chapters 3, 5).
6. We denote $\mathcal{X} = \mathbb{R}^n \times H^1([0, 1], \mathbb{R}^2) \times \mathbb{R}^{m+p}$ (Chapter 4).
7. For any Banach space B_1, B_2 , we denote $\mathcal{L}(B_1, B_2)$ the set of all bounded linear operators mapping B_1 to B_2 .

Norms

1. For any $X \in \mathbb{R}^n$, we denote $|X| \doteq \sqrt{X^\top X}$ the classical Euclidian norm.
2. For any $u \in C^0([0, T]; L^2([0, 1], \mathbb{R}^n))$, the L^2 -norm is defined by

$$\|u(t, \cdot)\|_{L^2} \doteq \sqrt{\int_0^1 u(t, \nu)^\top u(t, \nu) d\nu}.$$

3. For any $\tau > 0$, $z \in D_\tau$, for any $t > 0$, the D_τ -norm is defined by

$$\|z_{[t]}\|_{D_\tau} \doteq \sqrt{\left(\int_0^\tau z(t - \theta)^\top z(t - \theta) d\theta\right)} = \sqrt{\left(\int_{-\tau}^0 z(t + \theta)^\top z(t + \theta) d\theta\right)}.$$

4. For any $(u, X) \in \Xi$, the Ξ -norm is defined by $\|(u, X)\|_\Xi \doteq (\|u\|_{L^2}^2 + |X|^2)^{\frac{1}{2}}$.
5. For any $(X, u, Y) \in \mathcal{X}$, the \mathcal{X} -norm is defined by $\|(X, u, Y)\|_{\mathcal{X}} \doteq (\|X\|^2 + \|Y\|^2 + \|u\|_{L^2}^2)^{\frac{1}{2}}$.
6. For any bounded matrix-valued function F defined on \mathbb{K} , we define $\|F\|_\infty = \max_i \max_j \|F_{ij}\|_\infty$ the highest value of its components, where $\|F_{ij}\|_\infty = \max_{x \in \mathbb{K}} (|F_{ij}(x)|)$.

Frequency-domain analysis

1. We denote $\mathbb{C}^+ = \{s \in \mathbb{C} \mid \Re(s) \geq 0\}$ the closed right-half complex plane (RHP).
2. The letter s denotes the Laplace variable. For any complex $s \in \mathbb{C}$, $\Re(s)$ corresponds to the real part, and $\Im(s)$ the imaginary part.
3. For any proper and stable transfer matrix $G(s)$, $\bar{\sigma}(G(j\omega))$ stands for the largest singular value of $G(j\omega)$ at frequency ω , and the H_∞ -norm of G is $\|G\|_\infty = \text{ess sup}_{\omega \in \mathbb{R}} \bar{\sigma}(G(j\omega))$ (Chapter 4).

Préambule

Nous présentons en préambule le contexte de la thèse et les problématiques traitées. Afin de toucher une plus large communauté scientifique, cette thèse a été rédigée intégralement en anglais. Toutefois, des résumés introductifs sont disponibles en français en début de chaque chapitre, afin de pouvoir cibler facilement les problèmes considérés et les outils développés. Une liste des contributions publiées ou soumises au cours de cette thèse est également disponible à la fin du chapitre d'introduction (Chapitre 1).

Contexte

Cette thèse porte sur le contrôle de systèmes d'équations aux dérivées partielles (EDP) hyperboliques linéaires du premier ordre, interconnectés entre eux et/ou avec des équations différentielles ordinaires (EDO) selon une structure de chaîne. Ces systèmes se rencontrent naturellement lors de la modélisation de phénomènes physiques dont la dynamique dominante dépend du temps, mais également de l'espace (lois de conservation, flux, équations de transport, équations d'ondes...). Il peut être intuitif de considérer l'interconnexion de telles dynamiques distribuées avec des systèmes dont l'évolution dépend du temps uniquement. De telles structures apparaissent dans divers domaines de l'ingénierie: des réseaux électriques contenant des lignes de transmission [SWGR14, SWGR11], des réseaux routiers avec des modèles macroscopiques de trafic (modèle ARZ) [BYK19, YAK20], des écoulements non stationnaires dans des canaux [GL13, Hay19], des oscillations thermo-acoustiques (tube de Rijke) [dAVP18], le transport de charges à l'aide de câbles [WK20, WK21], ou des vibrations mécaniques dans des systèmes de forage [AS18, SMN⁺16]. La partie EDO peut modéliser efficacement les courants dans les inductances ou capacités, ou la dynamique d'une charge (modélisée comme une masse), ou de l'actionneur (dans un modèle classique de moteur électrique). Dans l'exemple du forage, le système d'EDP hyperboliques modélise la propagation de vibrations axiales et/ou torsionnelles, tandis que les EDO représentent la dynamique du moteur électrique en surface, de la tête de forage (BHA), ou son interaction avec la roche [AKIS20].

La stabilisation et le contrôle de telles **interconnexions entre EDP hyperboliques et EDO** sont donc des sujets de recherche avec un intérêt pratique, mais également théorique. En effet, stabiliser des systèmes en réseau tout en garantissant des performances satisfaisantes n'est pas facile, surtout lorsque l'actionneur n'est disponible qu'à des emplacements ponctuels, généralement à une extrémité du système. Dans la littérature, différentes approches ont été développées pour aborder de tels problèmes. Par exemple, le contrôleur Proportionnel intégral (PI) a été étendu à une chaîne de systèmes hyperboliques linéaires [BCT15]. Des méthodes basées sur la platitude [WRK09, MZ04] ou les dynamiques des lignes caractéristiques [SA17] ont été développées pour concevoir une loi de commande à rétroaction de sortie pour des systèmes hyperboliques interconnectés en série. En raison des retards inhérents à de telles structures en réseau, il est souvent nécessaire de concevoir des prédicteurs pour anticiper les valeurs futures de l'état [BL14].

La méthode du **backstepping** s'est révélée être prometteuse pour stabiliser les sys-

tèmes d'EDP hyperboliques. Son idée générale consiste à simplifier la structure du système considéré en déplaçant les termes de couplage (potentiellement déstabilisants) à la frontière actionnée. Pour ce faire, on utilise des transformations intégrales inversibles, en général de type Volterra. Cette méthode a été appliquée à des systèmes d'EDP hyperboliques du premier ordre dans [KSo8, VKC11, CVKB13], puis à des systèmes couplés entièrement actionnés [DMVK13]. Pour des systèmes d'EDP interconnectés, les premiers résultats ont été obtenus pour la stabilisation de réseaux composés de deux sous-systèmes [ABABS⁺18, ADMBA19]. Ils ont été étendus à un réseau en cascade avec un nombre arbitraire de sous-systèmes dans [Aur20], en introduisant une transformation complexe. Parallèlement, des contrôleurs basés sur le backstepping ont été développés pour des structures en chaîne contenant des systèmes d'EDO, type EDO-EDP-EDO [WKP18, DGK18, Geh21] ou EDP-EDO-EDP [AVDMK19, KK20]. Dans la plupart des cas, le design constructif est basé sur plusieurs transformations, utilisées pour annuler le terme de réflexion à la frontière actionnée de manière à ce que l'EDP n'ait plus d'impact sur l'état de l'EDO contrôlée [DGK18]. Cependant, supprimer le terme de réflexion peut entraîner des lois de commande non strictement propres. De même, il est nécessaire d'inverser la dynamique lorsque seul le système d'EDO est actionné, ce qui entraîne des **problèmes de robustesse**. En particulier, un retard arbitrairement petit dans la boucle peut provoquer l'instabilité du système en boucle fermée [DLP86]. Proposer des contrôleurs robustes aux retards (mais aussi aux incertitudes sur des paramètres ou des dynamiques négligées) est donc d'une préoccupation majeure pour une application ultérieure à des systèmes réels.

De manière intéressante, des notions de robustesse ont été développées dans le domaine des **systèmes à retard** [HVL13], qui sont étroitement liés aux systèmes d'EDP hyperboliques [KK14, ADM19]. Les propriétés de stabilité des systèmes d'EDP hyperboliques peuvent alors être analysées en utilisant la représentation équivalente sous forme de système à retard [Rus78a, Pee21].

Objectif général

Cette thèse vise à stabiliser des réseaux de systèmes d'EDP hyperboliques linéaires interconnectés avec des EDO selon une structure en chaîne. Nous présentons des méthodes constructives pour la conception de contrôleurs et d'observateurs.

Les approches proposées sont basées sur la méthode de backstepping et tirent parti des résultats d'analyse de stabilité développés pour les systèmes à retard.

Organisation de la thèse

Cette thèse introduit dans la **Partie I** deux classes de systèmes de dimension infinie: les systèmes d'EDP hyperboliques linéaires et les systèmes à retard (TDS) de type neutre. Dans le cas simple d'un système d'EDP hyperbolique linéaire scalaire, nous introduisons au **Chapitre 2** la relation entre ces deux classes et la *méthode de backstepping*. Elle induit des propriétés de stabilité asymptotique similaires. Ensuite, nous considérons au **Chapitre 3** une première interconnexion entre des équations de transport pures et une

EDO linéaire. Nous présentons les limites des approches de contrôle classiques Proportionnel et Proportionnel Intégral (PI), sur cette structure de chaîne simple. Cela souligne l'intérêt des contrôleurs basés sur le backstepping, qui prennent en compte la nature distribuée de la dynamique.

Après cette partie introductive, nous abordons différents problèmes de contrôle sur les structures en chaîne. Dans la **Partie II**, nous étudions le cas où l'actionnement disponible est situé **à une extrémité** du réseau. Nous considérons d'abord au **Chapitre 4** le cas d'une interconnexion EDO-EDP-EDO. La conception du contrôleur permettant le suivi de trajectoire et le rejet des perturbations s'appuie sur la méthode de backstepping et une analyse dans le domaine fréquentiel. Il est présenté dans [W1, B1, J2]. Ensuite, nous considérons dans le **Chapitre 5** le cas d'une chaîne composée d'un nombre arbitraire de systèmes d'EDP hyperboliques, interconnectés à l'extrémité non actionnée avec une EDO. Pour obtenir un contrôleur par réaction de sortie stabilisant, nous utilisons une approche *réursive*. Elle est présentée en [C8, J4] et appliquée aux systèmes de forage en [C5]. En effet, les systèmes de forage peuvent être modélisés par de tels réseaux, comme illustré au **Chapitre 6**.

Cependant, si dans certaines applications, comme le forage, l'actionneur est situé à une extrémité du réseau, ce n'est pas toujours le cas. Quelques exemples peuvent être trouvés dans le contrôle du trafic routier ou les dispositifs biomédicaux. Nous étudions donc dans la **Partie III** le cas où l'actionnement est disponible **à une jonction** du domaine. Dans le **Chapitre 7**, nous considérons le cas de deux systèmes d'EDP hyperboliques interconnectés avec actionneur à la frontière intermédiaire. En raison de nouveaux couplages, nous utilisons une transformation intégrale de *Fredholm*. Cela est présenté dans [C6, C7, J3]. Cette méthodologie est appliquée au **Chapitre 8** à la stabilisation de cordes [C1]. Ces deux parties se terminent par des perspectives et des extensions des approches proposées dans des cas de plus grande dimension ou des réseaux plus complexes.

Enfin, la **Partie IV** est dédiée aux **aspects négligés** des contrôleurs par backstepping. Tout d'abord, nous nous interrogeons dans le **Chapitre 9** sur le choix des systèmes cibles atteignables par des transformations inversibles. En utilisant une transformation affine en temps, nous montrons qu'une classe générale de systèmes d'EDP hyperboliques non scalaires peut être envoyée sur n'importe quel système arbitraire de la même classe. Un système cible adéquat doit être sélectionné parmi cette classe pour améliorer les performances en boucle fermée, par exemple obtenir une convergence plus rapide vers l'état d'équilibre. Nous montrons au **Chapitre 10** que des propriétés en boucle fermée ayant une signification physique peuvent être obtenues en utilisant le formalisme *Port Hamiltonien*. Cette stratégie a été présentée en [C4, C2]. Un design d'observateur pour le cas d'étude d'une poutre de Timoshenko considéré est proposé en annexe C. Enfin, nous introduisons au **Chapitre 11** l'utilisation de l'apprentissage automatique pour obtenir des estimations en temps réel de l'état distribué et des paramètres pour le cas d'étude du forage et de la poutre. Cette piste permettrait d'utiliser les contrôleurs distribués obtenus par backstepping pour des applications réelles.

1 - Introduction

Context

This thesis deals with the control of linear first-order hyperbolic Partial Differential Equations (PDE) systems interconnected with Ordinary Differential Equations (ODE) in a chain structure. Each elementary system consists in two scalar countervecing transport equations with in-domain couplings (balance laws). Networks of such interconnected elementary PDE systems naturally arise when modeling industrial processes for which the dominant dynamics involve a transport phenomenon or a delay. In a chain structure, they can be connected between themselves or with an ODE. We can cite as examples electrical networks containing transmission lines [Bra68, SWGR14, SWGR11], pneumatic systems [KGDM18], traffic flows [BYK19, YAK20, YAK20], density-flow systems [BCT15, BC16, HS21], unsteady flows on open canals [GL13, Hay19], thermo-acoustic oscillations in combustion dynamics such as Rijke tubes [dAVP18], transportation of loads using cables [WK20, WK21], or mechanical vibrations in drilling systems [AS18, SMAV16].

The PDE part can model the lossless transmission lines in electrical networks or any propagation phenomena such as vibrations or flow density. The ODE part can efficiently represent the dynamics of currents in inductors or voltages across capacitors, loads, actuators, or any lumped element connected to the distributed system. In the drilling example, the hyperbolic PDE system models axial and torsional stress propagation, with potential discontinuities due to the junctions between different types of pipes. At the same time, the ODE represents the Bottom hole Assembly (BHA) dynamics or the bit-rock interaction [AKIS20]. In the Rijke tube application, the PDEs correspond to the compressible gas dynamics, while the ODE represents the linearized heat power release [dAVP18]. Though the dynamics are primarily three-dimensional, we can usually only consider a dominant one along a specific dimension and approximate them as balance laws along a bounded one-dimensional spatial domain.

In this context, **interconnected ODEs and PDEs** are an intuitive structure that conserves the specific pointwise and distributed nature of the underlying dynamics. This explains why the stabilization and control of such systems is an **active research topic**. From an engineering point of view, interconnections between systems can be the source of multiple problems. They can create instabilities or vibrations nodes that are preferable to avoid since they destabilize the whole system [BPK14, ABP22]. Moreover, stabilizing networked systems while guaranteeing satisfying performance is not easy, especially when actuation is only available in discrete locations, usually at one end of the system. In the literature, various approaches have been developed to tackle such issues. For instance, the well-known PI controller was extended in [BCT15] to a chain of linear hyperbolic systems. A state-feedback controller for hyperbolic PDE networks was designed using a flatness-based analysis in [WRK09, MZo4]. The dynamics of characteristic lines were studied in [SA17] to design an output feedback control law for semi-linear hyperbolic systems interconnected in series. Due to the delays inherent to such networked structures, it is often necessary to design predictors to anticipate future values of the state [BL14].

Among these approaches, the **backstepping** proved to be a promising constructive

method to deal with hyperbolic PDEs. This framework consists in operating invertible coordinates changes to map the initial system to a target system with specific stability properties. Its general idea is simplifying the coupling structure by moving the destabilizing coupling terms at the actuated boundary, using successive integral invertible transformations. It was first proposed for the stabilization of various systems governed by PDEs such as chemical reactions [BKo2b], Burgers' equation with actuator dynamics [LKoo], heat equations [BKo2a] or parabolic partial integro-differential equations [SKo4]. This method takes advantage of the system's structure and allows the finding of adequate Lyapunov functions to assess the stability of the closed-loop system. It was then extended to flexible beams and wave equations [KSBGo7, KSSo6, KGBSo8, SGWK17]. Finally, it was extended to first-order hyperbolic PDEs in [KSo8, VKC11, CVKB13]. The backstepping methodology can also be applied to fully actuated coupled nonscalar systems [DMVK13, ADM16, CHO17].

This thesis deals with interconnections of such linear scalar first-order hyperbolic PDE systems. When only PDE systems are interconnected, the first results were obtained for stabilizing networks composed of two subsystems [ABABS⁺18, ADMBA19]. They were extended to a cascaded network with an arbitrary number of interconnected scalar PDEs in [Aur20], introducing a complex backstepping transformation. At the same time, backstepping-based controllers have been developed for chain structures containing ODE systems. First, only ODE-PDE interconnections were stabilized [DGK19, DMBAHK18]. Similarly, PDE-ODE-PDE interconnections [AVDMK19, KK20] were also considered. When the PDE system is fully actuated at one boundary, the strategy resumes as mapping the initial interconnected system to an exponentially stable cascaded system. Full-state feedback controllers were also designed to stabilize various ODE-PDE-ODE interconnections [WKP18, DGK18, Geh21]. In most cases, the constructive design is based on several invertible backstepping transforms, used to cancel the reflection term on the actuated boundary such that the PDE has no longer an impact on the state of the controlled ODE [BSBADLE17, DGK18]. However, they require restrictive structural assumptions.

A major concern for further application lies in the **implementability** of the proposed methods. Backstepping-based controllers require the knowledge of the distributed state to be computed. Usually, observers can be designed following a dual approach. Since they require know-how and a significant computational effort, their use must be justified by better closed-loop performances compared to classic boundary controllers (such as PI). Then, the **robustness** of the proposed solution, with regard to delays in the actuation or measurement, parameter uncertainties, or neglected dynamics or disturbances, must be considered. Indeed, the elementary linear interconnected systems under consideration do not encompass the complexity of real systems dynamics. More specifically, it has been long known that an arbitrarily small delay in the loop may cause the instability of the closed-loop system [DLP86]. When the ODE system is actuated, we might need to invert its dynamics, leading to non-strictly proper control inputs. Similarly, suppressing the reflection term using the backstepping-based controller may also lead to robustness issues. It was further shown in [AAMDM18] that hyperbolic PDE systems cannot always be exponentially stabilized or finite-time stabilized robustly to delays. Consequently, a focus has been made on robustly stabilizing such networks [BSBADLE19, AADMS21, ABADM23].

Interestingly, robustness analysis sometimes use a **time-delay systems representation** [HVL13]. Indeed, simplifying the coupling terms in the equivalent hyperbolic target system, it becomes possible to rewrite it as a time-delay system, generally of neutral type.

Using the method of characteristics, a linear first-order uncoupled hyperbolic PDE system can be rewritten as a difference equation. First mappings were proposed in [KK14] and extended to a general class of systems in [ADM19]. The stability properties of hyperbolic systems can then be analyzed using the equivalent Difference-Delay system representation [Rus78a]. It further led to the parametrization of the control input by a flat output [Woi13]. The advantages of considering different representations of the same system were recently emphasized in [Pee21]. We can therefore use specific tools developed for such delay-differential equations, for instance, take advantage of stability analysis results obtained in this formalism [HVL13, Nico1]. It can be combined with classic control design techniques (spectral analysis, pole placement, design of predictors) to stabilize interconnected networks.

Problems under consideration

Thesis Objective

This thesis aims to stabilize networks of linear scalar hyperbolic PDE systems interconnected with ODEs in a chain structure. We present constructive methods for the design of controllers and observers.

The proposed approaches are based on the backstepping methodology, and take advantage of stability analysis results for time-delay systems.

This thesis considers underactuated networks of hyperbolic PDE systems interconnected with linear ODE systems in a chain structure. As presented earlier, such networks have an interest in many practical applications. This thesis introduces in **Part I** existing results for two classes of infinite dimensional systems: linear hyperbolic Partial Differential Equations (PDE) systems and Time-Delay Systems (TDS) of the neutral type. In the simple case of a linear scalar hyperbolic PDE system, we introduce the strong relationship between these two classes, using an explicit mapping derived from the *backstepping methodology*. It induces similar asymptotic stability properties. Then we consider a first interconnection between pure transport equations and a linear ODE. Finite-dimensional systems may here correspond to the actuator or load dynamics. We present the limitations of classic control approaches, such as Proportional or Proportional Integral boundary feedbacks, on this simple chain structure. This emphasizes the interest in backstepping-based controllers, which consider the distributed nature of the dynamics.

After this introductory part, we address different stabilization problems on chain structures. In **Part II**, we study the case where the available actuation is located at one end of the network. We first consider in **Chapter 4** the case of an ODE-PDE-ODE interconnection. The output feedback design allowing output tracking and disturbance rejection combines backstepping and frequency analysis. It is presented in [W1, B1, J2]. Next, we consider in **Chapter 5** the case of a chain of arbitrary many scalar hyperbolic PDE systems interconnected at the unactuated end with an ODE. To obtain a stabilizing output-feedback controller, we propose an innovative *recursive dynamics interconnection framework*. It is presented in [C8, J4] and applied to drilling systems in [C5]. Indeed, drilling systems can be modeled by such chain structures. It is illustrated in **Chapter 6**, where we apply the

proposed methodology to the state estimation and trajectory tracking issues for two different well architectures.

However, though in some applications, such as drilling, the control input is available at one end of the network, it is not always the case. Some examples where the actuation is available *at a junction* of the domain can be found in traffic control or biomedical devices. We, therefore, study in **Part III** this situation. In **Chapter 7**, we consider the case of two interconnected hyperbolic PDE systems with actuation at the in-between boundary. Due to new couplings, we use an adequate Fredholm integral transform, whose well-posedness and invertibility are proved using an operator framework. It is presented in [C6, C7, J3]. This methodology is applied in **Chapter 8** to stabilize clamped-string dynamics with an actuation at the middle of the system [C1]. We end both parts by presenting perspectives and extensions of the proposed approaches to higher-dimensional cases and more complex networks.

Finally, **Part IV** is dedicated to under-considered aspects of backstepping-based controllers, such as controller tuning and implementation issues. First, we question in **Chapter 9** the choice of reachable target systems using the backstepping methodology. Using a creative time-affine transform, we show that a general class of nonscalar hyperbolic PDE systems can be mapped to any arbitrary system of the same class. An adequate target system should be selected among this class to improve the performances of actual designs based on the backstepping methodology regarding closed-loop properties, such as faster convergence. We show in **Chapter 10** that specified closed-loop properties can be obtained using the Port-Hamiltonian framework. This strategy was presented in [C4, C2]. An observer design for the considered test case is proposed in Appendix C. Finally, we introduce in **Chapter 11** the use of machine learning to obtain real-time estimations of the distributed state and parameters for some hyperbolic PDE systems. This could enable distributed backstepping-based controllers to be used for real applications.

Publications

The work presented in this thesis resulted in several publications listed below. We thank the researchers and associate editors who helped improve the overall quality of this work through the review process.

• Journal articles

- [J1] Jeanne Redaud, Jean Auriol, and Yann Le Gorrec. "In domain dissipation assignment of boundary controlled Port-Hamiltonian systems using backstepping". *Systems & Control Letters*, 2024 (submitted).
- [J2] Jeanne Redaud, Federico Bribiesca-Argomedo, and Jean Auriol. "Output Regulation and Tracking for Linear ODE-hyperbolic PDE-ODE Systems". *Automatica*, 2023 (provisionally accepted).
- [J3] Jeanne Redaud, Jean Auriol, and Silviu-Iulian Niculescu. "Stabilizing Output-feedback control law for Hyperbolic Systems using a Fredholm transformation". *IEEE Transactions on Automatic Control*. 2022, Vol.67 (12), pp. 6651-6666. [hal-03702316v1](#)
- [J4] Jeanne Redaud, Jean Auriol, and Silviu-Iulian Niculescu. "Output-feedback Control of an Underactuated Network of Interconnected Hyperbolic PDE-ODE Systems". *Systems & Control Letters*, 2021 154: 104984. [hal-03269701](#)

• Book Chapters

- [B1] Jeanne Redaud, Federico Bribiesca-Argomedo, and Jean Auriol. "Practical Output Regulation and Tracking for Linear ODE-hyperbolic PDE-ODE Systems". Springer, 2021. *Advances in Distributed Parameter Systems*. [hal-03419924v1](#)

• Conference papers

- [C1] Jeanne Redaud, and Jean Auriol. "Backstepping stabilization of a clamped string with actuation inside the domain" (2023). 22nd IFAC World Congress. [hal-04054149](#)
- [C2] Jeanne Redaud, Jean Auriol, and Yann Le Gorrec. "In-domain damping assignment of a Timoshenko-beam using state feedback boundary control" (2022). 61st IEEE Conference on Decision and Control (CDC). [hal-03798819v1](#)
- [C3] Jeanne Redaud, Jean Auriol, and Silviu-Iulian Niculescu. "Characterization of PI feedback controller gains for interconnected hyperbolic systems" (2022). 8th IFAC Symposium on System Structure and Control (SSSC). [hal-03798805v1](#)
- [C4] Jeanne Redaud, Jean Auriol, and Yann Le Gorrec. "Distributed Damping Assignment for a Wave Equation in the Port-Hamiltonian Framework" (2022). IFAC Workshop on Control of Systems Governed by Partial Differential Equations (CPDE). [hal-03702318v1](#)
- [C5] Jeanne Redaud, Jean Auriol, and Silviu-Iulian Niculescu. "Recursive Dynamics Interconnection Framework Applied to Angular Velocity Control of Drilling Systems" (2022). American Control Conference (ACC). [hal-03604406v1](#)
- [C6] Jeanne Redaud, Jean Auriol, and Silviu-Iulian Niculescu. "Stabilizing Integral Delay Dynamics and Hyperbolic Systems using a Fredholm Transformation" (2021). 60th IEEE Conference on Decision and Control (CDC). [hal-03357334](#)

[C7] Jeanne Redaud, Jean Auriol, and Silviu-Iulian Niculescu. "Observer Design for a Class of Delay Systems Using a Fredholm Transform" (2021). 16th IFAC Workshop on Time Delay Systems (TDS). [hal-03357349](#)

[C8] Jean Auriol, Federico Bribiesca Argomedo, Silviu-Iulian Niculescu, and Jeanne Redaud. "Stabilization of a Hyperbolic PDEs-ODE Network Using a Recursive Dynamics Interconnection Framework" (2021). European Control Conference (ECC). [hal-03185012](#)

- **Workshop presentation**

[W1] Jeanne Redaud, Federico Bribiesca-Argomedo, and Jean Auriol. "Practical Output Regulation and Tracking for Linear ODE-hyperbolic PDE-ODE Systems" (2021). 3rd DECOD — DELays and CONstraints in Distributed parameter systems.

Further contributions

At the end of my Ph.D., I had the opportunity to spend 3 months as a short-term postdoctoral fellow at Kobe University, under the supervision of Professor Hideki Sano. This collaboration resulted in the following contributions.

- **Journal articles**

[A1] Jeanne Redaud, Hideki Sano. "Numerical resolution of the inverse problem and unknown infection rate identification for a Kermack-McKendrick distributed model using singular value decomposition". Mathematical Biosciences and Engineering (AIMS), 2024 (submitted).

[A2] Hideki Sano, Jeanne Redaud. "Observers for hyperbolic systems with multiple delays in the nonlocal boundary condition and its application to secure image encryption". Systems & Control letters, 2024 (submitted).

[A3] Jeanne Redaud, Hideki Sano. "Enhanced image encryption algorithm based on chaotic hyperbolic PDE systems synchronization". Transactions on Image Processing, 2024 (submitted).

- **Conference papers**

[P1] Jeanne Redaud, Hideki Sano. "Synchronization of chaotic hyperbolic PDE systems for image encryption using backstepping observer design". European Control Conference (ECC), 2024 (submitted).

[P2] Jeanne Redaud, Hideki Sano. "Numerical analysis of a chaotic coupled hyperbolic PDE system for secure image encryption". 7th IFAC Conference on Analysis and Control of Nonlinear Dynamics and Chaos (ACNDC), 2024 (submitted).

- **Workshop presentation**

[R1] Hideki Sano, Jeanne Redaud. "Observers for hyperbolic systems with two delays in the nonlocal boundary condition and its application" (2023). RIMS Workshop on "Time-delay systems and mathematical sciences: new developments of theory and applications", Kyoto University.

Part I

Modélisation and preliminary results

Modélisation et résultats préliminaires

Introduction

As presented in the introduction, hyperbolic PDE systems (balance laws) interconnected with ODE systems allow for a comprehensive and accurate representation of a large class of systems involving spatial and temporal dynamics. This modeling facilitates system-level analysis, control design and provides valuable insights into the behavior and performance of interconnected systems. Considering the distributed dynamics in the design results in more complex infinite-dimensional controllers, compared to classic Proportional Integral Derivative (PID) boundary feedback laws, but can lead to better performance, such as fastest stabilization. In this introductory part, we give some insights into the systems under consideration, the methodology we use, and the stakes of this thesis.

First, **Chapter 2** introduces fundamental notions such as well-posedness and exponential stability for a scalar linear hyperbolic PDE system, actuated at one boundary. This simple hyperbolic PDE system corresponds to an elementary subsystem in the chain structures we consider throughout this thesis. We present some stability criteria from the literature for the case of conservation laws and constant anti-diagonal in-domain couplings. To deal with space-varying in-domain couplings, we present the backstepping methodology [Krs08]. It allows us to map the elementary subsystem to a target system where these couplings have been moved to the actuated boundary. Using the method of characteristics, we then present the close relation between hyperbolic PDE systems and *neutral* time-delay systems. As highlighted in [ADM19], this formulation can characterize the stability properties of hyperbolic systems in a more general setting. We end this chapter with perspectives on chain structures and briefly present the organization of the thesis.

Next, in **Chapter 3**, we focus on the simplest chain structure: hyperbolic PDE subsystem with no in-domain couplings (conservation laws) coupled at one end with an ODE system. As known, characterizing the stability of linear neutral time delay systems is a complex issue. Indeed, the characteristic equation associated with a delay system is *transcendental* and has infinitely many roots in the complex plane. Apart from the backstepping methodology [DGK18], several approaches have recently been developed for the control of coupled PDE-ODE systems, such as predictor-type feedback [Krs08], or flatness strategies [MK09]. Due to the complexity of their architecture, such controllers require know-how and computing power to be implemented on real systems. Therefore, their use must be justified by a failure of traditional controllers, such as Proportional (P) or Proportional Integral (PI) boundary output feedbacks [SDB05]. Using a frequency domain approach, we first characterize the open-loop and closed-loop stability of this simple chain structure using such simple feedback controllers. Their limitation emphasizes the interest in using more complex strategies, such as the backstepping methodology, to stabilize interconnected systems.

2 - Preliminary results on scalar linear hyperbolic PDE systems. Backstepping methodology.

This introductory chapter recalls general results on linear scalar hyperbolic Partial Differential Equations (PDE) systems [CVKB13, HVDMK15, BC16, Aur18]. We first present a class of balance laws using the classic PDE formalism. Such system will serve as an elementary component in chain structures further considered in this thesis. We also present the abstract operator framework that allows for stating their well-posedness. Then, we present general stability results for linear conservation laws and coupled hyperbolic PDE systems. Using the backstepping methodology, we can link this class of systems to neutral delay equations. It allows us to use some stability results obtained from frequency analysis and to derive a distributed controller stabilizing the system in finite time. Finally, we introduce the interconnections in a chain structure considered throughout this thesis and we present the organization of the manuscript.

Chapitre 2: Résultats préliminaires sur des systèmes scalaires linéaires d'EDP hyperboliques. Introduction à la méthode de backstepping. Ce chapitre introductif présente le cadre mathématique général des systèmes de dimension infinie que sont les systèmes d'équations aux dérivées partielles (EDP) de type hyperbolique. Nous présentons le formalisme classique considéré dans cette thèse, ainsi que le formalisme opérateur, utilisé pour montrer le caractère bien posé de ces systèmes. Nous présentons des résultats existants sur la stabilité de lois de conservations et de systèmes d'EDP hyperboliques couplés. Par la méthode de backstepping, nous pouvons réécrire un système d'EDP hyperbolique couplé sous la forme d'une équation à retard distribué de type neutre. Cela nous permet d'utiliser des résultats d'analyse fréquentielle pour établir leur stabilité. Nous introduisons finalement les systèmes interconnectés qui seront considérés au cours de cette thèse et présentons son organisation globale.

Contents

2.1	Well-posedness of the systems under consideration	16
2.1.1	Hyperbolic PDE formulation	16
2.1.2	Abstract operator framework formulation and well-posedness	17
2.2	Stability of linear hyperbolic systems	19
2.2.1	Scalar conservation laws	19
2.2.2	Coupled hyperbolic PDE systems	20
2.3	Stabilization of linear hyperbolic PDE system	27
2.3.1	Control input for finite-time stabilization	27
2.3.2	Delay-robust stabilizing controllers	29
2.4	Perspectives on more complex networks	30
2.4.1	Extension to chain structures	30
2.4.2	Thesis organization	31

2.1 . Well-posedness of the systems under consideration

This thesis will mostly consider scalar linear first-order hyperbolic PDE systems with constant transport speeds (except in Part IV). Before considering their interconnection in a chain structure, we present results for this class of systems using the classic PDE formulation. We also introduce the abstract operator formulation, which is used to assess the well-posedness of the hyperbolic PDE system and will further prove its interest in Chapter 7. Existing equivalent results for $(n+m) \times (n+m)$ hyperbolic systems are gathered in [Aur18], to which we refer any interested reader.

2.1.1 . Hyperbolic PDE formulation

General framework

For all $t \geq 0$, we consider a scalar hyperbolic PDE system of states $(u(t, \cdot), v(t, \cdot)) \in H^1([0, 1], \mathbb{R}^2)$, satisfying the following equations

$$\frac{\partial}{\partial t} u(t, x) + \lambda \frac{\partial}{\partial x} u(t, x) = \sigma^{++}(x)u(t, x) + \sigma^{+-}(x)v(t, x), \quad (2.1)$$

$$\frac{\partial}{\partial t} v(t, x) - \mu \frac{\partial}{\partial x} v(t, x) = \sigma^{-+}(x)u(t, x) + \sigma^{--}(x)v(t, x), \quad (2.2)$$

with the linear boundary conditions

$$u(t, 0) = qv(t, 0), \quad v(t, 1) = \rho u(t, 1) + V(t). \quad (2.3)$$

We assume that the right boundary is actuated by a control input $V(t)$, as schematically pictured in Figure 2.1. For the sake of simplicity, we assume we have constant transport speeds $\lambda, \mu > 0$ and constant boundary couplings q, ρ . The following results could be extended to space-dependent velocities [VKC11, HVDMK15, SA17]. We assume we have continuous in-domain couplings $\sigma^{\pm\mp} \in C^0([0, 1], \mathbb{R})$. We denote $(u_0, v_0) \in H^1([0, 1], \mathbb{R}^2)$ the corresponding initial conditions, which satisfy the following

Condition 2.1.1 *Compatibility conditions* $u_0(0) = qv_0(0), \quad v_0(1) = \rho u_0(1) + V(0)$.

As mentioned later in Remark 2.1.1 [HVDMK15], this condition is not restrictive for the choice of control input.

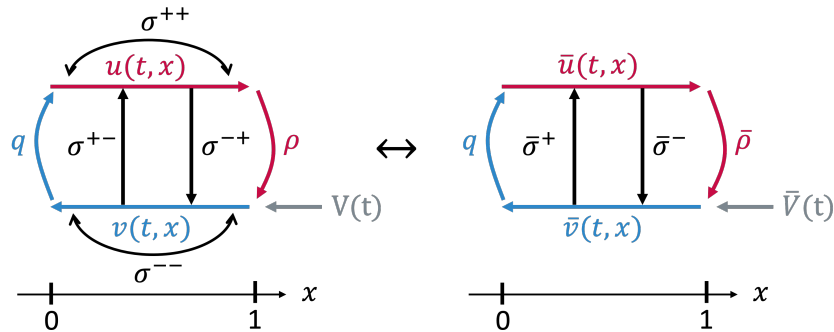


Figure 2.1 – Schematic representation of system (2.1)-(2.3) (left) and (2.4)-(2.5) (right).

First simplification

Note that the equations (2.1)-(2.2) can be first simplified using an exponential change of variables. Indeed, to apply the *backstepping* methodology introduced in Section 2.2.2, we need to suppress the coupling terms $\sigma^{\pm\pm}$ (similarly to what was done in the quasilinear or nonlinear case in [CVKB13, HVDMK15], or in [BC16, Section 5.3]). More precisely, since the functions $\sigma^{--}(\cdot)$, $\sigma^{++}(\cdot)$ are integrable, the following invertible exponential transformation is well defined for all $t > 0$ and all $x \in [0, 1]$:

$$\bar{u}(t, x) = u(t, x)e^{-\int_0^x \frac{\sigma^{++}(\nu)}{\lambda} d\nu}, \quad \bar{v}(t, x) = v(t, x)e^{+\int_0^x \frac{\sigma^{--}(\nu)}{\mu} d\nu}.$$

The new states satisfy

$$\begin{aligned} \frac{\partial}{\partial t} \bar{u}(t, x) + \lambda \frac{\partial}{\partial x} \bar{u}(t, x) &= \left(\frac{\partial}{\partial t} u(t, x) + \lambda \frac{\partial}{\partial x} u(t, x) - \sigma^{++}(x)u(t, x) \right) e^{-\int_0^x \frac{\sigma^{++}(\nu)}{\lambda} d\nu} \\ &= \sigma^{+-}(x)e^{-\int_0^x \frac{\sigma^{++}(\nu)}{\lambda} d\nu} v(t, x) = \bar{\sigma}^+(x)\bar{v}(t, x), \\ \frac{\partial}{\partial t} \bar{v}(t, x) - \mu \frac{\partial}{\partial x} \bar{v}(t, x) &= \bar{\sigma}^-(x)\bar{u}(t, x), \end{aligned} \quad (2.4)$$

with $\bar{\sigma}^+(x) = e^{-\int_0^x (\frac{\sigma^{++}(\nu)}{\lambda} + \frac{\sigma^{--}(\nu)}{\mu}) d\nu} \sigma^{+-}(x)$ and $\bar{\sigma}^-(x) = e^{\int_0^x (\frac{\sigma^{++}(\nu)}{\lambda} + \frac{\sigma^{--}(\nu)}{\mu}) d\nu} \sigma^{-+}(x)$.

The boundary conditions (2.3) rewrites

$$\bar{u}(t, 0) = q\bar{v}(t, 0), \quad \bar{v}(t, 1) = \bar{\rho}u(t, 1) + \bar{V}(t), \quad (2.5)$$

with $\bar{\rho} = \rho e^{\int_0^1 (\frac{\sigma^{++}(\nu)}{\lambda} + \frac{\sigma^{--}(\nu)}{\mu}) d\nu}$ and $\bar{V}(t) = e^{\int_0^1 \frac{\sigma^{--}(\nu)}{\mu} d\nu} V(t)$. Adjusting the corresponding initial conditions, system (2.1)-(2.3) and (2.4)-(2.5) are therefore equivalent. For this reason, we do not consider in this thesis the presence of diagonal coupling terms $\sigma^{\pm\pm}$ (i.e. σ^{++} , σ^{--}) in (2.1)-(2.3).

2.1.2 . Abstract operator framework formulation and well-posedness

The hyperbolic systems of form (2.1)-(2.3) belong to the general class of boundary control systems [Sal87]. They can be rewritten using the following abstract formulation

$$\frac{d}{dt} \begin{pmatrix} u \\ v \end{pmatrix} = A \begin{pmatrix} u \\ v \end{pmatrix} + BV, \quad (2.6)$$

where the operator A is defined by

$$\begin{aligned} A : D(A) \subset H^1([0, 1], \mathbb{R}^2) &\rightarrow H^1([0, 1], \mathbb{R}^2) \\ \begin{pmatrix} u \\ v \end{pmatrix} &\mapsto \begin{pmatrix} -\lambda \frac{\partial}{\partial x} u + \sigma^{+-}(\cdot)v \\ \mu \frac{\partial}{\partial x} v + \sigma^{-+}(\cdot)u \end{pmatrix}, \end{aligned}$$

on the domain $D(A) = \{(u, v) \in H^1([0, 1], \mathbb{R}^2) \mid u(0) = qv(0), v(1) = \rho u(1)\}$. The operator A is densely defined. The operators A and B can be identified through their adjoints. First, multiplying formally (2.1)-(2.2) by smooth test functions (ϕ, ψ) and integrating

by parts, we obtain

$$\begin{aligned}
0 = & - \int_0^T \int_0^1 \left(\frac{\partial}{\partial t} \phi(t, x) + \lambda \frac{\partial}{\partial x} \phi(t, x) + \psi(t, x) \sigma^{-+}(x) \right) u(t, x) \\
& + \left(\frac{\partial}{\partial t} \psi(t, x) - \mu \frac{\partial}{\partial x} \psi(t, x) + \phi(t, x) \sigma^{+-}(x) \right) v(t, x) dx dt \\
& + \int_0^1 \phi^T(T, x) u(T, x) + \psi(T, x) v(T, x) - (\phi(0, x) u_0(x) + \psi(0, x) v_0(x)) dx \\
& + \int_0^T (\lambda \phi(t, 1) - \mu \rho \psi(t, 1)) u(t, 1) - (\lambda q \phi(t, 0) - \mu \psi(t, 0)) v(t, 0) dt - \int_0^T \mu \psi(t, 1) V(t) dt.
\end{aligned}$$

Taking formally the canonical scalar product of (2.6) with the smooth test functions (ϕ, ψ) and comparing with the above equation, we define its adjoint A^* by

$$\begin{aligned}
A^* : D(A^*) \subset H^1([0, 1], \mathbb{R}^2) & \rightarrow H^1([0, 1], \mathbb{R}^2) \\
\begin{pmatrix} u \\ v \end{pmatrix} & \mapsto \begin{pmatrix} \lambda \frac{\partial}{\partial x} u + \sigma^{-+}(\cdot) v \\ -\mu \frac{\partial}{\partial x} v + \sigma^{+-}(\cdot) u \end{pmatrix},
\end{aligned}$$

with $D(A^*) = \{(u, v) \in H^1([0, 1], \mathbb{R}^2) \mid u(1) = \frac{\mu \rho}{\lambda} v(1), v(0) = \frac{\lambda q}{\mu} u(0)\}$. It has been proved in [Rus78b, Theorem 3.1] that A generates a C^0 -semigroup of bounded operators on $L^2([0, 1], \mathbb{R}^2)$. Since operator $B \in \mathcal{L}(\mathbb{R}, D(A^*)')$ satisfies $\langle BV, \begin{pmatrix} u \\ v \end{pmatrix} \rangle = \mu v(1) V$, its adjoint $B^* \in \mathcal{L}(D(A^*), \mathbb{R})$ is defined by

$$B^* \begin{pmatrix} u \\ v \end{pmatrix} = \mu v(1).$$

The operator B is well-defined since BV is continuous on $H^1([0, 1], \mathbb{R}^2)$ by the trace theorem. It satisfies

Condition 2.1.2 *Admissibility condition* [LT83, LT91, Wei89]

$$\exists M > 0, \int_0^T |B^* \mathcal{S}(T-t)^* z|^2 dt \leq M \|z\|_{L^2}^2, \quad \forall z \in D(A^*),$$

with \mathcal{S} the semigroup generated by the operator A . We have

Lemma 2.1.1: Well-posedness [Rus78b, Theorem 3.1]

For every initial condition $(u_0, v_0) \in H^1([0, 1], \mathbb{R}^2)$ satisfying condition 2.1.1, and every control laws $V \in L^2([0, t], \mathbb{R})$, the system (2.1)-(2.3) admits a unique solution $(u, v) \in C^0([0, +\infty), H^1([0, 1], \mathbb{R}^2))$.

Moreover, there exists constant M, γ and ρ_t such that

$$\|(u, v)\|_{L^2} \leq M e^{-\gamma t} (\|(u_0, v_0)\|_{L^2} + \rho_t \|V_{[t]}\|_{D_t}).$$

More generally, for initial conditions $(u_0, v_0) \in L^2([0, 1], \mathbb{R}^2)$, a general solution in $C([0, +\infty), L^2([0, 1], \mathbb{R}^2))$ [Rus78b] is of form

$$\begin{pmatrix} u(t, \cdot) \\ v(t, \cdot) \end{pmatrix} = \mathcal{S}(t) \begin{pmatrix} u_0 \\ v_0 \end{pmatrix} + C(t)V_{[t]},$$

where $V_{[t]}$ is the restriction of V to $[0, t]$, and $C(t) : L^2([0, t], \mathbb{R}) \rightarrow L^2([0, 1], \mathbb{R}^2)$ is a bounded linear operator for each t . Then, $\rho_t = \|C(t)\|$, $\forall t \geq 0$.

Remark 2.1.1 *In this thesis, we mostly consider the existence of H^1 solutions with H^1 initial conditions. However, we consider the exponential stability in the sense of the L^2 -norm given in Definition 2.2.1, which is less restrictive than the H^1 -norm. Using H^1 solutions allows considering pointwise values in Chapter 7. Considering L^2 -initial conditions would lead us to look for solutions in a weak formulation given in Section 2.1.2. Higher regularity of the solution would require additional compatibility conditions to condition 2.1.1, particularly on the time derivatives of (u_0, v_0) . As presented in [HVDMK15], it would only have a limited impact on the initial value of the control input, since a dynamical extension could be added.*

2.2 . Stability of linear hyperbolic systems

Next, we focus on the stability properties of scalar linear hyperbolic PDE systems. Since the approaches we present in this thesis mainly rely on the backstepping methodology, it is interesting to question first the stability properties of some hyperbolic systems in open-loop, that could be potential *target* systems. We give the following definition

Definition 2.2.1: Exponential stability [BC16]

The hyperbolic system (2.1)-(2.3) is exponentially stable, if there exist $\nu, C > 0$ such that, for every compatible initial condition $(u_0, v_0) \in H^1([0, 1], \mathbb{R}^2)$, the solution of (2.1)-(2.3) satisfies

$$\|(u, v)\|_{L^2} \leq Ce^{-\nu t} \|(u_0, v_0)\|_{L^2}.$$

2.2.1 . Scalar conservation laws

First, consider the simple case where $\sigma^{\pm\pm} \equiv 0 \leftrightarrow \sigma^{++} = \sigma^{--} = 0$. As seen in Section 2.2.2, the backstepping methodology corresponds to a mapping of system (2.1)-(2.3) to a target system where the in-domain couplings are usually moved to the actuated boundary. In the absence of in-domain coupling terms, system (2.1)-(2.3) reduces to a system of two *conservation laws*. Using the method of characteristics, we immediately have that,

$$\text{for all } t > \delta \doteq \frac{1}{\lambda} + \frac{1}{\mu}, v(t, 0) = \rho q v(t - \delta, 0). \quad (2.7)$$

Therefore, the boundary-coupled transport equations can be rewritten as a *neutral* system, and, more precisely, a difference equation. The stability properties of such a system

depend on the location of the roots of the corresponding complex characteristic equation [HVL13, Nico1], as seen in Chapter 3. It is given by

$$(1 - \rho q e^{-\delta s})v(s, 0) = 0.$$

From [HL02, Theorem 2.2], the difference equation (2.7) is exponentially stable iif

Condition 2.2.1 *The coefficients ρ, q satisfy $|\rho q| < 1$.*

Note that this condition is independent of delay δ . It prevents having infinitely many poles on the Right-Half Plane (RHP), which would hinder robust stabilization of the system [LRW96, HVL13, ABABS⁺18]. Similar conditions exist in a more general setting, as seen in the next chapters. In particular, the general case of neutral equations with multiple non-commensurate delays is given in [HL02, HVL13]. A Lyapunov approach led to an explicit sufficient condition in [CBdNo8]. More recently, necessary and sufficient conditions were derived for nonscalar difference equations in [ABP23], based on a Lyapunov functional constructed in [RCMDL18].

2.2.2 . Coupled hyperbolic PDE systems

Next, we take into account constant coupling terms σ^{+-}, σ^{-+} in (2.1)-(2.3). Using a Lyapunov approach, [BC16] derived sufficient conditions for the exponential stability of the open loop system. This could help to determine exponentially stable target systems (see Chapter 10 for further considerations) in the backstepping methodology. From [BC16, Corollary 5.5], [Aur18] derived the following

Lemma 2.2.1: Sufficient stability conditions [Aur18, Lemma 2.2.2]

If $q \neq 0$, system (2.1)-(2.3) is exponentially stable in open-loop if one condition is satisfied

1. $\sigma^{+-} = \sigma^{-+} = 0$,
2. $\sigma^{+-}\sigma^{-+} < 0$, and $\rho^2 < -\frac{\lambda\sigma^{-+}}{\mu\sigma^{+-}} < \frac{1}{q^2}$.

In the nonscalar case, the above conditions rewrite as Linear Matrices Inequalities (LMIs). This sufficient condition was extended in [BSBAA⁺19], rewriting system (2.1)-(2.3) as a neutral system with distributed delays. This is done using the *backstepping methodology*.

Introduction to the backstepping methodology

To avoid further case distinctions, assume $q \neq 0$ (this approach could be adapted to this situation [HVDMK15, Section 3.5]). We apply here the *backstepping methodology* [Krs08] for the coupled scalar linear hyperbolic PDE system (2.1)-(2.3). This methodology relies on an invertible change of variables, usually a Volterra integral transform.

Volterra integral transform We consider the following Volterra integral transform

$$\begin{aligned} \mathcal{K} : H^1([0, 1], \mathbb{R}^2) &\longrightarrow H^1([0, 1], \mathbb{R}^2) \\ \begin{pmatrix} u(t, \cdot) \\ v(t, \cdot) \end{pmatrix} &\mapsto \begin{pmatrix} u(t, \cdot) \\ v(t, \cdot) \end{pmatrix} - \int_0^\cdot \begin{pmatrix} K^{++} & K^{+-} \\ K^{-+} & K^{--} \end{pmatrix} (\cdot, y) \begin{pmatrix} u(t, y) \\ v(t, y) \end{pmatrix} dy \end{aligned} \quad (2.8)$$

The functions $K^{\pm\pm}, K^{\pm\mp}$ are referred to as the *kernels* of the transformation and are all defined on the triangular domain $\mathcal{T}^- = \{(x, y) \in \mathcal{S}, y \leq x\}$.

Theorem 2.2.1: Invertibility of Volterra integral transforms [Yos60]

Define a Volterra integral operator \mathcal{K} of form (2.8), with kernels $K \in C_{pw}^0(\mathcal{T}^-, \mathbb{R}^{2 \times 2})$. For any function $f \in H^1([0, 1], \mathbb{R}^2)$, the equation

$$f(\cdot) = \mathcal{K}(\varphi)$$

of unknown $\varphi \in H^1([0, 1], \mathbb{R}^2)$ admits a unique solution. The inverse transformation \mathcal{K}^{-1} is also a Volterra integral transform of form (2.8).

This boundedly invertible transform will map the initial system to a so-called *target system* with equivalent stability properties. Indeed, we have the following

Lemma 2.2.2: Equivalent stability properties

For any $(u, v) \in H^1([0, 1], \mathbb{R}^2)$ exponentially stable in the sense of Definition 2.2.1, the **target system** $(\alpha, \beta) = \mathcal{K}(u, v) \in H^1([0, 1], \mathbb{R}^2)$, with \mathcal{K} a Volterra integral transform defined by (2.8) is also exponentially stable in this sense. The converse holds.

Proof: The proof relies on the invertibility and boundedness of transform (2.8). Assume there exists $\nu, C > 0$ such that for all $t > 0$, $\|u(t, \cdot), v(t, \cdot)\|_{L^2}^2 \leq Ce^{-\nu t} \|u_0, v_0\|_{L^2}^2$. Let us show that $(\alpha, \beta) = \mathcal{K}(u, v)$ is exponentially stable.

For all $t > 0$, we have

$$\begin{aligned} \|\alpha(t, \cdot), \beta(t, \cdot)\|_{L^2}^2 &= \int_0^1 \alpha(t, \nu)^2 + \beta(t, \nu)^2 d\nu \\ &= \int_0^1 (u(t, \nu) - \int_0^\nu K^{++}(\nu, y)u(t, y) + K^{+-}(\nu, y)v(t, y)dy)^2 \\ &\quad + (v(t, \nu) - \int_0^\nu K^{-+}(\nu, y)u(t, y) + K^{--}(\nu, y)v(t, y)dy)^2 d\nu \\ &\leq 2 \int_0^1 A^+(\nu)u^2(t, \nu) + A^-(\nu)v^2(t, \nu)d\nu \\ &\leq \underbrace{\max_{\nu \in [0, 1]} (A^+(\nu)), \max_{\nu \in [0, 1]} (A^-(\nu))}_{A_M} \|u(t, \cdot), v(t, \cdot)\|_{L^2}^2 \leq Ke^{-\nu t} \|u_0, v_0\|_{L^2}^2, \end{aligned}$$

with $A^\pm(\nu) = 1 + \int_\nu^1 K^{\pm\pm}(y, \nu)^2 + K^{\mp\pm}(y, \nu)^2 dy$ and $K = CA_M$. Using the boundedness of the inverse transform, such that $(u_0, v_0) = \mathcal{K}^{-1}(\alpha_0, \beta_0)$, we show the existence of \bar{A}_0 such that $\|u_0, v_0\|_{L^2}^2 \leq \bar{A}_0 \|\alpha_0, \beta_0\|_{L^2}^2$, which concludes the proof. We can prove similarly the other implication. ■

The chosen target system must be *simple* enough to assess interesting stability properties easily and *reachable* by a **boundedly invertible** transform to share the same stability properties. In our simple case, the most natural choice of a target system would be to suppress the in-domain couplings.

Target system In the case of system (2.1)-(2.3), the potentially destabilizing terms are the in-domain couplings σ^{-+} , σ^{+-} [BC11, BC16]. Define a target system as two conservation laws

$$\frac{\partial}{\partial t} \alpha(t, x) + \lambda \frac{\partial}{\partial x} \alpha(t, x) = 0, \quad \frac{\partial}{\partial t} \beta(t, x) - \mu \frac{\partial}{\partial x} \beta(t, x) = 0, \quad (2.9)$$

with boundary conditions

$$\alpha(t, 0) = q\beta(t, 0), \quad \beta(t, 1) = \rho\alpha(t, 1) - \int_0^1 N^\alpha(y)\alpha(t, y) + N^\beta(y)\beta(t, y)dy + V(t), \quad (2.10)$$

with N^α , N^β continuous functions defined on $[0, 1]$, whom explicit expression is given later. It is represented in Figure 2.2 (left).

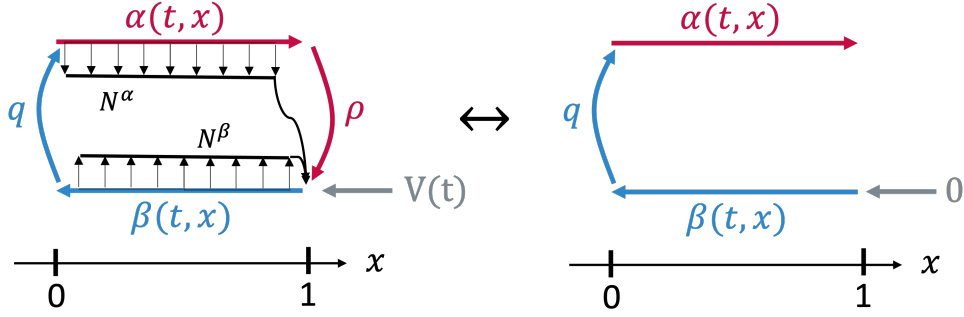


Figure 2.2 – Schematic representation of the target system (2.9)-(2.10) (left) and with control input (2.24) (right)

Well-posedness of an adequate transformation The first objective consists in proving the existence of a transformation of form (2.8), mapping the initial system (2.1)-(2.3) to the target system (2.9)-(2.10). By Lemma 2.2.2, the invertibility of transform (2.8) guarantees that both systems share equivalent stability properties. We want to obtain the equations satisfied by the kernels of the transform \mathcal{K} such that

$$\begin{pmatrix} \alpha(t, x) \\ \beta(t, x) \end{pmatrix} = \begin{pmatrix} u(t, x) \\ v(t, x) \end{pmatrix} - \int_0^x \begin{pmatrix} K^{++}(x, y) & K^{+-}(x, y) \\ K^{-+}(x, y) & K^{--}(x, y) \end{pmatrix} \begin{pmatrix} u(t, y) \\ v(t, y) \end{pmatrix} dy. \quad (2.11)$$

Introduce the following *kernel equations*

$$\begin{aligned} \lambda \frac{\partial}{\partial x} K^{++}(x, y) + \lambda \frac{\partial}{\partial y} K^{++}(x, y) &= -\sigma^{-+}(y) K^{+-}(x, y), \\ \lambda \frac{\partial}{\partial x} K^{+-}(x, y) - \mu \frac{\partial}{\partial y} K^{+-}(x, y) &= -\sigma^{+-}(y) K^{++}(x, y), \\ \mu \frac{\partial}{\partial x} K^{-+}(x, y) - \lambda \frac{\partial}{\partial y} K^{-+}(x, y) &= \sigma^{-+}(y) K^{--}(x, y), \\ \mu \frac{\partial}{\partial x} K^{--}(x, y) + \mu \frac{\partial}{\partial y} K^{--}(x, y) &= \sigma^{+-}(y) K^{-+}(x, y), \end{aligned} \quad (2.12)$$

with the boundary conditions

$$K^{+-}(x, x) = \frac{\sigma^{+-}(x)}{\lambda + \mu}, \quad K^{++}(x, 0) = \frac{\mu}{q\lambda} K^{+-}(x, 0), \quad (2.13)$$

$$K^{-+}(x, x) = -\frac{\sigma^{-+}(x)}{\lambda + \mu}, \quad K^{--}(x, 0) = \frac{q\lambda}{\mu} K^{-+}(x, 0). \quad (2.14)$$

We have the following lemma

Lemma 2.2.3: Well-posedness of kernel equations [CVKB13, A.1]

The system (2.12)-(2.14) admits a unique solution $K \in C^0(\mathcal{T}^-, \mathbb{R}^{2 \times 2})$.

Proof : The proof is quite usual [Krs08, HDMVK16] and [Aur18, Section 3.2.1]. Using the method of characteristics, we can write the integral equations associated with equations (2.12)-(2.14). They are then solved using the method of successive approximations (see Appendix A for more details on the numerical method). ■

Note that the regularity of the solution depends on one of the coupling terms $\sigma^{\pm\mp}$. For constant coefficients, an explicit solution to the kernel equations can be derived using Bessel and Marcum Q -functions [VK14]. Next, we have the following theorem

Theorem 2.2.2: Mapping of an adequate system

The transform (2.11) with kernels defined by (2.12)-(2.14) maps the initial system (2.1)-(2.3) to the target system (2.9)-(2.10).

Proof : Differentiating (2.11) with respect to time and integrating by parts, we obtain

$$\begin{aligned} \frac{\partial}{\partial t} \alpha(t, x) &= \frac{\partial}{\partial t} u(t, x) - \int_0^x K^{++}(x, y) \frac{\partial}{\partial t} u(t, y) + K^{+-}(x, y) \frac{\partial}{\partial t} v(t, y) dy \\ &= -\lambda \frac{\partial}{\partial x} u(t, x) + \sigma^{+-}(x) v(t, x) - \int_0^x K^{++}(x, y) \left(\sigma^{+-}(y) v(t, x) - \lambda \frac{\partial}{\partial y} u(t, y) \right) \\ &\quad + K^{+-}(x, y) \left(\mu \frac{\partial}{\partial y} v(t, y) + \sigma^{-+}(y) u(t, y) \right) dy \\ &= -\lambda \frac{\partial}{\partial x} u(t, x) + \sigma^{+-}(x) v(t, x) + \lambda K^{++}(x, x) u(t, x) - \lambda K^{++}(x, 0) u(t, 0) \\ &\quad - \mu K^{+-}(x, x) v(t, x) + \mu K^{+-}(x, 0) v(t, 0) - \int_0^x \left(K^{++}(x, y) \sigma^{+-}(y) \right. \\ &\quad \left. - \mu \frac{\partial}{\partial y} K^{+-}(x, y) \right) v(t, y) + \left(\lambda \frac{\partial}{\partial y} K^{++}(x, y) + K^{+-}(x, y) \sigma^{-+}(y) \right) u(t, y) dy. \end{aligned}$$

Similarly, differentiating (2.11) with respect to space, we obtain

$$\begin{aligned} \frac{\partial}{\partial x} \alpha(t, x) &= \frac{\partial}{\partial x} u(t, x) - K^{++}(x, x) u(t, x) - K^{+-}(x, x) v(t, x) \\ &\quad - \int_0^x \frac{\partial}{\partial x} K^{++}(x, y) u(t, y) + \frac{\partial}{\partial x} K^{+-}(x, y) v(t, y) dy. \end{aligned}$$

This yields

$$\begin{aligned} \frac{\partial}{\partial t} \alpha(t, x) + \lambda \frac{\partial}{\partial x} \alpha(t, x) &= (\sigma^{+-}(x) - \lambda K^{+-}(x, x) - \mu K^{+-}(x, x)) v(t, x) \\ &\quad + (\mu K^{+-}(x, 0) - \lambda K^{++}(x, 0)) v(t, 0) \\ &\quad - \int_0^1 \left(\lambda \frac{\partial}{\partial x} K^{++}(x, y) + \lambda \frac{\partial}{\partial y} K^{+-}(x, y) + \sigma^{-+}(y) K^{+-}(x, y) \right) u(t, y) dy \\ &\quad - \int_0^1 \left(\lambda \frac{\partial}{\partial x} K^{+-}(x, y) - \mu \frac{\partial}{\partial y} K^{+-}(x, y) + \sigma^{+-}(y) K^{++}(x, y) \right) v(t, y) dy \\ &= 0 \quad \text{by (2.12) - (2.13)}. \end{aligned}$$

Similarly, we apply the same operations on the second component of (2.11), and conclude by Lemma 2.2.3. ■

Thus, the existence of a unique solution to system (2.12)-(2.14) consequently, implies the existence of the transformation (2.11).

Explicit expression of the inverse transform In the following, we derive an explicit expression of the inverse transform $\mathcal{L} \doteq \mathcal{K}^{-1}$ such that

$$\forall t > 0, x \in [0, 1], \quad \begin{pmatrix} u(t, x) \\ v(t, x) \end{pmatrix} = \mathcal{L} \left(\begin{pmatrix} \alpha(t, x) \\ \beta(t, x) \end{pmatrix} \right).$$

As mentioned, it is also a Volterra integral transform [Krs08]. Following the same approach as in the previous section, we show that the kernels $L^{\pm\pm}$, $L^{\mp\pm}$ of the inverse transform are defined by the set of PDEs

$$\lambda \frac{\partial}{\partial x} L^{++}(x, y) + \lambda \frac{\partial}{\partial y} L^{++}(x, y) = \sigma^{+-}(x) L^{-+}(x, y), \quad (2.15)$$

$$\lambda \frac{\partial}{\partial x} L^{+-}(x, y) - \mu \frac{\partial}{\partial y} L^{+-}(x, y) = \sigma^{+-}(x) L^{--}(x, y), \quad (2.16)$$

$$\mu \frac{\partial}{\partial x} L^{-+}(x, y) - \lambda \frac{\partial}{\partial y} L^{-+}(x, y) = -\sigma^{-+}(x) L^{++}(x, y), \quad (2.17)$$

$$\mu \frac{\partial}{\partial x} L^{--}(x, y) + \mu \frac{\partial}{\partial y} L^{--}(x, y) = -\sigma^{-+}(x) L^{+-}(x, y), \quad (2.18)$$

with the boundary conditions

$$\begin{aligned} L^{++}(x, 0) &= \frac{\mu}{q\lambda} L^{+-}(x, 0), & L^{--}(x, 0) &= \frac{q\lambda}{\mu} L^{-+}(x, 0), \\ L^{+-}(x, x) &= \frac{\sigma^{+-}(x)}{\lambda + \mu}, & L^{-+}(x, x) &= -\frac{\sigma^{-+}(x)}{\lambda + \mu}. \end{aligned} \quad (2.19)$$

Similarly, from Theorem 2.2.3, there exists a unique solution to (2.15)-(2.19) in $C^0(\mathcal{T}^-, \mathbb{R}^{2 \times 2})$. A tutorial for the numerical resolution of (2.15)-(2.18) can be found in Appendix A. Using this inverse transformation, we can rewrite the boundary condition in $x = 1$ for the target system

$$\begin{aligned} \beta(t, 1) &= V(t) + \rho \alpha(t, 1) \\ &+ \int_0^1 (\rho L^{++}(1, y) - L^{-+}(1, y)) \alpha(t, y) + (\rho L^{+-}(1, y) - L^{--}(1, y)) \beta(t, y) dy. \end{aligned}$$

Defining $N^\alpha(y) = L^{-+}(1, y) - \rho L^{++}(1, y)$, $N^\beta(y) = L^{--}(1, y) - \rho L^{+-}(1, y)$, we obtain the expression (2.10).

Stability properties of the open-loop system

Distributed delay form Since the initial and target systems share the same stability properties, we can now study the stability properties of the target system (2.9)-(2.10). Note that for any initial conditions $(\alpha_0, \beta_0) = \mathcal{K}(u_0, v_0) \in H^1([0, 1], \mathbb{R}^2)$ satisfying a compatibility condition (2.1.1), it admits a unique solution $(\alpha(t, \cdot), \beta(t, \cdot)) \in H^1([0, 1], \mathbb{R}^2)$, for all $t \geq 0$. We now use the *method of characteristics* to determine the delay equation satisfied by $\beta(t, 1)$, when $t > \delta$. First, the transport equations (2.9) yields

$$\beta(t, x) = \beta\left(t - \frac{1-x}{\mu}, 1\right), \quad \alpha(t, x) = \alpha\left(t - \frac{x}{\lambda}, 0\right) = q\beta\left(t - \frac{x}{\lambda}, 0\right) = q\beta\left(t - \frac{x}{\lambda} - \frac{1}{\mu}, 1\right). \quad (2.20)$$

Consequently, replacing α, β by their delayed formulation (2.20) in the boundary condition (2.10), and performing two changes of variables in the integral terms, we obtain

$$\begin{aligned}\beta(t, 1) &= \rho q \beta(t - \delta, 1) - \int_0^1 q N^\alpha(y) \beta\left(t - \frac{y}{\lambda} - \frac{1}{\mu}, 1\right) + N^\beta(y) \beta\left(t - \frac{1-y}{\mu}, 1\right) dy \\ &= \rho q \beta(t - \delta, 1) - \int_0^{\frac{1}{\mu}} \mu N^\beta(1 - \mu s) \beta(t - s, 1) ds - \int_{\frac{1}{\mu}}^\delta q \lambda N^\alpha\left(\lambda\left(s - \frac{1}{\mu}\right)\right) \beta(t - s, 1) ds.\end{aligned}$$

Introducing $N(s) = \mathbb{1}_{[0, \frac{1}{\mu}]}(s) \mu N^\beta(1 - \mu s) + \mathbb{1}_{[\frac{1}{\mu}, \delta]}(s) q \lambda N^\alpha\left(\lambda\left(s - \frac{1}{\mu}\right)\right)$, we finally get for all $t \geq \delta$,

$$\beta(t, 1) = \rho q \beta(t - \delta, 1) - \int_0^\delta N(s) \beta(t - s, 1) ds. \quad (2.21)$$

Moreover, we can express $\beta(t, 1)$ as a function of the initial conditions for $t < \delta$.

Lemma 2.2.4: Expression for $t < \delta$ [Aur18, Lemma 5.1.1]

For $t < \delta$, the function $\beta(t, 1)$ can be expressed as a function of $(\alpha_0, \beta_0) \in H^1([0, 1], \mathbb{R}^2)$, the initial conditions of (2.9)-(2.10). Thus, $\beta_{[t]}(\cdot, 1) \in H^1((-\delta, 0], \mathbb{R})$, $\forall t \geq \delta$.

Proof: The complete proof for $\lambda \geq \mu$ is given in [Aur18, Lemma 5.1.1]. It consists of several steps. We solve $\alpha(t, x)$ and $\beta(t, x)$ for $t \in [0, \delta]$ through the method of characteristics as a function of the initial conditions and $\beta(\cdot, 1)$. We then solve $\beta(t, 1)$ using the solution of $\alpha(t, x)$ and $\beta(t, x)$ and the boundary condition (2.10). We show that it verifies a Volterra integral equation of the second kind, which admits a unique solution. ■

Since $(\alpha_0, \beta_0) = \mathcal{K}(u_0, v_0)$, there exists a function $\phi_{u_0, v_0}(\cdot) \in H^1((-\delta, 0], \mathbb{R})$ that depends on the initial condition (u_0, v_0) such that $\beta(\cdot, 1)$ is the solution of the initial value problem (2.21) with the initial data $\beta(\cdot, 1)_0 = \phi_{u_0, v_0}$.

From [ADM19, Aur18], we also have

Theorem 2.2.3: Comparable representations [Aur18, Theorem 5.1.1]

Consider the operator \mathcal{L}_0 defined by

$$\begin{aligned}\mathcal{L}_0 : H^1([-\delta, 0], \mathbb{R}) &\rightarrow \mathbb{R} \\ \phi_{[t]} &\mapsto \rho q \phi_{[t]}(\delta) - \int_0^\delta N(\nu) \phi_{[t]}(\nu) d\nu.\end{aligned}$$

The space generated by the solutions of

$$\phi_{[t]} = \mathcal{L}_0 \phi_{[t]}. \quad (2.22)$$

with the initial condition $\phi_0 = \phi_{u_0, v_0} \in H^1([-\delta, 0], \mathbb{R})$ is isomorphic to the space generated by the solutions of (2.9)-(2.10).

Theorem 2.2.4: Comparable stability properties [Aur18, Theorem 5.1.2]

Consider (u, v) the solution of (2.9)-(2.10) along with the initial condition (u_0, v_0) and $\phi_{[t]}$ the solution of (2.22) along with the initial condition ϕ_{u_0, v_0} . There exist $r > 0$ and two constants $C_1, C_2 > 0$ such that for all $t > \max(\delta, r)$, the following inequality holds

$$C_1 \|\phi_{[t]}\|_{D_r} \leq \|(u, v)\|_{L^2} \leq C_2 \|\phi_{[t]}\|_{D_\delta}.$$

Proof : The proof is given in the more general non-scalar case in [Aur18, Theorem 5.2.4] and in [ADM19]. ■

It proves that the stability of $\beta(t, 1)$ implies the stability of the states (u, v) . Therefore, we can establish sufficient stability criterion for the open-loop system (2.9)-(2.10) (or equivalently (2.1)-(2.3)) based on the stability analysis of delay equation (2.21).

Importance of the boundary couplings Consider the open-loop system (2.9)-(2.10). Rewriting (2.21) in the frequency domain, we obtain the associated *characteristic equation*

$$1 - \rho q e^{-\delta s} + \int_0^\delta N(\nu) e^{-\nu s} d\nu = 0. \quad (2.23)$$

For all $\sigma > 0$, denote $P_\sigma = \{s \in \mathbb{C} \mid \Re(s) > \sigma\}$. First, let us state

Lemma 2.2.5: Extension of Rouché's Theorem [Aur18, Section 6.1]

For all $\sigma > 0$, and two holomorphic functions F, H such that $|H(s)| \xrightarrow[|s| \rightarrow +\infty]{} 0$. If the function $\det(F)$ has an infinite number of zeros on P_σ , then the function $\det(F + H)$ has an infinite number of zeros whose real parts are strictly positive.

As a direct consequence, we have the following

Theorem 2.2.5: Instability of the open-loop system

If $|\rho q| > 1$, the characteristic equation (2.23) has an infinite number of roots with a positive real part. Consequently, system (2.1)-(2.3) cannot be delay-robustly stabilized.

Proof : Denote $F(s) = 1 - \rho q e^{-\delta s}$ and $H(s) = \int_0^\delta N(\nu) e^{-\nu s} d\nu$. Using the Riemann-Lebesgue theorem, we have $|H(s)| \xrightarrow[|s| \rightarrow +\infty]{} 0$. The function F has an infinite number of zeros whose real parts are equal to $\frac{\ln(|\rho q|)}{2\delta}$. By

Lemma 2.2.5, the holomorphic function $F + H$ has infinitely many roots in the complex Right Half Plane (RHP). It has been shown in [LRW96] that having an open-loop transfer function with infinitely many poles on the closed right half-plane implies no (delay-)robustness margins in closed-loop, that is introducing any arbitrarily small delay in the actuation destabilizes the closed-loop system. Thus, by [LRW96, Theorem 1.2], this neutral system cannot be delay-robustly stabilized. Consequently, system (2.1)-(2.3) cannot be delay-robustly stabilized by Theorem 2.2.4. ■

This emphasizes the further requirement that condition 2.2.1 is satisfied for the systems we consider in this thesis. We will refer to it as a *delay-robustness* condition.

Stability criteria for constant in-domain couplings Finally, in the case where the in-domain couplings are space-independent, explicit criteria for the stability of the system (2.1)-(2.3) in open-loop can be derived. To simplify the notations, we define the following parameters $a \doteq q \frac{1}{\mu} \sigma^{-+} + \rho \frac{1}{\lambda} \sigma^{+-}$, $R \doteq \frac{1}{\lambda \mu} \sigma^{+-} \sigma^{-+}$, and denote $I_n, n \in \mathbb{Z}$ the modified Bessel functions of the first kind. We have the following

Theorem 2.2.6: [BSBA⁺19, Proposition 3]

Consider system (2.1)-(2.3) in open-loop, with $q \neq 0$. If Condition 2. from Lemma 2.2.1 or one of the conditions below is satisfied

1. $\sigma^{+-}\sigma^{-+} \geq 0$, $\rho q \geq 0$, and $|a| + |R| \left(\frac{1}{1+|\rho q|} - \frac{1-|\rho q|}{2} \right) < 1 - |\rho q|$
2. $\sigma^{+-}\sigma^{-+} \geq 0$, $\rho q < 0$ and $|a| + |R| \frac{1+|\rho q|}{2} < 1 - |\rho q|$,
3. $\sigma^{+-}\sigma^{-+} < 0$, $\rho q \geq 0$ and $|a|I_0 \left(\sqrt{|R|} \right) + |R| \left(\frac{1}{1+|\rho q|} - \frac{1-|\rho q|}{2} \right) \times \left[I_0 \left(\sqrt{|R|} \right) - I_2 \left(\sqrt{|R|} \right) \right] < 1 - |\rho q|$,
4. $\sigma^{+-}\sigma^{-+} < 0$, $\rho q < 0$ and $|a|I_0 \left(\sqrt{|R|} \right) + |R| \frac{1+|\rho q|}{2} \times \left[I_0 \left(\sqrt{|R|} \right) - I_2 \left(\sqrt{|R|} \right) \right] < 1 - |\rho q|$.

then, system (2.1)-(2.3) is exponentially stable in the sense of the L^2 -norm.

This theorem can help to determine adequate open-loop unstable systems in simulations for an illustrative purpose, but also exponentially stable target systems.

2.3 . Stabilization of linear hyperbolic PDE system

2.3.1 . Control input for finite-time stabilization

Once we defined the backstepping transform (2.11) and the target system (2.9)-(2.10), a natural choice of control input is to **cancel all the terms** at the actuated boundary $x = 1$. To guarantee the *finite-time convergence* of the target system (2.9)-(2.10), we define

$$V(t) = -\rho u(t, 1) + \int_0^1 K^{-+}(1, y)u(t, y) + K^{--}(1, y)v(t, y)dy. \quad (2.24)$$

As represented in Figure 2.2 (right), it becomes a cascade of two transport equations with a zero-boundary condition. It converges, for any initial condition, to its equilibrium in finite time δ [VKC11, Theorem 1] as does the original system (2.1)-(2.3).

Implementability and observer design

Note that implementing the control law (2.24) requires knowledge of the distributed state. It is then necessary to design an *observer* to obtain a state estimation. This can be done following a dual approach, as presented in [VKC11, Section 4]. Backstepping-based controllers require higher computational effort than classic Proportional or Proportional Integral boundary feedbacks, which can be easily computed in real-time. Indeed, obtaining the distributed estimation is usually done by solving a finite element scheme. A trade-off must be found between a high mesh resolution (which lowers the implementation error) and an acceptable computation time (reducing the space mesh implies reducing the time mesh). This leads us to a first requirement

Requirement 2.3.1: Design of output-feedback controllers

Design an implementable controller $V(t)$ using a boundary measurement $y(t)$ to exponentially stabilize the system under consideration.

Robustness issues

Next, the control input (2.24) cancels all the reflection terms. It allows to map the initial system to the simplest target system and guarantees the best performance (lowest stabilization time). However, as the model given by equations (2.1)-(2.3) can result from an approximation of a more complex physical system, the **robustness** of the control input must be taken into account. Discrepancies with the real system can come from uncertainties in the physical parameters, neglected dynamics, disturbances acting on the system, and delays acting on the actuator or sensors. For instance, the disturbance rejection for this system class was considered in [Aam13]. This problem is also considered for a more complex chain structure in Chapter 4. Adaptive observers can be designed to estimate the system parameters jointly with the distributed state [ADAK16b]. Following [Aur18, Chapter 6], we study the impact of a small delay $\eta_\epsilon > 0$ on the stability of the closed-loop system, based on the stability results from Section 2.2. In the target system, the boundary condition (2.10) rewrites

$$\beta(t, 1) = \rho\alpha(t, 1) - \int_0^1 N^\alpha(y)\alpha(t, y) + N^\beta(y)\beta(t, y)dy + V(t - \eta_\epsilon).$$

For all $t \geq \delta$, using (2.21) in closed-loop with delayed control input (2.24), we obtain the delay differential equation satisfied by the boundary state $\beta(\cdot, 1)$

$$\beta(t, 1) = \rho q \beta(t - \delta, 1) - \rho q \beta(t - (\delta + \eta_\epsilon), 1) - \int_0^\delta N(s)(\beta(t - s, 1) - \beta(t - (s + \eta_\epsilon), 1))ds.$$

The characteristic equation associated to the above neutral DDE is

$$1 - \rho q e^{-\delta s} + \rho q e^{-(\delta + \eta_\epsilon)s} + (1 - e^{-\eta_\epsilon s}) \int_0^\delta N(\nu) e^{-\nu s} d\nu = 0. \quad (2.25)$$

Based on Lemma 2.2.5, [Aur18] showed the following

Theorem 2.3.1: Robust stabilization [Aur18, Theorem 6.2.3]

If $|\rho q| > \frac{1}{2}$, then for any $\eta_\epsilon > 0$, the system (2.1)-(2.3) along with the delayed backstepping control law $V(t - \eta_\epsilon)$ is unstable. It cannot be finite-time stabilized robustly to delays.

Therefore, in some cases, it appears necessary to avoid the total cancellation of the proximal reflection, and thereby to give up finite-time convergence. It leads us to a second requirement

Requirement 2.3.2: Design robust controllers

Design a stabilizing output-feedback controller $V(t)$ that is robust to small delays.

2.3.2 . Delay-robust stabilizing controllers

First, recall the following definition

Definition 2.3.1: Delay-robust stabilization [LRW96]

The controller $V(t) = \mathcal{V}(u, v)$ with \mathcal{V} linear operator, **delay-robustly** stabilizes the system (2.1)-(2.3) in the sense of [LRW96] if the closed-loop system is exponentially stable in the sense of Definition 2.2.1 and if there exists a delay $\eta^* > 0$ such that for any $0 \leq \eta_\epsilon \leq \eta^*$, the system (2.1)-(2.3) with the delayed control law $V(t - \eta_\epsilon)$ remains exponentially stable.

In [AAMD18], the authors proposed two solutions to guarantee the delay-robustness of the controller. First, to preserve some reflection terms at the actuated boundary, then to filter the control input.

Partial cancellation of the reflection term

To overcome the stability limitation given by Theorem 2.3.1, while maintaining the distributed nature of the controller (2.24), a first solution is to slightly modify the control law as follows

$$\begin{aligned} V_2(t) &= V(t) + (\rho - \tilde{\rho})(u(t, 1) - \int_0^1 K^{++}(x, y)u(t, y) + K^{+-}(x, y)v(t, y)dy, \quad (2.26) \\ &= -\tilde{\rho}\alpha(t, 1) + \int_0^1 N^\alpha(1, \nu)\alpha(t, \nu) + N^\beta(1, \nu)\beta(t, \nu)d\nu, \end{aligned}$$

with
$$|\tilde{\rho}| < \frac{1 - |\rho q|}{|q|}, \quad (2.27)$$

which is well-defined under condition 2.2.1. With this new control input, the boundary condition in $x = 1$ (2.10) rewrites $\beta(t, 1) = (\rho - \tilde{\rho})\alpha(t, 1)$, with $|\rho - \tilde{\rho}| < 1$ by (2.27). We have the following

Theorem 2.3.2: Robust stabilization [AAMD18, Theorem 4]

The control law defined by (2.26) with $\tilde{\rho}$ satisfying (2.27) delay-robustly stabilizes the system (2.1)-(2.3) in the sense of Definition 2.3.1.

This first solution has the disadvantage of adding complexity to the control design by introducing new parameters. This is all the more true for cascaded systems or nonscalar hyperbolic systems, where the boundary couplings are matrices and not scalar terms.

Filtering of the backstepping-based controller

In [AAMD18], the authors proposed a filtered boundary feedback, given in the Laplace domain by

$$U_3(s) = -\frac{1 + as}{1 + bs}\rho u(s, 1), \quad (2.28)$$

with $a, b > 0$ tuning coefficients. To keep the distributed structure of the controller, an alternative could be to filter the control input (2.24). Define a control $V_3(t)$ by its Laplace transform as

$$V_3(s) = \frac{1 + as}{1 + bs}V(s), \quad (2.29)$$

with $a, b > 0$. For any delay $\eta_\epsilon > 0$, the neutral characteristic equation associated with $\beta(t, 1) = \rho\alpha(t, 1) - \int_0^1 N^\alpha(y)\alpha(t, y) + N^\beta(y)\beta(t, y)dy + V_3(t - \eta_\epsilon)$ is given by

$$0 = s \left(1 - \frac{a}{b}e^{-\eta_\epsilon s} - \rho q e^{-\delta s} + \rho q \frac{a}{b}e^{-s(\delta + \eta_\epsilon)} + \left(1 - \frac{a}{b}e^{-\eta_\epsilon s} \right) H(s) \right) + \frac{1}{b}(1 - \rho q e^{-\delta s})(1 - e^{-\eta_\epsilon s}) + \frac{1}{b}(1 - e^{-\eta_\epsilon s})H(s),$$

with $H(s) = \int_0^\delta N(\nu)e^{-\nu s}d\nu$. By Riemann-Lebesgue lemma, $|H(s)| \xrightarrow[\Re(s) \geq 0]{|s| \rightarrow \infty} 0$.

Considering the neutral delay-differential equation with multiple delays of form $sF_1(s) + F_2(s) = 0$, a sharp sufficient condition for exponential stability is given by [HVL13, Fab13]

$$\begin{aligned} & \left| \frac{a}{b} \right| + |\rho q| + \left| \frac{a}{b} \rho q \right| < 1, \text{ and } \frac{1}{b} > (1 + 2|\rho q|) \\ \implies & \frac{a}{b} < \frac{1 - |\rho q|}{1 + |\rho q|}, \text{ and } b < \frac{1}{1 + 2|\rho q|}. \end{aligned}$$

With more insights on the stability of neutral delay-differential equation with integral terms and multiple pointwise delays, we could determine necessary and sufficient conditions for (2.29) to robustly stabilize the plant (2.1)-(2.3). This is out of the scope of this thesis. As seen in Chapter 4, filtering techniques can be used to robustify the controller designed for more complex interconnected chain structures.

2.4 . Perspectives on more complex networks

So far, we have only introduced stability and well-posedness results for the test case of a single linear scalar hyperbolic PDE system. As seen in the previous sections, many results exist to assess the stability or stabilize these *elementary* systems. Note also that most results presented in this introductory chapter are extended to nonscalar hyperbolic PDE systems in [Aur18].

2.4.1 . Extension to chain structures

Next, we will mainly focus on chain structures composed of the elementary hyperbolic PDE systems of the form (2.1)-(2.3), interconnected together through their boundaries or with ODE systems (except in Part IV where we consider nonscalar PDE systems). Such interconnected networks belong to the class of *under-actuated* systems. Though one subsystem might be fully actuated at this boundary, others are not. The dynamics of the actuated subsystem must be considered to stabilize the other subsystems and, consequently, the chain structure. These networks are also related to integral delay equations of the neutral type with several pointwise and distributed delays.

As mentioned in the introduction, some results already existed on the stabilization of chain structures, for instance, hyperbolic PDE-ODE interconnections [DMBAHK18, DGK19, ABABS⁺18, IGR21], or multiple PDE subsystems [SA17, Aur20]. However, in most, if not all, existing results, the control input is located at one end of the chain structure.

Thesis Objectives

This thesis aims at

- pursuing existing works on control of hyperbolic PDE systems interconnected with ODEs in a chain structure, satisfying Requirements 2.3.1-2.3.2,
- overcoming the limitation of actuation at the end of the chain structure by considering actuation at a junction,
- presenting some perspectives on under-considered implementation-related aspects of the backstepping methodology (reduction of the computation time, choice of a meaningful target system).

2.4.2 . Thesis organization

This thesis is organized as follows:

Chapter 3: Characterization of P/PI controllers for a simple chain structure. This chapter considers conservation laws interconnected at one end with a nonscalar ODE. It questions the effectiveness of the widely used Proportional and Proportional-Integral boundary feedback in this simple chain configuration. It introduces the frequency domain considerations proposed in the rest of the thesis and justifies the use of the backstepping methodology and the development of new tools to stabilize more complex chain structures.

Next, we focus in **Part II** on chain structures where the actuation is located at one end.

Chapter 4: Output regulation and tracking for linear ODE-hyperbolic PDE-ODE systems. This chapter considers an ODE-hyperbolic PDE-ODE interconnection (Figure 2.3). We propose an output-feedback controller to solve output regulation and disturbance rejection under some natural but restrictive structural assumptions. We use stability analysis in the frequency domain and the backstepping methodology. Robustness is guaranteed using filtering techniques.

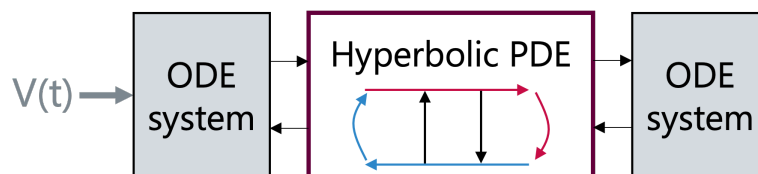


Figure 2.3 – System under consideration in Chapter 4. Output regulation and disturbance rejection. Focus on Requirements 2.3.1-2.3.2.

Chapter 5: Stabilizing a chain of N hyperbolic PDE systems interconnected with an ODE. In this chapter, we consider a chain of arbitrarily many hyperbolic PDE systems, actuated at one end and interconnected at the other end with an ODE system (Figure 2.4). We propose an output-feedback controller to stabilize the network using a *recursive dynamics interconnection framework*. We use the backstepping methodology and the method of characteristics to derive the delay equations satisfied by the boundary states. We use predictors to obtain real-time and future values of the distributed state.

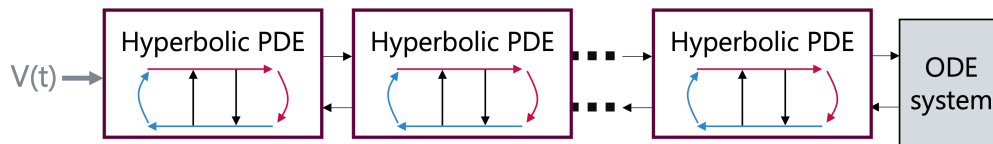


Figure 2.4 – System under consideration in Chapter 5. Exponential stabilization. Focus on Requirement 2.3.1.

Chapter 6: Application to drilling systems for state estimation and trajectory tracking. In this chapter, we illustrate the observer and controller designs proposed in the previous chapters in the context of drilling systems. We propose a state estimation of the axial motion for a vertical drilling system and a controller for trajectory tracking for the angular velocity in the case of a deviated well path.

At the end of this part, we present some natural extensions and the challenges that remain to be solved.

In **Part III**, we consider a chain structure where the actuation is not located at one end but at one in-between boundary.

Chapter 7: Stabilizing two hyperbolic PDE systems with in-between boundary actuation. This chapter considers a chain of two interconnected hyperbolic PDE systems, where the actuation is located at the in-between boundary (Figure 2.5). We propose an output feedback controller guaranteeing exponential stabilization of the system. We use the backstepping methodology with a Fredholm Integral transform that is proved to be invertible under a specific controllability assumption. Once again, our proposed methodology can also stabilize the solution of some integral delay equations.

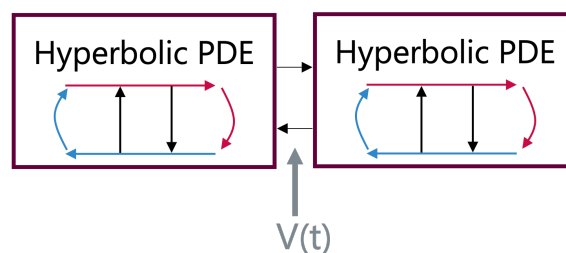


Figure 2.5 – System under consideration in Chapter 7. Exponential stabilization. Focus on Requirement 2.3.1.

Chapter 8: Application to the stabilization of a clamped string. In this chapter, we consider stabilizing a clamped string using a strain actuation at the middle of the string. This problem can be related to stabilizing an integral delay equation of the form considered in the previous chapter. We therefore adapt the methodology presented herein.

We end both Parts II and III by presenting some natural extensions to the systems considered (nonscalar case, more complex networks...)

Finally, in **Part IV**, we ponder on some current implementation-related limitations of the backstepping approach.

Chapter 9: Arbitrary target system for a general class of nonscalar hyperbolic PDE systems. In this chapter, we show that using a specific time-affine transform, we can map a general nonscalar linear hyperbolic PDE system to any target system of the same class. This offers a generalization of the backstepping methodology but questions the choice of an adequate target system.

Chapter 10: On the use of the Port-Hamiltonian framework to determine adequate target systems. In this chapter, we present the use of the Port-Hamiltonian framework to select an adequate target system in the class presented in the previous chapter. This guarantees specific closed-loop properties with a physical meaning (stability, energy decay rate). We illustrate this approach for the damping assignment of a clamped string and a Timoshenko beam. We present in Appendix C two observer designs for this latter system.

Chapter 11: Machine Learning techniques for distributed state and parameter estimation. In this chapter, we introduce some neural network-based architecture as a surrogate to classic backstepping-based observers in the same test case of a Timoshenko beam. We also present the potential of deep-learning-based solutions for parameter estimation in the case of drilling systems.

We gather in the Appendices some supplementary material that aims to understand this thesis better. First, in **Appendix A**, we present some numerical methods we used for kernel resolution. It could be read **after Chapter 2** and the introduction of the backstepping methodology. Next, we give in **Appendix B** the proof of Theorem 7.2.2. Before reading this proof, we advise any reader first to understand **Chapter 7**. It is pretty technical and requires some linear algebra and operator framework knowledge. Finally, we present in **Appendix C** some complementary results in the line of **Chapter 10**. We advise you to read this chapter first to understand this test case better. Here, we question the impact of the target system and the remaining degrees of freedom in the kernel equations for a backstepping-based observer design. This chapter gathers some numerical observations that might be obvious to researchers familiar with the backstepping methodology.

3 - Characterization of P/PI controllers for simple transport equations with load or actuator dynamics

This chapter aims to study the potential of widely used Proportional (P) or Proportional Integral (PI) boundary output feedback controllers to stabilize a simple class of interconnected systems. We consider first-order scalar hyperbolic PDE systems with no in-domain couplings (conservation laws) coupled at one end with an ODE system that can represent the finite-dimensional dynamics of an actuator or a load. This methodological chapter presents how frequency-domain approaches developed for delay-differential equations (DDEs) can be relevant for analyzing coupled hyperbolic PDE-ODE systems. Using a D-decomposition method [Nei49] developed for time-delay systems (TDS), we characterize the closed-loop stability intervals in the parameter space of the P/PI controller gains for two test cases. Using a frequency-domain representation, we study the location of the characteristic roots of the closed-loop systems. We can therefore define explicit criteria for the proportional and integral gains to ensure that all the poles have negative real parts [GKCo3]. These simple controllers can robustly stabilize the elementary chain structure if such criteria are met. However, they cannot always be satisfied. This emphasizes the limitations of low computational complexity controllers and justifies the interest in other methods, such as the backstepping methodology, to stabilize interconnected infinite-dimensional systems.

Chapitre 3: Caractérisation des contrôleurs P/PI pour une structure de chaîne simple lois de conservation-EDO. Ce chapitre a pour objectif d'étudier le potentiel des contrôleurs Proportionnel / Proportionnel-Intégral pour la stabilisation d'une classe simple de systèmes interconnectés. Nous considérons des systèmes d'EDP hyperboliques scalaires sans couplages dans le domaine (lois de conservation), couplés à une extrémité avec un système d'EDO, qui peut représenter la dynamique de dimension finie d'un actionneur ou d'une charge. Ce chapitre est d'abord méthodologique. Il présente comment les approches du domaine fréquentiel développées pour les équations différentielles à retard peuvent être pertinentes pour l'analyse des systèmes couplés EDP hyperboliques - EDO. En suivant la méthode de D-décomposition [Nei49] développée pour les systèmes à retard, nous caractérisons les intervalles de stabilité en boucle fermée en donnant des critères explicites sur les gains des contrôleurs. Nous étudions le placement des racines de l'équation caractéristique qualifiant la stabilité des systèmes en boucle fermée. Les gains doivent garantir qu'ils sont tous à partie réelle strictement négative [GKCo3]. Si cela n'est pas possible, de simples contrôleurs P/PI ne pourront pas stabiliser la chaîne de manière robuste. Cela met en lumière les limites de ces contrôleurs de faible complexité, et justifie l'intérêt de développer de nouvelles méthodes (telles que le backstepping) pour stabiliser des systèmes de dimension infinie interconnectés.

Contents

3.1 First elementary chain structure: ODE system coupled with pure transport equations	37
3.1.1 Systems under consideration	37
3.1.2 Overall strategy	37
3.1.3 Stability results for time-delay systems	38
3.2 Application to two test cases	41
3.2.1 Stabilization of transport equations with actuation dynamics	41
3.2.2 Stabilization of transport equations with load dynamics	45

Some of the results given herein were presented in:

- Jeanne Redaud, Jean Auriol, and Silviu-Iulian Niculescu "Characterization of PI feedback controller gains for interconnected hyperbolic systems" (2022). 8th IFAC Symposium on System Structure and Control (SSSC).

3.1 . First elementary chain structure: ODE system coupled with pure transport equations

3.1.1 . Systems under consideration

This section considers a scalar linear hetero-directional hyperbolic system corresponding to two transport equations coupled at one end with a scalar ODE. More precisely, we consider systems of state $(u, v, X) \in \Xi$ with the following structure

$$\frac{\partial}{\partial t}u(t, x) + \lambda \frac{\partial}{\partial x}u(t, x) = 0, \quad \frac{\partial}{\partial t}v(t, x) - \mu \frac{\partial}{\partial x}v(t, x) = 0, \quad (3.1)$$

$$\dot{X}(t) = aX(t) + bv(t, 0) + dV(t), \quad (3.2)$$

with the boundary conditions

$$u(t, 0) = qv(t, 0) + cX(t), \quad v(t, 1) = \rho u(t, 1) + (1 - d)V(t), \quad (3.3)$$

with $(t, x) \in [0, +\infty) \times [0, 1]$, $V(t)$ the control input, transport velocities $\lambda, \mu > 0$, and the coupling terms $a, b, c, q, \rho \in \mathbb{R}$. As in the previous chapter, we denote $\delta \doteq \frac{1}{\lambda} + \frac{1}{\mu}$ and define $r \doteq \rho q$. The initial conditions $(u(x, 0), v(x, 0), X(0)) = (u_0(x), v_0(x), X_0) \in \Xi$, satisfy compatibility conditions 2.1.1 (with additional term X_0). The output of the system is defined by $y(t) = dX(t) + (1 - d)v(t, 1)$. We use the boolean parameter $d \in \{0, 1\}$ to avoid unnecessary case distinctions. Consequently, in the first case $d = 1$, which characterizes actuator dynamics acting on a wave-like propagation system, the ODE system is actuated (Figure 3.1, left), while in the second case $d = 0$ (Figure 3.1, right) the PDE system is actuated. It is motivated by several industrial applications [PR01, WK20, GDD09].

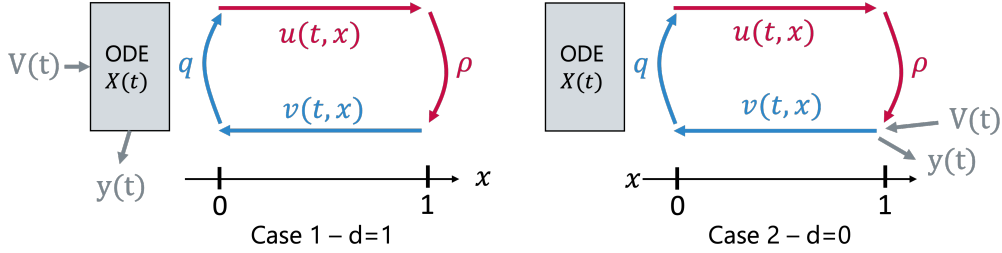


Figure 3.1 – Schematic representation of system (3.1)-(3.3)

We assume that the system satisfies the delay-robustness Condition 2.2.1, that rewrites here $|r| < 1$. The open-loop system is well-posed [BC16, Theorem A.6]. Note that even if the PDE and ODE systems are separately stable, their coupling can be the source of instabilities.

3.1.2 . Overall strategy

Comments on Proportional and PI feedback controllers

As mentioned in Chapter 2, backstepping-based controllers require know-how and an important computational effort to be implemented. The backstepping methodology can

be adapted to stabilizing ODE with input delay [Krs08, Chapter 9], a situation corresponding to case 2 if $\rho = 0$. However, their complexity limits their practical implementations. As a first step, it might be valuable to consider Proportional (P) or Proportional Integral (PI) controllers with low computational effort. More precisely, the control input is of form

$$V(t) = K_p y(t) + K_i \int_0^t y(\nu) d\nu, \quad (3.4)$$

the coefficient K_i being equal to zero for the proportional case. Indeed, in some cases, classic proportional controllers allow convergence to the desired setpoint. However, the integral term can suppress an eventual residual steady-state error and accelerate the convergence to the setpoint, with a risk of overshooting. Another problem, integrator windup, may occur when the actuator saturates, leading to very long transients. This can be seen in drilling applications, where mechanical constraints limit the input torque.

Tuning the best parameters results from a compromise between transient time and high stability. Since PI controllers are broadly applicable, many experimental methods exist to tune their parameters. To cite only a few: Ziegler-Nichols Step Response Method (open-loop tuning method applicable to open-loop stable plants only), Internal Model Controller Design Technique (uses an explicit model of the plant), Cohen-Coon Method (dominant Pole design). Some are detailed in [SDB05, Section 10]. However, such methods can be time-consuming. There are no explicit conditions guaranteeing appropriate gain values stabilizing ODE-PDE interconnected systems.

Control objective

The next section aims to derive general conditions on the controller gains (K_p, K_i) under which it is possible to stabilize the plant (3.1)-(3.3). The objective reads as follows

Objective 3.1.1: Exponential stabilization using P or PI feedback

For $d \in \{0, 1\}$, determine admissible bounds on (K_p, K_i) so that (3.1)-(3.3) is exponentially stabilized in the sense of the Ξ -norm. There exist $\nu > 0$, $C_0 \geq 1$, for all $(u_0, v_0, X_0) \in \Xi$, such that

$$\|(X, u, v)\|_{\Xi} \leq C_0 e^{-\nu t} \|(X_0, u_0, v_0)\|_{\Xi}.$$

First, we recall some general results regarding the stability of time-delay systems of neutral type with simple pointwise delay terms. In particular, we present the D-decomposition method and apply it to first-order neutral equations. As seen in Chapter 2, such equations can characterize the stability of hyperbolic PDE systems in the absence of in-domain couplings.

3.1.3 . Stability results for time-delay systems

Characteristic equation

In what follows, we consider a neutral delay-differential equation of the form

$$\frac{d}{dt} z(t) + \alpha z(t) + \gamma \frac{d}{dt} z(t - \delta) + \beta z(t - \delta) = 0, \quad (3.5)$$

where α, β, γ real coefficients and $\gamma \neq 0$. They will be related to the physical coefficients of system (3.1)-(3.3) in Section 3.2. The state z is defined on $[-\delta, 0]$ by an appropriate initial condition $z_0 \in L^2([-\delta, 0], \mathbb{R})$. The quasipolynomial characteristic equation associated with (3.5) is given in the Laplace domain by

$$\Delta(s, \delta) = d(s) + n(s)e^{-\delta s} = 0, \quad (3.6)$$

with $d(s) = s + \alpha$ and $n(s) = \gamma s + \beta$, two first-order quasi-polynomial, such that $\Delta(s, \delta)$ in (3.6) rewrites as:

$$\Delta(s, \delta) = s + \alpha + (\gamma s + \beta)e^{-\delta s} = s(1 + \gamma e^{-\delta s}) + \alpha + \beta e^{-\delta s}. \quad (3.7)$$

Having $\deg(d) = \deg(n)$ is a major difference with retarded systems, for which $\deg(d) > \deg(n)$. In neutral delay systems, the delays affect both the state variables and their derivatives, whereas in retarded delay systems, the delays affect only the state variables. It makes the study of the stability properties of such systems much more complicated. As discussed in [MN14], in the *neutral* case, there is an essential spectrum¹, such that the spectral abscissa function may exhibit discontinuities. This means that small changes in the system parameters can lead to sudden jumps or changes in the rightmost root of the spectrum. A delay in retarded systems can attenuate certain types of oscillations or disturbances in the system dynamics, leading to enhanced stability and robustness to parameter variations. In the neutral case, this *smoothing effect* disappears. The system may be unstable even if all the characteristic roots lie in the open left half complex plane (LHP), due to the presence of asymptotic chains of roots near the imaginary axis. The exponential stability of solutions then requires a stronger condition than having characteristic roots with strictly negative real parts.

Definition 3.1.1: Stability of a neutral type quasipolynomial [SDB05, GKCo3]

A quasi-polynomial $\Delta(s, \delta)$ is said to be **stable** if there exists $\sigma > 0$ such that the real parts of all its roots are less than $-\sigma$.

We show in the following that for the simple ODE-hyperbolic PDE interconnection (3.1)-(3.3) in open loop or subject to a proportional feedback controller, we obtain a first-order neutral equation yielding a characteristic quasi-polynomial of degree 3 of the form (3.7). We, therefore, present some general stability results for this class of characteristic equations.

Necessary condition

As discussed in [HVL13, Ste89], and presented in Chapter 2 as the *delay-robustness* Condition 2.2.1, the exponential stability of the trivial solution of the difference equation $z(t) + \gamma z(t - \delta) = 0$ is a *necessary condition* for the exponential stability of the scalar neutral equation (3.5). In our case, this condition rewrites as

Assumption 3.1.1 *The absolute value of coefficient γ is strictly less than 1, that is $|\gamma| < 1$.*

¹ The *essential spectrum* corresponds to a part of the spectrum of an operator that cannot be assigned to any isolated eigenvalues

If this assumption is not satisfied, the equation $\Delta(s, \delta) = 0$ admits an infinite number of roots with positive real parts, corresponding to delay-independent instability. As discussed in [MN14], increasing the delay in the closed-loop system induces instability.

D-decomposition method

In the study of hyperbolic PDE systems with no in-domain couplings, the delay term $\delta > 0$ in (3.5) results from the intrinsic transport time and depends on the transport speed and length of the space domain: it is determined by the physical properties of the system. Different criteria can be found to establish the stability of time-delay systems, such as Pontryagin criterion, Chebotarev criteria, Yesupovich-Svirskii criterion, or Michailov criterion [SDB05]. To analyze the stability of linear time-delay systems in the parameter space with constant delay δ , we follow the **D-decomposition approach** proposed in [Nei49]. The methodology can be resumed as follows [Nico1, Section 3.4.2]:

1. First, we consider the *delay-free* case $\delta = 0$ to determine a first stability condition for the system without delay. It would correspond to the ideal case of an infinitely high transport speed in the hyperbolic system.
2. By a continuity argument, the system will be stable for a time interval $\delta \in [0, \tau_c)$, depending on the existence of roots of (3.6) on the imaginary axis. We then determine the frequency of characteristic roots crossing the imaginary axis, corresponding to a switch in stability. If they exist, we define a stability interval $[0, \tau_c)$ on which the system is stable. The following shows that the critical delay τ_c in closed-loop depends on the controller gains. The PI feedback can therefore be used to guarantee stability properties.
3. Since the stability change can only occur through the imaginary axis if there are no crossing roots, we derive conditions for stability of the closed-loop system independently of the intrinsic delay δ .

Application to (3.7)

Under the first necessary Assumption 3.1.1, we apply the above methodology. In the *delay-free* case, the characteristic equation (3.7) rewrites as a first-order polynomial

$$\Delta(s, 0) = s(1 + \gamma) + \alpha + \beta. \quad (3.8)$$

The only root of (3.8) is given by $s^* = -\frac{\alpha+\beta}{1+\gamma}$. It belongs to the left half complex plane (LHP) under the following condition

Condition 3.1.1 *The coefficients satisfy*

$$\alpha + \beta > 0. \quad (3.9)$$

If this condition is not satisfied, the controller cannot even stabilize the closed-loop system in the ideal delay-free case. Next, consider the real delayed equation. Under Condition 3.1.1, by a continuity argument, the system is stable for $\delta \in [0, \tau_c)$, where τ_c corresponds to the frequency of the first imaginary axis crossing $s = j\omega$, with

$$\begin{cases} \alpha + \beta \cos(\delta\omega) + \omega\gamma \sin(\delta\omega) = 0 \\ \omega + \omega\gamma \cos(\delta\omega) - \beta \sin(\delta\omega) = 0 \end{cases}.$$

Using the fact that $|e^{-j\delta\omega}| = |-\frac{\alpha+j\omega}{\beta+j\gamma\omega}| = 1$, we also obtain that the pulsation at the imaginary axis crossing satisfies

$$(\alpha^2 + \omega^2) - (\gamma^2\omega^2 + \beta^2) = 0 \implies (1 - \gamma^2)\omega^2 = \beta^2 - \alpha^2. \quad (3.10)$$

If $\alpha^2 > \beta^2$, or equivalently $\alpha > |\beta|$ using Condition 3.1.1, under Assumption 3.1.1, equation (3.10) has no solution $\omega \in \mathbb{R}$. Since zero is not a solution of $\Delta(s, \delta) = 0$, the system is then stable with an infinite delay margin under the following condition

Condition 3.1.2 *The coefficients satisfy $\alpha \geq |\beta|$.*

Else, (3.10) admits a unique solution $\omega_c > 0$ corresponding to the frequency of the first crossing point on the imaginary axis. It is given by

$$\omega_c = \sqrt{\frac{\beta^2 - \alpha^2}{1 - \gamma^2}}. \quad (3.11)$$

The corresponding critical delay is then defined as

Definition 3.1.2: critical delay

The critical delay is defined by $\tau_c = \min\{\frac{\delta}{\omega_c} \mid s + \alpha + (\gamma s + \beta)z = 0, z = e^{-\delta s}\}$.

Solving the equation $z_c = e^{-j\omega_c\tau_c} = -\frac{\alpha+j\omega_c}{\beta+j\omega_c\gamma}$, we obtain

$$\tau_c = \frac{1}{\omega_c} \arctan\left(\frac{\omega_c(\alpha\gamma - \beta)}{\alpha\beta + \gamma\omega_c^2}\right) = \sqrt{\frac{1 - \gamma^2}{\beta^2 - \alpha^2}} \arctan\left(-\frac{\sqrt{(\beta^2 - \alpha^2)(1 - \gamma^2)}}{\alpha + \beta\gamma}\right). \quad (3.12)$$

Under Assumption 3.1.1 and Condition 3.1.1, the system is stable for $\delta \in [0, \tau_c)$. Else, the system is unstable. As seen next, the P/PI controller gains modify the coefficients of the characteristic equation of the closed-loop system. In some cases, they can ensure that the above conditions are satisfied.

3.2 . Application to two test cases

We now apply the methodology presented in Section 3.1.3 to derive conditions under which the system (3.1)-(3.3) can be stabilized by proportional feedback controllers. A similar analysis could be done to deal with the PI, and is only briefly presented for the two considered cases.

3.2.1 . Stabilization of transport equations with actuation dynamics

Neutral formulation and open-loop analysis

Consider system (3.1)-(3.3) with $d = 1$, satisfying Condition 2.2.1. Let us denote $z(t) = v(t, 0)$. Using the method of characteristics, we immediately obtain

$$z(t) = \rho q z(t - \delta) + c p X(t - \delta).$$

We now take the Laplace transform of (3.2) and the above equation, neglecting their initial conditions. Indeed, they only impact the transient behavior and do not modify the stability analysis [HVL13]. We get

$$(s - a)X(s) = bz(s) + V(s), \quad (3.13)$$

$$z(s)(1 - \rho q e^{-\delta s}) = c\rho e^{-\delta s} X(s). \quad (3.14)$$

This yields $X(s) = H_{XV}(s)V(s)$, where the transfer function is given by

$$H_{XV}(s) = \frac{1 - \rho q e^{-\delta s}}{(s - a) - \rho(qs + bc - qa)e^{-\delta s}}.$$

Open-loop stability The poles of the open-loop system are the solutions of the characteristic equation

$$\Delta_{OL}(s) = (s - a) - \rho(qs + bc - qa)e^{-\delta s} = 0. \quad (3.15)$$

It is a particular case of equation (3.7) with $\alpha = -a$, $\beta = \rho(qa - bc)$, $\gamma = -\rho q$. Following the methodology given in Section 3.1.3, the first necessary stability condition (3.9) is given by $a(1 - \rho q) + bc\rho < 0$. Then, applying condition 3.1.2, the system is open-loop stable with infinite delay margin iff $-a \geq |\rho(qa - bc)|$. Else, we must consider the crossing points of the imaginary axis to obtain a finite-delay margin. From (3.11)-(3.12) we get

$$\begin{cases} \omega_c = |a| + \sqrt{\frac{(\rho bc)^2 - 2abc\rho}{1-r^2}} \\ \tau_c = \sqrt{\frac{1-r^2}{(ra-bc\rho)^2 - a^2}} \arctan\left(\frac{-bc\rho\sqrt{(1-r^2)[(ra-bc\rho)^2 - a^2]}}{abc\rho - r(ra-bc\rho)^2}\right) \end{cases}.$$

If the necessary stability condition is verified, and if the second stability condition is satisfied or if $\delta < \tau_c$, the system is already open-loop stable, so the boundary feedback controller can be used to fasten convergence rate.

Boundary feedback stabilization with a proportional feedback controller

We first aim to stabilize system (3.1)-(3.3) using a proportional feedback controller $V(t) = K_p y(t)$. The characteristic equation of the closed-loop system is now given by

$$\Delta_{CL}(s) = s - (a + K_p) + (-\rho qs + \rho(q(a + K_p) - bc))e^{-\delta s} = 0.$$

It corresponds to equation (3.7) with $\alpha = -(a + K_p)$, $\beta = \rho[q(a + K_p) - bc]$, $\gamma = -\rho q$. Note that $|\gamma| = |r| < 1$ under Condition 2.2.1. Following the methodology given in Section 3.1.3, we obtain the first necessary stability condition

$$-(a + K_p) + \rho[q(a + K_p) - bc] > 0 \implies K_p < -a - \frac{bc\rho}{1 - \rho q}. \quad (3.16)$$

Next, we must determine the K_p -domain when the closed-loop system is stable with infinite delay margin, *i.e.* when $(a + K_p)^2 - \rho^2(q(a + K_p) - bc)^2 \geq 0$. This polynomial of

discriminant $(2\rho bc)^2 \geq 0$ admits one or two real solutions

$$K^\pm = -a - \frac{bc\rho(\rho q \pm 1)}{1 - (\rho q)^2},$$

such that condition 3.1.2 is satisfied on $(-\infty, K^-) \cup (K^+, +\infty)$. If this condition is not verified, the system can still be stabilized for some K_p , if the system delay δ is small enough. Finally, taking into account (3.16), we have the following theorem

Theorem 3.2.1: Stability regions for Proportional gain

Consider system (3.1)-(3.3) with the proportional feedback control law (3.4) ($K_i = 0$) under Condition 2.2.1. If the constant parameters of the system and the gain K_p satisfy either of the following set of inequalities

1. $bc\rho \geq 0$, and $K_p < -a - \frac{bc\rho}{1-\rho q}$;
2. $bc\rho < 0$, and $K_p < -a + \frac{bc\rho}{1+\rho q}$;
3. $bc\rho < 0$, $-a + \frac{bc\rho}{1+\rho q} \leq K_p < -a - \frac{bc\rho}{1-\rho q}$ and $\delta < \tau_c$ where

$$\begin{cases} \tau_c = \frac{1}{\omega_c} \arctan\left(-\frac{\omega_c bc\rho}{(a+K_p)(bc\rho - r(a+K_p)) - r\omega_c}\right), \\ \omega_c = \sqrt{\frac{(r(a+K_p) - bc\rho)^2 - (a+K_p)^2}{1-r^2}}. \end{cases}$$

then, the closed-loop system (3.1)-(3.3) is exponentially stable in the Ξ -norm.

Proof: Using the analysis presented above, the state X is exponentially stable. Then, since $|\rho q| < 1$, we obtain the exponential stability of the state $z(t)$, which in turn implies the exponential stability of the system (3.1)-(3.3). ■

For these values of K_p , the boundary feedback controller stabilizes the closed-loop system. One can notice that it is always possible to choose K_p negative enough to satisfy one of the two first conditions. However, the third condition allows choosing smaller absolute values of K_p , thus improving the robustness properties of the closed-loop system [Nico1].

Boundary feedback stabilization with a PI feedback controller

We now consider the interest of adding an integral term in the feedback controller $K_i \neq 0$. In the Laplace domain, using $V(s) = (K_p + \frac{K_i}{s})X(s)$, (3.13) rewrites

$$(s - a - K_p - \frac{K_i}{s})X(s) = bz(s).$$

Combining this equation with (3.14), we obtain $\Delta_{CL}(s) = Q(s, \delta) + P(s, \delta)(K_p + \frac{K_i}{s}) = 0$,

$$\text{with } \begin{cases} Q(s, \delta) = (s - a) - \rho[q(s - a) + bc]e^{-\delta s}, \\ P(s, \delta) = -1 + \rho q e^{-\delta s}. \end{cases} \quad (3.17)$$

Under Condition 2.2.1, P has no roots on the imaginary axis. Looking for solutions of the characteristic equation corresponding to imaginary axis crossings, we consider $s =$

$j\omega \in j\mathbb{R}$ and identify K_p (resp. K_i) with the real part (resp. imaginary part) of the second member. Indeed, we have

$$K_p = \Re\left(-\frac{Q(j\omega)}{P(j\omega)}\right), \quad K_i = \omega \Im\left(\frac{Q(j\omega)}{P(j\omega)}\right).$$

In particular, in the considered case, we obtain:

$$\begin{cases} K_p = -\frac{a+\rho(2aq-bc)\cos(\delta\omega)+\rho^2q(aq-bc)}{1+(\rho q)^2-2\rho q\cos(\delta\omega)}, \\ K_i = -\omega\frac{\omega(1+\rho^2q^2)-2\rho q\omega\cos(\delta\omega)+\rho bc\sin(\delta\omega)}{1+(\rho q)^2-2\rho q\cos(\delta\omega)}. \end{cases} \quad (3.18)$$

By continuity, the *instability degree*, i.e. the number of poles in the RHP, changes when a new pole crosses the imaginary axis.

Numerical simulations

We now illustrate our results with simulations. In what follows, the space domain $[0, 1]$ is discretized with a mesh of 100 points. We simulate the PDE system (3.1)-(3.3) using a Godunov Scheme [LeVo2] ($CFL = 1$) on the time interval $[0, 50]$ s. We solve the ODE using the Matlab method `ode45`. The parameters are given in Table 3.1, and are chosen such that the open-loop system is unstable. The Ξ -norm of the open-loop system is represented in Figure 3.5 (prune curve).

Param.	Value	Param.	Value	Param.	Value
a	-0.1	b	0.7	c	-0.7
q	0.5	ρ	0.8	δ	4

Table 3.1 – System parameters (Case 1)

We can select K_p so that the conditions of Prop. 3.2.1 are satisfied. Since $bc\rho < 0$, the closed-loop system is exponentially stable if $K_p < -0.18$ by condition (2). However, choosing $K_p \in [-0.18, -0.04]$, condition (3) can also be satisfied, as illustrated in Figure 3.2, which represents the admissible values for K_p under condition (3) of Theorem 3.2.1. The evolution of the Ξ -norm of the system is represented in Figure 3.5 for $K_p = -0.1$.

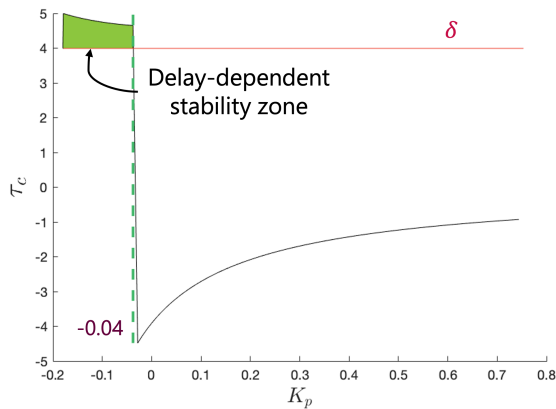


Figure 3.2 – Admissible values for K_p

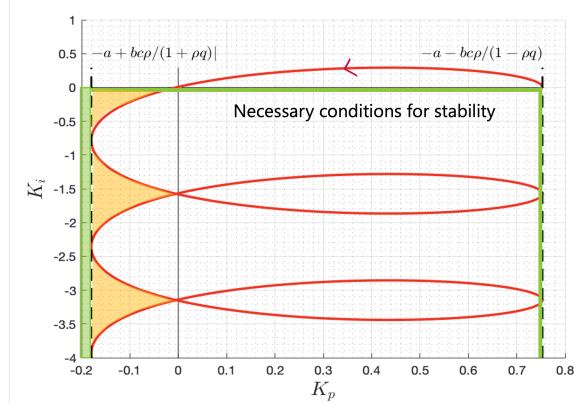


Figure 3.3 – Stability regions $(K_p(\omega), K_i(\omega))$

We now consider introducing an integral gain to improve the closed-loop performance. Plotting (3.18) as a function of the frequency, we obtain Figure 3.3. We can define stable regions delimited by the red curve $(K_p(\omega), K_i(\omega))$ for which the instability degree is constant and then select the controller gains on compact intervals inside the domains corresponding to stability regions.

Writing the characteristic equation of the closed-loop system in form (3.6), the necessary conditions for $d(s, K_p, K_i) + n(s, K_p, K_i)$ to be Hurwitz is $K_p < -a - \frac{bc\rho}{1-r}$, $K_i < 0$ (region delimited by green lines). The dotted lines correspond to the first stability condition (3.9). In our case, $bc\rho < 0$, the light green zone corresponds to a stability region, independently from the value of K_i . Finally, the light yellow regions correspond to stability regions with a finite delay margin. The critical delay must be computed beforehand for each (K_p, K_i) to ensure $\delta < \tau_c$. Using a gradient sampling algorithm [BLO05] accelerated by the Broyden–Fletcher Goldfarb–Shanno (BFGS) method, we can find values of K_p, K_i minimizing the spectral abscissa of the corresponding time-delay system². As illustrated in Figure 3.4, no roots lie in the right half complex plane in closed-loop. The distance with the axis $x = 0$ somehow corresponds to a robustness margin: the algorithm [AM23] maximizes the distance between the rightmost root and the imaginary axis.

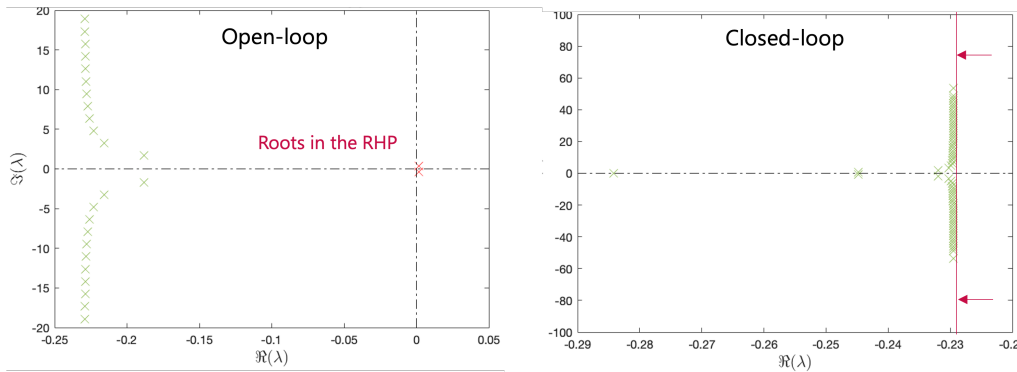


Figure 3.4 – Location of the roots of Δ_{OL} (left) and Δ_{CL} (right)

In this case, we obtain $K_i \approx -0.89$, $K_p \approx -1.89$, which belongs to the stability region as expected. As illustrated in Figure 3.5 (black curve), the stabilization is faster when we add an integral term in the controller. Finally, for comparison purposes, we also plotted in Figure 3.5 the closed-loop behavior using the controller developed in [BSBADLE19] (green dotted line). It has comparable performance to the well-tuned PI controller at the cost of higher complexity.

3.2.2 . Stabilization of transport equations with load dynamics

Neutral formulation and open-loop analysis

Consider now system (3.1)-(3.3) with $d = 0$, satisfying Condition 2.2.1. Let us denote $z(t) = v(t, 1)$. Using the method of characteristics, we obtain

$$z(t) = \rho q z(t - \delta) + \rho c X\left(t - \frac{1}{\lambda}\right) + V(t), \quad (3.19)$$

2. The TDS-control Matlab package we used can be found in <https://twr.cs.kuleuven.be/research/software/delay-control/> [AM23].

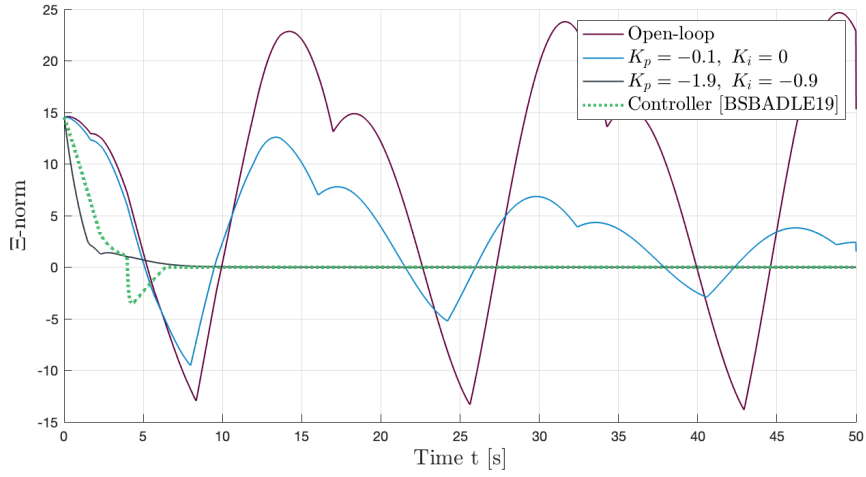


Figure 3.5 - Evolution of $\|(X, u, v)\|_{\Xi}$ ($d = 1$) for different control strategies

$$\dot{X}(t) = aX(t) + bz\left(t - \frac{1}{\mu}\right). \quad (3.20)$$

In the Laplace domain (neglecting, as before, the initial conditions), it gives

$$z(s) = \frac{s - a}{(s - a) - \rho(qs + bc - qa)e^{-\delta s}} V(s) \doteq H_{vV}(s)V(s).$$

Open-loop stability As expected, in an open loop, the poles of the transfer function are solutions of (3.15). Thus, the analysis follows the one presented in Section 3.2.1. We restrict the following study to $b \neq 0$, as acting on the ODE through the PDE is otherwise impossible.

Boundary feedback stabilization with a proportional feedback controller

We now aim to stabilize system (3.1)-(3.3) using a proportional feedback controller $V(t) = K_p y(t)$. From equations (3.19)-(3.20), we obtain

$$(s - a)X(s) = \frac{bc\rho e^{-\delta s}}{1 - K_p - re^{-\delta s}}.$$

The characteristic equation associated with the closed-loop system is then given by

$$\Delta_{CL}(s) = (1 - K_p)s - a(1 - K_p) + (-rs + \rho(qa - bc))e^{-\delta s} = 0.$$

Assuming $K_p \neq 1$, we rewrite the above equation in the form (3.7) with $\alpha = -a$, $\beta = \frac{\rho(qa - bc)}{1 - K_p}$, and $\gamma = -\frac{r}{1 - K_p}$. As explained in Section 3.1.3, it is necessary to have $|\gamma| < 1$, which implies $|1 - K_p| > |r|$. Following the proposed methodology, the closed-loop system is stable in the delay-free case under the condition

$$\frac{a(1 - K_p - r) + bc\rho}{1 - K_p - r} < 0 \iff \begin{cases} K_p < 1 - r \text{ and } aK_p > a(1 - r) + bc\rho, \\ \text{or } K_p > 1 - r \text{ and } aK_p < a(1 - r) + bc\rho. \end{cases}$$

$$\text{Define } \begin{cases} \theta_c = \sqrt{(\rho^2(aq - bc)^2 - a^2(1 - K_p)^2)((1 - K_p)^2 - (r)^2)} \\ \omega_c = \sqrt{\frac{\rho^2(aq - bc)^2 - a^2(1 - K_p)^2}{(1 - K_p)^2 - r^2}} \end{cases} . \text{ We have}$$

Theorem 3.2.2: Stability regions for Proportional controller

Consider system (3.1)-(3.3) with the control law (3.4) ($K_i = 0$) under Condition 2.2.1. Assume $a > 0$. If the constant parameters of the system and the gain K_p ($\neq 1$) satisfy either of the following set of inequalities

1. $bc\rho \geq 0$, $r \geq 0$ and $1 + r < K_p < 1 - r + \frac{bc\rho}{a}$,
2. $bc\rho \leq 0$, $r \geq 0$ and $1 - r + \frac{bc\rho}{a} < K_p < 1 - r$,
3. $bc\rho \geq 0$, $r \leq 0$ and $1 - r < K_p < 1 - r + \frac{bc\rho}{a}$,
4. $bc\rho \leq 0$, $r \leq 0$ and $1 - r + \frac{bc\rho}{a} < K_p < 1 + r$,

and if $\delta < \tau_c$, where $\tau_c = \frac{1}{\omega_c} \arctan\left(\frac{\theta_c}{a(1 - K_p)^2 + \rho^2 q(aq - bc)}\right)$. Then, the closed-loop system (3.1)-(3.3) is exponentially stable in the Ξ -norm.

Proof : The proof is identical to Theorem 3.2.1. The conditions rely on the following analysis. In this theorem, we consider the unstable case $a > 0$. Similar stability conditions could be obtained for $a = 0$ and $a < 0$ (even if, for this case, condition 3.1.2 needs to be verified). Here, we obtain $1 - r + \frac{bc\rho}{a} < K_p < 1 - r$ if $bc\rho < 0$ and $1 - r < K_p < 1 - r + \frac{bc\rho}{a}$, otherwise. We need to check condition 3.1.2 and the delay-dependent stability condition (finite delay margin) to obtain the stability domains. However, it is straightforward to show that condition 3.1.2 can never be verified if $a \leq 0$. The exponential stability of X is shown using the computations given above. It implies the one of $v(t, 1)$ and consequently of the whole PDE using the transport structure of the system. ■

Note that the two inequalities given in the proof can never be verified if $b = 0$, which is consistent with the fact that the ODE system cannot be stabilized. More interestingly, they cannot be verified if $c = 0$, which is a limitation of this control strategy compared to other approaches [ABABS⁺18].

Boundary feedback stabilization with a PI feedback controller

We now consider the interest of a PI controller. In the Laplace domain, the control feedback is given by $V(s) = (K_p + \frac{K_i}{s})z(s)$. Equations (3.19)-(3.20) become

$$-\rho ce^{-\delta s} X(s) + z(s)(1 - re^{-\delta s} - K_p - \frac{K_i}{s}) = 0, \quad (s - a)X(s) - be^{-\frac{1}{\mu}s} z(s) = 0.$$

As before, we rewrite the characteristic equation of the closed-loop system in the form

$$Q(s, \delta) + P(s, \delta)(K_p + \frac{K_i}{s}) = 0, \quad \text{with } \begin{cases} Q(s, \delta) = (s - a) + \rho(q(a - s) - bc)e^{-\delta s}, \\ P(s, \delta) = -s + a. \end{cases}$$

Under the same assumptions as in Section 3.2.1, we obtain the expression of (K_p, K_i) delimiting the stability regions.

$$\begin{cases} K_p = 1 + \frac{\rho(q(\omega^2 + a^2) + abc)}{a^2 + \omega^2} \cos(\delta\omega) + \omega\rho \frac{(-aq + bc + r)}{a^2 + \omega^2} \sin(\delta\omega), \\ K_i = \omega\rho \frac{q(a^2 + \omega^2) + abc}{a^2 + \omega^2} \sin(\delta\omega) - \omega bc \cos(\delta\omega). \end{cases}$$

Numerical simulations

To illustrate the specific case of an unstable ODE system, we give some simulation results for system (3.1)-(3.3) with parameters given in Table 3.2. The open-loop system is unstable, as seen in Figure 3.8 (prune curve).

Param.	Value	Param.	Value	Param.	Value
a	0.4	b	-0.5	c	1
q	0.5	ρ	0.5	δ	0.9

Table 3.2 – System parameters (Case 2)

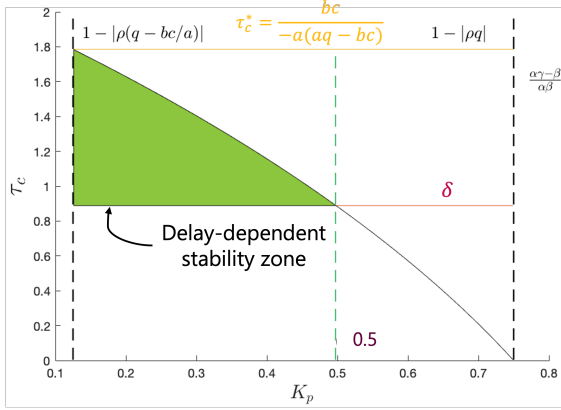


Figure 3.6 – Admissible values for K_p

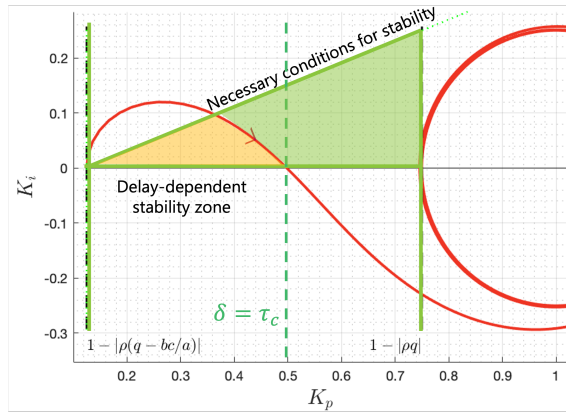


Figure 3.7 – Stability regions $(K_p(\omega), K_i(\omega))$

With $a > 0$, the system can only be stabilized by a proportional feedback controller if $\delta \leq \tau_c^* = \frac{bc}{-a(aq - bc)}$ (the maximum value of critical delay is independent of K_p). As represented in Figure 3.6, the system can only be stabilized by Proportional feedback only for $K_p \in (0.125, 0.5) \subset (1 - |\rho(q - \frac{bc}{a})|, 1 - |\rho|)$ with the chosen set of parameters.

Figure 3.8 shows that the system is stabilized for a gain $K_p = 0.4$ (blue curve). Next, to determine adequate integral gains for the controller, we first determine the necessary conditions for the characteristic polynomial $d(s, K_p, K_i) + n(s, K_p, K_i)$ of the closed-loop system ($\delta = 0$) to be Hurwitz. With the parameters given in Table 3.2, we obtain

$$0 < K_i < -a(1 - K_p - r) - bc\rho, \quad 1 - r > K_p > 1 - r + \frac{bc\rho}{a}.$$

The conditions are satisfied on the green light region in Figure 3.7. The only stability region (light yellow) corresponds to a stability region with a finite-delay margin. When K_i augments, the critical delay reduces, so the stability performances are worsened by adding $K_i \neq 0$, as illustrated in Figure 3.8 (black curve). Finally, the closed-loop performances are compared with a Predictor-based feedback controller [ABABS⁺18]. As seen in Figure 3.8 (green dotted curve), this controller induces oscillations and a high overrun of the initial values, which might be undesirable. However, it converges faster.

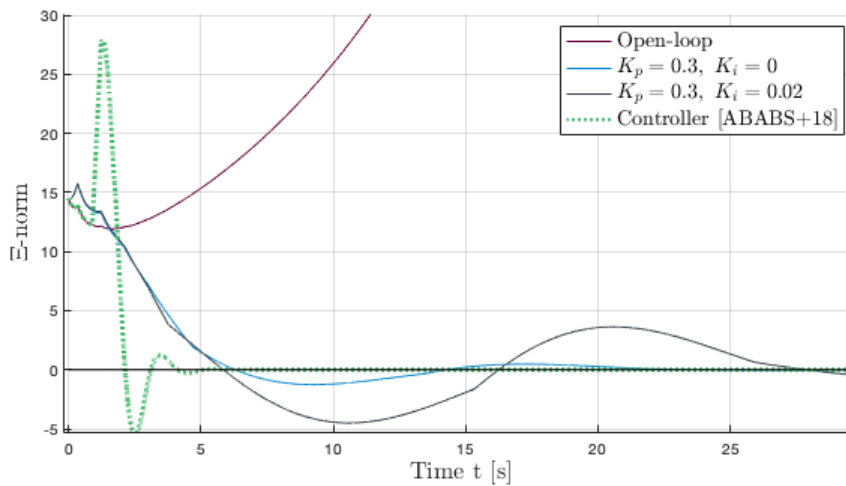


Figure 3.8 – Evolution of $\|(X, u, v)\|_{\Xi}$ ($d = 0$) for different control strategies.

Conclusion

This chapter shows that usual Proportional or PI boundary feedback controllers can be a satisfactory and easily implemented solution to stabilize hyperbolic PDE systems with no in-domain couplings interconnected with an ODE at one end. However, we also illustrate the limitations of this simple control design. Using a Proportional or PI controller only offers limited degrees of freedom. One must be aware that the plant (3.1)-(3.3) may not always be stabilizable by P or PI controllers. Simulations show that the resulting output-feedback laws may induce lower convergence speed than more complex controllers. Also, if the controller gains cannot be selected in the stability regions due to physical constraints, they might not be an appropriate solution.

Finally, we only considered here a system of two scalar hetero-directional transport equations. Deriving explicit criteria for the PI controller gains for interconnected systems of conservation laws becomes trickier [BCT15]. As shown in Chapter 2, adding in-domain couplings leads to Integral Delay Equations (IDE) with distributed delays. The methodology presented in this chapter cannot be straightforwardly applied. All these limitations justify the interest in the backstepping methodology further considered in this thesis.

Part II

Chain structure with actuation at one end

Structure de chaîne avec contrôle à une extrémité

Introduction

In Part I, we first presented simple systems of balance laws. In the presence of potentially destabilizing in-domain couplings, the *backstepping methodology* proved its interest since it allowed designing a stabilizing controller via the mapping to a simpler target system. Next, when the elementary hyperbolic PDE system is interconnected with an ODE, we showed that PI controllers do not always suffice to stabilize the structure.

As mentioned, hyperbolic PDE-ODE interconnections accurately represent transport phenomena and delays, that are common in industrial applications. Consequently, backstepping-based approaches have been used to control PDE-ODE interconnections [ABA19, IGR21] or ODE-PDE-ODE structures [WKP18, DGK18, Geh21]. We first focus on such hyperbolic PDE-ODE interconnections when the actuation is available at one end of the chain structure. In most cases, one can only measure a boundary value of the distributed state of the interconnected system. Usually, it corresponds to the actuated end. For control strategies to be applied to real systems, we also need to estimate the state, even in the presence of a disturbance. Stabilizing the system is also not always enough; output regulation to a reference trajectory is of higher interest in some contexts. Using the different equivalent representations (hyperbolic PDE systems and time-delay systems of the neutral type), we develop in this part control strategies for two kinds of interconnected systems.

Following [DMLA20, BSBADLE19], we propose in **Chapter 4** a constructive approach to design a robust, dynamic output-feedback controller solving disturbance rejection and output tracking for a broad class of interconnected ODE-hyperbolic PDE-ODE system. Solving this control objective is necessary for applications such as drilling since the objective is here to impose a specific trajectory to the unactuated bit at the end of the chain. Next, we consider a chain with arbitrarily many hyperbolic PDE subsystems. Such a system has been stabilized in [Aur20] using a complex backstepping transform or in [SA17] using the method of characteristics. In **Chapter 5**, the chain is interconnected at the unactuated end with an ODE system. So far, one major limitation of the backstepping approach for stabilizing general networks of interconnected ODE-PDE systems was its lack of genericity: adding a new subsystem into the network implies designing a completely new backstepping transform to encompass this new subsystem. Inspired by *modular approaches* from other research fields, such as electronics [ACMdC98] or bio-engineering [SKZ⁺92, SMHFoo], we design an output feedback control law using a *recursive dynamics interconnected framework*. It allows for a "plug-and-play"-like approach to control design since additional subsystems satisfying simple conditions can be added easily to the network. These two interconnected structures can be found in multiple applications: UAV-cable-payload structures [WK20], mining cables elevators [WK21], or drilling devices. Indeed, for this last example, the hyperbolic PDE subsystems represent axial or torsional vibrations along drill string sections. At the same time, the ODE systems model the non-negligible dynamics of the actuator, the bit-rock interaction, or the lumped dynamics of the Bottom Hole Assembly [AvdW19]. For such a system, measurement and actuation are usually only available at the surface ($x = 0$). This situation is illustrated in **Chapter 6**. Part II ends with some perspectives on the proposed approaches to more intricate networks.

4 - Output regulation for linear ODE - hyperbolic PDE - ODE systems

This chapter considers a generic class of interconnected ODE-hyperbolic PDE-ODE systems, presented in Section 4.1. This interconnected chain structure can be found in multiple applications: unmanned aerial vehicle (UAV)-cable-payload system [WK20], mining cable elevators [WK21] or drilling devices [RAN22a]. We propose a constructive approach to designing a robust, dynamic output-feedback controller that solves output regulation and tracking. The initial system is dynamically augmented with finite-dimensional exo-systems representing the reference trajectory and/or disturbance dynamics. Equivalently, the objective is to stabilize a virtual output depending on the states of the ODE opposite to the actuation. Based on some structural assumptions inspired by [BSBADLE19], we first design a full-state feedback controller stabilizing the virtual output in Section 4.2. We follow the backstepping methodology with a single general invertible integral transform to facilitate the implementation. The stability of the target system is analyzed in the frequency domain. We use filtering techniques [ABADM23] to guarantee the robustness of the proposed control law. Following a similar approach, we design a state observer for the augmented system in Section 4.3, reconstructing the system states and the disturbance. Finally, the full-state feedback controller and the observer are coupled to obtain the dynamic output-feedback controller in Section 4.4. Numerical limitations of the approach are illustrated in simulations in Section 4.5.

Chapitre 4: Régulation de sortie pour une chaîne EDO-EDP-EDO. Ce chapitre considère une large classe de systèmes interconnectés EDO - EDP hyperbolique - EDO (Section 4.1). La structure de chaîne est actionnée à une extrémité, où une mesure est également disponible. Nous proposons une approche constructive pour concevoir un contrôleur robuste utilisant la mesure disponible et permettant la régulation et le suivi de sortie. L'extrémité opposée est augmentée dynamiquement par un exo-système de dimension finie représentant la trajectoire de référence et/ou la dynamique des perturbations. De manière équivalente, l'objectif est de stabiliser une sortie virtuelle dépendant des états du système augmenté. Sous des hypothèses structurelles facilement vérifiables, nous déterminons dans un premier temps une loi de commande satisfaisant l'objectif, suivant [BSBADLE19] (Section 4.2). La stratégie est basée sur la méthode de backstepping, avec une unique transformation intégrale inversible afin de faciliter la mise en pratique de l'approche proposée. Puisque la loi de commande ainsi obtenue nécessite de connaître l'état du système, nous concevons ensuite un observateur d'état reconstruisant l'état du système et la perturbation (Section 4.3). Nous utilisons des techniques de filtrage [ABADM23] pour garantir la robustesse de la loi de commande proposée. Enfin, le contrôleur par retour d'état et l'observateur sont couplés pour obtenir le contrôleur par retour de sortie dynamique (Section 4.4). Des limites numériques sont illustrées en simulations (Section 4.5).

Contents

4.1 Problem description	57
4.1.1 System under consideration	57
4.1.2 Structural assumptions	58
4.1.3 Overall strategy	59
4.2 Full-state feedback control law design	60
4.2.1 Invertible transform and target system	60
4.2.2 Frequency analysis of the target system	63
4.2.3 Full-state feedback controller design	64
4.3 Observer design	67
4.3.1 Invertible transform and target system	67
4.3.2 Observer and error state	69
4.3.3 Frequency analysis of the error system	69
4.4 Dynamic output-feedback control law	72
4.5 Simulation results	73

Some of the results given herein were presented at the 3rd Workshop on DELays and CONstraints in Distributed parameter systems (DECOD) and were published in:

- Jeanne Redaud, Federico Bribiesca-Argomedo, and Jean Auriol. "Output Regulation and Tracking for Linear ODE-hyperbolic PDE-ODE Systems". *Automatica*, 2023 (provisionally accepted).
- _____. "Practical Output Regulation and Tracking for Linear ODE-hyperbolic PDE-ODE Systems". Springer, 2021. *Advances in Distributed Parameter Systems*.

4.1 . Problem description

4.1.1 . System under consideration

For all $t > 0$, we consider a system composed of a scalar hyperbolic PDE subsystem (states $(u(t, \cdot), v(t, \cdot)) \in H^1([0, 1], \mathbb{R}^2)$) coupled at both ends with ODEs, as illustrated in Figure 4.1. The first ODE system (state $X(t) \in \mathbb{R}^{n \times 1}$) represents the actuator dynamics. It is actuated by a control input $V(t) \in \mathbb{R}^{c \times 1}$ we want to determine and measured with $y(t) = C_{mes}X(t) \in \mathbb{R}^{n' \times 1}$. To encompass a disturbance and/or a reference trajectory, the state $Y(t)$ of the unactuated opposite ODE system is decomposed into two components. The state $Y_1(t) \in \mathbb{R}^{m \times 1}$ represents the dynamics of the load in the absence of perturbation. It is dynamically augmented by an exo-system of state $Y_2(t) \in \mathbb{R}^{p \times 1}$, such that $Y(t) = \begin{pmatrix} Y_1(t)^\top & Y_2(t)^\top \end{pmatrix}^\top \in \mathbb{R}^{(m+p) \times 1}$. The space-dependent states satisfy (2.1)-(2.2). It gives here

$$\dot{X}(t) = A_0X(t) + E_0v(t, 0) + B_0V(t), \quad \dot{Y}(t) = A_1Y(t) + \begin{pmatrix} E_1^\top & 0_{1 \times p} \end{pmatrix}^\top u(t, 1), \quad (4.1)$$

$$\frac{\partial}{\partial t}u(t, x) + \lambda \frac{\partial}{\partial x}u(t, x) = \sigma^+(x)v(t, x), \quad \frac{\partial}{\partial t}v(t, x) - \mu \frac{\partial}{\partial x}v(t, x) = \sigma^-(x)u(t, x), \quad (4.2)$$

with $A_1 = \begin{pmatrix} A_{11} & A_{12} \\ 0_{p \times m} & A_{22} \end{pmatrix}$ and the boundary conditions

$$v(t, 1) = \rho u(t, 1) + C_1Y(t), \quad u(t, 0) = qv(t, 0) + C_0X(t), \quad (4.3)$$

where $A_0 \in \mathbb{R}^{n \times n}$, $E_0 \in \mathbb{R}^{n \times 1}$, $B_0 \in \mathbb{R}^{n \times c}$, $A_{11} \in \mathbb{R}^{m \times m}$, $A_{12} \in \mathbb{R}^{m \times p}$, $A_{22} \in \mathbb{R}^{p \times p}$, $E_1 \in \mathbb{R}^{m \times 1}$, $C_0 \in \mathbb{R}^{1 \times n}$, $C_1 = [C_{11} \ C_{12}]$, with $C_{11} \in \mathbb{R}^{1 \times m}$ and $C_{12} \in \mathbb{R}^{1 \times p}$.

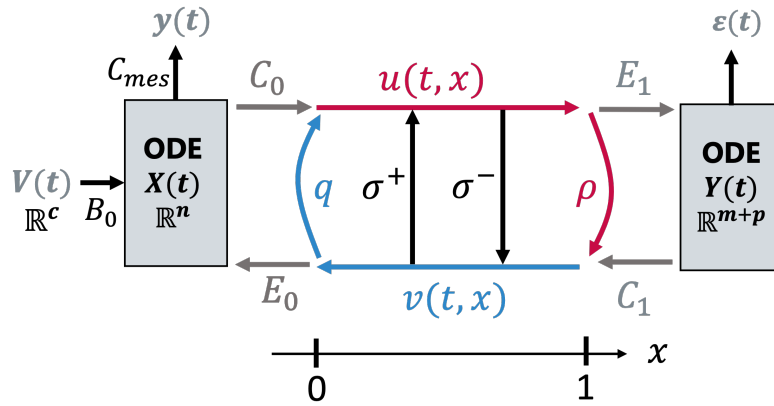


Figure 4.1 – Schematic presentation of the system

We consider constant transport velocities $\lambda, \mu > 0$, but the following results could be extended to space-dependent functions [VCKB11]. The in-domain couplings $\sigma^\pm \in C^0([0, 1], \mathbb{R})$ are space-dependent functions. The initial condition $(X_0, (u_0, v_0), Y_0)$ associated to system (4.1)-(4.3) belongs to \mathcal{X} and satisfy compatibility equations (2.1.1). The open-loop system (4.1)-(4.3) is well-posed [BC16, Appendix A].

4.1.2 . Structural assumptions

The methodology presented in this chapter requires several sufficient yet non-very restrictive assumptions. They are all gathered in this subsection.

Assumption 4.1.1 *The pairs (A_0, B_0) and (A_{11}, E_1) are stabilizable, or equivalently, there exist $F_0 \in \mathbb{R}^{p \times n}$ $F_1 \in \mathbb{R}^{1 \times m}$ such that $\bar{A}_0 \doteq A_0 + B_0 F_0$ and $\bar{A}_{11} \doteq A_{11} + E_1 F_1$ are Hurwitz.*

These two conditions are natural and can be easily numerically tested before implementing the overall strategy. The stabilizability of (A_0, B_0) allows for a simpler design of the control law (Section 4.2.1). However, the second condition on (A_{11}, E_1) is necessary. If unsatisfied, the distal ODE system cannot be stabilized, even without disturbance and independently of the interconnection structure.

Assumption 4.1.2 *The matrices (A_0, B_0, C_0) satisfy*

$$\text{rank}\left(\begin{pmatrix} sI - A_0 & B_0 \\ C_0 & 0_{1 \times c} \end{pmatrix}\right) = n + 1, \quad \forall s \in \mathbb{C}, \Re(s) \geq 0.$$

Again, this assumption simplifies the control design and serves several purposes. First, it implies that C_0 is not identically zero (which would obstruct the stabilization network). Then, under Assumption 4.1.1, the function $P_0(s) \doteq C_0(sI - \bar{A}_0)^{-1}B_0$ is stable and does not have any zeros in the right-half complex plane common to all its components. Consequently, $P_0(s)$ admits a stable right-inverse [Moy77], denoted $P_0^+(s)$, which is not necessarily proper. If the Moore-Penrose right inverse $P_0^\top(s)(P_0(s)P_0^\top(s))^{-1}$ is stable, it could be used. Else, a more involved stable inversion procedure is needed [ABA23].

Due to the duality between observation and stabilization, we need analogous assumptions to design the proposed state observer.

Assumption 4.1.3 *The pairs (A_0, C_{mes}) and (A_1, C_1) are detectable, or equivalently, there exist $L_X \in \mathbb{R}^{p \times n'}$, $\begin{pmatrix} L_1^\top & L_2^\top \end{pmatrix}^\top \in \mathbb{R}^{1 \times (p+m)}$ such that*

$$A_0^{obs} \doteq A_0 + L_X C_{mes}, \text{ and } A_1^{obs} \doteq A_1 + \begin{pmatrix} L_1 \\ L_2 \end{pmatrix} C_1 \text{ are Hurwitz.}$$

As before, only the detectability of (A_0, C_{mes}) is necessary, but the one of (A_1, C_1) allows for a simpler observer design.

Assumption 4.1.4 *The matrices (A_0, E_0, C_{mes}) satisfy*

$$\text{rank}\left(\begin{pmatrix} sI - A_0 & E_0 \\ C_{mes} & 0_{n' \times 1} \end{pmatrix}\right) = n + 1, \quad \forall s \in \mathbb{C}, \Re(s) \geq 0.$$

Symmetrically, the column vector E_0 is therefore not identically zero and admits a left inverse. The transfer matrix $P_{mes}(s) \doteq C_{mes}(sI - A_0^{obs})^{-1}E_0$ is stable and has no zeros in the right-half complex plane and admits a stable left-inverse, not necessarily proper.

Both assumptions can be easily checked before implementation, simplifying this methodology for field engineers. Finally, we have two easily tested assumptions on the boundary coupling coefficients:

Assumption 4.1.5 *The boundary coupling coefficients ρ and q do not equal 0.*

This assumption is only sufficient. It is not restrictive from an application perspective since the opposite corresponds to a perfect impedance matching between the PDE and the load or actuator. If not verified, the proposed strategy is not directly applicable but could be easily adapted by slightly modifying the target system, following similar ideas as the ones given in [VKC11]. As presented in Chapter 2, the (delay-) robustness condition (2.2.1) must be satisfied. It reads here as the following assumption:

Assumption 4.1.6 *The coupling coefficients product $|\rho q|$ is strictly less than 1.*

4.1.3 . Overall strategy

Define the virtual output by $\epsilon(t) \doteq C_e Y(t)$, with $C_e = [C_{e1} \ C_{e2}]$. The control objective reads as follows

Objective: Trajectory tracking - disturbance rejection

Design an output-feedback control law $V(t)$ such that, for all $(X_0, (u_0, v_0), Y_0) \in \mathcal{X}$, the virtual output $\epsilon(t)$ of the closed-loop system (4.1)-(4.3) converges exponentially to zero. There exists $C, \nu > 0$ such that

$$\forall t > 0, |\epsilon(t)| < C e^{-\nu t} |\epsilon(0)|.$$

Note that the virtual output is not necessarily scalar. This control objective encompasses different cases, as illustrated in Section 4.5. Indeed, the state $Y_2(t)$ represents the dynamics of the known trajectory, and/or the supposedly known disturbance model. For instance, taking $C_{e1} \neq 0_{\mathbb{R}^m}$, $C_{e2} = 0_{\mathbb{R}^p}$, we regulate to zero a linear combination of components of $Y_1(t)$ in the presence of a disturbance and solve an output regulation problem. Taking $C_{e1,i} - C_{e2,j} = 0$, $(i, j) \in \llbracket 1, m \rrbracket \times \llbracket 1, p \rrbracket$ (and the other components of the extended state equal to zero), we make the i^{th} component of the output Y_1 converge to the j^{th} component of a known trajectory of state Y_2 and solve an output tracking problem.

The proposed control strategy is the following. We use the backstepping methodology to map the original augmented system to a simpler target system. Then, we use frequency analysis techniques (under the Assumptions given above) to show that this constructive approach leads to a control law solving the output regulation-output tracking problem. Inspired by [BSBADLE19, ABADM23], we apply filtering techniques to guarantee the delay-robustness of the proposed controller.

Next, we solve the problem of state estimation and disturbance reconstruction following a dual approach. As in [ABA23], we first simplify the structure of the system using another backstepping transformation. We then design a Luenberger-like observer for the system, using the available colocated measurement $y(t)$. The convergence of the observer state towards the initial state is proved by an analysis of the error system in the frequency domain. Finally, we show that the observer can be combined with the control law to design a stabilizing output dynamic feedback control law. This strategy is schematically represented in Figure 4.2.

To solve the proposed control objective, we add one more assumption that gives a sufficient structural condition for the existence of a solution for the output regulation problem [FW75].

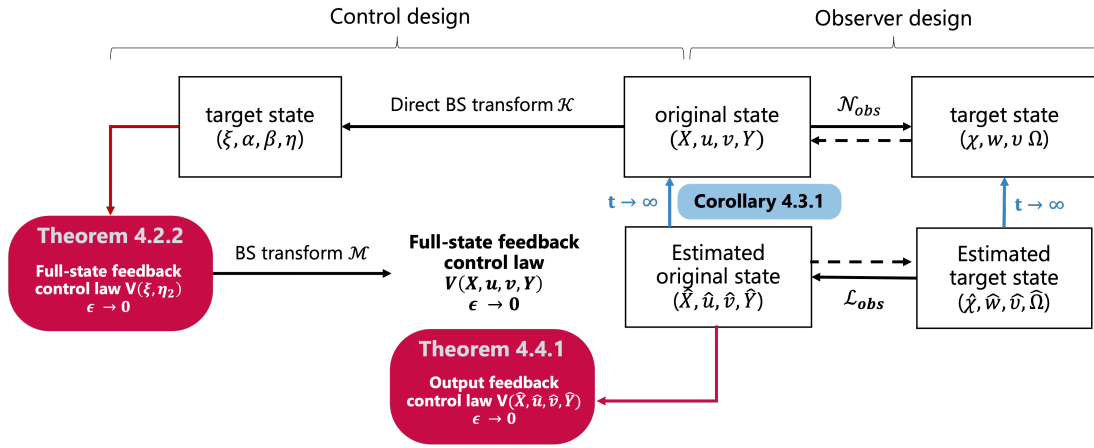


Figure 4.2 – Schematic presentation of output-feedback control design

Assumption 4.1.7 The matrix A_{22} is marginally stable, i.e., all its eigenvalues have zero real parts. For all initial conditions, the zero-input trajectories remain uniformly bounded. Also, there exist matrices $T_a \in \mathbb{R}^{m \times p}$, $F_a \in \mathbb{R}^{1 \times p}$ solutions to the **regulator equations**:

$$\begin{cases} -A_{11}T_a + T_a A_{22} + A_{12} = -E_1 F_a, \\ -C_{e1}T_a + C_{e2} = 0. \end{cases} \quad (4.4)$$

4.2 . Full-state feedback control law design

Inspired by [BSBADLE19], we first design a state-feedback controller following the backstepping methodology and using frequency analysis and filtering techniques [ABADM23].

4.2.1 . Invertible transform and target system

Backstepping transform

Let us map the original system (4.1)-(4.3) to a target system with a simplified structure, using the integral transformation $\mathcal{M} : \mathcal{X} \rightarrow \mathcal{X}$ defined by

$$X(t) = \xi(t) + \int_0^1 M^{12}(y)\alpha(t, y) + M^{13}(y)\beta(t, y)dy + \begin{pmatrix} M^{14} & M^{15} \end{pmatrix} \eta(t), \quad (4.5)$$

$$Y(t) = \eta(t),$$

$$u(t, x) = \alpha(t, x) + \int_x^1 M^{22}(x, y)\alpha(y) + M^{23}(x, y)\beta(y)dy + \begin{pmatrix} M^{24}(x) & M^{25}(x) \end{pmatrix} \eta(t),$$

$$v(t, x) = \beta(t, x) + \int_x^1 M^{32}(x, y)\alpha(y) + M^{33}(x, y)\beta(y)dy + \begin{pmatrix} M^{34}(x) & M^{35}(x) \end{pmatrix} \eta(t).$$

$$(4.6)$$

To highlight the structure of the transform, we use subindices for the different kernels. The kernels $M^{22}, M^{23}, M^{32}, M^{33} \in C^0(\mathcal{T}^+, \mathbb{R})$ are continuous functions. They satisfy

$$\begin{aligned}\lambda \frac{\partial}{\partial x} M^{22}(x, y) + \lambda \frac{\partial}{\partial y} M^{22}(x, y) &= \sigma^+(x) M^{32}(x, y), \\ \lambda \frac{\partial}{\partial x} M^{23}(x, y) - \mu \frac{\partial}{\partial y} M^{23}(x, y) &= \sigma^+(x) M^{33}(x, y), \\ \mu \frac{\partial}{\partial x} M^{32}(x, y) - \lambda \frac{\partial}{\partial y} M^{32}(x, y) &= -\sigma^-(x) M^{22}(x, y), \\ \mu \frac{\partial}{\partial x} M^{33}(x, y) + \mu \frac{\partial}{\partial y} M^{33}(x, y) &= -\sigma^-(x) M^{23}(x, y),\end{aligned}\tag{4.7}$$

with the boundary conditions

$$\begin{aligned}M^{23}(x, x) &= -\frac{\sigma^+(x)}{\lambda + \mu}, & M^{22}(x, 1) &= \frac{1}{\lambda} (M^{24}(x)E_1 + \rho\mu M^{23}(x, 1)), \\ M^{32}(x, x) &= \frac{\sigma^-(x)}{\lambda + \mu}, & M^{33}(x, 1) &= \frac{1}{\mu\rho} (\lambda M^{32}(x, 1) - M^{34}(x)E_1).\end{aligned}\tag{4.8}$$

The kernels $M^{24}, M^{34} \in C^0([0, 1], \mathbb{R}^{1 \times m})$ and $M^{25}, M^{35} \in C^0([0, 1], \mathbb{R}^{1 \times p})$, are defined on $[0, 1]$ by the set of ODEs

$$\begin{aligned}\lambda \frac{d}{dx} M^{24}(x) + M^{24}(x)\bar{A}_{11} &= \sigma^+(x) M^{34}(x), \\ \lambda \frac{d}{dx} M^{25}(x) + M^{25}(x)A_{22} &= \sigma^+(x) M^{35}(x) - M^{24}(x)\bar{A}_{12}, \\ \mu \frac{d}{dx} M^{34}(x) - M^{34}(x)\bar{A}_{11} &= -\sigma^-(x) M^{24}(x), \\ \mu \frac{d}{dx} M^{35}(x) - M^{35}(x)A_{22} &= -\sigma^-(x) M^{25}(x) + M^{34}(x)\bar{A}_{12},\end{aligned}$$

with the boundary conditions

$$M^{24}(1) = F_1, \quad M^{25}(1) = F_a + F_1 T_a, \quad M^{34}(1) = C_{11} + \rho F_1, \quad M^{35}(1) = C_{12} + \rho M^{25}(1),$$

where F_1 is defined by Assumption 4.1.1 and (F_a, T_a) by Assumption 4.1.7. Finally, kernels $M^{12}, M^{13} \in C^0([0, 1], \mathbb{R}^{n \times 1})$, $M^{14} \in \mathbb{R}^{n \times m}$, and $M^{15} \in \mathbb{R}^{n \times p}$ are defined by the following set of algebraic relations

$$\begin{aligned}C_0 M^{12}(y) &= M^{22}(0, y) - q M^{32}(0, y), \quad C_0 M^{13}(y) = M^{23}(0, y) - q M^{33}(0, y), \\ C_0 M^{14} &= M^{24}(0) - q M^{34}(0), \quad C_0 M^{15} = M^{25}(0) - q M^{35}(0).\end{aligned}\tag{4.9}$$

Lemma 4.2.1: Well-posedness of the kernel equations

The set of equations (4.7)-(4.9) is well-posed. The kernels of transform (4.5)-(4.6) are continuously defined on their respective definition domain.

Proof : First kernels $M^{24}, M^{34} \in C^0([0, 1], \mathbb{R}^{1 \times m})$ and $M^{25}, M^{35} \in C^0([0, 1], \mathbb{R}^{1 \times p})$, satisfy a well-posed set of coupled ODEs with boundary conditions in $x = 1$. The set of PDEs (4.7) with boundary conditions (4.8) in $y = x$ and $y = 1$ is well-posed, and $(M^{22}, M^{23}, M^{32}, M^{33})$ are continuously defined on \mathcal{T}^+ due to the regularity of the coupling terms [DMBAHK18, HVDMK15]. The right-invertibility of C_0 is guaranteed by Assumption 4.1.2. Though it seems counterintuitive at first glance, it allows us to find a solution for the algebraic

equation (4.9). Indeed, defining $M^{1i}(y) = C_0^+(M^{2i}(0, y) - qM^{3i}(0, y))$, for $i \in \{2, 3, 4, 5\}$, with $C_0C_0^+ = I$, guarantees that equations (4.9) are satisfied. ■

Note that the transform (4.5)-(4.6) is given in an inverse formulation because its kernels satisfy a simpler set of equations than the ones of the transform in a direct formulation. We have the following theorem

Theorem 4.2.1: Invertibility of the backstepping transform

The transform defined from $\mathcal{X} \rightarrow \mathcal{X}$ by (4.5)-(4.6) with kernels satisfying (4.7)-(4.9) is boundedly invertible. Its inverse transform has the same structure.

Proof : Since the transform comprises identity operators, integral operators with regular kernels, and products with bounded matrices, it is bounded. This change of variables is therefore well-defined and invertible due to its block triangular structure. The blocks on the diagonal, identity or Volterra integral operator, are all invertible [VKC11, Yos60]. The inverse transform $\mathcal{K} : \mathcal{X} \rightarrow \mathcal{X}$, has the same structure

$$\begin{aligned} \xi(t) &= X(t) - \int_0^1 K^{12}(y)u(t, y) + K^{13}(y)v(t, y)dy - \begin{pmatrix} K^{14} & K^{15} \end{pmatrix} Y(t), \quad \eta(t) = Y(t), \\ \alpha(t, x) &= u(t, x) - \int_x^1 K^{22}(x, y)u(y) + K^{23}(x, y)v(y)dy - \begin{pmatrix} K^{24} & K^{25} \end{pmatrix} (x)Y(t), \\ \beta(t, x) &= v(t, x) - \int_x^1 K^{32}(x, y)u(y) + K^{33}(x, y)v(y)dy - \begin{pmatrix} K^{34} & K^{35} \end{pmatrix} (x)Y(t), \end{aligned} \quad (4.10)$$

where the coefficients K^{ij} can be expressed in terms of M^{ij} (and reciprocally) [Krs08] by

$$\begin{aligned} K^{1i}(x) &= M^{1i}(x) - \int_0^x M^{12}(y)K^{2i}(y, x) + M^{13}(y)K^{3i}(y, x)dy, \\ K^{1j} &= M^{1j} - \int_0^1 M^{12}(y)K^{2j}(y) + M^{13}(y)K^{3j}(y)dy, \\ K^{ki}(x, y) &= M^{ki}(x, y) - \int_x^y M^{k2}(x, \nu)K^{2i}(\nu, y) + M^{k3}(x, \nu)K^{3i}(\nu, y)d\nu, \\ K^{ij}(x) &= M^{ij}(x) - \int_x^1 M^{i2}(x, y)K^{2j}(y) + M^{i3}(x, y)K^{3j}(y)dy. \end{aligned}$$

■

Target system

Differentiating the states defined by (4.5)-(4.6) with respect to time and space, and integrating by parts, we can show that the original system (4.1)-(4.3) is mapped to

$$\begin{aligned} \dot{\xi}(t) &= \bar{A}_0\xi(t) - \lambda M^{12}(0)C_0\xi(t) + \bar{E}_1\alpha(t, 1) + \bar{E}_0\beta(t, 0) \begin{pmatrix} M_1 & M_p \end{pmatrix} \eta(t) + B_0\tilde{V}(t) \\ &+ \int_0^1 M^\alpha(y)\alpha(t, y) + M^\beta(y)\beta(t, y)dy, \end{aligned} \quad (4.11)$$

$$\frac{\partial}{\partial t}\alpha(t, x) + \lambda \frac{\partial}{\partial x}\alpha(t, x) = 0, \quad \frac{\partial}{\partial t}\beta(t, x) - \mu \frac{\partial}{\partial x}\beta(t, x) = 0, \quad (4.12)$$

$$\dot{\eta}(t) = \begin{pmatrix} \bar{A}_{11} & \bar{A}_{12} \\ 0 & A_{22} \end{pmatrix} \eta(t) + \begin{pmatrix} E_1 \\ 0_{p \times 1} \end{pmatrix} \alpha(t, 1), \quad (4.13)$$

with the boundary conditions

$$\alpha(t, 0) = q\beta(t, 0) + C_0\xi(t), \quad \beta(t, 1) = \rho\alpha(t, 1), \quad (4.14)$$

where \bar{A}_0, \bar{A}_{11} are defined in Assumption 4.1.1. The distal ODE-state is decomposed into two parts $\eta(t) = \begin{pmatrix} \eta_1(t)^\top & \eta_2(t)^\top \end{pmatrix}^\top$. The different coefficients are defined by

$$\begin{aligned}\bar{A}_{12} &= A_{12} + E_1(F_a + F_1 T_a), \quad M^\alpha(y) = -\lambda \frac{d}{dy} M^{12}(y) + A_0 M^{12}(y) + E_0 M^{32}(0, y), \\ \bar{E}_0 &= E_0 - q\lambda M^{12}(0) + \mu M^{13}(0), \quad M^\beta(y) = \mu \frac{d}{dy} M^{13}(y) + A_0 M^{13}(y) + E_0 M^{33}(0, y), \\ \bar{E}_1 &= \lambda M^{12}(1) - M^{14} E_1 - \rho\mu M^{13}(1), \quad M_1 = -M^{14} \bar{A}_{11} + A_0 M^{14} + E_0 M^{34}(0), \\ M_p &= -M^{15} A_{22} - M^{14} \bar{A}_{12} + A_0 M^{15} + E_0 M^{35}(0).\end{aligned}$$

The initial condition is given by $(\xi_0, \alpha_0, \beta_0, \eta_0) = \mathcal{M}(X_0, u_0, v_0, Y_0) \in \mathcal{X}$. Finally, we defined $\tilde{V}(t) \doteq V(t) - F_0 \xi(t)$ in (4.11), with F_0 given in Assumption 4.1.1. Without disturbance ($\eta_2 \equiv 0$), this target system was stabilized in [BSBADLE19] using a dynamical controller.

4.2.2 . Frequency analysis of the target system

Let us denote $\tau = \frac{1}{\mu} + \frac{1}{\lambda}$, the total transport time induced by the transport equations. We now use the method of characteristics to rewrite the target system as a *time-delay system*. More precisely, the solutions of (4.12) satisfy, for $t > \tau, x \in [0, 1]$,

$$\alpha(t, x) = \alpha\left(t - \frac{x}{\lambda}, 0\right), \quad \beta(t, x) = \beta\left(t - \frac{1-x}{\mu}, 1\right). \quad (4.15)$$

Substituting these expressions in (4.14), we obtain

$$\alpha(t, 0) = \rho q \alpha(t - \tau, 0) + C_0 \xi(t), \quad \beta(t, 1) = \rho q \beta(t - \tau, 1) + \rho C_0 \xi\left(t - \frac{1}{\lambda}\right).$$

In the target system, the transport equations are equivalent to two continuous-time difference equations acting on the boundaries and coupled to the ODE-state $\xi(t)$. In what follows, we analyze the properties of such a system in the frequency domain using the Laplace transform. Since we focus on asymptotic properties, we assume all initial conditions equal zero to avoid complicating the expressions. We obtain

$$(1 - \rho q e^{-\tau s}) \alpha(s, 0) = C_0 \xi(s), \quad (1 - \rho q e^{-\tau s}) \beta(s, 1) = \rho C_0 e^{-\frac{s}{\lambda}} \xi(s). \quad (4.16)$$

The Laplace transform of (4.13) yields

$$(sI - \bar{A}_{11}) \eta_1(s) = \bar{A}_{12} \eta_2(s) + E_1 e^{-\frac{s}{\lambda}} \alpha(s, 0), \quad (sI - A_{22}) \eta_2(s) = 0. \quad (4.17)$$

Multiplying equation (4.17) by $(1 - \rho q e^{-\tau s})$, which has no zeros on the right-half plane by Assumption 4.1.6, and using (4.16), we obtain

$$(1 - \rho q e^{-\tau s})(sI - \bar{A}_{11}) \eta_1(s) = E_1 e^{-\frac{s}{\lambda}} C_0 \xi(s) + (1 - \rho q e^{-\tau s}) \bar{A}_{12} \eta_2(s).$$

Moreover, the matrix polynomial $(sI - \bar{A}_{11})$ is non-singular on the right-half plane from Assumption 4.1.1. Using the delay equation (4.15), and a change of variables in the integral

terms in (4.11), we obtain

$$\begin{aligned}\int_0^1 M^\alpha(y)\alpha(t, y)dy &= \int_0^{\frac{1}{\lambda}} \lambda M^\alpha(\lambda\theta)\alpha(t - \theta, 0)d\theta, \\ \int_0^1 M^\beta(y)\beta(t, y)dy &= \int_0^{\frac{1}{\mu}} \mu M^\beta(1 - \mu\theta)\beta(t - \theta, 1)d\theta.\end{aligned}$$

Consequently, the Laplace transform of (4.11) becomes

$$\begin{aligned}(sI - \bar{A}_0)\xi(s) &= -\lambda M^{12}(0)C_0\xi(s) + B_0\tilde{V}(s) + \left(\bar{E}_1 e^{-\frac{s}{\lambda}} + \int_0^{\frac{1}{\lambda}} \lambda M^\alpha(\lambda\theta)e^{-s\theta}d\theta\right)\alpha(s, 0) \\ &+ \left(\bar{E}_0 e^{-\frac{s}{\mu}} + \int_0^{\frac{1}{\mu}} \mu M^\beta(1 - \mu\theta)e^{-s\theta}d\theta\right)\beta(s, 1) + M_1\eta_1(s) + M_p\eta_2(s).\end{aligned}\quad (4.18)$$

Once again, multiplying by the quasipolynomial $(1 - \rho q e^{-\tau s})$ on both sides of (4.18), and using (4.16), we have

$$\begin{aligned}(1 - \rho q e^{-\tau s})(sI - \bar{A}_0)\xi(s) &= (1 - \rho q e^{-\tau s})B_0\tilde{V}(s) - (1 - \rho q e^{-\tau s})\lambda M^{12}(0)C_0\xi(s) \\ &+ [\bar{E}_1 e^{-\frac{s}{\lambda}} + \int_0^{\frac{1}{\lambda}} \lambda M^\alpha(\lambda\theta)e^{-s\theta}d\theta]C_0\xi(s) + [\bar{E}_0 e^{-\frac{s}{\mu}} + \int_0^{\frac{1}{\mu}} \mu M^\beta(1 - \mu\theta)e^{-s\theta}d\theta]\rho C_0 e^{-\frac{s}{\lambda}}\xi(s) \\ &+ M_1(sI - \bar{A}_{11})^{-1}E_1 e^{-\frac{s}{\lambda}}C_0\xi(s) + (1 - \rho q e^{-\tau s})[M_1(sI - \bar{A}_{11})^{-1}\bar{A}_{12} + M_p]\eta_2(s).\end{aligned}$$

Multiplying both sides by $(1 - \rho q e^{-\tau s})^{-1}$, we finally obtain for any $s \in \mathbb{C}$ with $\Re(s) \geq 0$

$$(sI - \bar{A}_0)\xi(s) = G(s)C_0\xi(s) + H(s)\eta_2(s) + B_0\tilde{V}(s), \quad (4.19)$$

$$\begin{aligned}\text{with } G(s) &= -\lambda M^{12}(0) + (1 - \rho q e^{-\tau s})^{-1} \left[e^{-\frac{s}{\lambda}} (\bar{E}_1 + M_1(sI - \bar{A}_{11})^{-1}E_1) \right. \\ &\quad \left. + \rho e^{-\tau s} \bar{E}_0 + \int_0^{\tau} M^\xi(\theta)e^{-s\theta}d\theta \right],\end{aligned}\quad (4.20)$$

$$\begin{aligned}M^\xi(\theta) &= \lambda \mathbf{1}_{[0, \frac{1}{\lambda}]}(\theta)M^\alpha(\lambda\theta) + \rho\mu \mathbf{1}_{(\frac{1}{\lambda}, \tau]}(\theta)M^\beta(1 - \mu\theta + \frac{\mu}{\lambda}), \\ H(s) &= M_1(sI - \bar{A}_{11})^{-1}\bar{A}_{12} + M_p.\end{aligned}\quad (4.21)$$

We now design a function $\tilde{V}(s)$ ensuring that $C_0\xi(s)$ in (4.19) exponentially converges to zero. We will show next that it ensures the virtual output ϵ convergence to zero.

4.2.3 . Full-state feedback controller design

Using the superposition principle, the control law is decomposed into two parts: $\tilde{V}(s) = U_\xi(s) + U_\eta(s)$. Using Assumption (4.1.1), equation (4.19) rewrites for any $s \in \mathbb{C}^+$

$$\begin{aligned}C_0\xi(s) &= C_0(sI - \bar{A}_0)^{-1}G(s)C_0\xi(s) + P_0(s)U_\xi(s) \\ &+ C_0(sI - \bar{A}_0)^{-1}H(s)\eta_2(s) + P_0(s)U_\eta(s).\end{aligned}\quad (4.22)$$

We can use each controller part to compensate for the inner dynamics. First, define the transfer function

$$F_\eta(s) \doteq -P_0^+(s)C_0(sI - \bar{A}_0)^{-1}H(s),$$

such that, knowing the values of η_2 , the control law $U_\eta(s) = F_\eta(s)\eta_2(s)$ cancels the effect of the disturbance on the output of the target system. As mentioned above, the obtained transfer function is not proper in general. However, we can use our prior knowledge of the disturbance or trajectory dynamics to regularize it and design a strictly proper transfer function $\tilde{F}_\eta(s)$, following the procedure presented in [ABA23] for instance. We then define

$$\tilde{U}_\eta(s) = \tilde{F}_\eta(s)\eta_2(s). \quad (4.23)$$

Once we have canceled the effects of the disturbance on the dynamics or taken into account the given trajectory, equation (4.22) rewrites

$$C_0\xi(s) = C_0(sI - \bar{A}_0)^{-1}G(s)C_0\xi(s) + P_0(s)U_\xi(s).$$

Next, we define the transfer function $F_\xi(s) = -P_0^+C_0(sI - \bar{A}_0)^{-1}G(s)$, and define $U_\xi(s) = F_\xi(s)C_0\xi(s)$. We would obtain $C_0\xi(s) = 0$ with this control law. However, the transfer function $F_\xi(s)$ may not be strictly proper. Thus, to make it strictly proper and guarantee the existence of robustness margins, we may use filtering techniques as in [BSBADLE19, ABADM23]. The resulting controller will be robust to small delays in the input and parameter uncertainties, which is not the case in some designs including derivative terms [WK20].

Let us decompose $G(s)$ in (4.20) into $G(s) = w(s)G(s) + (1 - w(s))G(s)$, with $w(s)$ a (SISO) stable low-pass filter of sufficient order, and define the proper transfer function $\tilde{F}_\xi(s)$ by

$$\tilde{F}_\xi(s) = -P_0^+(s)C_0(sI - \bar{A}_0)^{-1}w(s)G(s) = w(s)F_\xi(s). \quad (4.24)$$

We have the following lemma:

Lemma 4.2.2: Existence of a low-pass filter [BSBADLE19]

Let $w(s)$ be any low-pass filter, with a sufficiently high relative degree, and $0 < \delta < 1$ sufficiently small, such that

$$\forall x \in \mathbb{R}, |1 - w(jx)| \leq \frac{1 - \delta}{\|G\|_\infty \bar{\sigma}(C_0(jxI - \bar{A}_0)^{-1})}. \quad (4.25)$$

Then the dynamic output feedback $\tilde{U}_\xi(s) + \tilde{U}_\eta(s)$ with $\tilde{U}_\xi(s) = \tilde{F}_\xi(s)C_0\xi(s)$ where $\tilde{F}_\xi(s)$ is given in (4.24), and $\tilde{U}_\eta(s)$ in (4.23) exponentially stabilizes $C_0\xi(\cdot)$.

Proof : First, remark that the relative degree of $w(s)$ can always be chosen such that $F_\xi(s)$ becomes strictly proper in (4.24). Once the effects of the trajectory/disturbance have been canceled by $\tilde{U}_\eta(s)$, we can plug (4.24) into the simplified expression of (4.22). The closed-loop dynamics of $C_0\xi(\cdot)$ is then governed by

$$(1 - \Phi(s))C_0\xi(s) = 0, \quad (4.26)$$

where $\Phi(s) \doteq (1 - w(s))C_0(sI - \bar{A}_0)^{-1}G(s)$. Since $G(s)$ given in (4.20) is uniformly bounded in the right-

half complex plane, we have $\bar{\sigma}(G(jx)) \leq \|G\|_\infty$ for all x . Noting that $\Phi(s)$ is stable and strictly proper (\bar{A}_0 is Hurwitz by Assumption 4.1.1), we have by (4.25) that

$$\bar{\sigma}(\Phi(jx)) \leq |1 - w(jx)| \|G\|_\infty \bar{\sigma}(C_0(jxI - \bar{A}_0)^{-1}) \leq 1 - \delta, \quad \text{for all } x \in \mathbb{R}.$$

This implies that $\|\Phi\|_\infty < 1$, which is a sufficient condition for exponential stability of $C_0\xi(\cdot)$ in (4.26). Indeed, it implies that $1 - \Phi(s) = 0$ has no roots in the right-half complex plane. ■

We can then define the control input for the original system (4.1)-(4.3) as $V(t) = \tilde{V}(t) + F_0\xi(t)$. We now show that the output tracking-output regulation problems are solved.

Theorem 4.2.2: Stabilizing controller

Consider the extended control law $V(s) = (\tilde{F}_\xi(s)C_0 + F_0)\xi(s) + \tilde{F}_\eta(s)\eta_2(s)$, where $\tilde{F}_\xi(s), \tilde{F}_\eta(s)$ are two stable strictly proper transfer matrices respectively defined in equations (4.23)-(4.24). Then, under Assumptions 4.1.6, 4.1.1, 4.1.2, 4.1.7, the virtual output $\epsilon(t)$ exponentially converges to zero. The control action $V(t)$ and the trajectories of X, u, v , and Y remain bounded.

Proof : We have already proved in Lemma 4.2.2 that $C_0\xi(\cdot)$ is exponentially stabilized by the dynamic output feedback $\tilde{U}_\xi(s) + \tilde{U}_\eta(s) = \tilde{F}_\xi(s)C_0\xi(s) + \tilde{F}_\eta(s)\eta_2(s)$. Due to Assumption 4.1.6, $(1 - \rho qe^{-\tau s})$ has a stable inverse. Thus, the stability of $\alpha(\cdot, 0), \beta(\cdot, 1)$ is deduced from (4.16), which implies the exponential convergence to zero of α and β in the L^2 -norm. Let us now show that $C_{e1}\eta_1 + C_{e2}\eta_2 \rightarrow 0$. The dynamics of η_1 rewrites

$$\begin{aligned} \dot{\eta}_1(t) &= (A_{11} + E_1 F_1)\eta_1(t) + A_{12}\eta_2(t) + E_1(F_a + F_1 T_a)\eta_2(t) + E_1\alpha(t, 1), \\ &= (A_{11} + E_1 F_1)\eta_1(t) + (-E_1 F_a + A_{11} T_a - T_a A_{22})\eta_2(t) \\ &\quad + E_1(F_a + F_1 T_a)\eta_2(t) + E_1\alpha(t, 1) \quad \text{by Assumption 4.1.7} \\ &\implies \underbrace{(\eta_1 + T_a \eta_2)(t)} = \bar{A}_{11}(\eta_1 + T_a \eta_2) + \underbrace{E_1\alpha(t, 1)}_{\rightarrow 0}. \end{aligned}$$

Therefore, the dynamics of $\eta_1 + T_a \eta_2$ are exponentially stable. It implies that $C_{e1}(\eta_1 + T_a \eta_2)(t) = C_{e1}(Y_1 + T_a Y_2)(t) = C_{e1}Y_1(t) + C_{e2}Y_2(t) = \epsilon(t)$ converges to zero. The boundedness of the control input is guaranteed by the fact that functions $\tilde{F}_\xi, \tilde{F}_\eta$ are strictly proper (as $C_0\xi(s)$ exponentially converges to zero and $\eta_2(s)$ is bounded). The boundedness of the state η follows from equation (4.17). Finally, since $G(s)$ defined by (4.20) is a stable, proper transfer matrix and since \bar{A}_0 is Hurwitz (Assumption 4.1.1), we obtain from equation (4.19) that the state ξ remains bounded. This implies the boundedness of the original state using the invertibility and the boundedness of the backstepping transformation. ■

The control law $V(s)$ defined in Theorem 4.2.2 can be expressed in terms of the original coordinates as

$$\begin{aligned} V(s) &= (\tilde{F}_\xi(s)C_0 + F_0) \left(X(s) - \int_0^1 K^{12}(y)u(s, y) + K^{13}(y)v(s, y)dy - \begin{pmatrix} K^{14} & K^{15} \end{pmatrix} Y(s) \right) \\ &\quad + \tilde{F}_\eta(s)Y_2(s). \end{aligned}$$

Thus, its numerical implementation requires a temporal realization of $\tilde{F}_\xi(s)$ in (4.24) and $\tilde{F}_\eta(s)$ in (4.23), as well as a numerical approximation of the kernels of transform (4.10). It also requires the knowledge of all the states (X, u, v, Y) at any time. It is then necessary to *estimate* the state (X, u, v, Y_1) and reconstruct the disturbance Y_2 using the available measurement $y(t)$.

4.3 . Observer design

Following a dual approach, we now design a state observer for system (4.1)-(4.3). We first use an invertible backstepping transform to map the original system to a target system, in which the in-domain couplings are now local terms depending on the measure ODE state and the boundary term $v(t, 0)$ [ABA23]. It allows for a simpler observer design, using a copy of the target system dynamics with dynamical output injection gains. Using frequency analysis, their tuning guarantees the exponential convergence of the estimated state towards the real one. It is then possible to reconstruct the original state, including the disturbance term. The observer design strategy is summarized in Figure 4.3.

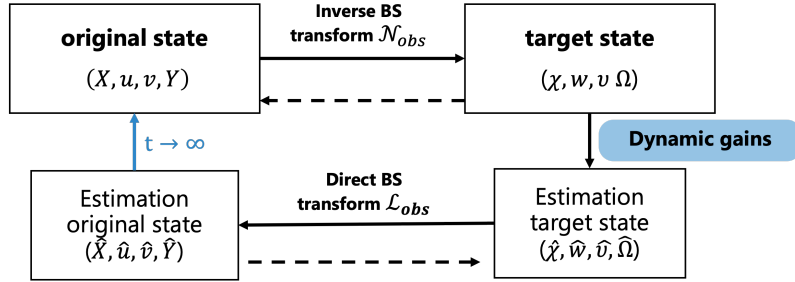


Figure 4.3 - Observer design strategy for system (4.1)-(4.3)

4.3.1 . Invertible transform and target system

Backstepping transform

Define the state $(\chi, w, v, \Omega) \in \mathcal{X}$, using the following transform \mathcal{L}_{obs}

$$X(t) = \chi(t), \quad Y(t) = \Omega(t) + \int_0^1 \begin{pmatrix} L^{42} \\ L^{52} \end{pmatrix} (y)w(y) + \begin{pmatrix} L^{43} \\ L^{53} \end{pmatrix} (y)v(y)dy, \quad (4.27)$$

$$\begin{aligned} u(t, x) &= w(t, x) + \int_0^x L^{22}(x, y)w(y) + L^{23}(x, y)v(y)dy, \\ v(t, x) &= v(t, x) + \int_0^x L^{32}(x, y)w(y) + L^{33}(x, y)v(y)dy, \end{aligned} \quad (4.28)$$

where $\Omega(t) = \begin{pmatrix} \Omega_1(t)^\top & \Omega_2(t)^\top \end{pmatrix}^\top$ is decomposed into two parts, and $(X, u, v, Y) \in \mathcal{X}$ is the solution of system (4.1)-(4.3). Similarly to Theorem 4.2.1, this transform is invertible, with inverse transform of the same form denoted \mathcal{N}_{obs} . The kernel functions $L^{i2}, L^{i3} \in C^0([0, 1], \mathbb{R}^{* \times 1})$ ($* = m$ if $i = 4$, $* = p$ if $i = 5$) and $L^{22}, L^{23}, L^{32}, L^{33} \in C(\mathcal{T}^-, \mathbb{R})$. They satisfy the following set of PDEs

$$\begin{aligned} \lambda \frac{\partial}{\partial x} L^{22}(x, y) + \lambda \frac{\partial}{\partial y} L^{22}(x, y) &= \sigma^+(x)L^{32}(x, y), \\ \lambda \frac{\partial}{\partial x} L^{23}(x, y) - \mu \frac{\partial}{\partial y} L^{23}(x, y) &= \sigma^+(x)L^{33}(x, y), \\ \mu \frac{\partial}{\partial x} L^{32}(x, y) - \lambda \frac{\partial}{\partial y} L^{32}(x, y) &= -\sigma^-(x)L^{22}(x, y), \\ \mu \frac{\partial}{\partial x} L^{33}(x, y) + \mu \frac{\partial}{\partial y} L^{33}(x, y) &= -\sigma^-(x)L^{23}(x, y), \end{aligned} \quad (4.29)$$

with the boundary conditions

$$\begin{aligned} L^{22}(1, y) &= \frac{1}{\rho} \left(L^{32}(1, y) - C_1 \left(L^{42}(y)^\top \quad L^{52}(y)^\top \right)^\top \right), \quad L^{23}(x, x) = \frac{\sigma^+(x)}{\lambda + \mu}, \\ L^{32}(x, x) &= -\frac{\sigma^-(x)}{\lambda + \mu}, \quad L^{33}(1, y) = \rho L^{23}(1, y) + C_1 \left(L^{43}(y)^\top \quad L^{53}(y)^\top \right)^\top, \end{aligned}$$

and the following set of ODEs

$$\begin{aligned} \lambda \frac{d}{dy} \begin{pmatrix} L^{42} \\ L^{52} \end{pmatrix} (y) &= \begin{pmatrix} A_{11} & A_{12} \\ 0_{p \times m} & A_{22} \end{pmatrix} \begin{pmatrix} L^{42} \\ L^{52} \end{pmatrix} (y) + \begin{pmatrix} E_1 \\ 0_{p \times 1} \end{pmatrix} L^{22}(1, y), \\ -\mu \frac{d}{dy} \begin{pmatrix} L^{43} \\ L^{53} \end{pmatrix} (y) &= \begin{pmatrix} A_{11} & A_{12} \\ 0_{p \times m} & A_{22} \end{pmatrix} \begin{pmatrix} L^{43} \\ L^{53} \end{pmatrix} (y) + \begin{pmatrix} E_1 \\ 0_{p \times 1} \end{pmatrix} L^{23}(1, y), \end{aligned}$$

with the boundary conditions

$$\begin{pmatrix} L^{42}(1) \\ L^{52}(1) \end{pmatrix} = -\frac{1}{\lambda} \left(\rho \begin{pmatrix} L_1 \\ L_2 \end{pmatrix} + \begin{pmatrix} E_1 \\ 0_{p \times 1} \end{pmatrix} \right), \quad \begin{pmatrix} L^{43}(1) \\ L^{53}(1) \end{pmatrix} = -\frac{1}{\mu} \begin{pmatrix} L_1 \\ L_2 \end{pmatrix}, \quad (4.30)$$

where the matrices L_1 and L_2 are defined in Assumption 4.1.3. Adjusting the proof from [DMBAHK18], which states the existence of a solution for a general class of kernel equations, this system admits a unique bounded solution.

Target system

Following the backstepping methodology, we derive equations (4.27)-(4.28) with respect to space and time and integrate by parts. We map the original system to this new target system

$$\begin{aligned} \dot{\chi}(t) &= A_0 \chi(t) + E_0 v(t, 0) + B_0 V(t), \quad \dot{\Omega}(t) = A_1^{\text{obs}} \Omega(t) + K_\Omega^{v,0} v(t, 0) + K_\Omega^\chi \chi(t), \quad (4.31) \\ \frac{\partial w}{\partial t}(t, x) + \lambda \frac{\partial w}{\partial x}(t, x) &= g_w(x) v(t, 0) + h_w(x) \chi(t), \\ \frac{\partial v}{\partial t}(t, x) - \mu \frac{\partial v}{\partial x}(t, x) &= g_v(x) v(t, 0) + h_v(x) \chi(t), \end{aligned}$$

with A_1^{obs} defined by Assumption 4.1.3 and the boundary conditions

$$w(t, 0) = qv(t, 0) + C_0 \chi(t), \quad v(t, 1) = \rho w(t, 1) + C_1 \Omega(t). \quad (4.32)$$

The functions g_w, g_v and h_w, h_v are uniquely defined [Yos60] by

$$\begin{aligned} g_w(x) + \int_0^x L^{22}(x, y) g_w(y) + L^{23}(x, y) g_v(y) dy &= \mu L^{23}(x, 0) - \lambda q L^{22}(x, 0), \\ g_v(x) + \int_0^x L^{32}(x, y) g_w(y) + L^{33}(x, y) g_v(y) dy &= \mu L^{33}(x, 0) - \lambda q L^{32}(x, 0), \\ h_w(x) + \int_0^x L^{22}(x, y) h_w(y) + L^{23}(x, y) h_v(y) dy &= -\lambda L^{22}(x, 0) C_0, \\ h_v(x) + \int_0^x L^{32}(x, y) h_w(y) + L^{33}(x, y) h_v(y) dy &= -\lambda L^{32}(x, 0) C_0. \end{aligned} \quad (4.33)$$

The terms $K_{\Omega}^{v,0}$, K_{Ω}^{χ} are then given by

$$K_{\Omega}^{v,0} = \mu \begin{pmatrix} L^{43}(0) \\ L^{53}(0) \end{pmatrix} - \lambda q \begin{pmatrix} L^{42}(0) \\ L^{52}(0) \end{pmatrix} - \int_0^1 \begin{pmatrix} L^{42}(y) & L^{43}(y) \\ L^{52}(y) & L^{53}(y) \end{pmatrix} \begin{pmatrix} g_w(y) \\ g_v(y) \end{pmatrix} dy,$$

$$K_{\Omega}^{\chi} = -\lambda \begin{pmatrix} L^{42}(0)C_0 \\ L^{52}(0)C_0 \end{pmatrix} - \int_0^1 \begin{pmatrix} L^{42}(y) & L^{43}(y) \\ L^{52}(y) & L^{53}(y) \end{pmatrix} \begin{pmatrix} h_w(y) \\ h_v(y) \end{pmatrix} dy.$$

4.3.2 . Observer and error state

Using the measurement $y(t) = C_{\text{mes}}X(t) = C_{\text{mes}}\chi(t) \in \mathbb{R}^{n'}$, we now design an observer for the target system. The observer state $(\hat{\chi}, \hat{w}, \hat{v}, \hat{\Omega})$ is the solution of a set of equations that is a copy of the original dynamics, to which we add dynamical output injection gains \mathcal{P} . They do not exactly correspond to static gains as in the usual Luenberger observer formulation. We use frequency analysis to determine their expression in the Laplace domain in the next section. The observer equations are

$$\begin{aligned} \dot{\hat{\chi}}(t) &= A_0\hat{\chi}(t) + E_0\hat{v}(t,0) + B_0V(t) - P_{\chi}(y(t) - C_{\text{mes}}\hat{\chi}(t)), \\ \frac{\partial \hat{w}}{\partial t} + \lambda \frac{\partial \hat{w}}{\partial x} &= g_w(x)\hat{v}(t,0) + h_w(x)\hat{\chi}(t) - \mathcal{P}_w(t,x), \\ \frac{\partial \hat{v}}{\partial t} - \mu \frac{\partial \hat{v}}{\partial x} &= g_v(x)\hat{v}(t,0) + h_v(x)\hat{\chi}(t) - \mathcal{P}_v(t,x), \\ \dot{\hat{\Omega}}(t) &= A_1^{\text{obs}}\hat{\Omega}(t) + K_{\Omega}^{v,0}\hat{v}(t,0) + K_{\Omega}^{\chi}\hat{\chi}(t) - \mathcal{P}_{\Omega}(t), \end{aligned} \quad (4.34)$$

with boundary conditions

$$\hat{w}(t,0) = q\hat{v}(t,0) + C_0\hat{\chi}(t) - \mathcal{P}_w^0(t), \quad \hat{v}(t,1) = \rho\hat{w}(t,1) + C_1\hat{\Omega}(t). \quad (4.35)$$

Initial conditions are arbitrarily chosen in \mathcal{X} . The corresponding error state is defined by $(\tilde{\chi}, \tilde{w}, \tilde{v}, \tilde{\Omega}) \doteq (\chi, w, v, \Omega) - (\hat{\chi}, \hat{w}, \hat{v}, \hat{\Omega})$. It satisfies

$$\dot{\tilde{\chi}}(t) = A_0\tilde{\chi}(t) + E_0\tilde{v}(t,0) + P_{\chi}C_{\text{mes}}\tilde{\chi}(t), \quad (4.36)$$

$$\begin{aligned} \frac{\partial \tilde{w}}{\partial t}(t,x) + \lambda \frac{\partial \tilde{w}}{\partial x}(t,x) &= g_w(x)\tilde{v}(t,0) + h_w(x)\tilde{\chi}(t) + \mathcal{P}_w(t,x), \\ \frac{\partial \tilde{v}}{\partial t}(t,x) - \mu \frac{\partial \tilde{v}}{\partial x}(t,x) &= g_v(x)\tilde{v}(t,0) + h_v(x)\tilde{\chi}(t) + \mathcal{P}_v(t,x), \end{aligned} \quad (4.37)$$

$$\dot{\tilde{\Omega}}(t) = A_1^{\text{obs}}\tilde{\Omega}(t) + K_{\Omega}^{v,0}\tilde{v}(t,0) + K_{\Omega}^{\chi}\tilde{\chi}(t) + \mathcal{P}_{\Omega}(t), \quad (4.38)$$

with the boundary conditions

$$\tilde{w}(t,0) = q\tilde{v}(t,0) + C_0\tilde{\chi}(t) + \mathcal{P}_w^0(t), \quad \tilde{v}(t,1) = \rho\tilde{w}(t,1) + C_1\tilde{\Omega}(t). \quad (4.39)$$

First, we can choose $P_{\chi} = L_X$, with L_X given in Assumption 4.1.3, such that (4.36) rewrites $\dot{\tilde{\chi}}(t) = A_0^{\text{obs}}\tilde{\chi}(t) + E_0\tilde{v}(t,0)$.

4.3.3 . Frequency analysis of the error system

Our objective is now to design the injected signals $\mathcal{P}_w, \mathcal{P}_v, \mathcal{P}_{\Omega}, \mathcal{P}_w^0$ guaranteeing that the error system (4.36)-(4.39) is exponentially stable in the sense of the \mathcal{X} -norm. We follow an approach similar to the one given in Section 4.2.2.

With the chosen P_χ and since $(sI - A_0^{\text{obs}})$ is non-singular on the complex right-half plane (Assumption 4.1.3), the Laplace transform of (4.36) gives

$$(sI - A_0^{\text{obs}})\tilde{\chi}(s) = E_0\tilde{v}(s, 0) \implies \tilde{\chi}(s) = (sI - A_0^{\text{obs}})^{-1}E_0\tilde{v}(s, 0) \quad \forall s \in \mathbb{C}^+. \quad (4.40)$$

Consider the function $P_{\text{mes}}(s)$ defined after Assumption 4.1.4, and denote $P_{\text{mes}}^-(s)$ any stable left-inverse. Equation (4.40) implies that $P_{\text{mes}}^-C_{\text{mes}}\tilde{\chi}(s) = \tilde{v}(s, 0)$. Let us now focus on equations (4.37). We want to choose signals $\mathcal{P}_w, \mathcal{P}_v$ to suppress the in-domain couplings, such that the two PDEs rewrite as pure transport equations. It implies that $\tilde{w}(t, x) \equiv \tilde{w}(t - \frac{x}{\lambda}, 0)$, $\tilde{v}(t, x) \equiv \tilde{v}(t - \frac{1-x}{\mu}, 1)$ or, in the frequency domain, $\tilde{w}(s, 1) \equiv e^{-\frac{s}{\lambda}}\tilde{w}(s, 0)$, $\tilde{v}(s, 0) \equiv e^{-\frac{s}{\mu}}\tilde{v}(s, 1)$. Applying the method of characteristics to (4.37), we have

$$\begin{aligned} \tilde{w}(t, 1) &= \tilde{w}(t - \frac{1}{\lambda}, 1) + \int_0^{\frac{1}{\lambda}} g_w(1 - \lambda\theta)\tilde{v}(t - \theta, 0) + h_w(1 - \lambda\theta)\tilde{\chi}(t - \theta) \\ &\quad + \mathcal{P}_w(t - \theta, 1 - \lambda\theta)d\theta, \\ \tilde{v}(t, 0) &= \tilde{v}(t - \frac{1}{\mu}, 0) + \int_0^{\frac{1}{\mu}} g_v(\mu\theta)\tilde{v}(t - \theta, 0) + h_v(\mu\theta)\tilde{\chi}(t - \theta) + \mathcal{P}_v(t - \theta, \mu\theta)d\theta. \end{aligned} \quad (4.41)$$

Taking the Laplace transform of (4.41), and incorporating (4.40), we have

$$\begin{aligned} \tilde{w}(s, 1) &= e^{-\frac{s}{\lambda}}\tilde{w}(s, 0) + \int_0^{\frac{1}{\lambda}} (g_w(1 - \lambda\theta) + h_w(1 - \lambda\theta)(sI - A_0^{\text{obs}})^{-1}E_0)\tilde{v}(s, 0)(s) \\ &\quad + \mathcal{P}_w(s, 1 - \lambda\theta)e^{-s\theta}d\theta, \\ \tilde{v}(s, 0) &= e^{-\frac{s}{\mu}}\tilde{v}(s, 1) + \int_0^{\frac{1}{\mu}} (g_v(\mu\theta) + h_v(\mu\theta)(sI - A_0^{\text{obs}})^{-1}E_0)\tilde{v}(s, 0) + \mathcal{P}_v(s, \mu\theta)e^{-s\theta}d\theta. \end{aligned}$$

We now consider that we have gains of the form $\mathcal{P}_w(s, x) = P_w(s, x)C_{\text{mes}}\tilde{\chi}(s)$, $\mathcal{P}_v(s, x) = P_v(s, x)C_{\text{mes}}\tilde{\chi}(s)$, which only depend on the available measurement and the observer state. To cancel the terms in the integral, we thus define the transfer functions

$$\begin{aligned} P_w(s, x) &\doteq -(g_w(x) + h_w(x)(sI - A_0^{\text{obs}})^{-1}E_0)P_{\text{mes}}^-(s), \\ P_v(s, x) &\doteq -(g_v(x) + h_v(x)(sI - A_0^{\text{obs}})^{-1}E_0)P_{\text{mes}}^-(s). \end{aligned} \quad (4.42)$$

Let us now consider the boundary condition (4.39). Taking its Laplace transform and incorporating therein (4.40), we have $\tilde{w}(s, 0) = (q + C_0(sI - A_0^{\text{obs}})^{-1}E_0)\tilde{v}(s, 0) + \mathcal{P}_w^0(s)$. Choosing $\mathcal{P}_w^0(s) \doteq P_w^0(s)C_{\text{mes}}\tilde{\chi}(s)$, we define $P_w^0(s) \doteq -(q + C_0(sI - A_0^{\text{obs}})^{-1}E_0)P_{\text{mes}}^-(s)$, such that the reflection terms at the boundary are cancelled. Finally, taking the Laplace transform of (4.38) and incorporating therein (4.40), we have

$$(sI - A_1^{\text{obs}})\Omega(s) = (K_\Omega^{v,0} + K_\Omega^\chi(sI - A_0^{\text{obs}})^{-1}E_0)\tilde{v}(s, 0) + \mathcal{P}_\Omega(s),$$

with $sI - A_1^{\text{obs}}$ non-singular on \mathbb{C}^+ by Assumption 4.1.3. With an input signal of form $\mathcal{P}_\Omega(s) = P_\Omega(s)C_{\text{mes}}\tilde{\chi}(s)$, the transfer function

$$P_\Omega(s) = -(K_\Omega^{v,0} + K_\Omega^\chi(sI - A_0^{\text{obs}})^{-1}E_0)P_{\text{mes}}^-(s), \quad (4.43)$$

guarantees the convergence of $\tilde{\Omega}$ to zero. Finally, we can use a low-pass filter $\omega(s)$ to ensure all the transfer functions defining the observer gains are strictly proper

$$\mathcal{P}_w(s, x) = \omega(s)P_w(s, x)C_{\text{mes}}\tilde{\chi}(s), \quad \mathcal{P}_v(s, x) = \omega(s)P_v(s, x)C_{\text{mes}}\tilde{\chi}(s), \quad (4.44)$$

$$\mathcal{P}_\Omega(s) = \omega(s)P_\Omega(s)C_{\text{mes}}\tilde{\chi}(s), \quad \mathcal{P}_w^0(s) = \omega(s)P_w^0(s)C_{\text{mes}}\tilde{\chi}(s). \quad (4.45)$$

The exponential stability of the error system is stated in the following theorem

Theorem 4.3.1: Exponential stability of the error system

Let $\omega(s)$ be any low pass filter with a sufficiently high relative degree, and $0 < \tilde{\delta} < 1$ sufficiently small, such that

$$\forall x \in \mathbb{R}, |1 - \omega(jx)| < \frac{1 - \tilde{\delta}}{|\rho q| + \bar{\sigma}(G_{\text{obs}}(jx))}, \quad (4.46)$$

with $G_{\text{obs}}(s) \doteq C_1(sI - A_1^{\text{obs}})^{-1} \left(K_\Omega^{\nu,0} + K_\Omega^\chi(sI - A_0^{\text{obs}})^{-1}E_0 \right)$

$$+ \rho \left[e^{-\tau s} C_0(sI - A_0^{\text{obs}})^{-1} + e^{-\frac{s}{\mu}} \int_0^{\frac{1}{\lambda}} (g_w(1 - \lambda\theta) + h_w(1 - \lambda\theta)(sI - A_0^{\text{obs}})^{-1}E_0) e^{-s\theta} d\theta \right]$$

$$+ \int_0^{\frac{1}{\mu}} (g_v(\mu\theta) + h_v(\mu\theta)(sI - A_0^{\text{obs}})^{-1}E_0) e^{-s\theta} d\theta;$$

Consider the dynamic output feedback gains (4.44)-(4.45) with $P_w(s, x)$, $P_v(s, x)$, $P_\Omega(s)$, $P_w^0(s)$ defined by (4.42)-(4.43). Then, under Assumptions 4.1.3 and 4.1.4, the error system (4.36)-(4.39), with any initial conditions in \mathcal{X} , is exponentially stable in the sense of the \mathcal{X} -norm.

Proof : First, we emphasize that we can always find a low pass filter ω and a coefficient $\tilde{\delta}$ such that condition (4.46) is satisfied. Indeed, the transfer function $G_{\text{obs}}(s)$ is strictly proper and uniformly bounded in the right-half complex plane as a sum of strictly proper transfer functions. The integral term goes to zero at high frequencies by the Riemann-Lebesgue lemma. Thus, at high frequency, $|G_{\text{obs}}(jx)| \rightarrow 0$ and the gain of the low-pass filter goes to zero $|\omega(jx)| \rightarrow 0$. Since $|\rho q| < 1$ by Assumption 4.1.6, we can choose $0 < \tilde{\delta} < 1 - |\rho q|$. An example of an adequate filter design is proposed in [ABADM23].

Plugging (4.44)-(4.45) into the Laplace transform of (4.36)-(4.39), we obtain

$$\tilde{\chi}(s) = (sI - A_0^{\text{obs}})^{-1}E_0\tilde{v}(s, 0), \quad (sI - A_1^{\text{obs}})\Omega(s) = (1 - \omega(s))[(K_\Omega^{\nu,0}\tilde{v}(s, 0) + K_\Omega^\chi\tilde{\chi}(s)),$$

$$\tilde{w}(s, 1) = e^{-\frac{s}{\lambda}}\tilde{w}(s, 0) - (1 - \omega(s)) \int_0^{\frac{1}{\lambda}} [g_w(1 - \lambda\theta) + h_w(1 - \lambda\theta)(sI - A_0^{\text{obs}})^{-1}E_0] e^{-s\theta} d\theta \tilde{v}(s, 0),$$

$$\tilde{v}(s, 0) = e^{-\frac{s}{\mu}}\tilde{v}(s, 1) - (1 - \omega(s)) \int_0^{\frac{1}{\mu}} [g_v(\mu\theta) + h_v(\mu\theta)(sI - A_0^{\text{obs}})^{-1}E_0] e^{-s\theta} d\theta \tilde{v}(s, 0),$$

$$\tilde{w}(s, 0) = (1 - \omega(s))[q\tilde{v}(s, 0) + C_0\tilde{\chi}(s)], \quad v(s, 1) = \rho\tilde{w}(s, 1) + C_1\Omega(s).$$

Combining the above equations, the closed-loop dynamics of $\tilde{v}(\cdot, 0)$ rewrite

$$\tilde{v}(s, 0) = (1 - \omega(s))[\rho q e^{-s\tau} + G_{\text{obs}}(s)]\tilde{v}(s, 0) = \Phi_{\text{obs}}(s)\tilde{v}(s, 0), \quad (4.47)$$

with $G_{\text{obs}}(s)$ defined in Theorem 4.3.1. Thus, $\Phi_{\text{obs}}(s)$ is stable and strictly proper. We have

$$\bar{\sigma}(\Phi_{\text{obs}}(jx)) \leq |1 - \omega(jx)| \bar{\sigma}(\rho q e^{-j\tau x} + G_{\text{obs}}(jx))$$

$$\leq |1 - \omega(jx)|(|\rho q| + \bar{\sigma}(G_{\text{obs}}(jx))) < 1 - \bar{\delta}, \quad \forall x \in \mathbb{R}, \text{ by (4.46).}$$

This implies that $\|\Phi_{\text{obs}}\|_{\infty} < 1$, which is a sufficient condition for exponential stability of $\tilde{v}(\cdot, 0)$ in (4.47).

If $\tilde{v}(s, 0)$ is exponentially stabilized, the error system becomes exponentially stable. Since A_0^{obs} is Hurwitz by Assumption 4.1.3, the dynamics in $\tilde{\chi}$ are stable and $\tilde{\chi}$ converges towards zero. Consequently, the boundary error state $\tilde{w}(\cdot, 0)$ converges to zero. It implies that the dynamics of \tilde{w} are stabilized.

Next, by Assumption 4.1.3, $\tilde{\Omega}$ is exponentially stabilized. ■

Note that due to the structure of the dynamic output feedback gains given in (4.44)-(4.45), and the properties of the filtered proper and stable transfer function $\omega(s)P(s, x)$, the convergence of the input $\tilde{\chi}$ to zero implies the one of the injection terms. Under Assumption 4.1.4, we thus designed dynamical observer gains stabilizing the target error system. Let us now define the original observer state

$$(\hat{X}, \hat{u}, \hat{v}, \hat{Y}) = \mathcal{L}_{\text{obs}}(\tilde{\chi}, \hat{w}, \hat{v}, \hat{\Omega}). \quad (4.48)$$

Corollary 4.3.1: Observer design

Let $\omega(s)$ be any low pass filter with a sufficiently high relative degree, satisfying (4.46) and the dynamic output feedback of form (4.44)-(4.45) with $P_w(s, x)$, $P_v(s, x)$, $P_{\Omega}(s)$ and $P_w^0(s)$ defined by (4.42)-(4.43). Then, under Assumptions 4.1.3, and 4.1.4, the observer state (4.48) exponentially converges to the original state (X, u, v, Y) .

Proof : Under the corollary assumptions, the target error state converges to zero at an exponential rate by Theorem 4.4.1. Consequently, the target observer state converges towards the target state. We, therefore, have access to an estimation of the state (χ, w, v, Ω) with the observer state. Using the invertible backstepping transform \mathcal{L}_{obs} defined by (4.27), we can reconstruct the original state (X, u, v, Y) . Indeed, we can define the original error state as $(\tilde{X}, \tilde{u}, \tilde{v}, \tilde{Y}) = (X, u, v, Y) - (\hat{X}, \hat{u}, \hat{v}, \hat{Y})$. Since the backstepping transform is invertible, the original error system shares the same stability properties with the target error system and is thus exponentially stable. Since the original error state converges to zero, the original observer is a correct estimation of the original state. ■

4.4 . Dynamic output-feedback control law

We can now fulfill the control objective

Theorem 4.4.1: Stabilization of the virtual output

Consider system (4.1)-(4.3) with the observer (4.34)-(4.35), (4.48) and the control law

$$\begin{aligned} \hat{V}(s) = & (\tilde{F}_{\xi}(s)C_0 + F_0) \left[\hat{X}(s) - K^{14}\hat{Y}_1(s) - \int_0^1 K^{12}(y)\hat{u}(s, y) + K^{13}(y)\hat{v}(s, y)dy \right] \\ & + \left[\tilde{F}_{\eta}(s) - (\tilde{F}_{\xi}(s)C_0 + F_0)K^{15} \right] \hat{Y}_2(s), \end{aligned} \quad (4.49)$$

with $\tilde{F}_{\xi}(t)$ defined by (4.24) and $\tilde{F}_{\eta}(s)$ defined in (4.23). Then, for all initial conditions $(X_0, u_0, v_0, Y_0) \in \mathcal{X}$, the virtual output $\epsilon(t)$ exponentially converges to zero, and the state of the system remains bounded in the \mathcal{X} -norm.

Proof : Using the previous results, we need to show that the dynamics of $C_0\xi$ are stabilized by the output feedback law (4.49). By Corollary 4.3.1, the error state $(\tilde{X}, \tilde{u}, \tilde{v}, \tilde{Y})$ exponentially converges to zero. Due to the invertibility of the backstepping transform \mathcal{K} defined in (4.10), the target error state $(\tilde{\xi}, \tilde{\alpha}, \tilde{\beta}, \tilde{\eta}) = \mathcal{K}(\tilde{X}, \tilde{u}, \tilde{v}, \tilde{Y})$ is exponentially stable.

Denote \mathcal{E} the well-defined linear operator such that $\hat{U} = \mathcal{E}(\hat{\xi}, \hat{\alpha}, \hat{\beta}, \hat{\eta}) = \mathcal{E}(\xi, \alpha, \beta, \eta) - \mathcal{E}(\tilde{\xi}, \tilde{\alpha}, \tilde{\beta}, \tilde{\eta})$. The dynamics of ξ and the error state have a cascaded structure (in other words, system $(\xi, \tilde{\xi}, \tilde{\alpha}, \tilde{\beta}, \tilde{\eta})$ has a triangular by blocks structure). Indeed, from (4.19), we have

$$(sI - \bar{A}_0)\xi(s) = G(s)C_0\xi(s) + H(s)\eta_2(s) + B_0(\hat{V}(s) - F_0\xi(s)),$$

and then by linearity

$$\begin{aligned} (sI - \bar{A}_0)\xi(s) &= G(s)C_0\xi(s) + H(s)\eta_2(s) + B_0\hat{V}(s) && : \text{exponentially stable dynamics} \\ &- B_0\mathcal{E}(\tilde{\xi}, \tilde{\alpha}, \tilde{\beta}, \tilde{\eta}) && : \text{autonomous exponentially stable system} \end{aligned}$$

The dynamics of (α, β, η) are not modified, and $C_0\xi$ converges to zero. We can apply the results from Section 4.2.3 to conclude. ■

4.5 . Simulation results

We conclude this chapter with some simulations illustrating the performance of the proposed output feedback controller in two test cases: the rejection of an exogenous sinusoidal disturbance and the tracking of a sinusoidal trajectory. For brevity, we consider the same plant in both cases. Only matrix C_e and the exogenous system pulsation ω_Y are changed. More test cases can be found in [J3].

The system, the observer, and the controller were implemented using Matlab and Simulink. The evolution of the PDE systems was simulated using an explicit in-time, first-order, upwind finite difference method. The ODE states were simulated using a variable step modified Rosenbrock solver ode23s. The evolution of the systems was computed on a 100s time scale, with a CFL number equal to 0.9. The space domain $[0, 1]$ is discretized with a mesh of $n_x = 101$ points.

We use the following parameters $\lambda = 1.8, \mu = 2.1, \rho = 0.5, q = 0.8$. For the sake of simplicity, we consider that there are no in-domain couplings. This allows computing the kernels of the Volterra integral transform using their explicit expression beforehand. The ODE dynamics are in dimension $n = 4, m = 3, c = 2$, and defined by the matrices

$$A_0 = \frac{1}{10} \begin{pmatrix} 0 & 0.14 & 0 & 0.1 \\ 0 & 0 & 0.14 & 0 \\ 0.3 & -0.4 & 0.2 & 0.2 \\ 0 & 0 & 0 & -1.1 \end{pmatrix}, B_0 = \begin{pmatrix} 0 & 0 \\ 0 & -0.1 \\ 0.1 & -0.1 \\ 0 & 0 \end{pmatrix}, A_{11} = \begin{pmatrix} 0.1 & 0 & 0 \\ 0.05 & -0.1 & -0.02 \\ 0 & 0 & -0.2 \end{pmatrix},$$

$$C_0 = \begin{pmatrix} 0.1 & 0 & 0 & -0.05 \end{pmatrix}, C_{11} = \begin{pmatrix} 1 & 0 & -0.2 \end{pmatrix}, C_{12} = \begin{pmatrix} 0 & 0 \end{pmatrix},$$

$$A_{12} = \begin{pmatrix} 0 & 0.1 \\ 0.2 & 0 \\ 0.01 & 0 \end{pmatrix}, A_{22} = \begin{pmatrix} 0 & 1 \\ -\omega_Y^2 & 0 \end{pmatrix}, E_0 = \begin{pmatrix} 0.2 \\ 0.1 \\ 0 \\ 0 \end{pmatrix}, E_1 = \begin{pmatrix} 0.1 \\ 0.01 \\ 0 \end{pmatrix}.$$

With these parameters, the open-loop system is unstable. Matrix A_{22} associated to the dynamics of state $Y_2 = \begin{pmatrix} y_2 & \dot{y}_2 \end{pmatrix}^\top \in \mathbb{R}^2$ corresponds to a sinusoidal signal of form $y_2(t) = A_{\text{mp}} \sin(\omega_y t)$. The matrices F_0, F_1, L_X, L_1, L_2 satisfying Assumptions 4.1.1 and 4.1.3 are obtained using the pole placement method `place`. The matrices T_a, F_a are computed using a Schur triangulation. Here, we have

$$T_a = \begin{pmatrix} -1 & 0 \\ -0.0924 & 0.0234 \\ -0.0002 & 0.001 \end{pmatrix}, F_a = \begin{pmatrix} -1 & 9 \end{pmatrix}.$$

The initial conditions are given by $X_0 = \begin{pmatrix} 0.1 & 0.1 & 0 & 0 \end{pmatrix}^\top, Y_0 = \begin{pmatrix} 1 & 0 & 0.1 & 0.1 & 0.1 \end{pmatrix}^\top, v_0(x) = 0.1 \sin(\frac{\pi}{2}x)$ and u_0 an affine function satisfying (4.3)

First test case: disturbance rejection

First, we consider the case where the distal system is subject to an exogenous sinusoidal disturbance of pulsation $\omega_Y = 0.1\pi$.

Objective 4.5.1: Disturbance rejection

With $C_e = \begin{pmatrix} 1 & 0 & 0 & 0 & 0 \end{pmatrix}$, the virtual output is defined by $\epsilon(t) = Y_{1,1}(t)$.

The proposed output-feedback control law stabilizes the first component of $Y_1(t)$ in presence of an exogenous sinusoidal disturbance.

As illustrated in Figure 4.4, the norm of the unstable open-loop system explodes. It remains bounded in closed-loop, as shown in Figure 4.5. In a closed loop, the virtual output $\epsilon(t)$, represented in Figure 4.8, converges to zero with the full state-feedback control law, even in the presence of the disturbance signal (dotted line).

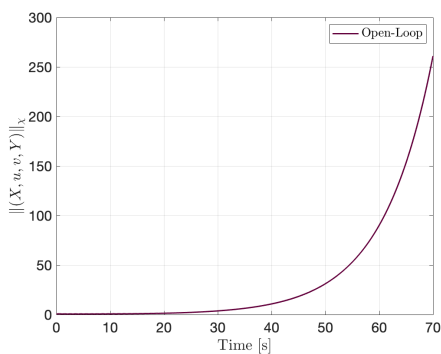


Figure 4.4 – Evolution of the \mathcal{X} -norm in open-loop

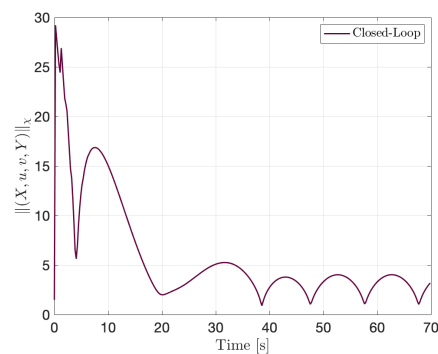


Figure 4.5 – Evolution of the \mathcal{X} -norm in closed-loop (test case 1)

The control inputs are pictured in Figure 4.6. They remain continuous but present high value at the beginning of the operation. The evolution of the PDE state $v(t, x)$ is pictured in Figure 4.7. It remains bounded as expected, but keeps oscillating to compensate the sinusoidal disturbance.

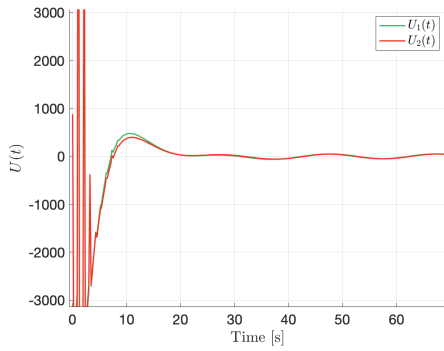


Figure 4.6 – Evolution of the control inputs (test case 1)

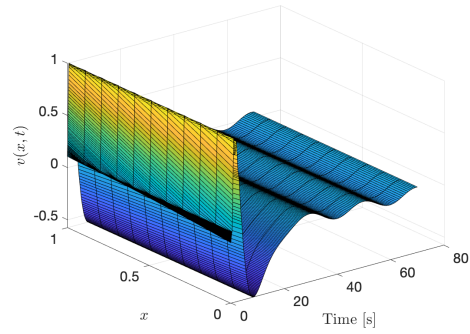


Figure 4.7 – Evolution of the PDE state $v(t, x)$ (test case 1)

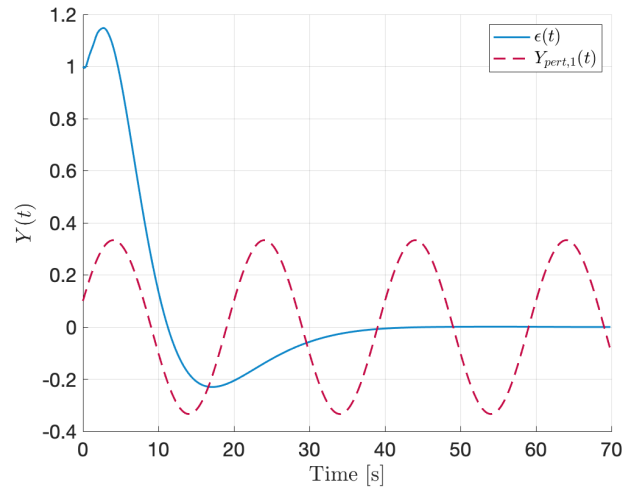


Figure 4.8 – Evolution of $\epsilon(t)$

Second test case: trajectory tracking

First, we consider the case of an exogenous sinusoidal trajectory of pulsation $\omega_Y = \pi$.

Objective 4.5.2: Reference trajectory tracking

With $C_e = \begin{pmatrix} 1 & 0 & 0 & -1 & 0 \end{pmatrix}$, the virtual output is defined by $\epsilon(t) = Y_{1,1}(t) - Y_{ref}(t)$. The proposed output-feedback control law makes the first component of $Y_1(t)$ follow the sinusoidal trajectory.

The open-loop system is still unstable. The norm of the state in a closed-loop is pictured in Figure 4.9. Although it does not converge to zero, it remains bounded while the system is excited to track the desired output.

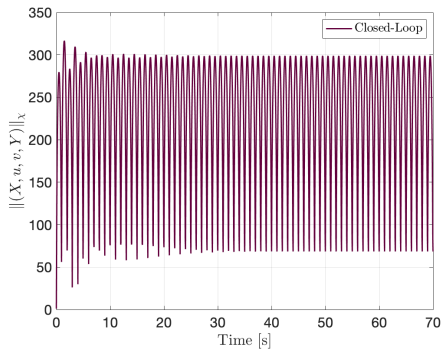


Figure 4.9 – Evolution of the \mathcal{X} –norm of the system (test case 2)

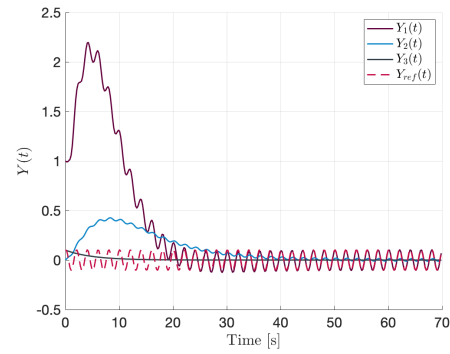


Figure 4.10 – Evolution of $Y_1(t)$ and reference trajectory (test case 2)

The evolution of the state Y_1 is pictured in Figure 4.10. As expected, the first component converges towards the sinusoidal trajectory (dotted red line).

Conclusion

In this chapter, we designed a strictly proper dynamic output-feedback controller allowing output regulation and output tracking for a class of interconnected ODE-PDE-ODE systems. The load dynamics at the unactuated end of the interconnection were dynamically augmented with a finite-dimensional exosystem modeling possible trajectory and disturbance inputs, as illustrated in two test cases in the simulation. The control and observer designs were based on the backstepping methodology, with a stability analysis in the frequency domain.

Though not given here, the simulation results from [RBAA23] raised some potential numerical limitations. In particular, the computation time to solve the observer system is essential since it requires refining the mesh grid. As mentioned in the perspectives closing Part II, model reduction techniques could be consequently investigated to ease the implementation of the proposed control strategies. Future contributions could also focus on leveraging the proposed assumptions. As mentioned in the introduction, an application of such ODE-PDE-ODE interconnection can be found in drilling systems. It is illustrated in Chapter 6. Natural extensions of the system considered herein include non-scalar PDE and are also presented at the end of Part II.

5 - Stabilizing a chain of N hyperbolic PDE systems interconnected with an ODE

This chapter considers a chain of linear scalar hyperbolic PDE subsystems interconnected at one end with an ODE. The opposite end is fully actuated. This network with arbitrarily many N subsystems is presented in Section 5.1. It can be used to model traffic flow dynamics on road sections with different configurations [YAK20] or drill strings with varying inclination or physical properties [AKIS20]. We propose a modular approach called **recursive dynamics interconnection framework** to design an output feedback stabilizing the chain. This new framework allows for a "plug-and-play"-like approach to control design since additional subsystems satisfying similar conditions can be added to the chain using the same procedure. It takes advantage of the interconnection between two consecutive subsystems. More precisely, for each subsystem considered independently, we determine a virtual input ensuring that its output tracks the virtual input stabilizing the downstream subsystem. Starting from the last subsystem, we recursively determine the control input stabilizing the whole chain (Section 5.5). However, due to the inherent transport time in each subsystem, each virtual input depends on the present and future values of the downstream states. To obtain an output feedback control law, we propose a similar approach to estimate the boundary states from the measurement available at the actuated end (Section 5.3). We then design a predictor ensuring that we have access to future values of the states. To ensure the applicability of the approach, the predicted values are computed using the boundary state estimations (Section 5.4).

Chapitre 5: Stabilisation d'un chaîne de N systèmes d'EDP hyperboliques interconnectée à une EDO. Ce chapitre traite de la stabilisation d'une chaîne constituée de N sous-systèmes d'EDP hyperboliques. Ce système, introduit en Section 5.1, est pleinement actionné à une extrémité, et connecté à l'autre extrémité à une EDO. Afin de généraliser l'approche par backstepping, nous proposons ici une **approche récursive** prenant en compte les interconnexions entre les différents sous-systèmes du réseau. Cette stratégie **modulaire** permet d'adapter simplement la loi de commande lorsqu'on ajoute au réseau un nouveau sous-système, sous réserve qu'il satisfasse certaines hypothèses. Plus précisément, pour chaque sous-système, nous cherchons à résoudre un problème de *tracking*, i.e de trouver une loi de commande virtuelle assurant que sa sortie (qui "actionne" le sous-système suivant) converge vers la commande virtuelle stabilisant le sous-système suivant. La loi de commande à l'entrée de la chaîne est obtenue récursivement (Section 5.5). A cause de l'inertie de chaque sous-système, son expression nécessite la connaissance des valeurs futures de l'état distribué de chaque sous-système. Pour pallier à cet inconvénient, nous utilisons une stratégie semblable pour obtenir une estimation retardée des états aux frontières de chaque sous-système, à partir de la mesure disponible à l'extrémité actionnée (Section 5.3). En utilisant des prédicteurs adéquats, nous pouvons finalement obtenir des valeurs présentes et futures de l'état distribué (Section 5.4). Cela permet d'implémenter la loi de commande et de stabiliser la chaîne.

Contents

5.1 Problem description	79
5.1.1 System under consideration	79
5.1.2 Structural assumptions	80
5.1.3 Overall strategy	81
5.2 Full-state backstepping-based output-tracking feedback	82
5.2.1 Stabilizing state-feedback controller	82
5.2.2 State-feedback controller for output-tracking of a known function	84
5.2.3 Predictor-based full-state feedback	85
5.3 Boundary state estimation	85
5.3.1 Generalization to a chain structure	85
5.3.2 Estimation of the ODE state	89
5.3.3 Recursive estimation of boundary states	89
5.4 Design of states predictors	90
5.4.1 Predictor design for the boundary states	90
5.4.2 Predictor design for the distributed states	93
5.5 Output-feedback control law design	93
5.5.1 Output-feedback control law	93
5.6 Simulation results	94

The results presented herein were published in:

- Jeanne Redaud, Jean Auriol, and Silviu-Iulian Niculescu. "Output-feedback Control of an Underactuated Network of Interconnected Hyperbolic PDE–ODE Systems". *Systems & Control Letters*, 2021 154: 104984.
- Jean Auriol, Federico Bribiesca Argomedeo, Silviu-Iulian Niculescu, and Jeanne Redaud. "Stabilization of a Hyperbolic PDEs-ODE Network Using a Recursive Dynamics Interconnection Framework" (2021). European Control Conference (ECC).

5.1 . Problem description

5.1.1 . System under consideration

This chapter considers a system composed of $N > 0$ interconnected hyperbolic PDE systems in a chain structure. It is actuated at the first end and coupled with an ODE at the other. The last unactuated ODE system can represent the dynamics of a load [WK20, WK21]. More specifically, in the context of drilling given in Chapter 6, it corresponds to the lumped collars and bit (BHA) at the end of the pipe or the interaction between the bit and the rock [AvdW19]. This system is schematically represented in Figure 5.1. Each hyperbolic PDE subsystem i , ($i \in \llbracket 1, N \rrbracket$) is modeled by (2.1)-(2.2):

$$\frac{\partial}{\partial t} u_i(t, x) + \lambda_i \frac{\partial}{\partial x} u_i(t, x) = \sigma_i^+(x) v_i(t, x), \quad (5.1)$$

$$\frac{\partial}{\partial t} v_i(t, x) - \mu_i \frac{\partial}{\partial x} v_i(t, x) = \sigma_i^-(x) u_i(t, x), \quad (5.2)$$

with in-domain coupling terms $\sigma_i^\pm(x)$ continuous functions, and $(t, x) \in [0, +\infty) \times [0, 1]$. As in Chapter 4, we assume constant transport speeds $\lambda_i > 0, \mu_i > 0$ for sake of simplicity. In this chain structure, each subsystem i is interconnected with its upstream subsystem $i - 1$ and downstream subsystem $i + 1$ following:

$$\begin{aligned} u_i(t, 0) &= q_{ii} v_i(t, 0) + q_{i,i-1} u_{i-1}(t, 1) + \delta_1^i V(t), \\ v_i(t, 1) &= \rho_{ii} u_i(t, 1) + \rho_{i,i+1} v_{i+1}(t, 0) + \delta_N^i CX(t), \end{aligned} \quad (5.3)$$

with constant couplings q_{ij}, ρ_{ij} . The last subsystem N is coupled with an ODE of dimension $p \in \mathbb{N}$ such that:

$$\dot{X}(t) = AX(t) + Bu_N(t, 1), \quad (5.4)$$

with $A \in \mathbb{R}^{p \times p}, B \in \mathbb{R}^{p \times 1}, C \in \mathbb{R}^{1 \times p}$ constant matrices. We denote $X_0 = X(0) \in \mathbb{R}^p$, and $u_i^0(\cdot) = u_i(0, \cdot), v_i^0(\cdot) = v_i(0, \cdot) \in H^1([0, 1], \mathbb{R})$ the corresponding initial conditions. Similarly to condition (2.1.1), they satisfy adequate compatibility equations. To avoid any useless case distinction, we also denote $q_{1,0} = 1, u_0(t, 1) = V(t), \rho_{N,N+1} = C$ and $v_{N+1}(t, 0) = X(t)$. We assume we can access a collocated measurement $y(t) = v_1(t, 0)$.

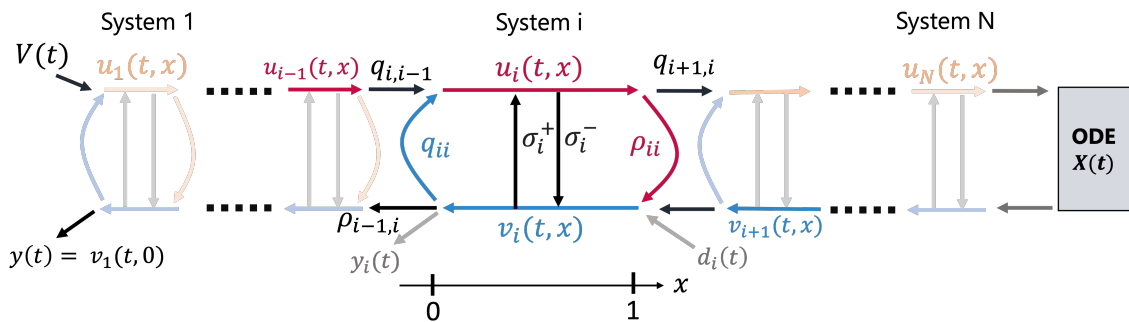


Figure 5.1 – Schematic representation of system (5.1)-(5.4)

The well-posedness of the system (5.1)-(5.4) in the sense of the L^2 -norm is guaranteed by [BC16, Appendix A], for any admissible control operator. Only the first subsystem is actuated through its boundary $x = 0$ by a real-valued control input $V(t)$ we want to design. Therefore, system (5.1)-(5.4) is said to be *under-actuated*. Contrary to [ABABS⁺18], where all the equations propagating in one direction are actuated, only one of the N rightward convecting equations is actuated. We then need to use the interconnections through the different subsystems' boundaries to act from one system to the downstream one.

5.1.2 . Structural assumptions

The design of a stabilizing full-state feedback law and a state observer requires several necessary and non-restrictive assumptions.

To guarantee that the whole system is stabilizable, we have

Assumption 5.1.1 *The ODE-state X is stabilizable, or equivalently, there exists $K \in \mathbb{R}^{1 \times p}$, such that $A + BK$ is Hurwitz.*

To stabilize the states of the downstream subsystems using actuation from the upstream subsystem, we need

Assumption 5.1.2 *For all $i \in \llbracket 2, N \rrbracket$, $q_{i,i-1} \neq 0$.*

It has been shown in [LRW96] that the open-loop transfer function must have a finite number of poles on the closed right half-plane to guarantee the existence of robustness margins for an arbitrary closed-loop system. For the system (5.1)-(5.4), [ABA19, ADM19] proved that this implies

Assumption 5.1.3 *The open loop system (5.1)-(5.4) in the absence of in-domain coupling terms ($\sigma_i \equiv 0$) and of the ODE ($X \equiv 0$) is exponentially stable in the sense of the L^2 norm.*

Some explicit conditions to verify such an assumption can be found in [HVL13, ADM19, Aur20]. This assumption is not restrictive as it is necessary for the existence of robustness margins for the closed-loop system. It is related to the robustness condition (2.2.1) given in Chapter I.

Next, to guarantee the observability of the whole system, we need that

Assumption 5.1.4 *The ODE-state X is detectable, or equivalently, there exists $L \in \mathbb{R}^{p \times 1}$ such that $A + LC$ is Hurwitz.*

To estimate the states of the downstream subsystems using the measurement from the upstream subsystem, we need the following

Assumption 5.1.5 *For all $i \in \llbracket 2, N \rrbracket$, $\rho_{i-1,i} \neq 0$.*

Under these structural assumptions, we propose the *recursive dynamics interconnection framework* described in the next sections.

5.1.3 . Overall strategy

Denote u (resp. v) the concatenation of the states u_i (resp. v_i). The control objective reads as follows:

Objective: Exponential stabilization in the Ξ -norm

Design an output-feedback control law $V(t)$ such that there exist $\nu > 0$, $C_0 > 0$, for all $(u^0, v^0) \in H^1([0, 1], \mathbb{R}^{2n})$, $X_0 \in \mathbb{R}^p$ verifying the compatibility conditions, all solutions of the closed-loop (5.1)-(5.4) satisfy

$$\|(u(t, \cdot), v(t, \cdot), X(t))\|_{\Xi} \leq C_0 e^{-\nu t} \|(u^0, v^0, X_0)\|_{\Xi}.$$

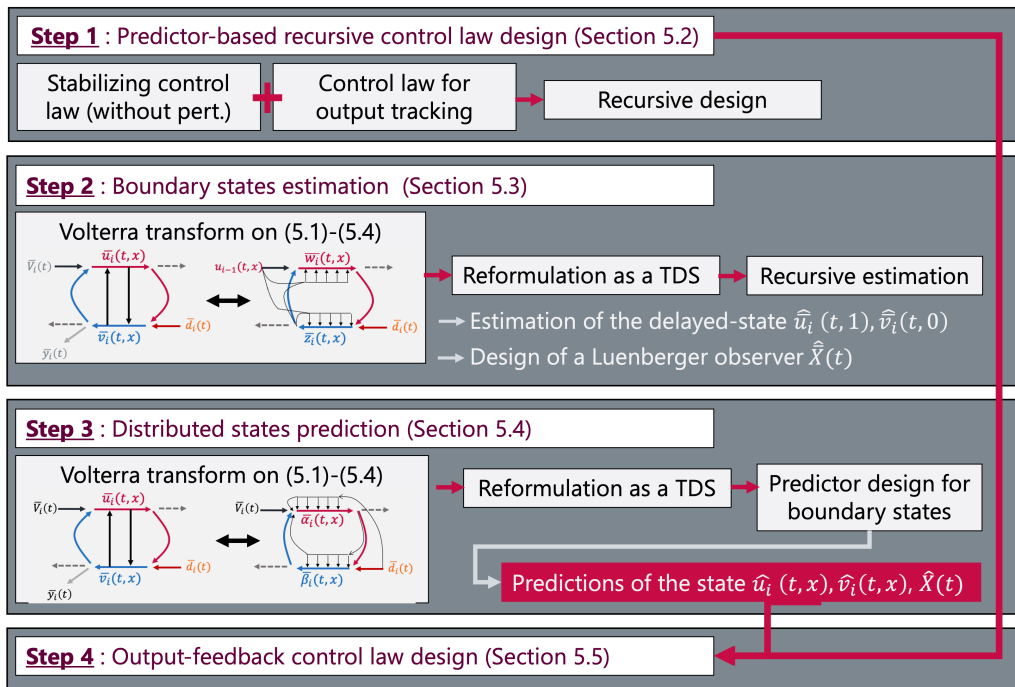


Figure 5.2 – Schematic representation of the proposed method

The proposed strategy is based on a *recursive interconnected dynamics framework*.

Under Assumptions 5.1.2 and 5.1.5, it can be seen that a system i acts on the downstream subsystem $i + 1$ through $u_i(t, 1)$, and on the upstream subsystem $i - 1$ through $v_i(t, 0)$. Let us define $\hat{V}_i(t) = q_{i,i-1}u_{i-1}(t, 1)$ as the *virtual input* acting on subsystem $i \in \llbracket 1, N \rrbracket$, and $\Phi_i(t)$ an arbitrary *virtual output* of subsystem i . Similarly, we call *virtual disturbance* the action of subsystem $i + 1$ on subsystem i , denoted $d_i(t) = \rho_{i,i+1}v_{i+1}(t, 0)$.

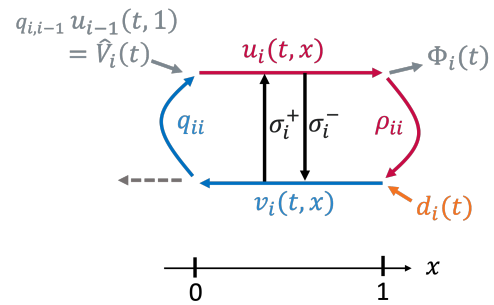


Figure 5.3 – Interactions of subsystem (5.1)-(5.2).

This control design takes advantage of the interactions between consecutive subsystems schematically illustrated in Figure 5.3.

The first step of our approach is designing a full-state feedback for output tracking in the presence of a supposedly known disturbance. For each subsystem, the resulting control input is the sum of two terms: a first backstepping-based control input for stabilizing each subsystem in the absence of perturbation, and a second recursively built control input for trajectory tracking of the virtual input for the downstream subsystem, with a supposedly known disturbance. Finally, the control input stabilizing the chain is obtained recursively, starting from the ODE at the end of the chain. To be computed, the resulting control law requires present and future values of the distributed states. One of the main advantages of this approach is that provided we can solve the tracking problem and correctly predict the distributed state for each subsystem, it becomes straightforward to add new subsystems. This results in a simpler and more generic control design procedure than the one developed in [Aur20].

The second step of our approach is estimating the boundary states using the available measurement $y(t)$. Starting from the first subsystem, we recursively estimate the states at each subsystem's boundaries. However, due to the natural inertia induced by the transport phenomenon, some delays appear, such that we can only obtain a delayed estimation of the states (\bar{u}_i, \bar{v}_i) . We use a first invertible backstepping transform (between o and x), to map each initial PDE subsystem to a target subsystem (\bar{w}_i, \bar{z}_i) . We rewrite it as a time-delay system and then estimate delayed values of the boundary PDE states and the ODE state using a classic Luenberger observer.

To obtain real-time estimations, we then design state predictors. Combining delayed estimations and state predictions, such an approach is similar to [KK17] (for finite dimensional systems). We use a second invertible backstepping transform (between x and 1), to map each initial PDE subsystem to a target subsystem $(\bar{\alpha}_i, \bar{\beta}_i)$. We rewrite the boundary states as a time-delay system and use this formulation to design the boundary states' predictor. Finally, combining the full-state feedback and the estimation-based predictors, we design a causal output feedback control law $V(t)$ exponentially stabilizing the entire chain. This strategy is schematically represented in Figure 5.2.

5.2 . Full-state backstepping-based output-tracking feedback

5.2.1 . Stabilizing state-feedback controller

Let us first consider subsystem (5.1)-(5.3) in absence of perturbation, $d_i(t) \equiv 0$, and subject to a virtual actuation $\hat{V}_i(t)$. The boundary conditions (5.3) rewrite $u_i(t, 0) = q_{ii}v_i(t, 0) + \hat{V}_i(t)$ and $v_i(t, 1) = \rho_{ii}u_i(t, 1)$. We have the following property:

Property 5.2.1 Stabilizability :

For all $i \in \llbracket 1, N \rrbracket$, in the absence of the virtual disturbance d_i (i.e. $d_i(t) \equiv 0$), subsystem i subject to the virtual actuation \hat{V}_i must be stabilizable by a state-feedback law, i.e there exists an operator \mathcal{H}^i , such that

$$\hat{V}_i(t) = \mathcal{H}^i(u_i(t, \cdot), v_i(t, \cdot)) \implies \|u_i(t), v_i(t)\|_{L^2} \xrightarrow[t \rightarrow +\infty]{} 0.$$

Moreover, there exists an operator \mathcal{K}_{N+1} , such that :

$$\hat{V}_{N+1}(t) = \mathcal{K}_{N+1}(X(t)) \implies |X| \xrightarrow[t \rightarrow +\infty]{} 0.$$

Following the backstepping methodology, we prove that the systems under consideration satisfy this property.

Lemma 5.2.1: Stabilizability of each subsystem in absence of perturbation

For all $i \in \llbracket 1, N \rrbracket$, in the absence of the virtual disturbance d_i (i.e. $d_i(t) \equiv 0$), there exists two continuous functions K_i^u, K_i^v defined on $[0, 1]$, such that the full-state feedback

$$\hat{V}_i(t) = -q_{ii}v_i(t, 0) + \int_0^1 K_i^u(y)u_i(t, y) + K_i^v(y)v_i(t, y)dy,$$

exponentially stabilizes subsystem (5.1)-(5.3) in the sense of the L^2 -norm.

Proof : The proof is based on the backstepping methodology. Consider the following Volterra integral transform $\mathcal{K}_i : H^1([0, 1], \mathbb{R}^2) \rightarrow H^1([0, 1], \mathbb{R}^2)$, and introduce the target state $\begin{pmatrix} \alpha_i(t, \cdot) \\ \beta_i(t, \cdot) \end{pmatrix} = \mathcal{K}_i\left(\begin{pmatrix} u_i(t, \cdot) \\ v_i(t, \cdot) \end{pmatrix}\right)$ by

$$\begin{cases} \alpha_i(t, x) = u_i(t, x) - \int_x^1 K_i^{++}(x, \nu)u_i(t, \nu) + K_i^{+-}(x, \nu)v_i(t, \nu)d\nu, \\ \beta_i(t, x) = v_i(t, x) - \int_x^1 K_i^{-+}(x, \nu)u_i(t, \nu) + K_i^{--}(x, \nu)v_i(t, \nu)d\nu, \end{cases} \quad (5.5)$$

where the kernels $K_i^{\cdot\cdot}$ are continuous functions defined on \mathcal{T}^+ as the unique solution [CVKB13, VCKB11] of

$$\begin{aligned} \lambda_i \frac{\partial}{\partial x} K_i^{++}(x, \nu) + \lambda_i \frac{\partial}{\partial \nu} K_i^{++}(x, \nu) &= -\sigma_i^-(y)K_i^{+-}(x, \nu), \\ \lambda_i \frac{\partial}{\partial x} K_i^{+-}(x, \nu) - \mu_i \frac{\partial}{\partial \nu} K_i^{+-}(x, \nu) &= -\sigma_i^+(y)K_i^{++}(x, \nu), \\ \mu_i \frac{\partial}{\partial x} K_i^{-+}(x, \nu) - \lambda_i \frac{\partial}{\partial \nu} K_i^{-+}(x, \nu) &= \sigma_i^-(y)K_i^{--}(x, \nu), \\ \mu_i \frac{\partial}{\partial x} K_i^{--}(x, \nu) + \mu_i \frac{\partial}{\partial \nu} K_i^{--}(x, \nu) &= \sigma_i^+(y)K_i^{-+}(x, \nu), \end{aligned} \quad (5.6)$$

$$K_i^{+-}(x, x) = -\frac{\sigma_i^+(x)}{\lambda_i + \mu_i}, K_i^{-+}(x, x) = \frac{\sigma_i^-(x)}{\lambda_i + \mu_i}, K_i^{++}(x, 1) = \rho_{ii} \frac{\mu_i}{\lambda_i} K_i^{+-}(x, 1), K_i^{--}(x, 1) = 0. \quad (5.7)$$

Following the backstepping methodology, we can define

$$\hat{V}_i^{BS}(t) = -q_{ii}v_i(t, 0) + \int_0^1 K_i^{++}(0, y)u_i(t, y) + K_i^{+-}(0, y)v_i(t, y)dy, \quad (5.8)$$

such that the target states satisfy the following

$$\frac{\partial}{\partial t} \alpha_i(t, x) + \lambda_i \frac{\partial}{\partial x} \alpha_i(t, x) = 0, \quad \frac{\partial}{\partial t} \beta_i(t, x) - \mu_i \frac{\partial}{\partial x} \beta_i(t, x) = \lambda_i K_i^{-+}(x, 1)\alpha_i(t, 1),$$

with the boundary conditions $\beta_i(t, 1) = \rho_{ii}\alpha_i(t, 1)$, and $\alpha_i(t, 0) = 0$. This target system is exponentially stable. This implies the exponential stability of the original system due to the invertibility of the transformation (5.5). Defining $\hat{V}_i(t) = \hat{V}_i^{BS}(t)$ in (5.8) concludes the proof. ■

Finally, the operator $\mathcal{K}_{N+1}(X)$ is simply defined by $\mathcal{K}_{N+1}(X) = KX$, with matrix K defined in Assumption 5.1.1.

5.2.2 . State-feedback controller for output-tracking of a known function

Next, we consider a subsystem i subject to a supposedly known perturbation $d_i(t) \neq 0$. Our next objective is to make the $q_{i+1,i}u_i(t, 1)$ converge towards the virtual input of the downstream subsystem $\hat{V}_{i+1}(t)$. We have the following property:

Property 5.2.2 Trackability :

For all $i \in \llbracket 1, N \rrbracket$, define $\Phi_i \in L^2(\mathbb{R}^+, \mathbb{R})$ an arbitrary known function and assume that the virtual disturbance d_i acting on subsystem i is known. Then, there exists a control law \hat{V}_i that exponentially tracks the function \hat{V}_{i+1} to the desired function Φ_i .

Moreover, if $d_i(t) \equiv \Phi_i(t) \equiv 0$, then, such a control law stabilizes subsystem i .

Lemma 5.2.2: Trajectory tracking [HDMVK16]

For $T > 0$ and all $i \in \llbracket 1, N \rrbracket$, assume that $\Phi_i(t)$ and $d_{i[t+\frac{1}{\lambda_i}]}$ are known for all $t > T$, and define the linear operator $\mathcal{L}^i : \mathbb{R} \times D_{\frac{1}{\lambda_i}} \rightarrow \mathbb{R}$ by

$$\mathcal{L}^i(\Phi_i(t + \frac{1}{\lambda_i}), d_{i[t+\frac{1}{\lambda_i}]}) = \frac{1}{q_{i,i+1}}\Phi_i(t + \frac{1}{\lambda_i}) + \mu_i \int_0^{\frac{1}{\lambda_i}} K_i^{+-}(x - \lambda_i s, 1)d_i(t + \frac{1}{\lambda_i} - s)ds, \quad (5.9)$$

with K_i^{+-} unique solution of (5.6)-(5.7). Then, for all $t > T$, the control law defined by

$$\hat{V}_i(t) = \mathcal{K}^i\left(\begin{pmatrix} u_i(t, \cdot) \\ v_i(t, \cdot) \end{pmatrix}\right) + \mathcal{L}^i(\Phi_i(t + \frac{1}{\lambda_i}), d_{i[t+\frac{1}{\lambda_i}]}) ,$$

where \mathcal{K}^i is the operator defined by Property 5.2.1, satisfies Property 5.2.2.

Proof : Under Assumption 5.1.1 and Assumption 5.1.2, let us prove that the operator defined in (5.9) satisfies Property 5.2.2. The strategy is once again based on the backstepping methodology. For $i \in \llbracket 1, N \rrbracket$, using the Volterra integral transform (5.5), we can map subsystem (5.1)-(5.3) to the target system

$$\frac{\partial}{\partial t}\alpha_i + \lambda_i \frac{\partial}{\partial x}\alpha_i = -\mu_i K_i^{+-}(x, 1)d_i(t), \quad \frac{\partial}{\partial t}\beta_i - \mu_i \frac{\partial}{\partial x}\beta_i = \lambda_i K_i^{-+}(x, 1)\alpha_i(t, 1),$$

with the boundary conditions $\alpha_i(t, 0) = \hat{V}_i(t) - \hat{V}_i^{BS}(t)$, $\beta_i(t, 1) = \rho_{ii}\alpha_i(t, 1) + d_i(t)$, where $\hat{V}_i^{BS}(t)$ is given in (5.8). Define, $V_i^{tr}(t) = \hat{V}_i(t) - \hat{V}_i^{BS}(t)$. Applying the method of characteristics on the above transport equation, we have

$$u(t, 1) = \alpha_i(t, 1) = \alpha_i(t - \frac{1}{\lambda_i}, 0) - \int_0^{\frac{1}{\lambda_i}} \mu_i K_i^{+-}(1 - \lambda_i s, 1)d_i(t - s)ds.$$

To guarantee that $u(t, 1) = \Phi_i(t)$, we therefore define $V_i^{tr}(t) = \mathcal{L}^i(\Phi_i(t + \frac{1}{\lambda_i}), d_{i[t+\frac{1}{\lambda_i}]})$ in (5.9). Note that the control input $\hat{V}_i(t)$ requires *future* values of the trajectory and disturbance to be computed.

Next, assume that Φ_i and d_i converge to zero, such that $\Phi_i(t) = d_i(t) \equiv 0$ for some $t > t^*$. Then, $V_i^{tr} \equiv 0$ for $t > t^*$, and so $\alpha_i(t, 0) \equiv 0$. The target system has a cascade structure from α_i into β_i , where α_i satisfies a pure transport equation. It converges to zero in finite time. Therefore, state β_i also converges to zero. Applying the inverse backstepping transform, the initial states (u_i, v_i) converge to zero. ■

Notice that the operator \mathcal{L}^i requires future values of the reference trajectory and the partial trajectory associated with the virtual disturbance $d_i(s)$, $\forall s \in [t, t + \frac{1}{\lambda_i}]$. This justifies the predictor design presented in Section 5.4.

5.2.3 . Predictor-based full-state feedback

Finally, assuming we have access to the future values of the states, we can apply our *recursive dynamics interconnection framework* and prove the following

Theorem 5.2.1: Existence of a predictor-based stabilizing controller

For $i \in \llbracket 1, N \rrbracket$, for all $x \in [0, 1]$, assume that we have access to a $\sum_{j=1}^{i-1} \frac{1}{\lambda_j} + \frac{x}{\lambda_i}$ units of time ahead prediction of the PDE states $u_i(t, x)$ and $v_i(t, x)$, and a $\sum_{j=1}^n \frac{1}{\lambda_j}$ units of time ahead prediction of the ODE X . Then, there exists a state feedback control law $V_{\Xi}^s(t)$ that exponentially stabilizes the system (5.1)-(5.4) in the sense of the Ξ -norm.

Proof : Let us apply our recursive dynamics interconnection framework. By assumption, we can access the values of $X(t)$. To stabilize the ODE, we want to make $u_N(t, 1)$ converge to $\Phi_N(t) = KX(t)$ where K is defined in Assumption 5.1.1. Under trackability of subsystem N (Property 5.2.2), in the presence of a perturbation converging to 0, we can then compute the virtual command $\hat{V}_N(t)$, towards which $u_{N-1}(t, 1)$ must converge. We then go up the whole chain until the first subsystem to recursively design the control law.

Starting from the last subsystem, define $\hat{V}_{N+1}(t) = KX(t)$, stabilizing the ODE system at the end of the chain. We have $d_N(t) = CX(t)$.

From then, we recursively define

$$\hat{V}_i(t) = \mathcal{K}^i \left(\begin{pmatrix} u_i(t, \cdot) \\ v_i(t, \cdot) \end{pmatrix} \right) + \mathcal{L}^i \left(\hat{V}_{i+1} \left(t + \frac{1}{\lambda_i} \right), d_{i \left[t + \frac{1}{\lambda_i} \right]} \right),$$

and $d_i(t) = \rho_{i, i+1} v_{i+1}(t, 0)$. To simplify the notation, we do not introduce specific notations for the predicted values of state (u_i, v_i, X) . More details are given in Section 5.5. Going back and forth along the chain, we finally have $V(t) = \hat{V}_1(t)$. The control law $V(t)$ is well-defined and causal due to the existence of the different predictors. Then, applying Lemma 5.2.1 on each subsystem, we obtain that $u_N(t, 1)$ exponentially converges to $\mathcal{K}_n(X(t))$. Consequently, $X(t)$ exponentially converges to zero. Using Lemma 5.2.2, we can recursively show that each subsystem exponentially converges to zero starting from $i = N$. This concludes the proof. ■

To apply this recursive dynamics interconnection framework, we must design adequate predictors for future values of the distributed states based on the available measurement. This is done in the following sections.

5.3 . Boundary state estimation

In this section, we estimate the values of the boundary PDE states using the available measurement $y(t)$. Due to the transport delay involved by each PDE subsystem, we can only estimate **past values** of the boundary states. The time ahead which an estimation of a boundary state is available depends on the transport velocities λ_i, μ_i .

5.3.1 . Generalization to a chain structure

Let us consider $\tau > 0$ a fixed, known delay, whose value will be given later. Define the τ -delay operator $\bar{\cdot}$, by

$$\forall \gamma \in C^1([0, +\infty), \mathbb{R}), \forall t > \tau, \bar{\gamma}(t) = \gamma(t - \tau).$$

Using this operator, we can rewrite the system (5.1)-(5.4) in its *delayed version* introducing the delayed states (\bar{u}_i, \bar{v}_i) , satisfying for all $t \geq \tau$, the coupled equations (2.1)-(2.2)

$$\begin{aligned} \frac{\partial}{\partial t} \bar{u}_i(t, x) + \lambda_i \frac{\partial}{\partial x} \bar{u}_i(t, x) &= \sigma_i^+(x) \bar{v}_i(t, x), \\ \frac{\partial}{\partial t} \bar{v}_i(t, x) - \mu_i \frac{\partial}{\partial x} \bar{v}_i(t, x) &= \sigma_i^-(x) \bar{u}_i(t, x), \end{aligned} \quad (5.10)$$

along with the boundary conditions

$$\bar{u}_i(t, 0) = q_{ii} \bar{v}_i(t, 0) + q_{i,i-1} \bar{u}_{i-1}(t, 1), \quad \bar{v}_i(t, 1) = \rho_{ii} \bar{u}_i(t, 1) + \rho_{i,i+1} \bar{v}_{i+1}(t, 0). \quad (5.11)$$

The delayed ODE state satisfies $\dot{\bar{X}}(t) = A\bar{X}(t) + B\bar{u}_N(t, 1)$. The available delayed measurement rewrites $\bar{y}(t) = y(t - \tau) \iff y(t) = \bar{y}(t + \tau)$. Thus, it means that we know τ -ahead future values of \bar{y} . Consider now an isolated subsystem i as illustrated in Figure 5.4.

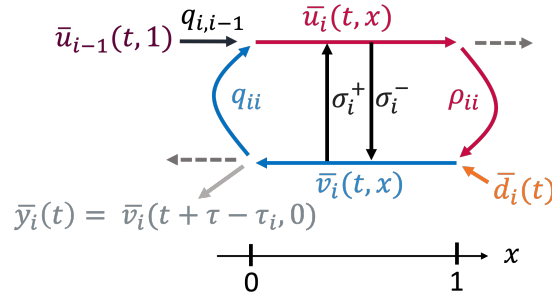


Figure 5.4 – Schematic representation of one subsystem i .

Define the delay τ_i inherent to the upstream dynamics as $\tau_i = \sum_{j=1}^{i-1} \frac{1}{\mu_j}$, and the intrinsic delay $\delta_i = \frac{1}{\lambda_i} + \frac{1}{\mu_i}$.

For any subsystem i , we assume we have access to a *virtual measurement* \bar{y}_i defined as $\bar{y}_i(t) = v_i(t - \tau_i, 0) = \bar{v}_i(t + \tau - \tau_i, 0)$. This definition is causal as it only requires past values of $\bar{v}_i(\cdot, 0)$. Note that $\bar{y}_1 = \bar{y}$, which is known on the time interval $[t, t + \tau]$. Our isolated subsystem i is also subject to a *virtual disturbance* $\bar{d}_i(t)$, defined as $\bar{d}_i(t) = \rho_{i,i+1} \bar{v}_{i+1}(t, 0)$.

For any function γ , we denote $\hat{\gamma}$ the corresponding *observer state* (or estimated state). In this section, we show that we can design an observer $\hat{u}_i(t, 1), \hat{v}_i(t, 0)$ for the delayed boundary states of each subsystem. More precisely, we prove the following

Property 5.3.1 Observability of the boundary states:

For all $i \in \llbracket 1, N \rrbracket$, there exists two functions $\hat{u}_i(\cdot, 1), \hat{v}_i(\cdot, 0)$, that causally depend on the measurement $y(t)$ and on the control law $V(t)$ such that: $\|\bar{u}_i(t, 1) - \hat{u}_i(t, 1)\|_{L^2} \xrightarrow{t \rightarrow +\infty} 0$ and $\|\bar{v}_i(t, 0) - \hat{v}_i(t, 0)\|_{L^2} \xrightarrow{t \rightarrow +\infty} 0$. Moreover, there exists \hat{X} that causally depends on the measurement $y(t)$ and on the control law $V(t)$ such that: $\|\bar{X}(t) - \hat{X}(t)\| \xrightarrow{t \rightarrow +\infty} 0$.

We obtain a more substantial result since the proposed estimation provides exact (delayed)-values of the PDE boundary states. We have

Lemma 5.3.1: Expressions of $\bar{u}_i(\cdot, 1)$, \bar{d}_i

Consider a subsystem $i \in \llbracket 1, N \rrbracket$, and assume that we have access to \bar{y}_i and $\bar{u}_{i-1}(\cdot, 1)$ on a time interval $[t, t + \tau - \tau_i]$.

Then, there exist two linear operators \mathcal{L}_{u_i} and \mathcal{L}_{d_i} , such that for $t > \tau + \frac{1}{\lambda_i}$,

$$\bar{u}_i(\nu, 1) = \mathcal{L}_{u_i}(\bar{y}_i(\cdot), \bar{u}_{i-1}(\cdot, 1)), \quad \bar{d}_i(\nu) = \mathcal{L}_{d_i}(\bar{y}_i(\cdot), \bar{u}_{i-1}(\cdot, 1)),$$

for all $\nu \in [t, t + \tau - \tau_{i+1}]$.

Note that the conditions of Lemma 5.3.1 are obviously satisfied for $i = 1$ since $\tau_1 = 0$.

Proof: The proof is based on the backstepping methodology inspired by [ABABS⁺18, CVKB13, VCKB11] coupled with a neutral-type time-delay formulation.

Backstepping transform

Consider subsystem $i \in \llbracket 1, N \rrbracket$, as represented in Figure 5.4. We first apply the invertible Volterra transform \mathcal{L}_i defined by

$$\begin{cases} \bar{u}_i(t, x) = \bar{w}_i(t, x) - \int_0^x L_i^{++}(x, \nu) \bar{w}_i(t, \nu) + L_i^{+-}(x, \nu) \bar{z}_i(t, \nu) d\nu, \\ \bar{v}_i(t, x) = \bar{z}_i(t, x) - \int_0^x L_i^{-+}(x, \nu) \bar{w}_i(t, \nu) + L_i^{--}(x, \nu) \bar{z}_i(t, \nu) d\nu, \end{cases} \quad (5.12)$$

where the kernels $L_i^{\cdot\cdot}$ are continuous functions defined on \mathcal{T}^- . They satisfy the following set of equations

$$\begin{aligned} \lambda_i \frac{\partial}{\partial x} L_i^{++}(x, \nu) + \lambda_i \frac{\partial}{\partial \nu} L_i^{++}(x, \nu) &= \sigma_i^+(x) L_i^{-+}(x, \nu), \\ \lambda_i \frac{\partial}{\partial x} L_i^{+-}(x, \nu) - \mu_i \frac{\partial}{\partial \nu} L_i^{+-}(x, \nu) &= \sigma_i^+(x) L_i^{--}(x, \nu), \\ \mu_i \frac{\partial}{\partial x} L_i^{-+}(x, \nu) - \lambda_i \frac{\partial}{\partial \nu} L_i^{-+}(x, \nu) &= -\sigma_i^-(x) L_i^{++}(x, \nu), \\ \mu_i \frac{\partial}{\partial x} L_i^{--}(x, \nu) + \mu_i \frac{\partial}{\partial \nu} L_i^{--}(x, \nu) &= -\sigma_i^-(x) L_i^{+-}(x, \nu), \end{aligned} \quad (5.13)$$

with the boundary conditions for all $x \in [0, 1]$, $L_i^{-+}(x, x) = \frac{\sigma_i^-(x)}{\lambda_i + \mu_i}$, $L_i^{+-}(x, x) = -\frac{\sigma_i^+(x)}{\lambda_i + \mu_i}$ and for all $\nu \in [0, 1]$, $L_i^{--}(1, \nu) = \rho_{ii} L_i^{+-}(1, \nu)$, $L_i^{++}(1, \nu) = 0$. This system admits a unique solution [CVKB13, VCKB11]. With this transformation, we can map the original system (5.10)-(5.11) to the target system :

$$\begin{aligned} \frac{\partial}{\partial t} \bar{w}_i(t, x) + \lambda_i \frac{\partial}{\partial x} \bar{w}_i(t, x) &= f_i(x) \bar{v}_i(t, 0) + h_i(x) \bar{u}_{i-1}(t, 1), \\ \frac{\partial}{\partial t} \bar{z}_i(t, x) - \mu_i \frac{\partial}{\partial x} \bar{z}_i(t, x) &= g_i(x) \bar{v}_i(t, 0) + k_i(x) \bar{u}_{i-1}(t, 1), \end{aligned} \quad (5.14)$$

with the following boundary conditions

$$\begin{aligned} \bar{w}_i(t, 0) &= q_{i,i-1} \bar{u}_{i-1}(t, 1) + q_{ii} \bar{v}_i(t, 0), \\ \bar{z}_i(t, 1) &= \rho_{ii} \bar{u}_i(t, 1) + \bar{d}_i(t) + \int_0^1 (L_i^{-+}(1, \nu) \bar{w}_i(t, \nu) + L_i^{--}(1, \nu) \bar{z}_i(t, \nu)) d\nu. \end{aligned} \quad (5.15)$$

Note that in-domain couplings have been moved to the right boundary $x = 1$ of subsystem i . The functions f_i, g_i, h_i, k_i are real-valued functions defined on $[0, 1]$. They are defined as the unique solution [Yos60] of the following Volterra integral equations of the second kind. For all $x \in [0, 1]$,

$$\begin{pmatrix} f_i(x) \\ g_i(x) \end{pmatrix} = \mathcal{L}_i^{-1} \left(\begin{pmatrix} \lambda_i q_{ii} L_i^{++}(x, 0) - \mu_i L_i^{+-}(x, 0) \\ \lambda_i q_{ii} L_i^{-+}(x, 0) - \mu_i L_i^{--}(x, 0) \end{pmatrix} \right), \quad \begin{pmatrix} h_i(x) \\ k_i(x) \end{pmatrix} = \mathcal{L}_i^{-1} \left(\begin{pmatrix} \lambda_i q_{i,i-1} L_i^{++}(x, 0) \\ \lambda_i q_{i,i-1} L_i^{-+}(x, 0) \end{pmatrix} \right). \quad (5.16)$$

Note that we have chosen to preserve the terms $\bar{u}_i(t, 1)$ and $\bar{v}_i(t, 0)$ in the target system (5.14) (instead of

replacing them by \bar{z}_i and \bar{w}_i) to simplify the estimation procedure.

Neutral-type formulation of the boundary states

In order to find the linear operators $\mathcal{L}_{u_i}, \mathcal{L}_{d_i}$, we now rewrite the new system (5.14)-(5.15) as a *functional differential equation of neutral type*. Using the method of characteristics, we have, $\forall x \in [0, 1], \forall t > \delta_i$:

$$\begin{aligned}\bar{w}_i(t, x) &= \bar{w}_i(t - \frac{x}{\lambda_i}, 0) + \int_0^{\frac{x}{\lambda_i}} f_i(x - \lambda_i s) \bar{v}_i(t - s, 0) + h_i(x - \lambda_i s) \bar{u}_{i-1}(t - s, 1) ds, \\ \bar{z}_i(t, x) &= \bar{z}_i(t - \frac{1-x}{\mu_i}, 1) + \int_0^{\frac{1-x}{\mu_i}} g_i(x + \mu_i s) \bar{v}_i(t - s, 0) + k_i(x + \mu_i s) \bar{u}_{i-1}(t - s, 1) ds.\end{aligned}\quad (5.17)$$

Consequently, we obtain, applying several changes of variable in the integral terms and from (5.17)

$$\begin{aligned}\bar{u}_i(t, 1) &= \bar{w}_i(t, 1) - \int_0^1 L_i^{+-}(1, \nu) \bar{z}_i(t, \nu) d\nu \quad \text{from (5.12) and since } L_i^{++}(1, \nu) = 0, \forall \nu \in [0, 1] \\ &= q_{i,i-1} \bar{u}_{i-1}(t - \frac{1}{\lambda_i}, 1) + q_{ii} \bar{v}_i(t - \frac{1}{\lambda_i}, 0) + \int_0^{\frac{1}{\lambda_i}} \bar{u}_{i-1}(t - s, 1) \mathcal{U}_i^-(s) + \bar{v}_i(t - s, 0) \mathcal{V}_i^-(s) ds \\ &\quad + \int_0^{\frac{1}{\mu_i}} \bar{u}_{i-1}(t + s, 1) \mathcal{U}_i^+(s) + \bar{v}_i(t + s, 0) \mathcal{V}_i^+(s) ds\end{aligned}\quad (5.18)$$

where

$$\begin{aligned}\forall s \in [0, \frac{1}{\lambda_i}] & \qquad \qquad \qquad \forall s \in [0, \frac{1}{\mu_i}] \\ \left\{ \begin{array}{l} \mathcal{U}_i^-(s) = h_i(1 - \lambda_i s), \\ \mathcal{V}_i^-(s) = f_i(1 - \lambda_i s), \end{array} \right. & \left\{ \begin{array}{l} \mathcal{U}_i^+(s) = \mu_i \int_s^{\frac{1}{\mu_i}} L_i^{+-}(1, \mu_i \nu) k_i(\mu_i(\nu - s)) d\nu, \\ \mathcal{V}_i^+(s) = \mu_i \left(-L_i^{+-}(1, \mu_i s) + \int_s^{\frac{1}{\mu_i}} L_i^{+-}(1, \mu_i \nu) g_i(\mu_i(\nu - s)) d\nu \right).\end{array} \right.\end{aligned}\quad (5.19)$$

Using the definition of the virtual measurement, we finally obtain

$$\begin{aligned}\bar{u}_i(t, 1) &= q_{i,i-1} \bar{u}_{i-1}(t - \frac{1}{\lambda_i}, 1) + \int_0^{\frac{1}{\lambda_i}} \mathcal{U}_i^-(s) \bar{u}_{i-1}(t - s, 1) + \mathcal{V}_i^-(s) \bar{y}_i(t - s - \tau + \tau_i) ds \\ &\quad + q_{ii} \bar{y}_i(t - \frac{1}{\lambda_i} - \tau + \tau_i) + \int_0^{\frac{1}{\mu_i}} \mathcal{U}_i^+(s) \bar{u}_{i-1}(t + s, 1) + \mathcal{V}_i^+(s) \bar{y}_i(t + s - \tau + \tau_i) ds.\end{aligned}$$

Similarly, we obtain

$$\begin{aligned}\bar{d}_i(t) &= \bar{v}_i(t, 1) - \rho_{ii} \bar{u}_i(t, 1) && \text{by definition} \\ &= \bar{v}_i(t + \frac{1}{\mu_i}, 0) - \int_0^{\frac{1}{\mu_i}} g_i(\mu_i s) \bar{v}_i(t + \frac{1}{\mu_i} - s, 0) + k_i(\mu_i s) \bar{u}_{i-1}(t + \frac{1}{\mu_i} - s, 1) ds && \text{from (5.17)} \\ &\quad - \rho_{ii} q_{i,i-1} \bar{u}_{i-1}(t - \frac{1}{\lambda_i}, 1) - \rho_{ii} q_{ii} \bar{v}_i(t - \frac{1}{\lambda_i}, 0) - \int_0^{\frac{1}{\lambda_i}} \bar{v}_i(t - s, 0) \mathcal{I}_{v_i}(s) + \bar{u}_{i-1}(t - s, 1) \mathcal{I}_{u_i}(s) ds, \\ &= \bar{y}_i(t - \tau + \tau_i + \frac{1}{\mu_i}) - \rho_{ii} q_{i,i-1} \bar{u}_{i-1}(t - \frac{1}{\lambda_i}, 1) - \rho_{ii} q_{ii} \bar{y}_i(t - \tau + \tau_i - \frac{1}{\lambda_i}) \\ &\quad - \int_0^{\frac{1}{\mu_i}} g_i(\mu_i s) \bar{y}_i(t - \tau + \tau_i + \frac{1}{\mu_i} - s) + k_i(\mu_i s) \bar{u}_{i-1}(t + \frac{1}{\mu_i} - s, 1) ds \\ &\quad - \int_0^{\frac{1}{\lambda_i}} \mathcal{I}_{v_i}(s) \bar{y}_i(t - \tau + \tau_i - s) + \mathcal{I}_{u_i}(s) \bar{u}_{i-1}(t - s, 1) ds,\end{aligned}\quad (5.20)$$

$$\text{where } \forall s \in [0, \frac{1}{\lambda_i}] : \left\{ \begin{array}{l} \mathcal{I}_{v_i}(s) = \rho_{ii} f_i(1 - \lambda_i s) + q_{ii} \lambda_i L_i^{-+}(1, \lambda_i s) + \int_{\lambda_i s}^1 L_i^{-+}(1, \nu) f_i(\nu - \lambda_i s) d\nu, \\ \mathcal{I}_{u_i}(s) = \rho_{ii} h_i(1 - \lambda_i s) + q_{i,i-1} \lambda_i L_i^{-+}(1, \lambda_i s) + \int_{\lambda_i s}^1 L_i^{-+}(1, \nu) h_i(\nu - \lambda_i s) d\nu.\end{array} \right.$$

Assuming that $\bar{u}_{i-1}(\cdot, 1)$ is known on a time interval $[t, t + \tau - \tau_i]$, it becomes possible to compute \bar{d}_i on the time interval $[t, t + \tau - \tau_{i+1}]$ and $\bar{u}_i(\cdot, 1)$ on $[t, t + \tau - \tau_{i+1}]$.

More precisely, for $\tau > \tau_i + \frac{1}{\mu_i} = \tau_{i+1}$, the expressions (5.18)-(5.20) define the linear operators $\mathcal{L}_{u_i}, \mathcal{L}_{d_i}$ satisfying Lemma 5.3.1. Moreover, with Assumption 5.1.5, we can now estimate $\bar{v}_{i+1}(\cdot, 0)$ on the time interval $[t, t + \tau - \tau_{i+1}]$, which gives us an estimation of \bar{y}_{i+1} . This concludes the proof. \blacksquare

5.3.2 . Estimation of the ODE state

We now consider the ODE system interconnected at the end of the chain with subsystem N . The corresponding delayed state satisfies the following:

$$\dot{\bar{X}}(t) = A\bar{X}(t) + B\bar{u}_N(t, 1), \quad \text{with} \quad \bar{d}_N(t) = C\bar{X}(t). \quad (5.21)$$

Assume that the functions \bar{d}_N and $\bar{u}_N(\cdot, 1)$ are known. Under Assumption 5.1.4, we design a *Luenberger-type* observer $\hat{\bar{X}}$ for the time-shifted ODE (5.21). It is defined by

$$\dot{\hat{\bar{X}}}(t) = A\hat{\bar{X}}(t) + B\bar{u}_N(t, 1) - L \left(\bar{d}_N(t) - C\hat{\bar{X}}(t) \right).$$

Using the matrix $L \in \mathbb{R}^{p \times 1}$ guaranteeing that $A + LC$ is Hurwitz, the error state defined as $\tilde{\bar{X}} = \bar{X} - \hat{\bar{X}}$ verifies the exponentially stable system

$$\dot{\tilde{\bar{X}}}(t) = (A + LC)\tilde{\bar{X}}(t).$$

Since the error state converges to zero, the designed observer $\hat{\bar{X}}$ converges to the real delayed state $\bar{X}(t)$. Thus, after a specific convergence delay, we can accurately estimate delayed values of the state $X(t)$.

Remark 5.3.1 *Note that if C is right invertible, $C^\top C$ invertible and $\bar{X}(t) = (C^\top C)^{-1}C^\top \bar{d}_N(t)$. Knowing the virtual disturbance \bar{d}_N on a time interval, we can directly reconstruct the delayed state $\bar{X}(t)$ on this time interval.*

5.3.3 . Recursive estimation of boundary states

Consider now the whole delayed system (5.10)-(5.11). We recursively apply Lemma 5.3.1 to obtain the following:

Theorem 5.3.1: Estimation of the delayed boundary states

Denote $\tau_i = \sum_{j=1}^{i-1} \frac{1}{\mu_j}$, for $i \in \llbracket 1, N \rrbracket$. If $\tau \geq \tau_{N+1}$, there exist causal linear operators $\mathcal{L}_u^i, \mathcal{L}_v^{i+1}$ such that, for all $t > \tau + \sum_{j=1}^i \frac{1}{\lambda_j}$, for all $\nu \in [t, t + \tau - \tau_{i+1}]$,

$$\forall i \in \llbracket 1, N \rrbracket, \bar{u}_i(\nu, 1) = \mathcal{L}_u^i(y(\cdot), V(\cdot)), \forall i \in \llbracket 0, N - 1 \rrbracket, \bar{v}_{i+1}(\nu, 0) = \mathcal{L}_v^{i+1}(y(\cdot), V(\cdot)).$$

Moreover, there exists a causal linear operator \mathcal{L}_X such that for all $t > \tau + \sum_{j=1}^N \frac{1}{\lambda_j}$, for all $\nu \in [t, t + \tau - \tau_N]$

$$\bar{X}(\nu) = \mathcal{L}_X(y(\cdot), V(\cdot)).$$

Proof : The proof is based on an induction argument. Note that we choose t large enough to properly obtain equations (5.18) and (5.20). We first consider $i = 1$. By definition, $v_1(t, 0) = y(t)$, so \mathcal{L}_v^1 is the identity operator. Equations (5.18) and (5.20) give us the two linear operators \mathcal{L}_u^1 , and \mathcal{L}_v^2 (since \bar{y} and \bar{V} are both known on the time interval $[t, t + \tau]$). Using the fact that $\bar{v}_2(t, 0)$ and $\bar{u}_1(t, 1)$ can be estimated on the time horizon $[t, t + \tau - \tau_2]$, we can apply Lemma 5.3.1. It then becomes possible to recursively define the linear operators $\mathcal{L}_u^i, \mathcal{L}_v^i$. ■

This theorem shows that Property 5.3.1 is satisfied for the interconnected chain under consideration. We can then define the observer states as $\hat{u}_i(t, 1) = \mathcal{L}_u^i(y(\cdot), V(\cdot))$, $\hat{v}_i(t, 0) = \mathcal{L}_v^i(y(\cdot), V(\cdot))$, and $\hat{X}(t) = \mathcal{L}_X(y(\cdot), V(\cdot))$. The proposed procedure gives exact, and not asymptotic delayed-values of the boundary states $u_i(t, 1)$ and $v_i(t, 0)$. However, the terminology *estimation* emphasizes that these values are not directly available but computed using the proposed recursive estimation procedure. If the measurement is corrupted by noise, these estimations will no longer be exact. Moreover, other approaches could be used to fulfill Property 5.3.1.

5.4 . Design of states predictors

We used the recursive dynamics interconnection framework in the previous section to estimate the delayed values of the boundary PDE and ODE states. However, to apply the methodology developed in Section 5.2 and design an output feedback control law satisfying the control objective, we need to estimate the non-delayed values of these boundary states and even predict future values. In this section, we design a predictor to obtain a $\tau + \sum_{j=1}^{i-1} \frac{1}{\lambda_j}$ ahead of time values of the delayed boundary states $\bar{u}_i(\cdot, 1)$ and $\bar{v}_i(\cdot, 0)$. We have the following property.

Property 5.4.1 Predictability

For all $x \in [0, 1]$, it is possible to obtain a $\tau + \sum_{j=1}^{i-1} \frac{1}{\lambda_j} + \frac{x}{\lambda_i}$ units of time ahead estimation of the PDE states $\bar{u}_i(t, x)$ and $\bar{v}_i(t, x)$, and a $\tau + \sum_{j=1}^N \frac{1}{\lambda_j}$ units of time ahead estimation of the ODE \bar{X} , using solely the measure $y(t)$ and the control law $V(t)$.

Using the boundary measurement, we can predict future values of the distributed PDE states on a time interval corresponding to the propagation time of the information from the boundary $x = 0$ of the first subsystem (where the measurement is available) to the desired point.

5.4.1 . Predictor design for the boundary states

Denote the total transport delay $\delta_{tot} \doteq \sum_{i=1}^N \delta_i$. First, we have

Lemma 5.4.1: Existence of boundary states predictions

Consider a subsystem $i \in \llbracket 1, N \rrbracket$, and assume we have access to all values of $y(\cdot), V(\cdot)$ on a time interval $[0, t]$.

Then, there exist causal boundary state predictors such that

$$\begin{aligned} \text{for all } s \in [t - \tau - \delta_{tot} - \sum_{j=1}^{i-1} \frac{1}{\lambda_j}, t], P_{\bar{v}_i}(t, s) &= \hat{v}_i(s + \tau + \sum_{j=1}^{i-1} \frac{1}{\lambda_j}, 0), \\ \text{for all } s \in [t - \tau - \delta_{tot} - \sum_{j=1}^i \frac{1}{\lambda_j}, t], P_{\bar{u}_i}(t, s) &= \hat{u}_i(s + \tau + \sum_{j=1}^i \frac{1}{\lambda_j}, 1), \\ \text{for all } s \in [t - \tau - \delta_{tot} - \sum_{j=1}^N \frac{1}{\lambda_j}, t], P_{\bar{X}}(t, s) &= \hat{X}(s + \tau + \sum_{j=1}^N \frac{1}{\lambda_j}). \end{aligned} \quad (5.22)$$

Proof : The proof follows four main steps. For each subsystem $i \in \llbracket 1, N \rrbracket$, we first use the backstepping transform \mathcal{K}_i defined in (5.5). Unlike transform (5.12), this transform preserve the terms $\bar{u}_i(t, 1)$ and $\bar{v}_i(t, 0)$ inside the target system. Most in-domain couplings are moved to the *left* boundary of each PDE subsystem. We then use the method of characteristics to obtain the neutral delay-equations satisfied by each boundary state. Inspired by, [BPDm16, KK17], we design a predictor and show that it matches the boundary states values.

Backstepping transform

Consider the following Volterra integral transforms \mathcal{K}_i (5.5) with kernels satisfying (5.6)-(5.7). The target states $\begin{pmatrix} \bar{\alpha}_i(t, \cdot) \\ \bar{\beta}_i(t, \cdot) \end{pmatrix} = \mathcal{K}_i \left(\begin{pmatrix} \bar{u}_i(t, \cdot) \\ \bar{v}_i(t, \cdot) \end{pmatrix} \right)$ satisfy

$$\frac{\partial}{\partial t} \bar{\alpha}_i(t, x) + \lambda_i \frac{\partial}{\partial x} \bar{\alpha}_i(t, x) = f_i^+(x) \bar{v}_{i+1}(t, 0), \quad \frac{\partial}{\partial t} \bar{\beta}_i(t, x) - \mu_i \frac{\partial}{\partial x} \bar{\beta}_i(t, x) = f_i^-(x) \bar{\alpha}_i(t, 1),$$

with the boundary conditions $\bar{\beta}_i(t, 1) = \rho_{ii} \bar{\alpha}_i(t, 1) + \rho_{i,i+1} \bar{v}_{i+1}(t, 0)$, and

$$\bar{\alpha}_i(t, 0) = q_{ii} \bar{v}_i(t, 0) + q_{i,i-1} \bar{u}_{i-1}(t, 1) + \int_0^1 M_i^{++}(0, \nu) \bar{\alpha}_i(t, \nu) + M_i^{+-}(0, \nu) \bar{\beta}_i(t, \nu), \quad (5.23)$$

where M_i^{\cdot} are the kernels of the inverse transform $\mathcal{M}_i = \mathcal{K}_i^{-1}$. The two gain functions f_i^-, f_i^+ are defined on $[0, 1]$ by $f_i^-(x) = \lambda_i K_i^{-+}(x, 1)$, $f_i^+(x) = -\mu_i \rho_{i,i+1} K_i^{+-}(x, 1)$.

Neutral-type formulation of the boundary states

We apply the method of characteristics on the target system to rewrite the boundary terms $\bar{u}_i(t, 1)$, $\bar{v}_i(t, 0)$ as solutions of difference equations.

We have for $i \in \llbracket 1, N \rrbracket$, $\bar{u}_i(t, 1) = \bar{\alpha}_i(t - \frac{1}{\lambda_i}, 0) + \int_0^{\frac{1}{\lambda_i}} f_i^+(1 - \nu \lambda_i) \bar{v}_{i+1}(t - \nu, 0) d\nu$. Following the approach given in [ADM19], we obtain

$$\begin{aligned} \bar{v}_i(t, 0) &= \rho_{ii} \bar{u}_i(t - \frac{1}{\mu_i}, 1) + \rho_{i,i+1} \bar{v}_{i+1}(t - \frac{1}{\mu_i}, 0) \\ &\quad + \int_0^{\delta_i} g_i^1(\nu) \bar{\alpha}_i(t - \nu, 0) + g_i^2(\nu) \bar{u}_i(t - \nu, 1) + g_i^3(\nu) \bar{v}_{i+1}(t - \nu, 0) d\nu, \end{aligned}$$

where the functions g_i^1 , g_i^2 and g_i^3 are defined by

$$\begin{aligned} g_i^1(\nu) &= -\mathbb{1}_{[0, \frac{1}{\lambda_i}]}(\nu) \lambda_i M_i^{-+}(0, \lambda_i \nu), \\ g_i^2(\nu) &= \mathbb{1}_{[0, \frac{1}{\mu_i}]}(\nu) (f_i^-(\mu_i \nu) - \mu_i \rho_{ii} M_i^{--}(0, 1 - \mu_i \nu) - \int_0^{1 - \mu_i \nu} M_i^{--}(0, \nu) f_i^-(\nu + \mu_i \nu) d\nu), \\ g_i^3(\nu) &= -\mathbb{1}_{[0, \frac{1}{\mu_i}]}(\nu) (\mu_i \rho_{i,i+1} M_i^{--}(0, 1 - \mu_i \nu)) - \mathbb{1}_{[0, \frac{1}{\lambda_i}]}(\nu) \left(\int_{\lambda_i \nu}^1 M_i^{-+}(0, \nu) f_i^+(\nu - \lambda_i \nu) d\nu \right). \end{aligned}$$

Similarly, we obtain

$$\begin{aligned} \bar{\alpha}_i(t, 0) &= q_{ii} \bar{v}_i(t, 0) + q_{i,i-1} \bar{u}_{i-1}(t, 1) \\ &\quad + \int_0^{\delta_i} k_i^1(\nu) \bar{\alpha}_i(t - \nu, 0) + k_i^2(\nu) \bar{u}_i(t - \nu, 1) + k_i^3(\nu) \bar{v}_{i+1}(t - \nu, 0) d\nu, \end{aligned}$$

where the functions k_i^1 , k_i^2 and k_i^3 are defined by

$$\begin{aligned} k_i^1(\nu) &= \mathbb{1}_{[0, \frac{1}{\lambda_i}]}(\nu) \lambda_i M_i^{++}(0, \lambda_i \nu), \\ k_i^2(\nu) &= \mathbb{1}_{[0, \frac{1}{\mu_i}]}(\nu) (\mu_i \rho_{ii} M_i^{+-}(0, 1 - \mu_i \nu) + \int_0^{1 - \mu_i \nu} M_i^{+-}(0, \nu) f_i^-(\nu + \mu_i \nu) d\nu), \\ k_i^3(\nu) &= \mathbb{1}_{[0, \frac{1}{\mu_i}]}(\nu) (\mu_i \rho_{i,i+1} M_i^{+-}(0, 1 - \mu_i \nu)) + \mathbb{1}_{[0, \frac{1}{\lambda_i}]}(\nu) \left(\int_{\lambda_i \nu}^1 M_i^{++}(0, \nu) f_i^+(\nu - \lambda_i \nu) d\nu \right). \end{aligned}$$

Note that the given expressions are still valid for $i = 0$, using $q_{1,0} \bar{u}_0(t, 1) = V(t - \tau)$ and for $i = N$ using $\bar{v}_{N+1}(t, 0) = X(t)$.

Estimation of the state $\bar{\alpha}_i(t, 0)$

To initialize the predictor for the boundary terms $\bar{u}_i(\cdot, 1)$, $\bar{v}_i(\cdot, 0)$, and $\bar{X}(\cdot)$, we can use the estimates $\hat{\bar{u}}_i(\cdot, 1)$, $\hat{\bar{v}}_i(\cdot, 0)$, and $\hat{\bar{X}}(\cdot)$ obtained in Section 5.3. For state $\bar{\alpha}_i(\cdot, 0)$, using equation (5.23) and integrating the states $(\bar{\alpha}_i, \bar{\beta}_i)$

along the characteristic lines, we immediately obtain

$$\begin{aligned}\bar{\alpha}_i(t, 0) &= q_{ii}\bar{v}_i(t, 0) + q_{i,i-1}\bar{u}_{i-1}(t, 1) \\ &+ \int_0^{\frac{1}{\lambda_i}} k_i^2(\nu)\bar{u}_i(t - \nu, 1) + \mu_i M_i^{+-}(0, 1 - \mu_i\nu)\rho_{i,i+1}\bar{v}_{i+1}(t - \nu, 0)d\nu \\ &+ \int_0^{\frac{1}{\lambda_i}} \lambda_i M_i^{++}(0, 1 - \lambda_i\nu)\bar{u}_i(t + \nu, 1) - \left(\int_0^{1-\lambda_i\nu} f_i^+(\nu + \lambda_i\nu)M_i^{++}(0, \nu)d\nu\right)\bar{v}_{i+1}(t + \nu, 0)d\nu.\end{aligned}$$

From Property 5.3.1, we have an estimation of $\bar{u}_i(\cdot, 1)$ and $\bar{v}_i(\cdot, 0)$ on $[t, t + \tau - \tau_N]$. We can use these estimates in the above expression to obtain $\hat{\alpha}_i(\cdot, 0)$ an estimation of $\bar{\alpha}_i(\cdot, 0)$, under the condition $\tau > \tau_N + \sup_i \{\frac{1}{\lambda_i}\}$.

Expression of the boundary-states predictors[ABP22]

We now design the predictors $P_{\bar{v}_i}(t, s)$, $P_{\bar{u}_i}(t, s)$ and $P_{\bar{\alpha}_i}(t, s)$ for the PDE boundary states $\bar{u}_i(t, 1)$, $\bar{v}_i(t, 0)$, $\bar{\alpha}_i(t, 0)$ and ODE state $\bar{X}(t)$.

For $t \geq 0$ and $s \in [t - \tau - \delta_{tot} - \sum_{j=1}^{i-1} \frac{1}{\lambda_j}, t]$, we denote $P_{\bar{v}_i}(t, s)$ (resp. $P_{\bar{\alpha}_i}(t, s)$) the state prediction of future values of $\bar{v}_i(t, 0)$ (resp. $\bar{\alpha}_i(t, 0)$) ahead a time $\tau + \sum_{j=1}^{i-1} \frac{1}{\lambda_j}$. They are defined by

$$P_{\bar{\alpha}_i}(t, s) = \begin{cases} \hat{\alpha}_i(s + \tau + \sum_{j=1}^{i-1} \frac{1}{\lambda_j}, 0) & \text{if } s \in [t - \delta_{tot} - \tau - \sum_{j=1}^{i-1} \frac{1}{\lambda_j}, t - \tau - \sum_{j=1}^{i-1} \frac{1}{\lambda_j}] \\ q_{ii}P_{\bar{v}_i}(t, s) + q_{i,i-1}P_{\bar{u}_{i-1}}(t, s) & \text{otherwise,} \end{cases} \quad (5.24)$$

$$+ \int_0^{\delta_i} k_i^1(\nu)P_{\bar{\alpha}_i}(t, s - \nu) + k_i^2(\nu)P_{\bar{u}_i}(t, s - \nu - \frac{1}{\lambda_i}) + k_i^3(\nu)P_{\bar{v}_{i+1}}(t, s - \nu - \frac{1}{\lambda_i})d\nu$$

$$P_{\bar{v}_i}(t, s) = \begin{cases} \hat{v}_i(s + \tau + \sum_{j=1}^{i-1} \frac{1}{\lambda_j}, 0) & \text{if } s \in [t - \delta_{tot} - \tau - \sum_{j=1}^{i-1} \frac{1}{\lambda_j}, t - \tau - \sum_{j=1}^{i-1} \frac{1}{\lambda_j}] \\ \rho_{i,i+1}P_{\bar{v}_{i+1}}(t, s - \frac{1}{\lambda_i} - \frac{1}{\mu_i}) + \rho_{ii}P_{\bar{u}_i}(t, s - \frac{1}{\lambda_i} - \frac{1}{\mu_i}) & \text{otherwise.} \end{cases} \quad (5.25)$$

$$+ \int_0^{\delta_i} g_i^1(\nu)P_{\bar{\alpha}_i}(t, s - \nu) + g_i^2(\nu)P_{\bar{u}_i}(t, s - \nu - \frac{1}{\lambda_i}) + g_i^3(\nu)P_{\bar{v}_{i+1}}(t, s - \nu - \frac{1}{\lambda_i})d\nu$$

Note that $P_{\bar{\alpha}_i}(t, s)$ is well-defined and causal, using the convention $q_{1,0}P_{\bar{u}_0}(t, s) = V(s)$, $s \in [t - \tau - \delta_{tot}, t]$. For $t \geq 0$ and for $s \in [t - \tau - \delta_{tot} - \sum_{j=1}^i \frac{1}{\lambda_j}, t]$, $P_{\bar{u}_i}(t, s)$ the state prediction of future values of $\bar{u}_i(t, 1)$ ahead a time $\tau + \sum_{j=1}^i \frac{1}{\lambda_j}$ is defined by

$$P_{\bar{u}_i}(t, s) = \begin{cases} \hat{u}_i(s + \tau + \sum_{j=1}^i \frac{1}{\lambda_j}, 0) & \text{if } s \in [t - \delta_{tot} - \tau - \sum_{j=1}^i \frac{1}{\lambda_j}, t - \tau - \sum_{j=1}^i \frac{1}{\lambda_j}] \\ P_{\bar{\alpha}_i}(t, s) + \int_0^{\frac{1}{\lambda_i}} f_i^+(1 - \nu\lambda_i)P_{\bar{v}_{i+1}}(t, s - \nu)d\nu & \text{otherwise.} \end{cases} \quad (5.26)$$

Following [BL14, BPDm16], we can also define $P_{\bar{X}}(t, s)$ as the classic state prediction of future values of $X(t)$ ahead a time $\sum_{j=1}^N \frac{1}{\lambda_j}$, for $s \in [t - \delta_{tot} - \sum_{j=1}^N \frac{1}{\lambda_j}, t]$, by

$$P_{\bar{X}}(t, s) = \begin{cases} \hat{X}(s + \tau + \sum_{j=1}^N \frac{1}{\lambda_j}) & \text{if } s \in [t - \delta_{tot} - \tau - \sum_{j=1}^N \frac{1}{\lambda_j}, t - \tau - \sum_{j=1}^N \frac{1}{\lambda_j}] \\ e^{A \sum_{j=1}^N \frac{1}{\lambda_j}} \left(\hat{X}(s) + \int_s^{s + \sum_{j=1}^N \frac{1}{\lambda_j}} e^{A(s-\nu)} B P_{\bar{u}_N}(t, \nu - \sum_{j=1}^N \frac{1}{\lambda_j}) d\nu \right) & \text{otherwise.} \end{cases} \quad (5.27)$$

The convergence of the predictor $P_{\bar{X}}(t, s)$ is guaranteed by [KK17, Part 1, Chapter 3].

From these definitions, we have, for all $s \in [t - \tau - \delta_{tot} - \sum_{j=1}^{i-1} \frac{1}{\lambda_j}, t]$, $P_{\bar{\alpha}_i}(t, s) = \hat{\alpha}_i(s + \tau + \sum_{j=1}^{i-1} \frac{1}{\lambda_j}, 0)$ and the expressions (5.22). This concludes the proof. ■

5.4.2 . Predictor design for the distributed states

We can now use the predictions of the PDE boundary states and the ODE to design a state observer for the whole system. We have the following

Theorem 5.4.1: Existence of states predictions

Consider the interconnected system (5.1)-(5.4) and assume that the measurement $y(\cdot) = v_1(\cdot, 0)$ and the control law $V(\cdot)$ are known on a time interval $[0, t]$, $t > 0$. Then, for all $i \in \llbracket 1, N \rrbracket$, there exist predictor functions $P_{\bar{v}_i}, P_{\bar{u}_i}$ such that for all $x \in [0, 1]$, $P_{\bar{v}_i}(t, x) = \bar{v}_i(t + \tau + \sum_{j=1}^{i-1} \frac{1}{\lambda_j} + \frac{x}{\lambda_i}, x)$, and $P_{\bar{u}_i}(t, x) = \bar{u}_i(t + \tau + \sum_{j=1}^{i-1} \frac{1}{\lambda_j} + \frac{x}{\lambda_i}, x)$.

Proof : With the predictors designed in 5.4, we have access to the values of the real boundary terms $u_i(\cdot, 1)$ on the time interval $[t, t + \sum_{j=1}^i \frac{1}{\lambda_j}]$, and $v_i(\cdot, 0)$ on the time interval $[t, t + \sum_{j=1}^{i-1} \frac{1}{\lambda_j}]$. We then use the predictors $P_{\bar{u}_i}(t, s), P_{\bar{v}_i}(t, s)$ in the delayed equations

$$\begin{aligned} \bar{\alpha}_i(t, x) &= \bar{\alpha}_i(t - \frac{x}{\lambda_i}, 0) + \int_0^{\frac{x}{\lambda_i}} f_i^+(x - \lambda_i \nu) \bar{v}_{i+1}(t - \nu, 0) d\nu, \\ \bar{\beta}_i(t, x) &= \rho_{ii} \bar{u}_i(t - \frac{1-x}{\mu_i}, 1) + \rho_{i, i+1} \bar{v}_{i+1}(t - \frac{1-x}{\mu_i}, 0) + \int_0^{\frac{1-x}{\mu_i}} f_i^-(x + \mu_i \nu) \bar{u}_i(t - \nu, 1) d\nu, \end{aligned}$$

to predict future values of the states $\alpha_i(t, x)$ and $\beta_i(t, x)$. Finally, using the invertibility of transforms (5.5), we can compute future values of the states $\bar{u}_i(t, x), \bar{v}_i(t, x)$, for all $x \in [0, 1]$, and thus finally have access to the whole states (u_i, v_i) . ■

Such predictors satisfy Property 5.4.1. We can now use the estimations of real-time and future values of the distributed states to derive an output-feedback control law.

5.5 . Output-feedback control law design

To obtain the control law $V(t)$ satisfying the control objective, we follow the recursive dynamics interconnection framework proposed in Section 5.2.

5.5.1 . Output-feedback control law

Here, we define an output-feedback control law following the same recursive design, but using the proposed predictor-observers designed in the previous section. More precisely, let us recursively define the sequence \hat{V}_i by

$$\hat{V}_{N+1}(t) = K P_{\bar{X}}(t + \tau - \sum_{j=1}^N \frac{1}{\lambda_j}),$$

and for $i \in \llbracket 1, N \rrbracket$

$$\begin{aligned} \hat{V}_i(t) &= \mathcal{K}^i \left(P_{\bar{u}_i}(t + \tau - \sum_{j=1}^{i-1} \frac{1}{\lambda_j} - \frac{x}{\lambda_i}, x), P_{\bar{v}_i}(t + \tau - \sum_{j=1}^{i-1} \frac{1}{\lambda_j} - \frac{x}{\lambda_i}, x) \right) \\ &\quad + \mathcal{L}^i \left(\hat{V}_{i+1}(t + \frac{1}{\lambda_i}), P_{\bar{v}_{i+1}}(t + \tau - \sum_{j=1}^{i-1} \frac{1}{\lambda_j}, 0) \right), \end{aligned}$$

where the operators \mathcal{H}^i and \mathcal{L}^i are defined in (5.8) and by equation (5.9) and the predictors $P_{\bar{u}_i}$, $P_{\bar{v}_i}$ and $P_{\bar{X}}$ are defined in Theorem 5.4.1 and Lemma 5.4.1. We finally define the control law $V_{\Xi}(t)$ as

$$V_{\Xi}(t) = \hat{V}_1(t). \quad (5.28)$$

First, we have the

Lemma 5.5.1: Convergence

If the control input $V_{\Xi}(t)$ asymptotically converges to $V_{\Xi}^s(t)$ defined in Theorem 5.2.1, then it stabilizes the system (5.1)-(5.4) in the sense of the Ξ -norm.

Proof : This can be seen by expressing the whole system in its neutral form [ADM19] and defining the difference between $V_{\Xi}(t)$ and $V_{\Xi}^s(t)$ as a disturbance. Then, using the variation-of-constants formula for a neutral differential equation (see [HVL13] page 31), we can guarantee the stabilization of the system (5.1)-(5.4). More details for complete proof can be found in [LADMA18]. ■

We are now able to prove that the output-feedback control law $V_{\Xi}(t)$ stabilizes the system (5.1)-(5.4). We have the following

Theorem 5.5.1: Existence of a stabilizing output-feedback controller

Consider the system (5.1)-(5.4). If Properties 5.2.1, 5.2.2, 5.3.1, 5.4.1 are verified, then the output-feedback control law $V_{\Xi}(t) = \hat{V}_1(t)$ defined by (5.28) exponentially stabilizes the system (5.1)-(5.4) in the sense of the Ξ -norm.

Proof : The control law $V_{\Xi}(t)$ is well-defined and causal due to the definition of the different predictors (Property 5.4.1). Let us consider that the predictors provide exact future values of the PDEs and ODE states. The corresponding control law is $V_{\Xi}^s(t)$. Then, applying Property 5.2.2 on each subsystem, we obtain that $u_N(\cdot, 1)$ exponentially converges to $\mathcal{H}_{N+1}(X(\cdot))$. Consequently, $X(t)$ exponentially converges to zero. Using Property 5.2.2, starting from the last subsystem $i = N$, each PDE subsystem exponentially converges to zero. Thus, the control law $V_{\Xi}(t)$ designed with exact predictions stabilizes the system (5.1)-(5.4). We now need to show that such a result still holds when using output measurements to define the predictors. Using Property 5.4.1, the designed predictors asymptotically converge to the real future values of the states (u_i, v_i) . Lemma 5.5.1 concludes the proof. ■

Note that Properties 5.3.1 and 5.2.1 are not directly used in the proof since they are usually required to show Properties 5.4.1 and 5.2.2.

5.6 . Simulation results

In this section, we illustrate the efficiency of the proposed recursive dynamics interconnection framework on a network of $N = 2$ hyperbolic PDE subsystems interconnected at one end with a scalar ODE. The numerical values of the parameters are given in Table 5.1, and chosen such that the open-loop system is slightly unstable. Note that Assumptions (5.1.1)-(5.1.5) are satisfied.

The simulations are run on Matlab on a time interval $[0, 30]$ s. The space domain $[0, 1]$ is discretized on a mesh with $\text{nx} = 51$ points.

Param.	Value	Param.	Value	Param.	Value	Param.	Value
λ_1	1	λ_2	2	q_{11}	0.5	ρ_{11}	0.3
μ_1	1.3	μ_2	1.8	q_{21}	0.3	ρ_{12}	0.4
σ_1^+	1	σ_2^+	-0.3	q_{22}	0.7	ρ_{22}	0.4
σ_1^-	0.4	σ_2^-	0.7	K	-3	L	-5
A	0.1	B	0.1	C	0.1		

Table 5.1 – Parameters used for simulation

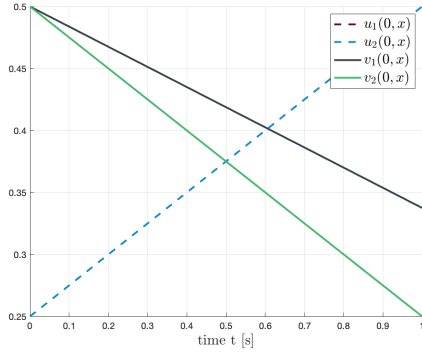


Figure 5.5 – Initial conditions $(u_i(0, x), v_i(0, x))$

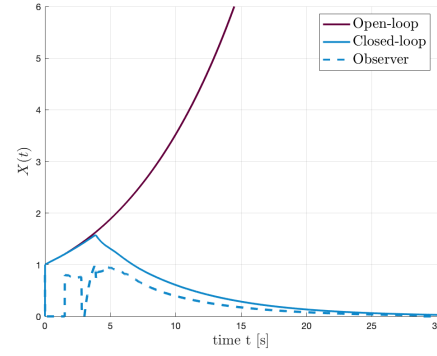


Figure 5.6 – Evolution of $X(t)$ and observer $\hat{X}(t)$

Beforehand, the kernel gains L_i^* , K_i^* corresponding to the invertible Volterra transforms (5.12) and (5.5) are computed using the successive approximation technique, with a precision $\epsilon = 10^{-8}$, and their values are stored in matrices of dimension $\mathbf{n}_x \times \mathbf{n}_x$ (see Appendix A). From them, using the same iterative method, in-domain coupling functions f_i, g_i, h_i, k_i defined in (5.16) are computed offline. All integral terms are computed using the trapezoidal approximation (`trapz`). Similar techniques are used to obtain the coupling terms $g_i^j, k_i^j, f_i^+, f_i^-$, $j \in \{1, 2, 3\}$. Their values are stored in vectors.

Next, we can simulate the evolution of the system using the classic finite volume method based on a Godunov scheme [LeVo2], and the Matlab medium order method `ode45`. The initial conditions of the states are affine functions represented in Figure 5.5. They satisfy the compatibility conditions. We chose $X_0 = 1$. The boundary observer values for the PDE states are initialized to 0.2, and $\hat{X}_0 = 0.8$.

To numerically compute the predictions, we first initialize the predictors using the estimations obtained in Section 5.3. These values are stored in a buffer. Then, it becomes possible to directly use equations (5.25)-(5.27) to compute the prediction at the next time step. After a delay $\tau > \tau_N + \sup_i \{ \frac{1}{\lambda_i} \}$, at each iteration, a buffer containing the values of the predictor is updated with the boundary state estimations at each iteration, and new values of the predictor are computed. The value of the control law is computed accordingly. A saturation has been added to avoid unrealistic high values.

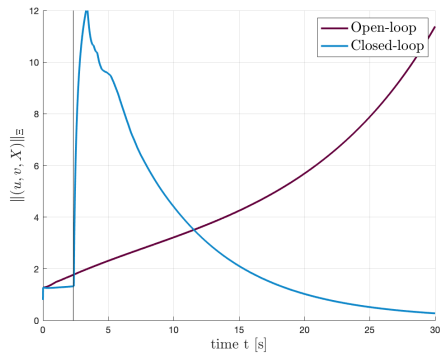


Figure 5.7 – Evolution of the Ξ -norm of system (5.1)-(5.4)

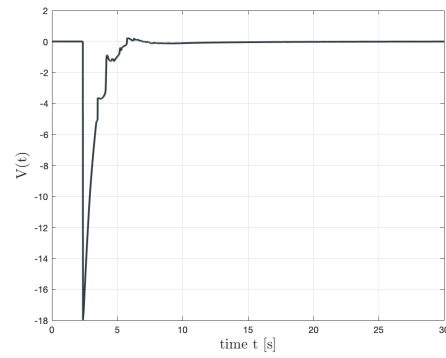


Figure 5.8 – Evolution of the control law defined in Theorem 5.5.1

In Figure 5.7 the evolution of the Ξ -norm defined in Section 5.1 is represented. As expected, the Ξ -norm of the open-loop system diverges, while it exponentially goes to 0 in closed-loop with the proposed controller. The control effort is represented in Figure 5.8. Since the actuation is only fully defined when we can compute the predicted values of the different states, the control input applied for $t < \tau = 2.3s$ is not reliable. The effect of saturation is also visible.

The evolution of the states $(u_i(t, x), v_i(t, x))$ in closed-loop is given in Figure 5.9.

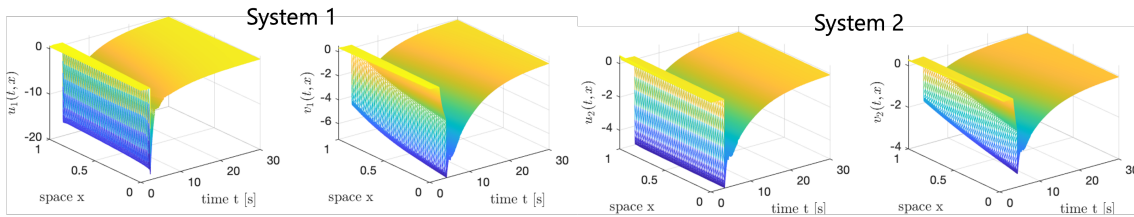


Figure 5.9 – Evolution of the states $(u_i(t, x), v_i(t, x))$ in closed-loop

Conclusion

In this chapter, we designed an output feedback control law stabilizing a chain of scalar linear hyperbolic systems coupled with an ODE at one end. We used backstepping transforms and a *recursive dynamics interconnection framework* to estimate the boundary states of each subsystem. We used these estimations to build predictors that allowed the recursive design of an output feedback control law.

We believe that the proposed approach could be easily adapted to different types of interconnected systems (including different subsystems or different types of chains) as long as some fundamental properties (trackability, predictability) are still verified. Perspectives are given at the end of Part II. Some numerical limitations arise from the use of predictors. Indeed, it is computationally expensive and difficult to implement for large values of N . Model-based predictions could be fastly obtained using machine learning techniques, in the line of the work presented in Chapter 11.

6 - Application to drilling systems for state estimation and trajectory tracking

In this chapter, we illustrate the practical interest of the interconnected systems considered in Part II. They can be used to represent the dynamics of drilling systems. More precisely, we aim at applying the *recursive dynamics interconnection framework* proposed in Chapter 5 to the control and state estimation of angular or torsional motion of the drill-string in two different contexts. Due to geopolitical instability and the inherent risk of an energy shortage, energy production stayed at high stake. At the same time, the depletion of raw materials made extracting and drilling oil or gas more and more difficult. It forces petroleum companies to reach very deep hydrocarbon reservoirs in areas with limited access and often in varying geological environments. From a more optimistic perspective, geothermal energy is also gaining attention as a renewable electricity resource with great potential. New closed-loop geothermal power plants (CGS) have emerged to overcome the drawbacks of conventional open-loop geothermal systems. To optimize their efficiency, they can require a deviated well path with a long horizontal section at a depth exceeding 2.5km [WMYY22]. In both situations, the main aspect that makes the control of the drilling system dynamics challenging is the extreme aspect ratio of the drill string. Indeed, the boreholes are usually very narrow, with a diameter of up to 50cm, and extend over several kilometers. Even though each drill pipe section is made of steel and thus rigid, the system behaves like a flexible structure and faces unwanted axial, torsional, and lateral vibrations [Jan93]. These vibrations have many negative impacts: they cause drill bit wear, premature motor failure, which imparts torque at the surface level, and damage to the borehole. In the worst case, it can lead to the rupture of the drill string, wasting costly drilling time. It also decreases the Rate Of Penetration (ROP) and thus reduces the process performance. Since they are an important source of economic loss, much effort has been made to allow control laws to avoid these unwanted oscillations.

The first simple models for the drilling systems were mass-spring models [Jan93]. The next step towards more precise modeling is to consider the drill string's distributed dynamics [SMAV16], using an Euler-Bernoulli beam model, for instance [GDD09]. However, to make the model more accurate, the effects of the stiffer drill collars and the bit on the overall dynamics can be considered. The Bottom Hole Assembly (BHA) can then be represented as a lumped element coupled at the end of the drill string. In the model proposed in [AvdW19], the axial and torsional motions of the drill string are modeled by two uncoupled sets of hyperbolic Partial Differential Equations (PDE). The bit-rock interaction or the dynamics of the BHA can be represented by an ordinary differential equation (ODE). The field-validated model [AS18] also separates the dynamics of the pipe and the collar. It was shown to be of high interest to consider the underlying distributed dynamics in the design of a stabilizing controller [ABS⁺22].

First, we consider in Section 6.1 the estimation of axial motion of the drill string in the situation of a vertical well-path without friction but bit-rock interaction. Then, in Section 6.2, we consider the control of the angular velocity of the drill bit, in the more complex case of a deviated well-path, for transient phases with the bit off-bottom.

Chapitre 6: Application de l'approche aux systèmes de forage. Estimation d'état et suivi de trajectoire. Dans ce chapitre, nous appliquons l'approche récursive développée au Chapitre 5 au contexte du forage. En effet, la dynamique des systèmes utilisés peut être modélisée par des équations d'onde ou sous forme de systèmes d'EDP hyperboliques. Le train de tiges est constitué de nombreux tubes (*pipes*) aux paramètres physiques (densité, diamètre, inclinaison) variables. Au bout de ce long système sont fixés des colliers (*collars*), plus courts et une tête de forage (*drill bit*). La dynamique de ces éléments massifs, celle du moteur en surface, mais également l'interaction de la roche avec la tête de forage, peuvent être modélisées par des équations aux dérivées ordinaires. On retrouve donc une structure de chaîne semblable à celle étudiée dans cette partie.

Plusieurs problématiques apparaissent lors du forage. L'extrême rapport d'aspect du train de tiges (10^{-4}) peut entraîner l'apparition d'oscillations (axiales et torsionnelles). En particulier, des vibrations du couple en torsion (phénomène de stick-slip) doivent être évitées car cela conduit à des détériorations des équipements et de la paroi du puits. Afin de prendre en compte l'apparition de ce phénomène, des modèles distribués ont été développés et validés expérimentalement [AS18, AvdW19]. Leur utilisation dans le design de la loi de commande a un intérêt dans la mitigation de vibrations indésirables [ABS⁺22], mais nécessite une estimation de l'état, à partir des mesures disponibles en surface. Dans un premier temps, nous illustrons l'utilisation de l'estimation d'état récursive du mouvement latéral d'un système de forage composé de deux sous-systèmes pour un puits vertical (Section 6.1). Dans un second temps, nous illustrons la loi de commande récursive afin de permettre le suivi d'une trajectoire de référence, dans le contexte de forage d'un puits avec une section horizontale (Section 6.2).

Contents

6.1 Axial motion of an offshore drilling system	99
6.1.1 Axial vibrations model	100
6.1.2 Application of the recursive framework	101
6.1.3 Simulation results	103
6.2 Torsional motion of a drill string in a deviated borehole . . .	105
6.2.1 Torsional vibrations model	107
6.2.2 Application of the recursive framework	109
6.2.3 Simulation results	113

The results presented herein were published in:

- Jeanne Redaud, Jean Auriol, and Silviu-Iulian Niculescu. "Recursive Dynamics Interconnection Framework Applied to Angular Velocity Control of Drilling Systems" (2022). American Control Conference (ACC).

6.1 . Axial motion of an offshore drilling system

Introduction

Context

As mentioned in the introduction, now that the most easily accessible oil resources have been depleted, petroleum companies must reach areas with limited access and great depths to find new reservoirs. An example can be found in offshore drilling with the giant Johan Sverdrup field, located 150 kilometers off the Norwegian coast. In this case, the water depth exceeds 110 meters, and the reservoir is at a depth of 1,900 meters. Figure 6.2 gives a picture of the Gudrun platform. In this situation, the platform can be built above the area of interest.

A drill string is used to create the borehole and access the reservoir. It is usually made of several long flexible pipes, connected at one end with heavier and shorter sections named collars. The collars are connected with a Bottom Hole Assembly (BHA), which ends with the drill bit chattering the rock. At the surface level, a rotary table with an electrical motor imparts a rotary and vertical motion of the drill string. Usually, the control input is the weight on the drill string and the torque at the end opposite to the bit. The objective is to improve the performance of the drilling operation, which is measured by the ROP, corresponding somehow to the drilling speed.

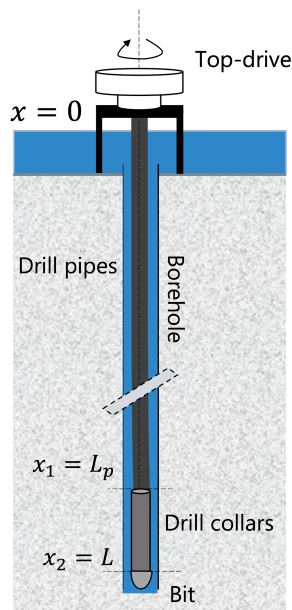


Figure 6.1 – Schematic drilling system

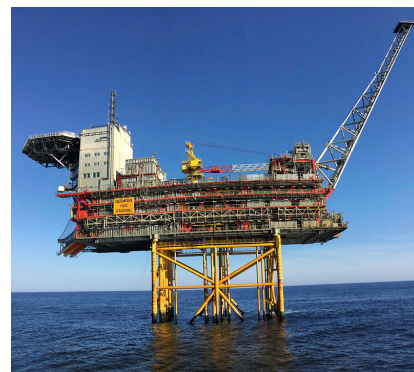


Figure 6.2 – Petter Andre Bøe
©Equinor

Objective: distributed state estimation

It was shown in [ABS⁺22] to be of high interest to consider the distributed dynamics in the design of a control input for output tracking. Moreover, the transition between pipe sections with different mechanical properties, particularly the transitions from the pipes to collars, cause reflections in the traveling waves due to the change in characteristic line

impedance [AA16]. For better accuracy, we can then distinguish the dynamics of the drill pipes and the drill collars [AS18].

However, controllers derived from the backstepping methodology usually require the knowledge of the state on its definition domain. We can therefore adapt the estimation strategy proposed in the previous chapter to obtain an accurate state estimation.

Objective 6.1.1: Distributed state estimation

Denote $c(t, x)$ the axial velocity along the drill string, and $w(t, x)$ the axial force (weight). Using surface measurement $(w(t, 0), c(t, 0))$, determine $(\hat{c}(t, x), \hat{w}(t, x))$ two distributed state estimations which exponentially converge to $(c(t, x), w(t, x))$.

6.1.1 . Axial vibrations model

We consider a vertical well with a drill string of length L , as illustrated in Figure 6.1. The depth is denoted $x \in [0, L]$, extending between the top drive at the surface level and the location of the drill bit.

Bi-sectional drill string model

The lower part of the drill string is usually made up of heavier drill collars with a shorter length and higher density, inertia, or Young's modulus than the pipe sections. This change of the characteristic line impedance may cause reflections in the traveling waves that may greatly impact the global dynamics [AA16, AdMS18a]. Let us assume we have 2 different sections and denote x_1 the spatial coordinate of the junction point between the pipe and the collar. We neglect the dynamics of the short portion of the drill string in the water. By convention, we have $x_0 = 0$, $x_1 = L_p$ and $x_2 = L = L_c + L_p$. For any variable or parameter, we denote \cdot^p its value along the drill pipes, and \cdot^c its value along the collars. We use \cdot^\star , with $\star = \{c, p\}$, or no subindex, to denote either variable.

Axial motion

Following the decoupled model given in [AvdW19], we only consider the axial motion of the drill string. Denote $\xi(t, x)$ the axial displacement depending on time and space in $[0, T] \times [0, L]$ with $T > 0$, and $c(t, x) = \frac{\partial \xi(t, x)}{\partial t}$ the axial velocity. For any infinitesimal axial position increment $dx \rightarrow 0$, the axial force associated with this displacement can be found from the strain, given as the local relative compression:

$$w^\star(t, x) = A^\star E^\star \frac{\xi^\star(t, x) - \xi^\star(t, x + dx)}{dx}, \text{ with } \begin{cases} A^\star : \text{cross-sectional area of section } \star, \\ E^\star : \text{Young's modulus of section } \star. \end{cases}$$

The axial motion is governed by the following

$$\frac{\partial w^\star(t, x)}{\partial t} + A^\star E^\star \frac{\partial c^\star(t, x)}{\partial x} = 0, \quad (6.1)$$

$$A^\star \rho^\star \frac{\partial c^\star(t, x)}{\partial t} + \frac{\partial w^\star(t, x)}{\partial x} = -k_a^\star(x) \rho^\star A^\star c^\star(t, x), \quad (6.2)$$

where k_a corresponds to viscous dissipation, varying with the environment of the drill string. The continuity of strain and axial velocity in $x = x_1$ implies

$$w^p(t, x_1) = w^c(t, x_1), \quad c^p(t, x_1) = c^c(t, x_1). \quad (6.3)$$

Coupling with the BHA

Neglecting the dynamics of the electrical motor imparting torque at the surface level, we assume that the operator controls the weight on the drill string, such that $V(t) = w^p(t, 0)$. The BHA can be lumped into an ODE coupled with the drill string [DMA15]. It is justified since it is much shorter than the drill string. Thus, the downhole boundary condition at $x = L$ can be obtained from a force balance on the lumped BHA. Denote $X(t) = \frac{\partial}{\partial t} \xi(t, L) = c(t, L)$. Following the models presented in [GDD09, AvdW19, AKIS20], under some simplifying assumptions, the interaction of the bit with the rock can lead to the following downhole boundary condition

$$M_b \dot{X}(t) = - \frac{a\zeta\epsilon}{\omega_{bit}} X(t) - w_f - w^c(t, L), \quad (6.4)$$

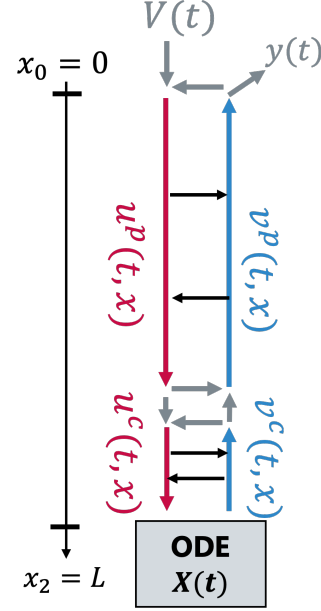


Figure 6.3 – System (6.6)-(6.8)

where M_b is the mass of the lumped BHA, ω_{bit} is the angular velocity of the bit (assumed constant), w_f is the friction weight (independent of the bit velocity), a is the bit radius, ζ is a characterization of the cutting angle and ϵ is the intrinsic specific energy of the rock.

6.1.2 . Application of the recursive framework

Riemann invariants

To rewrite system (6.1)-(6.2) in the form of a chain of hyperbolic PDE subsystems (5.1)-(5.4), we use the Riemann invariants and apply an exponential change of variable. Let us define $\lambda^* = \sqrt{\frac{E^*}{\rho^*}}$ and the new state variables

$$\begin{cases} u^*(t, x) = \frac{e^{\int_{x_i-1}^x \frac{k_a^*(s)}{2\lambda^*} ds}}{\sqrt{2}} (w^*(t, x) + A^* \sqrt{E^* \rho^*} c^*(t, x)), \\ v^*(t, x) = \frac{e^{-\int_{x_i-1}^x \frac{k_a^*(s)}{2\lambda^*} ds}}{\sqrt{2}} \left(-\frac{1}{A^* \sqrt{E^* \rho^*}} w^*(t, x) + c^*(t, x) \right). \end{cases} \quad (6.5)$$

They satisfy equations of form (2.1)-(2.2)

$$\frac{\partial}{\partial t} u^*(t, x) + \lambda^* \frac{\partial}{\partial x} u^*(t, x) = \sigma^{*+}(x) v^*(t, x) \quad (6.6)$$

$$\frac{\partial}{\partial t} v^*(t, x) - \lambda^* \frac{\partial}{\partial x} v^*(t, x) = \sigma^{*-}(x) u^*(t, x), \quad (6.7)$$

with the continuous in-domain coupling functions

$$\sigma^{*+}(x) = -\frac{k_a^*(x)}{2} A^* \sqrt{E^* \rho^*} e^{\int_{x_{i-1}}^x \frac{k_a^*(s)}{\lambda^*} ds}, \quad \sigma^{*-}(x) = -\frac{k_a^*(x)}{2A^* \sqrt{E^* \rho^*}} e^{-\int_{x_{i-1}}^x \frac{k_a^*(s)}{\lambda^*} ds},$$

and boundary conditions

$$u^p(t, 0) = A^p \sqrt{E^p \rho^p} v^p(t, 0) + \sqrt{2} V(t),$$

$$v^c(t, L) = \frac{1}{1 - \frac{1}{2} e^{-\int_{L_p}^L \frac{k_a^c(s)}{2\lambda^c} ds}} \frac{e^{-\int_{L_p}^L \frac{k_a^c(s)}{2\lambda^c} ds}}{\sqrt{2}} \left(-\frac{1}{A^c \sqrt{2E^c \rho^c}} u^c(t, L) + X(t) \right).$$

Injecting the above equation, (6.4) rewrites

$$\begin{aligned} \dot{X}(t) &= -\frac{a\zeta\epsilon}{\omega_{\text{bit}} M_b} X(t) - \frac{w_f}{M_b} - \frac{e^{\int_{L_p}^L \frac{k_a^c(s)}{2\lambda^c} ds}}{\sqrt{2}} \left(-A^c \sqrt{E^c \rho^c} v^c(t, L) + u^c(t, L) \right) \\ &= -\left(\frac{a\zeta\epsilon}{\omega_{\text{bit}} M_b} + \frac{A^c \sqrt{E^c \rho^c}}{2(1 - \frac{1}{2} e^{-\int_{L_p}^L \frac{k_a^c(s)}{2\lambda^c} ds})} \right) X(t) - \frac{w_f}{M_b} - \frac{e^{-\int_{L_p}^L \frac{k_a^c(s)}{2\lambda^c} ds}}{\sqrt{2}(1 - \frac{1}{2} e^{-\int_{L_p}^L \frac{k_a^c(s)}{2\lambda^c} ds})} u^c(t, L). \end{aligned} \quad (6.8)$$

Define the relative magnitude of the impedance $Z = \frac{A^p \sqrt{E^p \rho^p}}{A^c \sqrt{E^c \rho^c}}$ and $\alpha = \int_0^{L_p} \frac{k_a^p(s)}{2\lambda^p} ds$. In the Riemann coordinates, the continuity condition (6.3) gives the following boundary conditions at the junction $x = L_p$

$$\begin{aligned} v^p(t, L_p) &= \frac{1}{A^p \sqrt{E^p \rho^p}} \frac{Z e^{-\alpha} - e^\alpha}{Z e^{-\alpha} + e^\alpha} u^p(t, L_p) + \frac{2}{e^\alpha + Z e^{-\alpha}} v^c(t, L_p), \\ u^c(t, L_p) &= \frac{2}{Z e^{-\alpha} + e^\alpha} u^p(t, L_p) + A^c \sqrt{E^c \rho^c} \frac{e^\alpha - Z e^{-\alpha}}{Z e^{-\alpha} + e^\alpha} v^c(t, L_p). \end{aligned} \quad (6.9)$$

State estimation

Following the *recursive dynamics interconnection framework* proposed in Section 5.3, we can derive a predictor-based real-time estimation of the distributed state. Assuming that the friction weight is known, we design a Luenberger-type observer for the delayed ODE state. We can identify A and C quantifying the effect of $\tilde{X}(t)$ over $\bar{v}^c(t, L)$, using the previous equations

$$A = -\left(\frac{a\zeta\epsilon}{\omega_{\text{bit}} M_b} + \frac{A^c \sqrt{E^c \rho^c}}{2(1 - \frac{1}{2} e^{-\int_{L_p}^L \frac{k_a^c(s)}{2\lambda^c} ds})} \right), \quad C = \frac{e^{-\int_{L_p}^L \frac{k_a^c(s)}{2\lambda^c} ds}}{\sqrt{2}(1 - \frac{1}{2} e^{-\int_{L_p}^L \frac{k_a^c(s)}{2\lambda^c} ds})}.$$

Any negative real is an admissible value for L to make the dynamics of \tilde{X} exponentially stable. Using Theorem 5.3.1, we can determine an estimation of the delayed boundary states using the surface measurement

$$v^p(t, 0) = \frac{1}{\sqrt{2}} \left(c^p(t, 0) - \frac{1}{A^p \sqrt{E^p \rho^p}} w^p(t, 0) \right) \doteq y(t).$$

From the predictor design in Section 5.4, and Theorem 5.4.1, we have access to real-time values of $(u^*(t, x), v^*(t, x))$ using estimation-based predictors denoted $P_{\tilde{u}^*}(t, x)$, $P_{\tilde{v}^*}(t, x)$. Using the inverse change of variables, we have

$$\begin{cases} w^*(t, x) = \frac{1}{\sqrt{2}} \left(e^{-\int_{x_{i-1}}^x \frac{k_a^*(s)}{2\lambda^*} ds} P_{\tilde{u}^*}(t, x) - A^* \sqrt{E^* \rho^*} e^{\int_{x_{i-1}}^x \frac{k_a^*(s)}{2\lambda^*} ds} P_{\tilde{v}^*}(t, x) \right), \\ c^*(t, x) = \frac{1}{\sqrt{2}} \left(\frac{e^{-\int_{x_{i-1}}^x \frac{k_a^*(s)}{2\lambda^*} ds}}{A^* \sqrt{E^* \rho^*}} P_{\tilde{u}^*}(t, x) + e^{\int_{x_{i-1}}^x \frac{k_a^*(s)}{2\lambda^*} ds} P_{\tilde{v}^*}(t, x) \right). \end{cases} \quad (6.10)$$

We, therefore, have access to the real-time estimation of the distributed states along the drill string, satisfying Objective 6.1.1. This is illustrated next in numerical simulation on Matlab.

6.1.3 . Simulation results

As considered in this first example, and schematically illustrated in Figure 6.3, we have a vertical drill string divided into two subsystems: the drill pipe of length L_p and the collars of length $L_c = 230\text{m}$. The total length is $L = 2,000\text{m}$. The physical parameters taken from [AKIS20] are given in Table 6.1.

Param.	Value	Param.	Value	Param.	Value
A^p	$3.5 \times 10^{-3} \text{ m}^2$	A^c	$5 \times 10^{-3} \text{ m}^2$	M_b	$3.6 \times 10^4 \text{ kg}$
k_a^p	0.23 s^{-1}	k_a^c	0.3 s^{-1}	a	0.108 m
E^p	$2 \times 10^{11} \text{ Pa}$	E^c	$2.5 \times 10^{11} \text{ Pa}$	ϵ	$5.7 \times 10^6 \text{ J}$
ρ^p	8000 kg/m^3	ρ^c	8500 kg/m^3	ω_{bit}	31.5 m.s^{-1}

Table 6.1 – Parameters used for simulation

The simulation procedure is similar to the one described in Section 5.6. All kernel values are computed beforehand. The interconnected system is simulated on a timescale of 10s, using a Godunov schema and `ode45`. We use affine functions satisfying (6.9) for the initial conditions (Figure 6.4). Boundary observer values for the PDE states are initialized to 0.1. The drill string is decomposed on a mesh of $n_x = 500$ points. The open-loop system is here naturally stable.

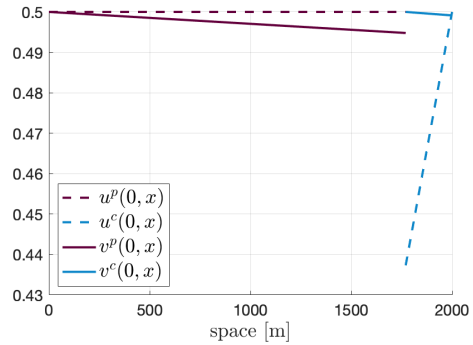


Figure 6.4 – Initial conditions

One can verify that Assumptions 5.1.1-5.1.5 are satisfied for this system. In particular, the scalar ODE state is controllable and observable, and the coupling coefficients in (6.9), (6.8) are non-zero. For the ODE-state observer, the gain $L_{\text{obs}} = -5$ is chosen. Figure 6.6 gives the evolution of the estimated and real down-hole axial velocity $\hat{X}(t)$ and $X(t)$ for the open-loop system. Note that the estimation is only available after $\delta = \frac{L_p}{\lambda^p} + \frac{L_c}{\lambda^c}$ which is approximately equal to 0.4s here. As expected, once we can correctly estimate the different PDE states using our recursive dynamics framework, we can obtain a reliable

estimation of the ODE state. The \mathcal{X} -norm of the error state converges quickly to zero, as represented in Figure 6.5.

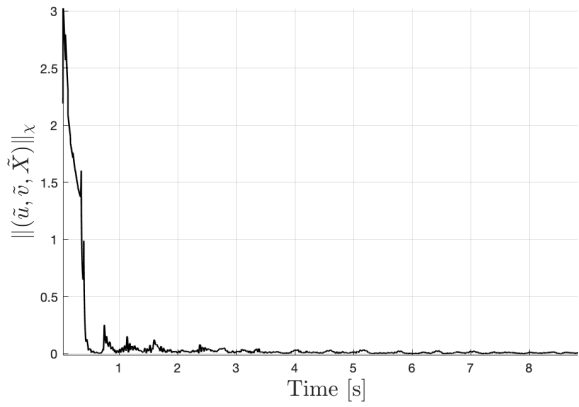


Figure 6.5 – Evolution of $\|(\tilde{u}, \tilde{v}, \tilde{X})\|_{\mathcal{X}}$

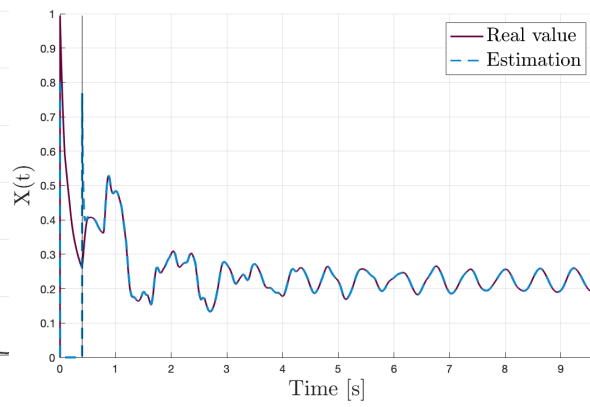


Figure 6.6 – Evolution of $X(t)$ and $\hat{X}(t)$

We represented in Figure 6.7 the evolution of the convergence time for several observer gains. As expected, the higher the value of $|L_{\text{obs}}|$, the faster the convergence. In practice, the value may be bounded by physical constraints.

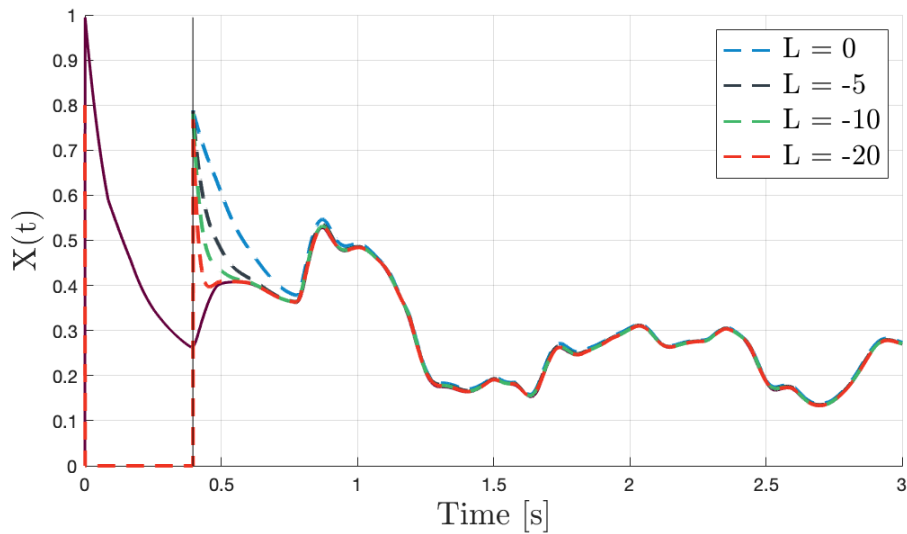


Figure 6.7 – Convergence of $\hat{X}(t)$ for several observer gains

6.2 . Torsional motion of a drill string in a deviated borehole

Next, we consider the torsional motion of a drill string in the case of a deviated well paths.

Introduction

Context

As for extracting fossil fuels, drilling for geothermal heat can lead to significant economic value and offers a promising alternative as a renewable energy resource. Similar engineering skills are needed. A new solution has been brought to reach the adequate depth and rock layers: drilling **directional** wells. Using complex deviated well paths is a potential landmark move to reach new energy sources. Usually deviated from a 60° to 75° angle, the first truly horizontal path was inaugurated in 2020 in Canada. The well was drilled to a depth of 3450m before turning at a 90° angle and drilling through sedimentary rock along a 2000m lateral route. This allows developing enhanced geothermal power systems with a U shape. Drilling horizontal is a feat of engineering: when deviation augments, so do friction along the borehole, especially in the top part of the drill string [Jan93]. A picture of the Precision Drilling Training Rig in Nisku, Alberta is given in Figure 6.8.



Figure 6.8 – ©Calgary University

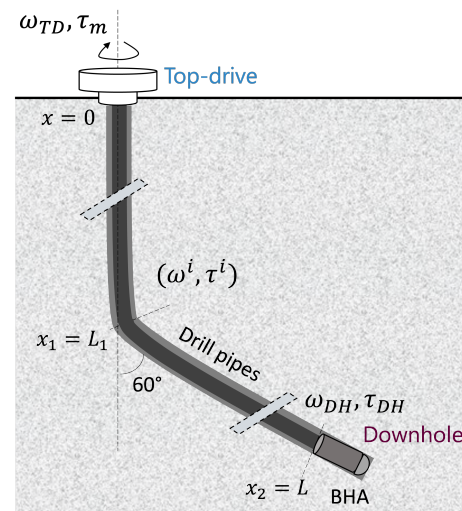


Figure 6.9 – Schematic representation

A second step towards better modeling the drill string dynamics is considering the varying environment, such as each section orientation. In particular, it has been pointed out that some unwanted oscillations were caused by the friction between the rotating drill string and the borehole wall [Jan93]. Among them, the most prevalent and destructive are torsional or rotational vibrations, known as *stick slip*. These oscillations are characterized by a sequence of *stick*, when the bit stops rotating while the top is still rotating, making the torque augment until the bit suddenly comes loose again or *slip*, with a sudden release of energy. Stick-slip oscillations may be caused by the speed-dependent nature of the contact forces (cutting and friction) or the coupling between the axial and torsional motions at the bit-rock interface [NW13]. Indeed, regardless of their complexity, most models consider that stick-slip is introduced as a discontinuous frictional force at the bit,

having a velocity-weakening effect [AA16]. However, since this phenomenon also appears when there is no such bit-rock interaction, it is assumed that it may also be caused by *along-string* Coulomb-type frictions [ZHS16]. Former models do not consider this phenomenon and fail to explain off-bottom stick-slip oscillations. Therefore, the Coulomb friction, which can be seen as a disturbance acting on each section, must be considered. Due to the high complexity and nonlinearity induced by the interaction between the drill bit and the rocks, we consider the bit off-bottom. This corresponds to transient phases required for drill pipe connections and the replacement of downhole tools. In this context, the torsional model presented below has been validated against field data [AS18].

Objective: reference trajectory tracking

For an industrial application, the objective is to control the downhole velocity or orientation of the drill string to optimize the ROP while avoiding undesired oscillations. Many stick-slip mitigation controllers have been developed through the last decades using the former understanding of this phenomenon. Most of those used in the field correspond to high gains PI control laws and follow the SoftSpeed and SoftTorque approaches [ASADM20]. Even though they are easy to analyze and implement and have a low computational effort, they do not help compensate the effects of Coulomb friction, as illustrated in Section 6.2.3. Some approaches are proposed to add new compensating terms to the existing PI controllers [ADMS18b], but are more adapted to uni-sectional drilling pipes.

Considering different pipe sections interconnected at the end with the ODE dynamics of the BHA, we can follow a *recursive dynamics interconnection framework* similar to the one proposed in the previous chapter to design a control law regulating the downhole angular velocity.

Objective 6.2.1: Reference trajectory tracking

Denote $\omega_{DH}(t)$ the downhole angular velocity. We aim at designing a torque control input that regulates the downhole angular velocity at the beginning of a drilling operation while avoiding entering a stick-slip limit cycle.

Our objective is to design a surface control law $V(t)$ such that $|\omega_{DH}(t) - \omega_{ref}(t)| \rightarrow 0$.

It is somehow related to the **disturbance rejection and tracking problem** considered in Chapter 4. To construct transition trajectories, [ADMS18b] uses semi-analytical functions (mollifier) for the downhole velocity ω_{DH} that are smooth and have vanishing derivatives in $\{0, L\}$. Their primary purpose is to avoid brutal changes in the reference signal. Let us introduce the *bump* function ϕ , defined by

$$\phi(t) = \begin{cases} \frac{\exp(-\frac{1}{1-t^2})}{\int_{-1}^1 \exp(-\frac{1}{1-\xi^2}) d\xi} & \text{for } t \in (-1, 1), \\ 0 & \text{otherwise.} \end{cases} \quad (6.11)$$

An appropriate mollifier is $m(t) = \int_0^t \phi(s-1) ds$. We define a reference trajectory using the mollifier with three degrees of freedom (amplitude A_m , switching time t_{st} , and switching duration t_{sd}).

As will be seen later, when the drilling device is in a slipping mode, *i.e* when the angular velocity is higher than a critical value ω_c , the estimation and rejection of the disturbance

terms are facilitated. It motivates a *switching mode* control law, in which we first increase the torque to break the static friction, and then apply the recursive control procedure presented in Section 6.2.2. With the reference trajectory $\omega_{ref}(t) = \omega_c + A_m m(\frac{t-t_{sd}}{t_{sr}})$, we must ensure that the angular velocity stays in the controllable zone $|\omega(t) > \omega_c|$. After the release of the BHA from the stick phase, the control objective 6.2.1 must be satisfied.

6.2.1 . Torsional vibrations model

First, we present the distributed model for the torsional motion of the drill string adjusted from [AS18]. It accurately describes the torsional movement of a multi-sectional drilling system in absence of bit-rock interaction. It comprises interconnected hyperbolic PDEs, coupled at both ends with an ODE, and includes distributed friction terms. Considering that we are at the beginning of the operation, we neglect the axial motion of the drill string. Moreover, we neglect the effects of pressure differential along the drill string and the Stribeck curve, such that the transition from static to dynamic Coulomb friction is not continuous.

Multi-section drill string model

We consider a deviating drilling device as illustrated in Figure 6.9 with curvilinear abscissa denoted $x \in [0, L]$, extending between the top-drive and the drill bit locations. The discontinuities between different sections of the drilling device are represented by a discontinuity in impedance. In the general framework presented in Chapter 5, we distinguish N sections. Apart from having different material properties (lengths, density, inertia or Young's modulus), the change in orientation induces different friction coefficients for each section. For any $i \in \llbracket 0, N - 1 \rrbracket$, the spatial coordinate x_i corresponds to the junction between section i and section $i + 1$. By convention, we have $x_0 = 0, x_N = L$. We use the subscript \cdot_i to denote a variable or physical parameter related to section i . When referring to general variables, it may be omitted. We use the subscript \cdot_{TD} to denote variables at the top of the drill string in $x = 0$, and \cdot_{DH} to denote variables at the downhole in $x = L$.

Torsional motion

The torsional dynamics are represented using the widely used distributed wave model [AS18, GDD09]. Denote $\Phi(t, x)$ the angular displacement depending on time and space in $[0, T] \times [0, L]$, and $\omega(t, x) = \frac{\partial \Phi(t, x)}{\partial t}$ the angular velocity. Considering an infinitesimal element of the drill string of length $dx \rightarrow 0$, we derive the angular torque $\tau(t, x)$ associated to Φ from the strain, given as the local relative compression:

$$\tau(t, x) = JG \frac{(\Phi(t, x) - \Phi(t, x + dx))}{dx}, \text{ with } \begin{cases} J : \text{polar moment of inertia,} \\ G : \text{shear modulus.} \end{cases}$$

Under the assumption of elastic deformations and using equations of continuity and state, we can derive the torsional dynamics. The state (ω_i, τ_i) on each section satisfies

$$\frac{\partial \tau_i(t, x)}{\partial t} + J_i G_i \frac{\partial \omega_i(t, x)}{\partial x} = 0, \quad J_i \rho_i \frac{\partial \omega_i(t, x)}{\partial t} + \frac{\partial \tau_i(t, x)}{\partial x} = S_i(t, x). \quad (6.12)$$

The source term $S_i(t, x)$ models the frictional contact with the borehole. Continuity of the angular velocity and torque is imposed at each boundary, such that

$$\tau_i(t, x_i) = \tau_{i+1}(t, x_i), \quad \omega_i(t, x_i) = \omega_{i+1}(t, x_i). \quad (6.13)$$

Coulomb friction model

Following [AS18], the interaction with the borehole along section i is modeled by

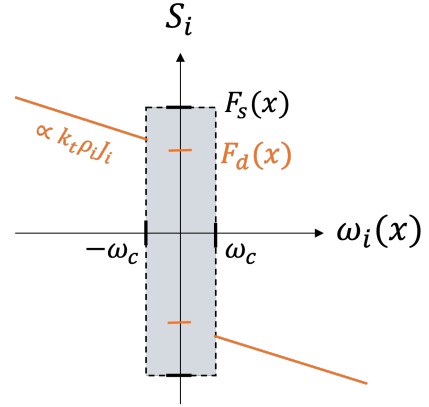
$$S_i(t, x) \doteq -\mathcal{F}_i(t, x) - k_t \rho_i J_i \omega_i(t, x),$$

where k_t is the viscous shear stress, and $\mathcal{F}_i(t, x)$ the alongside Coulomb friction between the drill string and the borehole. In practice, we can consider that the viscous shear stresses are negligible, such that for all sections $k_t \approx 0$.

The function \mathcal{F} is modeled by using the inclusion represented on the right

$$\begin{cases} \mathcal{F}(t, x) = \text{sign}(\omega(t, x))F_d(x), & |\omega(t, x)| > \omega_c, \\ \mathcal{F}(t, x) \in [-F_s(x), F_s(x)], & |\omega(t, x)| < \omega_c, \end{cases}$$

where $F_d(x) \doteq r_o(x)\mu_k F_N(x)$, $F_s(x) \doteq r_o(x)\mu_s F_N(x)$ correspond to the dynamic and static Coulomb torques. They depend on the outer drill string radius $r_o(x)$, the static (kinetic) friction coefficient μ_s (μ_k) and the normal force acting between the borehole wall and the drill string $F_N(x)$.



The angular velocity threshold ω_c corresponds to the transition from dynamic to static Coulomb friction. The function $\mathcal{F}(t, x) \in [-F_s(x), F_s(x)]$ denotes the inclusion where

$$\mathcal{F}(t, x) = -\frac{\partial \tau(t, x)}{\partial x} - k_t \rho J \omega(t, x) \in [-F_s(x), F_s(x)].$$

The expression of $F_N(x)$ can be deduced from the torque model presented in [SWB87], and, in our case study, is supposed to be known. Note that when $|\omega(t, x)| > \omega_c$, the alongside friction term \mathcal{F} only depends on the space. It is therefore easier to estimate and reject the disturbance caused by the side forces in this case. As previously mentioned, it motivates a *switching mode* control law, in which we first impose an important actuation guaranteeing the release of the BHA from the stick phase.

Coupling with the top-drive

As explained in Section 6.1, the top-drive of inertia I_{TD} is suspended from a traveling block. It is actuated by an electrical motor and travels vertically up and down to impart torque to the drill string. The motor torque is the control input $V(t) = \tau_m(t)$. Unlike in

the previous section, we do not neglect its dynamics, which are modeled by

$$\frac{d}{dt}\omega_{TD}(t) = \frac{1}{I_{TD}}(\tau_m(t) - \tau_{TD}(t)). \quad (6.14)$$

Coupling with the BHA

At the beginning of the operation, the bit is off-bottom such that there is no bit-rock interaction. As before, the dynamics of the lower part of the drill string are approximated as a single lumped element. The inertia of this set is given by $I_{DH} = \rho_{DH}L_{DH}J_{DH}$, with ρ_{DH} the average density, J_{DH} the polar moment of inertia, and L_{DH} the length of the downhole assembly. Their inertia explains why the collars and the bit still have a major impact on the drill string dynamics. Here, we consider such a lumped approximation for the lowest part of the drilling device. Assume that the downhole assembly is subject to the now lumped effect of the distributed source terms acting on the collars $D(t) = \int_{\text{collar}} S(t, x)dx$. The downhole boundary condition at $x = L$ can then be obtained from a force balance on the lumped BHA

$$\frac{d}{dt}\omega_{DH}(t) = \frac{1}{I_{DH}}(\tau_{DH}(t) - D(t)). \quad (6.15)$$

6.2.2 . Application of the recursive framework

Riemann invariants

We now rewrite the dynamics of the drill pipes sections (6.12) in the form of a chain of hyperbolic PDE systems of transport equations only coupled through the source terms. Define the standard *Riemann invariants* by

$$u_i(t, x) = \omega_i(t, x) + \frac{\lambda_i}{J_i G_i} \tau_i(t, x), \quad v_i(t, x) = \omega_i(t, x) - \frac{\lambda_i}{J_i G_i} \tau_i(t, x), \quad (6.16)$$

with $\lambda_i = \sqrt{\frac{\rho_i}{J_i}}$ the velocity of the torsional wave along section i . They satisfy

$$\frac{\partial u_i}{\partial t}(t, x) + \lambda_i \frac{\partial u_i}{\partial x}(t, x) = \frac{S_i(t, x)}{J_i \rho_i}, \quad \frac{\partial v_i}{\partial t}(t, x) - \lambda_i \frac{\partial v_i}{\partial x}(t, x) = \frac{S_i(t, x)}{J_i \rho_i}. \quad (6.17)$$

The continuity conditions (6.13) now read as

$$u_{i+1}(t, x_i) = a_1^i u_i(t, x_i) + a_2^i v_{i+1}(t, x_i), \quad (6.18)$$

$$v_i(t, x_i) = a_3^i u_i(t, x_i) + a_4^i v_{i+1}(t, x_i), \quad (6.19)$$

where $a_1^i = \frac{2}{1 + Z^i}$, $a_2^i = \frac{Z^i - 1}{1 + Z^i}$, $a_3^i = \frac{1 - Z^i}{1 + Z^i}$, $a_4^i = \frac{2Z^i}{1 + Z^i}$, and $Z^i = \frac{\lambda_i}{J_i G_i} / \frac{\lambda_{i+1}}{J_{i+1} G_{i+1}}$.

It corresponds to reflections of incoming waves from both sides. At the two ends, we have

$$u_1(t, 0) = -v_1(t, 0) + 2\omega_{TD}(t), \quad v_N(t, L) = 2\omega_{DH}(t) - u_N(t, L). \quad (6.20)$$

The boundary conditions (6.14)-(6.15) read

$$\dot{\omega}_{TD}(t) = \frac{1}{I_{TD}}V(t) - \frac{J_1 G_1}{\lambda_1 I_{TD}}(\omega_{TD}(t) - v_1(t, 0)), \quad (6.21)$$

$$\dot{\omega}_{DH}(t) = \frac{J_N G_N}{\lambda_N I_{DH}}(u_N(t, L) - \omega_{DH}(t)) - \frac{D}{I_{DH}}. \quad (6.22)$$

To avoid useless case distinctions, we use the following convention:

$$\begin{aligned} u_0(t, 0) &= \omega_{TD}(t), \quad a_1^0 = 2, \quad a_2^0 = -1, \quad a_3^0 = 0, \quad a_4^0 = \frac{J_1 G_1}{\lambda_1 I_{TD}}, \\ v_{N+1}(t, L) &= \omega_{DH}(t), \quad a_1^N = \frac{J_N G_N}{\lambda_N I_{DH}}, \quad a_2^N = 0, \quad a_3^N = -1, \quad a_4^N = 2. \end{aligned} \quad (6.23)$$

Note that we do not directly obtain subsystems of the form (5.1)-(5.4) in this case, since in-domain couplings do not linearly depend on $(u_i(t, x), v_i(t, x))$. However, we use a similar recursive framework. In this approach, we consider each drill pipe section as an independent subsystem, for which we solve a stabilization and output tracking problem. Using the method of characteristics in each section, we obtain

$$\begin{aligned} u_i(t, x_i) &= u_i(t - \frac{(x_i - x_{i-1})}{\lambda_i}, x_{i-1}) + d_i(t), \quad v_i(t, x_{i-1}) = v_i(t - \frac{(x_i - x_{i-1})}{\lambda_i}, x_i) + d_i(t), \\ \text{where } d_i(t) &= \int_{x_{i-1}}^{x_i} \frac{1}{J_i \rho_i \lambda_i} S_i(t - \frac{s - x_{i-1}}{\lambda_i}, s + x_i - x_{i-1}) dx. \end{aligned} \quad (6.24)$$

Thus, the effect of the Coulomb friction terms can be seen as disturbances acting at the different junctions. Note that if $|\omega| < \omega_c$ all over the drilling device, the terms d_i are constant. These notations are summarized in Figure 6.10.

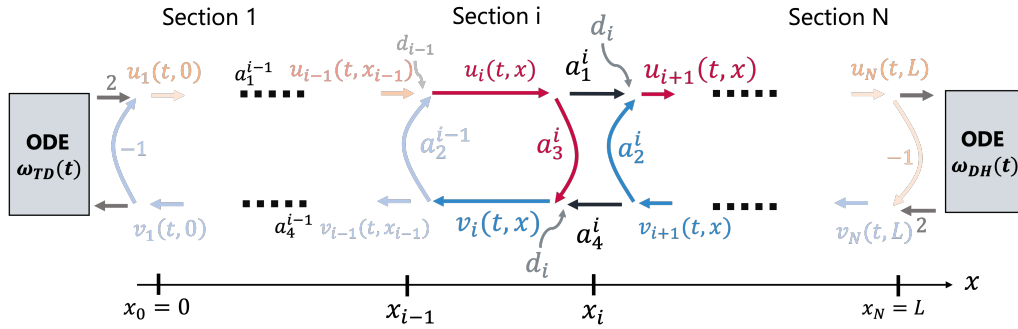


Figure 6.10 – Schematic representation of system (6.17)-(6.22)

Recursive definition of the control input

First, let us determine the virtual input $\hat{V}_{N+1} \equiv u_N(t, L)$ guaranteeing the convergence of $\omega_{DH}(t)$ to the reference trajectory $\omega_{ref}(t)$. With (6.23), (6.22) rewrites

$$\dot{\omega}_{DH}(t) = a_1^N(\hat{V}_{N+1}(t) - \omega_{DH}(t)) - \frac{D(t)}{I_{DH}}.$$

Then, defining $\hat{V}_{N+1}(t)$ as a sum of two terms

$$\begin{aligned} \hat{V}_{N+1}(t) \doteq & \frac{1}{a_1^N} (\dot{\omega}_{ref}(t) + a_1^N \omega_{ref}(t) - K_D(\omega_{DH}(t) - \omega_{ref}(t))) : \text{stabilization} & (6.25) \\ & + \frac{1}{a_1^N I_{DH}} D(t), & : \text{disturbance cancellation} \end{aligned}$$

with $D(t)$ supposedly known. For $K_D > 0$, we therefore ensure that $(\omega_{DH}(t) - \omega_{ref}(t))$ exponentially converges to zero. Next, we iterate the output tracking in the different sections. Denote $t_i = \frac{x_i - x_{i-1}}{\lambda_i}$ the transport time along section i . Using the boundary conditions (6.18) in (6.24), and applying the method of characteristics to (6.17), we obtain

$$u_i(t, x_i) = a_1^{i-1} u^{i-1}(t - t_i, x_{i-1}) + d_i(t) + a_2^{i-1} v_i(t - t_i, x_{i-1}).$$

To ensure that $u_i(t, x_i)$ tracks $\hat{V}_{i+1}(t)$, we define

$$\hat{V}_i(t) \doteq \frac{1}{a_1^{i-1}} (\hat{V}_{i+1}(t + t_i) - d_i(t + t_i)) - \frac{a_2^{i-1}}{a_1^{i-1}} v_i(t, x_i).$$

This paves the way for a recursive definition of the virtual inputs. Note that each \hat{V}_i requires future values of \hat{V}_{i+1} , and consequently, future values of the downstream section states. The causality of the control law will be guaranteed using state-predictors, described in Section 6.2.2. Iterating the procedure on the N sections, we return to the first section, whose state is interconnected with the top-drive ODE (6.21). To get $\omega_{TD}(t)$ converge to $\hat{V}_1(t)$, we define the control input $V(t)$ as

$$V(t) = I_{TD}(\dot{\hat{V}}_1(t) + a_4^0(\omega_{TD}(t) - v_1(t, 0)) - K_0(\omega_{TD} - \hat{V}_1(t))). \quad (6.26)$$

For any $K_0 > 0$, the output $(\omega_{TD}(t) - \hat{V}_1(t))$ exponentially converges to zero. Therefore, using the recursive definition of the virtual inputs $\hat{V}_i(t)$, starting from the downhole, and going up to $\hat{V}_1(t)$, we obtain a control input $V(t)$ satisfying the control objective.

Unlike simple control algorithms (such as PID controllers), the recursively designed control input requires the knowledge of future values of the PDE states and at the end of the downhole ODE state. For the sake of simplicity, we assumed here that the disturbance terms d_i are known and constant, considering the aforementioned switching-mode strategy. If not, we would need to estimate them and predict future values.

In the next section, we propose a state observer based on the recursive dynamics interconnection framework presented in the previous chapter, combined with a state-predictor.

Boundary state estimation

Consider the PDE system (6.17). We assume that the friction coefficients μ_k, μ_s are known. They could be estimated using one of the methods proposed in [ASNK22a]. If the disturbance terms are constant, then it is sufficient to know the boundary states $u_i(t, x_i)$ and $v_i(t, x_{i-1})$ to estimate the whole distributed states (u_i, v_i) . We then design a state observer for these boundary states. We have access to the measurement of the angular

velocity at the top drive $\omega_{TD}(t)$. We obtain $v^1(t, 0)$ from (6.21)

$$\hat{v}_1(t, 0) = \frac{\lambda_1 I_{TD}}{J_1 G_1} (\dot{\omega}_{TD}(t) - \frac{1}{I_{TD}} V(t)) + \omega_{TD}(t).$$

Then, we can compute an estimation of $u_1(t, 0)$ using the boundary condition (6.20)

$$\hat{u}_1(t, 0) = -\hat{v}_1(t, 0) + 2\omega_{TD}(t).$$

Injecting the boundary conditions (6.18)-(6.19) into (6.24), we obtain

$$\begin{aligned} u_i(t, x_i) &= a_1^{i-1} u^{i-1}(t - t_i, x_{i-1}) + a_2^{i-1} v_i(t - t_i, x_{i-1}) + d^i(t - t_i), \\ v_{i+1}(t, x_i) &= \frac{1}{a_4^i} v_i(t + \frac{x_i - x_{i-1}}{\lambda_i}, x_{i-1}) - \frac{a_3^i}{a_4^i} u_i(t, x_i) - d_i(t - \frac{x_i - x_{i-1}}{\lambda_i}). \end{aligned}$$

Consequently, it is possible to get an estimation of delayed values of the boundary states $u_i(t, x_i)$, $v_{i+1}(t, x_i)$, knowing $u_{i-1}(t, x_{i-1})$, $v_i(t, x_{i-1})$. The corresponding delay $\sum_{j=1}^i t_j$ depends on the section we consider. Let us denote δ_{tot} as the largest delay ($\delta_{tot} = \sum_{j=1}^N t_j$). Define the δ_{tot} -delay operator $\bar{\cdot}$ such that for any function γ , we have $\bar{\gamma}(t) = \gamma(t - \delta_{tot})$. Using the above expression, we can then define $\hat{\bar{u}}_i(t, x_i)$, $\hat{\bar{v}}_{i+1}(t, x_i)$ the estimations of the δ_{tot} -delayed states ($\bar{u}_i(t, x_i)$, $\bar{v}_{i+1}(t, x_i)$). These estimations are available on a time horizon $[t, t + \delta_{tot} - \sum_{j=1}^i t_j]$. We can finally estimate δ_{tot} -delayed values of the downhole ODE using these estimations. Indeed, assuming that we have estimates $\hat{\bar{u}}_N(t, L)$, $\hat{\bar{v}}_N(t, L)$, we can define an estimation of the downhole angular velocity as

$$\omega_{TD}^{\hat{\bar{\cdot}}} = \frac{\hat{\bar{u}}_N(t, L) + \hat{\bar{v}}_N(t, L)}{2}.$$

State-prediction

So far, we designed a state observer that provides a real-time estimation of the delayed ODE states and of the delayed boundary states. We now combine these estimations with state predictors to obtain a real-time estimation of the undelayed states. Moreover, as the virtual control inputs \hat{V}_i require the knowledge of future values of the states, the predictors of the boundary states $\bar{u}_i(t, x_i)$, $\bar{v}_i(t, x_i)$, will give $\delta_{tot} + \sum_{j=1}^i t_j$ ahead of time values of these delayed boundary states.

$$\begin{aligned} P_{\bar{u}_i}(t, s) &= \begin{cases} \hat{\bar{u}}_i(s + \delta_{tot} + \sum_{j=1}^i t_j, x_i) & \text{if } s \in [t - 3\delta_{tot} - \sum_{j=1}^i t_j, t - \delta_{tot} - \sum_{j=1}^i t_j] \\ a_1^{i-1} P_{\bar{u}_{i-1}}(t, s) + a_2^{i-1} P_{\bar{v}_i}(t, s) + d_i & \text{otherwise,} \end{cases} \\ P_{\bar{v}_i}(t, s) &= \begin{cases} \hat{\bar{v}}_i(s + \delta_{tot} + \delta_{i-1}, x_{i-1}) & \text{if } s \in [t - 3\delta_{tot} - \delta_{i-1}, t - \delta_{tot} - \delta_{i-1}] \\ a_4^i P_{\bar{v}_{i+1}}(t, s - 2t_i) + a_3^i P_{\bar{u}_i}(t, s - 2t_i) + d_i & \text{otherwise.} \end{cases} \end{aligned}$$

Finally, the state-prediction $P_{\bar{\omega}_{DH}}(t, s)$ of the downhole ODE $\bar{\omega}_{DH}$ ahead a time δ_N is defined for $s \in [t - 2\delta_{tot}, t]$ by

$$P_{\bar{\omega}_{DH}}(t, s) = \begin{cases} \hat{\omega}_{DH}(s + 2\delta_{tot}) & \text{if } s \in [t - 3\delta_{tot}, t - 2\delta_{tot}] \\ e^{-\frac{J_N G_N}{\lambda_N I_{DH}} \delta_{tot}} (\hat{\omega}_{DH}(s) & \text{otherwise.} \\ + \int_s^{s+\delta_{tot}} e^{-\frac{J_N G_N}{\lambda_N I_{DH}} (s-\nu)} \left(\frac{J_N G_N}{\lambda_N I_{DH}} P_{\bar{u}_N}(t, \nu - 2\delta_{tot}) - \frac{D}{I_{DH}} \right) d\nu \end{cases} .$$

These predictors are well-defined and causal. From these definitions, we have

$$\begin{aligned} P_{\bar{u}_i}(t, s) &= \hat{u}_i(s + \delta_{tot} + \delta_i, x_i), \quad s \in [t - 2\delta_{tot} - \delta_i, t], \\ P_{\bar{v}_i}(t, s) &= \hat{v}_i(s + \delta_{tot} + \delta_{i-1}, x_{i-1}), \quad s \in [t - 2\delta_{tot} - \delta_{i-1}, t], \\ P_{\bar{\omega}_{DH}}(t, s) &= \hat{\omega}_{DH}(s + 2\delta_{tot}), \quad s \in [t - 3\delta_{tot}, t]. \end{aligned}$$

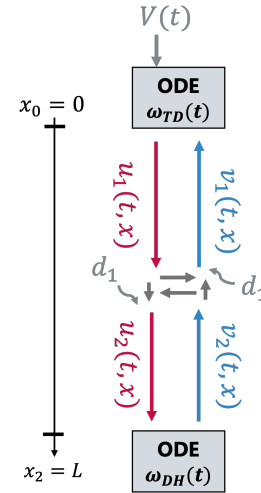
The numerical values of the predictors are updated at each time step, using past values stored in a buffer. They are initialized with the estimations.

6.2.3 . Simulation results

Test case

In this section, we illustrate the performances of our approach using simulated data representing a field scenario. We consider a $L = 3,000\text{m}$ long drilling device. It is composed of two sections $[0, L_1]$ and $[L_1, L_1 + L_2]$. The second section has a 60° deviation. The well is schematically represented in Figure 6.9 and corresponds to scenario *Well A* in [AS18].

It illustrates the case $N = 2$. In this situation, the side forces cannot be neglected. For sake of simplicity, we assume they are constant along the drill string with $(\mu_s, \mu_k) = (0.45, 0.28)$. The other parameters are given in Table 6.2. We use a spatial grid of $\Delta x = 500$ cells to discretize the drill string (CFL=0.99). To consider on-site physical constraints, the torque input is limited to 30 kNm. The transport equations are solved with Matlab using a first-order upwind scheme described in [AS18] to ensure numerical robustness and avoid spurious oscillations.



Trajectory tracking and control strategies

Initially, the drill string is at rest. The system is operated for 100s. After 20s, the velocity setpoint is changed to 120 RPM with a transition time of 10s. After 60s, it changes back to 60 RPM with the same transition time. The reference trajectory is represented in Figure 6.11 (dotted red line).

We apply the switching-mode controller to increase the torque to break the static friction before starting the recursive control procedure. The control input is computed using

Param.	Value	Param.	Value	Param.	Value
A_1	0.005m^2	A_2	0.01 m^2	I_{TD}	2900 kg.m^2
J_1	$2.28 \times 10^{-5}\text{ m}^4$	J_2	$1.49 \times 10^{-4}\text{ m}^4$	I_{DH}	152.9 kg.m^2
G_1	$6.1 \times 10^{10}\text{ m}$	G_2	$6.7 \times 10^{10}\text{ m}$	$\rho_1 = \rho_2$	7850kg/m^3
L_1	1700m	L_2	1300 m	gain K_0	10 (6.26)

Table 6.2 – Numerical parameters for simulation

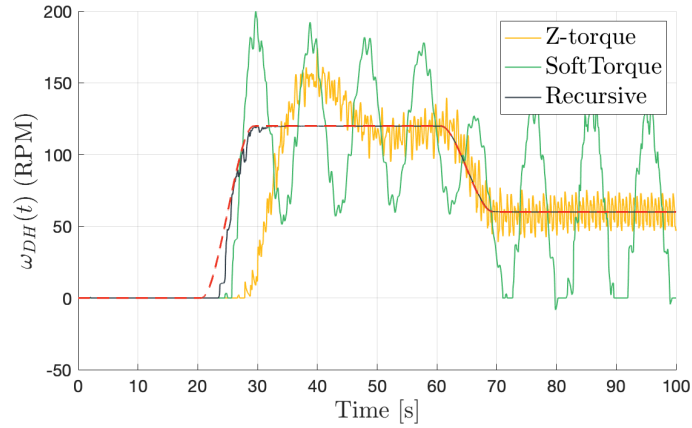


Figure 6.11 – Evolution of the downhole angular velocity $\omega_{DH}(t)$

the predictors based on boundary state estimations. As illustrated in Figure 6.12, the estimation error is relatively important during the transient time but quickly goes to zero when a setpoint is reached.

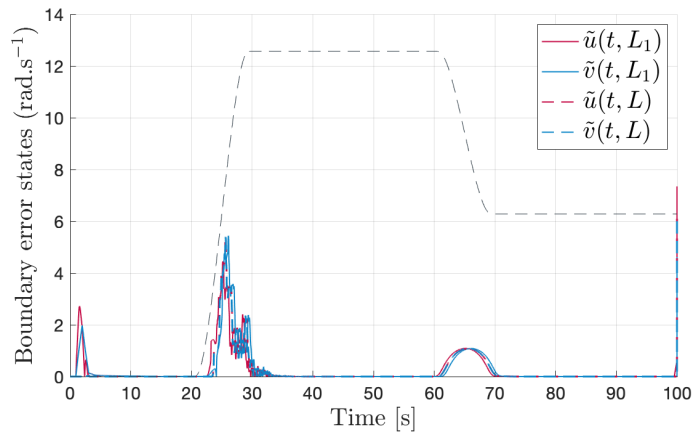


Figure 6.12 – Evolution of estimation error for boundary states

We compare the performance of the proposed controller with state-of-the-art PI controllers (soft-torque, Z-torque) classically used on the field. They correspond to PI controllers improved with fine-tuning of the gains, impedance matching, and filtering techniques. They were developed to mitigate stick-slip during drilling operation [ASADM20].

The time evolution of the downhole angular velocity for the three different control strategies is pictured in Figure 6.11. With the SoftTorque and Z-torque control law, the an-

gular velocity of the drill bit exceeds the reference values during the transient and keeps oscillating. However, one can quickly notice that the wide-band impedance (Z) matching used in this latter approach allow to reduce the oscillations induced by the Coulomb friction terms. With the new proposed controller, $\omega_{DH}(t)$ quickly converges to the reference trajectory as expected and has a smoother behavior. The apparition of stick-slip is therefore prevented¹.

Performance criteria

It is highly interesting to define several relevant specifications to compare the performances of the different controllers more precisely. We present some criteria in Table 6.3. First, the computation time (CT) is much higher for the proposed recursive strategy by comparison with state-of-the-art controllers. It is explained by the computational effort required to compute and update the predictors at each time step. However, it results in better performance in trajectory tracking. The average trajectory error (ATE) for the entire sequence and the last 25s is much lower with the proposed controller.

Control strategy	CT	ATE (total)	ATE (last 25s)	ACE
SoftTorque	1.8s	31RPM	46RPM	6.7kNm
Z-Torque	2.0s	15RPM	7.2RPM	12kNm
Recursive approach	19s	1.2RPM	0.02RPM	7.1kNm

Table 6.3 – Comparison of performance with state-of-the-art controllers

Finally, one can see that the average control effort (ACE) of the proposed approach is comparable with a SoftTorque. However, as represented in Figure 6.13, the control input reaches the thresholds $\pm\tau_{max}$ at the beginning of the operation.

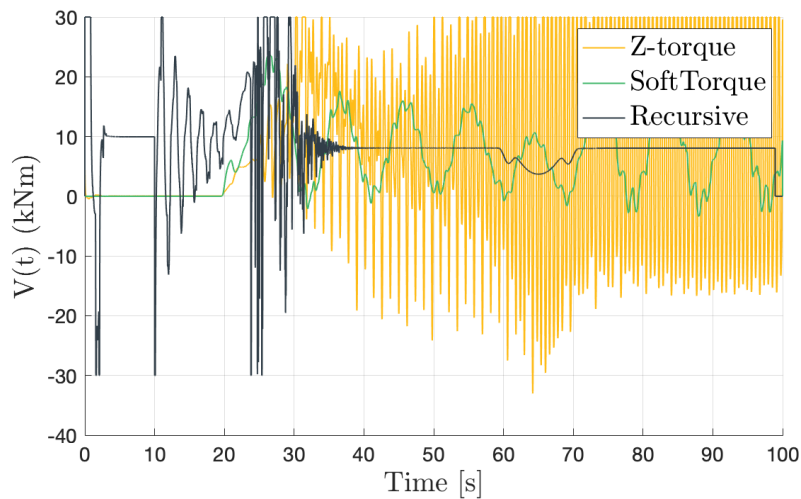


Figure 6.13 – Control effort for different strategies

1. The open-source code for torsional wave simulation can be found on <https://github.com/Open-Source-Drilling-Community/Aarsnes-and-Shor-Torsional-Model.git>.

Conclusion

In this chapter, we used a *recursive dynamics interconnection framework* for state estimation and controller design in the context of drilling. In the first example, this approach allowed us to estimate accurately the distributed axial motion of a drilling device in a vertical borehole. In the second example, it allowed us to ensure the downhole angular velocity to follow a specific trajectory, in a deviated path. Here, the torsional motion of the drill string was assumed to be the dominating dynamic behavior. The controller shown in simulations on a test case scenario to help avoiding torsional stick-slip vibrations at the beginning of drilling operations. Undeniably, the quality of the models can be improved by taking into account the couplings between torsional, longitudinal, and axial oscillations. One must not forget that this approach required known values of the different parameters, including the friction terms. Some of them may be difficult to evaluate, particularly the parameters that depend on the nature of the drilled rock as ϵ . Thus, the proposed approach could be combined with alternative techniques to estimate them as in [AKIS20]. Machine learning-based solutions for estimating the physical parameters are also proposed in Chapter 11.

Perspectives

In Part II, we focused on chain structures in which the control input and measurement were available at one end. First, we considered in Chapter 4 an ODE-linear scalar hyperbolic PDE-ODE interconnection. We presented a backstepping based output-feedback control design for output regulation and disturbance rejection. The robustness of the proposed approach was guaranteed using filtering techniques based on stability analysis in the frequency domain. Next, we considered in Chapter 5 a chain of arbitrary many linear scalar hyperbolic PDE systems, coupled at the unactuated end with an ODE. This network was exponentially stabilized using a predictor-based output feedback controller designed in a recursive dynamics interconnection framework. We finally illustrated in Chapter 6 the interest of such control strategies on two test cases inspired by drilling systems.

In this conclusion, we present some natural extensions of the chain structures we considered, such as non-scalar PDE systems (so-called $(n+m) \times (n+m)$ linear hyperbolic PDE systems), and chain structures with ODEs at both ends.

Chain of N nonscalar hyperbolic PDE subsystems coupled with an ODE at one end

A first natural extension of the work presented in Chapter 5 is to consider that each PDE subsystem i is not composed of two scalar hetero-directional transport equations but of the general form of $(n_i + m_i) \times (n_i + m_i)$ linear hyperbolic PDE systems. Such a model could represent coupled axial-torsional dynamics of a drill string with multiple sections, for instance. The last ODE subsystem could encompass the bit-rock interaction or the lumped effect of the BHA, as presented in Chapter 6. It is actuated at the first end by a control input $V(t) = B_0 u^1(t, 0)$, with $B_0 \in \mathbb{R}^{n_c \times n_1}$, where n_c is the number of available actuators. We assume we have access to a measurement at the actuated boundary $y(t) = C_{mes} v^1(t, 0)$, with $C_{mes} \in \mathbb{R}^{n_m \times m_1}$, where n_m is the number of available measurements.

This system is schematically represented in Figure 6.14. Each hyperbolic PDE subsystem i , ($i \in \llbracket 1, N \rrbracket$) is modeled by $(n+m)$ coupled scalar equations:

$$\frac{\partial}{\partial t} u^i(t, x) + \Lambda_i^+ \frac{\partial}{\partial x} u^i(t, x) = \Sigma_i^{++}(x) u^i(t, x) + \Sigma_i^{+-}(x) v^i(t, x), \quad (6.27)$$

$$\frac{\partial}{\partial t} v^i(t, x) - \Lambda_i^- \frac{\partial}{\partial x} v^i(t, x) = \Sigma_i^{-+}(x) u^i(t, x) + \Sigma_i^{--}(x) v^i(t, x), \quad (6.28)$$

with in-domain coupling terms $\Sigma_i^{-+} \in C([0, 1], \mathbb{R}^{m_i \times n_i})$, $\Sigma_i^{+-} \in C([0, 1], \mathbb{R}^{n_i \times m_i})$. The coupling terms $\Sigma_i^{++} \in C([0, 1], \mathbb{R}^{n_i \times n_i})$, $\Sigma_i^{--} \in C([0, 1], \mathbb{R}^{m_i \times m_i})$ satisfy $(\Sigma_i^{++})_{jj} = 0$, $j \in \llbracket 1, n_i \rrbracket$ and $(\Sigma_i^{--})_{jj} = 0$, $j \in \llbracket 1, m_i \rrbracket$. Each subsystem i is interconnected with its upstream subsystem $i-1$ and downstream subsystem $i+1$ following:

$$\begin{aligned} u^i(t, 0) &= Q^{ii} v^i(t, 0) + Q^{i, i-1} u^{i-1}(t, 1) + \delta_1^i B_0 V(t), \\ v^i(t, 1) &= R^{ii} u^i(t, 1) + R^{i, i+1} v^{i+1}(t, 0) + \delta_N^i C X(t), \end{aligned} \quad (6.29)$$

with constant couplings Q^{ij} , R^{ij} . The last subsystem N is coupled with an ODE of dimension $p \in \mathbb{N}$ such that:

$$\dot{X}(t) = AX(t) + Bu^N(t, 1), \quad (6.30)$$

with $A \in \mathbb{R}^{p \times p}$, $B \in \mathbb{R}^{p \times n_N}$, $C \in \mathbb{R}^{m_N \times p}$ constant matrices.

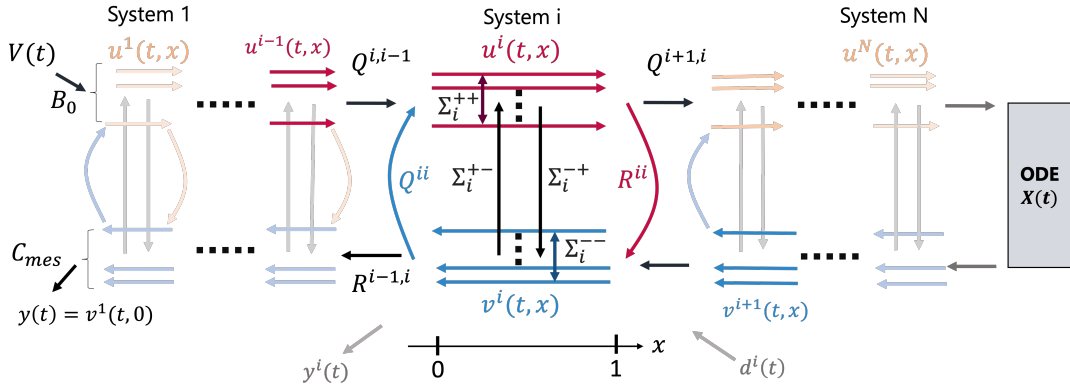


Figure 6.14 – Schematic representation of the system (6.27)-(6.30)

We believe the recursive dynamics interconnection framework proposed in Chapter 5 could be adapted to this more general case to the price of technical computations and structural assumptions on the different coupling matrices. For instance, matrices $R^{i-1,i}$ should be full-row rank ($\text{rank}(R^{i-1,i}) = m_{i-1}$) for the design of successive virtual control inputs. This condition implies that $m_{i-1} \leq m_i$, for all $i \in \llbracket 2, N \rrbracket$. The ODE system must also be stabilizable. Similar conditions would hold for the estimation design.

The case of a chain of two PDE subsystems of the form (6.27)-(6.29) was considered in [ABP22]. In the non-scalar case, the results from [Aur20, RAN21a] cannot be directly applied due to the remaining couplings in the target system obtained after the first Volterra integral transformation. With general coupling matrices ([ABP22] only considered diagonal coupling matrices) tracking and predictor design is even more difficult. Due to the multiple transport delays in each subsystem, the predictors designed in the previous chapters could be non-causal. We should therefore use another transform, that might lead to even more intricate computations.

Finally, as mentioned in Chapter 5, computing predictions at each time step in implementing a control input is computationally expensive. It prevents the use of such control laws for real-time application, highlighting the importance of the robustness of the proposed control design. Taking advantage of model reduction techniques [BSM22] to accelerate the computations could be highly interesting. Neural operators [LKA⁺21] have also proved to be a promising way to fasten the resolution of PDE systems [BSM22, SLY⁺22].

Chain of N scalar hyperbolic PDE subsystems coupled with an ODE at both ends

Next, a natural extension of systems studied in Chapters 4 and 5 are chains of $N > 0$ interconnected scalar hyperbolic PDE systems, coupled at both ends with an ODE. It is schematically illustrated in Figure 6.15.

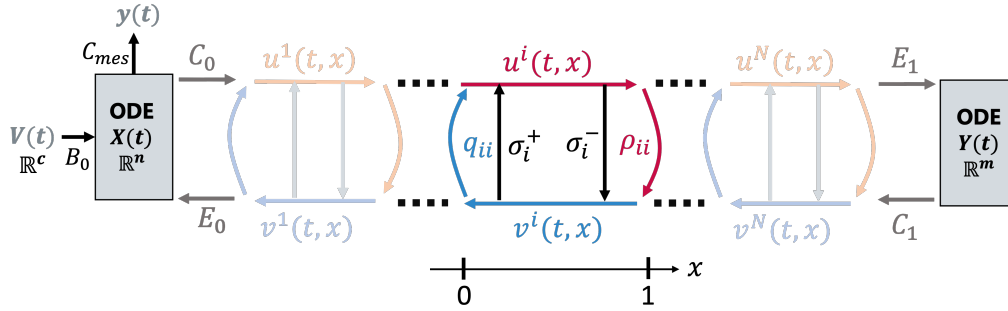


Figure 6.15 – Schematic representation of a chain with ODE at both ends

Applying results from Chapter 5, we can design a virtual control input $\hat{V}_1(t)$ to stabilize the PDE chain structure interconnected with the distal ODE system. Then, considering the actuated ODE system, it remains to solve an output-tracking/disturbance rejection problem. By designing a control input $V(t)$ such that $C_0 X(t)$ converges to $\hat{V}_1(t)$ in presence of a disturbance $E_0 v^1(t, 0)$.

Another difficulty arises in designing an output-feedback controller. Indeed, to develop the state estimation proposed in Section 5.3, we need a measurement of $v^1(\cdot, 0)$ on a certain time horizon. If we only access a partial measure of the ODE state $y(t) = C_{mes} X(t)$, we need to invert the proximal ODE dynamics. A frequency approach as the one proposed in Chapter 4 might be used to reconstruct the boundary state measurement. On the other hand, if a measurement of the first PDE state was available, results from [DGK18] could be considered.

Chain of N scalar hyperbolic PDE subsystems with ODE interconnections

Finally, one last example of a network to be considered would be the case where one or several ODE systems are interconnected inside the PDE chain structure. For instance, considering the system schematically illustrated in Figure 6.16, we would have the general form of equations ($E_0^1 = 0$, $E_1^0 = 0$)

$$\begin{cases} \frac{\partial}{\partial t} u^i(t, x) + \lambda_i \frac{\partial}{\partial x} u^i(t, x) = \sigma_i^+(x) v_i(t, x), & \text{if subsystem } i \text{ is a PDE,} \\ \frac{\partial}{\partial t} v^i(t, x) - \mu_i \frac{\partial}{\partial x} v^i(t, x) = \sigma_i^-(x) u_i(t, x), & \end{cases} \quad (6.31)$$

$$\dot{X}_i(t) = A_i X_i(t) + E_1^{i-1} u^{i-1}(t, 1) + E_0^i v^i(t, 0) + \delta_1^i B_0 V(t), \quad \text{else,} \quad (6.32)$$

with boundary conditions

$$u^i(t, 0) = q_{ii}v^i(t, 0) + \begin{cases} q_{i-1,i}u^{i-1}(t, 1) & \text{if the upstream subsystem is a PDE,} \\ C_0^{i-1}X_{i-1}(t) & \text{if the upstream subsystem is an ODE,} \end{cases}$$

$$v^i(t, 1) = \rho_{ii}u^i(t, 1) + \begin{cases} \rho_{i,i+1}v_{i+1}(t, 0) & \text{if the downstream subsystem is a PDE,} \\ C_1^{i+1}X_{i+1}(t) & \text{if the downstream subsystem is an ODE.} \end{cases}$$

Here we considered that the first and last subsystems are an ODE system.

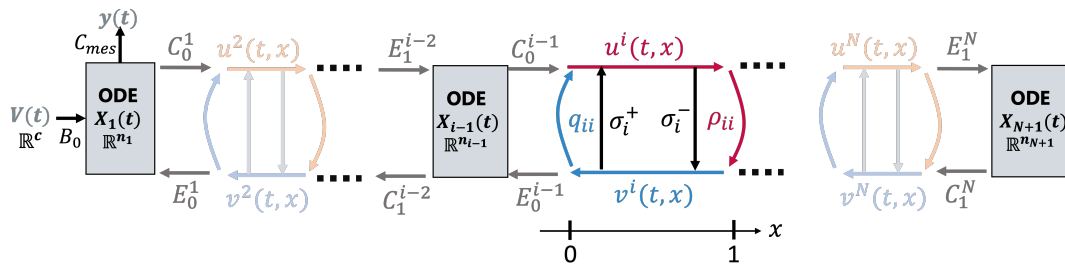


Figure 6.16 – Schematic representation of the system (6.31)-(6.32)

Adopting a 'plug and play' like approach as in Chapter 5 makes sense, but the presence of an ODE system inside the chain structure makes the tracking issue very delicate since the ODE dynamics need to be taken into account. A hypothesis of dynamics inversion for each ODE inside the chain structure could be added to the structural properties (trackability, predictability) already assumed in the recursive dynamics interconnection framework. Results from [AVDMK19, AADMS21], which focus on robust stabilization of PDE-ODE-PDE structures, should first be extended to output regulation.

Part III

Chain structure with actuation at the in-between boundary

Structure de chaîne avec contrôle à une jonction

Introduction

In Part II, we first considered networks of hyperbolic PDE systems interconnected with an ODE system at one (Chapter 5) or both (Chapter 4) ends. In all cases considered before, and in most networked systems found in the literature, the actuation was available at one end of the chain structure. Although such a configuration covers a wide range of applications, as for the UAV-cable-payload structure [WK20], mining cable elevators [WK21] or drilling pipes (Chapter 6), there are several situations for which the actuator is located at an arbitrary node of the network. In this part, we focus on the case where actuation is available at a *junction between two subsystems* in a chain structure. A first example can be found in traffic congestion control on vast road networks. Depending on the control strategy, the traffic model, or the road structure, the control input can either appear as an in-domain term [BLD21, YK21] or at a crossroad. For instance, this latter situation has been considered in [YAK22] in a simple configuration where several coupling terms are equal to zero. Another example of actuation at a junction between different subsystems can be found in biomedical devices, such as micro-endoscopes. Among other actuators, Electro-Active Polymer electrodes have proven to control their motion effectively [CRA14]. In [WLG18], micro endoscopes were modeled by a Timoshenko beam with distributed actuation inside the domain.

In **Chapter 7**, we first address the problem of output feedback stabilization of a chain of two linear hyperbolic PDE subsystems when actuation is located *at the in-between boundary*. It represents a significant difference from existing results. Here, we emphasize the difficulties arising when the actuator is not located at one end of the chain. The classic methods, such as [ADMBA19] or the recursive methodology presented in Part II cannot be applied. When applying the Volterra integral transforms classically used, integral terms appear at the unactuated boundary of the target system. Unlike in [SCWK20], the recirculation induced by the in-domain couplings depends on the control input; therefore, obtaining a stabilizing control law is not straightforward. It can be related to stabilizing a time delay system with pointwise and distributed actuation. Consequently, this configuration requires the development of a new control strategy, based on a Fredholm integral transform.

Next, we illustrate this approach in an example in **Chapter 8**, inspired by the aforementioned biomedical application. Here, we consider the case of a clamped string with in-domain damping and a discrete torque action inside the domain. As mentioned before, when the control input is located at one end of the system, several boundary feedback controllers already exist in the literature to stabilize the resulting wave equation [G22, KGBSo8]. Some controllability results exist for actuation at a junction between different strings when opposite ends are free [ATo1, LZoo]. The control strategy we propose is slightly different from the one presented in Chapter 7, since the control input appears twice at the junction $x_0 \in (0, 1)$, but the *concepts* behind are the same.

This is an excellent test case before generalizing results to more intricate networks. Part III ends with perspectives offered by the approaches developed herein.

7 - Stabilizing two hyperbolic PDE systems with in-between boundary actuation

This chapter considers an interconnection of two scalar hyperbolic systems with a boundary control input. As the introduction mentions, the actuation is not located at one end but at the **in-between boundary**. Our proposed control strategy is based on the backstepping methodology but introduces an original transform. First, we apply an invertible Volterra transform on each subsystem to map them on simpler intermediate subsystems without in-domain couplings. At the in-between boundary of the target system appear integral coupling terms. A change of variables allows rewriting the system as two hetero-directional hyperbolic PDEs. However, integral coupling terms that contain delayed actuation values remain at the unactuated boundary, when we reformulate it as a time delay system. To map the resulting system to an exponentially stable system without integral couplings, we use an appropriate **Fredholm integral transform**.

Unlike traditionally used Volterra integral transforms [HDMVK16], the existence and invertibility of such transforms are not guaranteed [Yos60]. Several results in the literature deal with the invertibility of Fredholm transforms when kernels satisfy specific boundary conditions [BAK15]. When their kernels are lower diagonal matrices [CHO17], invertibility also directly follows from the cascaded structure of the transform. As none of these conditions is fulfilled here, we use an operator framework, as suggested by [CHO16]. More precisely, we show in Section 7.2 that the well-posedness and invertibility of our transform can be related to a spectral controllability condition. The observer design follows a similar strategy and is presented in Section 7.3. The estimations are used in Section 7.4 to provide an output-feedback controller, stabilizing the interconnected system exponentially.

Chapitre 7: Contrôle à la jonction d'une chaîne de deux systèmes d'EDP hyperboliques par retour de sortie. Dans ce chapitre, nous considérons le cas d'une chaîne de deux sous-systèmes hyperboliques (Section 7.1). La commande est située à la jonction des deux sous-systèmes. La stratégie de contrôle s'inspire de la méthodologie de *backstepping*. Nous utilisons une transformation intégrale de type Volterra sur chaque sous-système, puis un changement de variables simple, afin de réécrire le système sous forme de deux équations de transport couplées hétérodirectionnelles. Cependant, cela induit des termes de couplage intégraux à la frontière non actionnée.

Pour supprimer ces couplages dans le domaine et envoyer le système résultant sur un système exponentiellement stable, nous utilisons une transformation intégrale de type Fredholm. Contrairement aux transformations de Volterra couramment employées et toujours inversibles, nous devons ici garantir l'existence et l'inversibilité de la transformation. Nous utilisons pour cela un formalisme opérateur [CHO16] (Section 7.2). Nous suivons une approche similaire pour obtenir une estimation d'état (Section 7.3). Cela nous permet finalement de proposer une loi de commande par retour de sortie (Section 7.4). Sa performance est illustrée par des simulations (Section 7.5).

Contents

7.1 Problem description	127
7.1.1 System under consideration	127
7.1.2 Structural assumptions	127
7.1.3 Structure simplification	128
7.2 Full-state feedback control law design	129
7.2.1 First target system without in-domain couplings	130
7.2.2 Operator formulation	132
7.2.3 Constructive design of a stabilizing control law	135
7.2.4 Invertibility of the Fredholm transform	137
7.2.5 Stabilizing control law	137
7.3 Observer design	138
7.3.1 Target system	139
7.3.2 Observer and error state	140
7.3.3 Constructive design of the observer gains	142
7.3.4 Convergence of the observer state	145
7.4 Output-Feedback control law	145
7.5 Simulation results	146

The results presented herein were published in:

- Jeanne Redaud, Jean Auriol, and Silviu-Iulian Niculescu. "Stabilizing Output-feedback control law for Hyperbolic Systems using a Fredholm transformation". IEEE Transactions on Automatic Control. 2022, Vol.67 (12), pp. 6651-6666.
- _____. "Stabilizing Integral Delay Dynamics and Hyperbolic Systems using a Fredholm Transformation" (2021). 60th IEEE Conference on Decision and Control (CDC).
- _____. "Observer Design for a Class of Delay Systems Using a Fredholm Transform" (2021). 16th IFAC Workshop on Time Delay Systems (TDS).

7.1 . Problem description

7.1.1 . System under consideration

We consider a system composed of two scalar hyperbolic PDE subsystems interconnected through their boundaries. However, contrary to previous results on chain structures with arbitrarily many hyperbolic PDE subsystems [SA17, AA17, Aur20], the actuation is here at the junction between two subsystems. Each subsystem $i \in \{1, 2\}$ is modeled by (5.1)-(5.2), where σ_i^+, σ_i^- are two continuous functions, which may be sources of instabilities. As previously, we assume we have normalized state variables such that $t > 0$, $x \in [0, 1]$ and constant transport velocities $\lambda_i > 0$, $\mu_i > 0$. The two subsystems are interconnected through their boundaries

$$u_1(t, 0) = q_{11}v_1(t, 0), \quad v_2(t, 1) = \rho_{22}u_2(t, 1), \quad (7.1)$$

$$v_1(t, 1) = V(t) + \rho_{11}u_1(t, 1) + \rho_{12}v_2(t, 0), \quad u_2(t, 0) = q_{22}v_2(t, 0) + q_{21}u_1(t, 1). \quad (7.2)$$

The different couplings terms q_{ij} and ρ_{ij} are assumed to be constant. As illustrated in Figure 7.1, the real-valued actuation $V(t)$ is located at the right boundary of the first subsystem. We assume that we measure the opposite boundary of the unactuated subsystem $y(t) = v_2(t, 0)$. We denote $u_i^0(\cdot) = u_i(0, \cdot), v_i^0(\cdot) = v_i(0, \cdot) \in H^1([0, 1], \mathbb{R})$ the initial conditions satisfying compatibility equations similar to (2.1.1) ((7.1)-(7.2) for $t = 0$). The existence of solutions in L^2 for the open-loop system is guaranteed by [BC16, Appendix A].

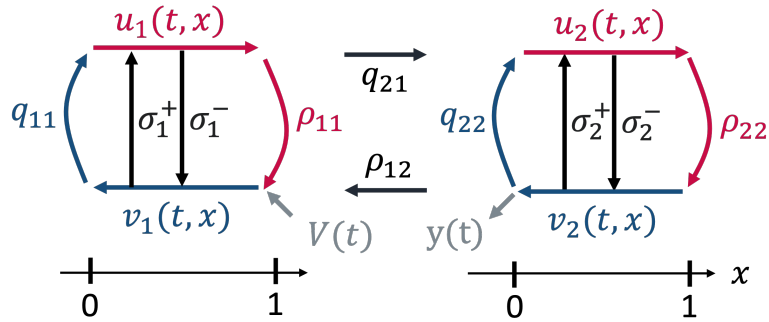


Figure 7.1 – Schematic representation of the system (5.1)-(7.2)

7.1.2 . Structural assumptions

As mentioned in the introduction, stabilizing the chain when the actuation is available at the in-between boundary is not as easy as when it is available at one end. Indeed, the different in-domain and boundary couplings somehow result in a re-circulation of past values of the control input, which must be considered in the design. We first make some structural assumptions on the boundary couplings to ensure the stabilizability of the interconnected system. The conditions that follow can be directly verified.

Assumption 7.1.1 *The boundary coupling coefficient q_{21} does not equal 0.*

This first assumption is crucial for stabilizing the whole system. In the case where $q_{21} = 0$, subsystem 2 evolves independently of subsystem 1. If not already stable in an open loop,

it cannot be stabilized by its interconnection with subsystem 1. Thus, this assumption is necessary if subsystem 2 is not stable. Also, in this case, subsystem 1 is undetectable if only the available measurement $v_2(t, 0)$ is used.

Assumption 7.1.2 *The boundary coupling coefficients q_{11} and ρ_{22} do not equal 0.*

If $q_{11} = 0$, the control input only acts on subsystem 2 through distributed terms resulting from in-domain couplings in (5.1). The backstepping methodology proposed here cannot be directly adjusted for this case. When solving the kernel equations, the resulting Fredholm equations become degenerate, and the proposed techniques do not apply. Similar considerations arise in the observer design when $\rho_{22} = 0$. It is so far a limitation of this approach. Finally, the (delay-) robustness condition (2.2.1) rewrites for the interconnected system as

Assumption 7.1.3 *The coupling coefficients $|\rho_{11}q_{11}|$ and $|\rho_{22}q_{22}|$ are strictly less than 1.*

In addition to these three general assumptions, some specific spectral controllability and spectral observability assumptions are added in Sections 7.2.2 and 7.3.2 respectively.

7.1.3 . Structure simplification

Under Assumption 7.1.2, we first define new variables to simplify the design of a stabilizing control law. We consider the bijective transformation

$$u'_1(t, x) = u_1(t, x), \quad v'_1(t, x) = q_{11}v_1(t, x), \quad u'_2(t, x) = \rho_{22}u_2(t, x), \quad v'_2(t, x) = v_2(t, x),$$

such that (5.1)-(5.2) hold for the new state $(u'_i, v'_i)_{i \in \{1,2\}}$ with the new coupling terms $\sigma'_i{}^\pm$ defined by

$$\sigma'_1{}^+(x) \doteq \frac{1}{q_{11}}\sigma_1^+(x), \quad \sigma'_1{}^-(x) \doteq q_{11}\sigma_1^-(x), \quad \sigma'_2{}^+(x) \doteq \rho_{22}\sigma_2^+(x), \quad \sigma'_2{}^-(x) \doteq \frac{1}{\rho_{22}}\sigma_2^-(x).$$

The boundary conditions are now written as follows:

$$u'_1(t, 0) = v'_1(t, 0), \quad v'_1(t, 1) = q_{11}(V(t) + \rho_{11}u'_1(t, 1) + \rho_{12}v'_2(t, 0)), \quad (7.3)$$

$$u'_2(t, 0) = q'_{22}v'_2(t, 0) + q'_{21}u'_1(t, 1), \quad v'_2(t, 1) = u'_2(t, 1), \quad (7.4)$$

with $q'_{22} \doteq \rho_{22}q_{22}$ and $q'_{21} \doteq \rho_{22}q_{21}$. We define the intermediate control input $V_S(t)$ by

$$V_S(t) = q_{11}(V(t) + \rho_{11}u'_1(t, 1) + \rho_{12}v'_2(t, 0)), \quad (7.5)$$

such that (7.3) rewrites as $v'_1(t, 1) = V_S(t)$. This new system is shown in Figure 7.2. With the changes above, we have two unitary boundary couplings and have included some boundary couplings in the control input. Although there is now a cascade structure from the first subsystem to the second one, the stabilization problem fundamentally differs from the one studied in Chapter 5. This system is well-posed for any continuous control input V_S and for any initial states $(u'_{i,0}, v'_{i,0})_{i \in \{1,2\}} = (u'_i(0, \cdot), v'_i(0, \cdot)) \in H^1([0, 1], \mathbb{R}^2)$ satisfying initial compatibility conditions.

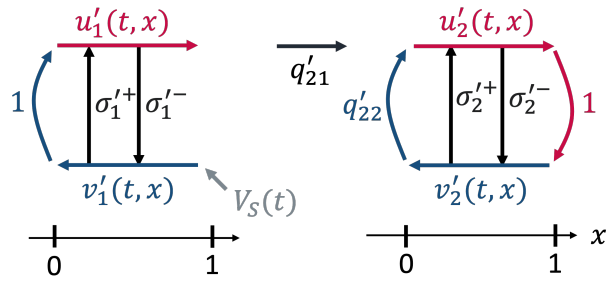


Figure 7.2 – Schematic representation of simplified system (5.1)-(7.4)

7.2 . Full-state feedback control law design

This section proposes a full-state feedback control law that exponentially stabilizes the system (5.1)-(7.2)¹. The control objective reads as follows:

Objective 7.2.1: Exponential stabilization in the L^2 -norm

Design an output-feedback control law $V(t)$ such that there exist $\nu > 0$, $C_0 \geq 1$, for all $(u_i^0, v_i^0) \in H^1([0, 1], \mathbb{R}^2)$ verifying the compatibility conditions, we have

$$\|(u(t, \cdot), v(t, \cdot))\|_{L^2} \leq C_0 e^{-\nu t} \|(u^0, v^0)\|_{L^2}.$$

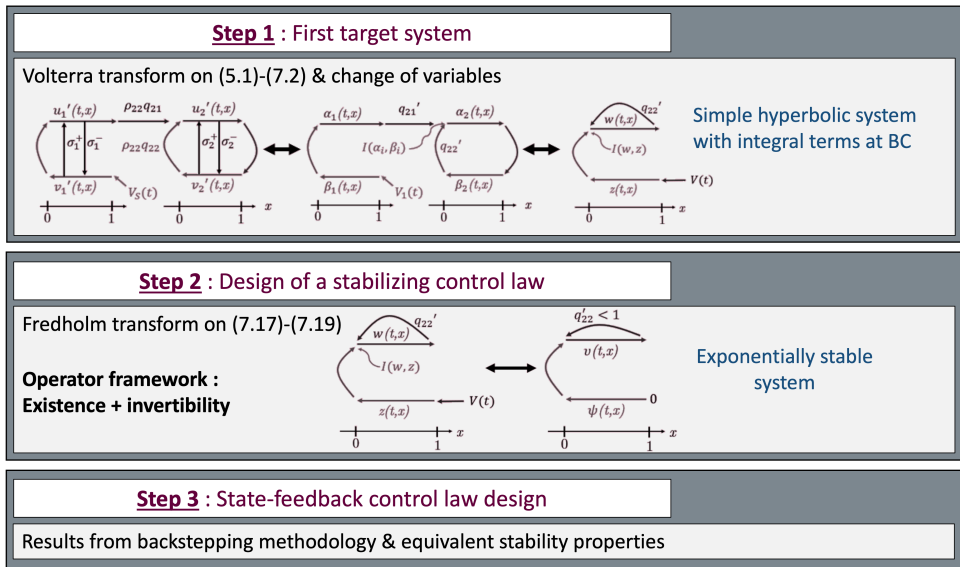


Figure 7.3 – Schematic representation of the control strategy

We follow the strategy schematically illustrated in Figure 7.3. Applying the classic backstepping methodology with Volterra transforms on each subsystem leads to a reformu-

1. This reference will denote the system (5.1)-(5.2) presented in Chapter 5, along with the boundary conditions (7.1)-(7.2)

lation of the chain as two coupled transport equations with integral couplings at the unactuated boundary. We then seek to map this new system to an exponentially stable target system, that is to say, to remove the potentially destabilizing re-circulation of the state feedback. We propose to use a Fredholm integral transform instead. To prove the existence and invertibility of such a transform, we follow the operator-framework-based approach given in [CHO16].

7.2.1 . First target system without in-domain couplings

Volterra transform

As mentioned in the introduction, the first step is to move the in-domain coupling terms to the in-between boundary using two different invertible Volterra backstepping transforms \mathcal{L}_i , $i \in \{1, 2\}$ acting on $H^1([0, 1], \mathbb{R}^2)$. More precisely, we have

$$\begin{cases} u'_1(t, x) = \alpha_1(t, x) - \int_0^x L_1^{++}(x, y)\alpha_1(t, y) + L_1^{+-}(x, y)\beta_1(t, y)dy, \\ v'_1(t, x) = \beta_1(t, x) - \int_0^x L_1^{-+}(x, y)\alpha_1(t, y) + L_1^{--}(x, y)\beta_1(t, y)dy, \end{cases} \quad (7.6)$$

$$\begin{cases} u'_2(t, x) = \alpha_2(t, x) - \int_x^1 L_2^{++}(x, y)\alpha_2(t, y) + L_2^{+-}(x, y)\beta_2(t, y)dy, \\ v'_2(t, x) = \beta_2(t, x) - \int_x^1 L_2^{-+}(x, y)\alpha_2(t, y) + L_2^{--}(x, y)\beta_2(t, y)dy, \end{cases} \quad (7.7)$$

where L_1^- (resp. L_2^-) are bounded piecewise continuous functions defined on the lower part of the unit square \mathcal{T}^- (resp. on its upper part \mathcal{T}^+). The kernels satisfy the following set of equations on their respective definition domain

$$\lambda_i \frac{\partial}{\partial x} L_i^{++}(x, y) + \lambda_i \frac{\partial}{\partial y} L_i^{++}(x, y) = \sigma_i'^+(x) L_i^{-+}(x, y), \quad (7.8)$$

$$\lambda_i \frac{\partial}{\partial x} L_i^{+-}(x, y) - \mu_i \frac{\partial}{\partial y} L_i^{+-}(x, y) = \sigma_i'^+(x) L_i^{--}(x, y),$$

$$\mu_i \frac{\partial}{\partial x} L_i^{-+}(x, y) - \lambda_i \frac{\partial}{\partial y} L_i^{-+}(x, y) = -\sigma_i'^-(x) L_i^{++}(x, y),$$

$$\mu_i \frac{\partial}{\partial x} L_i^{--}(x, y) + \mu_i \frac{\partial}{\partial y} L_i^{--}(x, y) = -\sigma_i'^-(x) L_i^{+-}(x, y), \quad (7.9)$$

with boundary conditions

$$L_1^{+-}(x, x) = -\frac{\sigma_1'^+(x)}{\lambda_1 + \mu_1}, \quad L_1^{-+}(x, x) = \frac{\sigma_1'^-(x)}{\lambda_1 + \mu_1}, \quad L_1^{++}(x, 0) = \frac{\mu_1}{\lambda_1} L_1^{+-}(x, 0), \quad (7.10)$$

$$L_1^{--}(x, 0) = \frac{\lambda_1}{\mu_1} L_1^{-+}(x, 0), \quad L_2^{+-}(x, x) = \frac{\sigma_2'^+(x)}{\lambda_2 + \mu_2}, \quad L_2^{-+}(x, x) = -\frac{\sigma_2'^-(x)}{\mu_2 + \lambda_2},$$

$$L_2^{++}(x, 1) = \frac{\mu_2}{\lambda_2} L_2^{+-}(x, 1), \quad L_2^{--}(x, 1) = \frac{\lambda_2}{\mu_2} L_2^{-+}(x, 1). \quad (7.11)$$

These two sets of equations admit a unique continuous solution [CVKB13]. The integral transform \mathcal{L}_i , $i \in \{1, 2\}$ is a bounded (and therefore continuous) operator from $H^1([0, 1], \mathbb{R}^2)$ to $H^1([0, 1], \mathbb{R}^2)$. The transformation is invertible as it is a Volterra transform [Yos60]. The inverse transforms \mathcal{L}_i^{-1} have the same structure.

Differentiating with respect to time and space (7.6)-(7.7), and integrating by part, we show

that the two Volterra transforms map the original system to

$$\frac{\partial}{\partial t}\alpha_i(t, x) + \lambda_i \frac{\partial}{\partial x}\alpha_i(t, x) = 0, \quad \frac{\partial}{\partial t}\beta_i(t, x) - \mu_i \frac{\partial}{\partial x}\beta_i(t, x) = 0, \quad (7.12)$$

with the boundary conditions

$$\alpha_1(t, 0) = \beta_1(t, 0), \quad \alpha_2(t, 0) = q'_{22}\beta_2(t, 0) + q'_{21}\alpha_1(t, 1) + \mathcal{I}(\alpha_i, \beta_i), \quad (7.13)$$

$$\beta_1(t, 1) = V_1(t), \quad \beta_2(t, 1) = \alpha_2(t, 1). \quad (7.14)$$

The resulting integral boundary couplings \mathcal{I} and control law V_1 are defined by

$$\mathcal{I}(\alpha_i, \beta_i) = -q'_{21} \int_0^1 L_1^{++}(1, y)\alpha_1(y) + L_1^{+-}(1, y)\beta_1(y)dy \quad (7.15)$$

$$+ \int_0^1 (L_2^{++}(0, y) - q'_{22}L_2^{-+}(0, y))\alpha_2(y) + (L_2^{+-}(0, y) - q'_{22}L_2^{--}(0, y))\beta_2(y)dy,$$

$$V_1(t) = V_S(t) + \int_0^1 L_1^{-+}(1, y)\alpha_1(y) + L_1^{--}(1, y)\beta_1(y)dy.$$

Denote by $(\alpha_i^0(\cdot), \beta_i^0(\cdot))^\top = \mathcal{L}_i^{-1}((u'_i(0, \cdot), v'_i(0, \cdot))^\top) \in H^1([0, 1], \mathbb{R}^2)$ the initial conditions associated to (7.12). This first target system (7.12)-(7.14) is therefore composed of two transport equations but presents integral terms (7.15) at the boundary $x = 0$, which may be sources of instabilities.

Change of variables

To simplify the problem, (7.12)-(7.14) can be reformulated as a single 2×2 hyperbolic PDE system whose state is denoted $(z(t, x), w(t, x))$. Indeed, each subsystem can be independently considered as a transport equation with a propagation time $\delta_i = \frac{1}{\lambda_i} + \frac{1}{\mu_i}$, and a velocity $\Lambda_i = \frac{\mu_i \lambda_i}{\lambda_i + \mu_i} = \frac{1}{\delta_i}$. Define the new set of coordinates $(w(t, x), z(t, x))$ by

$$\begin{cases} w(t, x) = \mathbf{1}_{[0, x_2]}(x)\alpha_2(t, \frac{x}{x_2}) + \mathbf{1}_{[x_2, 1]}(x)\beta_2(t, \frac{x-1}{x_2-1}), \\ z(t, x) = q'_{21} \left(\mathbf{1}_{[0, x_1]}(x)\alpha_1(t, 1 - \frac{x}{x_1}) + \mathbf{1}_{[x_1, 1]}(x)\beta_1(t, \frac{x-x_1}{1-x_1}) \right), \end{cases} \quad (7.16)$$

with $x_i = \frac{\mu_i}{\lambda_i + \mu_i}$. For any $t > 0$, for any $(\alpha_i(t, \cdot), \beta_i(t, \cdot))_{i \in \{1, 2\}} \in H^1([0, 1], \mathbb{R}^2)$, then $(w(t, \cdot), z(t, \cdot))$ defined by (7.16) is in $H^1([0, 1], \mathbb{R}^2)$. The new states $(w(t, x), z(t, x))$ satisfy

$$\frac{\partial}{\partial t}w(t, x) + \Lambda_2 \frac{\partial}{\partial x}w(t, x) = 0, \quad \frac{\partial}{\partial t}z(t, x) - \Lambda_1 \frac{\partial}{\partial x}z(t, x) = 0, \quad (7.17)$$

$$w(t, 0) = z(t, 0) + q'_{22}w(t, 1) + \int_0^1 N_w(y)w(t, y) + N_z(y)z(t, y)dy, \quad (7.18)$$

$$z(t, 1) = q'_{21}V_1(t) = V'_1(t), \quad (7.19)$$

where the integral coupling terms are defined by

$$N_w(x) = \mathbf{1}_{[0, x_2]}(x) \frac{1}{x_2} \left(L_2^{++}(0, \frac{x}{x_2}) - q'_{22}L_2^{-+}(0, \frac{x}{x_2}) \right)$$

$$\begin{aligned}
& + \mathbb{1}_{[x_2,1]}(x) \frac{1}{1-x_2} \left(L_2^{+-}(0, \frac{1-x}{1-x_2}) - q'_{22} L_2^{--}(0, \frac{1-x}{1-x_2}) \right), \\
N_z(x) = & - \mathbb{1}_{[0,x_1]}(x) \frac{1}{x_1} L_1^{++}(1, 1 - \frac{x}{x_1}) - \mathbb{1}_{[x_1,1]}(x) \frac{1}{1-x_1} L_1^{+-}(1, \frac{x-x_1}{1-x_1}).
\end{aligned}$$

Note that N_w (resp. N_z) is continuous by definition of x_i and due to the boundary conditions (7.10) and (7.11). In the following, we use system (7.17)-(7.19) to design the control law inspired by the backstepping methodology. A system of form (7.17)-(7.19) is used as a *comparison system* in Chapter 8.

Naive approach: Volterra integral transform

Using a Volterra integral transform (2.8), we try to map system (7.17)-(7.19) to a target system with no integral couplings at the unactuated boundary $x = 0$. Following the backstepping methodology, we notice that it imposes the boundary condition in $x = 1$ for some kernels. Then, no condition can be imposed along their boundary $x = y$. The kernels must satisfy coupled *nonlinear* PDEs, and some in-domain couplings appear in the target system. The integral coupling terms in (7.18) prevent a Volterra transform from mapping the system to an easily proven exponentially stable target system (a simple cascade structure for instance). Therefore, we propose to use a **Fredholm integral transform**, whose kernels are defined on the unit square \mathcal{S} . It offers more degrees of freedom, but is not always invertible [Yos60]. We then show that the invertibility of the transform is related to a controllability assumption for our system. The proof follows the approach proposed by [BC16] and relies on the operator framework introduced in Section 2.1.2.

7.2.2 . Operator formulation

Reformulation of system (7.17)-(7.19)

First, the system (7.17)-(7.19) is rewritten in the abstract form

$$\frac{d}{dt} \begin{pmatrix} w \\ z \end{pmatrix} = A \begin{pmatrix} w \\ z \end{pmatrix} + BV'_1, \tag{7.20}$$

where we can identify the operators A and B through their adjoints by taking the canonical scalar product of (7.20) formally with smooth test functions and comparing with the weak formulation [RAN21b]. The operator A is thus defined by

$$A : \begin{pmatrix} w \\ z \end{pmatrix} \mapsto \begin{pmatrix} -\Lambda_2 \frac{\partial w}{\partial x} \\ \Lambda_1 \frac{\partial z}{\partial x} \end{pmatrix}, \tag{7.21}$$

with $D(A) = \{(w, z) \in H^1([0, 1], \mathbb{R}^2) \mid z(1) = 0,$

$$w(0) = z(0) + q'_{22} w(1) + \int_0^1 N_w(y) w(y) + N_z(y) z(y) dy\}.$$

Its adjoint A^* is defined by

$$A^* : \begin{pmatrix} w \\ z \end{pmatrix} \mapsto \begin{pmatrix} \Lambda_2 \frac{\partial w}{\partial x} + \Lambda_2 N_w(\cdot) w(0) \\ -\Lambda_1 \frac{\partial z}{\partial x} + \Lambda_2 N_z(\cdot) w(0) \end{pmatrix}, \quad (7.22)$$

with $D(A^*) = \{(w, z) \in H^1([0, 1], \mathbb{R}^2) \mid w(1) = q'_{22} w(0), z(0) = \frac{\Lambda_2}{\Lambda_1} w(0)\}$.

The operator $B \in \mathcal{L}(\mathbb{R}, D(A^*))$ and its adjoint $B^* \in \mathcal{L}(D(A^*), \mathbb{R})$ are defined by

$$\langle BV'_1, \begin{pmatrix} w \\ z \end{pmatrix} \rangle = \Lambda_1 z(1) V'_1, \quad B^* \begin{pmatrix} w \\ z \end{pmatrix} = \Lambda_1 z(1). \quad (7.23)$$

Generalities on Fredholm integral operators

The stabilization of the PDE system (7.17)-(7.19) is done using an integral transform of the Fredholm type. Define the following operator \mathcal{T} by

$$\mathcal{T} : \begin{pmatrix} u \\ v \end{pmatrix} \mapsto \begin{pmatrix} u \\ v \end{pmatrix} - \int_0^1 K(\cdot, y) \begin{pmatrix} u(y) \\ v(y) \end{pmatrix} dy, \quad (7.24)$$

with $K \in C^0_{pw}(\mathcal{S}, \mathbb{R}^{2 \times 2})$. The following lemma, adjusted from [CHO16, Proposition 2.6], guarantees the invertibility of Fredholm integral transforms under several conditions.

Lemma 7.2.1: Invertibility of Fredholm integral operators [CHO16]

Consider two operators \mathcal{A}, \mathcal{B} , such that $D(\mathcal{A}) \subset H^1([0, 1], \mathbb{R}^2)$ and a Fredholm integral operator $\mathcal{T} : H^1([0, 1], \mathbb{R}^2) \rightarrow H^1([0, 1], \mathbb{R}^2)$ as defined by (7.24). Assume

- (a) $\ker(\mathcal{T}) \subset D(\mathcal{A})$,
- (b) $\ker(\mathcal{T}) \subset \ker(\mathcal{B})$,
- (c) $\forall z \in \ker(\mathcal{T}), \mathcal{T}\mathcal{A}z = 0$,
- (d) $\forall s \in \mathbb{C}, \ker(s - \mathcal{A}) \cap \ker(\mathcal{B}) = \{0\}$.

Then, the operator \mathcal{T} is invertible. Moreover, its inverse is a Fredholm integral operator whose kernels inherit the same regularity properties.

Proof : The proof follows the steps of [CHO16, Lemma 2.2, Proposition 2.6]. Since the integral part of \mathcal{T} is a compact operator, the Fredholm alternative [Bre10] implies that $\dim \ker(\mathcal{T}) < \infty$. Suppose that $\ker(\mathcal{T}) \neq \{0\}$. Due to condition (a), for all $z \in \ker(\mathcal{T})$ $\mathcal{A}z$ is well-defined, and condition (c) implies that $\ker(\mathcal{T})$ is stable by \mathcal{A} , that is to say, for all $z \in \ker(\mathcal{T})$, $\mathcal{A}z \in \ker(\mathcal{T})$. Since $\ker(\mathcal{T})$ is finite-dimensional and not reduced to $\{0\}$, the restriction $\mathcal{A}|_{\ker(\mathcal{T})}$ of \mathcal{A} to $\ker(\mathcal{T})$ has at least one eigenvalue $\nu \in \mathbb{C}$. Let ζ be the corresponding eigenfunction. Thus, $\zeta \in \ker(\nu - \mathcal{A})$ and $\zeta \in \ker(\mathcal{B})$ by condition (b). This is in contradiction with condition (d). Thus, $\ker(\mathcal{T}) = \{0\}$ and \mathcal{T} is injective. Using the Fredholm alternative [Bre10], we obtain that \mathcal{T} is invertible. The fact that the inverse operator is a Fredholm integral operator whose kernels inherit the same regularity properties comes from [CHO16, Section 2.4]. ■

Remark 7.2.1 Note that the operator \mathcal{T} is invertible if and only if its adjoint operator \mathcal{T}^* is invertible. It is given by

$$\mathcal{T}^* : \begin{matrix} H^1([0, 1], \mathbb{R}^2) \rightarrow H^1([0, 1], \mathbb{R}^2) \\ \begin{pmatrix} u \\ v \end{pmatrix} \mapsto \begin{pmatrix} u \\ v \end{pmatrix} - \int_0^1 \bar{K}^\top(y, \cdot) \begin{pmatrix} u(y) \\ v(y) \end{pmatrix} dy \end{matrix},$$

In some cases, the invertibility of the adjoint operator is easier to prove.

Spectral controllability assumption

Considering the four assumptions of Lemma 7.2.1, we note that the conditions (a)–(c) only depend on the choice of the integral operator \mathcal{T} . However, condition (d) corresponds to a fundamental property of the system that does not depend on the operator. Therefore, we make the following assumption:

Assumption 7.2.1 The operators A^* defined in (7.22) and B^* defined in (7.23) satisfy

$$\forall s \in \mathbb{C}, \ker(s - A^*) \cap \ker(B^*) = \{0\}.$$

This assumption is a controllability condition that is similar to the one given in [CHO16]. Interestingly, it can be reformulated using a time-delay systems formalism. Denote $\phi(t) = w(t, 0)$. Applying the method of characteristics to the transport equations (7.17), we obtain the *integral delay equation*

$$\begin{aligned} \phi(t) &= q'_{22}\phi(t - \delta_2) + \int_0^{\delta_2} \Lambda_2 N_w(\Lambda_2 \nu) \phi(t - \nu) d\nu \\ &\quad + V'_1(t - \delta_1) + \int_0^{\delta_1} \Lambda_1 N_z(1 - \Lambda_1 \nu) V'_1(t - \nu) d\nu. \end{aligned} \quad (7.25)$$

Let us formally take the Laplace transform of (7.25), with zero initial condition. We have $F_2(s)\phi(s) = F_1(s)V_1(s)$, where the holomorphic function F_2 and F_1 are defined by

$$\begin{aligned} F_2(s) &= 1 - q'_{22}e^{-\delta_2 s} - \int_0^{\delta_2} \Lambda_2 N_w(\Lambda_2 \nu) e^{-\nu s} d\nu, \\ F_1(s) &= e^{-\delta_1 s} + \int_0^{\delta_1} \Lambda_1 N_z(1 - \Lambda_1 \nu) e^{-\nu s} d\nu. \end{aligned}$$

To ensure that $F_2(s), F_1(s)$ cannot simultaneously be equal to zero, we are led to the following *spectral-like controllability* assumption [Mou98, Pan76]:

Assumption 7.2.2 For all $s \in \mathbb{C}$, $\text{rank}[F_2(s), F_1(s)] = 1$.

We can show the following

Lemma 7.2.2: Spectral Controllability

Under Assumption 7.2.2, Assumption 7.2.1 is satisfied.

Proof : Consider $s \in \mathbb{C}$ and $(w, z) \in \ker(s - A^*) \cap \ker(B^*)$. Since $(w, z) \in \ker(B^*)$, we have $z(1) = 0$. Since $(w, z) \in \ker(s - A^*)$, we have

$$sw(x) = \Lambda_2 w'(x) + \Lambda_2 N_w(x)w(0), \quad sz(x) = -\Lambda_1 z'(x) + \Lambda_2 N_z(x)w(0),$$

with the boundary conditions $w(1) = q'_{22}w(0)$, $\Lambda_1 z(0) = \Lambda_2 w(0)$. Solving these two equations, we obtain

$$\begin{aligned} w(x) &= e^{\frac{s}{\Lambda_2}x} w(0) - w(0) \int_0^x N_w(\nu) e^{\frac{s}{\Lambda_2}(x-\nu)} d\nu, \\ z(x) &= e^{-\frac{s}{\Lambda_1}x} z(0) + z(0) \int_0^x N_z(\nu) e^{-\frac{s}{\Lambda_1}(x-\nu)} d\nu. \end{aligned}$$

Using $z(1) = 0$, $w(1) = q'_{22}w(0)$, and evaluating the above equations in $x = 1$, one gets

$$w(0)F_2(s) = 0, \quad z(0)F_1(s) = 0.$$

Using Assumption 7.2.2, we cannot simultaneously have $F_2(s) = 0$ and $F_1(s) = 0$. It prevents pole-zero cancellation from V_1 to ϕ . Thus, we either have $w(0) = 0$ or $z(0) = 0$. Since $(w, z) \in D(A^*)$, $w(0) = z(0) = 0$ and $(w, z) = (0, 0)$. ■

This assumption can be verified using numerical methods for locating the zeros of analytical functions [DL67], for instance, the software package ZEAL [KVBR⁺00]. More insights are given in [RAN22b].

7.2.3 . Constructive design of a stabilizing control law

In this section, we design a full-state feedback controller for system (7.17)-(7.19) using the aforementioned strategy.

Presentation of the target system

Following the backstepping method, we want to map the PDE system (7.17)-(7.19) to a stable target system. Denote the target state as (v, ψ) , and define the integral operator \mathcal{N} of the form (7.24) with kernels $N^{\cdot\cdot} \in C^0_{pw}(\mathcal{S})$, such that

$$\begin{aligned} w(x) &= v(x) - \int_0^1 N^{++}(x, y)v(y) + N^{+-}(x, y)\psi(y)dy, \\ z(x) &= \psi(x) - \int_0^1 N^{-+}(x, y)v(y) + N^{--}(x, y)\psi(y)dy. \end{aligned} \quad (7.26)$$

The target state satisfies the following set of equations

$$\frac{\partial}{\partial t}v(t, x) + \Lambda_2 \frac{\partial}{\partial x}v(t, x) = 0, \quad \frac{\partial}{\partial t}\psi(t, x) - \Lambda_1 \frac{\partial}{\partial x}\psi(t, x) = 0, \quad (7.27)$$

with the boundary conditions

$$v(t, 0) = \psi(t, 0) + q'_{22}v(t, 1), \quad \psi(t, 1) = 0. \quad (7.28)$$

Denote now $(v^0(\cdot), \psi^0(\cdot))^\top = \mathcal{N}^{-1}((w^0(\cdot), z^0(\cdot))^\top) \in H^1([0, 1], \mathbb{R}^2)$ the initial conditions associated to (7.27). They satisfy the compatibility equations (7.28).

Theorem 7.2.1

For any initial conditions $(v^0(\cdot), \psi^0(\cdot)) \in H^1([0, 1], \mathbb{R}^2)$, system (7.27)-(7.28) is well-posed and exponentially converges to zero in the sense of the L^2 -norm.

Proof: The well-posedness of the target system (7.27)-(7.28) results from [BC16, Appendix A]. Due to the propagation of the boundary condition, ψ converges to 0 in finite time. For $t > \frac{1}{\Lambda_1}$, the first boundary condition becomes $v(t, 0) = q'_{22}v(t, 1) = q'_{22}v(t - \frac{1}{\Lambda_2}, 0)$. According to [BC16, HVL13], the system converges to 0 and is exponentially stable since $|q'_{22}| < 1$ by Assumption 7.1.1. ■

We now need to show that it is possible to map the system (7.17)-(7.19) to this target system using a bounded invertible transform. Indeed, this would guarantee that both systems share the same asymptotic stability properties. Once again, the proof of invertibility and existence of such transform will rely on an operator framework. Therefore, we first reformulate the target system using an abstract formulation

$$\frac{d}{dt} \begin{pmatrix} v \\ \psi \end{pmatrix} = A_0 \begin{pmatrix} v \\ \psi \end{pmatrix},$$

where A_0 satisfies (7.21), and is defined on $D(A_0) = \{(v, \psi) \in H^1([0, 1], \mathbb{R}^2) \mid v(0) = \psi(0) + q'_{22}v(1), \psi(1) = 0\}$. Its adjoint A_0^* is defined on $D(A^*) \subset H^1([0, 1], \mathbb{R}^2)$ by

$$A_0^* : \begin{pmatrix} u \\ v \end{pmatrix} \mapsto \begin{pmatrix} \Lambda_2 \frac{\partial u}{\partial x}(\cdot) \\ -\Lambda_1 \frac{\partial v}{\partial x}(\cdot) \end{pmatrix}.$$

Kernel equations

Following the backstepping methodology, we differentiate the expressions of (v, ψ) with respect to x and t and integrate them by parts. Plugging the resulting expressions into the target system, we obtain the equations satisfied by the kernels of the Fredholm integral transform \mathcal{N} , for all $(x, y) \in \mathcal{S}$,

$$\frac{\partial}{\partial x} N^{++}(x, y) + \frac{\partial}{\partial y} N^{++}(x, y) = 0, \quad \Lambda_2 \frac{\partial}{\partial x} N^{+-}(x, y) - \Lambda_1 \frac{\partial}{\partial y} N^{+-}(x, y) = 0, \quad (7.29)$$

$$\Lambda_1 \frac{\partial}{\partial x} N^{-+}(x, y) - \Lambda_2 \frac{\partial}{\partial y} N^{-+}(x, y) = 0, \quad \frac{\partial}{\partial x} N^{--}(x, y) + \frac{\partial}{\partial y} N^{--}(x, y) = 0, \quad (7.30)$$

with the boundary conditions

$$N^{++}(x, 0) = \frac{\Lambda_1}{\Lambda_2} N^{+-}(x, 0), \quad N^{--}(x, 0) = \frac{\Lambda_2}{\Lambda_1} N^{-+}(x, 0), \quad (7.31)$$

$$N^{++}(x, 1) = q'_{22} N^{++}(x, 0), \quad N^{-+}(x, 1) = q'_{22} N^{-+}(x, 0). \quad (7.32)$$

Evaluating (7.26) in $x = 0$, one gets

$$\begin{aligned} N_w(y) - \int_0^1 N_w(\nu) N^{++}(\nu, y) + N_z(\nu) N^{-+}(\nu, y) d\nu \\ = -N^{++}(0, y) + N^{-+}(0, y) + q'_{22} N^{++}(1, y), \end{aligned} \quad (7.33)$$

$$\begin{aligned}
N_z(y) - \int_0^1 N_w(\nu)N^{+-}(\nu, y) + N_z(\nu)N^{--}(\nu, y)d\nu \\
= -N^{+-}(0, y) + N^{--}(0, y) + q'_{22}N^{+-}(1, y).
\end{aligned}$$

To ensure the well-posedness of the problem, we add the two following conditions

$$N^{+-}(x, 1) = 0, \quad N^{--}(x, 1) = 0. \quad (7.34)$$

Unlike in other cases (see Appendix C), these boundary conditions do not correspond to a degree of freedom. Setting them to zero is necessary to satisfy condition (b) of Lemma 7.2.1, and further guarantee the invertibility of \mathcal{N} and its boundedness, as it appears in Appendix B. We have the following theorem

Theorem 7.2.2: Well-posedness of the kernel equations

The set of equations (7.29)-(7.34) admits a unique solution in $C_{pw}^0(\mathcal{S}, \mathbb{R}^{2 \times 2})$.

Proof : To avoid splitting this section, the extended proof is given in Appendix B. ■

7.2.4 . Invertibility of the Fredholm transform

We now show that the Fredholm integral transform \mathcal{N} is boundedly invertible.

Theorem 7.2.3: Invertibility of the Fredholm operator \mathcal{N}

Consider the Fredholm integral operator \mathcal{N} of the form (7.24) defined on $H^1([0, 1], \mathbb{R}^2)$, with kernels defined on $C_{pw}^0(\mathcal{S})$ as the unique solution of (7.29)-(7.34). Then the operator \mathcal{N} is boundedly invertible.

Proof : The adjoint operator \mathcal{N}^* associated to \mathcal{N} , is also of the form (7.24). We have

$$\mathcal{N}^* \begin{pmatrix} v(x) \\ \psi(x) \end{pmatrix} = \begin{pmatrix} v(x) \\ \psi(x) \end{pmatrix} - \int_0^1 \bar{N}(y, x)^\top \begin{pmatrix} v(y) \\ \psi(y) \end{pmatrix} dy.$$

Due to the regularity of the integral and of the kernels $N^{\cdot\cdot}$, we have $\ker(\mathcal{N}^*) \subset H^1([0, 1], \mathbb{R}^2)$. Taking any $z \in \ker(\mathcal{N}^*)$, and evaluating it in $x = 0$, $x = 1$, we directly obtain conditions (a), (b) of Lemma 7.2.1. Since \mathcal{N} maps the original system (7.17)-(7.19) to the target system (7.27)-(7.28), we have for all $z \in \ker(\mathcal{N}^*)$, $\mathcal{N}^*A^*z = A_0^*\mathcal{N}^*z$ (see [CHO16] for instance). From (b), we therefore obtain condition (c). Condition (d) does not depend on the operator \mathcal{N} . We can then conclude that \mathcal{N}^* is invertible. Following Remark 7.2.1, so is \mathcal{N} .

The inverse operator \mathcal{N}^{-1} associated to \mathcal{N} is of form (7.24), with kernels \check{N} defined on $C_{pw}^0(\mathcal{S}, \mathbb{R}^{2 \times 2})$ as the unique solution of $\check{N}(x, y) = -N(x, y) + \int_0^1 N(x, \nu)\check{N}(\nu, y)d\nu$. ■

7.2.5 . Stabilizing control law

Using the inverse transform, we define the full-state feedback controller $V_1'(t)$ by

$$V_1'(t) = - \int_0^1 \check{N}^{-+}(1, \nu)w(\nu, t) + \check{N}^{--}(1, \nu)z(\nu, t)d\nu.$$

We can then compute the control law $V(t)$ stabilizing the initial system

$$V(t) = \frac{1}{q_{11}} V_S(t) - \rho_{12} v_2(t, 0) - \rho_{11} u_1(t, 1), \quad (7.35)$$

with the intermediate control input $V_S(t)$ introduced in (7.5) defined by

$$\begin{aligned} V_S(t) = & -\frac{1}{q'_{21}} \left(\int_0^1 x_2 \check{N}^{-+}(1, x_2 \nu) \alpha_2(t, \nu) + (1 - x_2) \check{N}^{-+}(1, 1 - (1 - x_2) \nu) \beta_2(t, \nu) d\nu \right) \\ & - \int_0^1 \left(L_1^{-+}(1, \nu) + x_1 \check{N}^{-}(1, x_1(1 - \nu)) \right) \alpha_1(t, \nu) \\ & + \left(L_1^{-}(1, \nu) + (1 - x_1) \check{N}^{-}(1, x_1 + (1 - x_1) \nu) \right) \beta_1(t, \nu) d\nu. \end{aligned}$$

Since the two Volterra backstepping transforms $\mathcal{L}_1, \mathcal{L}_2$ are invertible, we can express the control law defined above as a function of the original states (u_i, v_i) . We can conclude this section with the following theorem

Theorem 7.2.4: Exponential stability of the closed-loop system

The state-feedback control law $V(t)$ defined by (7.35) exponentially stabilizes the hyperbolic system (5.1)-(7.2) in the sense of the L^2 -norm.

Proof: First, let us show that state-feedback control law $V'_1(t)$ defined above exponentially stabilizes the hyperbolic system (7.17)-(7.19) in the sense of the L^2 -norm. Any initial condition of (7.17)-(7.19) in $H^1([0, 1], \mathbb{R}^2)$ is mapped to an initial condition for (7.27)-(7.28) in $H^1([0, 1], \mathbb{R}^2)$. The target system (7.27)-(7.28) admits a unique solution with adequate regularity. As justified earlier, it is exponentially stable in the sense of the L^2 -norm. Due to the bounded invertibility of the Fredholm integral transform \mathcal{N} (Theorem 7.2.3) in $H^1([0, 1], \mathbb{R}^2)$, the intermediate system (7.17)-(7.19) admits a unique solution with desired regularity. With the control law $V'_1(t)$, the hyperbolic system (7.17)-(7.19) and the target system (7.27)-(7.28) share the same stability properties. Then, let us show that it implies the exponential stability of (7.12)-(7.14). For all $x \in [0, 1]$, the initial target states rewrite $\alpha_1(t, x) = \frac{1}{q'_{21}} z(t, x_1(1 - x))$, $\beta_1(t, x) = \frac{1}{q'_{21}} z(t, x_1 + (1 - x_1)x)$, and $\beta_2(t, x) = w(t, 1 - (1 - x_2)x)$, $\alpha_2(t, x) = w(t, x_2 x)$.

Therefore, the convergence of (w, z) to zero at an exponential rate immediately implies the exponential stability of (α_i, β_i) . Then, with the continuous control law $V_S(t)$ defined above, the hyperbolic system (5.1)-(7.2) is equivalent to the target systems (7.12)-(7.14). Due to the bounded invertibility of the Volterra integral transforms \mathcal{L}_i , the original states (u_i, v_i) share the same stability properties. ■

This proof can be easily adjusted to show that the well-posedness of the target system (7.27)-(7.28) implies the well-posedness of the closed-loop system (5.1)-(7.2).

7.3 . Observer design

In this section, we design a state observer for the system (5.1)-(7.2), using the measurement $y(t) = v_2(0, t)$. First, we use two invertible Volterra integral transforms \mathcal{M}_i and a change of variable to map the interconnected system (5.1)-(7.2) to a simpler target system (ω, γ) . We define an observer state $(\hat{\omega}, \hat{\gamma})$ as a copy of the dynamics of this target system plus output injection terms to be designed. The strategy we follow is similar to the one presented in Section 7.2. It relies on the backstepping methodology, with a Fredholm-type integral transform \mathcal{K} , whose existence and invertibility are shown following the same operator formalism.

7.3.1 . Target system

Volterra transform and kernel equations

As before, we first use classic Volterra integral transforms to modify the in-domain couplings. Define two integral transforms \mathcal{M}_i , $i \in \{1, 2\}$ on $H^1([0, 1], \mathbb{R}^2)$ by

$$\begin{cases} u_1(t, x) = a_1(t, x) + \int_x^1 M_1^{++}(x, y)a_1(t, y) + M_1^{+-}(x, y)b_1(t, y)dy, \\ v_1(t, x) = b_1(t, x) + \int_x^1 M_1^{-+}(x, y)a_1(t, y) + M_1^{--}(x, y)b_1(t, y)dy, \\ u_2(t, x) = a_2(t, x) + \int_0^x M_2^{++}(x, y)a_2(t, y) + M_2^{+-}(x, y)b_2(t, y)dy, \\ v_2(t, x) = b_2(t, x) + \int_0^x M_2^{-+}(x, y)a_2(t, y) + M_2^{--}(x, y)b_2(t, y)dy, \end{cases}$$

where the kernels M_1^{\cdot} (resp. M_2^{\cdot}) are piecewise continuous bounded functions defined on \mathcal{T}^+ (resp. \mathcal{T}^-). They satisfy the same set of equations (7.8)-(7.9) as kernels L_i (except that the coupling terms are now σ_i^{\pm}), with the boundary conditions

$$\begin{aligned} M_1^{+-}(x, x) &= -\frac{\sigma_1^+(x)}{\lambda_1 + \mu_1}, M_1^{-+}(x, x) = \frac{\sigma_1^-(x)}{\lambda_1 + \mu_1}, M_2^{+-}(x, x) = \frac{\sigma_2^+(x)}{\lambda_2 + \mu_2}, \\ M_2^{-+}(x, x) &= -\frac{\sigma_2^-(x)}{\mu_2 + \lambda_2}, M_1^{++}(0, y) = q_{11}M_1^{-+}(0, y), M_1^{--}(0, y) = \frac{1}{q_{11}}M_1^{+-}(0, y), \\ M_2^{++}(1, y) &= \frac{1}{\rho_{22}}M_2^{-+}(1, y), M_2^{--}(1, y) = \rho_{22}M_2^{+-}(1, y). \end{aligned}$$

These two sets of equations admit a unique piecewise continuous solution [VKC11]. Applying the above transforms to both subsystems, we obtain the target system

$$\begin{aligned} \frac{\partial}{\partial t}a_i(t, x) + \lambda_i \frac{\partial}{\partial x}a_i(t, x) &= H_i^a(x)a_1(t, 1) + F_i^a(x)b_2(t, 0) + K_i^a(x)V(t), \\ \frac{\partial}{\partial t}b_i(t, x) - \mu_i \frac{\partial}{\partial x}b_i(t, x) &= H_i^b(x)a_1(t, 1) + F_i^b(x)b_2(t, 0) + K_i^b(x)V(t), \end{aligned} \quad (7.36)$$

with the boundary conditions

$$\begin{aligned} a_1(t, 0) &= q_{11}b_1(t, 0), a_2(t, 0) = q_{22}b_2(t, 0) + q_{21}a_1(t, 1), \\ b_1(t, 1) &= \rho_{11}a_1(t, 1) + \rho_{12}b_2(t, 0) + V(t), b_2(t, 1) = \rho_{22}a_2(t, 1). \end{aligned} \quad (7.37)$$

Denote $(a_i^0(\cdot), b_i^0(\cdot))^\top = \mathcal{M}_i^{-1}((u_i^0(\cdot), v_i^0(\cdot))^\top) \in H^1([0, 1], \mathbb{R}^2)$ the initial conditions associated to (7.36)-(7.37), satisfying the adequate compatibility equations (2.1.1). The in-domain coupling terms $F_i^a, F_i^b, H_i^a, H_i^b$ are defined by the set of equations

$$\begin{aligned} F_1^*(x) + \int_x^1 M_1^{++}(x, \nu)F_1^a(\nu) + M_1^{+-}(x, \nu)F_1^b(\nu)d\nu &= -\mu_1\rho_{12}M_1^-(x, 1), \\ F_2^*(x) + \int_0^x M_2^{++}(x, \nu)F_2^a(\nu) + M_2^{+-}(x, \nu)F_2^b(\nu)d\nu &= \mu_2M_2^-(x, 0) - \lambda_2q_{22}M_2^+(x, 0) \\ H_1^*(x) + \int_x^1 M_1^{++}(x, \nu)H_1^a(\nu) + M_1^{+-}(x, \nu)H_1^b(\nu)d\nu &= \lambda_1M_1^+(x, 1) - \mu_1\rho_{11}M_1^-(x, 1), \\ H_2^*(x) + \int_0^x M_2^{++}(x, \nu)H_2^a(\nu) + M_2^{+-}(x, \nu)H_2^b(\nu)d\nu &= -\lambda_2q_{21}M_2^+(x, 0), \end{aligned} \quad (7.38)$$

with $\cdot = +$ if $*$ = a , and $\cdot = -$ if $*$ = b . The coupling terms K are defined by

$$\begin{pmatrix} K_1^a(x) \\ K_1^b(x) \end{pmatrix} = \mathcal{M}_1^{-1} \left(\begin{pmatrix} -\mu_1 M_1^{+-}(x, 1) \\ -\mu_1 M_1^{-}(x, 1) \end{pmatrix} \right), \quad \begin{pmatrix} K_2^a(x) \\ K_2^b(x) \end{pmatrix} = 0. \quad (7.39)$$

The Volterra integral equations (7.38)-(7.39) admit a unique solution in $L^2([0, 1], \mathbb{R}^4)$. Due to the piecewise continuity of the kernels M^* and the regularizing property of the integral operator, H_i^* , F_i^* , K_1^* are piecewise continuous functions.

Change of variables

Consider a new set of coordinates $(\omega(t, x), \gamma(t, x))$ given by

$$\begin{cases} \omega(t, x) = q_{21} \left(q_{11} \mathbb{1}_{[0, \xi_1]}(x) b_1(t, 1 - \frac{x}{\xi_1}) + \mathbb{1}_{[\xi_1, 1]}(x) a_1(t, \frac{x - \xi_1}{1 - \xi_1}) \right), \\ \gamma(t, x) = \mathbb{1}_{[0, \xi_2]}(x) b_2(t, \frac{x}{\xi_2}) + \mathbb{1}_{[\xi_2, 1]}(x) \rho_{22} a_2(t, \frac{x - 1}{\xi_2 - 1}), \end{cases}$$

with $\xi_i = \frac{\lambda_i}{\lambda_i + \mu_i} = 1 - x_i$. Note that the boundary value in $\gamma(0, t)$ corresponds to $y(t)$. These new variables satisfy the following set of equations

$$\begin{aligned} \frac{\partial}{\partial t} \omega(t, x) + \Lambda_1 \frac{\partial}{\partial x} \omega(t, x) &= H_1(x) \omega(t, 1) + F_1(x) \gamma(t, 0) + K_1(x) V(t), \\ \frac{\partial}{\partial t} \gamma(t, x) - \Lambda_2 \frac{\partial}{\partial x} \gamma(t, x) &= H_2(x) \omega(t, 1) + F_2(x) \gamma(t, 0), \end{aligned} \quad (7.40)$$

where $\Lambda_i = \frac{\mu_i \lambda_i}{\mu_i + \lambda_i}$ is defined in Section 7.2.1, and where the functions verify

$$\begin{aligned} H_1(x) &= q_{11} \mathbb{1}_{[0, \xi_1]}(x) H_1^b(1 - \frac{x}{\xi_1}) + \mathbb{1}_{[\xi_1, 1]}(x) H_1^a(\frac{x - \xi_1}{1 - \xi_1}), \\ F_1(x) &= q_{21} (q_{11} \mathbb{1}_{[0, \xi_1]}(x) F_1^b(1 - \frac{x}{\xi_1}) + \mathbb{1}_{[\xi_1, 1]}(x) F_1^a(\frac{x - \xi_1}{1 - \xi_1})), \\ H_2(x) &= \frac{1}{q_{21}} (\mathbb{1}_{[0, \xi_2]}(x) H_2^b(\frac{x}{\xi_2}) + \mathbb{1}_{[\xi_2, 1]}(x) \rho_{22} H_2^a(\frac{x - 1}{\xi_2 - 1})), \\ F_2(x) &= \mathbb{1}_{[0, \xi_2]}(x) F_2^b(\frac{x}{\xi_2}) + \mathbb{1}_{[\xi_2, 1]}(x) \rho_{22} F_2^a(\frac{x - 1}{\xi_2 - 1}), \\ K_1(x) &= q_{21} (\mathbb{1}_{[0, \xi_1]}(x) q_{11} K_1^b(1 - \frac{x}{\xi_1}) + \mathbb{1}_{[\xi_1, 1]}(x) K_1^a(\frac{x - \xi_1}{1 - \xi_1})). \end{aligned}$$

They satisfy the boundary conditions

$$\begin{aligned} \omega(t, 0) &= \rho_{11} q_{11} \omega(t, 1) + q_{21} \rho_{12} q_{11} \gamma(t, 0) + q_{21} q_{11} V(t), \\ \gamma(t, 1) &= q_{22} \rho_{22} \gamma(t, 0) + \omega(t, 1). \end{aligned} \quad (7.41)$$

7.3.2 . Observer and error state

Definition

In this subsection, we define an observer for the system (7.40)-(7.41), as a copy of the original system with output injection terms (Luenberger-type observer). Note that the measurement $y(t)$ corresponds to $\gamma(t, 0) = b_2(t, 0) = v_2(t, 0)$. The different variable changes turned the measurement at the in-between boundary into a classic measure-

ment at one end of the resulting system. The observer state $(\hat{\omega}, \hat{\gamma})$ satisfies the following set of equations

$$\begin{aligned}\frac{\partial}{\partial t}\hat{\omega}(t, x) + \Lambda_1 \frac{\partial}{\partial x}\hat{\omega}(t, x) &= H_1(x)\hat{\omega}(t, 1) + F_1(x)\hat{\gamma}(t, 0) + G_1(x)(\hat{\gamma}(t, 0) - y(t)) + K_1(x)V(t), \\ \frac{\partial}{\partial t}\hat{\gamma}(t, x) - \Lambda_2 \frac{\partial}{\partial x}\hat{\gamma}(t, x) &= H_2(x)\hat{\omega}(t, 1) + F_2(x)\hat{\gamma}(t, 0) + G_2(\hat{\gamma}(t, 0) - y(t)),\end{aligned}\tag{7.42}$$

with the boundary conditions

$$\begin{aligned}\hat{\omega}(t, 0) &= \rho_{11}q_{11}\hat{\omega}(t, 1) + q_{21}\rho_{12}q_{11}\gamma(t, 0) + q_{21}q_{11}V(t), \\ \hat{\gamma}(t, 1) &= q_{22}\rho_{22}\gamma(t, 0) + \hat{\omega}(t, 1).\end{aligned}\tag{7.43}$$

Define the error state $(\tilde{\omega}, \tilde{\gamma}) = (\omega, \gamma) - (\hat{\omega}, \hat{\gamma})$ satisfying

$$\begin{aligned}\frac{\partial}{\partial t}\tilde{\omega}(t, x) + \Lambda_1 \frac{\partial}{\partial x}\tilde{\omega}(t, x) &= \tilde{H}_1(x)\tilde{\omega}(t, 1) + \tilde{G}_1(x)\tilde{\gamma}(t, 0), \\ \frac{\partial}{\partial t}\tilde{\gamma}(t, x) - \Lambda_2 \frac{\partial}{\partial x}\tilde{\gamma}(t, x) &= \tilde{H}_2(x)\tilde{\omega}(t, 1) + \tilde{G}_2(x)\tilde{\gamma}(t, 0),\end{aligned}\tag{7.44}$$

where $\tilde{G}_i \doteq F_i + G_i$ are two bounded piecewise continuous functions defined on $[0, 1]$, and the boundary conditions

$$\tilde{\omega}(t, 0) = \rho_{11}q_{11}\tilde{\omega}(t, 1), \quad \tilde{\gamma}(t, 1) = \tilde{\omega}(t, 1).\tag{7.45}$$

We aim to determine the gains \tilde{G}_i such that (7.44)-(7.45) is exponentially stable.

Operator framework

We rewrite system (7.44)-(7.45) in the abstract form

$$\frac{d}{dt} \begin{pmatrix} \tilde{\omega} \\ \tilde{\gamma} \end{pmatrix} = \tilde{A} \begin{pmatrix} \tilde{\omega} \\ \tilde{\gamma} \end{pmatrix} + \mathcal{G}\tilde{C} \begin{pmatrix} \tilde{\omega} \\ \tilde{\gamma} \end{pmatrix},$$

where the operator \tilde{A} is defined by

$$\tilde{A} : \begin{pmatrix} \tilde{\omega} \\ \tilde{\gamma} \end{pmatrix} \mapsto \begin{pmatrix} -\Lambda_1 \frac{\partial \tilde{\omega}}{\partial x} + H_1(\cdot)\tilde{\omega}(1) \\ \Lambda_2 \frac{\partial \tilde{\gamma}}{\partial x} + H_2(\cdot)\tilde{\omega}(1) \end{pmatrix}, \tag{7.46}$$

with $D(\tilde{A}) = \{(\tilde{\omega}, \tilde{\gamma}) \in H^1([0, 1], \mathbb{R}^2) \mid \tilde{\omega}(0) = \rho_{11}q_{11}\tilde{\omega}(1), \tilde{\gamma}(1) = \tilde{\omega}(1)\}$. The operator \tilde{A} is well-posed and densely defined [BC16]. We can already draw a parallel with the definition of the operator \tilde{A} in (7.46) and the adjoint operator A^* defined in Section 7.2 by (7.22). The trace operator \tilde{C} and operator \mathcal{G} are defined by

$$\tilde{C} : \begin{pmatrix} \tilde{\omega} \\ \tilde{\gamma} \end{pmatrix} \mapsto \tilde{\gamma}(0), \quad \mathcal{G} : \begin{matrix} D(\tilde{A}) \subset H^1([0, 1], \mathbb{R}^2) \rightarrow \mathbb{R} \\ \mathbb{R} \rightarrow C_{pw}^0([0, 1], \mathbb{R}^2) \\ x \mapsto \begin{pmatrix} \tilde{G}_1(\cdot) \times x \\ \tilde{G}_2(\cdot) \times x \end{pmatrix} \end{matrix}. \tag{7.47}$$

Spectral observability condition

Similarly to what has been done in Section 7.2.2, we need to formulate an observability assumption to guarantee the possibility of estimating the PDE states.

Assumption 7.3.1 *The operators \tilde{A} and \tilde{C} respectively defined in (7.46) and (7.47) satisfy for any $s \in \mathbb{C}$, $\ker(s - \tilde{A}) \cap \ker(\tilde{C}) = \{0\}$.*

This is analogous to the *controllability* Assumption 7.2.1. Rewriting equations (7.40) in the time-delay framework, it can be similarly reformulated using the holomorphic functions

$$\begin{aligned}\tilde{F}_1(s) &= 1 - \rho_{11}q_{11}e^{-\delta_1 s} - \int_0^{\delta_1} H_1(\Lambda_1\nu)e^{(\nu-\delta_1)s} d\nu, \\ \tilde{F}_2(s) &= e^{-\delta_2 s} + e^{\delta_2 s} \int_0^{\delta_2} H_2(\Lambda_2\nu)e^{-\nu s} d\nu.\end{aligned}$$

Using the variation of constant formula, and taking the Laplace transform in (7.46), we obtain $\tilde{\omega}(1)\tilde{F}_1(s) = \tilde{\omega}(1)\tilde{F}_2(s) = 0$. We have

Assumption 7.3.2 spectral observability *For all $s \in \mathbb{C}$, $\text{rank}[\tilde{F}_1(s), \tilde{F}_2(s)] = 1$.*

Similarly to what has been done before, Assumption 7.3.2 implies 7.3.1.

7.3.3 . Constructive design of the observer gains

In this section, we design the observer gains \tilde{G}_1, \tilde{G}_2 to stabilize the error system (7.44)-(7.45). First, we use a Fredholm integral transform to map it to an exponentially stable target system. We give the equations satisfied by the kernels of this transformation. Assuming the transformation is well-defined, we prove its invertibility using the operator framework. Finally, we show that the existence of solutions for some integral equations implies the existence of the kernels defining the Fredholm integral transform.

Presentation of the target system

Consider the target system

$$\frac{\partial}{\partial t}\tilde{\zeta}(t, x) + \Lambda_1 \frac{\partial}{\partial x}\tilde{\zeta}(t, x) = 0, \quad \frac{\partial}{\partial t}\tilde{\eta}(t, x) - \Lambda_2 \frac{\partial}{\partial x}\tilde{\eta}(t, x) = 0, \quad (7.48)$$

with the boundary conditions

$$\tilde{\zeta}(t, 0) = \rho_{11}q_{11}\tilde{\zeta}(t, 1), \quad \tilde{\eta}(t, 1) = \tilde{\zeta}(t, 1). \quad (7.49)$$

Denote $(\tilde{\zeta}^0, \tilde{\eta}^0) \in H^1([0, 1], \mathbb{R}^2)$ the initial conditions associated to (7.48) satisfying the compatibility conditions (2.1.1) ((7.49) for $t = 0$). The well-posedness of the error system (7.48)-(7.49) implies the one of the error system (7.42)-(7.43) and consequently of the observer system (7.44)-(7.45). This target system (7.48)-(7.49) is exponentially stable in the sense of the L^2 -norm, since $|\rho_{11}q_{11}| < 1$ by Assumption 7.1.3 [BC16]. Define now the Fred-

holm integral transform \mathcal{K} of the form (7.24), such that $\begin{pmatrix} \tilde{\zeta} \\ \tilde{\eta} \end{pmatrix} = \mathcal{K} \begin{pmatrix} \tilde{\omega} \\ \tilde{\gamma} \end{pmatrix}$. More precisely,

we have

$$\begin{cases} \tilde{\zeta}(t, x) = \tilde{\omega}(t, x) - \int_0^1 K^{++}(x, \nu)\tilde{\omega}(t, \nu) + K^{+-}(x, \nu)\tilde{\gamma}(t, \nu)d\nu, \\ \tilde{\eta}(t, x) = \tilde{\gamma}(t, x) - \int_0^1 K^{-+}(x, \nu)\tilde{\omega}(t, \nu) + K^{--}(x, \nu)\tilde{\gamma}(t, \nu)d\nu, \end{cases} \quad (7.50)$$

where $K^{\cdot\cdot}$ are four bounded piecewise continuous functions defined on \mathcal{S} .

Kernel equations

Following the backstepping methodology, we show that the kernels $K^{\cdot\cdot}$ must satisfy

$$\begin{aligned} \frac{\partial}{\partial x}K^{++}(x, y) + \frac{\partial}{\partial y}K^{++}(x, y) = 0, \quad \frac{\partial}{\partial x}K^{+-}(x, y) - \frac{\Lambda_2}{\Lambda_1}\frac{\partial}{\partial y}K^{+-}(x, y) = 0, \\ \frac{\partial}{\partial x}K^{-+}(x, y) - \frac{\Lambda_1}{\Lambda_2}\frac{\partial}{\partial y}K^{-+}(x, y) = 0, \quad \frac{\partial}{\partial x}K^{--}(x, y) + \frac{\partial}{\partial y}K^{--}(x, y) = 0, \end{aligned} \quad (7.51)$$

where we have

$$\begin{aligned} H_1(x) + \Lambda_1(K^{++}(x, 1) - \rho_{11}q_{11}K^{++}(x, 0)) - \Lambda_2K^{+-}(x, 1) \\ = \int_0^1 K^{++}(x, \nu)H_1(\nu) + K^{+-}(x, \nu)H_2(\nu)d\nu, \\ H_2(x) + \Lambda_1(K^{-+}(x, 1) - \rho_{11}q_{11}K^{-+}(x, 0)) - \Lambda_2K^{--}(x, 1) \\ = \int_0^1 K^{-+}(x, \nu)H_1(\nu) + K^{--}(x, \nu)H_2(\nu)d\nu, \end{aligned} \quad (7.52)$$

and the boundary conditions

$$\begin{aligned} K^{++}(0, y) = \rho_{11}q_{11}K^{++}(1, y), \quad K^{+-}(0, y) = \rho_{11}q_{11}K^{+-}(1, y), \\ K^{-+}(1, y) = K^{-+}(1, y), \quad K^{--}(1, y) = K^{+-}(1, y). \end{aligned} \quad (7.53)$$

To these conditions, we add the two following boundary conditions,

$$K^{-+}(0, y) = 0, \quad K^{--}(0, y) = 0. \quad (7.54)$$

The boundary conditions (7.54) are necessary to ensure that condition (b) of Lemma 7.2.1 is satisfied for the operator \mathcal{K} . If we manage to show that (7.51)-(7.54) admit a solution, we will be able to prove that (7.44)-(7.45) can be mapped to (7.48)-(7.49). Indeed, differentiating (7.50) with respect to time and space, integrating by parts, and using the fact that the state $(\tilde{\omega}, \tilde{\gamma})$ verifies (7.44)-(7.45), we directly obtain the target system (7.48)-(7.49).

Well-posedness of kernel equations

Theorem 7.3.1: Well-posedness of the kernel equations

The set of equations (7.51)-(7.54) admits a unique solution in $C_{pw}^0(\mathcal{S}, \mathbb{R}^{2 \times 2})$.

Proof : The proof is similar to the one of Theorem 7.2.3 given in Appendix B. Indeed, let us define the kernels

$\tilde{N}^{\cdot\cdot}$ on \mathcal{S} by

$$\begin{aligned}\tilde{N}^{++}(x, y) &= K^{++}(1 - y, 1 - x), & \tilde{N}^{+-}(x, y) &= \frac{\Lambda_1}{\Lambda_2} K^{+-}(1 - y, 1 - x), \\ \tilde{N}^{-+}(x, y) &= \frac{\Lambda_2}{\Lambda_1} K^{-+}(1 - y, 1 - x), & \tilde{N}^{--}(x, y) &= K^{--}(1 - y, 1 - x).\end{aligned}\quad (7.55)$$

The kernels $\tilde{N}^{\cdot\cdot}$ satisfy the same set of PDEs (7.29)-(7.30) than kernels $N^{\cdot\cdot}$ (that define the invertible Fredholm integral transform \mathcal{N} (7.26)). Moreover, they satisfy the same boundary conditions (7.31), (7.32) and (7.34), the only difference being the name of the coupling coefficient (q'_{22} or $\rho_{11}q_{11}$), that are both strictly less than 1 by Assumption 7.1.3. Finally, the kernels $\tilde{N}^{\cdot\cdot}$ satisfy similar integral equations

$$\begin{aligned}\tilde{N}_w(y) - \int_0^1 \tilde{N}_w(\nu)\tilde{N}^{++}(\nu, y) + \tilde{N}_z(\nu)\tilde{N}^{-+}(\nu, y)d\nu \\ &= -\tilde{N}^{++}(0, y) + \tilde{N}^{-+}(0, y) + \rho_{11}q_{11}\tilde{N}^{++}(1, y), \\ \tilde{N}_z(y) - \int_0^1 \tilde{N}_w(\nu)\tilde{N}^{+-}(\nu, y) + \tilde{N}_z(\nu)\tilde{N}^{--}(\nu, y)d\nu \\ &= -\tilde{N}^{+-}(0, y) + \tilde{N}^{--}(0, y) + \rho_{11}q_{11}\tilde{N}^{+-}(1, y),\end{aligned}$$

with $\tilde{N}_w(y) \doteq \frac{1}{\Lambda_1} H_1(1 - y)$ and $\tilde{N}_z(y) \doteq \frac{1}{\Lambda_2} H_2(1 - y)$. Under the spectral observability Assumption 7.3.1, we prove the well-posedness and the existence of kernels $\tilde{N}^{\cdot\cdot}$ on \mathcal{S} , following the approach presented in Section 7.2.3. Since the change of variables (7.55) is invertible, we immediately state the well-posedness of (7.51)-(7.54). Since we have $(H_1, H_2) \in C_{pw}^0([0, 1], \mathbb{R}^2)$, and due to the regularizing properties of the integral operator, the kernel equations (7.51)-(7.54) admit a unique piecewise continuous solution on \mathcal{S} . ■

Invertibility of the Fredholm transform

Similarly to what was done in Section 7.2.4, we have the following:

Theorem 7.3.2: Invertibility of integral operator \mathcal{K}

The Fredholm integral transform \mathcal{K} with kernels defined by (7.51)-(7.54) is invertible.

Proof : We show that this operator satisfies the conditions of Lemma 7.2.1. Since operator \mathcal{K} is of form (7.24) with

$$K(x, y) = \begin{pmatrix} K^{++}(x, y) & K^{+-}(x, y) \\ K^{-+}(x, y) & K^{--}(x, y) \end{pmatrix},$$

we can use Lemma 7.2.1 to show its invertibility. Condition (d) is given by Assumption 7.3.2. The boundary conditions (7.53)-(7.54) imply that conditions (a) – (b) hold. Condition (c) is a direct consequence of (7.51)-(7.52) and assumptions (a) – (b). ■

Definition of the observer gains

Following the backstepping procedure, we obtain the expressions of the observer gains \tilde{G}_i . Indeed, in order to map the original system (7.44)-(7.45) to the target system (7.48)-(7.49), the observer gains must satisfy the integral equations

$$\begin{aligned}\tilde{G}_1(x) - \int_0^1 K^{++}(x, \nu)\tilde{G}_1(\nu) + K^{+-}(x, \nu)\tilde{G}_2(\nu)d\nu &= -\Lambda_2 K^{+-}(x, 0), \\ \tilde{G}_2(x) - \int_0^1 K^{-+}(x, \nu)\tilde{G}_1(\nu) + K^{--}(x, \nu)\tilde{G}_2(\nu)d\nu - \Lambda_2 K^{--}(x, 0), \\ \iff \mathcal{K}\left(\begin{pmatrix} \tilde{G}_1(x) \\ \tilde{G}_2(x) \end{pmatrix}\right) &= \begin{pmatrix} -\Lambda_2 K^{+-}(x, 0) \\ -\Lambda_2 K^{--}(x, 0) \end{pmatrix}.\end{aligned}\quad (7.56)$$

Since \mathcal{K} is invertible, the observer gains \tilde{G}_1 and \tilde{G}_2 defined by (7.56) exist and are uniquely defined as piecewise continuous functions on $[0, 1]$. They satisfy

$$\begin{pmatrix} \tilde{G}_1(x) \\ \tilde{G}_2(x) \end{pmatrix} = \mathcal{K}^{-1} \begin{pmatrix} -\Lambda_2 K^{+-}(x, 0) \\ -\Lambda_2 K^{--}(x, 0) \end{pmatrix}, \forall x \in [0, 1].$$

7.3.4 . Convergence of the observer state

We can now show the convergence of the observer state $(\hat{\omega}, \hat{\gamma})$ to the real state (ω, γ) . First, we have the following:

Lemma 7.3.1: Exponential stability of the error system

Any solution $(\hat{\omega}, \hat{\gamma})$ of (7.44)-(7.45) converges to zero in the sense of the L^2 -norm.

Proof : System (7.48)-(7.49) is exponentially stable in the sense of the L^2 -norm. Since the backstepping transform \mathcal{K} is bounded and invertible by Theorem 7.3.2, system (7.44)-(7.45) shares equivalent stability properties. ■

Thus, the error system (7.44)-(7.45) is exponentially stable. The observer state (7.42)-(7.43) defined with gains $G_i = \tilde{G}_i - F_i$ converges towards the initial state (ω, γ) . We then define observer states for (a_i, b_i) by

$$\begin{aligned} \hat{a}_1(t, x) &= \frac{1}{q_{21}} \hat{\omega}(t, \xi_1 + (1 - \xi_1)x), \quad \hat{a}_2(t, x) = \frac{1}{\rho_{22}} \hat{\gamma}(t, 1 - (1 - \xi_2)x), \\ \hat{b}_1(t, x) &= \frac{1}{q_{21}q_{11}} \hat{\omega}(t, \xi_1(1 - x)), \quad \hat{b}_2(t, x) = \hat{\gamma}(t, \xi_2x). \end{aligned}$$

We have the following theorem:

Theorem 7.3.3: Convergence of the estimates

The state estimates defined by $\begin{pmatrix} \hat{u}_i \\ \hat{v}_i \end{pmatrix} = \mathcal{M}_i \begin{pmatrix} \hat{a}_i \\ \hat{b}_i \end{pmatrix}$ converge exponentially towards the original states (u_i, v_i) in the sense of the L^2 -norm.

Proof : It is a direct consequence of the properties of the Volterra integral transforms \mathcal{M}_i . ■

7.4 . Output-Feedback control law

We can now combine the state observer designed in Section 7.3 with the full state feedback control law $V(t)$ designed in Section 7.2.5, to obtain an output feedback controller. We can state the main theorem of this chapter

Theorem 7.4.1: Stabilizing output-feedback controller

The output-feedback control law $\hat{V}(\hat{u}_1(\cdot), \hat{u}_2(\cdot), \hat{v}_1(\cdot), \hat{v}_2(\cdot))$ defined by

$$\hat{V}(t) = \frac{1}{q_{11}} \hat{V}_S(t) - \rho_{12} y(t) - \rho_{11} \hat{u}_1(t, 1), \quad (7.57)$$

$$\text{with } \hat{V}_S(t) = -\frac{1}{q_{12}} \int_0^1 \begin{pmatrix} x_2 \check{N}^{-+}(1, x_2 \nu) \\ (1 - x_2) \check{N}^{-+}(1, 1 - (1 - x_2) \nu) \end{pmatrix}^\top \mathcal{L}_2^{-1} \begin{pmatrix} \hat{u}_2(t, \nu) \\ \hat{v}_2(t, \nu) \end{pmatrix} d\nu \\ + \int_0^1 \begin{pmatrix} L_1^{-+}(1, \nu) - x_1 \check{N}^{-+}(1, x_1(1 - \nu)) \\ L_1^{-+}(1, \nu) - (1 - x_1) \check{N}^{-+}(1, x_1 + (1 - x_1) \nu) \end{pmatrix}^\top \mathcal{L}_1^{-1} \begin{pmatrix} \hat{u}_1(t, \nu) \\ \hat{v}_1(t, \nu) \end{pmatrix} d\nu$$

exponentially stabilizes system (5.1)-(7.2) in the sense of the L^2 -norm.

Proof : Similarly to what has been done in [LADMA18], we define $(\tilde{u}_i, \tilde{v}_i) = (\hat{u}_i - u_i + u_i, \hat{v}_i - v_i + v_i) = (-\tilde{u}_i + u_i, -\tilde{v}_i + v_i)$. By linearity of the integral operators, we obtain

$$\hat{V}(t) = V(t) + \tilde{V}(t), \quad (7.58)$$

where $\tilde{V}(t) = -\frac{1}{q_{11}} \hat{V}_S(t) + \rho_{11} \tilde{u}_1(t, 1)$, is the difference between the output feedback law and the previously designed state feedback law. By Lemma 7.3.1, and since the integral control operator is bounded, we have $|\hat{V}_S(t)| \xrightarrow{t \rightarrow \infty} 0$ and $\|\tilde{u}_1(t)\|_{L^2} \xrightarrow{t \rightarrow \infty} 0$ as the error states converge to zero. Thus, the term $\tilde{V}(t)$ can be seen as a disturbance that converges to zero. Using Theorem 7.2.4, and the input-to-state stability of the system (as it is done in [ADM20, LADMA18] for two equations), we can conclude to the exponential stability of the system. Indeed, the closed-loop system would rewrite as a neutral system subject to a disturbance that goes to zero [ADM19]. Applying the variations of constants formula yields the expected result. ■

7.5 . Simulation results

We conclude this chapter with some simulation results to illustrate the relevance of the proposed output-feedback controller. First, the parameters are chosen such that the interconnected systems are highly unstable in open-loop, and Assumptions 7.1.1-7.1.3 are satisfied. Their numerical values are given in Table 7.1.

Param.	Value	Param.	Value	Param.	Value	Param.	Value
λ_1	1.5	λ_2	1.2	q_{11}	1	ρ_{11}	0.3
μ_1	1.3	μ_2	1.8	q_{21}	0.6	ρ_{12}	0.8
σ_1^+	-0.2	σ_2^+	-0.3	q_{22}	0.9	ρ_{22}	0.9
σ_1^-	0.4	σ_2^-	0.7				

Table 7.1 – Parameters used for simulation

The initial conditions of the states are affine functions satisfying the compatibility conditions. The observer values are initialized to 0. As illustrated in Figure 7.6, the L^2 -norm of the open-loop system diverges.

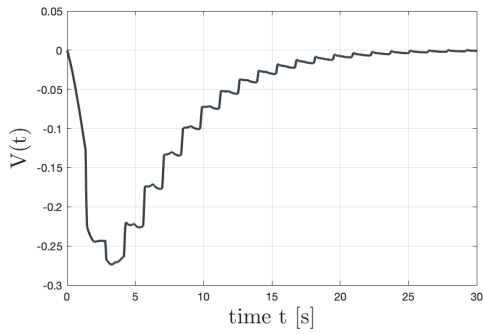


Figure 7.4 – Evolution of control effort $V(t)$

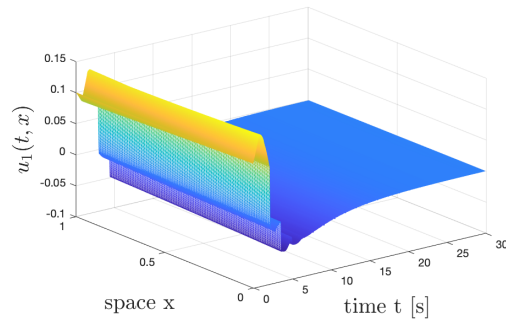


Figure 7.5 – Evolution of $u_1(t, x)$

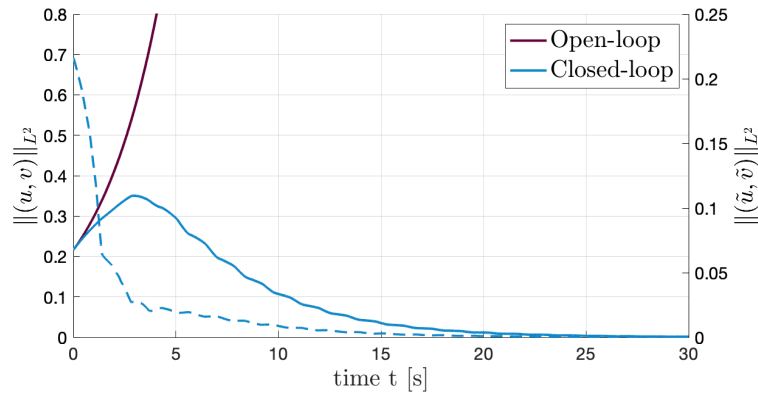


Figure 7.6 – Evolution of the L^2 -norm of state and error

Beforehand, the kernel of the invertible Volterra transforms $\mathcal{L}_i, \mathcal{M}_i$ and Fredholm transforms \mathcal{N}, \mathcal{K} (and their inverse) are computed using the successive approximation technique [ADM16], with a precision $\epsilon = 10^{-10}$, on a space mesh with $n_x = 101$ points. It takes about 450s to converge, which could not be achieved if Assumption 7.2.2 was unsatisfied. As represented in Figure 7.7, they show discontinuities along some specific characteristic lines given in the proof of Theorem 7.2.3. Then, the functions H_i^*, F_i^*, K_i^*, G_i are computed using the same method. The integral terms are approximated using a trapezoidal method. As illustrated in Figure 7.7b, they are continuous on $[0, 1]$.

Next, we can simulate the evolution of the system $(u_i, v_i)_{i \in \{1,2\}}$ on Matlab using the classic finite volume method based on a Godunov scheme [LeVo2], on a 30s timescale. As illustrated in Figure 7.6, the parameters are chosen such that the whole interconnected system remains unstable in open-loop. In the presence of the control law (7.57) represented in Figure 7.4, the system (u, v) becomes exponentially stable. The evolution of component $u_1(t, x)$ is given in Figure 7.5. As illustrated in Figure 7.6, its L^2 -norm converges to zero as expected. The control input represented on the right converges to zero. In figure 7.6 (dotted line), we also represent the performance of our observer design: the L^2 -norm of the error state (\tilde{u}, \tilde{v}) converges to zero, such that the estimation converges towards the actual value as expected.

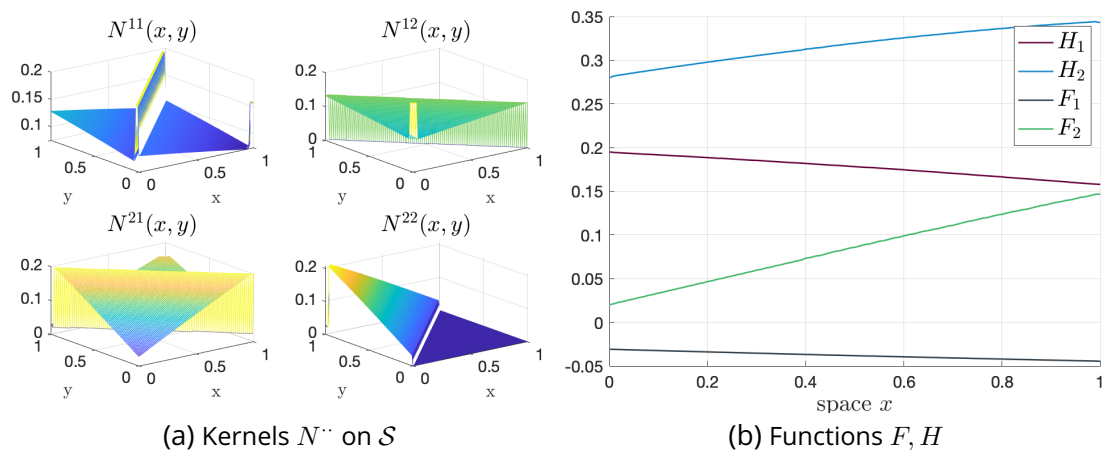


Figure 7.7 – Illustration of kernel computations

Conclusion

This chapter presented a novel methodology for stabilizing a chain of two interconnected hyperbolic PDE subsystems. The actuator and measurement are located at the in-between boundary. The proposed approach involved designing a full-state feedback controller using classic Volterra transforms and a change of variables to rewrite the chain as a scalar hyperbolic system. We then followed the backstepping approach to map this PDE system to a simple (exponentially stable) target system. However, we encountered a challenge in the configuration considered herein as it required a Fredholm transform, which is not always invertible, unlike the commonly used Volterra transforms. To address this challenge, we demonstrated the invertibility of the Fredholm transform using an operator framework inspired by the work of [CHO16]. We also proved the well-posedness of the kernels defining the Fredholm transform using similar ideas. Finally, we applied a similar approach to design a state observer, which resulted in an output-feedback controller that was tested using numerical simulations.

Next, in Chapter 8, we show how this strategy can be adapted for the in-domain stabilization of a clamped string. Finally, as presented in the perspectives ending Part III, the proposed approach paves the way for future contributions to networks with actuation inside the graph structure. We believe it could be combined with results from Part II to tackle a wider diversity of physical systems with an arbitrary number of PDEs or ODEs. It is also a milestone toward the stabilization of under-actuated systems.

8 - Application to the stabilization of a clamped string

In this chapter, we apply the control strategy presented in Chapter 7 to the case of a clamped string with actuation inside the domain. Using the Riemann invariants of the energy states, we reformulate it as a chain of two coupled hyperbolic subsystems with actuation at the in-between boundary. The resulting system differs from (5.1)-(7.2) since the control input appears at the in-between boundary of both subsystems. However, after applying successive transforms, it is shown to be equivalent to stabilizing a neutral-type delay-differential equation. We can therefore use (7.17)-(7.19) as a *comparison system* and derive a suitable controller from the methodology presented in Chapter 7.

Chapitre 8: Application au contrôle au milieu d'une corde fixée en une extrémité. Dans ce chapitre, nous adaptons la stratégie de commande présentée au chapitre 7 au cas d'une corde fixée en un point avec actionnement à l'intérieur du domaine. Ce problème peut être reformulé comme la stabilisation d'une chaîne de deux sous-systèmes hyperboliques couplés avec actionnement à la frontière au milieu. Le système résultant diffère de (5.1)-(7.2) en ce que la loi de commande apparaît à la frontière intermédiaire entre les deux sous-systèmes. Cependant, après application de transformations successives, on montre que la stabilisation de ce système revient à celle d'une équation différentielle à retard de type neutre. Nous pouvons donc utiliser (7.17)-(7.19) comme *système de comparaison* et déduire un contrôleur approprié à partir de la méthodologie présentée au chapitre précédent.

Contents

8.1 System under consideration	150
8.1.1 Vibrating string model	150
8.1.2 Control objective	151
8.1.3 Reformulation as interconnected hyperbolic systems . . .	151
8.2 Controller design	153
8.2.1 Application of the backstepping methodology	153
8.2.2 Reformulation as a time delay system	155
8.2.3 Application of the control strategy	158
8.3 Simulation results	161

The results given herein were presented in:

- Jeanne Redaud, and Jean Auriol. "Backstepping stabilization of a clamped string with actuation inside the domain" (2023). 22nd IFAC World Congress.

8.1 . System under consideration

8.1.1 . Vibrating string model

Consider a vibrating string of length $\ell = 1$, clamped at one end ($x = 0$) and free at the other ($x = 1$). We assume that the actuator imparts a compressive stress in a pointwise location inside the domain $x_0 \in (0, 1)$. It is shown schematically in Figure 8.1.

Denote $w(t, x)$ the lateral displacement of the string from a steady-state reference position. The space and time variables are evolving in $[0, +\infty) \times [0, 1]$. Its dynamics are derived from Hooke's law.

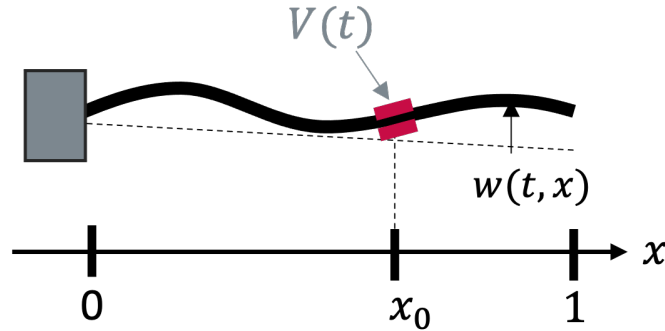


Figure 8.1 – Schematic representation of system (8.1)-(8.3)

The string parameters are ρ the mass density, c characterizing some in-domain damping, and E the Young's modulus. We only consider the case where the transport delays on both sides of the actuator are equal, corresponding to actuation in the middle of the beam $x_0 = \frac{1}{2}$, but still, present the more general equations. The displacement $w(t, x)$ satisfies the following PDE

$$\frac{\partial^2}{\partial t^2} w(t, x) = \frac{E}{\rho} \frac{\partial^2}{\partial x^2} (w(t, x)) - c \frac{\partial}{\partial t} w(t, x). \quad (8.1)$$

The first end of the string is clamped, while the opposite end is free. The boundary conditions therefore read

$$\frac{\partial w}{\partial t} \Big|_{x=0}(t) = 0, \quad E \frac{\partial w}{\partial x} \Big|_{x=1}(t) = 0. \quad (8.2)$$

Two additional constraints are derived from the continuity of speed $x = x_0$, and a discontinuity in force due to the presence of the control input

$$\frac{\partial w}{\partial t} \Big|_{x=x_0^-}(t) = \frac{\partial w}{\partial t} \Big|_{x=x_0^+}(t), \quad \frac{\partial w}{\partial x} \Big|_{x_0^-}(t) = \frac{V(t)}{E} + \frac{\partial w}{\partial x} \Big|_{x_0^+}(t). \quad (8.3)$$

The initial position and velocity of the string are given by $(w(x, 0) = w_0(x), w_t(x, 0) = w_1(x)) \in H^1([0, 1], \mathbb{R}) \times H^1([0, 1], \mathbb{R})$ and satisfy adequate compatibility conditions (2.1.1) ((8.2)-(8.3) for $t = 0$).

8.1.2 . Control objective

Define the strain $X_1(t, x) = \frac{\partial w}{\partial x}(t, x)$ and momentum $X_2(t, x) = \rho(x) \frac{\partial w}{\partial t}(t, x)$ of the string. The control objective reads as follows:

Objective 8.1.1: Exponential stabilization of the energy

Design an output-feedback control law $V(t)$ such that there exist $C, \nu > 0, \forall t > 0$, for all initial conditions $(X_1)_0(x) = w'_0(x)$ and $(X_2)_0(x) = \rho(x)w_1(x)$, we have

$$\|(X_1(t), X_2(t))\|_{L^2} \leq Ce^{-\nu t} \|(X_1)_0, (X_2)_0\|_{L^2}. \quad (8.4)$$

In the case $c \geq 0$ under consideration, the open-loop system is naturally exponentially stable. However, we can use the control input $V(t)$ to fasten the convergence of the string to its reference position. In a general wave equation stemming from the linearization of an unstable system ($c < 0$), the control input can be used for stabilization purposes.

The strategy reads as follows

1. We use a first change of variables to rewrite the energy states (X_1, X_2) in *Riemann* coordinates. The new states (ξ^+, ξ^-) satisfy transport equations with in-domain couplings. The ones on the diagonal are removed using an exponential change of variables. The new states are denoted $(\bar{\xi}^+, \bar{\xi}^-)$ (Section 8.1.3).
2. We use two classic Volterra integral transforms to map $(\bar{\xi}^+, \bar{\xi}^-)$ to a simpler target system (γ^+, γ^-) . The in-domain couplings have been moved to the actuated boundary $x = x_0$ (Section 8.2.1). The interconnected system differs from (5.1)-(7.2) since the control input appears at the in-between boundary of both subsystems.
3. Using the method of characteristics, we derive the integral delay equations satisfied by the boundary states (Section 8.2.2). We show their stabilization is closely related to the one of a *comparison system* of the form (7.17)-(7.19). We can apply the stability results from Chapter 7 under a specific controllability condition. We determine the stabilizing feedback law (Section 8.2.3).

8.1.3 . Reformulation as interconnected hyperbolic systems

From now on, we decompose the space domain into two intervals $\mathcal{I}_1 \doteq [0, x_0)$ and $\mathcal{I}_2 \doteq [x_0, 1]$. The restriction of the displacement w on \mathcal{I}_1 (resp. \mathcal{I}_2) is denoted with subscript \cdot_1 (resp. \cdot_2). We first rewrite system (8.1) in Riemann coordinates. Denote $\lambda = \sqrt{\frac{E}{\rho}}$, $\eta = \sqrt{E\rho}$, and the invertible matrix $Q_1 = \frac{1}{\sqrt{2}} \begin{pmatrix} 1 & \frac{1}{\eta} \\ -\eta & 1 \end{pmatrix}$. The *Riemann variables* are defined by

$$\forall (t, x) \in [0, +\infty) \times [0, 1], \begin{pmatrix} \xi^+(t, x) \\ \xi^-(t, x) \end{pmatrix} = Q_1^{-1} \begin{pmatrix} X_1(t, x) \\ X_2(t, x) \end{pmatrix}.$$

The exponential stability of the state (X_1, X_2) is equivalent to the one of (ξ^+, ξ^-) . Each subsystem $i \in \{1, 2\}$ satisfies

$$\frac{\partial}{\partial t} \xi_i^+(t, x) + \lambda \frac{\partial}{\partial x} \xi_i^+(t, x) = \sigma^{++} \xi_i^+(t, x) + \sigma^{+-} \xi_i^-(t, x), \quad (8.5)$$

$$\frac{\partial}{\partial t} \xi_i^-(t, x) - \lambda \frac{\partial}{\partial x} \xi_i^-(t, x) = \sigma^{-+} \xi_i^+(t, x) + \sigma^{--} \xi_i^-(t, x), \quad (8.6)$$

with boundary conditions

$$\begin{aligned} \xi_1^+(t, 0) &= \eta^{-1} \xi_1^-(t, 0), \quad \xi_2^-(t, 1) = -\eta \xi_2^+(t, 1), \\ \xi_1^-(t, x_0) &= \frac{1}{\sqrt{2\lambda}} V(t) + \xi_2^-(t, x_0), \quad \xi_2^+(t, x_0) = \xi_1^+(t, x_0) - \frac{1}{\sqrt{2E}} V(t). \end{aligned} \quad (8.7)$$

The in-domain couplings $\sigma^{\cdot\cdot}$ are identical for both subsystems, and given by

$$\sigma^{++} = -\frac{c}{2}, \quad \sigma^{+-} = \frac{c}{2\eta}, \quad \sigma^{-+} = \frac{\eta c}{2}, \quad \sigma^{--} = -\frac{c}{2}.$$

The interconnected system is schematically represented in Figure 8.2.

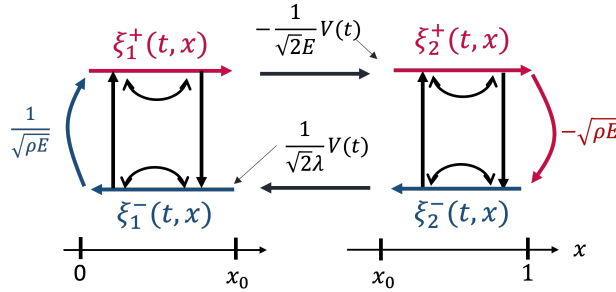


Figure 8.2 – Schematic representation of system (8.5)-(8.7)

The initial conditions associated to the interconnected system (8.5)-(8.7) are H^1 functions. With the appropriate compatibility conditions (2.1.1), the open-loop system is well-posed [BC16].

To rewrite the system as a time-delay system, we first use an exponential change of variables [HVDKM15] to remove the in-domain couplings $\sigma^{\pm\pm}$, as explained in Section 2.1.1. Define $I_0(x) = \frac{cx}{2\lambda}$, $I_1(x) = \frac{1-x}{2} \frac{c}{\lambda}$, and the new sets of variables $\bar{\xi}_1^-(t, x)$ and $\bar{\xi}_2^-(t, x)$ as

$$\begin{pmatrix} \bar{\xi}_1^+ \\ \bar{\xi}_1^- \end{pmatrix} = \begin{pmatrix} e^{I_0(x)} & 0 \\ 0 & e^{-I_0(x)} \end{pmatrix} \begin{pmatrix} \xi_1^+ \\ \xi_1^- \end{pmatrix}, \quad \begin{pmatrix} \bar{\xi}_2^+ \\ \bar{\xi}_2^- \end{pmatrix} = \begin{pmatrix} e^{-I_1(x)} & 0 \\ 0 & e^{I_1(x)} \end{pmatrix} \begin{pmatrix} \xi_2^+ \\ \xi_2^- \end{pmatrix}. \quad (8.8)$$

By applying this change of variables to system (8.5)-(8.7), the new states satisfy

$$\begin{aligned} \frac{\partial}{\partial t} \bar{\xi}_i^+(t, x) + \lambda \frac{\partial}{\partial x} \bar{\xi}_i^+(t, x) &= \bar{\sigma}_i^+(x) \bar{\xi}_i^-(t, x), \\ \frac{\partial}{\partial t} \bar{\xi}_i^-(t, x) - \lambda \frac{\partial}{\partial x} \bar{\xi}_i^-(t, x) &= \bar{\sigma}_i^-(x) \bar{\xi}_i^-(t, x), \end{aligned} \quad (8.9)$$

and boundary conditions

$$\begin{aligned} \bar{\xi}_1^+(t, 0) &= \eta^{-1} \bar{\xi}_1^-(t, 0), \quad \bar{\xi}_2^-(t, 1) = -\eta \bar{\xi}_2^+(t, 1), \\ \bar{\xi}_1^-(t, x_0) &= -\alpha U^+(t) + q^- \bar{\xi}_2^-(t, x_0), \quad \bar{\xi}_2^+(t, x_0) = q^+ \bar{\xi}_1^+(t, x_0) + U^+(t), \end{aligned} \quad (8.10)$$

with $U^+(t) = -1/(\sqrt{2E})e^{-I_1(x_0)}V(t)$, $q^+ = e^{-I_0(1)} = q^-$ and $\alpha = \sqrt{E\rho} = \eta$. The coupling terms are now space-dependent and rewrite

$$\begin{aligned}\forall x \in \mathcal{I}_1, \bar{\sigma}_1^+(x) &= e^{2I_0(x)}\sigma^{+-}, \bar{\sigma}_1^-(x) = e^{-2I_0(x)}\sigma^{-+}, \\ \forall x \in \mathcal{I}_2, \bar{\sigma}_2^+(x) &= e^{-2I_1(x)}\sigma^{+-}, \bar{\sigma}_2^-(x) = e^{2I_1(x)}\sigma^{-+}.\end{aligned}$$

This system is schematically illustrated in Figure 8.3. Note that, contrary to (5.1)-(7.2), the control input simultaneously appears in two boundary conditions.

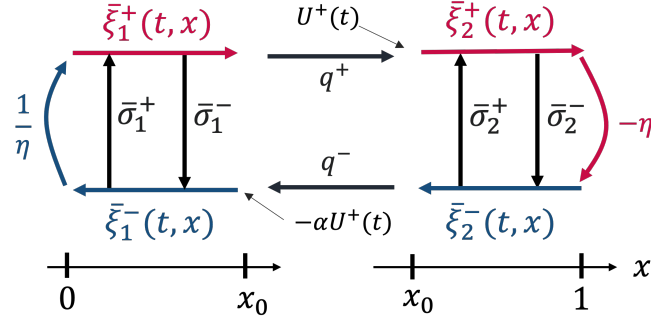


Figure 8.3 – Schematic representation of system (8.9)-(8.10)

8.2 . Controller design

To design the control input, we aim to rewrite the interconnected system as a *time-delay system*, whose stability is equivalent to the one of a *comparison system* of form (7.17)-(7.19). We can then apply the strategy presented in Chapter 7. To do so, we first use an invertible integral transform on each subsystem to move the in-domain couplings at the actuated boundary, and use the method of characteristics.

8.2.1 . Application of the backstepping methodology

First Volterra integral transforms

Inspired by the backstepping approach [VKC11], we define the two following Volterra integral operators $\mathcal{K}_i : H^1(\mathcal{I}_i, \mathbb{R}^2) \longrightarrow H^1(\mathcal{I}_i, \mathbb{R}^2)$, $i \in \{1, 2\}$, such that for all $t > 0$,

$$\forall x \in \mathcal{I}_1, \begin{pmatrix} \bar{\xi}_1^+(t, x) \\ \bar{\xi}_1^-(t, x) \end{pmatrix} = \begin{pmatrix} \bar{\xi}_1^+(t, x) \\ \bar{\xi}_1^-(t, x) \end{pmatrix} - \int_0^x \begin{pmatrix} K_1^{++} & K_1^{+-} \\ K_1^{-+} & K_1^{--} \end{pmatrix} (x, y) \begin{pmatrix} \bar{\xi}_1^+(t, x) \\ \bar{\xi}_1^-(t, x) \end{pmatrix} (y) dy, \quad (8.11)$$

$$\forall x \in \mathcal{I}_2, \begin{pmatrix} \bar{\xi}_2^+(t, x) \\ \bar{\xi}_2^-(t, x) \end{pmatrix} = \begin{pmatrix} \bar{\xi}_2^+(t, x) \\ \bar{\xi}_2^-(t, x) \end{pmatrix} - \int_x^1 \begin{pmatrix} K_2^{++} & K_2^{+-} \\ K_2^{-+} & K_2^{--} \end{pmatrix} (x, y) \begin{pmatrix} \bar{\xi}_2^+(t, x) \\ \bar{\xi}_2^-(t, x) \end{pmatrix} (y) dy, \quad (8.12)$$

where K_1 (resp. K_2) are bounded piecewise continuous functions defined on the lower part of the unit square \mathcal{T}^- (resp. on the upper part \mathcal{T}^+). We then introduce the target states

$$\begin{pmatrix} \gamma_i^+ \\ \gamma_i^- \end{pmatrix} = \mathcal{K}_i \left(\begin{pmatrix} \bar{\xi}_i^+ \\ \bar{\xi}_i^- \end{pmatrix} \right), \quad i \in \{1, 2\}.$$

Kernels equations

The kernels satisfy the following set of equations

$$\begin{aligned} \lambda \frac{\partial}{\partial x} K_i^{++} + \lambda \frac{\partial}{\partial y} K_i^{++} &= -\bar{\sigma}_i^-(y) K_i^{+-}, \quad \lambda \frac{\partial}{\partial x} K_i^{+-} - \lambda \frac{\partial}{\partial y} K_i^{+-} = -\bar{\sigma}_i^+(y) K_i^{++}, \\ \lambda \frac{\partial}{\partial x} K_i^{-+} - \lambda \frac{\partial}{\partial y} K_i^{-+} &= \bar{\sigma}_i^-(y) K_i^{--}, \quad \lambda \frac{\partial}{\partial x} K_i^{--} + \lambda \frac{\partial}{\partial y} K_i^{--} = \bar{\sigma}_i^+(y) K_i^{-+}, \end{aligned}$$

with boundary conditions

$$K_1^{+-}(x, x) = \frac{\bar{\sigma}_1^+(x)}{2\lambda}, \quad K_1^{-+}(x, x) = -\frac{\bar{\sigma}_1^-(x)}{2\lambda}, \quad (8.13)$$

$$K_1^{++}(x, 0) = \eta K_1^{+-}(x, 0), \quad K_1^{--}(x, 0) = \eta^{-1} K_1^{-+}(x, 0), \quad (8.14)$$

$$K_2^{+-}(x, x) = -\frac{\bar{\sigma}_2^+(x)}{2\lambda}, \quad K_2^{-+}(x, x) = \frac{\bar{\sigma}_2^-(x)}{2\lambda}, \quad (8.15)$$

$$K_2^{++}(x, 1) = -\eta K_2^{+-}(x, 1), \quad K_2^{--}(x, 1) = -\eta^{-1} K_2^{-+}(x, 1). \quad (8.16)$$

The two sets of equations admit a unique continuous solution on their definition domain [CVKB13, DMBAHK18]. Transforms \mathcal{K}_i , for $i \in \{1, 2\}$, are Volterra integral transforms. They are invertible [Yos60], and the inverse operators $\mathcal{L}_i \doteq \mathcal{K}_i^{-1}$ have the same form.

Equivalent target systems

The two Volterra transforms (8.11)-(8.12) map system (8.9)-(8.10) to

$$\frac{\partial}{\partial t} \gamma_i^+(t, x) + \lambda \frac{\partial}{\partial x} \gamma_i^+(t, x) = 0, \quad \frac{\partial}{\partial t} \gamma_i^-(t, x) - \lambda \frac{\partial}{\partial x} \gamma_i^-(t, x) = 0, \quad (8.17)$$

with the boundary conditions

$$\gamma_1^+(t, 0) = \eta^{-1} \gamma_1^-(t, 0), \quad \gamma_1^-(t, x_0) = q^- \gamma_2^-(t, x_0) - \alpha U^+(t) + I^-(t), \quad (8.18)$$

$$\gamma_2^-(t, 1) = -\eta \gamma_2^+(t, 1), \quad \gamma_2^+(t, x_0) = q^+ \gamma_1^+(t, x_0) + U^+(t) + I^+(t), \quad (8.19)$$

where $I^+(t), I^-(t)$ are defined on $[0, +\infty)$ using the inverse kernels:

$$\begin{aligned} \begin{pmatrix} I^+(t) \\ I^-(t) \end{pmatrix} &= \int_0^{x_0} \begin{pmatrix} -q^+ L_1^{++} & -q^+ L_1^{+-} \\ L_1^{-+} & L_1^{--} \end{pmatrix} (x_0, y) \begin{pmatrix} \gamma_1^+(y) \\ \gamma_1^-(y) \end{pmatrix} dy \\ &+ \int_{x_0}^1 \begin{pmatrix} L_2^{++} & L_2^{+-} \\ -q^- L_2^{-+} & -q^- L_2^{--} \end{pmatrix} (x_0, y) \begin{pmatrix} \gamma_2^+(y) \\ \gamma_2^-(y) \end{pmatrix} dy. \end{aligned}$$

The initial conditions $(\gamma_{i,0}^+, \gamma_{i,0}^-) \in H^1(\mathcal{I}_i, \mathbb{R}^2)$ are obtained from the Volterra transforms of the initial conditions $(\bar{\xi}_{i,0}^+, \bar{\xi}_{i,0}^-)$. As illustrated in Figure 8.4, the in-domain coupling terms have been replaced by integral terms at the actuated boundary $x = x_0$.

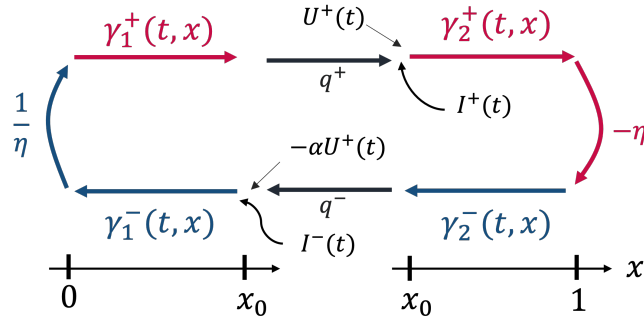


Figure 8.4 – Schematic representation of system (8.17)-(8.19)

8.2.2 . Reformulation as a time delay system

We now reformulate the hyperbolic system as a time-delay system. Introduce

$$\begin{cases} y(t) = \gamma_2^+(t, x_0), \\ z(t) = \gamma_1^-(t, x_0) + \alpha \gamma_2^+(t, x_0). \end{cases} \quad (8.20)$$

The function z has been defined to verify a time-delay equation that does not directly depend on the control input u^+ . Define $\phi(x) = \frac{x}{\lambda}$ on \mathcal{I}_1 and $\psi(x) = \frac{x-x_0}{\lambda}$ on \mathcal{I}_2 , and $t_F = 2\frac{x_0}{\lambda} = \frac{1}{\lambda}$ and $\tau = \frac{x_0}{\lambda} = \frac{t_F}{2}$. Using the method of characteristics, the solution of (8.17) is given by

$$\begin{aligned} \gamma_1^+(t, x) &= \begin{cases} \gamma_{1,0}^+(x - \lambda t), & \text{if } t \leq \frac{x}{\lambda}, \\ \gamma_1^+(t - \frac{x}{\lambda}, 0), & \text{else,} \end{cases} \quad , \quad \gamma_2^+(t, x) = \begin{cases} \gamma_{2,0}^+(x - \lambda t), & \text{if } t \leq \frac{x-x_0}{\lambda}, \\ \gamma_2^+(t - \frac{x-x_0}{\lambda}, x_0), & \text{else,} \end{cases} \\ \gamma_1^-(t, x) &= \begin{cases} \gamma_{1,0}^-(x + \lambda t), & \text{if } t \leq \frac{x_0-x}{\lambda}, \\ \gamma_1^-(t - (\frac{x_0}{\lambda} - \frac{x}{\lambda}), x_0), & \text{else,} \end{cases} \quad , \quad \gamma_2^-(t, x) = \begin{cases} \gamma_{2,0}^-(x + \lambda t), & \text{if } t \leq \frac{1-x}{\lambda}, \\ \gamma_2^-(t - (\frac{1-x}{\lambda}), 1), & \text{else.} \end{cases} \end{aligned}$$

From there, using the boundary conditions (8.18)-(8.19), we have for $t > t_F$,

$$\gamma_1^+(t, x) = \eta^{-1}(z - \alpha y)(t - \frac{x}{\lambda} - \frac{x_0}{\lambda}), \quad \gamma_2^-(t, x) = -\eta y(t + \frac{x}{\lambda} - \frac{3x_0}{2\lambda}).$$

We can also rewrite the integral terms appearing in (8.18)-(8.19) in terms of delayed values of (y, z) , to finally derive the equations satisfied by functions y, z . For all $t > t_F$, using the boundary condition (8.19), we have

$$y(t) = U^+(t) + q^+ \eta^{-1}(z - \alpha y)(t - \frac{1}{\lambda}) \quad (8.21)$$

$$\begin{aligned} &- q^+ \int_0^{x_0} \eta^{-1} L_1^{++}(x_0, \nu)(z - \alpha y)(t - \frac{\nu}{\lambda} - \frac{x_0}{\lambda}) + L_1^{+-}(x_0, \nu)(z - \alpha y)(t + \frac{\nu}{\lambda} - \frac{x_0}{\lambda}) d\nu \\ &+ \int_{x_0}^1 L_2^{++}(x_0, \nu)y(t - \frac{\nu - x_0}{\lambda}) - \eta L_2^{+-}(x_0, \nu)y(t + \frac{\nu - x_0}{\lambda} - \frac{1}{\lambda}) d\nu, \end{aligned}$$

$$\doteq U^+(t) + \mathcal{F}(y, z)(t). \quad (8.22)$$

Similarly, from (8.18), we obtain

$$\begin{aligned}
z(t) &= \frac{\alpha q^+}{\eta} (z - \alpha y) \left(t - \frac{1}{\lambda}\right) - \eta q^- y \left(t - \frac{1}{\lambda}\right) \\
&+ \int_0^{x_0} \eta^{-1} [L_1^{-+}(x_0, \nu) - \alpha q^+ L_1^{++}(x_0, \nu)] (z - \alpha y) \left(t - \frac{\nu}{\lambda} - \frac{x_0}{\lambda}\right) \\
&\quad + [L_1^{--}(x_0, \nu) - \alpha q^+ L_1^{+-}(x_0, \nu)] (z - \alpha y) \left(t + \frac{\nu}{\lambda} - \frac{x_0}{\lambda}\right) d\nu \\
&+ \int_{x_0}^1 [\alpha L_2^{++}(x_0, \nu) - q^- L_2^{-+}(x_0, \nu)] y \left(t - \frac{\nu - x_0}{\lambda}\right) \\
&\quad - \eta [\alpha L_2^{+-}(x_0, \nu) - q^- L_2^{--}(x_0, \nu)] y \left(t + \frac{\nu - x_0}{\lambda} - \frac{1}{\lambda}\right) d\nu. \tag{8.23}
\end{aligned}$$

Though these expressions are defined for $t > t_F$ for sake of simplicity, we have the following

Lemma 8.2.1: Well-posedness of (y, z)

Consider that system (8.17)-(8.19) is in open loop for $t \leq t_F$. For $t \leq t_F$, the terms $(y(t), z(t))$ defined by (8.20) can be expressed as a function of $(\gamma_{i,0}^+, \gamma_{i,0}^-)_{i \in \{1,2\}}$, the initial conditions of (8.17)-(8.19). Thus, $(y_{[t]}(\cdot), z_{[t]}(\cdot)) \in D_{t_F}$, $\forall t \geq 0$.

Proof : For any admissible control input $U^+(t)$, system (8.17)-(8.19) is well-posed and admits a unique solution in $C([0, +\infty), H^1([0, 1], \mathbb{R}^2))$. Due to definition (8.20), for any $t \geq t_F$, (y, z) can be expressed as boundary states and the partial trajectories belong to D_{t_F} .

Using technical computations, we can express (y, z) on $[0, \tau]$ as combinations of the initial values $(\gamma_{i,0}^+, \gamma_{i,0}^-)_{i \in \{1,2\}}$. To give more insights, let us define $y(t)$, $t \in [0, t_F]$:

$$\begin{aligned}
y(t) &= \gamma_2^+(t, x_0), \text{ by definition,} \\
&= q^+ \gamma_1^+(t, x_0) - q^+ \int_0^{x_0} L_1^{++}(x_0, y) \gamma_1^+(y) + L_1^{+-}(x_0, y) \gamma_1^-(y) dy \\
&\quad + \int_{x_0}^t L_2^{++}(x_0, y) \gamma_2^+(y) + L_2^{+-}(x_0, y) \gamma_2^-(y) dy, \text{ using (8.18),} \\
&= q^+ \left[\mathbf{1}_{[0, \tau]}(t) \gamma_{1,0}^+(x_0 - \lambda t) + \frac{1}{\eta} \mathbf{1}_{[\tau, t_F]}(t) \gamma_{1,0}^-(\lambda(t - \tau)) \right] + \mathcal{I}^+(t).
\end{aligned}$$

We then decompose similarly the different terms in $\mathcal{I}^+(t)$, using the method of characteristics on small time intervals until reaching the initial conditions. Since we can go back in time from τ each time, we can mechanically express all the terms, despite the apparition of intricate integral terms.

For instance, the first term in $\mathcal{I}^+(t)$ rewrites, $\forall y \in [0, x_0]$, $\forall t \in [0, t_F]$,

$$\begin{aligned}
\gamma_1^+(t, y) &= \mathbf{1}_{[0, \frac{y}{\lambda}]}(t) \gamma_{1,0}^+(y - \lambda t) + \mathbf{1}_{[\frac{y}{\lambda}, \frac{y}{\lambda} + \tau]}(t) \frac{1}{\eta} \gamma_{1,0}^-(\lambda t) + \mathbf{1}_{[\frac{y}{\lambda} + \tau, t_F]}(t) \frac{1}{\eta} \left(q^- \gamma_{2,0}^- (1 + y - \lambda t) \right. \\
&+ \int_0^{x_0} L_1^{--}(x_0, \nu) \gamma_{1,0}^-(\nu - y - x_0 + \lambda t) d\nu - q^- \int_{x_0}^1 L_2^{-+}(x_0, \nu) \gamma_{2,0}^+(\nu + y + x_0 - \lambda t) d\nu \left. \right) \\
&+ \frac{1}{\eta} \int_0^{x_0} L_1^{-+}(x_0, \nu) \left(\left(\mathbf{1}_{[\frac{y}{\lambda} + \tau, \frac{y+\nu}{\lambda} + \tau]}(t) \gamma_{1,0}^+(\nu - \lambda t + y + x_0) + \mathbf{1}_{[\frac{y+\nu}{\lambda} + \tau, t_F]}(t) \frac{1}{\eta} \gamma_{1,0}^-(\lambda t - y - x_0 - \nu) \right) \right. \\
&\left. - \frac{q^-}{\eta} \int_{x_0}^1 L_2^{--}(x_0, \nu) \left(\mathbf{1}_{[\frac{y}{\lambda} + \tau, \frac{y-\nu}{\lambda} + 3\tau]}(t) \gamma_{2,0}^-(\nu + \lambda t + y + x_0) - \eta \mathbf{1}_{[\frac{y-\nu}{\lambda} + 3\tau, t_F]}(t) \gamma_{2,0}^+(2 - \lambda t + y + x_0 - \nu) \right) d\nu \right).
\end{aligned}$$

Alternatively, we could prove following [Aur18, Lemma 5.1.1] that $(\gamma_2^+(\cdot, x_0), \gamma_1^-(\cdot, x_0))$ is the solution of a Volterra integral equation of the second kind, which admits a unique solution in H^1 . ■

By assuming we have access to past values of the functions (y, z) , we can define for all $t > t_F$ the following new control input $V(t) = U^+(t) + \mathcal{F}(z, y)(t)$. From now on, if $t \leq t_F$, we choose $U^+(t) = 0$. After several changes of variables in the integral terms, the above expression (8.23) rewrites

$$z(t) = a_0 z(t - t_F) + a_1 V(t - t_F) + \int_0^{t_F} N_z(s) z(t - s) + N_V(s) V(t - s) ds, \quad (8.24)$$

with $a_0 = \frac{\alpha q^+}{\eta} = q^+$, $a_1 = -(\frac{\alpha^2 q^+}{\eta} + \eta q^-) = -2\eta q^+$ and

$$\begin{aligned} N_z(s) &= \mathbb{1}_{[0, \tau]}(s) \lambda (L_1^-(x_0, \lambda(\tau - s)) - \alpha q^+ L_1^{+-}(x_0, \lambda(\tau - s))) \\ &\quad + \mathbb{1}_{[\tau, t_F]}(s) \frac{\lambda}{\eta} (L_1^{-+}(x_0, \lambda(s - \tau)) - \alpha q^+ L_1^{++}(x_0, \lambda(s - \tau))), \end{aligned} \quad (8.25)$$

$$\begin{aligned} N_V(s) &= -\alpha N_z(s) + \mathbb{1}_{[0, \tau]}(s) \lambda (\alpha L_2^{++}(x_0, \lambda s + x_0) - q^- L_2^{-+}(x_0, \lambda s + x_0)) \\ &\quad - \mathbb{1}_{[\tau, t_F]}(s) \eta \lambda (q^- L_2^{--}(x_0, 1 - \lambda s + x_0) - \alpha L_2^{+-}(x_0, 1 - \lambda s + x_0)). \end{aligned} \quad (8.26)$$

Equation (8.24) corresponds to an integral delay equation with pointwise and distributed actuation. To fasten the stabilization and avoid robustness issues, we want to cancel a part of the reflection term $a_0 z(t - t_F)$ that appears in equation (8.24). More precisely, for $\bar{a}_0 \in (0, a_0)$, define $\bar{V}(t) = V(t) + \frac{\bar{a}_0}{a_1} z(t)$. It rewrites

$$z(t) = (a_0 - \bar{a}_0) z(t - t_F) + a_1 \bar{V}(t - t_F) + \int_0^{t_F} \bar{N}_z(s) z(t - s) + N_V(s) \bar{V}(t - s) ds, \quad (8.27)$$

with $\bar{N}_z(s) = N_z(s) - \frac{\bar{a}_0}{a_1} N_V(s)$. In what follows, we denote $\bar{a}_0 = a_0 - \bar{a}_0$. We have the following result

Lemma 8.2.2: Relation between two norms

Consider that there exists a control input $U^+(t)$, such that (y, z) exponentially converge to zero in the sense of the D_{t_F} -norm. Then the states $(\gamma_i^+, \gamma_i^-)_{i \in \{1, 2\}}$ exponentially converge to zero in the sense of the spatial L^2 -norm.

Proof : Assume that the functions (y, z) exponentially converge to zero in the sense of the D_{t_F} -norm. Then there exists $C_1, \nu_1 > 0$, for all $t > t_F$,

$$\|(y_{[t]}, z_{[t]})\|_{D_{t_F}}^2 = \int_0^{t_F} y(t - \theta)^2 + z(t - \theta)^2 d\theta \leq C_1 e^{-\nu_1 t} \|(y_{[t_F]}, z_{[t_F]})\|_{D_{t_F}}^2.$$

Let us show that (γ^+, γ^-) exponentially converges to zero in the sense of the spatial L^2 -norm. By definition, we have $\|(\gamma^+(t, \cdot), \gamma^-(t, \cdot))\|_{L^2}^2 = \int_0^{x_0} \gamma_1^+(t, y)^2 + \gamma_1^-(t, y)^2 dy + \int_{x_0}^1 \gamma_2^+(t, y)^2 + \gamma_2^-(t, y)^2 dy$. For sake of brevity, we consider the first term only, similar relations can be obtained for the other state components γ_2^+, γ_2^- and γ_1^- . For all $t > t_F$, we have

$$\begin{aligned} \int_0^{x_0} (\gamma_1^+(t, \nu)^2) d\nu &= \frac{1}{\eta^2} \int_0^{x_0} (z - \alpha y)^2 (t - \frac{\nu}{\lambda} - \tau) d\nu, \text{ using the characteristics line, and (8.20)} \\ &= \int_\tau^{t_F} \frac{\lambda}{\eta^2} (z - \alpha y)^2 (t - s) ds \text{ using a change of variables in the integral} \\ &\leq \frac{2\lambda}{\eta^2} \int_0^{t_F} z^2(t - s) + \alpha^2 y^2(t - s) ds \text{ since } \tau > 0, \end{aligned}$$

$$\leq 2\lambda \max(1, \eta^2) \|(z_{[t]}, y_{[t]})\|_{D_{t_F}}^2 \leq 2\lambda \max(1, \eta^2) C_1^2 e^{-\nu_1 t} \|(y_{[t_F]}, z_{[t_F]})\|_{D_{t_F}}^2.$$

Due to Lemma 8.2.1, there exists a bounded operator \mathcal{O} such that, for all $0 \leq s \leq t_F$, $(z, y) = \mathcal{O}(\gamma_{i,0}^+, \gamma_{i,0}^-)$. Therefore, there exists $C_0 > 0$ such that

$$\int_0^{t_F} z^2(s) + y^2(s) ds \leq C_0 \|(\gamma_0^+, \gamma_0^-)\|_{L^2}^2.$$

Consequently, there exists $C_1^+ > 0$ such that for all $t \geq t_F$, $\int_0^{x_0} (\gamma_1^+(t, \nu)^2) d\nu \leq C_1^+ e^{-\nu_1 t} \|(\gamma_0^+, \gamma_0^-)\|_{L^2}^2$. We obtain similar inequalities for the other terms of $\|(\gamma^+(t, \cdot), \gamma^-(t, \cdot))\|_{L^2}^2$, with same exponential rate and constants denoted C_i^\pm by analogy. Adding the four resulting inequalities, we obtain the exponential convergence of state (γ^+, γ^-) to zero in the sense of the spatial L^2 -norm, with a decay rate $\frac{\nu_1}{2}$ and an admissible constant given by $\sqrt{C_1^+ + C_1^- + C_2^+ + C_2^-}$. ■

We finally have the following theorem

Theorem 8.2.1: Exponential stabilization of the initial energy states

Consider that there exists a control input $U^+(t)$, such that (y, z) exponentially converge to zero in the sense of the D_{t_F} -norm. Then the original energy states (X_1, X_2) exponentially converge to zero in the sense of the spatial L^2 -norm (8.4). Therefore, the control objective 8.1.1 is fulfilled.

Proof : Assume that the functions (y, z) exponentially converge to zero in the sense of the D_{t_F} -norm. From Lemma 8.2.2 stated above, it implies the convergence of states (γ^+, γ^-) in the sense of the L^2 -norm. The invertibility and boundedness of the Volterra integral transforms \mathcal{K}_i directly imply the exponential stability of the hyperbolic system (8.9)-(8.10), and consequently the one of the initial states (ξ^+, ξ^-) defined in (8.8). The exponential stabilization of energy states (X_1, X_2) directly follows, using the definition of the Riemann coordinates. From $U^+(t)$, we can then directly derive an adequate control input satisfying control objective 8.1.1. ■

To solve our initial problem, we therefore need to determine an adequate state-feedback controller that exponentially stabilizes the integral delay system (8.21)-(8.24).

8.2.3 . Application of the control strategy

The control strategy developed in Chapter 7 can be applied to the stabilization of the clamped string under several conditions listed in

Assumption 8.2.1 *The system parameters must satisfy*

- $|\tilde{a}_0| < 1$ and $a_1 \neq 0$,
- For all $s \in \mathbb{C}$, $\text{rank}[1 - \tilde{a}_0 e^{-t_F s} - \int_0^{t_F} \bar{N}_z(\nu) e^{-\nu s} d\nu, a_1 e^{-t_F s} + \int_0^{t_F} N_V(\nu) e^{-\nu s} d\nu] = 1$.

Comparison system

Let us denote $\lambda_F = \frac{1}{t_F}$ and define the $L^\infty([0, 1])$ -functions N_u, N_v by $N_u(x) = t_F \bar{N}_z(t_F x)$ and $N_v(x) = \frac{t_F}{a_1} N_V(t_F(1-x))$. We introduce the hyperbolic system of form (7.17)-(7.19) as a *comparison system*

$$\begin{aligned} \frac{\partial}{\partial t} u(t, x) + \lambda_F \frac{\partial}{\partial x} u(t, x) &= 0, \\ \frac{\partial}{\partial t} v(t, x) - \lambda_F \frac{\partial}{\partial x} v(t, x) &= 0, \end{aligned} \tag{8.28}$$

with the boundary conditions

$$u(t, 0) = v(t, 0) + \tilde{a}_0 u(t, 1) + \int_0^1 N_u(\nu) u(\nu) + N_v(\nu) v(\nu) d\nu, \quad (8.29)$$

$$v(t, 1) = a_1 \bar{V}(t) \doteq V_1(t). \quad (8.30)$$

This comparison system is illustrated in Figure 8.5. System (8.28)-(8.30) corresponds to a balance law system [BC16] actuated through one boundary.

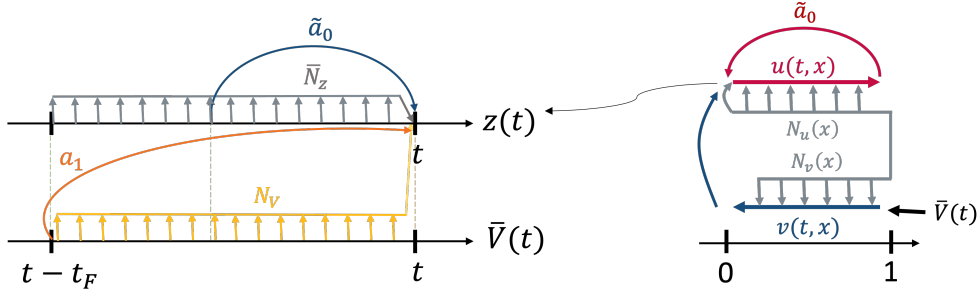


Figure 8.5 – Schematic representation of IDE (8.27) and comparison system (8.28)-(8.30).

Applying the method of characteristics, one can verify that $u(t, 0)$ verifies equation (8.27) and corresponds to z for adequate initial conditions in D_{t_F} . We have the following

Lemma 8.2.3: Use of a comparison system

For any admissible feedback law $V_1(t)$, for any initial conditions $(u_0, v_0) \in H^1([0, 1], \mathbb{R}^2)$ satisfying the compatibility conditions, system (8.28)-(8.29) admits a unique solution in $C^0([0, +\infty); H^1([0, 1], \mathbb{R}^2))$.

If the solution of (8.28)-(8.30), such that $u_{[t_F]}(\cdot, 0) = z_{[t_F]}(\cdot)$, exponentially converges to zero in the sense of the L_2 -norm, then the solution of (8.27) exponentially converges to zero in the sense of the D_{t_F} -norm.

Proof : From Chapter 7, it was shown that system (8.28)-(8.30) can be obtained from a well-posed system using boundedly invertible transforms. Therefore, it admits a unique solution in $H^1([0, 1], \mathbb{R}^2)$, for all $t \geq 0$. First, let us show that $u(\cdot, 0)$ satisfies (8.27) for $t \geq t_F$. Applying the method of characteristics on (8.28), we have for $t > t_F$, $u(t, x) = u(t - \frac{x}{\lambda_F}, 0)$ and $v(t, x) = a_1 \bar{V}(t - \frac{1-x}{\lambda_F})$. Injecting these in (8.29), and using the definition of N_u, N_v implies, for all $t > t_F$, $u(t, 0) = a_1 \bar{V}(t - t_F) + \tilde{a}_0 u(t - t_F, 0) + \int_0^{t_F} \bar{N}_z(\nu) u(t - \nu, 0) N_V(\nu) \bar{V}(t - \nu) d\nu$. Therefore, $u(\cdot, 0)$ is solution of (8.27) for $t \geq t_F$. Moreover, $u(\cdot, 0)$ is uniquely defined on $[0, t_F]$ by the initial conditions $(u_0, v_0) \in H^1([0, 1], \mathbb{R}^2)$. Indeed, we have, for all $t \leq t_F$,

$$u(t, 0) = v_0(\lambda_F t) + \tilde{a}_0 u_0(1 - \lambda_F t) + \int_0^1 N_u(\nu) \left[\mathbb{1}_{[0, \frac{\nu}{\lambda_F}]}(t) u_0(\nu - \lambda_F t) + \mathbb{1}_{[\frac{\nu}{\lambda_F}, t_F]}(t) u(t - \frac{\nu}{\lambda_F}, 0) \right] + N_v(\nu) \mathbb{1}_{[0, \frac{1-\nu}{\lambda_F}]}(t) v_0(\nu + \lambda_F t) d\nu,$$

since the system is in open-loop for $t \leq t_F$. It implies that $u(\cdot, 0)$ is defined on $[0, t_F]$ as the unique solution

of the Volterra integral equation of the second kind

$$u(t, 0) - \int_0^t N_u(\lambda_F(t-s))u(s, 0)ds \doteq \mathcal{L}(u(\cdot, 0))(t) = f(u_0, v_0)(\lambda_F t),$$

with \mathcal{L} an invertible transform from D_{t_F} to D_{t_F} and with $f(u_0, v_0)(x) = v_0(x) + \bar{a}_0 u_0(1-x) + \int_0^{1-x} N_u(s+x)u_0(s)ds + \int_x^1 N_v(s-x)v_0(s)ds$, an operator from $H^1([0, 1], \mathbb{R}^2) \rightarrow D_{t_F}$. Indeed, since transform f is a composition of continuous functions (and the regularizing properties of the integral, with piecewise continuous kernel functions) its image belongs to D_{t_F} . Denote, $u(\cdot, 0) = \mathcal{L}(f(u_0, v_0)) \in D_{t_F}$. We can define on $[0, 1]$ an adequate initial conditions satisfying the compatibility equations in the pre-image of $\mathcal{L}^{-1}(z_{[t_F]})$.

Then, let us prove that the exponential convergence of the unique solution of (8.28)-(8.30) defined with the above initial condition in the sense of the L^2 -norm implies the convergence of $u(\cdot, 0)$ (and consequently, z) in the sense of the D_{t_F} -norm. Consider $t > t_F$ big enough. Assuming the exponential stability of (u, v) in the sense of the L^2 -norm, there exist $C, \nu > 0$, such that $\|(u, v)\|_{L^2}^2 \leq C e^{-\nu t} \|(u_0, v_0)\|_{L^2}^2$. Since (8.28)-(8.30) is well-posed on $[0, t_F]$, there also exists C_F such that $\|(u, v)\|_{L^2}^2 \leq C_F e^{-\nu t} \|(u(t_F, \cdot), v(t_F, \cdot))\|_{L^2}^2$. We have

$$\begin{aligned} \|z_{[t]}\|_{D_{t_F}}^2 &= \int_0^{t_F} z^2(t-s)ds = \int_0^{t_F} u(t-s, 0)^2 ds \\ &= t_F \int_0^1 u\left(t - \frac{x}{\lambda_F}, 0\right)^2 dx = t_F \int_0^1 u(t, x)^2 dx \text{ using the characteristic equation in (8.28)} \\ &\leq t_F C_F e^{-\nu t} \|(u(t_F, \cdot), v(t_F, \cdot))\|_{L^2}^2 = t_F C_F e^{-\nu t} \int_0^1 u(t_F, x)^2 + v(t_F, x)^2 dx \\ &= t_F C_F e^{-\nu t} \int_0^1 u\left(t_F - \frac{x}{\lambda_F}, 0\right)^2 + v\left(\frac{x}{\lambda_F}, 1\right)^2 dx \\ &= t_F C_F e^{-\nu t} \int_0^{t_F} \lambda_F u^2(t-s, 0)ds \text{ using a change of variable and } \bar{V}(t) \equiv 0, t \leq t_F \\ &= C_F e^{-\nu t} \|z_{[t_F]}\|_{D_{t_F}}^2. \end{aligned}$$

Consequently, the L^2 -exponential stability of (u, v) implies the D_{t_F} -exponential stability of z . ■

Expression of the control input

Under Assumption 8.2.1, we can now apply the results from Chapter 7.

Theorem 8.2.2: Exponential stabilization

There exist two piecewise continuous functions M^1, M^2 defined on $[0, 1]$, such that the state-feedback controller $\bar{V}(t)$ defined for all $t > t_F$ by

$$\bar{V}(t) = -\frac{1}{a_1} \int_0^1 M^1(\nu)z\left(t - \frac{\nu}{\lambda}\right) + M^2(\nu)y\left(t - \frac{1-\nu}{\lambda}\right)d\nu. \quad (8.31)$$

exponentially stabilizes the integral delay dynamics (8.27) in the sense of the D_{t_F} -norm. Consequently, it exponentially stabilizes the original (X_1, X_2) in the spatial L^2 -norm.

Proof : Following the approach given in Chapter 7, we use a Fredholm integral transform to map the comparison system (8.28)-(8.29) to an exponentially stable system. We obtain a control input which rewrites in our case (8.31), using the functions (y, z) . The expressions of functions M^1, M^2 , correspond to boundary values of the kernels of the transform. From Lemma 8.2.3, we therefore obtain a control input (8.31) exponentially stabilizing z in the sense of the D_{t_F} -norm. Moreover, the control input exponentially converges to zero. Consequently, $V(t) = \bar{V}(t) - \frac{\bar{a}_0}{a_1} z(t)$ exponentially converges to zero. The function $y(t)$, defined by equation (8.21) and that corresponds to $V(t)$, then exponentially converges to zero in the sense of the D_{t_F} -norm. Applying Theorem 8.2.1 completes the proof. ■

From the control input $\bar{V}(t)$, it is possible to obtain the adequate control input $V(t)$ stabilizing the initial system. It can be expressed with the energy states using the different

transforms. Indeed, by definition $V(t) = -\sqrt{2}Ee^{I_1}U^+(t)$ and $U^+(t) = \bar{V}(t) - \frac{\bar{a}_0}{a_1}z(t) - \mathcal{F}(y, z)$, where \mathcal{F} is a pointwise and distributed delay operator defined in (8.21), using past values of (y, z) over a time $[0, t_F]$. Using definition (8.20), it rewrites with past values of $(\gamma_1^-(\cdot, x_0), \gamma_2^+(\cdot, x_0))$. Therefore, the initial control input $V(t)$ can be computed using the history of the boundary outputs $(\gamma_1^-(\cdot, x_0), \gamma_2^+(\cdot, x_0))$.

8.3 . Simulation results

In order to illustrate the proposed control strategy, we present some simulations implemented using Matlab. The coefficients of the wave equation (8.1) are given by $\rho = 0.9, E = 2.2$, and $c = 0.1$. It models a slightly damped clamped string of length $\ell = 2$. This initial system is then naturally stable due to the presence of dissipative terms. However, our approach could also work in the case of unstable systems with antidamping (e.g. systems resulting from linearization of Saint-Venant equation [BC16]).

The initial string position is $w_0(x) = \frac{2}{\pi} \cos(\frac{\pi}{2}(1 - x))$. Each space domain \mathcal{I}_i is discretized with a mesh of $\mathbf{nx} = 100$ points. We first compute offline the values of the different coupling terms and solve the kernel equations for the two Volterra integral transforms and the Fredholm integral transform. The unique solution of the kernel for direct and inverse transforms is obtained using the successive approximation technique with an error threshold $\epsilon = 10^{-8}$. The computations converge after 17 steps. The values are stored in matrices of size $\mathbf{nx} \times \mathbf{nx}$. All integral terms are approximated using the trapezoidal method. We also compute and store the couplings N_V, N_z and N_u, N_v . First, we simulated system (8.9)-(8.10) in open-loop on a time horizon of 10s using a Godunov Scheme [LeVoz] ($CFL = 1$). It allows to obtain partial trajectories $(y_{[t_F]}, z_{[t_F]})$. Next, we solve (8.27), with the control input (8.31) computed at each time step. We can illustrate the evolution of the virtual output $z(t)$ defined on $[0, 10]$ s. The control input is then applied for $t \geq t_F$. Figure 8.6 shows that the more we cancel the reflection term, the faster the amplitude of the oscillations decreases to the price of higher numerical instabilities (as illustrated by the green dotted line).

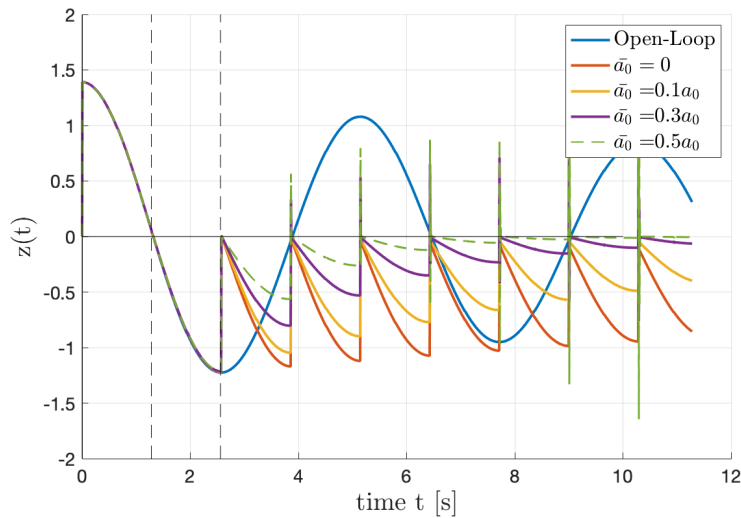


Figure 8.6 – Evolution of the output $z(t)$ for different \bar{a}_0

We can also compute the evolution of the energy of the system $\mathcal{E}(t)$ in closed-loop and open-loop. It is equivalent to the L^2 -norm of the energy states (see Chapter 10). The control input cancels a part of the reflection with $\bar{a}_0 = 0.2a_0$. As illustrated in Figures 8.7 and 8.8 (dotted line), it converges to zero. From $z(t)$ in open-loop and closed-loop, we can reconstruct the evolution of the whole state (γ^+, γ^-) and, from there, apply the successive transform to obtain the initial energy states (X) . The evolution of $X_2(t, x)$ in open-loop and closed-loop (after t_F) for $\bar{a}_0 = 0.1a_0$ is represented in Figure 8.9.

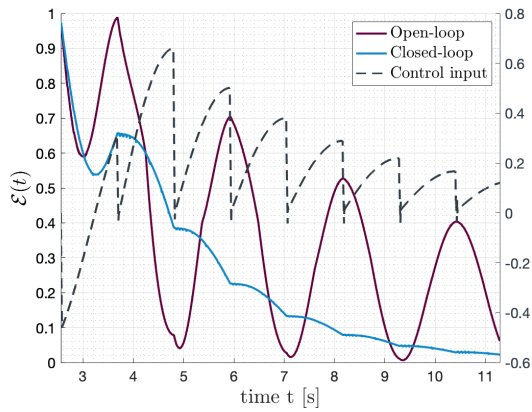


Figure 8.7 – Stable case

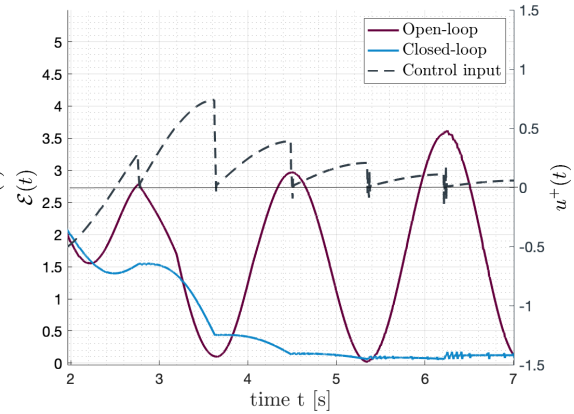


Figure 8.8 – Unstable case

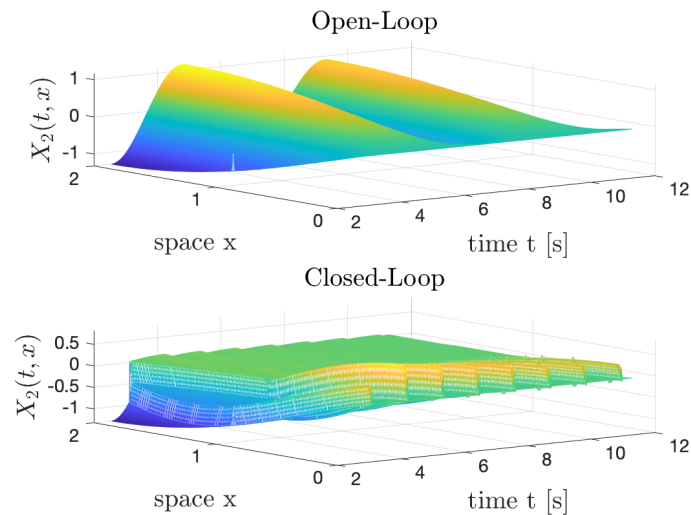


Figure 8.9 – Evolution of state component X_2 in open-loop (top) and closed-loop (bottom)

Finally, we consider the case of a naturally slightly unstable system with antidamping, e.g. systems resulting from the linearization of Saint-Venant equation [BC16]. Here, the physical parameters are $\rho = 0.9$, $E = 4$, and $c = -0.1$. We cancel 10% of the reflection term to guarantee that $\bar{a}_0 < 1$. As illustrated in Figure 8.8, the open-loop energy of the system diverges, while the one in closed-loop goes to 0.

Conclusion

In this chapter, we applied the methodology proposed in Chapter 7 to a clamped string with actuation located inside the domain. We used Riemann invariants to rewrite the initial wave equation as an interconnection of two systems of first-order hyperbolic PDE systems. We then combined the backstepping approach with the method of characteristics to rewrite the hyperbolic system as an integral delay equation with distributed actuation. We were finally able to adjust the results from the previous chapter to derive a stabilizing control law under a controllability condition. An estimation of the whole state is necessary to be implemented on real systems. As shown in Section 7.3, a state observer could be designed using a similar approach. In order to get a more complete work, we need to design an observer. By defining an adequate output, an approach similar to Section 7.3 could be applied.

In future work, we wish to extend this approach to more complex beam models such as Euler-Bernoulli or Timoshenko beams. The performance of the full-state feedback could then be compared with boundary feedbacks obtained from frequency domain approaches for beams coupled by dissipative joints [CDKP87, Reb95] or energy based controllers [AT00, AT01].

Perspectives

In Part III, we considered a chain structure of two scalar hyperbolic systems where the control input is located at the in-between boundary. As seen in Chapter 7, the stabilization of this simple network was a challenging issue. In this situation, we could not rely on the classic invertible transforms used in the backstepping methodology. An operator framework was introduced to guarantee the existence and invertibility of the Fredholm transform proposed instead. Interestingly, this stabilization problem is highly related to the stabilization of Integral Delay Equations (IDE) with pointwise and distributed actuation. This work then also offers an alternative approach for the stabilization of under-actuated systems, such as $1 + 2$ hyperbolic systems.

This approach paves the way for future network contributions with actuation inside the graph structure. A natural extension is to consider the case of two non-scalar PDE systems with actuation at some in-between boundaries. Another natural extension is to consider a chain of $N > 2$ subsystems with actuation at one or several in-between boundaries. We believe this approach could be combined with approaches seen in Part II to tackle a wider diversity of physical systems with an arbitrary number of PDEs or ODEs. For instance to consider the actuator dynamics at the junction of a chain of several hyperbolic PDE systems or additional loads at the end of a chain structure.

Underactuated $1 + 2$ linear hyperbolic system

A class of systems that can be stabilized with the approach presented in Chapter 7 are underactuated $1 + 2$ hyperbolic systems, where only one of the two leftward-convecting equations is actuated. In [ADMEA14], this system models the flow of liquid and gas along a drillstring in a Drif-Flux Model (DFM). It could also model an underactuated network of open channels [dHPC⁺03].

Such a system was considered in [CVK17], in the simpler case of a wave equation coupled to a transport equation, and in [ABABP20]. In the latter, the underactuated system was stabilized under the more restrictive assumption of exponentially stable actuation dynamics, using successive state transformations. It is illustrated in Figure 8.10.

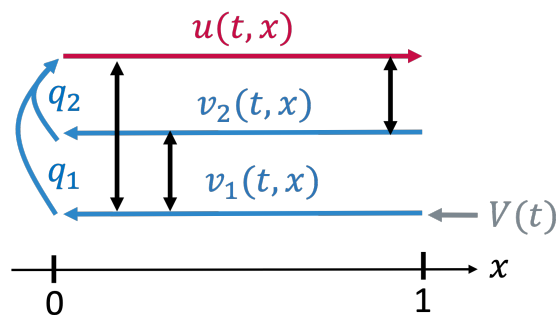


Figure 8.10 – Schematic representation of the system (8.32)-(8.33)

It corresponds to a state $w(t, x) = (u(t, x), v_1(t, x), v_2(t, x))^T$ satisfying

$$\frac{\partial}{\partial t} w(t, x) + \Lambda \frac{\partial}{\partial x} w(t, x) = \Sigma(x) w(t, x), \quad (8.32)$$

where the different arguments evolve in $(0, +\infty) \times [0, 1]$, and with the following boundary conditions

$$u(t, 0) = q_1 v_1(t, 0) + q_2 v_2(t, 0), \quad v_1(t, 1) = \rho_1 u(t, 1) + V(t), \quad v_2(t, 1) = \rho_2 u(t, 1). \quad (8.33)$$

The diagonal matrix Λ is given by $\Lambda = \text{diag}(\lambda, -\mu_1, -\mu_2)$, where the different positive velocities λ, μ_1, μ_2 are assumed to be constant, as the boundary couplings q_1, q_2, ρ_1 and ρ_2 . The components of the matrix Σ are continuous functions. Following the backstepping approach in [ADM19], the stabilization of this underactuated system is shown in [ABABP20] equivalent to the one of an integral delay equation of the form

$$z(t) = \rho_2 q_1 \bar{V}(t - \tau_1) + \rho_2 q_2 z(t - \tau_2) + \int_0^{\max(\tau_1, \tau_2)} N_z(\nu) z(t - \nu) + N_V(\nu) \bar{V}(t - \nu) d\nu,$$

with $\bar{V}(t)$ a full-state feedback depending on the distributed states. It is closely related to the IDE given in (7.25), and considered in [RAN21b]. Thus the proposed methodology is of high interest for stabilizing underactuated hyperbolic systems.

Chain of two multidimensional hyperbolic subsystems with actuation at the in-between boundary

Next, a natural extension of the interconnection of two scalar hyperbolic PDE subsystems with actuation at the in-between boundary is to consider non-scalar PDE systems. This situation appears when using a Timoshenko beam model with in-domain actuation instead of a string model for the clamped system studied in Chapter 8. Writing the energy states in the Riemann coordinates and assuming we have a torque and bending control input in the middle of the beam, we can reformulate the system as

$$\begin{aligned} \frac{\partial}{\partial t} \xi_i^+(t, x) + \Lambda \frac{\partial}{\partial x} \xi_i^+(t, x) &= \Sigma^{++}(x) \xi_i^+(t, x) + \Sigma^{+-}(x) \xi_i^-(t, x), \\ \frac{\partial}{\partial t} \xi_i^-(t, x) - \Lambda \frac{\partial}{\partial x} \xi_i^-(t, x) &= \Sigma^{-+}(x) \xi_i^+(t, x) + \Sigma^{--}(x) \xi_i^-(t, x), \end{aligned} \quad (8.34)$$

with boundary conditions

$$\begin{aligned} \xi_1^+(t, 0) &= -R^{-1} \xi_1^-(t, 0), \quad \xi_1^-(t, 1) = V(t) + \xi_2^-(t, 0), \\ \xi_2^-(t, 1) &= R \xi_2^+(t, 1), \quad \xi_2^+(t, 0) = R^{-1} V(t) + \xi_1^+(t, 1). \end{aligned} \quad (8.35)$$

It is schematically represented in Figure 8.11. Following a backstepping methodology similar to the one in Chapter 8, we can move the in-domain couplings to the in-between boundary. Next, using the method of characteristics, we can rewrite the equations satisfied by the boundary functions $z_2^+(t, 0), z_1^-(t, 1)$. Defining $z(t) = z_1^-(t, 1) - R z_2^+(t, 0)$ and a new control input such that $z_1^-(t, 1) = \bar{V}(t)$ (which cancels the reflection terms), we show

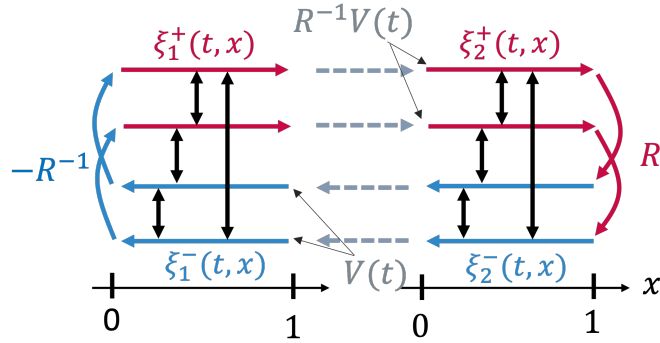


Figure 8.11 – Schematic representation of the system (8.34)-(8.35)

that it is the solution of an IDE of form

$$\begin{pmatrix} z_1(t) \\ z_2(t) \end{pmatrix} = 2 \begin{pmatrix} \bar{V}_1(t - \tau_\lambda) \\ \bar{V}_2(t - \tau_\mu) \end{pmatrix} - \begin{pmatrix} z_1(t - \tau_\lambda) \\ z_2(t - \tau_\mu) \end{pmatrix} + \int_0^{\max(\tau_\lambda, \tau_\mu)} H(s) \bar{V}(t - s) + G(s) z(t - s) ds$$

with $G, H \in C_{pw}^0([0, \max(\tau_\lambda, \tau_\mu)], \mathbb{R}^{2 \times 2})$. If $\tau_\mu \neq \tau_\lambda$, we cannot straightforwardly use a simple hyperbolic PDE system as a comparison system and apply results from Chapter 7. A third rightward or leftward convecting transport equation could be used in the comparison system to compensate for the remaining delayed terms. This would lead to more intricate computations.

In a more general setting of two $(n + m)$ linear hyperbolic subsystems with control at the in-between boundary, we would have to deal with many more delays, non necessarily commensurate. If all leftward or rightward convecting transport equations are actuated, the stabilization of the two interconnected subsystems may result in stabilizing an IDE of the form

$$z(t) = Q \begin{pmatrix} z_1(t - \tau_1) \\ z_i(t - \tau_i) \\ \dots \\ z_n(t - \tau_n) \end{pmatrix} + R \begin{pmatrix} V_1(t - \tau_1) \\ V_i(t - \tau_i) \\ \dots \\ V_n(t - \tau_n) \end{pmatrix} + \int_0^{\max(\tau_i)} N_V V(t - s) + N_z(s) z(t - s) ds,$$

with Q, R not necessarily diagonal invertible matrices. When not all rightward or leftward equations are actuated, or for mixed actuation, the stabilization would require additional technical developments.

Chain of two scalar hyperbolic subsystems with actuation at the in-between boundary and actuator dynamics

For application purposes, another extension of the works developed in Chapters 7 and 4 is to consider the actuator dynamics. It would correspond to a chain of an actuated ODE sandwiched between two scalar hyperbolic PDE subsystems, as illustrated in Figure 8.12. An example of such interconnection can be found in [ZLW⁺22], which con-

siders the control of a flexible beam using Ionic polymer–metal composites (IPMC) actuators. A simplified lumped RLC control-oriented mode models their electric dynamics. The voltage input results in torque applied to the beam. Both systems are coupled using power-preserving interconnection. The new interconnections and the actuator dynam-

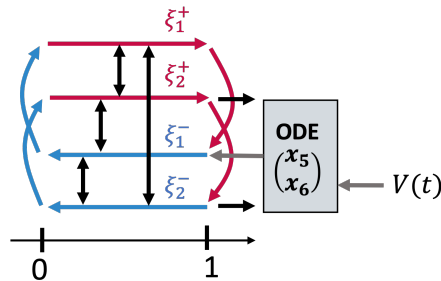


Figure 8.12 – Schematic representation of ODE actuator dynamics

ics make the approach proposed in Part III not directly applicable. The Fredholm integral transform would move the integral coupling terms in the ODE. Note that the stabilization of an ODE-PDE-ODE chain structure with actuation of the PDE boundary was considered in [ABADM23].

Chain of scalar hyperbolic subsystems with actuation at an in-between boundary

Another natural extension is an underactuated chain of $N > 2$ scalar hyperbolic PDE subsystems with boundary actuation at one in-between boundary. This finds applications in open channels or electrical networks.

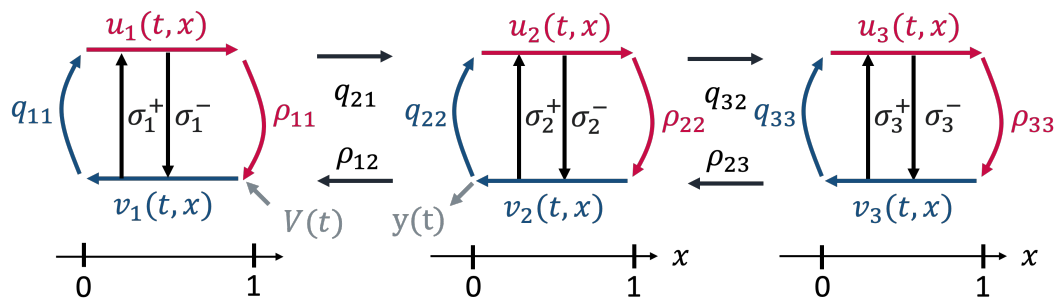


Figure 8.13 – Schematic representation of the system (5.1),(8.37)

We illustrate this situation with $N = 3$ hyperbolic PDE subsystems, schematically represented in Figure 8.13. Following the approach from Chapter 7, we could use different integral transforms to move the in-domain couplings at each boundary. Using the method of characteristics in the target systems and under some assumptions, the stabilization of

the chain could be related to the one of the following integral delay equation

$$\begin{aligned} \alpha(t) - q_2\alpha(t - \tau_2) - q_3\alpha(t - \tau_3) - q_{23}\alpha(t - (\tau_2 + \tau_3)) - \int_0^{\tau_2 + \tau_3} N_\alpha(s)\alpha(t - s)ds \\ = q_1\bar{V}(t - (\tau_1 + \frac{1}{\lambda_2})) + \int_{\frac{1}{\lambda_2}}^{\tau_1 + \frac{1}{\lambda_2}} N_V(s)\bar{V}(t - s)ds. \end{aligned} \quad (8.36)$$

Due to multiple, not necessarily commensurate delays, this IDE cannot be straightforwardly stabilized [DDLM15]. In the general case of N subsystems, each state i satisfies (5.1) with boundary conditions

$$\begin{aligned} u_i(t, 0) &= q_{ii}v_i(t, 0) + q_{i,i-1}u_{i-1}(t, 1), \\ v_i(t, 1) &= \rho_{ii}u_i(t, 1) + \rho_{i,i+1}v_{i+1}(t, 0) + \delta_c^i V(t), \end{aligned} \quad (8.37)$$

such that subsystem $c \in \llbracket 1, N-1 \rrbracket$ is actuated. Following the system studied in Section 7.1, we assume we have a boundary measurement $y(t) = v_{c+1}(t, 0)$.

In the case of a cascaded network, [Aur20] proposed a general invertible transform on each PDE subsystem to move all in-domain couplings to the actuated boundary $x = 1$ of subsystem c . In the more general case, we could apply a transform composed of a Volterra plus an affine term for each downstream subsystem to move all in-domain couplings to one boundary. Due to the inherent transport delay in each subsystem, a reformulation as a time delay system would result in a general integral delay equation of form (8.36) with multiple pointwise delayed terms.

We could also combine this approach with [RAN21a] to tackle a wider diversity of physical systems with an arbitrary number of PDEs or ODEs. For applications such as microendoscopes, the localization and the number of control inputs available is of high interest [WLG18]. We could also ponder more general controllability properties and the optimal location of several actuators along the network. Note that the control of a string with in-domain actuation considered in Chapter 8, in the general case where the actuator is not located in the middle of the string, resulting in the control of an integral delay equation of form (8.36), with 2 pointwise delay terms corresponding to the transport time on each side of the actuator.

Chains of scalar hyperbolic subsystems containing loops

Finally, a last extension of the proposed approach could be considering chain networks containing loops (cycles). It corresponds to the chain of N hyperbolic scalar PDE subsystems introduced in the previous section, where the first and last PDE subsystems are also interconnected. Such systems can represent networks of pipes transporting fluids [WA22].

Part IV

Exploring under-considered aspects of backstepping-based controllers

Different case studies

**Exploration d'aspects négligés dans la conception
de contrôleurs par backstepping**

Divers cas d'études

Introduction

In parts II and III, we presented backstepping-based controller designs for different classes of interconnected hyperbolic PDE systems. We raised some difficulties regarding numerical implementation (such as computation time). In Part IV, we aim to focus on these under-considered aspects of the backstepping-based controllers.

The backstepping methodology proved its efficiency as a constructive method, and in some cases may offer better closed-loop performances than classic finite dimension controllers [ABS⁺22]. So far, emphasis was placed on stabilizing systems, and not on controller tuning. As already mentioned, finding an adequate target system requires some expertise. Indeed, it must be simple enough to grant stability properties easily. First, all the in-domain couplings were suppressed in the target system. Though it allowed for finite-time stabilization, it was shown to have a negative impact on the robustness with regard to small delays. It might then be necessary to keep some in-domain coupling terms, or not to completely cancel the reflection term. However, the target system must be reachable by an invertible transform. As seen in Part III, the classic Volterra integral transforms cannot handle some integral couplings, preventing a mapping to the easily-assessable exponentially target system. We give clues and new frameworks to answer the following questions:

1. What is the class of reachable target systems?
2. How to define a target system with specific stability properties?
3. How to ease the numerical implementation of backstepping-based controllers to obtain real-time implementable control laws?

To broaden the use of backstepping-based controllers, a concern may be the choice of a reachable class of target systems that can be mapped from an initial plant. Since the closed-loop performance depends on the choice of a target system, it is a crucial step in the controller design. In **Chapter 9**, we introduce an innovative time-affine transform that maps a linear first-order hyperbolic PDE system to an arbitrary target system of the same class. This considerably simplifies concerns about the choice of a target system and eases the design procedure. Indeed, it allows mapping any target system within a specific class. Among this class of reachable target systems, we must then determine the ones presenting adequate closed-loop properties. To do so, we can use sufficient criteria as given in Chapter 2 in the scalar case or more broadly gathered in [Aur18]. In **Chapter 10**, we show how the Port Hamiltonian framework [JZ12] can help design target systems with specified asymptotic properties by adding tuning parameters with a physical meaning. We illustrate the methodology proposed in Chapter 9 on two simple test cases. Since the backstepping-based controllers require the knowledge of all distributed states, an observer state must also be designed, usually following a dual approach.

Finally, one major drawback of the backstepping-based controllers remains their numerical limitations. If real-time control (or online control for adaptive controllers) is desired, the computation time becomes crucial. Output-feedback controllers often involve solving the observer PDE system at each time step, which can be computationally demanding [ADAK16a, ADAK16b, SA17]. It usually requires numerical discretization schemes

such as finite difference, finite element, or spectral methods [LeVo2]. As emphasized in Chapter 4, a trade-off must be found to ensure the stability of the numerical scheme while limiting the size of the mesh. It is even more accurate when the control design requires using predictors as in Chapter 5. Recently, advances in machine learning allowed mapping parameters to infinite dimensional operators [LJK21, LKA⁺21]. To downplay the necessary computation time required to implement backstepping-based controllers, it might be of high interest [BSK23, SLY⁺22]. Following this trend, we ponder in **Chapter 11** on using Machine Learning-based solutions to fasten a PDE model resolution drastically. First, in the wake of [SLY⁺22], we consider using neural networks as a surrogate for classical backstepping-based observers. Next, inspired by [AKN21], we consider their interest in estimating unknown physical parameters for one drilling example given in Chapter 6.

9 - Arbitrary target system for a general class of non-scalar hyperbolic PDE systems

In this chapter, we propose a methodology to map a general class of nonscalar hyperbolic PDE systems to any target system of the same class with different in-domain couplings. We consider linear hyperbolic PDE systems from Chapter 2, extended in the general nonscalar framework. This general class of $(n+m) \times (n+m)$ linear hyperbolic PDE systems is fully actuated at one end. It contains potentially destabilizing in-domain and boundary couplings and is presented in Section 9.1. They can model the coupled torsional and axial dynamics of a drillstring [AvdW18] or the motion of a Timoshenko beam [Tim74], as illustrated in Chapter 10. Using a full-state feedback control law, we want to map a system in this class to an arbitrary target system with a similar structure. More precisely, we modify the in-domain couplings, while the transport speeds and unactuated boundary couplings remain unchanged. The backstepping methodology inspires the approach proposed in Section 9.2. We apply a classic Volterra integral transform from the initial and target systems to replace the distributed in-domain couplings with local terms. We introduce an innovative time-affine transform to map the two simplified equivalent systems. This transform requires past values of one boundary state. Composing all these boundedly invertible transforms, we can derive in Section 9.3 a distributed controller. It allows the initial system in closed loop to share asymptotic stability properties with a specified target system.

Chapitre 9: Système cible arbitraire pour une classe générale de systèmes d'EDP hyperboliques non scalaires.

Ce chapitre porte sur les systèmes d'EDP hyperboliques linéaires considérés dans le Chapitre 2, étendus dans le cadre général non scalaire. Cette classe générale de systèmes hyperboliques, avec des couplages potentiellement déstabilisants à l'intérieur du domaine et aux frontières, est actionnée à une extrémité (Section 9.1). Ils peuvent modéliser la dynamique torsionnelle et axiale couplée d'un système de forage [AvdW18] ou le mouvement d'une poutre de Timoshenko [Tim74], comme illustré dans le Chapitre 10. En utilisant une loi de commande de rétroaction d'état complet, nous souhaitons envoyer un système de cette classe sur un système cible arbitraire. L'approche proposée est inspirée de la méthodologie de backstepping (Section 9.2). À partir du système initial et du système cible, une transformation intégrale de Volterra classique est d'abord utilisée pour remplacer les couplages répartis dans le domaine par des termes locaux. Pour mapper les deux systèmes équivalents simplifiés, nous introduisons ensuite une nouvelle transformation affine en temps. Elle nécessite les valeurs passées d'un état à la frontière. En composant toutes ces transformations inversibles et bornées, une loi de commande distribuée est obtenue (Section 9.3). Elle garantit que le système initial en boucle fermée partage les mêmes propriétés asymptotique qu'un autre système cible de la même classe avec des termes de couplage à l'intérieur du domaine choisis arbitrairement.

Contents

9.1 Problem description	177
9.1.1 System under consideration	177
9.1.2 Control objective	178
9.1.3 Overall strategy	179
9.2 Full-state feedback control law design	180
9.2.1 classic backstepping transforms	180
9.2.2 Time-space affine change of variable	183
9.3 Control law	191

Some of the results given herein were submitted to Systems & Control Letters [J1].

9.1 . Problem description

In this section, we first present the class of hyperbolic systems under consideration. Then, we present the control objective and the overall control design strategy.

9.1.1 . System under consideration

Consider a linear $(n + m) \times (n + m)$ hyperbolic PDE system defined by

$$\begin{aligned} \frac{\partial}{\partial t} \xi^+(t, x) + \Lambda^+ \frac{\partial}{\partial x} \xi^+(t, x) &= \Sigma^{++}(x) \xi^+(t, x) + \Sigma^{+-}(x) \xi^-(t, x), \\ \frac{\partial}{\partial t} \xi^-(t, x) - \Lambda^- \frac{\partial}{\partial x} \xi^-(t, x) &= \Sigma^{-+}(x) \xi^+(t, x) + \Sigma^{--}(x) \xi^-(t, x), \end{aligned} \quad (9.1)$$

and the boundary conditions

$$\xi^+(t, 0) = Q_0 \xi^-(t, 0), \quad \xi^-(t, 1) = R_1 \xi^+(t, 1) + V(t), \quad (9.2)$$

with coupling matrices $Q_0 \in \mathbb{R}^{m \times n}$, $R_1 \in \mathbb{R}^{n \times m}$. It corresponds to a generalization in the nonscalar case of system (2.1)-(2.3). The positive constant transport velocity matrices, denoted $\Lambda^+ = \text{diag}(\lambda_i) \in D_n^+$, $\Lambda^- = \text{diag}(\mu_i) \in D_m^+$, are sorted by decreasing order, i.e. $\lambda_1 > \lambda_2 > \dots > \lambda_n$ and $\mu_1 > \mu_2 > \dots > \mu_m$. As mentioned in previous chapters, the following approach can be adapted to the space-dependent case to the price of more technical computations. We have in-domain coupling matrix-valued functions $\Sigma^{+-} \in C^1([0, 1], \mathbb{R}^{n \times m})$, $\Sigma^{-+} \in C^1([0, 1], \mathbb{R}^{m \times n})$, $\Sigma^{++} \in C^1([0, 1], \mathbb{R}^{n \times n})$, and $\Sigma^{--} \in C^1([0, 1], \mathbb{R}^{m \times m})$. As classically considered, [VKC11, HVDMK15, Aur18], we have, for all $x \in [0, 1]$, $\forall 1 \leq i \leq n$, $\Sigma_{ii}^{++}(x) = 0$ and $\forall 1 \leq i \leq m$, $\Sigma_{ii}^{--}(x) = 0$. We have the following

Lemma 9.1.1: well-posedness of the system [Rus78b, Corog]

For any initial conditions $(\xi_0^+, \xi_0^-) \in H^1([0, 1], \mathbb{R}^{n+m})$, every control input $V(t) \in \mathbb{R}^m$ regular enough, satisfying appropriate compatibility conditions (2.1.1), system (9.1) along with boundary condition (9.2) admits a unique solution $\xi = [\xi^{+\top}, \xi^{-\top}]^\top \in C^0([0, +\infty); H^1([0, 1], \mathbb{R}^{n+m}))$.

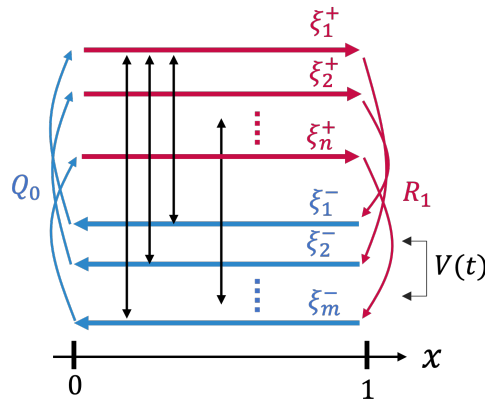


Figure 9.1 – Schematic representation of (9.1)-(9.2)

9.1.2 . Control objective

Class of reachable target system

In this chapter, we aim at mapping the system (9.1)-(9.2) to a target system of the same class with specific asymptotic stability properties. The general class of target systems is defined by the following set of PDEs

$$\begin{aligned} \frac{\partial}{\partial t} \bar{\xi}^+(t, x) + \Lambda^+ \frac{\partial}{\partial x} \bar{\xi}^+(t, x) &= \bar{\Sigma}^{++}(x) \bar{\xi}^+(t, x) + \bar{\Sigma}^{+-}(x) \bar{\xi}^-(t, x), \\ \frac{\partial}{\partial t} \bar{\xi}^-(t, x) - \Lambda^- \frac{\partial}{\partial x} \bar{\xi}^-(t, x) &= \bar{\Sigma}^{-+}(x) \bar{\xi}^+(t, x) + \bar{\Sigma}^{--}(x) \bar{\xi}^-(t, x), \end{aligned} \quad (9.3)$$

with boundary conditions

$$\bar{\xi}^+(t, 0) = Q_0 \bar{\xi}^-(t, 0), \quad \bar{\xi}^-(t, 1) = \bar{V}(t), \quad (9.4)$$

with $\bar{V}(t)$ a regular enough arbitrary function that can depend on the boundary or distributed state. As shown in Chapter 2, if we find boundedly invertible transforms mapping the closed-loop system (9.1)-(9.2) to (9.3)-(9.4), they will share the same stability properties.

The control objective reads as follows

Objective 9.1.1: Target closed-loop behaviour

Design a full-state feedback control law $V(t) \in L^2([0, +\infty), \mathbb{R}^m)$ such that the closed-loop system (9.1)-(9.2) has the same asymptotic stability properties that the target system defined by (9.3)-(9.4).

First considerations

In this target system, the boundary couplings at the unactuated boundary $x = 0$ remain the same, since they cannot be modified by Volterra integral transforms. Here, we introduce new in-domain coupling terms $\bar{\Sigma}$, which are also assumed to be continuous and differentiable matrix-valued functions. As before, $\bar{\Sigma}^{++}, \bar{\Sigma}^{--}$ must have no term on their diagonal. This defines a class of **reachable target systems**, with in-domain couplings and couplings at the actuated boundary considered as degrees of freedom.

We are interested in specifying these degrees of freedom to ensure that the target system has specified asymptotic properties. The main criterion remains exponential stability of the closed-loop system. For instance, one can choose

$$\bar{V}(t) = \bar{R}_1 \bar{\xi}^+(t, 1), \quad (9.5)$$

with \bar{R}_1 ensuring asymptotic stability of the system (9.3)-(9.5) in the sense of the L^2 -norm. Thanks to a Lyapunov approach, we can derive sufficient conditions from Linear Matrices Inequalities (LMIs) to do so. We have the following

Theorem 9.1.1: Linear Matrices Inequalities [BC16, Proposition 5.2]

The solution of (9.3)-(9.5) with initial condition $(\bar{\xi}_0^+, \bar{\xi}_0^-)$ is exponentially stable (for the L^2 -norm) if there exist some reals $\mu \neq 0$, $p_i > 0$, $i = 1, \dots, n$ and $q_j > 0$, $j = 1, \dots, m$ such that

$$\begin{pmatrix} P^+ \Lambda^+ e^{-\mu} & 0 \\ 0 & P^- \Lambda^- \end{pmatrix} - \begin{pmatrix} 0 & Q_0 \\ R_1 & 0 \end{pmatrix}^\top \begin{pmatrix} P^+ \Lambda^+ & 0 \\ 0 & P^- \Lambda^- e^{\mu} \end{pmatrix} \begin{pmatrix} 0 & Q_0 \\ R_1 & 0 \end{pmatrix} \geq 0,$$

and for all $x \in [0, 1]$, $\mu P(\mu x) \begin{pmatrix} \Lambda^+ & 0 \\ 0 & \Lambda^- \end{pmatrix} - \bar{\Sigma}(x)^\top P(\mu x) - P(\mu x) \bar{\Sigma}(x) > 0$, with $P^+ = \text{diag}\{p_1, \dots, p_n\}$, $P^- = \text{diag}\{q_1, \dots, q_m\}$ and $P(\mu x) = \text{diag}\{P^+ e^{-\mu x}, P^- e^{\mu x}\}$.

More explicit conditions can be derived when the in-domain couplings have a specific structure, e.g. constant. To solve LMIs numerically, a feasibility solver such as `fesap` [GN97] is required. Its complexity depends quadratically on the problem size. Note that LMI can be used to derive sufficient stability conditions for neutral time-delay systems too [KMC05]. We can also impose a specific **closed-loop behavior** using the Port-Hamiltonian framework, as presented in Chapter 10.

9.1.3 . Overall strategy

Overall transform

Using a classic Volterra integral transform, it is not possible to map directly (9.1)-(9.2) to (9.3)-(9.4), in the nonscalar case. We have the following

Proposition 9.1.1 For all $t > 0$, for any initial conditions, for any $V(t)$, $\bar{V}(t)$, let us denote $[\bar{\xi}^+(t, \cdot)^\top \bar{\xi}^-(t, \cdot)^\top]^\top \in H^1([0, 1], \mathbb{R}^{n+m})$ the solution of (9.3)-(9.4) and $[\xi^+(t, \cdot)^\top \xi^-(t, \cdot)^\top]^\top \in H^1([0, 1], \mathbb{R}^{n+m})$ the solution of (9.1)-(9.2). If $n > 1$, $m > 1$, it is not always possible to find a transform \mathcal{K} of form (2.8) such that

$$\forall t > 0, \begin{pmatrix} \bar{\xi}^+(t, \cdot) \\ \bar{\xi}^-(t, \cdot) \end{pmatrix} = \mathcal{K} \left(\begin{pmatrix} \xi^+(t, \cdot) \\ \xi^-(t, \cdot) \end{pmatrix} \right).$$

Proof : For all $x \in [0, 1]$, define the Volterra integral transform $\mathcal{K} : H^1([0, 1], \mathbb{R}^{n+m}) \rightarrow H^1([0, 1], \mathbb{R}^{n+m})$

$$\mathcal{K}(\xi)(x) = \xi(x) - \int_0^x K(x, y) \xi(y) dy, \quad (9.6)$$

with kernels $K = \begin{pmatrix} K^{++} & K^{+-} \\ K^{-+} & K^{--} \end{pmatrix} \in C_{pw}^1(\mathcal{T}^-, \mathbb{R}^{(n+m) \times (n+m)})$.

Following the backstepping methodology, we show that kernels K^{++} , K^{+-} must satisfy

$$\begin{aligned} \Lambda^+ \frac{\partial}{\partial x} K^{++} + \frac{\partial}{\partial y} K^{++} \Lambda^+ &= \bar{\Sigma}^{++}(x) K^{++} + \bar{\Sigma}^{+-}(x) K^{+-} - K^{++} \Sigma^{++}(y) - K^{+-} \Sigma^{-+}(y), \\ \Lambda^+ \frac{\partial}{\partial x} K^{+-} - \frac{\partial}{\partial y} K^{+-} \Lambda^- &= \bar{\Sigma}^{++}(x) K^{+-} + \bar{\Sigma}^{--}(x) K^{--} - K^{++} \Sigma^{+-}(y) - K^{+-} \Sigma^{--}(y), \end{aligned}$$

with boundary conditions

$$K^{++}(x, x) \Lambda^+ - \Lambda^+ K^{++}(x, x) = \bar{\Sigma}^{++}(x) - \Sigma^{++}(x), \quad (9.7)$$

$$\Lambda^+ K^{+-}(x, x) + K^{+-}(x, x) \Lambda^- = \Sigma^{+-}(x) - \bar{\Sigma}^{+-}(x), \quad (9.8)$$

$$K^{+-}(x, 0) \Lambda^- - K^{++}(x, 0) \Lambda^+ Q_0 = 0. \quad (9.9)$$

We can easily show that kernels K^{-+} , K^{--} satisfy a similar set of equations. With no further conditions on the couplings, this system is **ill-posed**. Indeed, the boundary condition (9.8) in $x = y$ entirely defines K^{+-} on \mathcal{T}^- . Then, boundary conditions (9.7), (9.9) do not suffice to entirely define K^{++} on \mathcal{T}^- . If Q_0 admits a left invert $Q_{0,l}^{-1}$, that is if its lines are spanning vectors for \mathbb{R}^n , (9.9) rewrites $K^{++}(x, 0) = K^{+-}(x, 0) \Lambda^- Q_{0,l}^{-1} (\Lambda^+)^{-1}$. Components K_{ij}^{++} , for $j \geq i$ are then well-defined. However, along the segment $\{y = 0, 0 \leq x \leq 1 - \frac{\lambda_j}{\lambda_i}\}$, the component must satisfy (9.9) but is also defined by (9.7) using the method of characteristics. Complex compatibility conditions should be satisfied to ensure the well-posedness. Similarly, with no assumption on Q_0 , some components of K^{++} might not be entirely defined on \mathcal{T}^- . The well-posedness of this set of equations is therefore not guaranteed in the general case. ■

Consequently, in the general case, we cannot directly use the backstepping methodology with a classic Volterra integral transform to fulfill objective 9.1.1. However, it is possible for $n = m = 1$, as illustrated in Chapter 10.

Step by step approach

To simplify the analysis, we propose to apply a step-by-step approach with different successive transforms:

1. In section 9.2.1, we use two classic backstepping Volterra transforms of form (9.6)
 - \mathcal{K} to map the system ξ to a simpler target system γ for which most of the in-domain coupling terms have been moved at the actuated boundary;
 - $\bar{\mathcal{K}}$ to map the target system $\bar{\xi}$ to a system $\bar{\gamma}$, for which most of the in-domain coupling terms have been moved at the boundary $x = 1$.

It simplifies the structure.

2. Next, in Section 9.2.2, we use a specific invertible time-affine transform \mathcal{F} to map the system γ to the system $\bar{\gamma}$ of the same form.

Composing the different transforms, it becomes straightforward to design the corresponding feedback law in Section 9.3.

9.2 . Full-state feedback control law design

9.2.1 . classic backstepping transforms

Inspired by [HVDMK15, CHO17], we use a classic Volterra transform on system (9.1)-(9.2) to map it to a simpler system, where most of the in-domain coupling terms have been moved to the actuated boundary.

First Volterra integral transform

Define $\Gamma^+ \in C_{pw}^0([0, 1], \mathbb{R}^{n \times m})$, $\Gamma^- \in C_{pw}^0([0, 1], \mathbb{R}^{m \times m})$ two piecewise continuous matrix-valued functions. For all $x \in [0, 1]$, define the Volterra integral transform \mathcal{K} of form

(9.6), with kernels $K = \begin{pmatrix} K^{++} & K^{+-} \\ K^{-+} & K^{--} \end{pmatrix}$ satisfying the following partial differential equations

$$\begin{aligned} \Lambda^+ \frac{\partial}{\partial x} K^{++}(x, y) + \frac{\partial}{\partial y} K^{++}(x, y) \Lambda^+ &= -K^{++}(x, y) \Sigma^{++}(y) - K^{+-}(x, y) \Sigma^{-+}(y), \\ \Lambda^+ \frac{\partial}{\partial x} K^{+-}(x, y) - \frac{\partial}{\partial y} K^{+-}(x, y) \Lambda^- &= -K^{++}(x, y) \Sigma^{+-}(y) - K^{+-}(x, y) \Sigma^{--}(y), \\ \Lambda^- \frac{\partial}{\partial x} K^{-+}(x, y) - \frac{\partial}{\partial y} K^{-+}(x, y) \Lambda^+ &= K^{-+}(x, y) \Sigma^{++}(y) + K^{--}(x, y) \Sigma^{-+}(y), \\ \Lambda^- \frac{\partial}{\partial x} K^{--}(x, y) + \frac{\partial}{\partial y} K^{--}(x, y) \Lambda^- &= K^{-+}(x, y) \Sigma^{+-}(y) + K^{--}(x, y) \Sigma^{--}(y). \end{aligned} \quad (9.10)$$

They satisfy the boundary conditions for all $x \in [0, 1]$,

$$\begin{aligned} \Lambda^+ K^{++}(x, x) - K^{++}(x, x) \Lambda^+ &= \Sigma^{++}(x), \quad \Lambda^+ K^{+-}(x, x) + K^{+-}(x, x) \Lambda^- = \Sigma^{+-}(x), \\ \Lambda^- K^{-+}(x, x) + K^{-+}(x, x) \Lambda^+ &= -\Sigma^{-+}(x), \quad \Lambda^- K^{--}(x, x) - K^{--}(x, x) \Lambda^- = -\Sigma^{--}(x). \end{aligned} \quad (9.11)$$

The two following equations must also be satisfied in $y = 0$, for all $x \in [0, 1]$,

$$\begin{aligned} -K^{++}(x, 0) \Lambda^+ Q_0 + K^{+-}(x, 0) \Lambda^- &= \Gamma^+(x), \\ -K^{-+}(x, 0) \Lambda^+ Q_0 + K^{--}(x, 0) \Lambda^- &= \Gamma^-(x). \end{aligned} \quad (9.12)$$

As mentioned earlier, some components of Γ^\pm are degrees of freedom, while others are imposed by the boundary conditions (9.11). To guarantee the well-posedness of the kernel equations, we must impose arbitrary conditions in $x = 1$ for $K_{ij}^{\pm\pm}$, $i > j$. To guarantee the continuity of the kernels along the boundary $y = z$, we can impose

$$K_{ij}^{++}(1, y) = \frac{\Sigma_{ij}^{++}(1)}{\lambda_i - \lambda_j}, \quad K_{ij}^{--}(1, y) = \frac{\Sigma_{ij}^{--}(1)}{\mu_j - \mu_i}, \quad i > j. \quad (9.13)$$

Following the considerations presented in Appendix C, we could rather impose

$$K_{ij}^{++}(1, y) = 0, \quad K_{ij}^{--}(1, y) = 0.$$

Some components of the coupling matrix Γ^- can also be simplified using the remaining degrees of freedom in $y = 0$ for $K_{ij}^{\pm\pm}$, $i \leq j$. Imposing for $i \leq j$,

$$\Gamma_{ij}^-(x) = 0 \Leftrightarrow K_{ij}^{--}(x, 0) = (K^{-+}(x, 0) \Lambda^+ Q_0 (\Lambda^-)^{-1})_{ij}, \quad (9.14)$$

simplifies the structure of the target system. It guarantees that the in-domain coupling matrices in the target system for the leftward convecting equation are strictly triangular [HVD⁺15]. Similarly, if the boundary coupling matrix Q_0 is invertible, we can simplify the couplings in the target system by imposing

$$\Gamma_{ij}^+(x) = 0 \Leftrightarrow K_{ij}^{++}(x, 0) = (K^{+-}(x, 0) \Lambda^- (\Lambda^+ Q_0)^{-1})_{ij}, \quad i \leq j. \quad (9.15)$$

We have the following lemma

Lemma 9.2.1: Well-posedness of the kernel equations [HVDMK15]

The system defined by (9.10)-(9.13) with $\frac{n(n+1)}{2}$ (resp. $\frac{m(m+1)}{2}$) continuous boundary conditions defining $K_{ij}^{++}(\cdot, 0)$ (resp. $K_{ij}^{--}(\cdot, 0)$), for $i \leq j$ admits a unique solution in $C_{pw}^1(\mathcal{T}^-, \mathbb{R}^{(n+m) \times (n+m)})$. The Volterra integral transform \mathcal{K} defined by (9.6) is boundedly invertible. Its inverse transform $\mathcal{L} = \mathcal{K}^{-1}$ is also a Volterra integral transform.

Proof: The proof can be adjusted from [HVDMK15, Theorem A.1]. The kernels' regularity derives from the one of the coupling terms. The kernel $L \in C_{pw}^1(\mathcal{T}^-, \mathbb{R}^{(n+m) \times (n+m)})$ of the inverse transform are related to the ones of the direct transform by $L(x, y) = -K(x, y) + \int_y^x K(x, s)L(s, y)ds$. ■

Mapped target system

We next define a new state $\gamma = [\gamma^{+\top}, \gamma^{-\top}]^\top = \mathcal{K}(\xi)$ obtained using the invertible transform (9.6). It satisfies

$$\begin{aligned} \frac{\partial}{\partial t} \gamma^+(t, x) + \Lambda^+ \frac{\partial}{\partial x} \gamma^+(t, x) &= \Gamma^+(x) \gamma^-(t, 0), \\ \frac{\partial}{\partial t} \gamma^-(t, x) - \Lambda^- \frac{\partial}{\partial x} \gamma^-(t, x) &= \Gamma^-(x) \gamma^-(t, 0), \end{aligned} \quad (9.16)$$

with the boundary conditions

$$\gamma^+(t, 0) = Q_0 \gamma^-(t, 0), \quad \gamma^-(t, 1) = R_1 \gamma^+(t, 1) + V(t) + I_1(t). \quad (9.17)$$

The integral term $I_1(t)$ is given by

$$I_1(t) = \int_0^1 (L^{+-}(1, y) - R_1 L^{++}(1, y)) \gamma^+(t, y) + (L^{-+}(1, y) - R_1 L^{--}(1, y)) \gamma^-(t, y) dy, \quad (9.18)$$

while the coupling matrix-valued functions are defined by

$$\begin{aligned} \Gamma_{ij}^+(x) &= \begin{cases} 0, & \text{for } j \leq i \text{ if } Q_0 \text{ invertible} \\ (K^{+-}(x, 0)\Lambda^- - K^{++}(x, 0)\Lambda^+ Q_0)_{ij}, & \text{else,} \end{cases} \\ \Gamma_{ij}^-(x) &= \begin{cases} 0, & \text{if } j \leq i, \\ (K^{-+}(x, 0)\Lambda^- - K^{--}(x, 0)\Lambda^+ Q_0)_{ij}, & \text{else.} \end{cases} \end{aligned}$$

Second Volterra Integral transform

As in the previous section, we use another Volterra integral transform to map the target system (9.3)-(9.4) to a simpler system (9.21)-(9.22). Define the integral operator $\bar{\mathcal{K}} : H^1([0, 1], \mathbb{R}^{n+m}) \rightarrow H^1([0, 1], \mathbb{R}^{n+m})$ by, for all $x \in [0, 1]$,

$$\bar{\gamma}(x) = \bar{\mathcal{K}}(\bar{\xi}(x)) = \bar{\xi}(x) - \int_0^x \bar{K}(x, y) \bar{\xi}(y) dy. \quad (9.19)$$

For any kernels $\bar{K} \in C_{pw}^1(\mathcal{T}^-, \mathbb{R}^{(n+m) \times (n+m)})$, this transform is boundedly invertible, and its inverse transform, denoted $\bar{\mathcal{L}}$ is also a Volterra integral transform of the form (9.6). The kernels $\bar{K} = \begin{pmatrix} \bar{K}^{++} & \bar{K}^{+-} \\ \bar{K}^{-+} & \bar{K}^{--} \end{pmatrix}$ satisfy analogous equations to the ones given by (9.10)-(9.14)

(except that terms Σ^{\cdot} are replaced by functions $\bar{\Sigma}^{\cdot}$ in equations (9.10)-(9.11),(9.13)). Now, define the matrix-valued functions $\bar{\Gamma}^+ \in C_{pw}^0([0, 1], \mathbb{R}^{n \times m})$ and $\bar{\Gamma}^- \in C_{pw}^0([0, 1], \mathbb{R}^{m \times m})$ by

$$\begin{aligned} \bar{\Gamma}_{ij}^+(x) &= \begin{cases} 0, & \text{for } j \leq i, \text{ if } Q_0 \text{ invertible} \\ (\bar{K}^{+-}(x, 0)\Lambda^- - \bar{K}^{++}(x, 0)\Lambda^+Q_0)_{ij}, & \text{else,} \end{cases} \\ \bar{\Gamma}_{ij}^-(x) &= \begin{cases} 0, & \text{if } j \leq i, \\ (\bar{K}^{--}(x, 0)\Lambda^- - \bar{K}^{-+}(x, 0)\Lambda^+Q_0)_{ij}, & \text{else.} \end{cases} \end{aligned} \quad (9.20)$$

Note that $\bar{\Gamma}^-$ (as Γ^-) is strictly lower triangular. Differentiating with respect to time and space (9.19), and since $\bar{\xi} = [\bar{\xi}^{+\top}, \bar{\xi}^{-\top}]^\top$ is the unique solution of (9.3)-(9.4), we show, that $\bar{\gamma} = [\bar{\gamma}^{+\top}, \bar{\gamma}^{-\top}]^\top$ satisfies

$$\begin{aligned} \frac{\partial}{\partial t} \bar{\gamma}^+(t, x) + \Lambda^+ \frac{\partial}{\partial x} \bar{\gamma}^+(t, x) &= \bar{\Gamma}^+(x) \bar{\gamma}^-(t, 0), \\ \frac{\partial}{\partial t} \bar{\gamma}^-(t, x) - \Lambda^- \frac{\partial}{\partial x} \bar{\gamma}^-(t, x) &= \bar{\Gamma}^-(x) \bar{\gamma}^-(t, 0), \end{aligned} \quad (9.21)$$

with boundary conditions

$$\bar{\gamma}^+(t, 0) = Q_0 \bar{\gamma}^-(t, 0), \quad \bar{\gamma}^-(t, 1) = \bar{V}_\gamma(t), \quad (9.22)$$

with $\bar{V}_\gamma(t) = \bar{V}(t) - \int_0^1 \bar{K}^{-+}(1, y) \bar{\xi}^+(t, y) + \bar{K}^{--}(1, y) \bar{\xi}^-(t, y) dy$. For any initial conditions $\bar{\gamma}_0 = \bar{K}(\bar{\xi}_0) \in H^1([0, 1], \mathbb{R}^{n+m})$ satisfying the compatibility conditions, this system admits a unique solution in $C^0([0, +\infty); H^1([0, 1], \mathbb{R}^{n \times m}))$.

9.2.2 . Time-space affine change of variable

In the following, we denote $\bar{\tau} = \max\{\frac{1}{\mu_m}, \frac{1}{\lambda_n}\}$. Define $\chi \doteq H^1([0, 1], \mathbb{R}^{n+m}) \times \mathcal{D}_\tau$, with $\mathcal{D}_\tau \doteq D_{\tau_1} \times D_{\tau_2} \times \dots \times D_{\tau_m}$, and $\tau_i = (m - i + 1)\bar{\tau}$. We now map the solution of (9.16)-(9.17) to the solution of (9.21)-(9.22), for any initial condition. Define for all $x \in [0, 1]$, $t \geq t^* \doteq m\bar{\tau} > 0$, a *time-affine* change of variables by

$$\text{for } 1 \leq i \leq m, \quad (9.23)$$

$$\bar{\gamma}_i^-(t, x) = \gamma_i^-(t, x) + \int_0^{\frac{1-x}{\mu_i}} \sum_{j=1}^{i-1} F_{ij}^-(x, y) \gamma_j^-(t-y, 0) + \sum_{j=2}^{i-1} H_{ij}^-(x, y) \bar{\gamma}_j^-(t-y, 0) dy,$$

$$\text{for } 1 \leq i \leq n, \quad (9.24)$$

$$\begin{aligned} \bar{\gamma}_i^+(t, x) &= \gamma_i^+(t, x) + \int_0^{\frac{x}{\lambda_i}} \sum_{j=1}^m F_{ij}^+(x, y) \gamma_j^-(t-y, 0) + \sum_{j=2}^m H_{ij}^+(x, y) \bar{\gamma}_j^-(t-y, 0) dy \\ &+ \int_{\frac{x}{\lambda_i}}^{\frac{1}{\mu_m} + \frac{x}{\lambda_i}} \sum_{j=1}^{m-1} M_{ij}^+(x, y) \gamma_j^-(t-y, 0) + \sum_{j=2}^{m-1} N_{ij}^+(x, y) \bar{\gamma}_j^-(t-y, 0) dy. \end{aligned}$$

Notice that this transform requires the past values of the boundary state $\bar{\gamma}(\cdot, 0)$. As explained later, this transform is only defined for $t > m\bar{\tau}$ due to its recursive form. Also, note that the first component of the leftward convecting state $\gamma_1^-(t, x)$ is not modified here.

For all $1 \leq i \leq n$, $1 \leq j \leq m$ (resp. $2 \leq j \leq m$), F_{ij}^+ , (resp. H_{ij}^+) is a real-valued function

in $C_{pw}^1(\mathcal{T}_{\lambda_i}^+, \mathbb{R})$, and for all $1 \leq i \leq n$, $1 \leq j \leq m-1$ (resp. $2 \leq j \leq m-1$), M_{ij}^+ (resp. N_{ij}^+) is a real-valued function in $C_{pw}^1(\mathcal{P}_{\frac{1}{\mu_m}, \lambda_i}^+, \mathbb{R})$. For all $1 \leq i \leq m$, $1 \leq j \leq i-1$ (resp. $2 \leq j \leq i-1$), function F_{ij}^- (resp. H_{ij}^-) is defined in $C_{pw}^1(\mathcal{T}_{\mu_i}^-, \mathbb{R})$. Transform (9.23)-(9.24) can be rewritten in a more condensed form

$$\bar{\gamma}^-(x) = \gamma^-(x) + \int_0^{\frac{1-x}{\mu_m}} F^-(x, y) \gamma^-(t-y, 0) + H^-(y) \bar{\gamma}^-(t-y, 0) dy, \quad (9.25)$$

$$\begin{aligned} \bar{\gamma}^+(x) &= \gamma^+(x) + \int_{\frac{x}{\lambda_n}}^{\frac{1}{\mu_m} + \frac{x}{\lambda_n}} M^+(x, y) \gamma^-(t-y, 0) + N^+(x, y) \bar{\gamma}^-(t-y, 0) dy \\ &+ \int_0^{\frac{x}{\lambda_n}} F^+(x, y) \gamma^-(t-y, 0) + H^+(x, y) \bar{\gamma}^-(t-y, 0) dy. \end{aligned} \quad (9.26)$$

Matrices F^-, H^- have a strictly lower triangular form and are defined for all $x \in [0, 1]$, for all $y \in [0, \frac{1-x}{\mu_m}]$ by

$$\begin{aligned} (F^-(x, y))_{ij} &= \mathbb{1}_{[0, \frac{1-x}{\mu_i}]}(y) F_{ij}^-(x, y), \quad \forall 2 \leq i \leq m, 1 \leq j \leq i-1, \\ (H^-(x, y))_{ij} &= \mathbb{1}_{[0, \frac{1-x}{\mu_i}]}(y) H_{ij}^-(x, y), \quad \forall 2 \leq i \leq m, 2 \leq j \leq i-1. \end{aligned}$$

Similarly, matrices F^+, H^+ are defined component-wise for all $x \in [0, 1]$ by:

$$\begin{aligned} \forall y \in [0, \frac{x}{\lambda_n}], \forall 1 \leq i \leq n, \quad & (F^+(x, y))_{ij} = \mathbb{1}_{[0, \frac{x}{\lambda_i}]}(y) F_{ij}^+(x, y), \quad 1 \leq j \leq m, \\ & (M^+(x, y))_{ij} = \mathbb{1}_{[\frac{x}{\lambda_i}, \frac{1}{\mu_m} + \frac{x}{\lambda_i}]}(y) M_{ij}^+(x, y), \quad 1 \leq j \leq m-1, \\ \forall y \in [\frac{x}{\lambda_1}, \frac{1}{\mu_m} + \frac{x}{\lambda_n}], \forall 1 \leq i \leq n, \quad & (H^+(x, y))_{ij} = \mathbb{1}_{[0, \frac{x}{\lambda_i}]}(y) H_{ij}^+(x, y), \quad 2 \leq j \leq m, \\ & (N^+(x, y))_{ij} = \mathbb{1}_{[\frac{x}{\lambda_i}, \frac{1}{\mu_m} + \frac{x}{\lambda_i}]}(y) N_{ij}^+(x, y), \quad 2 \leq j \leq m-1. \end{aligned}$$

The different kernels satisfy the following pure transport equations

$$\begin{aligned} \text{for } 1 \leq i \leq n, \quad & 1 \leq j \leq m, \quad 1 \leq j \leq m-1, \\ & \frac{\partial F_{ij}^+}{\partial x} + \frac{1}{\lambda_i} \frac{\partial F_{ij}^+}{\partial y} = 0, \quad \frac{\partial M_{ij}^+}{\partial x} + \frac{1}{\lambda_i} \frac{\partial M_{ij}^+}{\partial y} = 0, \\ & 2 \leq j \leq m, \quad 2 \leq j \leq m-1, \\ & \frac{\partial H_{ij}^+}{\partial x} + \frac{1}{\lambda_i} \frac{\partial H_{ij}^+}{\partial y} = 0, \quad \frac{\partial N_{ij}^+}{\partial x} + \frac{1}{\lambda_i} \frac{\partial N_{ij}^+}{\partial y} = 0, \\ \text{for } 2 \leq i \leq m, \quad & 1 \leq j \leq i-1, \quad 2 \leq j \leq i-1, \\ & \frac{\partial F_{ij}^-}{\partial x} - \frac{1}{\mu_i} \frac{\partial F_{ij}^-}{\partial y} = 0, \quad \frac{\partial H_{ij}^-}{\partial x} - \frac{1}{\mu_i} \frac{\partial H_{ij}^-}{\partial y} = 0, \end{aligned} \quad (9.27)$$

with boundary conditions defined for all $x \in [0, 1]$,

$$\begin{aligned} \text{if } 1 \leq i \leq n, \quad F_{ij}^+(x, 0) &= \begin{cases} \bar{\Gamma}_{i1}^+(x) - \Gamma_{i1}^+(x), & \text{if } j = 1, \\ -\Gamma_{ij}^+(x), & \text{if } 2 \leq j \leq m, \end{cases} \\ H_{ij}^+(x, 0) &= \bar{\Gamma}_{ij}^+(x), \quad 2 \leq j \leq m, \end{aligned} \quad (9.28)$$

$$\text{if } 2 \leq i \leq m, F_{ij}^-(x, 0) = \begin{cases} \bar{\Gamma}_{i1}^-(x) - \Gamma_{i1}^-(x), & \text{if } j = 1, \\ -\Gamma_{ij}^-(x), & \text{if } 1 < j \leq i - 1, \end{cases}$$

$$3 \leq i \leq m, H_{ij}^-(x, 0) = \bar{\Gamma}_{ij}^-(x), 1 \leq j \leq i - 1,$$

and for all $y \in [0, \frac{1}{\mu_m}]$, for $1 \leq i \leq n$,

$$M_{ij}^+(0, y) = \sum_{k=j+1}^m \mathbb{1}_{[0, \frac{1}{\mu_k}]}(y) (Q_0)_{ik} F_{kj}^-(0, y), 1 \leq j \leq m - 1,$$

$$N_{ij}^+(0, y) = \sum_{k=j+1}^m \mathbb{1}_{[0, \frac{1}{\mu_k}]}(y) (Q_0)_{ik} H_{kj}^-(0, y), 2 \leq j \leq m - 1. \quad (9.29)$$

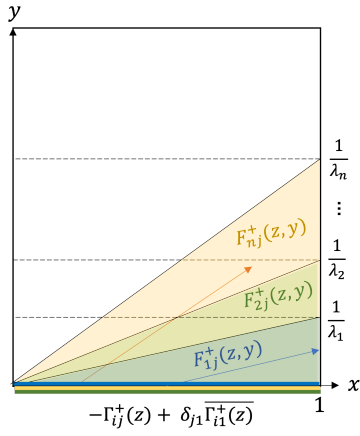


Figure 9.2 – Schematic representation of kernels F_{1j}^+ , F_{2j}^+ , F_{nj}^+ on their definition domain

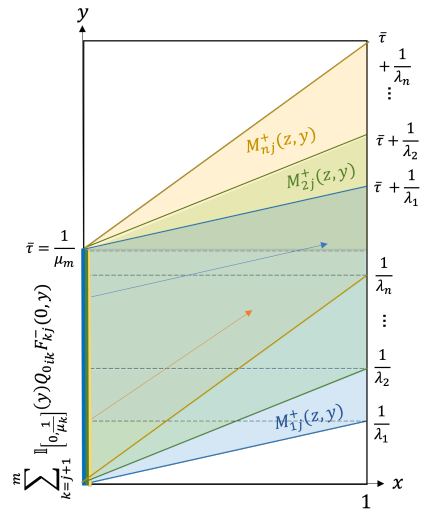


Figure 9.3 – Schematic representation of kernels M_{1j}^+ , M_{2j}^+ , M_{nj}^+ on their definition domain

We have the following Lemma

Lemma 9.2.2: Well-posedness of the kernels equations

The system of $4nm + (m - 1)^2$ transport equations (9.27) with boundary conditions (9.28)-(9.29) admits a unique piecewise continuous solution on its definition domain.

Proof : First, there are $4 \times nm$ kernels defined in (9.26) and $\frac{m(m-1)}{2} + \frac{(m-1)(m-2)}{2} = (m - 1)^2$ in (9.25), which all satisfy pure transport equations on their definition domain. Using the method of characteristics in the transport equations (9.27), we prove that each kernel is entirely defined by the corresponding boundary condition (9.28)-(9.29). This is schematically illustrated in Figures 9.2-9.3. We first define kernels F_{ij}^+ , H_{ij}^+ using their boundary value in $x \in [0, 1]$, $y = 0$. Their regularity depends on the coupling matrices $\bar{\Gamma}$, Γ on $[0, 1]$. Then, we define kernels M_{ij}^+ , N_{ij}^+ using their value in $y \in [0, \frac{1}{\mu_m}]$. We finally obtain

$$\text{for } 1 \leq i \leq n, \forall (x, y) \in \mathcal{T}_{\lambda_i}^+, \quad \begin{aligned} F_{ij}^+(x, y) &= \delta_{j1} \bar{\Gamma}_{i1}^+(x - \lambda_i y) - \Gamma_{ij}^+(x - \lambda_i y), 1 \leq j \leq m, \\ H_{ij}^+(x, y) &= \bar{\Gamma}_{ij}^+(x - \lambda_i y), 2 \leq j \leq m, \end{aligned}$$

$$\begin{aligned} \forall (x, y) \in \mathcal{P}_{\frac{1}{\mu_m}, \lambda_i}^+, \quad & M_{ij}^+(x, y) = \sum_{k=j+1}^m \mathbb{1}_{[\frac{x}{\lambda_i}, \frac{1}{\mu_k} + \frac{x}{\lambda_i}]}(y) (Q_0)_{ik} F^-(0, y - \frac{x}{\lambda_i}), \quad (1 \leq j \leq m-1), \\ & N_{ij}^+(x, y) = \sum_{k=j+1}^m \mathbb{1}_{[\frac{x}{\lambda_i}, \frac{1}{\mu_k} + \frac{x}{\lambda_i}]}(y) (Q_0)_{ik} H^-(0, y - \frac{x}{\lambda_i}), \quad (1 \leq j \leq m-1). \\ \text{for } 2 \leq i \leq m, \forall (x, y) \in \mathcal{T}_{\mu_i}^-, \quad & F_{ij}^-(x, y) = \delta_{j1} \bar{\Gamma}_{i1}^-(x + \mu_i y) - \Gamma_{ij}^-(x + \mu_i y), \quad 1 \leq j \leq i-1, \\ & H_{ij}^-(x, y) = \bar{\Gamma}_{ij}^-(x + \mu_i y), \quad 2 \leq j \leq i-1. \end{aligned}$$

All kernels are bounded by boundedness of functions $\Gamma^\pm, \bar{\Gamma}^\pm$ on $[0, 1]$. ■

Note that, due to the strict triangular structure of the kernels in (9.23), we can get rid of the dependence in $\bar{\gamma}(\cdot, 0)$ in (9.23)-(9.24). More precisely, we have the following lemma

Lemma 9.2.3: Expression of an equivalent transform

There exist piecewise continuous functions \mathcal{F}_{ij}^- ($1 \leq j < i$), \mathcal{M}_{ij}^- ($1 \leq j \leq i-2$), for $i \leq m$, defined on $\mathcal{T}_{\mu_i}^-, \mathcal{P}_{b_{ij}, \mu_i}^-$ respectively, with $b_{ij} = \sum_{k=j+1}^{i-1} \frac{1}{\mu_k}$; and \mathcal{F}_{ij}^+ ($1 \leq j \leq m$), \mathcal{M}_{ij}^+ ($1 \leq j \leq m-1$), for $i \leq n$, defined on $\mathcal{T}_{\lambda_i}^+, \mathcal{P}_{\bar{\tau}, \lambda_i}^+$ respectively, such that the transform defined in (9.23)-(9.24) can be rewritten equivalently as

$$\begin{aligned} \bar{\gamma}_i^-(t, x) &= \gamma_i^-(t, x) + \int_0^{\frac{1-x}{\mu_i}} \sum_{j=1}^{i-1} \mathcal{F}_{ij}^-(x, y) \gamma_j^-(t-y, 0) dy \\ &+ \sum_{j=1}^{i-2} \int_{\frac{1-x}{\mu_i}}^{b_{ij} + \frac{1-x}{\mu_i}} \mathcal{M}_{ij}^-(x, y) \gamma_j^-(t-y, 0) dy, \end{aligned} \quad (9.30)$$

$$\begin{aligned} \bar{\gamma}_i^+(t, x) &= \gamma_i^+(t, x) + \int_0^{\frac{x}{\lambda_i}} \sum_{j=1}^m \mathcal{F}_{ij}^+(x, y) \gamma_j^-(t-y, 0) dy \\ &+ \sum_{j=1}^{m-1} \int_{\frac{x}{\lambda_i}}^{A_j + \frac{x}{\lambda_i}} \mathcal{M}_{ij}^+(x, y) \gamma_j^-(t-y, 0) dy, \quad \text{with } A_j = \frac{1}{\mu_m} + \sum_{k=j+1}^m \frac{1}{\mu_k}. \end{aligned} \quad (9.31)$$

Proof: The expression of the kernels defined in Lemma 9.2.3 are obtained recursively. For any integer $i \leq m$, consider the recursive proposition \mathcal{P}_i^- : "there exist piecewise continuous functions \mathcal{F}_{ij}^- ($1 \leq j < i-1$), \mathcal{M}_{ij}^- ($1 \leq j \leq i-2$) defined on $\mathcal{T}_{\mu_i}^-, \mathcal{P}_{b_{ij}, \mu_i}^-$ respectively, such that, for all $\gamma^- \in \chi_t$, functions $\bar{\gamma}_i^-$ defined in (9.23) and (9.30) are equal".

Initialisation: First, \mathcal{P}_1^- is satisfied. Indeed, we have, for all $(t, x) \in [0, +\infty) \times [0, 1]$,

$$\begin{aligned} \bar{\gamma}_1^-(t, x) &= \gamma_1^-(t, x) \quad \text{from (9.23)} \\ &= \bar{\gamma}_1^-(t, x) \quad \text{from (9.30),} \end{aligned}$$

so the two transforms define the same function.

Heredity: Now assume that \mathcal{P}_k^- is satisfied for $k < i$, and let us show that \mathcal{P}_i^- is satisfied. Starting from (9.23), we have

$$\begin{aligned} \bar{\gamma}_i^-(t, x) &= \gamma_i^-(t, x) + \int_0^{\frac{1-x}{\mu_i}} \sum_{j=1}^{i-1} F_{ij}^-(x, y) \gamma_j^-(t-y, 0) + \sum_{j=2}^{i-1} H_{ij}^-(x, y) \bar{\gamma}_j^-(t-y, 0) dy, \\ &= \gamma_i^-(t, x) + \int_0^{\frac{1-x}{\mu_i}} \sum_{j=1}^{i-1} F_{ij}^-(x, y) \gamma_j^-(t-y, 0) dy \\ &+ \int_0^{\frac{1-x}{\mu_i}} \sum_{j=2}^{i-1} H_{ij}^-(x, y) \left[\gamma_j^-(t-y, 0) + \int_0^{\frac{1}{\mu_j}} \sum_{k=1}^{j-1} \mathcal{F}_{jk}^-(0, s) \gamma_k^-(t-y-s, 0) ds \right. \\ &\left. + \sum_{k=1}^{j-2} \int_{\frac{1}{\mu_j}}^{b_{jk} + \frac{1}{\mu_j}} \mathcal{M}_{jk}^-(0, s) \gamma_k^-(t-y-s, 0) ds \right] dy \quad \text{by induction hypothesis.} \end{aligned}$$

We then use (a) a change of variables in the two double integral terms, then (b) we invert the two integrals, taking care of several case disjunctions on the domain, (c) we invert the terms of the sum, and finally (d) we decompose the integral term to obtain

$$\begin{aligned}\bar{\gamma}_i^-(t, x) &= \gamma_i^-(t, x) + \int_0^{\frac{1-x}{\mu_i}} \sum_{j=1}^{i-1} \left[F_{ij}^-(x, y) + \delta_{j \geq 2} H_{ij}^-(x, y) \right. \\ &\quad \left. + \sum_{k=j+1}^{i-1} \delta_{j \leq i-2} I_{ijk}^{\mathcal{F}}(x, y) + \delta_{j \leq i-3} I_{ijk}^{\mathcal{M}}(x, y) \right] \gamma_j^-(t-y, 0) dy \\ &\quad + \sum_{j=1}^{i-2} \int_{\frac{1-x}{\mu_i}}^{b_{ij} + \frac{1-x}{\mu_i}} \left[\sum_{k=j+1}^{i-1} J_{ijk}^{\mathcal{F}}(x, y) + \delta_{j \leq i-3} J_{ijk}^{\mathcal{M}}(x, y) \right] \gamma_j^-(t-y, 0) dy,\end{aligned}$$

with for all $z \in [0, 1]$, $y \in [0, b_{ij} + \frac{1-x}{\mu_i}]$ and $j \leq i-2$, $j+1 \leq k \leq i-1$, denote $H_{ijk}^f(x, y, s) = H_{ik}^-(x, s) \mathcal{F}_{jk}^-(0, y-s)$,

$$\begin{aligned}I_{ijk}^{\mathcal{F}}(x, y) &= \mathbb{1}_{[1-\frac{\mu_i}{\mu_k}, 1]}(x) \int_0^y H_{ijk}^f(x, y, s) ds \\ &\quad + \mathbb{1}_{[0, 1-\frac{\mu_i}{\mu_k}]}(x) \left[\mathbb{1}_{[0, \frac{1}{\mu_k}]}(y) \int_0^y H_{ijk}^f(x, y, s) ds + \mathbb{1}_{[\frac{1}{\mu_k}, \frac{1-x}{\mu_i}]}(y) \int_{y-\frac{1}{\mu_k}}^y H_{ijk}^f(x, y, s) ds \right], \\ J_{ijk}^{\mathcal{F}}(x, y) &= \mathbb{1}_{[0, 1-\frac{\mu_i}{\mu_k}]}(x) \left[\mathbb{1}_{[\frac{1-x}{\mu_i}, \frac{1-x}{\mu_i} + \frac{1}{\mu_k}]}(y) \int_{y-\frac{1}{\mu_k}}^{\frac{1-x}{\mu_i}} H_{ijk}^f(x, y, s) ds \right] \\ &\quad + \mathbb{1}_{[1-\frac{\mu_i}{\mu_k}, 1]}(x) \left[\mathbb{1}_{[\frac{1-x}{\mu_i}, \frac{1}{\mu_k}]}(y) \int_0^{\frac{1-x}{\mu_i}} H_{ijk}^f(x, y, s) ds + \mathbb{1}_{[\frac{1}{\mu_k}, \frac{1}{\mu_k} + \frac{1-x}{\mu_i}]}(y) \int_{y-\frac{1}{\mu_k}}^{\frac{1-x}{\mu_i}} H_{ijk}^f(x, y, s) ds \right],\end{aligned}$$

and for all $z \in [0, 1]$, $y \in [0, b_{ij} + \frac{1-x}{\mu_i}]$ and $j \leq i-3$, $j+1 \leq k \leq i-1$, denote $H_{ijk}^m(x, y, s) = H_{ik}^-(x, s) \mathcal{M}_{jk}^-(0, y-s)$,

$$\begin{aligned}I_{ijk}^{\mathcal{M}}(x, y) &= \mathbb{1}_{[1-\mu_i b_{kj}, 1]}(x) \left[\mathbb{1}_{[\frac{1}{\mu_k}, \frac{1-x}{\mu_i}]}(y) \int_0^{y-\frac{1}{\mu_k}} H_{ijk}^m(x, y, s) ds \right] \\ &\quad + \mathbb{1}_{[0, 1-\mu_i b_{kj}]}(x) \left[\mathbb{1}_{[\frac{1}{\mu_k}, b_{k+1, j}]}(y) \int_0^{y-\frac{1}{\mu_k}} H_{ijk}^m(x, y, s) ds + \mathbb{1}_{[b_{k+1, j}, \frac{1-x}{\mu_i}]}(y) \int_{y-b_{k+1, j}}^{y-\frac{1}{\mu_k}} H_{ijk}^m(x, y, s) ds \right], \\ J_{ijk}^{\mathcal{M}}(x, y) &= \mathbb{1}_{[0, 1-\mu_i b_{kj}]}(x) \left[\mathbb{1}_{[\frac{1-x}{\mu_i}, \frac{1-x}{\mu_i} + b_{k+1, j}]}(y) \int_{y-b_{k+1, j}}^{\frac{1-x}{\mu_i}} H_{ijk}^m(x, y, s) ds \right] \\ &\quad + \mathbb{1}_{[1-\mu_i b_{kj}, 1]}(x) \left[\mathbb{1}_{[\frac{1-x}{\mu_i}, \frac{1}{\mu_k} + \frac{1-x}{\mu_i}]}(y) \int_0^{y-\frac{1}{\mu_k}} H_{ijk}^m(x, y, s) ds \right. \\ &\quad \left. + \mathbb{1}_{[\frac{1}{\mu_k} + \frac{1-x}{\mu_i}, b_{k+1, j}]}(y) \int_0^{\frac{1-x}{\mu_i}} H_{ijk}^m(x, y, s) ds + \mathbb{1}_{[b_{k+1, j}, b_{k+1, j} + \frac{1-x}{\mu_i}]}(y) \int_{y-b_{k+1, j}}^{\frac{1-x}{\mu_i}} H_{ijk}^m(x, y, s) ds \right].\end{aligned}$$

From there, we can derive the expression

$$\begin{aligned}\mathcal{F}_{ij}^-(x, y) &= F_{ij}^-(x, y) + \delta_{j \geq 2} H_{ij}^-(x, y) + \sum_{k=j+1}^{i-1} \delta_{j \leq i-2} I_{ijk}^{\mathcal{F}}(x, y) + \delta_{j \leq i-3} I_{ijk}^{\mathcal{M}}(x, y), \\ \mathcal{M}_{ij}^-(x, y) &= \sum_{k=j+1}^{i-1} J_{ijk}^{\mathcal{F}}(x, y) + \delta_{j \leq i-3} J_{ijk}^{\mathcal{M}}(x, y),\end{aligned}$$

to match definition (9.30).

By induction, the proposition \mathcal{P}_k^- is true for all $1 \leq k \leq m$. From then, we can obtain the expressions of \mathcal{F}_{ij}^+ , \mathcal{M}_{ij}^+ in (9.31). Starting from (9.24), we replace $\bar{\gamma}_j(t-y, 0)$ in the affine terms by the expression (9.30).

As before, to rewrite the corresponding expression in the form (9.31), we do (a) a change of variables in the two double integral terms, then (b) we invert the two integrals, taking care of several case disjunctions on the domain, that results in the use of indicator function, (c) we invert the terms of the sum and exchange the indices, and finally (d) we decompose the integral term on $[0, \frac{x}{\lambda_i}]$ and $[\frac{x}{\lambda_i}, A_j + \frac{x}{\lambda_i}]$. After these technical computations, we obtain the expressions of $\mathcal{F}_{ij}^+, \mathcal{M}_{ij}^+$ as functions of $F_{ij}^+, H_{ij}^+, \mathcal{F}_{jk}^-, \mathcal{M}_{jk}^-$ and $H_{ij}^+, M_{ij}^+, N_{ij}^+, \mathcal{F}_{jk}^-, \mathcal{M}_{jk}^-$, $k \leq j - 1$ respectively. ■

Note that the proposed affine transformation is defined and invertible for $t > t^* = m\bar{\tau}$. Therefore, the stability properties of the closed-loop system are equivalent to the one of the target system only after a transient time. Finally, we have the following theorem

Theorem 9.2.1: Invertibility of the time-affine transform

The transform defined component-wise by (9.23)-(9.24) is boundedly invertible on χ , for all $t > m\bar{\tau}$.

Proof : We prove the invertibility of the transform defined by (9.23)-(9.24) by induction component-wise. Consider the following proposition, for $1 \leq i \leq m$, \mathcal{P}_i : "For all $t \in [m\bar{\tau}, +\infty)$, $\bar{\gamma}_i^-(t, \cdot)$ can be expressed in function of $\gamma_j^-(t, \cdot) \in H^1([0, 1], \mathbb{R}^{n+m})$, $\gamma_i^-(\cdot, 0) \in D_{\tau_j}$, for $1 \leq j \leq i$ and $\bar{\gamma}_{j'}^-(\cdot, 0) \in D_{\tau_{j'}}$, for $1 \leq j' < i$." First, since $\gamma_1^-(t, x) = \bar{\gamma}_1^-(t, x)$, proposition \mathcal{P}_1 is true. Next, assume \mathcal{P}_j is satisfied for $j < i$, and let us prove that \mathcal{P}_i is true. By induction, the terms in (9.23) are well defined. In particular, we have

$$\bar{\gamma}_i^-(t, 0) = \underbrace{\gamma_i^-(t, 0)}_{\text{known on } [t - \tau_i, t]} + \underbrace{\int_0^{\frac{1-x}{\mu_i}} \sum_{j=1}^{i-1} F_{ij}^-(0, y) \gamma_j^-(t - y, 0) + \sum_{j=2}^{i-1} H_{ij}^-(0, y) \bar{\gamma}_j^-(t - y, 0) dy}_{\text{known on } [t - \tau_j + \frac{1}{\mu_i}, t] \subset [t - \tau_i, t]}$$

such that \mathcal{P}_i is satisfied. The inverse transform is immediately given by

$$\gamma_i^-(t, x) = \bar{\gamma}_i^-(t, x) + \int_0^{\frac{1-x}{\mu_i}} \sum_{j=1}^{i-1} \bar{F}_{ij}^-(x, y) \bar{\gamma}_j^-(t - y, 0) + \sum_{j=2}^{i-1} \bar{H}_{ij}^-(x, y) \bar{\gamma}_j^-(t - y, 0) dy,$$

with $\bar{H}_{ij}^-(x, y) = -F_{ij}^-(x, y)$ and $\bar{F}_{ij}^-(x, y) = -\delta_{j1} F_{i1}^-(x, y) - \delta_{j>1} H_{ij}^-(x, y)$.

Next, the transform (9.24) is a well-defined affine transform. For all $1 \leq i \leq n$, we have

$$\begin{aligned} \bar{\gamma}_i^+(t, x) &= \gamma_i^+(t, x) + \underbrace{\int_0^{\frac{x}{\lambda_i}} \sum_{j=1}^m F_{ij}^+(x, y) \gamma_j^-(t - y, 0) + \sum_{j=2}^m H_{ij}^+(x, y) \bar{\gamma}_j^-(t - y, 0) dy}_{\text{known on } [t - \tau_j + \frac{1}{\lambda_i}, t]} \\ &+ \underbrace{\int_{\frac{x}{\lambda_i}}^{\frac{1}{\mu_m} + \frac{x}{\lambda_i}} \sum_{j=1}^{m-1} M_{ij}^+(x, y) \gamma_j^-(t - y, 0) + \sum_{j=2}^{m-1} N_{ij}^+(x, y) \bar{\gamma}_j^-(t - y, 0) dy}_{\text{known on } [t - \tau_j + \frac{1}{\mu_m} + \frac{1}{\lambda_i}, t]} \end{aligned}$$

which is well defined since, $\forall 1 \leq j \leq m$, $\tau_j > \tau_m \leq \frac{1}{\lambda_i}$ and $\forall 1 \leq j \leq m - 1$, $\tau_j > \tau_{m-1} \leq \frac{1}{\mu_m} + \frac{1}{\lambda_i}$. The expression of the inverse transform is straightforward. The boundedness of the transform is derived from the boundedness of the kernels and integral operators. ■

Note that though the general operator derived from transform (9.23)-(9.24) is defined on χ , we only here consider the particular case where for $t \geq t^*$, the function in $\mathcal{D}_\tau[t]$ corresponds to the past values of a subpart of the boundary state at time t defined in $H^1([0, 1], \mathbb{R}^{n+m})$ (more precisely, the subpart solution of the leftward convecting equations defined in $H^1([0, 1], \mathbb{R}^m)$). We restrict the use of this transform on the space $\chi^* = H^1([0, 1], \mathbb{R}^{n+m}) \times D_\tau^*$, with $D_\tau^* = H^1([t^* - \tau_1, t^*], \mathbb{R}) \times H^1([t^* - \tau_2, t^*], \mathbb{R}) \times \dots \times$

$H^1([t^* - \tau_m, t^*], \mathbb{R})$. This will imply specific asymptotic stability properties in the different norms.

Alternative formulation

An alternative definition to the affine transform can be found, which does not necessitate a recursive definition of the state, to the price of more intricated kernel equations. Define the quadrilateral domains $\mathcal{Q}_{b_{ij}, \mu_i}^- = \mathcal{T}_{\mu_i}^- \cup \mathcal{P}_{b_{ij}, \mu_i}^-$ and $\mathcal{Q}_{A_j, \lambda_i}^+ = \mathcal{T}_{\lambda_i}^+ \cup \mathcal{P}_{A_j, \lambda_i}^+$.

Lemma 9.2.4: Alternative expression of the time-affine transform

There exist piecewise continuous functions \mathcal{N}_{ij}^- , for $2 \leq i \leq m$, and $1 \leq j < i$, defined on $\mathcal{Q}_{b_{ij}, \mu_i}^-$ with $b_{ij} = \sum_{k=j+1}^{i-1} \frac{1}{\mu_k}$, and \mathcal{N}_{ij}^+ for $1 \leq i \leq n$, $1 \leq j \leq m$, defined on $\mathcal{Q}_{A_j, \lambda_i}^+$, such that the transform defined in (9.23)-(9.24) can be rewritten equivalently as

$$\bar{\gamma}_i^-(x) = \gamma_i^-(x) + \int_0^{b_{ij} + \frac{1-x}{\mu_i}} \sum_{j=1}^{i-1} \mathcal{N}_{ij}^-(x, y) \gamma_j^-(t-y, 0) dy, \quad (9.32)$$

$$\bar{\gamma}_i^+(x) = \gamma_i^+(x) + \sum_{j=1}^m \int_0^{A_j + \frac{x}{\lambda_i}} \mathcal{N}_{ij}^+(x, y) \gamma_j^-(t-y, 0) dy. \quad (9.33)$$

Proof : Using Lemma 9.2.3, it is equivalent to show that transforms (9.30)-(9.31) and (9.32)-(9.33) are equivalent. Introduce $\mathcal{D}_{\mu_i}^- = \{(x, y) \in \mathcal{T}_{\mu_i}^- \mid y = \frac{1-x}{\mu_i}\}$ and $\mathcal{D}_{\lambda_i}^+ = \{(x, y) \in \mathcal{T}_{\lambda_i}^+ \mid y = \frac{x}{\lambda_i}\}$ two one-dimensional spaces. This can be seen directly by defining

$$\begin{aligned} \text{for all } 2 \leq i \leq m, 1 \leq j \leq i-1, \quad \mathcal{N}_{ij}^-(x, y) &= \begin{cases} \mathcal{F}_{ij}^-(x, y), \forall (x, y) \in \mathcal{T}_{\mu_i}^- \\ \mathcal{M}_{ij}^-(x, y), \forall (x, y) \in \mathcal{P}_{b_{ij}, \mu_i}^- \setminus \mathcal{D}_{\mu_i}^- \end{cases} \\ \text{for all } 1 \leq i \leq n, 1 \leq j \leq m, \quad \mathcal{N}_{ij}^+(x, y) &= \begin{cases} \mathcal{F}_{ij}^+(x, y), \forall (x, y) \in \mathcal{T}_{\lambda_i}^+ \\ \mathcal{M}_{ij}^+(x, y), \forall (x, y) \in \mathcal{P}_{A_j, \lambda_i}^+ \setminus \mathcal{D}_{\lambda_i}^+ \end{cases}. \end{aligned}$$

■

Equivalently, using the backstepping methodology, the kernels are defined as the unique solution of the following set of equations

$$\begin{aligned} \text{for } 1 \leq i \leq n, 1 \leq j \leq m, \forall (x, y) \in \mathcal{Q}_{A_j, \lambda_i}^+, \\ \frac{\partial \mathcal{N}_{ij}^+}{\partial y} + \lambda_i \frac{\partial \mathcal{N}_{ij}^+}{\partial x} = \sum_{k=j+1}^m \mathbf{1}_{[0, \frac{1}{\mu_k}]}(y) \bar{\Gamma}_{ik}^+(x) \mathcal{N}_{kj}^-(0, y), \end{aligned} \quad (9.34)$$

$$\begin{aligned} \text{for } 2 \leq i \leq m, 1 \leq j \leq i-1, \forall (x, y) \in \mathcal{Q}_{b_{ij}, \mu_i}^-, \\ \frac{\partial \mathcal{N}_{ij}^-}{\partial y} - \mu_i \frac{\partial \mathcal{N}_{ij}^-}{\partial x} = \sum_{k=j+1}^{i-1} \mathbf{1}_{[0, \frac{1}{\mu_k}]}(y) \bar{\Gamma}_{ik}^-(x) \mathcal{N}_{kj}^-(0, y), \end{aligned} \quad (9.35)$$

with boundary conditions

$$\begin{aligned} \text{for } 1 \leq i \leq n, 1 \leq j \leq m, \\ \forall z \in [0, 1], \mathcal{N}_{ij}^+(x, 0) = \bar{\Gamma}_{ij}^+(x) - \Gamma_{ij}^+(x), \\ \forall y \in (0, A_j], \mathcal{N}_{ij}^+(0, y) = \sum_{k=j+1}^m \mathbf{1}_{[0, \frac{1}{\mu_k}]}(y) (Q_0)_{ik} \mathcal{N}_{kj}^-(0, y), \end{aligned} \quad (9.36)$$

$$\text{for } 2 \leq i \leq m, 1 \leq j \leq i-1, \quad \begin{aligned} \forall z \in [0, 1], \mathcal{N}_{ij}^-(x, 0) &= \bar{\Gamma}_{ij}^-(x) - \Gamma_{ij}^-(x), \\ \forall y \in (\frac{1}{\mu_i}, b_{ij} + \frac{1}{\mu_i}], \mathcal{N}_{ij}^-(0, y) &= 0. \end{aligned} \quad (9.37)$$

Lemma 9.2.5: Well-posedness of the kernel equations

The system of $nm + \frac{m(m+1)}{2}$ transport equations (9.34)-(9.35) with boundary conditions (9.36)-(9.37) admits a unique bounded C_{pw}^1 solution on its definition domain.

Proof : We recursively prove the well-posedness of the kernel equations (9.34)-(9.35). Let us first prove the existence of a unique solution for the $\frac{m(m+1)}{2}$ partial differential equations (9.35), with $m(m+1)$ boundary conditions (9.37). Their quadrilateral domain is illustrated on Figure 9.4 (left), in the case $b_{ij} \leq \frac{1}{\mu_i}$. For any integer $i \leq m$, consider the recursive proposition \mathcal{P}_i^- : "For all $1 \leq j \leq i-1$, equation (9.35)_{ij} with boundary condition (9.37)_{ij} admits a unique solution $\mathcal{N}_{ij}^- \in C_{pw}^1(\mathcal{Q}_{b_{ij}, \mu_i}^-)$ ".

Initialisation: For $i = 2$, \mathcal{N}_{21} satisfies a pure transport equation. By the method of characteristics, we can express its values on its definition domain \mathcal{T}_{μ_1} using the boundary value in $y = 0$: $\forall (x, y) \in \mathcal{T}_{\mu_1}$, $\mathcal{N}_{21} = \bar{\Gamma}_{21}(z + \mu_1 y) - \Gamma_{21}(z + \mu_1 y)$. Its regularity depends on the one of Γ_{21} , $\bar{\Gamma}_{21}$.

Heredity: We now assume that proposition \mathcal{P}_{i-1}^- is satisfied, and show that \mathcal{P}_i^- is true. Starting from $j = i-1$, $\mathcal{N}_{i, i-1}^-$ is entirely defined on \mathcal{T}_{μ_i} by $\mathcal{N}_{i, i-1}^- = \bar{\Gamma}_{i, i-1}(z + \mu_i y) - \Gamma_{i, i-1}(z + \mu_i y)$. Next, for any $j \leq i-2$, using the method of characteristics in (9.35), we have

$$\forall (x, y) \in \mathcal{T}_{\mu_i}, \mathcal{N}_{ij}^-(x, y) = (\bar{\Gamma}_{ij}^- - \Gamma_{ij}^-)(z + \mu_i y) + \int_0^y \sum_{k=j+1}^{i-1} \mathbb{1}_{[0, \frac{1}{\mu_k}]}(y-s) \bar{\Gamma}_{ik}^-(z + \mu_i s) \mathcal{N}_{kj}^-(0, y-s) ds,$$

$$\forall (x, y) \in \mathcal{P}_{b_{ij}, \mu_i}^- \setminus \mathcal{D}_{\mu_i}^-, \mathcal{N}_{ij}^-(x, y) = \int_0^{\frac{x}{\mu_i}} \sum_{k=j+1}^{i-1} \mathbb{1}_{[0, \frac{1}{\mu_k}]}(y+s) \bar{\Gamma}_{ik}^-(z - \mu_i s) \mathcal{N}_{kj}^-(0, y+s) ds.$$

By induction, the kernel \mathcal{N}_{ij}^- is then uniquely defined on its definition domain. It is piecewise continuous since a discontinuity can, for instance, occur along $\mathcal{D}_{\mu_i}^- = \mathcal{T}_{\mu_i} \cap \mathcal{P}_{b_{ij}, \mu_i}^-$.

We proceed similarly to prove the well-posedness of the $n \times m$ kernel equations (9.34), (9.36). ■

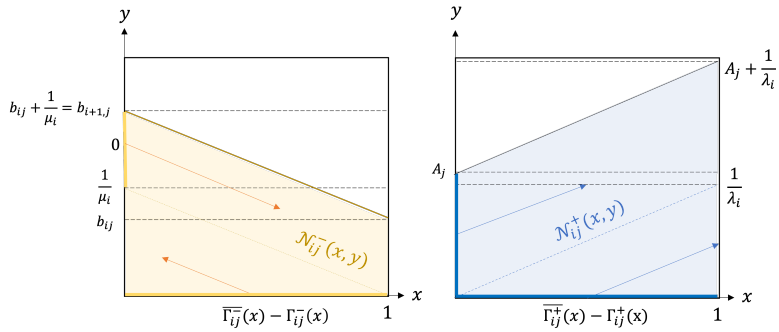


Figure 9.4 – Schematic representation of kernels \mathcal{N}_{ij}^+ , \mathcal{N}_{ij}^- on their definition domain

Remark 9.2.1 Similarly to what was done in (9.25)-(9.26), the transform (9.32)-(9.33) or equivalently (9.30)-(9.31) can be rewritten in a condensed matrix form

$$\begin{aligned} \bar{\gamma}^-(t, x) &= \gamma^-(t, x) + \int_0^{b_{m1} + \frac{1-x}{\mu_m}} \mathcal{N}^-(x, y) \gamma^-(t-y, 0) dy, \\ \bar{\gamma}^+(t, x) &= \gamma^+(t, x) + \int_0^{A_1 + \frac{x}{\lambda_m}} \mathcal{N}^+(x, y) \gamma^-(t-y, 0) dy. \end{aligned} \quad (9.38)$$

defining adequate matrix kernels \mathcal{N}^- , \mathcal{N}^+ using indicator functions.

9.3 . Control law

We can finally determine the adequate control input $V(t)$ to ensure that transform (9.19) with the kernels defined above map system (9.21)-(9.22) with in-domain coupling terms given by (9.20) to the initial target system (9.3)-(9.4). We could recursively define each control law component using (9.23). For the sake of simplicity, we use expression (9.38). We can then define the control input as

$$V(t) = \bar{V}_\gamma(t) - R_1 \gamma^+(t, 1) - I_1(t) - \int_0^{b_{m1}} \mathcal{N}^-(x, y) \gamma^-(t - y, 0) dy. \quad (9.39)$$

Using the different transforms and the definition of $\bar{V}_\gamma(t)$, the control law (9.39), defined for $t > m\bar{\tau}$, could be rewritten with distributed values of the original and target states.

$$\begin{aligned} V(t) = & \bar{V}(t) - R_1 \xi^+(t, 1) - \int_0^1 \bar{K}^{-+}(1, y) \bar{\xi}^+(t, y) + \bar{K}^{--}(1, y) \bar{\xi}^-(t, y) dy \\ & + \int_0^1 K^{-+}(1, y) \xi^+(t, y) + K^{--}(1, y) \xi^-(t, y) dy - \int_0^{b_{m1}} \mathcal{N}^-(1, y) \xi^-(t - y, 0) dy. \end{aligned} \quad (9.40)$$

To implement the control law, we need access to the distributed values of the states $\xi(t, x)$ and $\bar{\xi}(t, x)$ and the history of $\xi^-(\cdot, 0)$ over an interval $[0, b_{m1}] \subset [0, m\tau]$. An observer design could be proposed using boundary measurements to solve this drawback [HDMVK16, AA19]. An output-feedback control law can then be obtained. Using the superposition principle, we can show that if the error converges exponentially to zero, then the closed-loop system (9.1)-(9.2) with control input (9.39) is still exponentially stable.

Let us prove that the initial and target systems have equivalent asymptotic stability properties. First, we have the following lemma

Lemma 9.3.1: Equivalent asymptotic norm properties

There exists two constants κ_0 and κ_1 , such that for any $t > t^*$, and $0 < r < \min(\frac{1}{\mu_1}, \frac{1}{2m\|\Gamma^-\|_\infty^2})$,

$$\kappa_0 \|\gamma_{[t+r]}^-(\cdot, 0)\|_r \leq \|\gamma^-(t, \cdot)\|_{L^2} \leq \kappa_1 \|\gamma_{[t+\frac{1}{\mu_m}]}^-(\cdot, 0)\|_{\frac{1}{\mu_m}}. \quad (9.41)$$

The exponential stability of $\gamma^-(t, \cdot)$ in the sense of the L^2 -norm is equivalent to the exponential stability of $\gamma_{[t]}^-(\cdot, 0)$ in the sense of the $\mathcal{D}_{\frac{1}{\mu_m}}$ -norm.

Proof: This lemma is inspired from [ADM19]. The right member of inequality (9.41) derives from rewriting of $\gamma^-(t, x)$ as future values of $\gamma^-(\cdot, 0)$. In what follows, C will be an overloaded constant. Using the methods of characteristics, we have, for $t > t^*$,

$$\begin{aligned} \|\gamma^-(t, \cdot)\|_{L^2}^2 &= \int_0^1 \sum_{i=1}^m \gamma_i^-(t, \nu)^2 d\nu \text{ by definition} \\ &= \sum_{i=1}^m \int_0^1 (\gamma_i^-(t + \frac{\nu}{\mu_i}, 0) + \int_0^{\frac{\nu}{\mu_i}} \sum_{k=1}^{i-1} \Gamma_{ik}^-(\nu - \mu_i s) \gamma_k^-(t + s, 0) ds)^2 d\nu \\ &\leq 2 \left(\sum_{i=1}^m \int_0^1 \gamma_i^{-2}(t + \frac{\nu}{\mu_i}, 0) d\nu + \sum_{i=1}^m \int_0^1 \int_0^{\frac{\nu}{\mu_i}} \sum_{k=1}^{i-1} \Gamma_{ik}^{-2}(\nu - \mu_i s) \gamma_k^{-2}(t + s, 0) ds d\nu \right) \end{aligned}$$

$$\begin{aligned}
&\leq 2 \left(\mu_1 \int_0^{\frac{1}{\mu_m}} \sum_{i=1}^m \gamma_i^{-2}(t+s, 0) ds + m \int_0^{\frac{1}{\mu_i}} \sum_{k=1}^m \|\Gamma^-\|_\infty^2 \gamma_k^{-2}(t+s, 0) ds \right) \\
&\leq C \|\gamma_{[t+\frac{1}{\mu_m}]}^-(\cdot, 0)\|_{\frac{1}{\mu_m}}^2 \text{ using a time translation.}
\end{aligned}$$

Similarly, we can obtain the left-hand side of inequality (9.41)

$$\begin{aligned}
&\int_0^r \sum_{i=1}^m \gamma_i^-(t+s, 0)^2 ds = \int_0^r \sum_{i=1}^m (\gamma_i^-(t, \mu_i s) - \int_0^s \sum_{k=1}^{i-1} \Gamma_{ik}^-(\mu_i(s-\nu)) \gamma_k^-(t+\nu, 0) d\nu)^2 ds \\
&\leq 2 \sum_{i=1}^m \int_0^{\mu_i r} \frac{1}{\mu_i} \gamma_i^{-2}(t, s) ds + \sum_{i=1}^m \int_0^r \int_0^s \|\Gamma^-\|_\infty^2 \sum_{k=1}^{i-1 < m} \gamma_k^{-2}(t+\nu, 0) d\nu ds \\
&\leq 2 \sum_{i=1}^m \int_0^1 \frac{1}{\mu_i} \gamma_i^{-2}(t, s) ds + \sum_{i=1}^m \int_0^r \int_0^r \|\Gamma^-\|_\infty^2 \sum_{k=1}^{i-1 < m} \gamma_k^{-2}(t+\nu, 0) d\nu ds \\
&\leq \frac{2}{\mu_m} \|\gamma^-(t, \cdot)\|_{L^2}^2 + 2mr \|\Gamma^-\|_\infty^2 \|\gamma_{[t+r]}^-(\cdot, 0)\|_r^2 \\
&\implies 0 < \frac{\mu_m}{2} (1 - 2mr \|\Gamma^-\|_\infty^2) \|\gamma_{[t+r]}^-(\cdot, 0)\|_r^2 \leq \|\gamma^-(t, \cdot)\|_{L^2}^2 \text{ since } r < \frac{1}{2m \|\Gamma^-\|_\infty^2}.
\end{aligned}$$

Let us now show that the exponential stability of $\|\gamma^-(t, \cdot)\|$ in the sense of the L^2 -norm is equivalent to the exponential stability of $\|\gamma_{[t]}^-(\cdot, 0)\|$ in the sense of the $\mathcal{D}_{\frac{1}{\mu_m}}$ -norm. Let us consider first that $\gamma^-(\cdot, 0)$ is exponentially stable in the sense of the $\mathcal{D}_{\frac{1}{\mu_m}}$ -norm. By definition, for any $\eta > 0$, there exists $C_0 > 0, \nu > 0$ such that for all $t > \max\{t^*, \eta\}$,

$$\|\gamma_{[t]}^-(\cdot, 0)\|_{\frac{1}{\mu_m}} \leq C_0 e^{-\nu t} \|\gamma_{[\eta]}^-(\cdot, 0)\|_{\frac{1}{\mu_m}}.$$

Then, for all $t > t^*$,

$$\begin{aligned}
\|\gamma^-(t, \cdot)\|_{L^2} &\leq \kappa_1 \|\gamma_{[t+\frac{1}{\mu_m}]}^-(\cdot, 0)\|_{\frac{1}{\mu_m}} \text{ by (9.41)} \\
&\leq C_0 e^{-\frac{\nu}{\mu_m} t} \kappa_1 e^{-\nu t} \|\gamma_{[\eta]}^-(\cdot, 0)\|_{\frac{1}{\mu_m}}.
\end{aligned}$$

We can decompose the term $\|\gamma_{[\eta]}^-(\cdot, 0)\|_{\frac{1}{\mu_m}}$ using a finite number of terms defined on intervals of length r , with r defined in Lemma 9.3.1. Define $n_r = \max_{k \in \mathbb{N}} (kr \leq \frac{1}{\mu_m})$. We have

$$\begin{aligned}
\|\gamma_{[\eta]}^-(\cdot, 0)\|_{\frac{1}{\mu_m}}^2 &= \sum_{i=1}^m \int_{-\frac{1}{\mu_m}}^0 \gamma_i^{-2}(\eta+s, 0) ds \\
&\leq \sum_{i=1}^m \sum_{k=0}^{n_r} \int_{-(k+1)r}^{-kr} \gamma_i^{-2}(\eta+s, 0) ds = \sum_{i=1}^m \sum_{k=0}^{n_r} \int_{-r}^0 \gamma_i^{-2}(\eta+s-kr, 0) ds \\
&= \sum_{k=0}^{n_r} \|\gamma_{[\eta-kr]}^-(\cdot, 0)\|_r^2 \leq \sum_{k=0}^{n_r} \frac{1}{\kappa_0^2} \|\gamma^-(\eta-(k+1)r, \cdot)\|_{L^2}^2. \tag{9.42}
\end{aligned}$$

Choosing η such that $n_r + 1 \leq \eta < 2t^*$ and since system (9.16)-(9.17) is well-posed, there exists $\kappa > 0$, such that $\|\gamma^-(\eta-(k+1)r, \cdot)\|_{L^2} \leq \kappa \|\gamma_0^-\|_{L^2}$. We finally obtain

$$\|\gamma^-(t, \cdot)\|_{L^2} \leq C_0 \frac{\kappa_1}{\kappa_0} \kappa (n_r + 1) e^{-\frac{\nu}{\mu_m} t} e^{-\nu t} \|\gamma_0^-\|_{L^2}^2.$$

This implies the exponential stability of γ^- in the sense of the L^2 -norm. We can use the same arguments to prove that the exponential stability of γ^- in the sense of the L^2 -norm implies the exponential stability of $\gamma^-(\cdot, 0)$ in the sense of the $\mathcal{D}_{\frac{1}{\mu_m}}$ -norm. \blacksquare

We finally have the theorem

Theorem 9.3.1: Asymptotic stability properties of the solutions

Let us choose $\bar{\Sigma}^{\pm\pm}$, $\bar{\Sigma}^{\mp\pm}$ and $\bar{V}(t)$ such that, for all initial conditions $(\bar{\xi}_0^+(x), \bar{\xi}_0^-(x)) \in H^1([0, 1], \mathbb{R}^{(n+m)})$ satisfying the appropriate compatibility conditions, the solution of (9.3)-(9.4) is exponentially stable in the sense of the L^2 -norm. Then, for any initial conditions $(\xi_0^+(x), \xi_0^-(x)) \in H^1([0, 1], \mathbb{R}^{(n+m)})$ satisfying the appropriate compatibility conditions, the solution of (9.1)-(9.2) with control input defined by (9.39) is exponentially stable in the sense of the L^2 -norm.

Proof : First, we can straightforwardly extend the definitions of transforms $\mathcal{K}, \bar{\mathcal{K}}$ on χ^* . Indeed, these Volterra integral transforms do not affect the boundary value in $x = 0$, and remain, therefore boundedly invertible on χ^* . From [CVKB13], the exponential stability of state (γ^+, γ^-) satisfying closed-loop target system (9.16)-(9.17), in the sense of the L^2 -norm, is equivalent to the one of the initial state (ξ^+, ξ^-) satisfying the closed loop initial system (9.1)-(9.2). Similarly, the exponential stability of state $(\bar{\xi}^+, \bar{\xi}^-)$ satisfying target system (9.3)-(9.4), in the sense of the L^2 -norm, is equivalent to the one of the initial state $(\bar{\gamma}^+, \bar{\gamma}^-)$ satisfying system (9.21)-(9.22). Let us now prove that the exponential stability of state $(\bar{\gamma}^+, \bar{\gamma}^-)$ in the sense of the L^2 -norm implies the one of state (γ^+, γ^-) using Lemma 9.3.1. First, let us extend definition (9.23)-(9.24) for $t \in [0, t^*]$ by the identity function. We prove the exponential stability of γ^- . The exponential stability of γ^+ and consequently the one of the state (γ^-, γ^+) is proven similarly.

For $\eta > t^*$ sufficiently big, there exists $C_\eta, \nu > 0$, such that $\|\gamma^-(t, \cdot)\|_{L^2} \leq C_\eta e^{-\nu t} \|\bar{\gamma}^-(\eta, \cdot)\|_{L^2}$. Next, using the inverse transform of (9.30), we have

$$\begin{aligned} \int_0^1 \sum_{i=1}^m \gamma_i^{-2}(t, s) ds &= \int_0^1 \sum_{i=1}^m \left(\bar{\gamma}_i^-(t, s) + \int_0^{\frac{1-s}{\mu_i}} \sum_{j=1}^{i-1} \bar{\mathcal{F}}_{ij}^-(s, y) \bar{\gamma}_j^-(t-y, 0) dy \right. \\ &\quad \left. + \sum_{j=1}^{i-2} \int_{\frac{1-s}{\mu_i}}^{\frac{1-s}{\mu_j}} \bar{\mathcal{M}}_{ij}^-(s, y) \bar{\gamma}_j^-(t-y, 0) dy \right)^2 ds, \\ &\leq 2 \left(\int_0^1 \sum_{i=1}^m \bar{\gamma}_i^{-2}(t, s) ds + m \|\bar{\mathcal{F}}^-\|_\infty^2 \|\bar{\gamma}_{[\bar{t}]}^-(\cdot, 0)\|_{\frac{1}{\mu_m}}^2 + m \|\bar{\mathcal{M}}^-\|_\infty^2 \|\bar{\gamma}_{[\bar{t}]}^-(\cdot, 0)\|_{\frac{m}{\mu_m}}^2 \right). \end{aligned} \quad (9.43)$$

Using inequality (9.42), there exists $k_1 > 0$ such that $\|\bar{\gamma}_{[\bar{t}]}^-(\cdot, 0)\|_{\frac{1}{\mu_m}}^2 \leq k_1 e^{-\nu t} \|(\gamma_0^+, \gamma_0^-)\|_{L^2}^2$.

Similarly, we can show that there exists $k_2 > 0$ such that $\|\bar{\gamma}_{[\bar{t}]}^-(\cdot, 0)\|_{\frac{m}{\mu_m}}^2 \leq k_2 e^{-\nu t} \|(\gamma_0^+, \gamma_0^-)\|_{L^2}^2$.

Injecting this in the above equation implies that

$$\|\gamma^-(t, \cdot)\|_{L^2}^2 \leq \|\bar{\gamma}^-(t, \cdot)\|_{L^2}^2 + m(k_1 \|\bar{\mathcal{F}}^-\|_\infty^2 + k_2 \|\bar{\mathcal{M}}^-\|_\infty^2) \|\bar{\gamma}_{[\bar{t}]}^-(\cdot, 0)\|_{\frac{1}{\mu_m}}^2 \leq \bar{C}_\eta e^{-\nu t} \|\bar{\gamma}^-(\eta, \cdot)\|_{L^2}^2.$$

Injecting in equation (9.43), there exists a constant $C_1 > 0$ such that for all $t > 2t^*$, we have

$$\|\bar{\gamma}^-(t, \cdot)\|_{L^2}^2 \leq e^{-\nu t} \|(\gamma_0^+, \gamma_0^-)\|_{L^2}^2.$$

This last inequality still holds when $t \leq 2t^*$ due to the well-posedness of the open-loop system. Similarly, using transformation (9.24), we can show the existence of a constant C_2 such that for all $t > 0$

$$\|\bar{\gamma}^+(t, \cdot)\|_{L^2}^2 \leq e^{-\nu t} \|(\gamma_0^+, \gamma_0^-)\|_{L^2}^2.$$

Consequently, the system (9.21)-(9.22) is exponentially stable. The converse can be proved using the inverse transformation defined in the proof of Theorem 9.2.1. ■

Conclusion

This chapter presented a full-state feedback boundary controller design inspired by the backstepping methodology. The methodology is based on successive classic Volterra integral transforms and an innovative time-affine transform. As a result, implementing the control input requires the knowledge of past values of some boundary terms. It allows mapping a general linear hyperbolic PDE system actuated at one boundary to another target system of the same structure with arbitrarily chosen in-domain coupling terms. In particular, we could remove all in-domain couplings by imposing $\bar{\Sigma} = 0$. Choosing such simple target systems allows for a simpler analysis of closed-loop properties. In particular, the design of Lyapunov functionals is simplified for conservation laws. It could be highly interesting for event triggered control [WK21]. However, for robustness concerns or reduction of the control effort, keeping the in-domain couplings that tend to stabilize the initial system could be more relevant. In Chapter 10, we study how the Port Hamiltonian Framework can greatly help design target systems with a physical meaning. The asymptotic stability properties of the closed-loop system follow the ones of the target system. As already mentioned, the proposed controller should be coupled with an observer, such as the one proposed in [HDMVK16, WAA21].

10 - On the use of the Port-Hamiltonian framework to determine adequate target systems

In Chapter 9, we introduced an innovative time-affine transform to design a full-state feedback boundary controller. It allowed to map a general class of hyperbolic PDE systems to an arbitrary target system with the same structure, and ensured that both systems share the same asymptotic stability properties. We briefly discussed adequate choices of target systems, such as exponentially stable target systems derived from LMIs. This chapter presents how the **Port Hamiltonian framework** can be used to derive target systems with a *physical meaning*, allowing trade-offs between different performance specifications. Port-Hamiltonian systems (PHS) [MvdS93] were first introduced to represent non-resistive physical systems in interaction with their environment. This framework was extended to infinite dimensional systems as *distributed PHS* [vdSM02], and has since been widely used to model and control systems described by PDEs [Vil07, JZ12]. Indeed, this approach has proven very efficient in establishing the well-posedness and stability properties of infinite dimensional systems controlled at one boundary [VZLGM09]. As shown in Section 10.1, it offers a physical framework that could match the class of hyperbolic target systems (9.3)-(9.4) considered in Chapter 9. Under some structural assumptions, choosing a target system with interesting stability properties is possible. We state general results on boundary-controlled systems following the formalism used in [Vil07, LGZMo5]. We then present the steps necessary to match the general class of target systems. Introducing natural tuning parameters and adding degrees of freedom (e.g., the dissipation rate) with a clear energy interpretation is essential for the practical implementation of backstepping controllers. This strategy can be applied to add in-domain damping to vibrating strings or flexible beams. It is illustrated in Section 10.2 on the low-dimensional case of a clamped string with space-varying coefficients and then in Section 10.3 in the more complex case of a clamped Timoshenko beam. In both cases, the open-loop systems are already stable. Here, we apply the strategy from Chapter 9 to assign them a **specified closed-loop behavior**. More precisely, we ensure the exponential stability of the closed-loop systems by imposing a specific decay rate on their energy. The target systems, defined in the Port-Hamiltonian framework, correspond to a copy of the original one with additional in-domain damping terms with a clear energy interpretation. Both examples are illustrated with numerical simulations.

Chapitre 10: Utilisation du formalisme Port-Hamiltonien pour le choix d'un système cible adéquat. Au chapitre 9, une transformation temporelle affine innovante a été introduite. Elle permet d'envoyer une classe générale de systèmes d'EDP hyperboliques en boucle fermée sur un système cible arbitraire de même structure. Nous avons brièvement discuté des choix adéquats de systèmes cibles exponentiellement stables dérivés d'Inégalités Matricielles Linéaires (LMI). Dans ce chapitre, nous montrons comment le formalisme **Port Hamiltonien** permet de déterminer des systèmes cibles ayant une *signification physique*. Sous certaines hypothèses, il permet d'obtenir un système cible de la classe considérée au chapitre précédent, avec des propriétés de stabilité intéressantes (comme la passivité). Le cadre des systèmes Port-Hamiltoniens (PHS)

a été étendu aux systèmes de dimension infinie en tant que *PHS distribués* [vdSMo2]. Il est depuis largement utilisé pour modéliser et contrôler des systèmes d'EDP [Vil07, JZ12]. En suivant le formalisme utilisé dans [Vil07, LGZMo5], nous présentons des résultats généraux sur les PHS contrôlés à la frontière. Nous présentons les différentes transformations leur permettant de correspondre à la classe générale de systèmes cibles (9.3)-(9.4) (Section 10.1). Cela permet d'utiliser la méthode du chapitre 10 en introduisant des paramètres d'ajustement naturels et en ajoutant des degrés de liberté (par exemple, le taux de dissipation) avec une interprétation énergétique claire. Le système cible peut être choisi en utilisant les résultats du formalisme Port-Hamiltonien pour garantir sa stabilité exponentielle en imposant un taux de décroissance spécifique sur l'énergie. Cela est illustré par deux cas d'études appuyés de simulations numériques. Nous présentons d'abord une corde avec paramètres physiques variables (Section 10.2), puis une poutre de Timoshenko encastree (Section 10.3). Dans les deux cas, le système cible est défini comme le système initial dans le formalisme port-hamiltonien, mais contient des termes d'amortissement supplémentaires dans le domaine.

Contents

10.1 Problem description	197
10.1.1 General framework	197
10.1.2 Stability considerations	198
10.1.3 Structural assumptions	198
10.1.4 Reformulation as a system of balance laws	199
10.2 Application to a clamped string with space-varying coefficients	200
10.2.1 Reformulation in the Port-Hamiltonian framework	201
10.2.2 Matching a system of balance laws	202
10.2.3 Control design	203
10.2.4 Simulation results	204
10.3 Application to a clamped Timoshenko beam	205
10.3.1 Reformulation in the Port-Hamiltonian framework	207
10.3.2 Matching a system of balance laws	209
10.3.3 Control design	210
10.3.4 Simulation results	211

Some of the results given herein were submitted to System & Control letters [J1] and presented in:

- Jeanne Redaud, Jean Auriol, and Yann Le Gorrec. "In-domain damping assignment of a Timoshenko-beam using state feedback boundary control" (2022). 61st IEEE Conference on Decision and Control (CDC).
- _____. "Distributed Damping Assignment for a Wave Equation in the Port-Hamiltonian Framework" (2022). IFAC Workshop on Control of Systems Governed by Partial Differential Equations (CPDE).

10.1 . Problem description

This section presents a first-order distributed parameter *Port-Hamiltonian system* on a one-dimensional space domain and some of its properties. Under some structural assumptions, we show that they correspond to the general class of hyperbolic PDE systems (9.1)-(9.2) and (9.3)-(9.4) considered in Chapter 9. Using several invertible transforms, we establish the relationship between the PHS framework and the Riemann framework considered in the previous chapter.

10.1.1 . General framework

Following the general formalism given in [VZLGM09, JZ12], denote $X(t, x) = [X_1^\top, X_2^\top]^\top \in H^1([0, 1], \mathbb{R}^{2n})$ the *energy state* defined on $[0, +\infty) \times [0, 1]$. It satisfies

$$\frac{\partial X}{\partial t} = P_1 \frac{\partial}{\partial x} (\mathcal{H}(x)X(t, x)) + (P_0 - \Pi_0)\mathcal{H}(x)X(t, x), \quad (10.1)$$

with $P_1 \in \mathbb{R}^{2n \times 2n}$ a non singular symmetric matrix, and $P_0 \in \mathbb{R}^{2n \times 2n}$ a skew adjoint matrix. The Hamiltonian $\mathcal{H} = \text{diag}(\mathcal{H}_1, \mathcal{H}_2)$ is a bounded, symmetric and Lipschitz continuous strictly positive matrix-valued function defined on $[0, 1]$, such that for all $x \in [0, 1]$, $\mathcal{H}(x) \geq mI$ with constant $m > 0$. Matrix $\Pi_0 \in \mathbb{R}^{2n \times 2n}$ is a positive semidefinite matrix, corresponding to in-domain dissipation. The case $\Pi_0 = 0$ corresponds to lossless hyperbolic systems [LGZM05]. The boundary port variables associated to (10.1), known as *boundary effort* e_∂ and *boundary flow* f_∂ are defined by

$$\begin{bmatrix} f_\partial(t) \\ e_\partial(t) \end{bmatrix} = \frac{1}{\sqrt{2}} \begin{bmatrix} P_1 & -P_1 \\ I_{2n} & I_{2n} \end{bmatrix} \begin{bmatrix} \mathcal{H}(1)X(t, 1) \\ \mathcal{H}(0)X(t, 0) \end{bmatrix} \doteq P \begin{bmatrix} \mathcal{H}(1)X(t, 1) \\ \mathcal{H}(0)X(t, 0) \end{bmatrix}. \quad (10.2)$$

Define $\Xi = \begin{pmatrix} 0_{2n} & I_{2n} \\ I_{2n} & 0_{2n} \end{pmatrix} \in \mathbb{R}^{4n \times 4n}$, and $W \in \mathbb{R}^{2n \times 4n}$ a full-row rank matrix satisfying $W\Xi W^\top \geq 0$. From [VZLGM09, Theorem II.3], system (10.1) with boundary conditions

$$u_\partial(t) = W \begin{bmatrix} f_\partial(t) \\ e_\partial(t) \end{bmatrix}, \quad (10.3)$$

is a boundary control system [CZ12]. Next, define $\tilde{W} \in \mathbb{R}^{2n \times 4n}$ full rank matrix with $\begin{pmatrix} W \\ \tilde{W} \end{pmatrix}$ invertible, and introduce the output of the system as

$$y(t) = \tilde{W} \begin{bmatrix} f_\partial(t) \\ e_\partial(t) \end{bmatrix}. \quad (10.4)$$

For any energy state $X \in H^1([0, 1], \mathbb{R}^{2n})$, $\mathcal{H}X$ denotes the co-energy variable associated with X , and $\|X\|_{\mathcal{H}}^2$ corresponds to its Hamiltonian. This norm is equivalent to the standard

L^2 -norm, and corresponds to the total energy of the system $\mathcal{E}(t)$. It is defined by

$$\mathcal{E}(t) = \frac{1}{2} \int_0^1 \left(X^\top(t, x) \mathcal{H}(x) X(t, x) \right) dx = \|X\|_{\mathcal{H}}^2.$$

10.1.2 . Stability considerations

To define a class of adequate exponentially stable target systems for (10.1)-(10.3), consider that $u_\partial(t) = 0$, for all $t \geq 0$. It was shown in [VZLGMog] that the exponential stability of (10.1) with (10.3)-(10.4), which is related to the supply rate of energy, is determined by the input and output coupling matrices W, \tilde{W} . Indeed, in the Port-Hamiltonian framework, the interaction between different systems can be interpreted as an energy exchange through a set of well-defined power ports [MLGRZ17]. We have the following

Theorem 10.1.1: Exponential stability of BCS [VZLGMog, Theorem III.2]

Consider a boundary control system defined by (10.1) with (10.3)-(10.4), and $u(t) = 0$ for $t \geq 0$. If the (2, 2)-block of the matrix

$$P_{W, \tilde{W}} = \begin{bmatrix} W \Xi W^\top & W \Xi \tilde{W}^\top \\ \tilde{W} \Xi W^\top & \tilde{W} \Xi \tilde{W}^\top \end{bmatrix}^{-1}$$

is negative definite, then the system is exponentially stable.

From Theorem [JZ12, Lemma 9.1.4], a natural class of exponentially stable target systems is defined by

$$\frac{\partial}{\partial t} \bar{X} = P_1 \frac{\partial}{\partial x} (\mathcal{H}(x) \bar{X}) + \bar{P}_0 (\mathcal{H}(x) \bar{X}), \text{ with } W \begin{bmatrix} \bar{f}_\partial \\ \bar{e}_\partial \end{bmatrix} = 0_{2n}, \quad (10.5)$$

with $\bar{P}_0 \in \mathbb{R}^{2n \times 2n}$ a skew-adjoint matrix, and W satisfying $W \Xi W^\top > 0$. Alternatively, if \bar{P}_0 is not skew-adjoint, as in the case considered in Section 10.3, it suffices to ensure that there exists $k_1 > 0$, such that the energy decays as

$$\frac{d\mathcal{E}}{dt} \leq -k_1 \|(\mathcal{H}(1) \bar{X}(t, 1))\|^2 \text{ or } \frac{d\mathcal{E}}{dt} \leq -k_1 \|(\mathcal{H}(0) \bar{X}(t, 0))\|^2, \quad (10.6)$$

to prove the exponential stability of (10.5) by [VZLGMog, Theorem III.2]. Selecting Port-Hamiltonian systems with a strictly decaying energy as a target system (9.3)-(9.4) offers an interesting perspective. Instead of suppressing most in-domain couplings, we could modify them to guarantee a faster exponential decay rate. This change of paradigm is illustrated in two test cases in Sections 10.2-10.3.

10.1.3 . Structural assumptions

To apply the strategy presented in Chapter 9, we need the considered PHS (10.1)-(10.3) (or (10.1)-(10.5)) with interesting stability properties to match the class of reachable target systems (9.3)-(9.4). To do so, we express their Riemann coordinates and suppress some of the in-domain couplings. First, for constant Hamiltonian, we have the following conjecture

Conjecture 10.1.1 For all $\lambda \in \sigma(P_1\mathcal{H})$, then $-\lambda \in \sigma(P_1\mathcal{H})$.

If zero is not one of its eigenvalues, matrix $P_1\mathcal{H}$ is invertible since it has $2 \times n$ opposite (distinct) eigenvalues. Consequently, $P_1\mathcal{H}$ is diagonalizable if $0 \notin \text{sp}(P_1\mathcal{H}(x))$ and if all eigenvalues are of multiplicity one. More generally, the PHS must satisfy the following assumption:

Assumption 10.1.1 For all $x \in [0, 1]$, the matrix-valued function $P_1\mathcal{H}(x)$ is diagonalizable, and 0 is not one of its eigenvalues.

Note that Assumption 10.1.1 is implied by P_1 being full-row rank. If $0 \in \sigma(P_1\mathcal{H}(x))$, system (10.1) cannot be rewritten in the general form (9.1), since the dynamics of the corresponding components of state $X(t, x)$ would be described by an ODE. The proposed approach should be adapted to ODE-hyperbolic PDE interconnections, such as systems considered in Chapter 4. A second assumption concerns the form of the boundary matrix W . To rewrite the target system in the hyperbolic PDE formalism with boundary conditions (9.4), we need the boundary conditions at both ends of the spatial domain to be decoupled. A sufficient condition is given by

Assumption 10.1.2 Define $W = \begin{bmatrix} \Xi_1 & \Xi_2 \end{bmatrix}$ a full row rank matrix with $W\Xi W^\top \geq 0$. Then, there exists $R_1 \in \mathbb{R}^{n \times n}$, $Q_0 \in \mathbb{R}^{n \times n}$ such that $W_P \doteq WP$ is diagonal by block, that is, there exist $\mathcal{R} = \begin{bmatrix} -R_1 & I_n \end{bmatrix} \in \mathbb{R}^{n \times 2n}$, $\mathcal{Q} = \begin{bmatrix} I_n & -Q_0 \end{bmatrix} \in \mathbb{R}^{n \times 2n}$ such that

$$W_P = \begin{bmatrix} \Xi_2 + \Xi_1 P_1 & \Xi_2 - \Xi_1 P_1 \end{bmatrix} = \begin{bmatrix} \mathcal{R} & 0_{\mathbb{R}^{n \times 2n}} \\ 0_{\mathbb{R}^{n \times 2n}} & \mathcal{Q} \end{bmatrix}.$$

Moreover, the control input is of form $u_\partial(t) = \begin{bmatrix} V(t) \\ 0 \end{bmatrix}$.

This implies that $\begin{bmatrix} V(t) \\ 0 \end{bmatrix} = \begin{bmatrix} \mathcal{R}\mathcal{H}(1)\bar{X}(t, 1) \\ \mathcal{Q}\mathcal{H}(0)\bar{X}(t, 0) \end{bmatrix}$. Indeed, to apply the approach proposed in Chapter 9, we need one boundary to be **fully-actuated**.

10.1.4 . Reformulation as a system of balance laws

Under the assumptions given in the previous section, we can define an exponentially stable system in the Port Hamiltonian framework (for instance, of the form (10.5)) and reformulate it as a hyperbolic PDE system of the form (9.3)-(9.4). We first define the Riemann coordinates associated with states $\bar{X}(t, x)$ and then perform an exponential change of variables to suppress some coupling terms.

Riemann Coordinates

By Assumption 10.1.1, there exist an invertible matrix-valued function $Q(x) \in \mathbb{R}^{2n \times 2n}$, and a diagonal matrix valued function $\Lambda(x)$ defined on $[0, 1]$, such that for all $x \in [0, 1]$, $P_1\mathcal{H}(x) = Q(x)\Lambda(x)Q^{-1}(x)$. From conjecture 10.1.1, in the case of constant Hamiltonian, we would have $\Lambda = \text{diag}(\lambda_1, \dots, \lambda_n, -\lambda_1, \dots, -\lambda_n)$ with $\lambda_1 > \lambda_2 > \dots > \lambda_n$. To rewrite the target system with adequate asymptotic stability properties of the form (10.5), we first

define a new set of variables $\bar{\zeta}(t, x) = Q^{-1}(x)\bar{X}(t, x) \in H^1([0, 1], \mathbb{R}^{2n})$. It satisfies a similar set of PDEs with in-domain space-dependent couplings terms

$$\frac{\partial \bar{\zeta}}{\partial t}(t, x) + \Lambda(x) \frac{\partial \bar{\zeta}}{\partial x}(t, x) = \bar{\Sigma}(x) \bar{\zeta}(t, x), \text{ with } W_P \begin{bmatrix} \mathcal{H}(1)Q(1)\bar{\zeta}(t, 1) \\ \mathcal{H}(0)Q(0)\bar{\zeta}(t, 0) \end{bmatrix} = 0, \quad (10.7)$$

where $\bar{\Sigma}(x) = [Q^{-1}(x)(P_1 \frac{\partial \mathcal{H}}{\partial x} + \bar{P}_0 \mathcal{H}(x)) - \frac{\partial Q^{-1}(x)}{\partial x}]Q(x)$.

Exponential change of variables

To apply the strategy presented in Chapter 9, we first need to suppress the diagonal coupling terms of $\bar{\Sigma}(x)$. To do so, we apply an exponential change of variables [CVKB13]. For all $x \in [0, 1]$, we define the invertible matrix-valued function $\bar{A}(x) \in D_{2n}^+([0, 1])$ with diagonal functions defined for all $i \in \llbracket 1, 2n \rrbracket$ by

$$\bar{A}_{ii}(x) = e^{\bar{I}_i(x)}, \text{ with } \bar{I}_i(x) = - \int_0^x \frac{\bar{\Sigma}_{ii}(s)}{\Lambda_{ii}(s)} ds.$$

We then define the new state variable by $\bar{\xi}(t, x) = \bar{A}(x)\bar{\zeta}(t, x)$. It satisfies

$$\frac{\partial \bar{\xi}}{\partial t}(t, x) + \Lambda(x) \frac{\partial \bar{\xi}}{\partial x}(t, x) = \bar{\Sigma}(x) \bar{\xi}(t, x), \text{ with } W_P \begin{bmatrix} \mathcal{H}(1)Q(1)\bar{A}(1)^{-1}\bar{\xi}(t, 1) \\ \mathcal{H}(0)Q(0)\bar{\xi}(t, 0) \end{bmatrix} = 0, \quad (10.8)$$

where $\bar{\Sigma}_{ij}(x) = [\bar{A}(x)\bar{\Sigma}(x)\bar{A}^{-1}(x)]_{ij}$ for $i \neq j$, and 0 else. Under Assumption 10.1.2, the boundary condition rewrites

$$\begin{cases} \mathcal{H}_2(1)\bar{X}_2(t, 1) = R_1 \mathcal{H}_1(1)\bar{X}_1(t, 1), \\ \mathcal{H}_1(0)\bar{X}_1(t, 0) = Q_0 \mathcal{H}_2(0)\bar{X}_2(t, 0), \end{cases} \implies \begin{cases} \bar{X}_2(t, 1) = \mathcal{H}_2(1)^{-1} R_1 \mathcal{H}_1(1)\bar{X}_1(t, 1), \\ \bar{X}_1(t, 0) = \mathcal{H}_1(0)^{-1} Q_0 \mathcal{H}_2(0)\bar{X}_2(t, 0), \end{cases}$$

which is of form 9.4. We can now proceed further in the control design.

Using this approach, we were then able to match the class of systems considered in the previous chapter. Using the Port Hamiltonian framework allows to select target systems with a physical meaning. Instead of suppressing all the in-domain couplings (which can be source of instability), we can keep some of them. It can reduce the control effort by avoiding to cancel terms that naturally tend to stabilize the system. We apply the proposed methodology on two low dimensional boundary controlled distributed Port Hamiltonian systems.

10.2 . Application to a clamped string with space-varying coefficients

A first application to the proposed strategy can be found in damping assignment for a clamped string. This section gathers results presented in [RALG22a].

Consider a vibrating string clamped at the first end $x = 0$ and actuated at the other in $x = 1$. We denote $w(t, x)$ the vertical position of the string at point x and time $t > 0$. It

satisfies

$$\rho(x) \frac{\partial^2 w}{\partial t^2}(t, x) = \frac{\partial}{\partial x} \left(E(x) \frac{\partial w}{\partial x}(t, x) \right) - \kappa(x) \frac{\partial w}{\partial t}(t, x),$$

with $\rho(x), E(x) \in C^1([0, 1], \mathbb{R})^+$ being the mass density and Young's modulus, which are here space-dependent. The sign of term $\kappa(x) \in C^0([0, 1], \mathbb{R})$ characterizes the damping properties of the system. Note that we do not assume its positiveness. If the above string equation derives from the linearization of an unstable system, it could be negative (anti-damping). Initially, the position of the string is given by $w(\cdot, 0) = w_0 \in H^1([0, 1], \mathbb{R})$, and its speed by $\frac{\partial w}{\partial t}|_{t=0} = w_1 \in H^1([0, 1], \mathbb{R})$, with $w_0(0) = 0 = w_1(0)$.

10.2.1 . Reformulation in the Port-Hamiltonian framework

We first rewrite the model as a Port-Hamiltonian system in the general framework given in Section 10.1, with $n = 1$. The energy state variables $X = [X_1, X_2]^\top \in H^1([0, 1], \mathbb{R}^2)$ are defined by

$$X_1(t, x) = \frac{\partial w}{\partial x}(t, x), \quad X_2(t, x) = \rho(x) \frac{\partial w}{\partial t}(t, x), \quad (10.9)$$

where $X_1(t, x)$ (resp. $X_2(t, x)$) corresponds to the strain (resp. to the momentum). They satisfy

$$\frac{\partial}{\partial t} \begin{pmatrix} X_1 \\ X_2 \end{pmatrix} = \begin{pmatrix} 0 & \frac{\partial}{\partial x} \left(\frac{1}{\rho(x)} \cdot \right) \\ \frac{\partial}{\partial x} (E(x) \cdot) & -c(x) \end{pmatrix} \begin{pmatrix} X_1 \\ X_2 \end{pmatrix}, \quad (10.10)$$

with $c(x) = \frac{\kappa(x)}{\rho(x)}$. The first end of the string is clamped, while the other is actuated. It gives the following boundary conditions

$$X_2(0, t) = 0, \quad E(1)X_1(1, t) = u_\partial(t). \quad (10.11)$$

Following [JZ12], the equation satisfied by the states is given by (10.1) with $n = 1$, $P_0 = 0_{\mathbb{R}^2 \times 2}$, $P_1 = \begin{pmatrix} 0 & 1 \\ 1 & 0 \end{pmatrix}$ and $\Pi_0 = \begin{pmatrix} 0 & 0 \\ 0 & \kappa(x) \end{pmatrix}$.

The Hamiltonian density is given by $\mathcal{H}(x) = \text{diag}(E(x), \frac{1}{\rho(x)}) \in D_2^+([0, 1])$. The *boundary effort* e_∂ and *boundary flow* f_∂ are given by

$$\begin{cases} e_\partial = \frac{1}{\sqrt{2}}((\mathcal{H}X)(1) + (\mathcal{H}X)(0)), \\ f_\partial = \frac{1}{\sqrt{2}}(P_1(\mathcal{H}X)(1) - P_1(\mathcal{H}X)(0)). \end{cases}$$

The boundary conditions rewrite, for all $t \geq 0$,

$$W \begin{pmatrix} f_\delta(t) \\ e_\delta(t) \end{pmatrix} = \begin{pmatrix} V(t) \\ 0 \end{pmatrix}, \quad \text{with } W = \frac{1}{\sqrt{2}} \begin{pmatrix} 0 & 1 & 1 & 0 \\ 1 & 0 & 0 & -1 \end{pmatrix}. \quad (10.12)$$

Using the proposed strategy, we want to impose a specific decay rate to the energy

of the system \mathcal{E} , using a *distributed damping assignment*. More precisely, we want to make the dynamics of X equivalent to the dynamics of $\bar{X} = [\bar{X}_1, \bar{X}_2]^\top$ satisfying (10.5) with

$$\bar{P}_0(x) = \begin{pmatrix} 0 & 0 \\ 0 & -K(x) \end{pmatrix}.$$

The closed-loop system will, therefore, asymptotically behave as a damped string with strictly positive space-varying damping term $K(x) > 0$. The energy of the closed-loop system decreases proportionally to this term

$$\frac{d\bar{\mathcal{E}}}{dt} = - \int_0^1 K(y) \left(\frac{\bar{X}_2(t, y)}{\rho(y)} \right)^2 dy. \quad (10.13)$$

Therefore, we guarantee that the target system has a strictly decreasing energy, with decay rate related to the damping variable K introduced.

10.2.2 . Matching a system of balance laws

By analogy with results from Chapter 9, we define

$$\Lambda^+(x) = \Lambda^-(x) \doteq \lambda(x) = \sqrt{E(x)/\rho(x)} \in \mathbb{R}^+.$$

To simplify the notations, we introduce the following functions $r(x) = \sqrt{E(x)\rho(x)}$ and $\delta(x) = \left(\frac{\rho'}{\rho} + \frac{E'}{E} \right) (x)$, $\delta_1^3(x) = \left(3\frac{\rho'}{\rho} - \frac{E'}{E} \right) (x)$, $\delta_3^1(x) = \left(\frac{\rho'}{\rho} - 3\frac{E'}{E} \right) (x)$.

Assumptions 10.1.1-10.1.2 are satisfied. Indeed, since the matrix $P_1\mathcal{H}(x)$ admits two opposite eigenvalues $\pm\lambda(x)$, there exists $Q \in C^1([0, 1], \mathbb{R}^{2 \times 2})$ invertible, such that $P_1\mathcal{H}(x) = Q(x)\text{diag}(\lambda(x), -\lambda(x))Q(x)^{-1}$. Next, the boundary $x = 1$ is fully actuated, and the couplings at the boundary are non-zero scalars, so all hypotheses are satisfied for this low dimensional case.

Original system

First, we rewrite system (10.10)-(10.11) in the Riemann coordinates. The new state variables $[\zeta^+(t, x), \zeta^-(t, x)]^\top = Q^{-1}(x)[X_1(t, x), X_2(t, x)]^\top$ satisfy two hetero-directional hyperbolic PDEs of form (9.1)-(9.2) with in-domain spatially varying continuous coupling terms

$$\begin{cases} \Sigma^{++}(x) = \frac{1}{2} \left(-c(x) + \frac{\lambda}{2} \delta_3^1(x) \right), \\ \Sigma^{+-}(x) = \frac{1}{2\rho(x)} \left(\frac{c(x)}{\lambda(x)} - \frac{1}{2} \delta(x) \right), \\ \Sigma^{-+}(x) = \frac{E(x)}{2} \left(\frac{c(x)}{\lambda(x)} + \frac{1}{2} \delta(x) \right), \\ \Sigma^{--}(x) = \frac{1}{2} \left(-c(x) - \frac{\lambda}{2} \delta_1^3(x) \right), \end{cases}$$

and boundary couplings by $Q_0 \equiv q_0 = \frac{1}{r(0)}$ and $R_1 \equiv r_1 = -r(1)$. The control input is defined by $V(t) = \frac{\sqrt{2}}{\lambda(1)} u_\partial(t)$. The exponential change of variables $[\xi^+(t, x), \xi^-(t, x)]^\top = A(x)[\zeta^+(t, x), \zeta^-(t, x)]^\top$ from Section 10.1.4 is given by $A(x) = \text{diag}(f(x)e^{I_c(x)}, g(x)e^{-I_c(x)})$, with $\forall x \in [0, 1]$, $I_c(x) = \int_0^x \frac{c(s)}{2\lambda(s)} ds$ and $f(x) = \sqrt{\frac{E(x)\lambda(x)}{E(0)\lambda(0)}}$, $g(x) = \sqrt{\frac{\lambda(x)\rho(0)}{\rho(x)\lambda(0)}}$. The new variables satisfy the hyperbolic PDEs of form (9.1)-(9.2), with new in-domain cou-

pling terms defined by

$$\begin{cases} \Sigma^{++}(x) = \Sigma^{--}(x) = 0, \\ \Sigma^{+-}(x) = \frac{1}{2r(0)} e^{2I_c(x)} (c(x) - \frac{\lambda}{2} \delta(x)), \\ \Sigma^{-+}(x) = \frac{r(0)}{2} e^{-2I_c(x)} (c(x) + \frac{\lambda}{2} \delta(x)), \end{cases}$$

and a new coupling term $r_1 = -r(0)e^{-2I_c(1)}$ at the boundary $x = 1$. The control input is given by

$$V(t) = g(1)e^{-I_c(1)} \frac{\sqrt{2}}{\lambda(1)} u_\partial(t).$$

Target system

Similarly, we apply the same change of variables on the target system to rewrite it in Riemann coordinates. We define $[\bar{\zeta}^+(t, x), \bar{\zeta}^-(t, x)]^\top = Q^{-1}(x)[\bar{X}_1(t, x), \bar{X}_2(t, x)]^\top$. Next, we use an exponential change of variable to suppress the antidiagonal in-domain couplings. Define $\forall x \in [0, 1]$, $\bar{A}(x) = \text{diag}(f(x)e^{I_K(x)}, g(x)e^{-I_K(x)})$, $I_K(x) = \int_0^x \frac{K(s)}{2\lambda(s)} ds$. The new state $[\bar{\xi}^+(t, x), \bar{\xi}^-(t, x)]^\top = \bar{A}(x)[\bar{\zeta}^+(t, x), \bar{\zeta}^-(t, x)]^\top$ satisfies hetero-directional hyperbolic PDEs of form (9.3)-(9.4) with in-domain couplings defined by

$$\begin{cases} \bar{\Sigma}^{++}(x) = \bar{\Sigma}^{--}(x) = 0, \\ \bar{\Sigma}^{+-}(x) = \frac{1}{2r(0)} e^{2I_K(x)} (K(x) - \frac{\lambda(x)}{2} \delta(x)), \\ \bar{\Sigma}^{-+}(x) = \frac{r(0)}{2} e^{-2I_K(x)} (K(x) + \frac{\lambda(x)}{2} \delta(x)), \end{cases}$$

and boundary coupling term $\bar{R}_1 \doteq a_1 = -r(0)e^{-2I_K(1)}$.

10.2.3 . Control design

Following Chapter 9, we use a classic invertible Volterra integral transform (9.6) to replace the in-domain coupling terms. In this low-dimensional case, there is no need for an affine transform. Indeed, since the coupling term q_0 is invertible, we could map both systems to targets with no in-domain couplings and use the control input to compensate for the resulting integral terms at the actuated boundary. More precisely, we have

Theorem 10.2.1: Existence of a mapping

For all $t > 0$, for any initial conditions satisfying appropriate compatibility conditions, for any $V(t)$, let us denote $[\bar{\xi}^+(t, \cdot), \bar{\xi}^-(t, \cdot)]^\top \in H^1([0, 1], \mathbb{R}^2)$ the solution of (9.3)-(9.4) and $[\xi^+(t, \cdot), \xi^-(t, \cdot)]^\top \in H^1([0, 1], \mathbb{R}^2)$ the solution of (9.1)-(9.2), with the couplings defined above. Then there exists a Volterra integral transform \mathcal{K} such that

$$\begin{pmatrix} \bar{\xi}^+ \\ \bar{\xi}^- \end{pmatrix} = \begin{pmatrix} \xi^+ \\ \xi^- \end{pmatrix} - \int_0^x \begin{pmatrix} K^{++} & K^{+-} \\ K^{-+} & K^{--} \end{pmatrix} (x, y) \begin{pmatrix} \xi^+ \\ \xi^- \end{pmatrix} (y) dy.$$

Proof : We can show, following the backstepping methodology, that the kernels $K^{\pm\mp}$ must satisfy on \mathcal{T}^- the following set of equations

$$\lambda(x) \frac{\partial}{\partial x} K^{++}(x, y) + \frac{\partial}{\partial y} \lambda(y) K^{++}(x, y) = \bar{\Sigma}^{+-}(x) K^{-+}(x, y) - \Sigma^{-+}(y) K^{+-}(x, y),$$

$$\begin{aligned}
\lambda(x) \frac{\partial}{\partial x} \partial K^{+-}(x, y) - \frac{\partial}{\partial y} \lambda(y) K^{+-}(x, y) &= \bar{\Sigma}^{+-}(x) K^{--}(x, y) - \Sigma^{+-}(y) K^{++}(x, y), \\
\lambda(x) \frac{\partial}{\partial x} K^{-+}(x, y) - \frac{\partial}{\partial y} \lambda(y) K^{-+}(x, y) &= \Sigma^{-+}(y) K^{--}(x, y) - \bar{\Sigma}^{-+}(x) K^{++}(x, y), \\
\lambda(x) \frac{\partial}{\partial x} K^{--}(x, y) + \frac{\partial}{\partial y} \lambda(y) K^{--}(x, y) &= \Sigma^{+-}(y) K^{-+}(x, y) - \bar{\Sigma}^{-+}(x) K^{+-}(x, y),
\end{aligned}$$

with boundary conditions

$$\begin{aligned}
K^{+-}(x, x) &= \frac{\Sigma^{+-}(x) - \bar{\Sigma}^{+-}(x)}{2\lambda(x)}, \quad K^{++}(x, 0) = q_0^{-1} K^{+-}(x, 0), \\
K^{-+}(x, x) &= \frac{\bar{\Sigma}^{-+}(x) - \Sigma^{-+}(x)}{2\lambda(x)}, \quad K^{--}(x, 0) = q_0 K^{-+}(x, 0).
\end{aligned}$$

The well-posedness of the kernel equations is proved in [DMBAHK18]. The set of above equations admits a unique piecewise continuous solution on \mathcal{T}^- . We, therefore, guarantee the existence of an adequate transformation. ■

Note that the transform defined above corresponds to the composition of \mathcal{K} defined in (9.6) and $\bar{\mathcal{L}}$ defined under (9.19). Consequently, the equations satisfied by the kernels slightly differ from (9.10)-(9.15) given in Chapter 9.

Remark 10.2.1 *In this low dimensional case, by composition of the above-mentioned transforms, we were able to derive directly an overall boundedly invertible transform, given by*

$$\begin{pmatrix} \bar{X}_1(t, x) \\ \bar{X}_2(t, x) \end{pmatrix} = C(x) \begin{pmatrix} X_1(t, x) \\ X_2(t, x) \end{pmatrix} - \int_0^x \begin{pmatrix} N^{++} & N^{+-} \\ N^{-+} & N^{--} \end{pmatrix}(x, y) \begin{pmatrix} X_1(t, y) \\ X_2(t, y) \end{pmatrix} dy.$$

with, for all $x \in [0, 1]$, $I(x) = I_c(x) - I_K(x)$ and

$$C(x) = \begin{pmatrix} \cosh(I(x)) & -\frac{1}{\gamma(x)} \sinh(I(x)) \\ -\gamma(x) \sinh(I(x)) & \cosh(I(x)) \end{pmatrix}.$$

The control input is directly obtained from the backstepping methodology. It is given by

$$\begin{aligned}
u_\partial(t) &= \frac{\lambda(1)}{\sqrt{2}g(1)e^{-I_c(1)}} \left[(a_1 - r_1) \xi^+(1, t) \right. \\
&\quad \left. + \int_0^1 (K^{-+}(1, y) - a_1 K^{++}(1, y)) \xi^+(y) + (K^{--}(1, y) - a_1 K^{+-}(1, y)) \xi^-(y) dy \right]. \tag{10.14}
\end{aligned}$$

10.2.4 . Simulation results

We illustrate the performances of the proposed control approach on simulation using Matlab. We consider a soft PVC string of length 1m, with constant physical parameters $\rho = 1.35 \times 10^3 \text{kg.m}^{-3}$, $E = 0.9 \text{GPa}$. Its initial position is $w_0(x) = 0.1 \sin(\frac{2x}{\pi})$, and no initial speed. We simulated system (9.1)-(9.2) on a time horizon of 20s using a Godunov Scheme [LeVo2] ($CFL = 0.99$). The space domain $[0, 1]$ is discretized with a mesh of 200 points. Beforehand, the kernels $K^{\pm\mp}$ are computed offline using a fixed-point algorithm (see Appendix A). The control input is computed at each time step using (10.14).

We consider a case where the string is naturally slightly damped ($c = 0.1$). Using the proposed control input, we want to artificially assign a higher damping coefficient

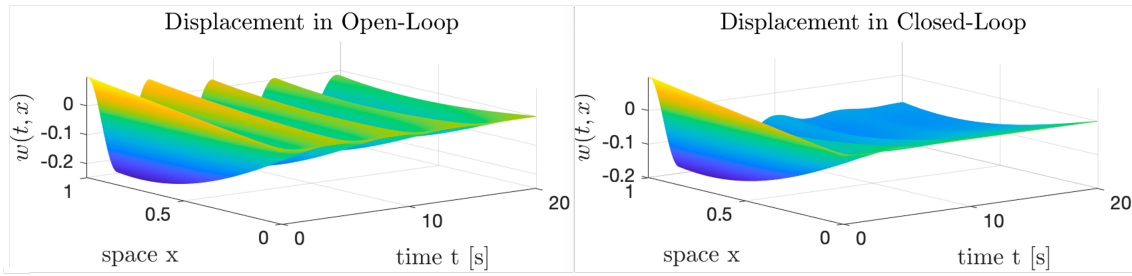


Figure 10.1 – 3D-displacement $w(t, x)$ in open-loop (left), and closed-loop (right) (10.14)

$K = 5c > 0$ to the closed-loop system. We compare the performance of the proposed control law with a simple boundary feedback $X_1(t, 1) = -0.1X_2(t, 1)$. From the values of $(\bar{\xi}^+, \bar{\xi}^-)$, we can numerically compute the evolution of the displacement $w(t, x)$ along the string. As illustrated in Figure 10.1, the oscillations naturally present in open-loop (top) are substantially damped in closed-loop (bottom). The string is stabilized around a stable position.

We represent the energy evolution for both the open-loop and closed-loop systems with the two controllers in Figure 10.2. The black vertical line gives the value $\tau = 2\lambda = 2.45$. With the control input we propose (blue), the energy of the closed-loop system decays faster than with arbitrary proportional feedback (black) or naturally in open-loop (purple). It follows the reference energy decay of an open-loop system with in-domain damping K (dotted red). We represented in Figure 10.3 the evolution of the proportional boundary feedback (green) and full-state feedback (10.14) (blue). As expected, both control efforts go to zero.

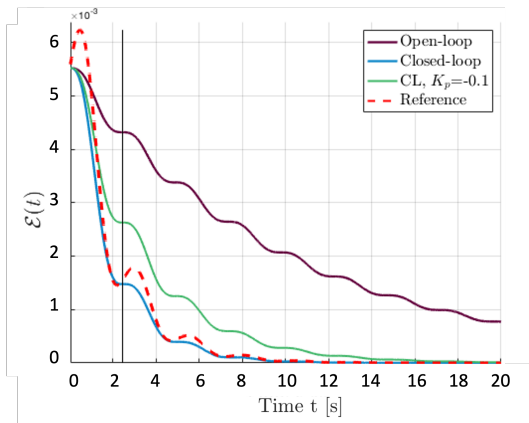


Figure 10.2 – Evolution of the energy $\mathcal{E}(t)$

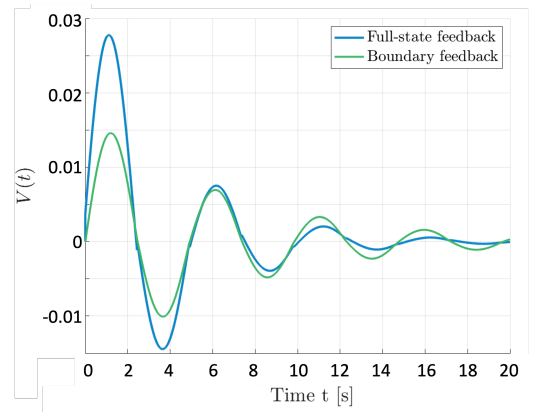


Figure 10.3 – Evolution of the control effort

10.3 . Application to a clamped Timoshenko beam

Next, we apply the methodology proposed in Chapter 9 for in-domain damping assignment of a clamped Timoshenko beam. An extended version of the work presented herein can be found in [RALG22b]. It emphasizes on a second low-dimensional test case the great potential of the Port-Hamiltonian framework in selecting target systems with

specific stability properties.

10.3.1 . Reformulation in the Port-Hamiltonian framework

We consider the clamped actuated Timoshenko beam model proposed in [Tim74]. This model usually represents compliant mechanical structures such as cantilevers or flexible endoscopes [WLG18]. It takes into account shear deformation and rotational inertia of the structure. We denote $w(t, x)$ (resp. $\phi(t, x)$) the transverse normalized displacement (resp. rotation angle) defined on $[0, \infty) \times [0, 1]$. From the balance equations on the momenta, they satisfy

$$\rho \frac{\partial^2 w}{\partial t^2}(t, x) = \frac{\partial}{\partial x} \left(K_s \left(\frac{\partial w}{\partial x}(t, x) - \phi(t, x) \right) \right), \quad (10.15)$$

$$I_\rho \frac{\partial^2 \phi}{\partial t^2}(t, x) = \frac{\partial}{\partial x} \left(EI \frac{\partial \phi}{\partial x}(t, x) \right) + K_s \left(\frac{\partial w}{\partial x}(t, x) - \phi(t, x) \right). \quad (10.16)$$

For the sake of simplicity, we assume that all physical parameters (mass per length unit ρ , rotary moment of inertia of a cross-section I_ρ , Young's modulus of elasticity E , moment of inertia I and shear modulus K_s) are constant. The first end of the beam ($x = 0$) is clamped, such that no movement is allowed and $\frac{\partial w}{\partial t}|_{x=0} = 0$, $\frac{\partial \phi}{\partial t}|_{x=0} = 0$. The opposite end ($x = 1$) is fully actuated, such that $K_s(\frac{\partial w}{\partial x}|_{x=1} - \phi(t, 1)) = V_{\partial 1}(t)$, $EI \frac{\partial \phi}{\partial x}|_{x=1} = V_{\partial 2}(t)$. The initial positions of the beam is given by $w(x, 0) = w_0(x) \in H^1([0, 1], \mathbb{R})$, $\phi(x, 0) = \phi_0(x) \in H^1([0, 1], \mathbb{R})$ and initial speeds in the same space. We define the energy state variables $X = [X_1^\top, X_2^\top]^\top \in H^1([0, 1], \mathbb{R}^4)$ by

$$X_1(t, x) = \begin{pmatrix} \frac{\partial w}{\partial x}(t, x) - \phi(t, x) \\ \frac{\partial \phi}{\partial x}(t, x) \end{pmatrix}, \quad X_2(t, x) = \begin{pmatrix} \rho \frac{\partial w}{\partial t}(t, x) \\ I_\rho \frac{\partial \phi}{\partial t}(t, x) \end{pmatrix}, \quad (10.17)$$

where $X_1(t, x)$ represents shear and angular displacements, while $X_2(t, x)$ represents momentum and angular momentum. Here, the original system (10.15)-(10.16) rewrites in the form (10.1), with $n = 2$ and

$$P_i = \begin{bmatrix} 0 & G_i \\ (-1)^{i+1} G_i^\top & 0 \end{bmatrix}, \quad \text{with } G_0 = \begin{bmatrix} 0 & -1 \\ 0 & 0 \end{bmatrix}, G_1 = \begin{bmatrix} 1 & 0 \\ 0 & 1 \end{bmatrix}, \quad (10.18)$$

and $\Pi_0 = 0_{\mathbb{R}^2 \times 2}$. The boundary matrix is given by $W = \begin{bmatrix} 0_2 & I_2 & I_2 & 0_2 \\ -I_2 & 0_2 & 0_2 & I_2 \end{bmatrix}$, and the Hamiltonian density

$$\mathcal{H} = \text{diag} \left(K_s, EI, \frac{1}{\rho}, \frac{1}{I_\rho} \right) \in D_4^+.$$

In the Port Hamiltonian framework, the boundary conditions rewrite

$$X_2(t, 0) = 0_{\mathbb{R}^2}, \quad X_1(t, 1) = V_\partial(t) \in \mathbb{R}^2, \quad \text{with } V_\partial(t) = \begin{pmatrix} \frac{V_{\partial 1}(t)}{K_s} \\ \frac{V_{\partial 2}(t)}{EI} \end{pmatrix}. \quad (10.19)$$

For any control input $V_\partial \in C^2([0, T], \mathbb{R}^2)$, for any initial conditions satisfying the *compatibility conditions*, [Z12, Lemma 13.2.1] guarantees the existence of a unique classic solution of (10.1)-(10.19). As mentioned in introduction, the Port-Hamiltonian framework offers an

easily interpretable physical framework to define a target system with dissipative terms. The control objective reads as follows

Objective: Specific energy decay rate in closed-loop

Design a full-state boundary feedback $V_{\partial}(t)$ such that $\mathcal{E}(t)$, the energy of the closed-loop system decays following

$$\frac{d\mathcal{E}}{dt} = - \int_0^1 \left(\begin{bmatrix} c_3 & c_4 \\ \rho & I_\rho \end{bmatrix} X_2^\top X_2(t, x) \right) dx, \quad (10.20)$$

with $c_3, c_4 > 0$ two arbitrary in-domain damping coefficients.

In other words, we want the closed-loop system to behave as the exponentially stable target system (10.5) with $\bar{P}_0 = P_0 - \text{diag}(0, 0, c_3\rho, c_4I_\rho)$ and boundary condition

$$\bar{X}_2(t, 0) = 0_{\mathbb{R}^2}, \quad \bar{X}_1(t, 1) = 0_{\mathbb{R}^2}. \quad (10.21)$$

In the target system (10.1)-(10.3), we decided to add dissipative terms by choosing $\Pi_0 > 0$, such that the closed-loop system behaves as a Timoshenko beam with in-domain damping. Using Theorem 10.1.1, we could have alternatively stabilized the beam by applying a velocity feedback of form $\bar{X}_1(t, 1) = \text{diag}(-c_1, -c_2)\bar{X}_2(t, 1)$, with $c_1, c_2 > 0$.

To fulfill our control objective, we first reformulate the initial and target systems in the hyperbolic PDE formalism following Section 10.1.4, and then apply the control design strategy proposed in Chapter 9. It is illustrated in Figure 10.4.

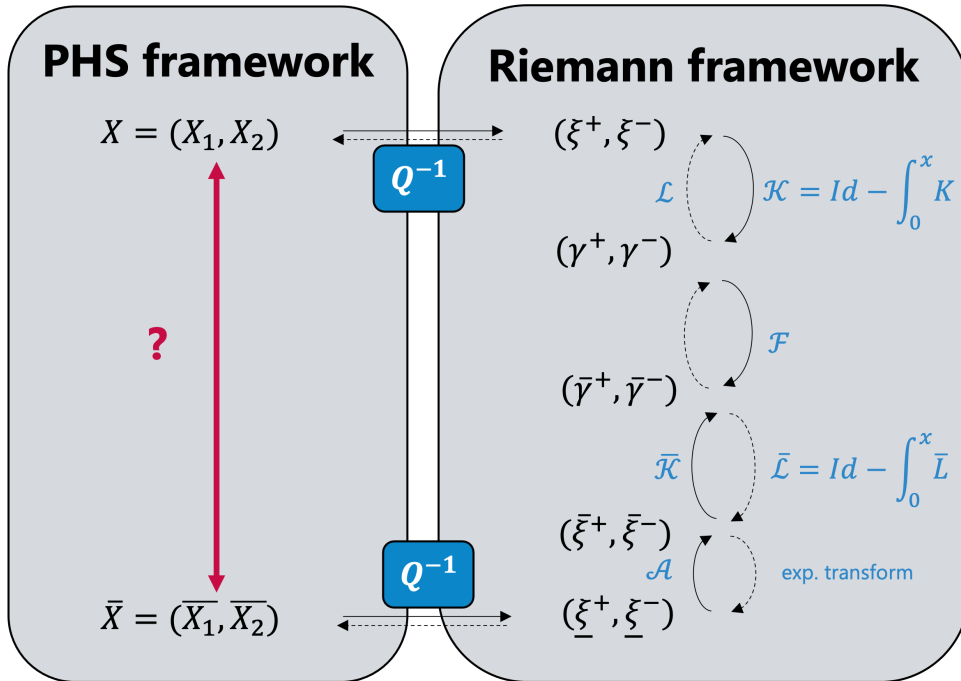


Figure 10.4 – Overall strategy

10.3.2 . Matching a system of balance laws

In what follows, we define the transport velocities $\lambda = \sqrt{\frac{K_s}{\rho}} > 0$, $\mu = \sqrt{\frac{EI}{I_\rho}} > 0$ and the matrix $\Lambda = \Lambda^+ = \Lambda^- = \text{diag}(\lambda, \mu)$, with $\lambda > \mu$ and $R = \text{diag}(\frac{\lambda}{K_s}, \frac{1}{\mu I_\rho}) \in D_2^+$. Assumptions 10.1.1-10.1.2 are satisfied, and $P_1 \mathcal{H} = Q \text{diag}(-\Lambda, \Lambda) Q^{-1}$ with $Q = \frac{1}{\sqrt{2}} \begin{pmatrix} -R & I_2 \\ I_2 & R^{-1} \end{pmatrix}$. The boundary $x = 1$ is fully actuated.

Original system

The state $\xi(t, x) = [\xi^{+\top}(t, x), \xi^{-\top}(t, x)]^\top = Q^{-1} X(t, x) \in H^1([0, 1], \mathbb{R}^4)$ verifies system (9.1)-(9.2), with $Q_0 = -R^{-1}$, $R_1 = R$, $V(t) = \sqrt{2} V_\partial(t)$, and the following in-domain coupling terms

$$\begin{aligned} \Sigma^{++} &= \frac{1}{2} \begin{pmatrix} 0 & \frac{K_s}{\lambda I_\rho} \\ -\lambda & 0 \end{pmatrix}, \quad \Sigma^{+-} = \frac{1}{2} \begin{pmatrix} 0 & \frac{\mu K_s}{\lambda} \\ K_s & 0 \end{pmatrix}, \\ \Sigma^{-+} &= \frac{1}{2} \begin{pmatrix} 0 & -\frac{1}{I_\rho} \\ -\frac{\lambda}{\mu I_\rho} & 0 \end{pmatrix}, \quad \Sigma^{--} = \frac{1}{2} \begin{pmatrix} 0 & -\mu \\ \frac{K_s}{\mu I_\rho} & 0 \end{pmatrix}. \end{aligned}$$

Target system

Similarly, we define $\underline{\xi}(t, x) = Q^{-1} \bar{X}(t, x)$, where $\underline{\xi} = [\underline{\xi}^{+\top}, \underline{\xi}^{-\top}]^\top \in H^1([0, 1], \mathbb{R}^4)$. It satisfies (9.1) where the coupling terms are defined by

$$\begin{aligned} \underline{\Sigma}^{++} &= \frac{1}{2} \begin{pmatrix} -c_3 & \frac{K_s}{\lambda I_\rho} \\ -\lambda & -c_4 \end{pmatrix}, \quad \underline{\Sigma}^{+-} = \frac{1}{2} \begin{pmatrix} -\frac{K_s}{\lambda} c_3 & \frac{K_s \mu}{\lambda} \\ K_s & -\mu I_\rho c_4 \end{pmatrix}, \\ \underline{\Sigma}^{-+} &= \frac{1}{2} \begin{pmatrix} -\frac{\lambda}{K_s} c_3 & -\frac{1}{I_\rho} \\ -\frac{\lambda}{\mu I_\rho} & -\frac{c_4}{\mu I_\rho} \end{pmatrix}, \quad \underline{\Sigma}^{--} = \frac{1}{2} \begin{pmatrix} -c_3 & -\mu \\ \frac{K_s}{\mu I_\rho} & -c_4 \end{pmatrix}, \end{aligned}$$

with boundary conditions $\underline{\xi}^+(t, 0) = -R^{-1} \underline{\xi}^-(t, 0)$, $\underline{\xi}^-(t, 1) = R \underline{\xi}^+(t, 1)$. We then perform the exponential change of coordinates, $\bar{\xi} = [\bar{\xi}^{+\top}, \bar{\xi}^{-\top}]^\top = \bar{A}(x) \underline{\xi}$, with $\forall x \in [0, 1]$, $\bar{A}(x) = \text{diag}(e^{\alpha x}, e^{\beta x}, e^{-\alpha x}, e^{-\beta x})$ and $\alpha \doteq \frac{c_3}{2\lambda}$, $\beta \doteq \frac{c_4}{2\mu}$. The new state satisfies (9.1) where the now space-dependent in-domain coupling terms are

$$\begin{aligned} \bar{\Sigma}^{++}(x) &= \frac{1}{2} \begin{pmatrix} 0 & \frac{K_s}{\lambda I_\rho} e^{(\alpha-\beta)x} \\ -\lambda e^{-(\alpha-\beta)x} & 0 \end{pmatrix}, \quad \bar{\Sigma}^{+-}(x) = \frac{1}{2} \begin{pmatrix} -\frac{K_s}{\lambda} c_3 e^{2\alpha x} & \frac{K_s \mu}{\lambda} e^{(\alpha+\beta)x} \\ K_s e^{(\alpha+\beta)x} & -\mu I_\rho c_4 e^{2\beta x} \end{pmatrix}, \\ \bar{\Sigma}^{-+}(x) &= \frac{1}{2} \begin{pmatrix} -\frac{\lambda}{K_s} c_3 e^{-2\alpha x} & -\frac{1}{I_\rho} e^{-(\alpha+\beta)x} \\ -\frac{\lambda}{\mu I_\rho} e^{-(\alpha+\beta)x} & -\frac{c_4}{\mu I_\rho} e^{-2\beta x} \end{pmatrix}, \quad \bar{\Sigma}^{--}(x) = \frac{1}{2} \begin{pmatrix} 0 & -\mu e^{-(\alpha-\beta)x} \\ \frac{K_s}{\mu I_\rho} e^{(\alpha-\beta)x} & 0 \end{pmatrix}. \end{aligned}$$

The boundary conditions are now given by $\bar{\xi}^+(t, 0) = -R^{-1} \bar{\xi}^-(t, 0)$, $\bar{\xi}^-(t, 1) = \bar{R} \bar{\xi}^+(t, 1)$, with $\bar{R} = \text{diag}(e^{-2\alpha}, e^{-2\beta}) R$. Applying the strategy proposed in the previous chapter, we want to determine the control input $V(t)$ so that the closed-loop system behaves asymptotically as the Timoshenko beam with in-domain damping.

10.3.3 . Control design

classic backstepping transformations

We now map the initial and target systems to simpler systems, where most coupling terms have been moved to the boundary. We do not give here the explicit expression of the kernel equations for brevity, which can be found in Section 9.2.1. Starting from the initial states ξ , define $\gamma = \mathcal{K}(\xi) = [\gamma^{+\top}, \gamma^{-\top}]^\top$, with \mathcal{K} a first Volterra integral transform. Following the backstepping methodology, we show in [RALG22b] that for kernels satisfying a set of well-posed equations, the initial system (9.1)-(9.2) with couplings defined above, can be mapped to (9.16)-(9.17), with Γ^+, Γ^- strictly lower triangular matrices, since R is invertible. We define similarly a transform $\bar{\mathcal{K}}$ of form (9.6) to map the target system to a simpler system. The state $\bar{\gamma} = \bar{\mathcal{K}}(\bar{\xi})$ verifies (9.21)-(9.22), with strictly lower triangular in-domain coupling matrices $\bar{\Gamma}^+, \bar{\Gamma}^-$.

Affine transformation

Next, we define component-wise a time-affine transform \mathcal{F} such that $\bar{\gamma} = \mathcal{F}(\gamma)$ by

$$\bar{\gamma}_1^+(t, x) = \gamma_1^+(t, x), \quad \bar{\gamma}_1^-(t, x) = \gamma_1^-(t, x), \quad (10.22)$$

$$\bar{\gamma}_2^+(t, x) = \gamma_2^+(t, x) + \int_0^{\frac{x}{\mu}} F_{21}^+(x, y) \gamma_1^-(t - y, 0) dy + \int_{\frac{x}{\mu}}^{\frac{1}{\mu}(1+x)} M_{21}^+(x, y) \gamma_1^-(t - y, 0) dy,$$

$$\bar{\gamma}_2^-(t, x) = \gamma_2^-(t, x) + \int_0^{\frac{1}{\mu}(1-x)} F_{21}^-(x, y) \gamma_1^-(t - y, 0) dy. \quad (10.23)$$

Note that this transform requires the knowledge of past values of the boundary state $\gamma_1^-(t, 0)$ and is only defined for $t \geq t^* = \frac{2}{\mu}$. By Theorem 9.2.1, it is invertible on a specific domain. The kernels $F_{21}^\pm \in C_{pw}^1(\mathcal{T}_\mu^\pm, \mathbb{R}^{2 \times 2})$ and $M_{21}^+ \in C_{pw}^1(\mathcal{P}_{\frac{1}{\mu}, \mu}^+, \mathbb{R}^{2 \times 2})$ satisfy a well-posed set of equations by Lemma 9.2.2. Using the method of characteristics, they can be expressed using the non-zero components of the in-domain couplings

$$\begin{cases} F_{21}^+(x, y) = \bar{\Gamma}_{21}^+(x - \mu y) - \Gamma_{21}^+(x - \mu y), \quad \forall (x, y) \in \mathcal{T}_\mu^+, \\ F_{21}^-(x, y) = \bar{\Gamma}_{21}^-(x + \mu y) - \Gamma_{21}^-(x + \mu y), \quad \forall (x, y) \in \mathcal{T}_\mu^-, \\ M_{21}^+(x, y) = -\mu I_\rho (\bar{\Gamma}_{21}^-(\mu y - z) - \Gamma_{21}^-(\mu y - z)), \quad \forall (x, y) \in \mathcal{P}_{\frac{1}{\mu}, \mu}^+. \end{cases} \quad (10.24)$$

Full-state feedback control law

The control input directly derives from the different transforms and (9.39)

$$\forall t > t^*, \quad V(t) = (\bar{R} - R)\gamma^+(t, 1) - I_1(t) + I_2(t) + \bar{R} \left(\begin{array}{c} 0 \\ \int_0^{\frac{2}{\mu}} \mathcal{I}(y) dy \end{array} \right), \quad (10.25)$$

where the integral term \mathcal{I} is defined on $[0, \frac{2}{\mu}]$ by

$$\mathcal{I}(y) = \left(\mathbb{1}_{[0, \frac{1}{\mu}]}(y) F_{21}^+(1, y) + \mathbb{1}_{[\frac{1}{\mu}, \frac{2}{\mu}]}(y) M_{21}^+(1, y) \right) \gamma_1^-(t - y, 0),$$

and the integral terms I_1, I_2 depend on the kernels of the two Volterra transforms and the distributed states $\gamma, \bar{\gamma}$. It could be rewritten with distributed values of the original states $X(t, x)$ using the different transforms.

10.3.4 . Simulation results

We finally illustrate the performance of our control strategy for the test case presented in Section 10.3. We consider a Timoshenko beam of length $\ell = 1\text{m}$, with physical parameters given in Table 10.1. It is initially at rest at a position $w_0(x) = 0.1 \sin(\frac{\pi}{2}z)$, $\phi_0(x) = 0$. Using the above control strategy, we want the closed-loop beam to behave as (10.5)-(10.21) with $c_3 = 0.5 \text{ USI}$, $c_4 = 0.8 \text{ USI}$.

Param.	Value	Param.	Value
EI	$0.5 \text{ kg m}^3\text{s}^{-2}$	I_ρ	0.9 kg m
K_s	1.2 kg m s^{-2}	ρ	0.9 kg m^{-1}

Table 10.1 – Numerical values for simulation

As illustrated in Figure 10.5, the position of the open-loop system oscillates around an equilibrium. Its energy is approximately constant due to the absence of dissipative terms. It is represented in Figure 10.7 (red).

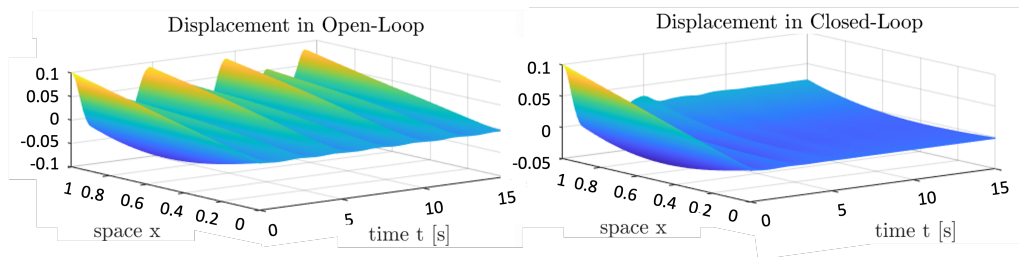


Figure 10.5 – 3D-displacement $w(t, x)$ in open-loop (left) and closed-loop (right)

Unlike in [RALG22b], where the control input is computed for all time steps using a buffer, we here only apply the control input (10.25) for $t \geq t^*$, with $t^* = \frac{2}{\mu}$. The evolution of its first component (blue) and second (red) is represented in Figure 10.6, as well as its norm (black). Since it requires the computation of state $\gamma, \bar{\gamma}$ at each time step, it is more computationally expensive than traditional PI controllers.

The system is in open loop on $[0, t^*]$. After the control input is applied, the position of the closed-loop system converges quickly to an equilibrium. As illustrated in Figure 10.7 (blue), its energy decreases at the same rate as the target system (dotted red).

Conclusion

This chapter illustrates how the Port-Hamiltonian formalism can be used to determine a target system with interesting stability properties. It offered a physical framework that could match a class of hyperbolic PDE systems under some assumptions. We were

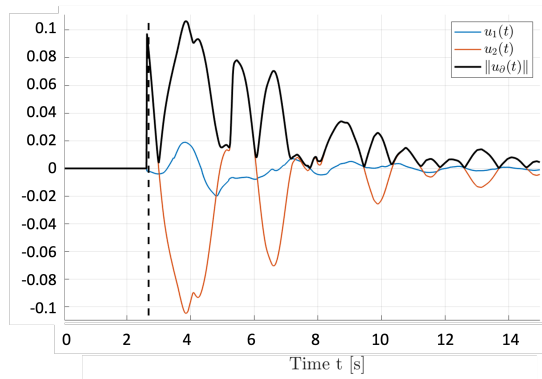


Figure 10.6 – Evolution of the control effort

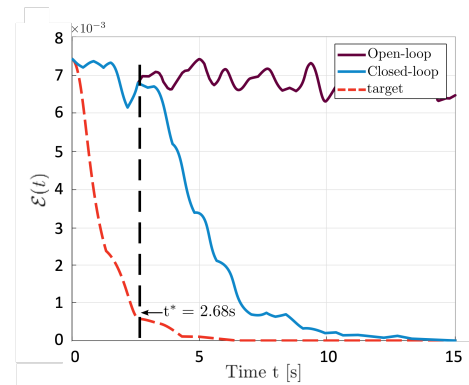


Figure 10.7 – Evolution of the energy $\mathcal{E}(t)$

then able to apply the methodology proposed in Chapter 9 while introducing natural tuning parameters and adding degrees of freedom (e.g., the dissipation rate) with a clear energy interpretation. This is an essential step for the practical implementation of backstepping controllers. Using the Port-Hamiltonian framework allowed the design of easily parametrizable (and attainable) target systems for which the closed-loop behaviors are perfectly known and match performance specifications. In particular, we imposed the energy decay rate using an in-damping assignment for two test cases: a clamped string with space-varying coefficients and a clamped Timoshenko beam.

So far the results presented in this chapter are only preliminary results. They should be followed by a *quantitative* analysis of the target system properties. This could be done by defining specific performance criteria, similar to what is proposed in Appendix C. As already mentioned, implementing the full-state feedback controller (10.25) requires the knowledge of all the states. We should then design a state observer [HDMVK16, AA19]. An example of such an observer is studied in Appendix C for the study case of a Timoshenko beam with space-varying coefficients. More generally, observers have been proposed in the port-Hamiltonian framework in [TRWLG20]. Moreover, we could take advantage of the intrinsic modularity of the Port-Hamiltonian framework to adapt this approach to more extensive networks of interconnected systems. We could also combine this approach with the one presented in Part III to consider the case when one boundary is not fully actuated.

11 - Machine learning techniques for distributed state and parameter estimation

This chapter aims to take advantage of recent advances in machine-learning techniques to solve drawbacks inherent to backstepping-based controllers. The resolution of a PDE observer system at each time-step, necessary to implement an output-feedback controller, is time consuming. Our first objective is to propose a surrogate to generate an estimation of the distributed state in real-time using the available measurements. Deep learning-based techniques to solve PDE systems [BHS20, NS21, LJK21] have recently gained attention. They offer a faster solution than classic numerical schemes, such as the Godunov scheme [LeV02] used in simulations. Following [SLY⁺22], we focus on the use of Fourier Neural Operators [LKA⁺21] to obtain a fast estimation of the Timoshenko beam energy states considered in Chapter 10. Following the promising results of physics-informed neural networks [RPK19, LZK⁺23], we propose to extend this approach by adding physical loss terms in the training process.

In some situations, a direct measurement of physical parameters that appear in the dynamical model is not possible or uneasy. In an evolving environment, they might also vary with time. This is the case for drilling, where the friction coefficients depend on the nature of the rocks being drilled. Different numerical methods can be proposed, but using neural networks seemed promising [ASNK22a]. Our second objective is to estimate unknown physical parameters from the available measurement. As a test case, we aim to estimate static and kinetic Coulomb friction terms for drilling systems considered in Chapter 6. Using Transformers [VSP⁺17], the state-of-the-art architecture for processing temporal series, we propose an innovative method to estimate them at the beginning of a drilling operation. As a perspective, we combine both architectures to provide a combined parameter and distributed state estimation in a two-branches network [LJK21, BSK23]. This offers a first step toward using such estimations in a closed-loop with a full-state feedback controller.

Chapitre 11: Apprentissage automatique pour l'estimation d'un état distribué et des paramètres du système. Dans ce chapitre, nous visons à tirer parti des avancées récentes en apprentissage automatique pour résoudre différents problèmes inhérents à l'utilisation des contrôleurs proposés, basés sur le backstepping. Notre premier objectif est d'envisager un substitut aux systèmes d'observateurs classiques, qui pourrait générer une estimation en temps réel de l'état distribué, en utilisant les mesures disponibles. Les techniques d'apprentissage profond pour résoudre les systèmes d'EDP [BHS20, NS21, LJK21] ont récemment suscité l'attention. Elles offrent une solution plus rapide que les schémas numériques classiques, tels que le schéma de Godunov [LeV02] utilisé dans nos simulations. Inspirés par [SLY⁺22], nous nous concentrons sur l'utilisation d'opérateurs neuronaux de Fourier [LKA⁺21] pour obtenir une estimation rapide de l'état distribué de la poutre de Timoshenko considérée au chapitre 10.

Suite aux résultats prometteurs des réseaux neuronaux intégrant des connaissances physiques [RPK19, LZK⁺23], nous proposons d'étendre cette approche en ajoutant des termes de perte physique dans le processus d'entraînement.

Dans cette thèse, nous avons jusqu'à présent négligé la question de la robustesse par rapport aux incertitudes des paramètres. Cependant, il s'agit d'une préoccupation cruciale pour une application pratique. Notre deuxième objectif est d'estimer les paramètres physiques inconnus à partir des mesures disponibles. Cette question a été soulevée par [ASNK22a], dans le contexte des systèmes de forage considérés au chapitre 6. En utilisant les Transformers [VSP⁺17], l'architecture de pointe pour le traitement des séries temporelles, nous proposons une méthode innovante pour estimer les coefficients de frottement au début d'une opération de forage.

En perspective, nous combinons les deux architectures pour fournir une estimation simultanée des paramètres et de l'état distribué dans un réseau à deux branches [LJK21, BSK23]. Cela constitue une première étape vers l'utilisation de telles estimations en boucle fermée avec un contrôleur à rétroaction d'état complet.

Contents

11.1 Distributed state estimation using a neural network	215
11.1.1 Review on recent advances	215
11.1.2 Test case: estimation of the distributed state of a Timoshenko beam	216
11.1.3 Perspectives	225
11.2 Parameter estimation using a neural network	226
11.2.1 Review on recent advances	227
11.2.2 Test case: estimation of friction parameters while drilling	227
11.2.3 Perspectives: combined approach	230

A conference paper based on results presented in Section 11.2 was accepted at the 43rd IEEE International Geoscience and Remote Sensing Symposium (IGARSS).

The results presented herein derive from a collaboration with Maxime Darrin, during a 2-month research project in LIVIA, Laboratoire d'imagerie, de vision et d'intelligence artificielle in Ecole de Technologie Supérieure (ETS), Montreal, Canada. It was funded by the CNRS International Research Laboratory (IRL) *International Laboratory on Learning Systems* (ILLS). I am very grateful to the CNRS for this opportunity.

11.1 . Distributed state estimation using a neural network

In this section, we present a neural network-based strategy to surrogate the resolution of the observer system at each time step. It aims to replace the resolution of a finite element scheme. This allows to fasten the computation time drastically and could ease the use of output-feedback backstepping-based controllers for real systems.

11.1.1 . Review on recent advances

Approximating operators between infinite dimensional spaces

In recent years, there has been a growing interest in neural-network-based approaches to solve PDEs. Historically, neural networks have first focused on learning mappings between finite-dimensional spaces, solving, therefore, simple tasks such as regression. The objective is to use the network as a universal approximator to determine correlations between input-output pairs. If correctly trained, it can map new inputs to a suitable output. Recently, this approach has been generalized to learn mappings between infinite-dimensional function spaces, using the *random feature model* [NS21] or model reduction techniques such as principal component analysis [BHKS20]. Such neural networks (NN), called **neural operators** [LKA⁺20], are therefore able to learn the abstract representation of the PDE model to obtain the solution and are usually mesh-independent. Based on the universal theorem of operators [CC95], another architecture called *DeepONet* was also proposed in [LJK21] to learn operators from a small dataset. Such neural networks could solve PDE systems **much faster** than traditional solvers (Godunov scheme, finite element methods...) [SLY⁺22]. These solvers are usually mesh-dependent, so obtaining an accurate solution is often time-consuming. A first strategy has been to use *Fourier Neural Operators* introduced in [LKA⁺21]. Indeed, spectral methods [CHQZ88] have appeared to be a promising solution to enforce linear spatial PDEs into convolutional neural networks [JKB20]. Their architecture will be described in more detail later on. It was shown to have very good approximation results on several PDE systems (Burgers' Equation, Darcy Flow), with a consistent error rate (independent of the resolution). This formulation has been recently applied in a feedforward and a recurrent architecture to replace traditional solvers in obtaining a state estimation from backstepping-based observer systems. In [SLY⁺22], the authors proved that recurrent or feed-forward neural networks could greatly accelerate the estimation time while keeping high accuracy. In particular, the **recurrent** architecture seems intuitively more adequate since it only requires the state estimation and measurement on the previous timestep.

Adding a priori knowledge of the underlying physics

All these approaches were first only **data-driven**, and did not use the underlying dynamics. The question of how to best enforce physical constraints in the solution recently raised a high interest. It could ensure the trustworthiness of the model output by guaranteeing physical consistency. It would then make such networks useable to obtain estimations of PDE systems, for real-time implementation of backstepping-based controllers for instance. In the wake of Physics-informed neural networks (PINNs) [RPK19], the next step was to add a priori knowledge of the underlying dynamics. Taking advantage of automatic differentiation [BPRS15], the training procedure of a DeepONet was modified in [WWP21] to add loss terms representing the discrepancy of the output with the physical model.

Similarly, Physics-Informed Neural Operators (PINO) [LZK⁺23] have proved promising results in several applications, such as solving Burger equations or modeling flows in heterogeneous environments [RAMH22]. A general overview of existing techniques is given in [GBYK22]. It paves the way toward physically consistent predictions with higher accuracy, generalization performance, and data efficiency.

11.1.2 . Test case: estimation of the distributed state of a Timoshenko beam

Overall objective

To avoid using computationally expensive classic numerical solvers, an alternative could be to model the initial PDE system **or** the observer PDE system by a neural network. At first glance, one might naively question the interest in using observers like the ones designed in Appendix C, if the PDE system modeling the state behavior is already known. The main interest lies in the independence of the initial condition in the observer system. It allows it to converge to the real state regardless of the initial condition using available measurements $Y(t)$ solely. It is a crucial property since the distributed initial condition is usually unknown. In [SLY⁺22], the authors also argue that combining the backstepping approach with ML-based resolution guarantees the convergence of the NN output to the real state.

Our objective reads as follows

Objective 11.1.1

For $T > 0$, approximate the function $X \in C^1((0, T] \times H^1([0, 1], \mathbb{R}^4))$, defined as a solution of (10.1)-(10.19) with given initial conditions X_0 satisfying the compatibility conditions, by a neural network of parameters θ , defined by $f_\theta : (Y_T, X_0) \mapsto \hat{X}_{\theta, T}$. More precisely, we want

$$\| \|X(\cdot, \cdot) - \hat{X}_{\theta, T}(\cdot, \cdot)\|_{L^2}^2 \|_{D_\tau} \rightarrow 0$$

for some $0 < \tau < T$.

In other words, we need to find the parameters θ (also known as *weights*), such that the output of the NN is a *good* estimation of the distributed state. The choice of the norm to consider is somehow arbitrary. Here, we consider that the D_τ -norm of the L^2 -norm of the *discrepancy* between the real state and the output from the NN goes to zero. Taking an average on time is justified by the use of time sequences.

The neural network takes as inputs sequences of measurements Y_T (depending on a recurrent or convolutional architecture as explained later) and the initial state (or state predicted at the previous time step). It could also take as inputs known physical parameters. First, we generate a dataset, containing inputs and reference outputs. The NN is trained on a part of this dataset. The weights θ are modified to minimize a specific loss as described later. Following [SLY⁺22], we use different NN architectures. Once they are trained, they can serve as a surrogate to obtain a fast estimation of the state.

Generating a first dataset

The first consideration is to generate an adequate dataset for training and testing the neural networks. This can be done offline using classic numerical schemes. We assume that physical parameters are known and constant, with values given in Table 11.1.

Parameter	Value	Parameter	Value
2 nd moment of area I	0.5	Length ℓ	1
Young's modulus E	1	shear modulus K_s	1.2
rotary moment of inertia I_ρ	0.9	linear density ρ	0.9

Table 11.1 – Numerical values for simulation

We neglect the damping terms such that $\eta_1 = \eta_2 = 0$. To generate a dataset with different state evolutions, it remains to choose the initial conditions. The random realizations of the initial conditions are generated by sampling a **Gaussian random field** [RWo6]. They are distributed as a *Gaussian Process* with mean function m and covariance function k , and denoted $(\xi_0^+(x), \xi_0^-(x)) \sim \mathcal{GP}(m, k)$. The covariance function is defined by $k(x_1, x_2) = \exp(-\frac{1}{2l}(x_1 - x_2)^2)$, with length scale parameter $l > 0$ chosen to control the complexity of the sampled input functions (here kept equal to one). The mean function is defined by $m : [0, \ell] \rightarrow \mathbb{R}^4$, with $m_1(x) = \frac{A}{\sqrt{2}} \frac{\pi}{2\ell} \sin(\frac{\pi}{2\ell}(\ell - x))$, $m_3 = \frac{K_s}{\lambda} m_1(x)$ and $m_2(x) = m_4(x) = 0$, with amplitude $\frac{A\pi}{2\ell} = 0.1$. It corresponds to an initial position $w(x) = A \cos(\frac{\pi}{2\ell}(\ell - x))$ and a constant reference angular position and no velocity. The resulting function is then projected to a specific null space so that the initial conditions satisfy the compatibility conditions (2.1.1).

A set of $N = 1200$ samples is generated. It is split into a set of $N_{\text{train}} = 1000$ training samples and $N_{\text{test}} = 200$ testing samples. From the random initial condition, the evolution of the four states $(\xi^+(t, x), \xi^-(t, x))$ is computed on a time scale $[0, T]$, with $T = 10$ s. The space discretization is $dx = 0.01$, so the space mesh D_x contains $N_x = 101$ points. We chose a CFL number equal to 1. As in previous simulations, we use a Godunov scheme [LeVo2] to solve the coupled hyperbolic PDE system on Matlab. As a reminder, they are given by (9.1)-(9.2)

$$\begin{aligned} \frac{\partial}{\partial t} \xi^+(t, x) + \Lambda \frac{\partial}{\partial x} \xi^+(t, x) &= \Sigma^{++}(x) \xi^+(t, x) + \Sigma^{+-}(x) \xi^-(t, x), \\ \frac{\partial}{\partial t} \xi^-(t, x) - \Lambda \frac{\partial}{\partial x} \xi^-(t, x) &= \Sigma^{-+}(x) \xi^+(t, x) + \Sigma^{--}(x) \xi^-(t, x), \end{aligned}$$

with boundary conditions

$$\xi^+(t, 0) = -R^{-1} \xi^-(t, 0), \quad \xi^-(t, 1) = R \xi^+(t, 1),$$

with in-domain and boundary couplings given in Section 10.3, and boundary measurement $Y(t) = \sqrt{2} D \xi^+(1)$ defined in Appendix C. With the parameters in Table 11.1, we obtain a time discretization D_t with $N_t = 1167$ points. We then compute the values of the energy states $(X(t, x))$ using the adequate changes of variables. A 3D representation for one example is given in Figure 11.1. With a processor 2,3 GHz Intel Core i5, generating and storing the dataset takes approximately 10min.

The resulting tensor is, therefore, of dimension $N \times N_t \times N_x \times 4$. We also define a measurement tensor of dimension $N \times N_t \times 2$ corresponding to $X^+(t, \ell)$. To reduce the size of the state tensor (4.3Go), we first operate a subsampling in time to obtain data at approximately 25Hz, and a new time discretization D_{tt} with N_{tt} points. One limitation of these data-based approaches lies in their need for storage and computation capacities.

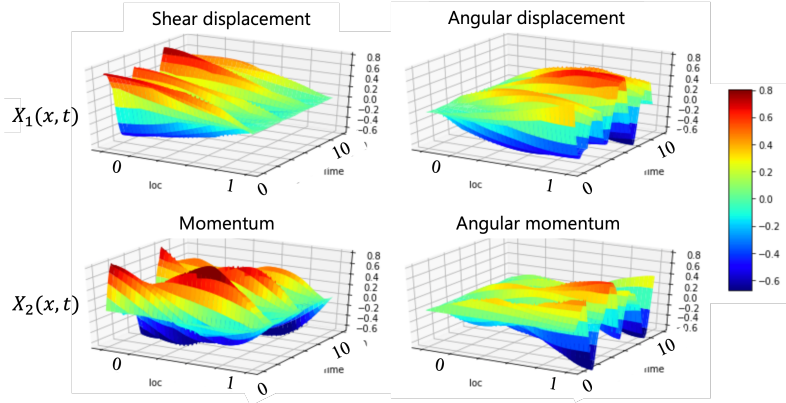


Figure 11.1 – One example of state evolution

Parameter	Interpretation
N (resp. $N_{\text{train/test}}$)	number of samples (in train/test sets)
N_t (resp. N_{tt})	number of points in time discretization D_t (resp. D_{tt})
N_x	number of points in space discretization D_x
N_b	batch size
N_p	number of parameters (4)

Table 11.2 – Parameter interpretation

The interpretation of different parameters introduced are gathered in Table 11.2.

Limitation of the classic recurrent architectures

In a naive approach, we first use classic recurrent architectures developed to learn time sequences. For instance, Long-Short-Term-Memory (LSTM) [HS97] is a recurrent neural network capable of learning order dependence in sequence prediction problems. It was modified in [CvMG⁺14] to create simpler and less computationally expensive Gated Recurrent Units (GRU). As seen in [SLY⁺22], the neural network cannot adequately estimate the distributed PDE state. In particular, it fails to match the oscillation amplitude. This results in an oscillatory density error function. In Figure 11.2, we first represent the 3-D evolution of the first component of state $X_1(t, x)$ (shear displacement), computed using the Godunov scheme (reference) and by an LSTM neural network.

For better visualization, we represented the error between the reference and predicted values for 9 random samples, projected on $D_x \times D_{tt}$ in Figure 11.3.

We also represent the evolution of the estimation error averaged on the test samples for each state component. As seen in Figure 11.4, the mean L^2 -norm oscillates around a relatively high value (between 2 and 3). Therefore, we could expect that such estimations might not be used to generate output-state feedback controllers.

Fourier Neural Operators

Following what was done in [SLY⁺22], we then focused on a new type of neural network known as *Fourier Neural Operators* [LKA⁺21]. As mentioned in the previous section, it follows the recent trend of using NN to learn mesh-independent infinite-dimensional

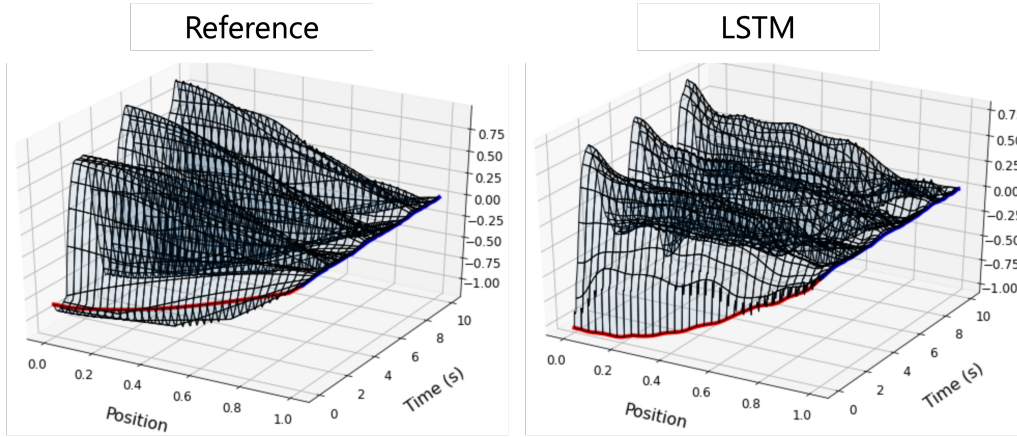


Figure 11.2 – Evolution of state component $X_{1,1}(t, x)$ for one test sample

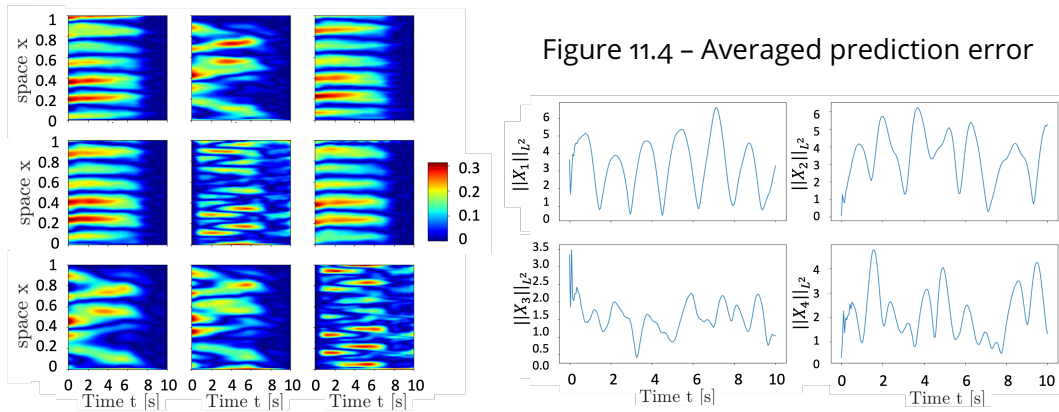


Figure 11.4 – Averaged prediction error

Figure 11.3 – Projected prediction error

operators, not just a discretized solution [BKS20, NS21, LJK21]. This structure relies on the neural operator proposed in [LKA⁺20], where the integral kernel operator is replaced by a convolution operator defined in Fourier space. More precisely, the neural operator is formulated as an iterative architecture. First, the input is lifted to a higher dimensional hidden representation using a linear transform (grey rectangle). Several iterations of an FNO unit (such as schematically illustrated in Figure 11.5) are then operated. Each update corresponds to an integral convolution operator (upper branch of Figure 11.5 summed up with a convolution \mathcal{W} (orange box), composed with a nonlinear activation function (green circle). The convolution operator is defined in Fourier space. Finally, the last update is projected back to the output space using a linear transform. More details will be given for each specific architecture in the following sections. The structure presented in [LKA⁺21] cannot be directly applied to our problem since the available functions are not distributed over the spatial domain: the measurement is only available at one boundary. We next present the two first solutions we implemented, inspired by the approach proposed in [SLY⁺22].

Convolutional FNO

We first propose a convolutional FNO-based neural network (convFNO). It relies on the strong assumptions that the initial conditions of all states $X_0(x)$ are known on a given

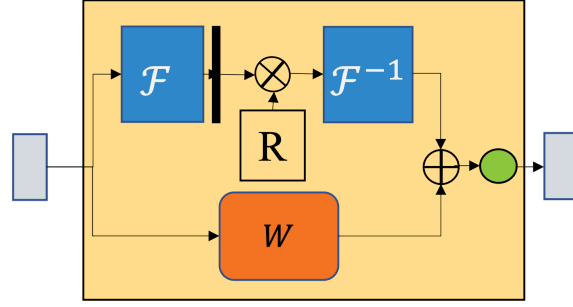


Figure 11.5 – Structure of a FNO-unit (Fourier Layer) [LKA⁺21]

mesh D_x , and that we have access to all boundary measurements over D_t .

Figure 11.6 illustrates the different components of the convolutional FNO.

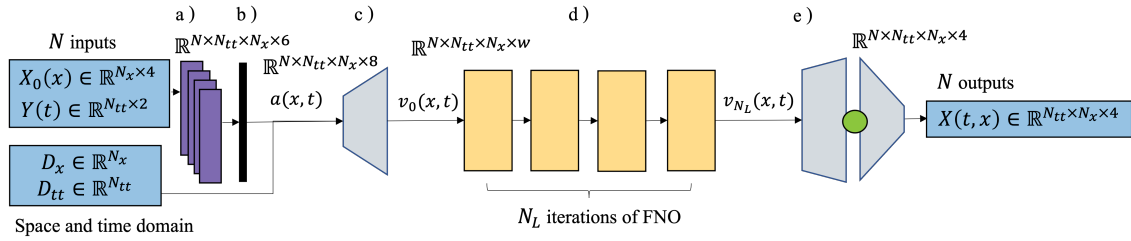


Figure 11.6 – Architecture of the convolutional FNO

The N samples of discretized inputs $X_0 \in \mathbb{R}^{N_x \times 4}$ and $Y(t) \in \mathbb{R}^{N_{tt} \times 2}$ are first reshaped into a tensor (a), whose values are normalized using *unit gaussian normalization* (b). The tensor is then stacked with the discretized definition domain $D_x \times D_{tt}$ and fed to a first linear operator of width w . The resulting tensor is obtained by the transform $v_0(t, x) = a(t, x)A_0^T + b_0$ with values of tensor $A_0 \in \mathbb{R}^{w \times 8}$ and bias b_0 initialized from $\mathcal{U}(-\sqrt{\frac{1}{8}}, \sqrt{\frac{1}{8}})$ (c). The values (weights) of (A_0, b_0) are learned during training. We then perform $N_L = 4$ iterations of 2D FNO-units, considering a time \times space definition domain (d). As recommended in [LKA⁺21], since the discretization is uniform, we keep the $k_{\max} = 12$ Fourier modes in the Fast Fourier Transform of $v_0(t, x)$. The initial weights of R the tensor of dimension $N_{tt} \times N_x \times w \times w$ are randomly initialized. The operator \mathcal{W} is a 2D convolution operator. The nonlinear activation function is a Gaussian Error Linear Unit (GELU) [HG16]. Finally, the last output $v_{N_L}(t, x)$ is projected to a higher dimensional space $\mathbb{R}^{f_{c1}}$, applied another GELU, and projected back to the output space, such that $X(t, x) = (\text{GELU}(v_4(t, x)A_1^T + b_1))A_2^T + b_2$ (e). The hyperparameters are summarized in Table 11.3.

Step	Param.	Value	Step	Param.	Value
c) Projection width	w	32	d) # FNO-units	N_L	4
d) # modes in FFT	k_{\max}	12	d) Activation func.	●	GELU
e) Projection width	f_{c1}	128	e) Activation func.	●	GELU

Table 11.3 – Hyperparameters used for simulation

The common loss term corresponds to the **mean-squared error** over a batch of N_b data during training. Knowing the expected state values, we can compute

$$\mathcal{L}_{MSE} = \frac{1}{N_b N_x N_t} \sum_{k=1}^{N_b} \sum_{i=1}^{N_t} \sum_{j=1}^{N_x} \|X(t_i, x_j) - f_{\theta}(Y_{[-T+t_i-dt, t_i-dt]}, \hat{X}_{[-T+t_i-dt]})(t_i, x_j)\|^2.$$

Following [SLY⁺22], we define the relative norm of the approximation error ε_{L^2} by

$$\varepsilon_{L^2} = \frac{1}{N_b} \sum_{k=1}^{N_b} \sum_{i=1}^{N_x} \sum_{j=1}^{N_{tt}} \frac{\|\hat{X}(j, i) - X(i, j)\|_2}{\|X(i, j)\|_2}.$$

This network is trained on $N_{\text{train}} = 1000$ samples to minimize ε_{L^2} . We use Adam optimizer to train for 500 epochs with an initial learning rate of 0.001 halved every 100 epochs.

The training time is 65 min (approx. 8sec/epochs). In Figure 11.7, we represent the evolution of the MSE (red) and relative norm error ε_{L^2} (blue) during training. We then test the trained neural network on $N_{\text{test}} = 200$ samples. The computation time was 0.09s.

We obtain a good approximation, with $MSE = 0.026$ and $\varepsilon_{L^2} = 6.7 \times 10^{-3}$.

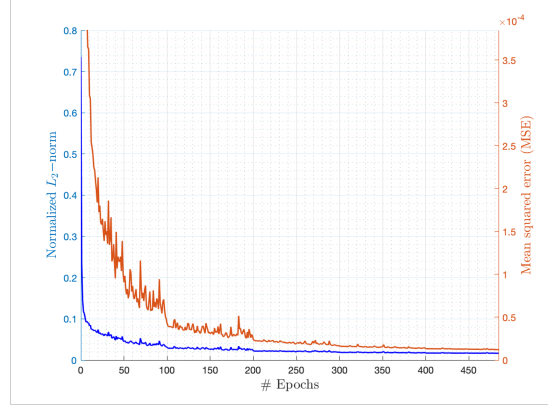


Figure 11.7 – Loss evolution during training

We represent in Figure 11.8 the reference 3D evolution of $X_1(t, x)$ computed using the Godunov scheme (left) and the evolution predicted by the convFNO network (right) from initial conditions and boundary measurements, for one random sample set.

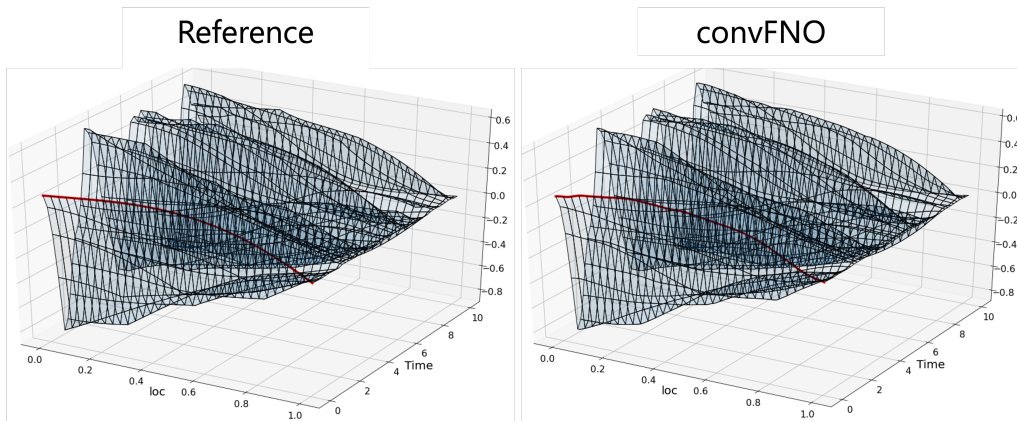


Figure 11.8 – Comparison of 3D evolution for PDE state and convolutional FNO prediction

As for the LSTM, we represented the projection of the error. The dark blue regions correspond to an error inferior to 2×10^{-3} , which is promisingly low. The highest prediction errors correspond to smoothing the dynamics in the high amplitude oscillations.

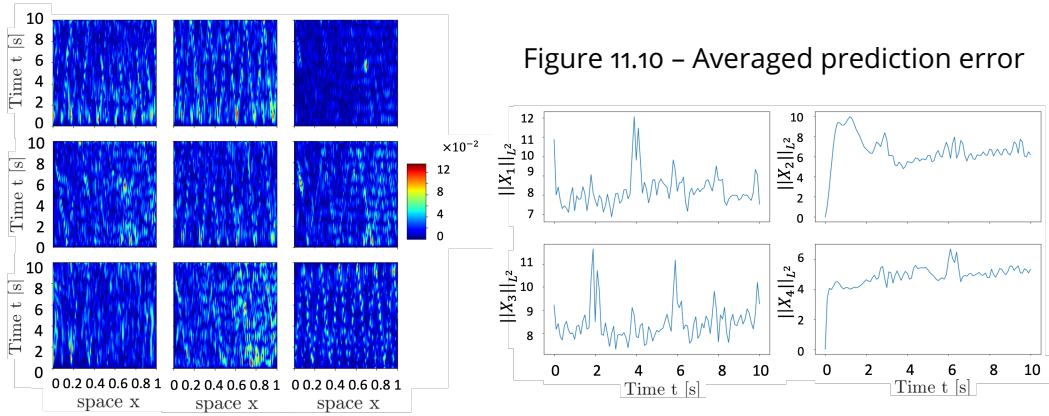


Figure 11.9 – Projected prediction error

In Figure 11.10, we represented the evolution of the L^2 -norm of the prediction error for each state component, averaged over the test set. As expected, it does not evolve significantly in time but is higher than using classic backstepping-based observers.

Recurrent FNO

However, though the convolutional architecture showed a small estimation error, it is not entirely satisfactory for application purposes. In real situations, we only have access to boundary measurements. The neural network should therefore be able to estimate the whole state given the new measure, using the past information (past measures or past state estimations) eventually. Following [SLY⁺22], we compare the previous predictions with the ones obtained using a recurrently implemented FNO unit. Unlike the convolutional architecture Figure 11.6, the recurrent FNO (recFNO) represented in Figure 11.11 is trained to learn the state evolution at the next time step, using the state values and the boundary measurement at the previous time step as inputs. We use the Adam optimizer to train the recFNO on the training set for 82 epochs with an initial learning rate of 0.001 that is halved every 20 epochs (it was reduced after consideration of the evolution of the norm).

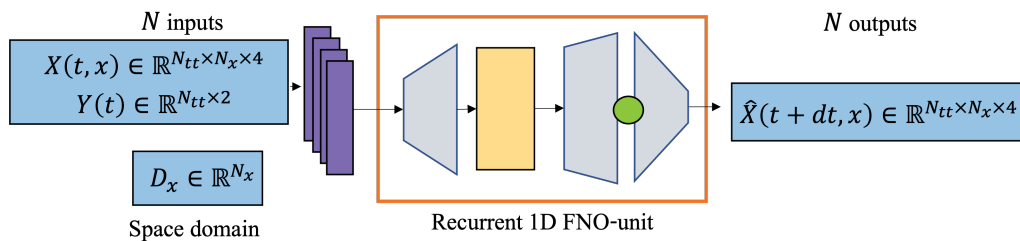


Figure 11.11 – Architecture of the recurrent FNO implementation

The training time is 138min (approx. 98sec/epochs). Using state values as inputs, we obtain very accurate state estimation at the next step. In Figure 11.7, we represent the evolution of the MSE (red) and relative norm error ε_{L^2} (blue) during training. We obtain a good approximation, with $MSE = 1.5 \times 10^{-6}$ and $\varepsilon_{L^2} = 4.8 \times 10^{-3}$.

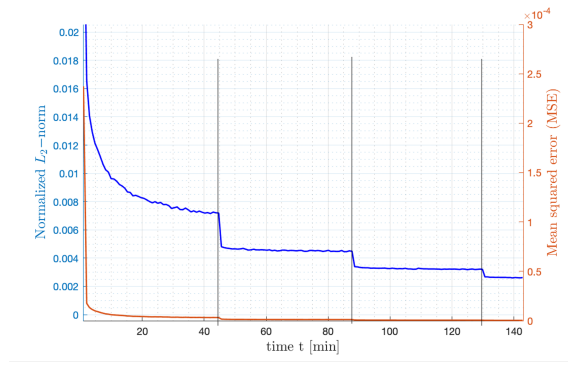


Figure 11.12 – Loss evolution during training

The hyperparameters are summarized in Table 11.4.

Step	Param.	Value	Step	Param.	Value
c) Projection width	w	64	d) # FNO-units	N_L	1
d) # modes in FFT	k_{\max}	16	d) Activation func.	●	GELU
e) Projection width	fc_1	128	e) Activation func.	●	GELU

Table 11.4 – Hyperparameters used for simulation

The training performances are gathered at Table 11.5.

Criteria	unit	convFNO	recFNO
Training time	s/epoch	8	98
MSE		0.026	1.5×10^{-6}
ε_{L^2}		6.7×10^{-3}	4.8×10^{-3}

Table 11.5 – Summary of training performances

We then test the trained neural network on $N_{\text{test}} = 200$ samples. In testing, recFNO is evaluated using the previous state estimation and the new measurement value at each time step. It is illustrated in Figure 11.13.

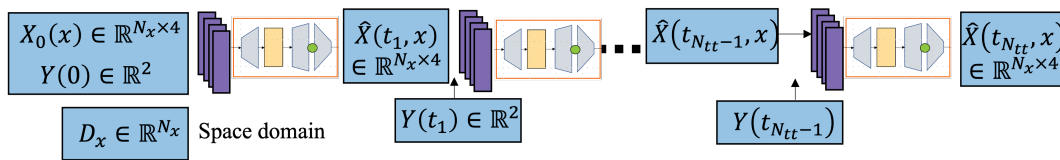


Figure 11.13 – Testing procedure for recFNO

We represent in Figure 11.8 the reference 3D evolution of $X_1(t, x)$ computed using the Godunov scheme (left) and the evolution predicted by the recFNO network recursively, for one random sample set. As for convFNO, we represent the projection of the error between the reference and predicted values for 9 random samples (Figure 11.15) and the prediction error, averaged on 50 test samples (Figure 11.16).

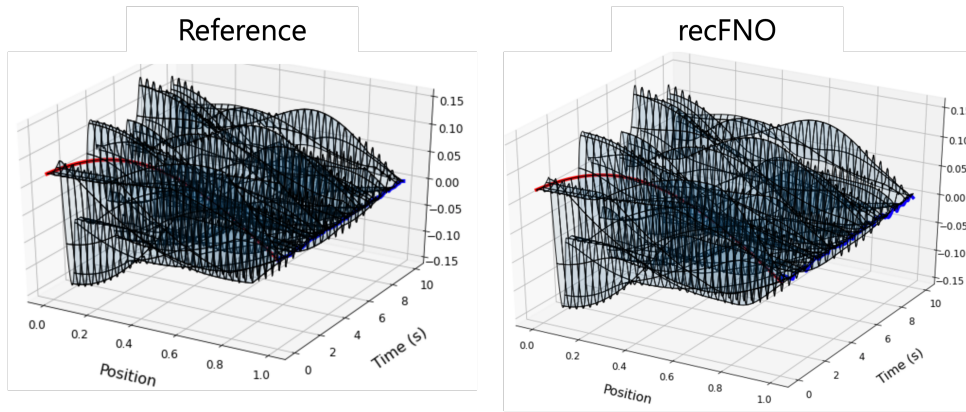


Figure 11.14 – Comparison of 3D evolution for PDE state and recurrent FNO prediction

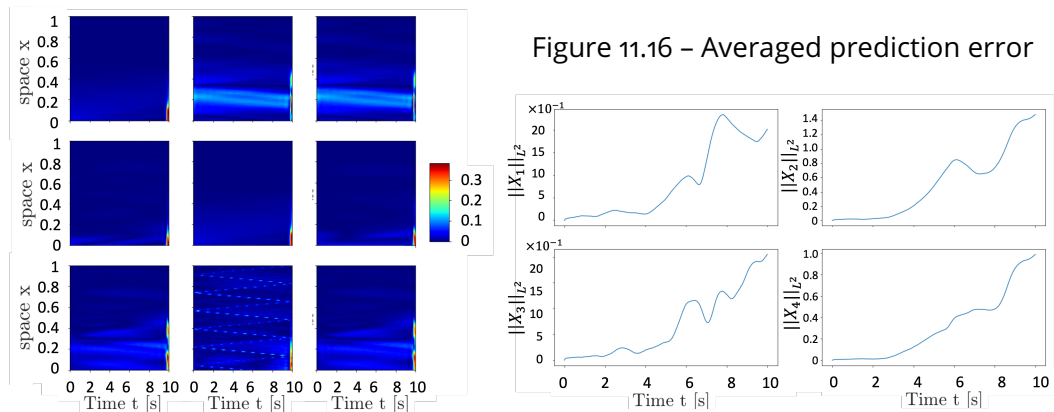


Figure 11.16 – Averaged prediction error

Figure 11.15 – Projected prediction error

We see that the error seems to explode. To illustrate discrepancies among the test samples, we also plot the MSE error for 10 different samples in Figure 11.17. As represented on the right side of the graph, the error is below 10^{-5} ($\leq 0.1\%$) for 80% of the samples over the first 2sec. Depending on the sample, the error explodes after a critical time ranging from 3 to 8sec. This emphasizes the need to develop a robust state prediction and a mixed convolutional-recurrent framework.

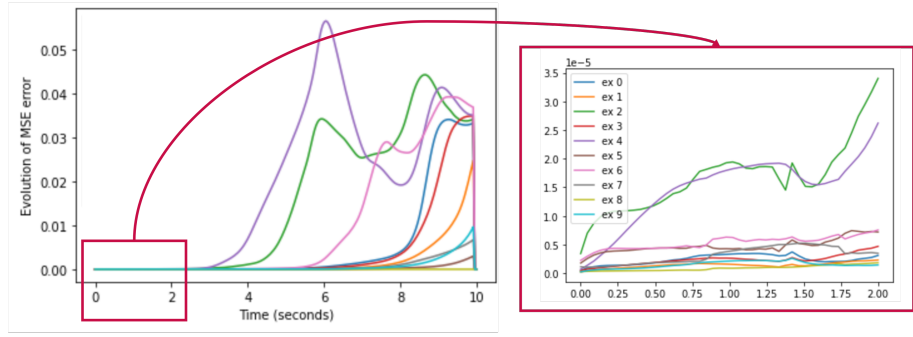


Figure 11.17 – Evolution of MSE for 10 test samples

11.1.3 . Perspectives

FNO-inspired architectures

First, the results presented in Section 11.1.2 emphasized the interest and limitations of pure convolutional and recurrent architectures. It emphasizes the need to develop a mixed convolutional-recurrent framework. Instead of using solely one new measurement and the state prediction at the last time step (as represented in Figure 11.13), the architecture we propose in Figure 11.18 takes as input a sequence of measurement $Y_T \in \mathbb{R}^{N_t \times 2}$, as well as the physical parameters $P \in \mathbb{R}^{N_p}$. Here, $N_p = 4$ since the Timoshenko beam is characterized by four physical parameters $\rho, K_s, EI, I\rho$.

Using a recurrent neural network, we obtain a summary of the time sequence of dimension \mathbb{R}^{h_0} . This input is concatenated with physical parameters. We project this input on three different branches (denseNet) to obtain the amplitude A , the frequency f , and the phase ϕ of the continuous Fourier Decomposition. We then learn the spectral decomposition of the output. We finally project to the space of adequate dimension. We can, therefore, compute the value of the state for any $x \in [0, 1]$.

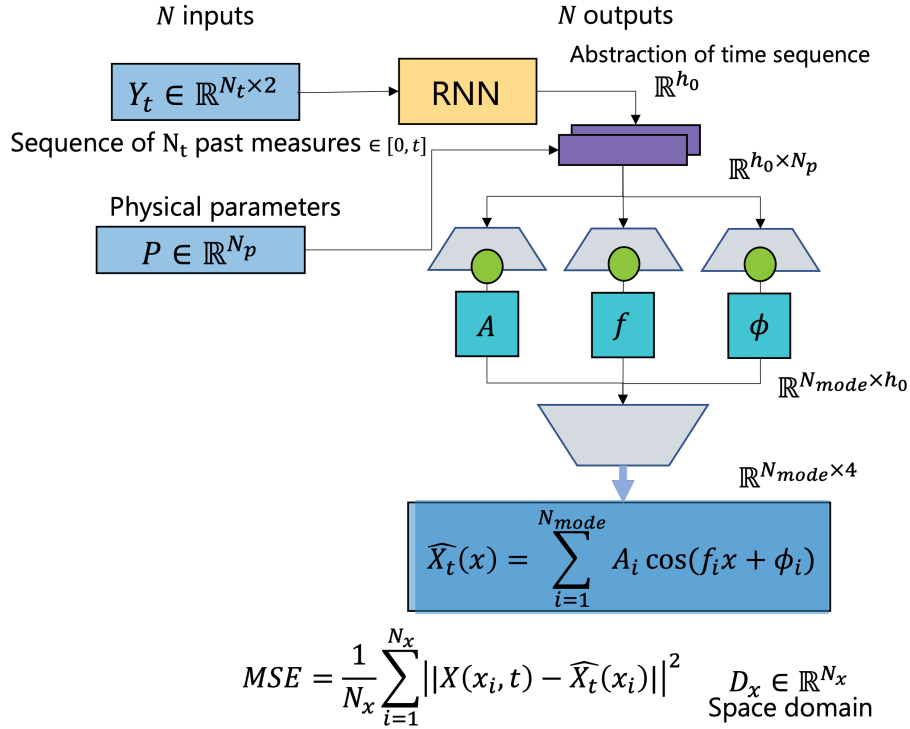


Figure 11.18 – Schematic representation of an alternative architecture

It is still subject to investigation.

Integration of soft physical constraints

Inspired by model-driven physics-informed neural networks [RPK19], we ponder on the efficiency of adding soft constraints (additional loss terms) to improve the physical consistency of the given output. To obtain the estimated state in real-time, which is a necessary step towards using backstepping-based controllers on real systems, a *model-aware* NN could be more performant [LZK+23]. Denote $\widehat{X}_{\theta, T}^+ = f_{\theta}^+(Y, X_0)$ and $\widehat{X}_{\theta, T}^- = f_{\theta}^-(Y, X_0)$

the state estimations obtained as outputs of one of the proposed neural network. We define different loss terms

- *Consistency with measurement*: the output must correspond to the measurements on the boundary. We select N_Y random subpoints $t_i \in [0, T]$ from the measurements and compute an average error

$$\mathcal{L}_{meas}(\theta) = \frac{1}{N_Y} \sum_{i=1}^{N_Y} \|Y(t_i) - Df_{\theta}^{-}(Y, X_0)(t_i, 1)\|^2.$$

- *Consistency with boundary conditions*: the output must satisfy the boundary conditions. We select N_{BC} random points $t_i \in [0, T]$ and compute an average error

$$\mathcal{L}_{BC}(\theta) = \frac{1}{N_{BC}} \sum_{i=1}^{N_{BC}} \|f_{\theta}^{-}(Y, X_0)(t_i, 0)\|^2 + \|f_{\theta}^{+}(Y, X_0)(t_i, 1)\|^2.$$

- *Consistency with the dynamics*: the output must satisfy (10.1). We select N_t time points $t_i \in [0, T]$ and N_x mesh points $x_j \in [0, 1]$ and evaluate the term

$$\begin{aligned} \mathcal{L}_{PDE}(\theta) = \frac{1}{N_t N_x} \sum_{i=1}^{N_t} \sum_{j=1}^{N_x} & \left\| \frac{\partial}{\partial t} f_{\theta}(Y, X_0)|_{(t_i, x_j)} - P_1 \mathcal{H} \frac{\partial}{\partial x} f_{\theta}(Y, X_0)|_{(t_i, x_j)} \right. \\ & \left. - P_0 \mathcal{H} f_{\theta}(Y, X_0)(t_i, x_j) \right\|^2. \end{aligned}$$

Using spectral methods simplifies the computation of the derivatives. Indeed, when the original state (at fixed time) is decomposed into a linear combination of trigonometric basis functions of varying frequencies, the spatial derivative is directly obtained by multiplying the coefficients by a complex number [JKBM20, CHQZ88]. However, this should be done inside the FNO unit. An alternative is to take advantage of the powerful *automatic differentiation* techniques [BPRS15], that enable us to obtain the gradients of the output with respect to the different variables. However, since the values of the gradients are used in the loss expression, the values must be differentiated again when using a gradient-based method for minimizing the loss with respect to the NN parameters.

Adopting new loss terms could slow down the training process, but at the same time reduce the number of necessary training samples for better generalizability. The choice of a trade-off between the different loss terms must also be subject to investigation [WWP21, SIH21].

11.2 . Parameter estimation using a neural network

As shown in the previous section, machine-learning-based solutions can be of high interest to palliate the slow resolution time of PDE systems using finite elements or finite volume methods [LeVo2]. Another problem such data-driven methods can handle is

parameter estimation from available measurements, also known as the *inverse problem*.

11.2.1 . Review on recent advances

Parameter estimation using machine learning has raised much interest in recent years. It is challenging to reconstruct accurate estimates of the PDE parameters from available measurements to produce consistent dynamics [Kut23]. Different solutions have been explored. classic architectures such as convolutional neural networks (CNN) [SMN⁺23, ASNK22b] or recurrent neural networks (RNN) [SIH21] have proved their interest. To ensure that physical constraints of the models were satisfied, new architectures were proposed, such as PINNs [RPK19, TMP⁺20], enhanced with deep spectral feature aggregation [WWLL22] and other variants as PGNN [KWRK21] or PhyCNN [ZLS20].

Recently, transformers [VSP⁺17] have gained significant attention and have become a cornerstone in handling temporal series. Their attention-based architecture allows them to capture complex patterns and dependencies. They offer several advantages. First, recurrent networks, such as LSTM presented in Section 11.1.2, are to be run sequentially. This is not the case for transformer architectures, which enable better parallelization while outperforming recurrent networks in all domains. In addition, standard automatic differentiation libraries such as Pytorch do not support higher order differentiation (computation of Jacobian) required to compute PDE-based losses for recurrent networks. This eases the implementation of physical loss terms.

11.2.2 . Test case: estimation of friction parameters while drilling

In this section, we adapt the ideas mentioned above to the context of drilling. As seen in Chapter 6, the torsional motion of a drill bit is subject to undesired oscillations due to the presence of nonlinear friction terms, characterized by a couple (μ_k, μ_s) , that correspond to kinetic and static friction coefficients respectively. Control strategies based on more accurate distributed dynamics of the drillstring have proven more efficient than classic approaches to prevent stick-slip apparition during operation [ASADM20]. However, implementing such strategies requires knowledge of physical parameters, state estimations, and predictions.

Data-driven methods have been proposed to estimate these parameters while drilling [ASNK22b]. Though they have shown to be a promissive alternative to former model-based methods, they still lack generalizability. We propose a dual architecture of transformer-based neural networks to overcome this limitation. We could obtain physics-guided estimations of the angular velocity and torque by adding physical constraints during the training phase.

Overall objective

In this second test case, we consider the **off-bottom torsional** motion of a drilling device of length L . As explained in Chapter 6, this corresponds to transient phases when the bit is not in contact with the rock, for instance, when a new pipe section is added to the drilling system or when the drill string is removed from the borehole to fix a failure. We use the distributed model from [AS18] and given in Section 6.2. As a reminder, the torsional dynamics of torque and angular velocity were given by

$$\frac{\partial \tau(t, x)}{\partial t} + JG \frac{\partial \omega(t, x)}{\partial x} = 0, \quad J\rho \frac{\partial \omega(t, x)}{\partial t} + \frac{\partial \tau(t, x)}{\partial x} = S(t, x),$$

with source term $S(t, x)$ a nonlinear term depending on the angular velocity and friction coefficients.

On the field, the available measurements mainly consist of surface data, for instance, surface rotation per minute (RPM) or motor torque. As seen in Section 6.2.3, estimation strategies using predictors based on the aforementioned distributed model require a high computational effort, such that the estimated state cannot be obtained in real time. Thus, it prevents this approach from being used on the field. Moreover, they require all parameters of the system (and, in particular, subsurface physical properties) to be known, which is not the case in practice. Our objective reads as follows

Objective 11.2.1: Parameter estimation

From sequences Y_t of surface measurements, estimate the physical parameters (μ_s, μ_k) of the model using a neural network of parameters θ , defined by $g_\theta : Y_t \mapsto \hat{M}_\theta \in \mathbb{R}^p$. More precisely, we want

$$|M - \hat{M}_\theta| \longrightarrow 0.$$

Transformer-based architecture

The first neural network aims at estimating the physical parameters $M = (\mu_k, \mu_s) \in \mathbb{R}^2$. It is a Transformer [VSP⁺17] characterized by parameters θ , and denoted $T_\theta(\cdot)$. It aggregates the sequence of inputs $Y_i \in \mathbb{R}^{N_p+2N_t}$, and outputs an estimation $\hat{M} \in \mathbb{R}^2$ of the physical parameters. We obtain the adequate parameters θ by minimizing the following L_2 -loss function $\mathcal{L}_{L_2}(\theta)$

$$\mathcal{L}_{L_2}(\theta) = \frac{1}{N_b} \sum_{i=1}^{N_b} \|M_i - T_\theta(Y_i)\|_2^2.$$

The chosen architecture is schematically represented in Figure 11.19.

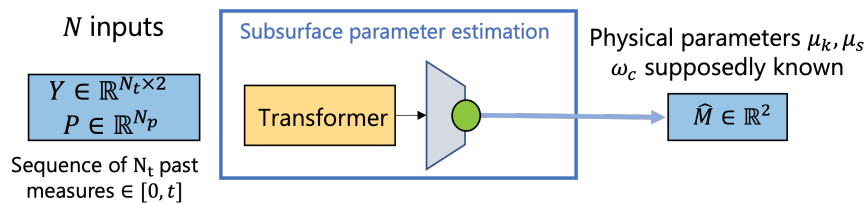


Figure 11.19 – Schematic representation of transformer-based parameter estimation

Generation of a dataset

To train and validate our estimation algorithm, we generated a wide dataset following the numerical scheme¹ presented in [AS18]. To obtain representative data, we use a real well geometry J1. It is illustrated in Figure 11.20. The red and blue dots correspond to depths where we can access real data. We also represent the friction parameters profile. We generate 1000 sequences of 100s of 20Hz surface measurements (motor torque and surface angular velocity), for $L \in [2500, 4000]$ m, $\mu_s \in [0.2, 0.8]$, $\mu_k \in [0.06, 0.72]$.

1. The Matlab implementation can be found on <https://github.com/Open-Source-Drilling-Community/Aarsnes-and-Shor-Torsional-Model>.

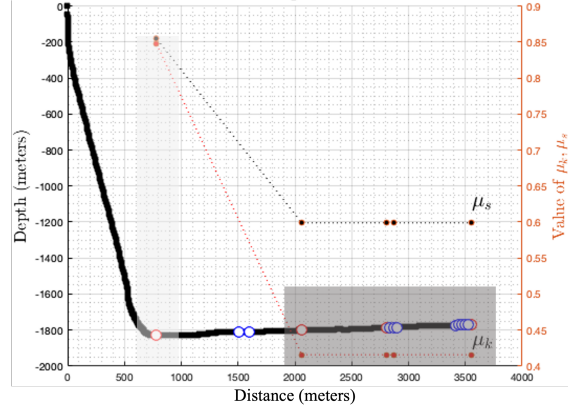


Figure 11.20 – Well J1 schematic profile

We point out that this dataset contains only samples for a single value of angular velocity threshold $\omega_c = 1.5\text{rad.s}^{-1}$ and null initial conditions. In a further approach, this parameter should also be estimated by the NN, and initial conditions should vary. The approach proposed in Section 11.1.2 could be used. As mentioned, generating exhaustive datasets requires an important computation time and storage capacity. This is, so far, a limitation of the approach. The reference trajectory is constant (60RPM with slope). The implemented control input is a PI control with fixed gains.

Network design and Training process

Training process. The dataset is split 80% – 20% to separate training and validation datasets. To obtain the parameters (θ, Θ) minimizing the losses $\mathcal{L}_{L_2}(\theta), \mathcal{L}(\Theta)$, we use AdamW [LH17] with an initial learning rate of 10^{-3} . The training is done on 100 epochs, with a batch size $N_b = 16$.

Hyperparameters tuning. We designed several models using a broad range of hyperparameters. We trained each model and observed the evolution of the average error on the same validation dataset. We selected the best configuration among the 48 configurations tested in Table 11.21.

Hyperparameters	Values
hidden dimension	32, 64, 256, 1024
train-validation ratio	0.2, 0.4, 0.6, 0.8
learning rate	10^{-3}
L_2 regularization	$10^{-1}, 10^{-2}, 10^{-3}$

Figure 11.21 – Range of hyperparameters

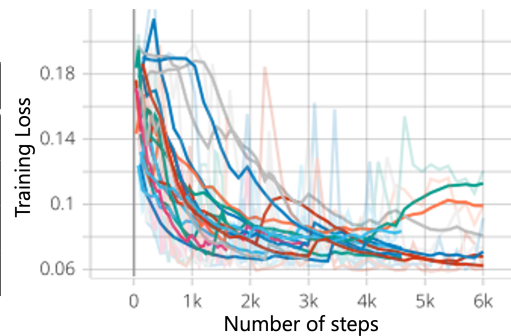


Figure 11.22 – Loss evolution (μ_s)

The performance of the trained neural networks is evaluated on simulated and field data. The friction coefficients were estimated on the validation dataset ($N_{\text{test}} = 200$) with an average relative error of $\delta(\mu_k) = 2.3\%$ (resp. $\delta(\mu_s) = 3.3\%$) and a standard deviation of $5.2e^{-3}$ (resp. $1.8e^{-2}$) after 2500 steps. Our proposed method outperformed the existing estimation methods based on convolutional neural networks [ASNK22a]. As illustrated in

Figure 11.23, the standard deviation is reduced and the average estimated value is closer to the real one for both μ_k (red) and μ_s (blue).

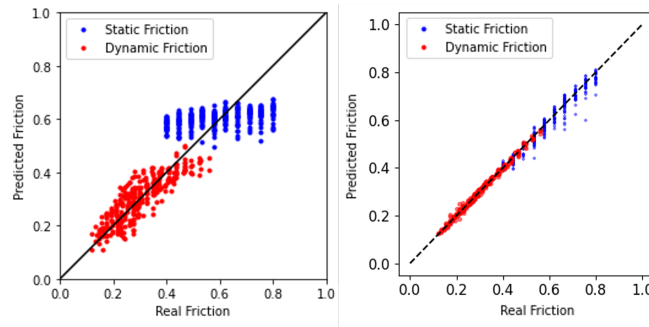


Figure 11.23 – Regression performance: CvNN [ASNK22a] (left), Transformer (right)

11.2.3 . Perspectives: combined approach

Once the parameter estimation has been obtained, it can be used as the input of the network proposed in Section 11.1.3. We obtain the two-branches architecture schematically represented in Figure 11.24.

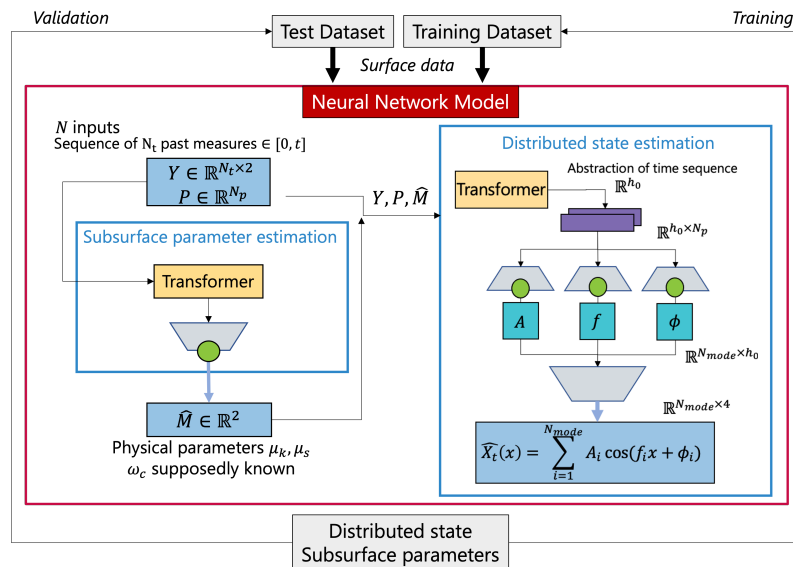


Figure 11.24 – schematic representation of the two branches architecture

Estimation of the distributed state

Inspired by [LJK21], we propose to estimate the distributed state $(\omega(t, x), \tau(t, x))$ at time t using sequences of past measurements, using a two branches architecture. Our goal is to select the most appropriate state representation under physical constraints using sets of discrete inputs Y_i . The first branch relies on a transformer encoder to aggregate the input sequences Y_i augmented with \hat{M} . It produces an abstract representation of the system, which is combined with an abstract representation of the requested coordinates. Inspired by FNO [LKA⁺21], the obtained summary is used to output the intensity,

frequency, and phase of the Fourier decomposition representing the distributed state $X(t, x) \doteq (\omega(t, x), \tau(t, x))$ along the drillstring. The second branch builds the spatiotemporal grid mesh $(t, x) \in [0, T] \times [0, L]$, where the estimation is evaluated.

One example of distributed state estimation using the proposed strategy is given in Figure 11.25. On the right map, showing the error between expected and predicted value, we note that the discontinuity between the pipe and the collar dynamics is not well considered. One proposition to palliate this difficulty could be to add physical loss terms.

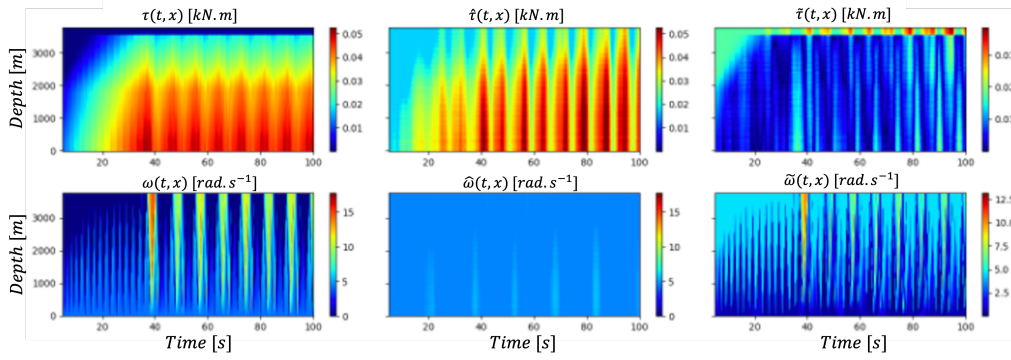


Figure 11.25 – Preliminary results

Physic-informed neural networks

Following [RPK19, SIH21, WWP21], we define a composite loss that takes into account experimental data (\mathcal{L}_O) as well as a physical error. While the former is the usual error term when training a neural network on a dataset, the latter ensures that the solution verifies theoretical PDEs (\mathcal{L}_{PDE}) and boundary conditions (\mathcal{L}_{BC}):

$$\mathcal{L}(\Theta) = \mathcal{L}_O(\Theta) + \mathcal{L}_{\text{PDE}}(\Theta) + \mathcal{L}_{\text{BC}}(\Theta). \quad (11.1)$$

It should be seen as data and physics-driven losses. This adds *a priori* knowledge of the underlying dynamics (6.12)-(6.14) during training. As before, the first loss term corresponds to the state estimation residual in the squared L_2 -norm

$$\mathcal{L}_O(\Theta) = \frac{1}{N_x} \frac{1}{N_t} \frac{1}{N_b} \sum_{i=1}^{N_b} \sum_{j=1}^{N_x} \sum_{k=1}^{N_t} \|X^i(t_k, x_j) - S_{Y_i, \Theta}(t_k, x_j)\|_2^2.$$

The squared L^2 -norm tends to efficiently penalize bigger discrepancies between the output and real value. Other loss terms (regularization) can be added.

The following term ensures that (6.12) are satisfied

$$\mathcal{L}_{\text{PDE}}(\Theta) = \frac{1}{N_x} \frac{1}{N_t} \frac{1}{N_b} \sum_{i=1}^{N_b} \sum_{j=1}^{N_x} \sum_{k=1}^{N_t} \|\mathcal{O}(f_{Y_i, \Theta}(t_k, x_j))\|_2^2.$$

$$\text{with } \mathcal{O}(S_{Y_i, \Theta}(t, x)) = \left(\begin{array}{c} \frac{\partial \hat{\tau}^i}{\partial t}(t, x) + JG \frac{\partial \hat{\omega}^i}{\partial x}(t, x) \\ \frac{\partial \hat{\tau}^i}{\partial x}(t, x) + J\rho \frac{\partial \hat{\omega}^i}{\partial t}(t, x) + \mathcal{F}(\hat{\omega}^i, x) \end{array} \right).$$

We want the solution to meet the boundary condition (6.14)

$$\mathcal{L}_{\text{BC}}(\Theta) = \frac{1}{N_t} \frac{1}{N_b} \sum_{i=1}^{N_b} \sum_{k=1}^{N_t} \|\mathcal{B}(S_{Y_i, \Theta}(t_k))\|_2^2 + |\hat{\tau}^i(t_k, L)|^2,$$

with $\mathcal{B}(S_{Y_i, \Theta}(t)) = \frac{\partial \hat{\tau}^i}{\partial t}(t, 0) - \frac{1}{I_{TD}}(\tau_m^i(t) - \hat{\tau}^i(t, 0))$. We believe that integrating physical loss terms into the training process will improve the overall estimation. This is still subject to investigation.

Conclusion

This chapter presented several interests in machine-learning-based techniques for distributed state and parameter estimation. We obtained promising results for estimating unknown physical parameters and distributed states based on the available measurements. We illustrated the proposed solutions for two test cases studied in this thesis: a clamped Timoshenko beam and a bi-sectional drilling system. All architectures can be easily adapted to other PDE systems by redefining the training set and input dimensions. In both cases, we proposed to add physical loss terms to generate a physic-informed neural estimator. This raised new computational difficulties.

Many questions remain open. First, we only used simulated datasets so far. This naturally leads to a bias in the learning process since the training data are generated using the physical model. If real data were available, it would be possible to construct a hybrid physics-data model. For instance, using the experimental setup presented in [WLG18], or field data from drilling companies or online resources².

This would allow us to confront the obtained physical parameters or predicted boundary values to measurements. This perspective is schematically represented in Figure 11.26. Moreover, the current architectures contain many hyper-parameters that can be optimized to enhance the performance of the estimations. In particular, the trade-off between the empirical loss of model predictions, the complexity of the model, and the physical loss are of high interest [SIH21]. This could help improve generalization performance since the real training data are small and not fully representative.

In future work, the state estimations might be used to compute backstepping-based control laws. So far, the neural networks have only been used to learn dynamics from open-loop systems or given inputs. To efficiently mitigate undesired stick-slip oscillations or more generally, stabilize the system, the impact of a control law must be considered. The robustness of the control law with regard to state estimation error is also of primary interest. The transformer-based architecture proposed in Section 11.2 could also be combined with *Fourier neural operators* [LKA⁺21] presented in Section 11.1 to approximate the model and predict future values of the distributed state.

2. Some drilling data are made available freely. See <https://www.equinor.com/energy/volve-data-sharing> or <https://data.world/us-doe.gov/>. In this work, I worked on real data from ©Eavor, in partnership with the University of Calgary. For confidentiality reasons, the outcomes of this research are not presented herein.

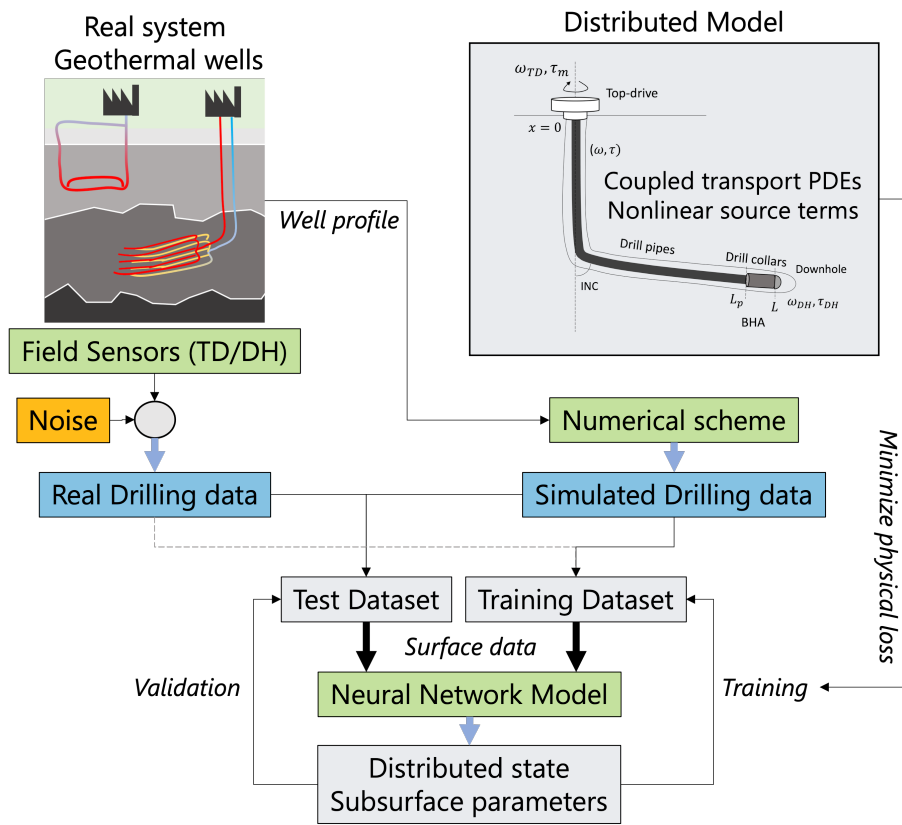


Figure 11.26 - Perspectives

Conclusions

This thesis focused on controlling underactuated networks of hyperbolic partial differential equations (PDE) systems interconnected with linear ordinary differential equations (ODE) systems in a chain structure. Such networks have practical applications in various fields, making their study essential and relevant.

In Part I, we introduced two classes of infinite-dimensional systems: linear scalar hyperbolic PDE systems and time-delay systems (TDS) of the neutral type. Since they are closely related, this thesis aims at taking advantage of control approaches developed for both. We presented in Chapter 2 how the backstepping methodology can be used to establish a mapping between them. In Chapter 3, we then discussed the limitations of the classic Proportional or PI boundary feedback in the context of a simple chain structure made of conservation laws coupled with actuator or load ODE dynamics. It legitimated the interest in infinite-dimensional controllers.

In Part II, we investigated the case where the available actuation is located at one network end. In Chapter 4, we examined an ODE-PDE-ODE interconnection and presented an output feedback design based on backstepping and frequency analysis to achieve trajectory tracking and disturbance rejection. In Chapter 5, we considered a chain of arbitrarily many hyperbolic PDE systems interconnected at the unactuated end with an ODE. To stabilize this structure, we proposed a recursive dynamics interconnection framework. We also discussed in Chapter 6 the application of these control strategies to drilling systems.

In Part III, the focus shifted to controlling hyperbolic PDE systems with actuation at a junction in a chain structure. The difficulties in controlling systems with actuation at the in-between boundary were emphasized in Chapter 7 on the case of two interconnected hyperbolic PDE systems. A new control approach was proposed, based on a Fredholm integral transform, whose invertibility is guaranteed using an operator framework. This approach was applied in Chapter 8 to the in-domain control of a clamped string. Both parts II and III ended with perspectives on more complex chain structures. This thesis paves the way to more general considerations of networks of hyperbolic PDE systems.

Finally, Part IV addressed some under-considered aspects of backstepping-based controllers. It discussed the complexity of implementing infinite-dimensional controllers on real systems. First, the question of a reachable target system for a general class of non-scalar hyperbolic PDE systems was raised in Chapter 9. By introducing an innovative time-affine transform, choosing reachable target systems was simplified, enabling the easier implementation of backstepping-based controllers. The Port Hamiltonian framework also proved its interest in Chapter 10 to design target systems with specified stability properties. Furthermore, the numerical limitations associated with backstepping-based controllers for real-time control were challenged in Chapter 11. To address this challenge, the potential of machine learning-based solutions was explored. We proposed different architectures for fast and adaptive state estimation for the drilling systems and Timoshenko beams already presented in this thesis. This opened up exciting possibilities for significantly reducing computation time and enhancing the efficiency of the backstepping-based controllers.

Overall, this thesis provided a comprehensive analysis of backstepping-based con-

trollers for interconnected hyperbolic PDE systems, shedding light on their benefits and limitations. Different strategies were proposed, combining frequency analysis developed for time-delay systems and backstepping design. Several chain structures combining linear ODEs and hyperbolic PDE systems were considered. The innovative approaches presented in this work offer valuable insights into stability analysis, observer and target system designs, and the integration of machine learning techniques. Our results pave the way for further advancements and applications of backstepping-based control strategies in various fields, including the drilling industry.

Conclusions

Cette thèse s'est concentrée sur le contrôle de réseaux sous-actionnés composés de systèmes d'équations aux dérivées partielles (EDP) hyperboliques interconnectés avec des systèmes d'équations différentielles ordinaires (EDO) linéaires dans une structure en chaîne. De tels réseaux trouvent des applications pratiques dans divers domaines: leur étude est ainsi pertinente.

Dans la Partie I, nous avons introduit deux classes de systèmes de dimension infinie : les systèmes d'EDP hyperboliques linéaires scalaires et les systèmes à retard (TDS) de type neutre. Cette thèse vise à tirer parti des approches de contrôle développées pour ces deux classes de systèmes étroitement liées. Nous avons présenté dans le Chapitre 2 comment la méthodologie de backstepping peut être utilisée pour établir une telle correspondance. Dans le Chapitre 3, nous avons ensuite discuté des limitations des contrôleurs de type Proportionnel ou Proportionnel-Intégral dans le contexte d'une structure en chaîne simple constituée de lois de conservation couplées à des dynamiques d'actionneurs ou de charges.

Dans la Partie II, nous avons étudié le cas où l'actionnement disponible se trouve à une extrémité du réseau. Dans le Chapitre 4, nous avons examiné une interconnexion ODE-PDE-ODE et présenté une conception de rétroaction de sortie basée sur le backstepping et l'analyse fréquentielle pour atteindre le suivi de trajectoire et le rejet des perturbations. Dans le Chapitre 5, nous avons considéré une chaîne constituée d'un nombre arbitraire de systèmes d'EDP hyperboliques interconnectés à l'extrémité non actionnée avec une EDO. Pour stabiliser cette structure, nous avons proposé une approche récursive basée sur les dynamiques d'interconnexion. Nous avons également discuté dans le Chapitre 6 l'application de ces stratégies de contrôle et d'estimation aux systèmes de forage.

Dans la Partie III, l'accent a été mis sur le contrôle de systèmes d'EDP hyperboliques avec actionnement au niveau d'une jonction entre deux sous-systèmes. Les difficultés de contrôle des systèmes avec actionnement à la frontière intermédiaire ont été soulignées dans le Chapitre 7 sur le cas de deux systèmes d'EDP hyperboliques interconnectés. Une nouvelle approche de contrôle a été proposée, basée sur une transformation intégrale de type Fredholm, dont l'inversibilité est garantie en utilisant un formalisme opérateur. Cette approche a été appliquée dans le Chapitre 8 au contrôle dans le domaine d'une corde fixée à une extrémité. Les parties II et III se sont terminées par des perspectives sur des structures en chaîne plus complexes. Cette thèse ouvre la voie à des considérations plus générales sur les réseaux de systèmes d'EDP hyperboliques.

Enfin, la Partie IV aborde certains aspects négligés des contrôleurs basés sur le backstepping. Elle aborde la complexité de la mise en œuvre de contrôleurs de dimension infinie sur des systèmes réels. Tout d'abord, la question d'un système cible atteignable pour une classe générale de systèmes d'EDP hyperboliques non scalaires a été soulevée dans le Chapitre 9. En introduisant une transformation affine temporelle novatrice, le processus de sélection des systèmes cibles atteignables a été simplifié, permettant une mise en œuvre plus simple des contrôleurs par backstepping. Le cadre des systèmes Hamiltoniens à Port a également démontré son intérêt dans le Chapitre 10 pour concevoir des systèmes cibles avec des propriétés de stabilité spécifiées. Il a été utilisé pour améliorer davantage les performances des contrôleurs dans deux cas d'étude. De plus, les limitations numériques des contrôleurs par backstepping pour du contrôle en temps réel ont été soulevées dans le Chapitre 11. Pour relever ce défi, le potentiel des solutions basées sur l'apprentissage automatique a été exploré. Nous avons proposé différentes architectures pour l'estimation rapide et adaptative de l'état des systèmes de forage et des poutres de Timoshenko déjà présentés dans cette thèse. Cela ouvre des possibilités passionnantes pour réduire considérablement le temps de calcul et améliorer l'efficacité des contrôleurs par backstepping.

Dans l'ensemble, cette thèse a fourni une analyse de contrôleurs par backstepping pour des systèmes d'EDP hyperboliques interconnectés, en mettant en évidence leurs avantages et leurs limites. Différentes stratégies ont été proposées, combinant l'analyse fréquentielle développée pour les systèmes à retard et la méthode de backstepping. Plusieurs structures en chaîne combinant des EDO linéaires et des systèmes d'EDP hyperboliques ont été envisagées. Les approches novatrices présentées dans ce travail offrent des perspectives précieuses sur l'analyse de stabilité, la conception d'observateurs et de systèmes cibles, ainsi que l'intégration des techniques d'apprentissage automatique. Nos résultats ouvrent la voie à de nouvelles avancées et applications des stratégies de contrôle par backstepping dans différents domaines, notamment l'industrie du forage.

Bibliography

- [AA16] U. J. F. Aarsnes and O. M. Aamo. Linear stability analysis of self-excited vibrations in drilling using an infinite dimensional model. *Journal of Sound and Vibration*, 360:239–259, 2016.
- [AA17] H. Anfinsen and O.M. Aamo. Model reference adaptive control of $n+1$ coupled linear hyperbolic PDEs. *Systems & Control Letters*, 109:1–11, 2017.
- [AA19] H. Anfinsen and O. M. Aamo. *Adaptive Control of Hyperbolic PDEs*. Communications and Control Engineering. Springer, Cham, 2019.
- [AADMS21] J. Auriol, U. J. F. Aarsnes, F. Di Meglio, and R. Shor. Robust control design of underactuated 2×2 PDE-ODE-PDE systems. *IEEE control systems letters*, 5(2):469–474, 2021.
- [Aam13] O.M Aamo. Disturbance rejection in 2×2 linear hyperbolic systems. *IEEE Transactions on Automatic Control*, 58(5):1095–1106, May 2013.
- [AAMDM18] J. Auriol, U. J. F. Aarsnes, P. Martin, and F. Di Meglio. Delay-robust control design for heterodirectional linear coupled hyperbolic PDEs. *IEEE Transactions on Automatic Control*, 63(10):3551–3557, 2018.
- [ABA19] J. Auriol and F. Bribiesca-Argomedo. Delay-robust stabilization of an $n+m$ PDE-ODE system. In *IEEE 58th Conference on Decision and Control (CDC)*, page 4964–4970, 2019.
- [ABA23] J. Auriol and F. Bribiesca Argomedo. Observer design for $n + m$ linear hyperbolic ODE-PDE-ODE systems. *IEEE control systems letters*, 7:283–288, 2023.
- [ABABP20] J. Auriol, F. Bribiesca-Argomedo, and D. Bresch-Pietri. Backstepping stabilization of an underactuated $1+2$ linear hyperbolic system with a proper control. In *IEEE 59th Conference on Decision and Control (CDC)*. IEEE, 2020.
- [ABABS⁺18] J. Auriol, F. Bribiesca Argomedo, D. Bou Saba, M. Di Loreto, and F. Di Meglio. Delay-robust stabilization of a hyperbolic PDE–ODE system. *Automatica*, 95:494–502, 2018.
- [ABADM23] J. Auriol, F. Bribiesca Argomedo, and F. Di Meglio. Robustification of stabilizing controllers for ODE-PDE-ODE systems: A filtering approach. *Automatica*, 147:110724, 2023.
- [ABP22] J. Auriol and D. Bresch Pietri. Robust state-feedback stabilization of an underactuated network of interconnected $n+m$ hyperbolic PDE systems. *Automatica*, 136:110040, 2022.
- [ABP23] J. Auriol and D. Bresch-Pietri. On input-to-state stability of linear difference equations and its characterization with a Lyapunov functional. In *IFAC World Congress 2023*, 2023.
- [ABS⁺22] J. Auriol, I. Boussaada, R. J. Shor, H. Mounier, and S.-I. Niculescu. Comparing advanced control strategies to eliminate stick-slip oscillations in drillstrings. *IEEE access*, 10:10949–10969, 2022.

- [ACMdC98] A. Araujo, A. Carvalho, and J. L. Martins de Carvalho. A modular approach for modeling and simulation of semiconductor power devices. In *24th Annual Conference of the IEEE Industrial Electronics Society*, volume 1, pages 331–335 vol.1, 1998.
- [ADAK16a] H. Anfinsen, M. Diagne, O. M. Aamo, and M. Krstic. An adaptive observer design for $n+1$ coupled linear hyperbolic PDEs based on swapping. *IEEE Transactions on Automatic Control*, 61(12):3979–3990, 2016.
- [ADAK16b] H. Anfinsen, M. Diagne, O. M. Aamo, and M. Krstic. Boundary parameter and state estimation in general linear hyperbolic PDEs. *IFAC-PapersOnLine*, 49(8):104–110, 2016.
- [ADM16] J. Auriol and F. Di Meglio. Minimum time control of heterodirectional linear coupled hyperbolic PDEs. *Automatica*, 71:300–307, 2016.
- [ADM19] J. Auriol and F. Di Meglio. An explicit mapping from linear first order hyperbolic PDEs to difference systems. *Systems & Control Letters*, 123:144–150, 2019.
- [ADM20] J. Auriol and F. Di Meglio. Robust output feedback stabilization for two heterodirectional linear coupled hyperbolic PDEs. *Automatica*, 115:108896, 2020.
- [ADMBA19] J. Auriol, F. Di Meglio, and F. Bribiesca-Argomedo. Delay robust state feedback stabilization of an underactuated network of two interconnected PDE systems. In *2019 American Control Conference (ACC)*, pages 593–599. IEEE, 2019.
- [ADMEA14] U. J. F. Aarsnes, F. Di Meglio, S. Evje, and O. M. Aamo. Control-oriented drift-flux modeling of single and two-phase flow for drilling. In *IEEE/ACM International Conference on Human-Robot Interaction*, 2014.
- [AdMS18a] U. J. F. Aarsnes, F. di Meglio, and R. Shor. Benchmarking of industrial stick-slip mitigation controllers. *IFAC-PapersOnLine*, 51(8):233–238, 2018.
- [ADMS18b] U. J. F. Aarsnes, F. Di Meglio, and R. J. Shor. Avoiding stick-slip vibrations in drilling through startup trajectory design. *Journal of Process Control*, 70:24–35, 2018.
- [AKIS20] J. Auriol, N. Kazemi, K. Innanen, and R. Shor. Combining formation seismic velocities while drilling and a PDE-ODE observer to improve the drill-string dynamics estimation. In *2020 American Control Conference (ACC)*, pages 3120–3125. IEEE, 2020.
- [AKN21] J. Auriol, N. Kazemi, and S.-I. Niculescu. Sensing and computational frameworks for improving drill-string dynamics estimation. *Mechanical systems and signal processing*, 160:107836, 2021.
- [AM23] P. Appeltans and W. Michiels. Analysis and controller-design of time-delay systems using TDS-CONTROL. A tutorial and manual. *arXiv:2305.00341*, 2023.
- [AS65] M. Abramowitz and I. A. Stegun. *Handbook of mathematical functions with formulas, graphs, and mathematical tables*. U.S. Govt. Print. Off., 1965.
- [AS18] U. J. F. Aarsnes and R. J. Shor. Torsional vibrations with bit off bottom: Modeling, characterization and field data validation. *Journal of Petroleum Science and Engineering*, 163:712–721, 2018.

- [ASADM20] J. Auriol, R. J. Shor, J. U. F. Aarsnes, and F. Di Meglio. Closed-loop tool face control with the bit off-bottom. *Journal of Process Control*, 90:35–45, 2020.
- [ASNK22a] J. Auriol, R. Shor, S.-I. Niculescu, and N. Kazemi. Estimating drill string friction: Comparing model-based and data-driven methods. In *American Control Conference (ACC)*, pages 3464–3469. IEEE, 2022.
- [ASNK22b] J. Auriol, R. Shor, S.-I. Niculescu, and N. Kazemi. Estimating drill string friction with model-based and data-driven methods. In *2022 American Control Conference (ACC)*, pages 3464–3469, 2022.
- [AToo] K. Ammari and M. Tucsnak. Stabilization of Bernoulli–Euler beams by means of a pointwise feedback force. *SIAM journal on control and optimization*, 39(4):1160–1181, 2000.
- [ATo1] S. Avdonin and M. Tucsnak. Simultaneous controllability in sharp time for two elastic strings. *ESAIM. Control, optimisation and calculus of variations*, 6(6):259–273, 2001.
- [Aur18] J. Auriol. *Robust design of backstepping controllers for systems of linear hyperbolic PDEs*. PhD thesis, PSL Research University, 2018.
- [Aur20] J. Auriol. Output feedback stabilization of an underactuated cascade network of interconnected linear PDE systems using a backstepping approach. *Automatica*, 117:108964, 2020.
- [AVDMK19] U.J.F. Aarsnes, R. Vazquez, F. Di Meglio, and M. Krstic. Delay robust control design of under-actuated PDE-ODE-PDE systems. In *2019 American and Control Conference (ACC)*, pages 3200–3205. IEEE, 2019.
- [AvdW18] U. J. F. Aarsnes and N. van de Wouw. Dynamics of a distributed drill string system: Characteristic parameters and stability maps. *Journal of sound and vibration*, 417:376–412, 2018.
- [AvdW19] U. J. F. Aarsnes and N. van de Wouw. Axial and torsional self-excited vibrations of a distributed drill-string. *Journal of Sound and Vibration*, 444:127–151, 2019.
- [BAK15] F. Bribiesca-Argomedo and M. Krstic. Backstepping-forwarding control and observation for hyperbolic PDEs with Fredholm integrals. *IEEE Transactions on Automatic Control*, 60(8):2145–2160, 2015.
- [BC11] G. Bastin and J.-M. Coron. On boundary feedback stabilization of non-uniform linear 2×2 hyperbolic systems over a bounded interval. *Systems & Control Letters*, 60(11):900–906, 2011.
- [BC16] G. Bastin and J.-M. Coron. *Stability and boundary stabilization of 1-D hyperbolic systems*. Springer, 2016.
- [BCT15] G. Bastin, J.-M. Coron, and S.O. Tamasoiu. Stability of linear density-flow hyperbolic systems under PI boundary control. *Automatica*, 53:37–42, 2015.
- [BHKS20] K. Bhattacharya, B. Hosseini, N. B. Kovachki, and A. M. Stuart. Model reduction and neural networks for parametric PDEs. *arXiv:2005.03180*, 2020.
- [BKo2a] A. Balogh and M. Krstic. Infinite dimensional backstepping-style feedback transformations for a heat equation with an arbitrary level of instability. *European journal of control*, 8(2):165–175, 2002.

- [BK02b] D.M Boskovic and M Krstic. Backstepping control of chemical tubular reactors. *Computers & Chemical Engineering*, 26(7):1077–1085, 2002.
- [BL14] N. Bekiaris-Liberis. Simultaneous compensation of input and state delays for nonlinear systems. *Systems & Control Letters*, 73:96–102, 2014.
- [BLD21] N. Bekiaris-Liberis and A. I. Delis. PDE-based feedback control of freeway traffic flow via time-gap manipulation of ACC-equipped vehicles. *IEEE transactions on control systems technology*, 29(1):461–469, 2021.
- [BLO05] J.V. Burke, A.S. Lewis, and M.L. Overton. A robust gradient sampling algorithm for nonsmooth, nonconvex optimization. *SIAM journal on optimization*, 15(3):751–779, 2005.
- [BPDM16] D. Bresch-Pietri and F. Di Meglio. Prediction-based control of linear input-delay system subject to state-dependent state delay-application to suppression of mechanical vibrations in drilling. *IFAC-PapersOnLine*, 49(8):111–117, 2016.
- [BPK14] D. Bresch-Pietri and M. Krstic. Adaptive output feedback for oil drilling stick-slip instability modeled by wave PDE with anti-damped dynamic boundary. In *2014 American Control Conference (ACC)*, pages 386–391. IEEE, 2014.
- [BPRS15] A. G. Baydin, B. A. Pearlmutter, A. A. Radul, and J. M. Siskind. Automatic differentiation in machine learning: a survey. *arXiv:1502.05767*, 2015.
- [Bra68] R. K. Brayton. Small-signal stability criterion for electrical networks containing lossless transmission lines. *IBM J. Research Develop.*, 12(6):431–440, 1968.
- [Bre10] H. Brezis. *Functional analysis, Sobolev spaces and partial differential equations*. Springer Science & Business Media, 2010.
- [BSBAA⁺19] D. Bou Saba, F. Bribiesca-Argomedo, J. Auriol, M. Di Loreto, and F. Di Meglio. Stability analysis for a class of linear 2×2 hyperbolic PDEs using a backstepping transform. *IEEE Transactions on Automatic Control*, 65(7):2941–2956, 2019.
- [BSBADLE17] D. Bou Saba, F. Bribiesca Argomedo, M. Di Loreto, and D. Eberard. Backstepping stabilization of 2×2 linear hyperbolic PDEs coupled with potentially unstable actuator and load dynamics. In *IEEE 56th Annual Conference on Decision and Control (CDC)*, pages 2498–2503, 2017.
- [BSBADLE19] D. Bou Saba, F. Bribiesca-Argomedo, M. Di Loreto, and D. Eberard. Strictly proper control design for the stabilization of 2×2 linear hyperbolic ODE-PDE-ODE systems. In *IEEE 58th Conference on Decision and Control (CDC)*, pages 4996–5001, 2019.
- [BSK23] L. Bhan, Y. Shi, and M. Krstic. Neural operators for bypassing gain and control computations in PDE backstepping, 2023.
- [BSM22] H. Baumann, A. Schaum, and T. Meurer. Data-driven control-oriented reduced order modeling for open channel flows. *IFAC-PapersOnLine*, 55(26):193–199, 2022. 4th IFAC Workshop on Control of Systems Governed by Partial Differential Equations CPDE 2022.
- [BYK19] M. Burkhardt, H. Yu, and M. Krstic. Stop-and-go suppression in two-class congested traffic. *arXiv:1905.06476*, 2019.

- [CBdNo8] J.-M. Coron, G. Bastin, and B. d'Andréa Novel. Dissipative boundary conditions for one-dimensional nonlinear hyperbolic systems. *SIAM Journal on Control and Optimization*, 47(3):1460–1498, 2008.
- [CC95] T. Chen and H. Chen. Universal approximation to nonlinear operators by neural networks with arbitrary activation functions and its application to dynamical systems. *IEEE transactions on neural networks*, 6 4:911–7, 1995.
- [CDKP87] G. Chen, M. C. Delfour, A. M. Krall, and G. Payre. Modeling, stabilization and control of serially connected beams. *SIAM Journal on Control and Optimization*, 25(3):526–546, 1987.
- [CHO16] J.-M. Coron, L. Hu, and G. Olive. Stabilization and controllability of first-order integro-differential hyperbolic equations. *Journal of Functional Analysis*, 271(12):3554–3587, 2016.
- [CHO17] J.-M. Coron, L. Hu, and G. Olive. Finite-time boundary stabilization of general linear hyperbolic balance laws via Fredholm backstepping transformation. *Automatica*, 84:95–100, 2017.
- [CHQZ88] C. Canuto, M. Y. Hussaini, A. Quarteroni, and T. A. Zang. *Spectral Methods in Fluid Dynamics*. Springer Berlin Heidelberg, Berlin, Heidelberg, 1988.
- [Cor09] J.-M. Coron. *Control and nonlinearity*, volume 136 of *Mathematical surveys and Monographs*. American Mathematical Soc., 2009.
- [CRA14] M. T. Chikhaoui, K. Rabenorosoa, and N. Andreff. Kinematic modeling of an EAP actuated continuum robot for active micro-endoscopy. *Advances in Robot Kinematics*, pages 457–465, 2014.
- [CVK17] S. Chen, R. Vazquez, and M. Krstic. Stabilization of an underactuated coupled transport-wave PDE system. In *2017 American Control Conference (ACC)*, pages 2504–2509, 2017.
- [CVKB13] J.-M. Coron, R. Vazquez, M. Krstic, and G. Bastin. Local exponential H^2 stabilization of a 2×2 quasilinear hyperbolic system using backstepping. *SIAM Journal on Control and Optimization*, 51(3):2005–2035, 2013.
- [CvMG⁺14] K. Cho, B. van Merriënboer, C. Gulcehre, D. Bahdanau, F. Bougares, H. Schwenk, and Y. Bengio. Learning phrase representations using RNN encoder-decoder for statistical machine translation. *arXiv:1406.1078*, 2014.
- [CZ12] R.F. Curtain and H. Zwart. *An introduction to infinite-dimensional linear systems theory*, volume 21. Springer Science & Business Media, 2012.
- [dAVP18] G. A. de Andrade, R. Vazquez, and D. J. Pagano. Backstepping stabilization of a linearized ODE–PDE rijke tube model. *Automatica*, 96:98–109, oct 2018.
- [DDL15] S. Damak, M. Di Loreto, and S. Mondié. Stability of linear continuous-time difference equations with distributed delay: Constructive exponential estimates. *International Journal of Robust and Nonlinear Control*, 25(17):3195–3209, 2015.
- [DGK18] J. Deutscher, N. Gehring, and R. Kern. Output feedback control of general linear heterodirectional hyperbolic ODE–PDE–ODE systems. *Automatica*, 95:472–480, 2018.

- [DGK19] J. Deutscher, N. Gehring, and R. Kern. Output feedback control of general linear heterodirectional hyperbolic PDE-ODE systems with spatially-varying coefficients. *International journal of control*, 92(10):2274–2290, 2019.
- [dHPC⁺03] J. de Halleux, C. Prieur, J.-M. Coron, B. d’Andréa Novel, and G. Bastin. Boundary feedback control in networks of open channels. *Automatica*, 39(8):1365–1376, 2003.
- [DL67] L.M. Delves and J.N. Lyness. A numerical method for locating the zeros of an analytic functions. *Math. Comput.*, 21:543–560, 1967.
- [DLP86] R. Datko, J. Lagnese, and M.P. Polis. An example on the effect of time delays in boundary feedback stabilization of wave equations. *SIAM Journal on Control and Optimization*, 24(1):152–156, 1986.
- [DMA15] F. Di Meglio and Ulf J. F. Aarsnes. A distributed parameter systems view of control problems in drilling. *IFAC-PapersOnLine*, 48(6):272–278, 2015.
- [DMBAHK18] F. Di Meglio, F. Bribiesca Argomedo, L. Hu, and M. Krstic. Stabilization of coupled linear heterodirectional hyperbolic PDE-ODE systems. *Automatica*, 87:281–289, 2018.
- [DMLA20] F. Di Meglio, P.-O. Lamare, and U. J. F Aarsnes. Robust output feedback stabilization of an ODE-PDE-ODE interconnection. *Automatica*, 119:109059, 2020.
- [DMVK13] F. Di Meglio, R. Vazquez, and M. Krstic. Stabilization of a system of $n+1$ coupled first-order hyperbolic linear PDEs with a single boundary input. *IEEE Transactions on Automatic Control*, 58(12):3097–3111, 2013.
- [Fab13] R.H. Fabiano. A stability result for a scalar neutral equation with multiple delays. In *IEEE 52nd Annual Conference on Decision and Control (CDC)*, pages 1089–1094. IEEE, 2013.
- [FW75] B. A. Francis and W. M. Wonham. The internal model principle for linear multivariable regulators. *Applied mathematics and optimization*, 2(2):170–194, 1975.
- [GBYK22] S. Goswami, A. Bora, Y. Yu, and G. E. Karniadakis. Physics-informed deep neural operator networks. *arXiv:2207.05748*, 2022.
- [GDD09] C. Germy, V. Denoël, and E. Detournay. Multiple mode analysis of the self-excited vibrations of rotary drilling systems. *Journal of Sound and Vibration*, 325(1-2):362–381, 2009.
- [Geh21] N. Gehring. A systematic design of backstepping-based state feedback controllers for ODE-PDE-ODE systems. *IFAC-PapersOnLine*, 54(9):410–415, 2021. 24th International Symposium on Mathematical Theory of Networks and Systems MTNS 2020.
- [GKC03] K. Gu, V.-L. Kharitonov, and J. Chen. *Stability of Time-Delay Systems*. Control Engineering. Springer Basel AG, Boston, MA, 2003.
- [GL13] Q. Gu and T. Li. Exact boundary controllability of nodal profile for unsteady flows on a tree-like network of open canals. *Journal de Mathématiques Pures et Appliquées*, 99(1):86–105, 2013.

- [GN97] P. Gahinet and A. Nemirovski. The projective method for solving linear matrix inequalities. *Mathematical programming*, 77(1):163–190, 1997.
- [Hay19] A. Hayat. PI controller for the general saint-venant equations. *Journal de l'Ecole Polytechnique*, 2019.
- [HDMVK16] L. Hu, F. Di Meglio, R. Vazquez, and M. Krstic. Control of homodirectional and general heterodirectional linear coupled hyperbolic PDEs. *IEEE Transactions on Automatic Control*, 61(11):3301–3314, 2016.
- [HG16] D. Hendrycks and K. Gimpel. Gaussian error linear units (gelus). *arXiv:1606.08415*, 2016.
- [HL02] J. Hale and S.M. Verduyn Lunel. Strong stabilization of neutral functional differential equations. *IMA Journal of Mathematical Control and Information*, 19(1 and 2):5–23, 2002.
- [HS97] S. Hochreiter and J. Schmidhuber. Long short-term memory. *Neural Computation*, 9:1735–1780, 1997.
- [HS21] A. Hayat and P. Shang. Exponential stability of density-velocity systems with boundary conditions and source term for the H^2 norm. *Journal de mathématiques pures et appliquées*, 153:187–212, 2021.
- [HVDKM15] L. Hu, R. Vazquez, F. Di Meglio, and M. Krstic. Boundary exponential stabilization of 1-D inhomogeneous quasi-linear hyperbolic systems. *SIAM Journal on Control and Optimization*, 57(2):963–998, 2015.
- [HVL13] J.K Hale and S.M Verduyn Lunel. *Introduction to Functional Differential Equations*, volume 99 of *Applied Mathematical Sciences*. Springer, 2013.
- [IGR21] A. Irscheid, N. Gehring, and J. Rudolph. Trajectory tracking control for a class of 2×2 hyperbolic PDE-ODE systems. *IFAC-PapersOnLine*, 54(9):416–421, 2021. 24th International Symposium on Mathematical Theory of Networks and Systems MTNS 2020.
- [Jan93] J. D. Jansen. *Nonlinear dynamics of oilwell drillstrings*. PhD thesis, Delft University of Technology, 1993.
- [JG22] F.-F. Jin and W. Guo. Boundary stabilization of a 1-D wave equation with multi-point velocity recirculations. *Systems & control letters*, 164:105230, 2022.
- [KBM20] C. Jiang, K. Kashinath, J. Bendavid, and P. Marcus. Enforcing hard physical constraints in CNNs through differentiable PDE layer. In *ICLR 2020 Workshop on Integration of Deep Neural Models and Differential Equations*, 2020.
- [JZ12] B. Jacob and H. J. Zwart. *Linear Port-Hamiltonian Systems on Infinite-dimensional Spaces*. Springer Basel, Dordrecht, 2012.
- [Ker21] S. Kerschbaum. *Backstepping control of coupled parabolic systems with varying parameters*. doctoral thesis, FAU University Press, 2021.
- [KGBSo8] M. Krstic, B.-Z. Guo, A. Balogh, and A. Smyshlyaev. Output-feedback stabilization of an unstable wave equation. *Automatica*, 44(1):63–74, 2008.
- [KGDM18] R. Kern, N. Gehring, J. Deutscher, and M. Meissner. Design and experimental validation of an output feedback controller for a pneumatic system with distributed parameters. In *18th International Conference on Control, Automation and Systems (ICCAS)*, pages 1391–1396, 2018.

- [KK14] I. Karafyllis and M. Krstic. On the relation of delay equations to first-order hyperbolic partial differential equation. *ESAIM: Control, Optimisation and Calculus of Variations*, 20(3):894–923, 2014.
- [KK17] I. Karafyllis and M. Krstic. *Predictor feedback for delay systems: Implementations and approximations*, volume 1. Birkhäuser Cham, 2017.
- [KK20] S. Koga and M. Krstic. Single-boundary control of the two-phase stefan system. *Systems & control letters*, 135:104573, 2020.
- [KMC05] V. Kharitonov, S. Mondie, and J. Collado. Exponential estimates for neutral time-delay systems: an LMI approach. *IEEE transactions on automatic control*, 50(5):666–670, 2005.
- [Krs08] M. Krstic. *Boundary control of PDEs. A course on backstepping designs.*, volume 16 of *Advances in design and control*. Siam, 2008.
- [KSo8] M. Krstic and A. Smyshlyaev. Backstepping boundary control for first-order hyperbolic PDEs and application to systems with actuator and sensor delays. *Systems & Control Letters*, 57(9):750–758, 2008.
- [KSBG07] M. Krstic, A.A. Siranosian, A. Balogh, and Bao-Zhu Guo. Control of strings and flexible beams by backstepping boundary control. In *2007 American Control Conference*, pages 882–887. IEEE, 2007.
- [KSS06] M. Krstic, A.A. Siranosian, and A. Smyshlyaev. Backstepping boundary controllers and observers for the slender Timoshenko beam: Part I - design. In *2006 American Control Conference (ACC)*, pages 2412–2417. IEEE, 2006.
- [Kut23] J N. Kutz. Machine learning for parameter estimation. *Proceedings of the National Academy of Sciences*, 120(12):e2300990120, 2023.
- [KVBR⁺00] P. Kravanja, M. Van Barel, O. Ragos, M.N. Vrahatis, and F.A. Zafiropoulos. ZEAL: A mathematical software package for computing zeros of analytic functions. *Comput. Phys. Comm.*, 124:212–232, 2000.
- [KWRK21] A. Karpatne, W. Watkins, J. Read, and V. Kumar. Physics-guided neural networks (PGNN): An application in lake temperature modeling. *arXiv:1710.11431*, 2021.
- [LADMA18] P.-O Lamare, J. Auriol, F. Di Meglio, and U.J.F Aarsnes. Robust output regulation of 2x2 hyperbolic systems: Control law and input-to-state stability. In *2018 American and Control Conference (ACC)*, pages 1732–1739. IEEE, 2018.
- [LeVo2] R. J. LeVeque. *Finite volume methods for hyperbolic problems*. Cambridge university press, 2002.
- [LGZM05] Y. Le Gorrec, H. Zwart, and B. Maschke. Dirac structures and boundary control systems associated with skew-symmetric differential operators. *SIAM journal on control and optimization*, 44(5):1864–1892, 2005.
- [LH17] I. Loshchilov and F. Hutter. Decoupled weight decay regularization. In *International Conference on Learning Representations*, 2017.
- [LJK21] L. Lu, P. Jin, and G. E. Karniadakis. DeepONet: Learning nonlinear operators for identifying differential equations based on the universal approximation theorem of operators. *Nature Machine Intelligence*, 3(3):218–229, 2021. arXiv:1910.03193.

- [LK00] W.-J. Liu and M. Krstic. Backstepping boundary control of Burgers' equation with actuator dynamics. *Systems & control letters*, 41(4):291–303, 2000.
- [LKA⁺20] Z. Li, N. Kovachki, K. Azizzadenesheli, B. Liu, K. Bhattacharya, A. Stuart, and A. Anandkumar. Neural operator: Graph kernel network for partial differential equations. *arXiv:2003.03485*, 2020.
- [LKA⁺21] Z. Li, N. Kovachki, K. Azizzadenesheli, B. Liu, K. Bhattacharya, and A. Stuart. Fourier neural operators for parametric partial differential equations. *arXiv:2010.08895*, 2021.
- [LRW96] H. Logemann, R. Rebarber, and G. Weiss. Conditions for robustness and nonrobustness of the stability of feedback systems with respect to small delays in the feedback loop. *SIAM Journal on Control and Optimization*, 34(2):572–600, 1996.
- [LT83] I. Lasiecka and R. Triggiani. Regularity of hyperbolic equations under $l_2(0, t; l_2(\gamma))$ -Dirichlet boundary terms. *Applied mathematics & optimization*, 10(1):275–286, 1983.
- [LT91] I. Lasiecka and R. Triggiani. Differential and algebraic Riccati equations with application to boundary/point control problems: continuous theory and approximation theory. *Lecture notes in control and Information Sciences*, 164:1–160, 1991.
- [LZ00] G. Leugering and E. Zuazua. On exact controllability of generic trees. *ESAIM. Proceedings*, 8:95–105, 2000.
- [LZK⁺23] Z. Li, H. Zheng, N. Kovachki, D. Jin, H. Chen, B. Liu, K. Azizzadenesheli, and A. Anandkumar. Physics-informed neural operator for learning partial differential equations. *arXiv:2111.03794*, 2023.
- [MK09] T. Meurer and A. Kugi. Tracking control for boundary controlled parabolic PDEs with varying parameters: Combining backstepping and differential flatness. *Automatica*, 45(5):1182–1194, 2009.
- [MLGRZ17] A. Macchelli, Y. Le Gorrec, H. Ramirez, and H. Zwart. On the synthesis of boundary control laws for distributed port-hamiltonian systems. *IEEE transactions on automatic control*, 62(4):1700–1713, 2017.
- [MN14] W. Michiels and S.-I. Niculescu. *Stability, Control, and Computation for Time-Delay Systems. An Eigenvalue-Based Approach*. SIAM, Philadelphia, 2014.
- [Mou98] H. Mounier. Algebraic interpretations of the spectral controllability of a linear delay system. In *Forum Mathematicum*, volume 10, pages 39–58. De Gruyter, 1998.
- [Moy77] P. Moylan. Stable inversion of linear systems. *IEEE Transactions on Automatic Control*, 22(1):74–78, 1977.
- [MvdS93] B.M. Maschke and A.J. van der Schaft. Port-controlled hamiltonian systems: Modelling origins and system theoretic properties. *Control engineering practice*, 1(5):359–365, 1993.
- [MZ04] T. Meurer and M. Zeitz. Flatness-based feedback control of diffusion-convection-reaction systems via k-summable power series. *IFAC Proceedings Volumes*, 37(13):177–182, 2004.

- [Nei49] J. Neimark. D-subdivisions and spaces of quasi-polynomials. *Prikladnaya Matematika i Mekhanika*, 13(4):349–380, 1949.
- [Nico1] S.-I. Niculescu. *Delay Effects on Stability: A Robust Control Approach*, volume 269 of *LNCIS*. Springer-Verlag, London, 2001.
- [NS21] N. H. Nelsen and A. M. Stuart. The Random Feature Model for input-output maps between Banach spaces. *SIAM journal on scientific computing*, 43(5):A3212–A3243, 2021.
- [NW13] K. Nandakumar and M. Wiercigroch. Stability analysis of a state dependent delayed, coupled two DOF model of drill-string vibration. *Journal of Sound and Vibration*, 332(10):2575–2592, 2013.
- [Pan76] L. Pandolfi. Stabilization of neutral functional differential equations. *Journal of Optimization Theory and Applications*, 20(2):191–204, 1976.
- [Pee21] M. Peet. Representation of networks and systems with delay: DDEs, DDFs, ODE–PDEs and PIEs. *Automatica*, 127:109508, 2021.
- [PR01] N. Petit and P. Rouchon. Flatness of heavy chain systems. *SIAM Journal on Control and Optimization*, 40(2):475–495, 2001.
- [RALG22a] J. Redaud, J. Auriol, and Y. Le Gorrec. Distributed damping assignment for a wave equation in the port-hamiltonian framework. In *IFAC-PapersOnLine*, volume 55-26, pages 155–161, 2022. 4th IFAC Workshop on Control of Systems Governed by Partial Differential Equations (CPDE).
- [RALG22b] J. Redaud, J. Auriol, and Y. Le Gorrec. In-domain damping assignment of a Timoshenko-beam using state feedback boundary control. In *IEEE 61st Conference on Decision and Control (CDC)*, pages 5405–5410, 2022.
- [RAMH22] S. G Rosofsky, H. Al Majed, and E. A Huerta. Applications of physics-informed neural operators. *arXiv:2203.12634*, 2022.
- [RAN21a] J. Redaud, J. Auriol, and S.-I. Niculescu. Output-feedback control of an under-actuated network of interconnected hyperbolic PDE–ODE systems. *Systems & control letters*, 154:104984, 2021.
- [RAN21b] J. Redaud, J. Auriol, and S.-I. Niculescu. Stabilizing integral delay dynamics and hyperbolic systems using a Fredholm transformation. In *IEEE 60th Conference on Decision and Control (CDC)*, pages 2595–2600, 2021.
- [RAN22a] J. Redaud, J. Auriol, and S.-I. Niculescu. Recursive dynamics interconnection framework applied to angular velocity control of drilling systems. In *American Control Conference (ACC)*, pages 5308–5313, 2022.
- [RAN22b] J. Redaud, J. Auriol, and S.-I. Niculescu. Stabilizing output-feedback control law for hyperbolic systems using a Fredholm transformation. *IEEE Transactions on Automatic Control*, 67(12):6651–6666, 2022.
- [RBAA23] J. Redaud, F. Bribiesca-Argomedo, and J. Auriol. Output regulation and tracking for linear ODE-hyperbolic PDE-ODE systems. *Automatica*, 2023. prov. accepted.
- [RCMDL18] E. Rocha Campos, S. Mondié, and M. Di Loreto. Necessary stability conditions for linear difference equations in continuous time. *IEEE Transactions on Automatic Control*, 63:4405–4412, 2018.

- [Reb95] R. Rebarber. Exponential stability of coupled beams with dissipative joints: A frequency domain approach. *SIAM Journal on Control and Optimization*, 33(1):1–28, 1995.
- [RPK19] M. Raissi, P. Perdikaris, and G.E. Karniadakis. Physics-informed neural networks: A deep learning framework for solving forward and inverse problems involving nonlinear partial differential equations. *Journal of Computational Physics*, 378:686–707, 2019.
- [Rus78a] D. L Russell. Canonical forms and spectral determination for a class of hyperbolic distributed parameter control systems. *Journal of Mathematical Analysis and Applications*, 62:186–225, 1978.
- [Rus78b] D.L. Russell. Controllability and stabilizability theory for linear partial differential equations: recent progress and open questions. *Siam Review*, 20(4):639–739, 1978.
- [RWo6] C. E. Rasmussen and C.K.I. Williams. *Gaussian Processes in Machine Learning*. MIT Press, 2006.
- [SA17] T. Strecker and O. M. Aamo. Output feedback boundary control of series interconnections of 2×2 semilinear hyperbolic systems. *IFAC-PapersOnLine*, 50(1):663–670, 2017.
- [Sal87] D. Salamon. Infinite-dimensional linear systems with unbounded control and observation: a functional analytic approach. *Transactions of the American Mathematical Society*, 300(2):383–431, 1987.
- [SCWK20] L. Su, S. Chen, J.-M. Wang, and M. Krstic. Stabilization of a 2×2 system of hyperbolic PDEs with recirculation in the unactuated channel. *Automatica*, 120:109147, 2020.
- [SDB05] G.J. Silva, A. Datta, and S.P. Bhattacharyya. *PID Controllers for Time-Delay Systems*. Control Engineering. Birkhäuser Boston, MA, 1st ed. 2005 edition, 2005.
- [SGWK17] L. Su, W. Guo, J.-M. Wang, and M. Krstic. Boundary stabilization of wave equation with velocity recirculation. *IEEE Transactions on Automatic Control*, 62(9):4760–4767, 2017.
- [SIH21] J. Sun, K. A. Innanen, and C. Huang. Physics-guided deep learning for seismic inversion with hybrid training and uncertainty analysis. *GEOPHYSICS*, 86(3):R303–R317, 2021.
- [SKo4] A. Smyshlyaev and M. Krstic. Closed-form boundary state feedbacks for a class of 1-D partial integro-differential equations. *IEEE Transactions on Automatic Control*, 49(12):2185–2202, 2004.
- [SKZ⁺92] R. Simon, R. Kania, R. Zuckermann, V. Huebner, D. Jewell, S. Banville, S. Ng, L. Wang, S. Rosenberg, C. Marlowe, D. Spellmeyer, R. Tan, A. Frankel, D. Santi, F. Cohen, and P. Bartlett. Peptoids: A modular approach to drug discovery. *Proc. Natl. Acad. Sci. U. S. A.*, 89:9367–9371, 10 1992.
- [SLY⁺22] Y. Shi, Z. Li, H. Yu, D. Steeves, A. Anandkumar, and M. Krstic. Machine learning accelerated PDE backstepping observers. *IEEE 61th Conference on Decision and Control*, page 8, 2022.

- [SMAV16] B; Saldivar, S. Mondié, and J. C. Avila Vilchis. The control of drilling vibrations: A coupled PDE-ODE modeling approach. *International journal of applied mathematics and computer science*, 26(2):335–349, 2016.
- [SMHFoo] A. Sunder, R. Mülhaupt, R. Haag, and H. Frey. Hyperbranched polyether polyols: A modular approach to complex polymer architectures. *Advanced Materials*, 12:235 – 239, 2000.
- [SMN⁺16] B. Saldivar, S. Mondié, S.-I. Niculescu, H. Mounier, and I. Boussaada. A control oriented guided tour in oilwell drilling vibration modeling. *Annual Reviews in Control*, 42:100 – 113, 2016.
- [SMN⁺23] I Sgura, L. Mainetti, F. Negro, M. G Quarta, and B. Bozzini. Deep-learning based parameter identification enables rationalization of battery material evolution in complex electrochemical systems. *Journal of Computational Science*, 66:101900, 2023.
- [Ste89] G. Stepan. *Retarded Dynamical Systems: Stability and Characteristic Functions*, volume 210 of *Pitman research notes in mathematics series*. Longman Scientific & Technical, 1989.
- [SWB87] M C Sheppard, C Wick, and T Burgess. Designing well paths to reduce drag and torque. *SPE Drilling Engineering*, 2:344–350, 1987.
- [SWGR11] C. Schmuck, F. Woittennek, A. Gensior, and J. Rudolph. Flatness-based feed-forward control of an HVDC power transmission network. In *IEEE 33rd International Telecommunications Energy Conference (INTELEC)*, pages 1–6. IEEE, 2011.
- [SWGR14] C. Schmuck, F. Woittennek, A. Gensior, and J. Rudolph. Feed-forward control of an HVDC power transmission network. *IEEE Transactions on Control Systems Technology*, 22(2):597–606, 2014.
- [Tim74] S.P. Timoshenko. *Vibration problems in engineering*. Wiley, 4e. edition, 1974.
- [TMP⁺20] A. M. Tartakovsky, C. Ortiz Marrero, Paris Perdikaris, G. D. Tartakovsky, and D. Barajas-Solano. Physics-informed deep neural networks for learning parameters and constitutive relationships in subsurface flow problems. *Water resources research*, 56(5):n/a, 2020.
- [TRWLG20] J. Toledo, H. Ramirez, Y. Wu, and Y. Le Gorrec. Passive observers for distributed port-hamiltonian systems. *IFAC-PapersOnLine*, 53(2):7587–7592, 2020. 21st IFAC World Congress.
- [VCKB11] R. Vazquez, J.-M. Coron, M. Krstic, and G. Bastin. Local exponential H^2 stabilization of a 2×2 quasilinear hyperbolic system using backstepping. In *IEEE 50th IEEE Conference on Decision and Control and European Control Conference (CDC-ECC)*, pages 1329–1334. IEEE, 2011.
- [vdSM02] A.J van der Schaft and B.M Maschke. Hamiltonian formulation of distributed-parameter systems with boundary energy flow. *Journal of geometry and physics*, 42(1):166–194, 2002.
- [Vilo7] J.A Villegas. *A Port-Hamiltonian Approach to Distributed Parameter Systems*. PhD thesis, Univesity of Twente, 2007.

- [VK14] R. Vazquez and M. Krstic. Marcum Q-functions and explicit kernels for stabilization of 2×2 linear hyperbolic systems with constant coefficients. *Systems & Control Letters*, 68:33–42, 2014.
- [VKC11] R. Vazquez, M. Krstic, and J.-M. Coron. Backstepping boundary stabilization and state estimation of a 2×2 linear hyperbolic system. In *Conference on Decision and Control and European Control Conference*, pages 4937–4942. IEEE, 2011.
- [VSP⁺17] A. Vaswani, N. Shazeer, N. Parmar, J. Uszkoreit, L. Jones, A. N. Gomez, L. Kaiser, and I. Polosukhin. Attention is all you need. In *Advances in Neural Information Processing Systems*, volume 30, 2017.
- [VZLGM09] J.A. Villegas, H. Zwart, Y. Le Gorrec, and B. Maschke. Exponential stability of a class of boundary control systems. *IEEE transactions on automatic control*, 54(1):142–147, 2009.
- [WA22] N. c. A. Wilhelmsen and O. M. Aamo. Leak detection, size estimation and localization in water distribution networks containing loops. In *IEEE 61st Conference on Decision and Control (CDC)*, pages 5429–5436, 2022.
- [WAA21] N. C. A Wilhelmsen, H. Anfinsen, and O. M Aamo. Minimum time observer designs for $n+m$ linear hyperbolic systems with unilateral, bilateral or point-wise in-domain sensing. *European Journal of Control*, 61:50–67, 2021.
- [Wei89] G. Weiss. Admissibility of unbounded control operators. *SIAM Journal on Control and Optimization*, 27(3):527–545, 1989.
- [WK20] J. Wang and M. Krstic. Delay-compensated control of sandwiched ODE-PDE-ODE hyperbolic systems for oil drilling and disaster relief. *Automatica*, 120:109131, 2020.
- [WK21] J. Wang and M. Krstic. Event-triggered output-feedback backstepping control of sandwich hyperbolic pde systems. *IEEE Transactions on Automatic Control*, 67(1):220–235, 2021.
- [WKP18] J. Wang, M. Krstic, and Y. Pi. Control of a 2×2 coupled linear hyperbolic system sandwiched between 2 ODEs. *International Journal of Robust and Nonlinear Control*, 28(13):3987–4016, 2018.
- [WLG18] Y. Wu and Y. Le Gorrec. Optimal actuator location for electro-active polymer actuated endoscope. In *6th IFAC Workshop on Lagrangian and Hamiltonian Methods for Nonlinear Control LHMNC*, volume 51-3, pages 199–204, 2018.
- [WMYY22] C. Wei, L. Mao, C. Yao, and G. Yu. Heat transfer investigation between well-bore and formation in U-shaped geothermal wells with long horizontal section. *Renewable energy*, 195:972–989, 2022.
- [Woi13] F. Woittennek. Flatness based feedback design for hyperbolic distributed parameter systems with spatially varying coefficients. *IFAC Proceedings Volumes*, 46(26):37–42, 2013.
- [WRK09] F. Woittennek, J. Rudolph, and T. Knüppel. Flatness based trajectory planning for a semi-linear hyperbolic system of first order PDE modeling a tubular reactor. *PAMM*, 9(1):3–6, 2009.

- [WWLL22] Y. Wang, Q. Wang, W. Lu, and H. Li. Physics-Constrained Seismic Impedance Inversion Based on Deep Learning. *IEEE Geoscience and Remote Sensing Letters*, 19:1–5, 2022.
- [WWP21] S. Wang, H. Wang, and P. Perdikaris. Learning the solution operator of parametric partial differential equations with physics-informed DeepONets. *Science Advances*, 7(40):8605, 2021.
- [YAK20] H. Yu, J. Auriol, and M. Krstic. Simultaneous stabilization of traffic flow on two connected roads. In *2020 American Control Conference (ACC)*, pages 3443–3448, 2020.
- [YAK22] H. Yu, J. Auriol, and M. Krstic. Simultaneous downstream and upstream output-feedback stabilization of cascaded freeway traffic. *Automatica*, 136:110044, 2022.
- [YK21] H. Yu and M. Krstic. Output feedback control of two-lane traffic congestion. *Automatica*, 125:109379, 2021.
- [Yos60] K. Yoshida. *Lectures on differential and integral equations*, volume 10. Interscience Publishers, 1960.
- [ZHS16] D. Zhao, S. Hovda, and S. Sangesland. Abnormal downhole pressure variation by axial stick-slip of drillstring. *Journal of Petroleum Science and Engineering*, 145:194–204, 2016.
- [ZLS20] R. Zhang, Y. Liu, and H. Sun. Physics-guided convolutional neural network (PhyCNN) for data-driven seismic response modeling. *Engineering Structures*, 215:110704, July 2020.
- [ZLW⁺22] W. Zhou, N. Liu, Y. Wu, H. Ramirez, and Y. Le Gorrec. Energy-based modeling and hamiltonian LQG control of a flexible beam actuated by IPMC actuators. *IEEE access*, 10:12153–12163, 2022.

Appendices

We gather in this part some supplementary material. It aims for a better understanding of this thesis.

First, in **Appendix A**, we present some of the numerical methods we used. It aims to give a general overview of numerical methods we used for any reader unfamiliar with hyperbolic PDE systems and the numerical resolution of coupled equations. It helps to understand the notions of well-posedness for the kernel equations and subtleties not mentioned when presenting the simulations. It also explains the computational methodology I used during my thesis, which is necessary for the reproducibility of the simulation results. It could be read *after Chapter 2* and the introduction of the backstepping methodology.

Next, we give in **Appendix B** the proof of Theorem 7.2.2. We advise any reader first to understand *Chapter 7* before reading this proof. We decided to present the complete proof in Appendix, to avoid splitting the overall reading of this chapter. It is quite technical and requires some linear algebra and operator framework knowledge.

Finally, we present in **Appendix C** some complementary results in the line of *Chapter 10*. We advise the reader to read it before to understand this test case better. Here, we question the choice of the target system for a backstepping-based observer design. We also comment on the impact of arbitrarily fixing the boundary conditions that remain degrees of freedom for the kernel definition. This chapter gathers some numerical observations that might be obvious to researchers familiar with the backstepping methodology.

A - A tutorial on numerical methods for solving kernel equations

Throughout this thesis, we illustrated the proposed backstepping-based controllers on simulations using ©Matlab. In this appendix, we present the computation methods we used to solve the kernel equations, necessary to compute the control law. This appendix is intended for a public not familiar with numerical methods and hyperbolic PDE resolution.

Kernels are usually defined on a 2–D grid representing the definition domain, which is the unit square \mathcal{S} for kernels of Fredholm integral transforms (in Chapter 7) or triangular subparts \mathcal{T}^\pm for kernels of Volterra integral transforms. We divide the segment $[0, 1]$ into p intervals to create the space mesh. The values of the kernels on \mathcal{S} are then stored on a $(p+1) \times (p+1) = n_x \times n_x$ matrix.

A.1 . Method of characteristics

Let us first consider a simplified case in the form of a general first-order hyperbolic equation

$$\frac{\partial}{\partial x} K(x, y) + a \frac{\partial}{\partial y} K(x, y) = H(x, y). \quad (\text{A.1})$$

In the case of kernel equations derived from scalar hyperbolic PDE systems, the parameter a is usually equal to 1, or strictly negative. Functions H, K are regular (usually continuous) and defined on a part of the unit square \mathcal{S} . To solve (A.1), we use the *method of characteristics*.

It consists in using a specific parametrization $(X(s), Y(s))$, for which the PDE rewrites as an ODE, i.e (A.1) rewrites

$$\frac{d}{ds} K(X(s), Y(s)) = H(X(s), Y(s)).$$

The solution propagates through the characteristic lines in first-order hyperbolic PDEs. The choice of the characteristic line we follow to obtain the value of $K(x, y)$ inside its definition domain depends on the boundary conditions available, as illustrated in Figure A.3. We can then integrate along the characteristic line between a value $s = 0$, for which we obtain the value in (x, y) , and a value s_f that depends on the boundary condition. Here, we only present two cases that appear frequently when solving kernel equations for scalar hyperbolic systems.

Case $a = 1$ In this case, the characteristic lines are parallel to the first diagonal of \mathcal{S} . On \mathcal{T}^+ (resp. \mathcal{T}^-), one boundary condition is enough in $y = 1$ or $x = 0$ (resp. $x = 1$ or $y = 0$) to define the value of K on the definition domain, assuming that H is known.

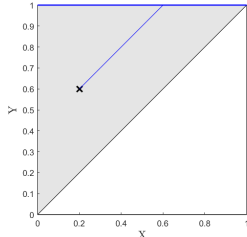
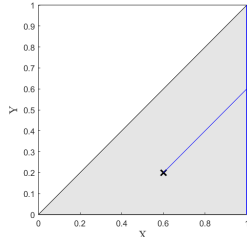
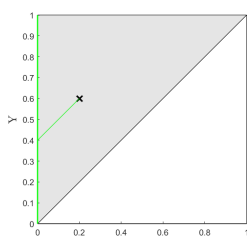
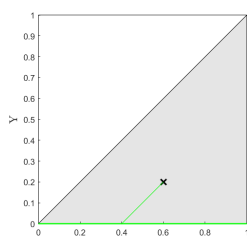
Cl. \ Dom	\mathcal{T}^+	\mathcal{T}^-
$X(s) = x + s$ $Y(s) = y + s$	$K(x, y) = K(x + 1 - y, 1) - \int_0^{1-y} H(x + s, y + s) ds$  <p>Boundary condition in $y = 1$</p>	$K(x, y) = K(1, y + 1 - x) - \int_0^{1-x} H(x + s, y + s) ds$  <p>Boundary condition in $x = 1$</p>
$X(s) = x - s$ $Y(s) = y - s$	$K(x, y) = K(0, y - x) + \int_0^x H(x - s, y - s) ds$  <p>Boundary condition in $x = 0$</p>	$K(x, y) = K(x - y, 0) + \int_0^y H(x - s, y - s) ds$  <p>Boundary condition in $y = 0$</p>

Figure A.3 – Different situations in the case $a = 1$

Case $a < 0$ In this case, the slope of the characteristic lines depends on the value of $|a|$ (relative to 1). A boundary condition in $y = x$ is required, or two boundary conditions on the side of the square.

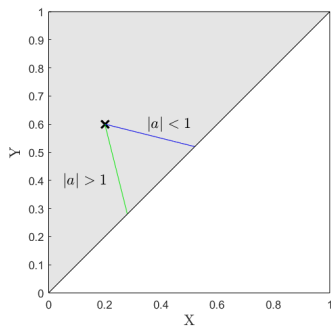


Figure A.1 – Characteristic $(x + s, y - |a|s)$ on \mathcal{T}^+

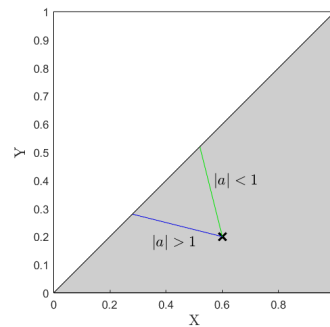


Figure A.2 – Characteristic $(x - s, y + |a|s)$ on \mathcal{T}^-

A.1.1 . Computation of the characteristics

To compute the integral term along the characteristics, we can use a function `solve_charac` that stores in a $(p + 1) \times (p + 1)$ cell. We start from a point of the domain and compute the characteristic line that starts at the point and stops at the boundary of the domain.

Algorithm: Kernels defined on \mathcal{S}^+

Variables: k corresponds to x , l corresponds to y

Inputs: number of points on the characteristic S_k

1 **For** $1 \leq k \leq p + 1$ **do**

2 **For** $k \leq l \leq p + 1$ **do**

3 starting point: $X0 = [(k-1)/p; (1-1)/p]$ ($s_0 = 0$)

• Boundary condition in $y = 1$:

$s_F = (1 - X0(2)) / \text{abs}(a)$, Update the values of S with
 $X(s) = x + |a|s, Y(s) = y + |a|s.$

• Boundary condition in $x = 0$:

$s_F = X0(1) / \text{abs}(a)$, Update the values of S with
 $X(s) = x - |a|s, Y(s) = y - |a|s.$

Outputs: $SK\{i, j\} = S$, $S[:, 1]$ contains N points corresponding to s ,
 $S[:, 2]$ corresponds to $X(s)$, $S[:, 3]$ to $Y(s)$

Algorithm: Kernels defined on \mathcal{S}^-

Variables: k corresponds to x , l corresponds to y

Inputs: number of points on the characteristic S_k

1 **For** $k \leq p + 1$ **do**

2 **For** $1 \leq l \leq k$ **do**

3 starting point: $X0 = [(k-1)/p; (1-1)/p]$ ($s_0 = 0$)

• Boundary condition in $x = 1$:

$s_F = (1 - X0(1)) / \text{abs}(a)$, Update the values of S with
 $X(s) = x + |a|s, Y(s) = y + |a|s.$

• Boundary condition in $y = 0$:

$s_F = X0(2) / \text{abs}(a)$, Update the values of S with
 $X(s) = x - |a|s, Y(s) = y - |a|s.$

Outputs: $SK\{i, j\} = S$, $S[:, 1]$ contains N points corresponding to s ,
 $S[:, 2]$ corresponds to $X(s)$, $S[:, 3]$ to $Y(s)$

A.1.2 . Approximating the integral term

We project the value of H on a one-dimensional integration domain \mathcal{S} . The integral term may be approximated as the limit of a Riemann's sum

$$\int_0^{s_F} H(X(s), Y(s)) ds = \lim_{N \rightarrow \infty} \frac{\text{length}(\mathcal{S})}{N} \sum_{k=0}^{N-1} H(X(s_k), Y(s_k)), \quad (\text{A.2})$$

with $(s_k)_{k \in \llbracket 0, N-1 \rrbracket}$ a partition of the characteristic line \mathcal{S} , such that $H(X(s_{N-1}), Y(s_{N-1})) = H(X(s_F), Y(s_F))$ and $s_0 = 0$ such that $H(X(s_0), Y(s_0)) = H(x, y)$. In implementation, we can then approximate the value of H along the characteristic line \mathcal{S} by

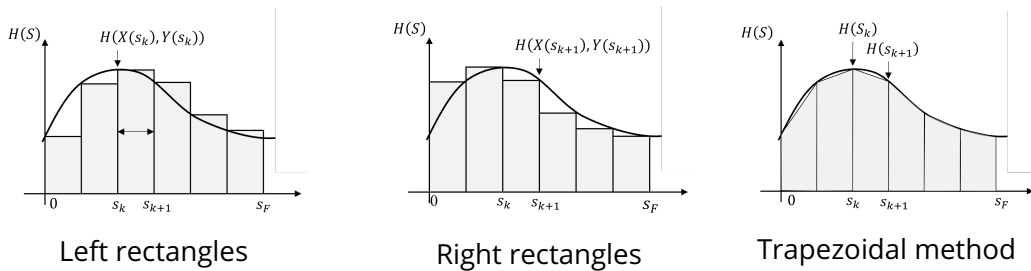
$$\int_{\mathcal{S}} H(X(s), Y(s)) ds \simeq \|(X(s_k), Y(s_k)) - (X(s_{k+1}), Y(s_{k+1}))\| \sum_{k=0}^{n-2} H(X(s_k), Y(s_k)),$$

$$\simeq \|(X(s_k), Y(s_k)) - (X(s_{k+1}), Y(s_{k+1}))\| \sum_{k=0}^{n-2} H(X(s_{k+1}), Y(s_{k+1})).$$

However, the quality of the approximation highly depends on the number of points N discretizing \mathcal{S} . A better way to compute the integral term is to use a second-order method, for instance, the *trapezoidal method* (`trapz` in Matlab¹). It approximates the integral term by a pointwise linear function

$$\int_{\mathcal{S}} H(X(s), Y(s)) ds \simeq \sum_{k=0}^{n-2} d(\mathcal{S}_{k+1}, \mathcal{S}_k) \frac{H(\mathcal{S}_k) + H(\mathcal{S}_{k+1})}{2}. \quad (\text{A.3})$$

We represent below three ways of approximating the integral term along \mathcal{S} :



A.1.3 . Approximating the function along the characteristic line

Since values of the function H are only available on a predefined grid $n_x \times n_x$ values, there is no value stored for all points S_k of the characteristic line. On Figures A.4-A.5, we schematically represented a characteristic line \mathcal{S} in \mathcal{T}^+ , starting from the point $(0.2, 0.4)$ with a mesh of 0.02 ($p = 50$). We see that the function H is only defined in three points along the characteristic (black dots). To compute an approximation of the integral term $\int_0^{s_F} H(X(s), Y(s)) ds$, we, therefore, need to find good approximations of $H(s_k)$.

1. More details can be found here <https://fr.mathworks.com/help/matlab/numerical-integration-and-differentiation.html>

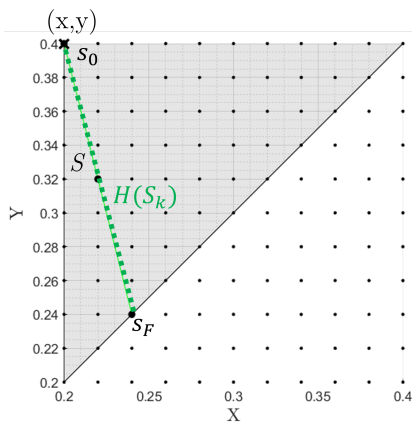


Figure A.4 – Discretization of the definition domain

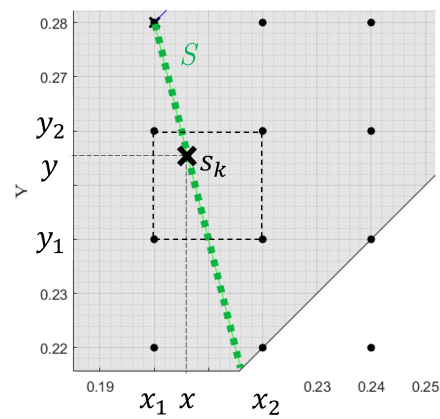


Figure A.5 – Evaluation of $H(X(s_k), Y(s_k))$

Different methods are already implemented on ©Matlab for interpolation of functions on 2-D grids (`griddata`, `gridfit`, `interp2`). To avoid errors on the boundaries of the domain, we defined two different functions on \mathcal{T}^+ and \mathcal{T}^- that linearly approximate the value of $H(x, y)$ by ponderating the values of the two to four nearest grid points. Two functions (`InterpolateLow` (resp. `InterpolateHigh`) for functions defined on \mathcal{S}^- (resp. \mathcal{S}^+) are defined using the bivariate interpolation method given in [AS65, Chapter 25]. Different situations are possible, depending on the number of points available, two points b_1 or a_2 is outside of the triangular domain, or three points $i = j$ near the first diagonal.

Algorithm: `InterpolateLow`, on \mathcal{S}^-

- Inputs:** Z : a $(p + 1) \times (p + 1)$ lower triangular matrix,
 x, y : coordinates where we want an approximation,
 p : $1/p$ is the step of the regular mesh on $[0, 1]^2$
- 1 **Initialisation:** compute the four points on the grid around (x,y) the points of coordinates $ip, (i + 1)p$ around x , indices a_1, a_2 , and $jp, (j + 1)p$ around y , indices b_1, b_2
 - 2 **If** a_2, b_2 are outside the grid **then**
 - 3 | $(x,y)=(1,1)$, **return** $Z(p,p)$
 - 4 **Else**
 - 5 | (x,y) inside the domain **then** According to the number of points available, compute a pondered mean res
 - 6 **return** res
-

A.1.4 . Application to kernel equations

Let us consider the general kernel equations given in (2.15)-(2.18). First, assume kernels L^\cdot are defined on \mathcal{T}^+ . The integration domain of the integral part of the Volterra transform is between $y \in [x, 1]$. Consider (2.15), and assume we have a boundary condition defined for $x = 0$. We define the *characteristic lines* parameterized by s , as $X(s) =$

$x - \lambda s$, $Y(s) = y - \lambda s$. We have

$$\frac{d}{ds}L^{++}(X(s), Y(s)) = \frac{\partial L^{++}}{\partial X} \frac{\partial X}{\partial s} + \frac{\partial L^{++}}{\partial Y} \frac{\partial Y}{\partial s} \quad (\text{A.4})$$

$$= -\lambda \frac{\partial}{\partial x} L^{++}(X, Y) - \lambda \frac{\partial}{\partial y} L^{++}(X, Y) \quad (\text{A.5})$$

$$= -\sigma^{+-}(x) L^{-+}(X, Y). \quad (\text{A.6})$$

Integrating along the characteristics line, between a value $s_F = \frac{x}{\lambda}$ for which we have the boundary condition, and the initial value $s = 0$ (for which we obtain the value $L^{++}(x, y)$), we therefore have

$$L^{++}(x, y) = L^{++}(0, y - x) + \int_0^{\frac{x}{\lambda}} \sigma^{+-}(x - \lambda s) L^{-+}(x - \lambda s, y - \lambda s) ds \quad (\text{A.7})$$

Assume that we now have a boundary condition in $y = 1$. We define the characteristic lines $X(s) = x + \lambda s$, $Y(s) = y + \lambda s$. We have

$$\frac{d}{ds}L^{++}(X(s), Y(s)) = \sigma^{+-}(x) L^{-+}(X, Y). \quad (\text{A.8})$$

Integrating along the characteristics line, between a value $s_F = \frac{1-y}{\lambda}$ and $s = 0$ we have

$$L^{++}(x, y) = L^{++}(x + 1 - y, 1) - \int_0^{\frac{1-y}{\lambda}} \sigma^{+-}(x + \lambda s) L^{-+}(x + \lambda s, y + \lambda s) ds \quad (\text{A.9})$$

We obtain a similar expression for (2.18). However, for (2.16)-(2.17), the slope of the characteristic lines depends of the ratio $\frac{\lambda}{\mu}$. Usually, the boundary condition is taken in $x = y$, to guarantee the boundary condition is available for any $(x, y) \in \mathcal{T}^+$. For (2.16), we have the characteristic $X(s) = x + \lambda s$, $Y(s) = y - \mu s$, and

$$L^{+-}(x, y) = L^{+-}(x, x) - \int_0^{\frac{y-x}{\lambda+\mu}} \sigma^{+-}(x + \lambda s) L^{--}(x + \lambda s, y - \mu s) ds. \quad (\text{A.10})$$

For (2.17), we have the characteristic $X(s) = x + \mu s$, $Y(s) = y - \lambda s$, and

$$L^{-+}(x, y) = L^{-+}(x, x) + \int_0^{\frac{y-x}{\lambda+\mu}} \sigma^{-+}(x + \mu s) L^{++}(x + \mu s, y - \lambda s) ds. \quad (\text{A.11})$$

Similarly, when the kernels are computed on \mathcal{T}^- , the lower part of the unit square \mathcal{S} , i.e when the integration domain is between $y = 0$ and $y = x$, the boundary condition is given in $y = 0$ (or $x = 1$) for (2.15)-(2.18) and in $x = y$ for (2.16)-(2.17).

To keep in mind

In this thesis, we will regularly compute kernels with different boundary conditions, defined on different domains. A first consideration on their well-posedness consists in analyzing the available boundary conditions (imposed by the backstepping methodology), to determine the remaining degrees of freedom (to be given an arbitrary value, as presented in Appendix C). All in all, the boundary conditions must allow to define the kernels on their entire definition domain.

A.2 . Successive approximations

There are many ways of computing functions satisfying integral equations. The proof of the existence of such functions relies on the fixed point method or *successive approximation method* (see [Yos60, Chapter 1], [Krs08, Section 4.4]). The existence of a solution to the kernel equations in the backstepping methodology has been widely studied. Proofs can be found in the literature, for different regularity, and with space-varying velocities (see [CVKB13, Appendix A] or the general setup proposed in [DMBAHK18, Section 3]).

A.2.1 . Volterra integral equations of the second kind

Let $K(s, t)$ be a real-valued continuous (or piecewise continuous) function defined on $\mathcal{S} = [0, 1]^2$; and $f(s)$ be a real-valued continuous (or piecewise continuous) function defined on the interval $[0, 1]$, $\lambda \in \mathbb{R}$. A *Volterra integral equation of the second kind* with unknown φ is defined by

$$f(s) = \varphi(s) - \lambda \int_a^s K(s, t)\varphi(t)dt$$

Such an equation admits a unique solution that can be expressed in two ways:

- as a power series in λ : $\varphi(s) = \sum_{n=0}^{\infty} \lambda^n \varphi_n(s)$
with φ_n defined by $\varphi_0(s) = f(s)$, $\varphi_n(s) = \int_a^s K(s, t)\varphi_{n-1}(t)dt$;
- using the resolvent kernel Γ : $\varphi(s) = f(s) + \lambda \int_a^s \Gamma(s, t; \lambda)f(t)dt$
with $\Gamma(s, t; \lambda) = \sum_{n=1}^{\infty} \lambda^{n-1} K^{(n)}(s, t)$ defined using the **iterated kernels** recursively defined by $K^{(1)}(s, t) = K(s, t)$, \dots , $K^{(n)}(s, t) = \int_t^s K(s, r)K^{(n-1)}(r, t)dt$.

The existence (convergence of the series) and uniqueness are proven using iterated increase.

Application to kernel equations

Using the method of characteristics, we showed in Section A.1.4 that the kernels satisfy coupled Volterra integral equations of the second kind. Interestingly, we also have to solve similar equations when defining observers of the Luenberger type (in (4.33), (7.38) for instance). An example is

$$f(x) - \int_0^x L(x, \xi)f(\xi)d\xi = \lambda qL(x, 0)$$

with unknown f (can be multidimensional) and kernel L previously computed.

A.2.2 . Numerical implementation

There are two main ways of computing solutions of such equations by the method of successive approximations. First, let us consider the case of 1-D functions (f, g) defined on $[0, 1]$. The space domain is discretized with space step p on $n_x = 1/(p+1)$ discrete values. To solve the kernel equations, we use the following algorithm:

Algorithm: Method of successive approximation

Inputs: number of space values n_x , kernels L , parameters λ, μ, q, \dots

- 1 **Initialisation:** build $f, f_{bis}, f_{ter} = \text{zeros}(n_x, 1)$
- 2 **While** $\text{eps} \leq \text{thres} \ \& \ n_{iter} \leq \text{max_iter}$ **do**
- 3 **For** x from 0 to 1 (with step p) **do**
 - compute an approximation of the integral term

$$\int_0^x L(x, \xi) f(\xi) + K(x, \xi) g(\xi) d\xi$$
 - compute f_{bis} using $f(x) \leftarrow \int_0^x L(x, \xi) f(\xi) d\xi + \lambda q L(x, 0)$
- 4 Update the values : $f_{ter} = f, f = f_{bis}$
- 5 Update the number of iterations $n_{iter} += 1$, update eps

While the error eps is inferior to a certain threshold (typically $\epsilon = 10^{-5}$) and the number of iterations is inferior to a maximum (typically 20), the algorithm iterates the recursive construction. The error is computed as the maximum value of the difference between f_{ter} and f_{bis} over the discretized definition domain. As presented in Section A.1.2, we can use different methods to compute the integral terms:

- sum the values and multiply by dx , without changing the space step;
- discretize $[0, x]$ with a thinner step, and use 1-D or 2-D approximations of the kernels to obtain the integral as a sum;
- compute the function $L(x, \xi) f(\xi)$ on $\text{space_mesh}(1:i)$ and use a `trapz` method for instance.

It could be interesting to compare the resulting functions and the values of the integral terms at each step using different methods. Machine-learning based methods have also been investigated [BSK23]. Each method has its advantages and inconveniences, in terms of computation time and implementation complexity. We noticed that some points (matrices products, bounds on the interval, or sums...) are sources of recurrent errors.

Quality of the computation

To keep in mind

Usually, the kernels are used in the main simulation to compute the full-state boundary feedback controller (see (2.24), (5.8) or (7.57)). A *bad* approximation of the kernels could lead to a bad expression of the stabilizing control input, which could impact the performance of the closed-loop system.

The impact of ϵ (eps) and nx (n_x) on the **quality** of the kernels can be subject to investigation. They have a high impact on the offline computation time and for nx on the simulation time afterward. Especially for adaptive control, the kernel equations must be solved online to consider the varying physical parameters. Innovative resolution methods must be sought, such as using neural networks as a surrogate [BSK23]. This aligns with the work presented in Chapter 11. However, it is not yet clear if taking more time to compute kernels greatly impacts the simulation itself.

		p		
eps	# iter.	20	50	100
10^{-5}	11	2.01	27.9	247
10^{-8}	17	3.39	44.1	362
10^{-10}	21	3.91	61.9	462

Table A.1 – Evolution of the computation time (s) for some kernels equations

Another difficulty is that in the general case (non-constant/non-zero in-domain couplings), we do not have a "theoretical value" that could serve as a reference. Evaluating the "quality" of the kernels obtained using the method of successive approximations given in the above algorithm is therefore not straightforward. To check if the computed kernels correspond to their theoretical values and usually detect mistakes in the algorithms, we can numerically verify:

1. if they satisfy the PDEs,
2. if they satisfy the boundary conditions.

We can first search on a 2D grid if the PDEs are satisfied, using the differentiation tool `diff`. Except along the discontinuity lines, the error should remain under 10^{-2} . It is illustrated in Figure A.6 for two kernels (transform (C.8)).

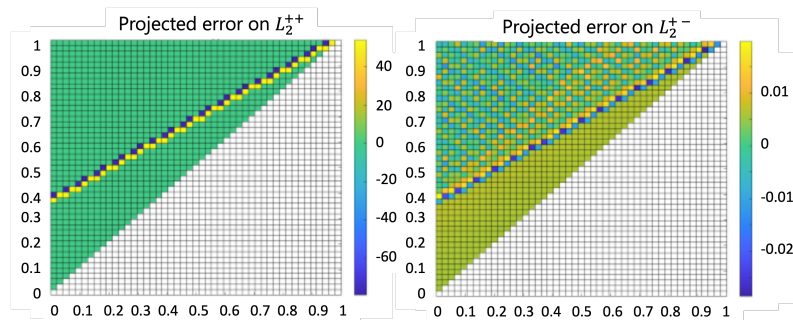


Figure A.6 – 2D error map for component (12) of two kernels

Similarly, when computing the inverse kernels (kernels of the inverse transform), we usually compose both transforms and check if the results give the identity by computing the L^2 -norm of the difference between the initial state and the state obtained after the two transforms. The error should be of order 10^{-4} maximum.

Moreover, in some cases, we have some degrees of freedom on the boundary conditions we chose for the kernels. We could also ponder on the impact of these boundary conditions on the quality of the resulting controller. Preliminary work in this direction for the observer design is presented in Appendix C.

A.2.3 . Perspectives

A very interesting toolbox has been developed by Jakob Gabriel from Ulm University, to automatize the computation of backstepping-based controllers². This library is a collection of Matlab scripts, functions, and classes to simplify the implementation of control laws for infinite dimensional systems. The authors provide an object-oriented framework to use time and space-dependent functions and operators. This significantly simplifies calculations with matrix-valued functions, since there is no need here to re-write "by hand" resolution algorithms. Though it offers fewer degrees of freedom in the implementation, it highly helps in most cases. In particular, when considering space-varying velocities, it gives an intuitive representation of the kernel resolution along the characteristic lines (Figure A.7).

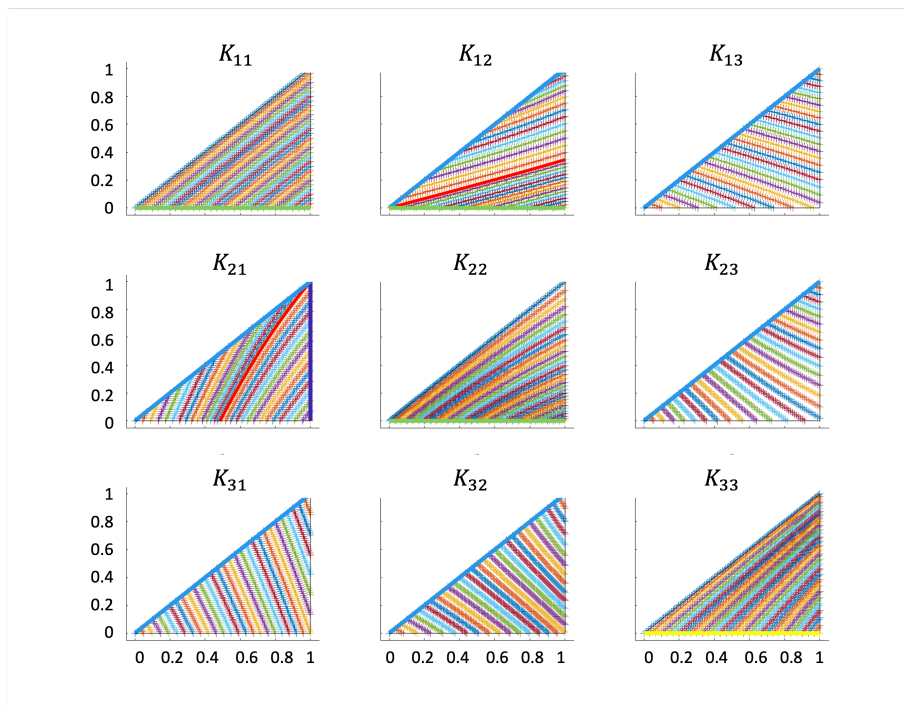


Figure A.7 – Example of 2D projection of space varying kernels using Coni

2. The Matlab code can be found on <https://zenodo.org/record/6420876> or <https://gitlab.com/control-system-tools/coni>. Similarly, efficient algorithms for solving kernels of parabolic PDEs are available at <https://doi.org/10.5281/zenodo.4274739> [Ker21]

B - Proof of Theorem 7.2.2

In this Appendix, we give the complete proof of Theorem 7.2.2. As a reminder, it reads as follows

Theorem: Well-posedness of the kernel equations 7.2.2

The set of equations (7.29)-(7.34) admits a unique solution in $C_{pw}^0(\mathcal{S}, \mathbb{R}^{2 \times 2})$.

Due to the integral terms in the boundary conditions (7.33), we cannot apply classical methods [DMBAHK18] to prove the existence of a unique solution to (7.29)-(7.34). The proof is decomposed into several steps:

- First, we express all the kernels as functions of the boundary terms $N^{+-}(0, y)$ and $N^{-+}(0, y)$. We show that the existence of $N^{+-}(0, \cdot), N^{-+}(0, \cdot)$ implies the existence of all kernels on \mathcal{S} . Moreover, they share the same regularity properties.
- Then, we show that $N^{+-}(0, \cdot), N^{-+}(0, \cdot)$ are defined by an integral equation of the form (7.24).
- We show that the conditions of Lemma 7.2.1 are satisfied for this operator. It concludes the proof.

B.1 . Expression of the kernels as functions of the boundary terms

First, we prove the following

Lemma B.1.1: Kernels reduction

For all $(x, y) \in \mathcal{S}$, $N^{\cdot\cdot}(x, y)$ can be expressed as functions of $N^{+-}(0, \cdot)$ and $N^{-+}(0, \cdot)$.

Proof : Applying the method of characteristics on the transport equations (7.29)-(7.30), we can express $N^{\cdot\cdot}$ on \mathcal{S} as functions of their boundary values.

First, for kernels N^{++}, N^{--} represented on Figure B.1, the slope of the characteristic lines does not depend on Λ_i . The kernels are defined by their boundary values in $y = 1$ and $y = 0$. Using the boundary conditions

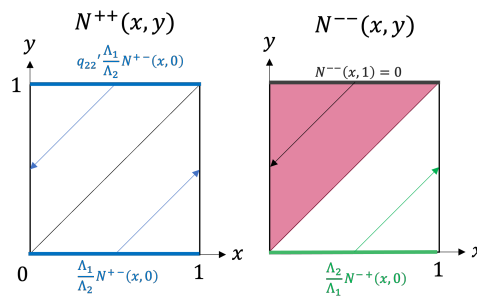


Figure B.1 – Representation of the kernels N^{++}, N^{--}

(7.31)-(7.34), direct computations give

$$N^{++}(x, y) = \frac{\Lambda_1}{\Lambda_2} (\mathbb{1}_{[0, y]}(x) q_{22}' N^{+-}(x - y + 1, 0) + \mathbb{1}_{[y, 1]}(x) N^{+-}(x - y, 0)),$$

$$N^{--}(x, y) = \frac{\Lambda_2}{\Lambda_1} \mathbb{1}_{[y, 1]}(x) N^{-+}(x - y, 0).$$

To express the two other kernels as functions of their boundary terms, we need to look closely at their characteristics, whose slope depends on the ratio $\frac{\Lambda_1}{\Lambda_2}$. The case $\Lambda_2 = \Lambda_1$ is the easiest to handle since the characteristic lines parallel the antidiagonal of \mathcal{S} . In the other cases, the characteristic lines for kernels N^{-+} , N^{+-} do not divide \mathcal{S} into two equal triangular domains, as illustrated in Figure B.2. In particular, in the case

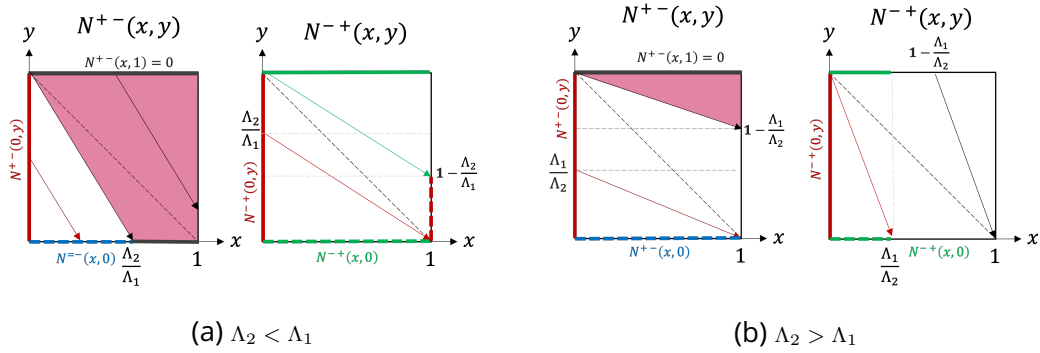
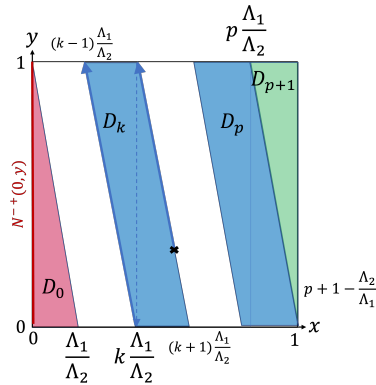


Figure B.2 – Representation of kernels N^{-+} , N^{+-}

$\Lambda_2 > \Lambda_1$ the boundary condition $N^{+-}(x, 1) = 0$ defines the values of $N^{+-}(1, y)$ for the triangular domain $x \in [0, 1]$, $y \in [1 - \frac{\Lambda_2}{\Lambda_1}x, 1]$ only, and the boundary condition $N^{-+}(0, y)$ directly defines the kernels' values for the triangular domain $x \in [0, \frac{\Lambda_1}{\Lambda_2}]$, $y \in [0, 1 - \frac{\Lambda_2}{\Lambda_1}x]$ only. One can note that the boundary condition $N^{+-}(x, 1) = 0, \forall x \in [0, 1]$ propagates along the characteristic lines, such that N^{+-} is equal to 0 on the right upper part of \mathcal{S} , as illustrated by the red domains on Figure B.2.

To determine the values on \mathcal{S} in that case, we use an iterative procedure. Let us define p as the unique integer verifying $p \frac{\Lambda_1}{\Lambda_2} \leq 1 < (p + 1) \frac{\Lambda_1}{\Lambda_2}$. We can divide the square \mathcal{S} into different sub-domains $D_k, k \in \llbracket 0, p + 1 \rrbracket$, as illustrated below.



More precisely, we have:

- $D_0 = \{0 \leq y \leq 1, 0 \leq x \leq \frac{\Lambda_1}{\Lambda_2}(1 - y)\}$,
- $\forall k \in \llbracket 1, p - 1 \rrbracket$,
 $D_k = \{0 \leq y \leq 1, \frac{\Lambda_1}{\Lambda_2}(k - y) \leq x < \frac{\Lambda_1}{\Lambda_2}(k + 1 - y)\}$,
- $D_p = \{0 \leq y \leq 1, \frac{\Lambda_1}{\Lambda_2}(p - y) \leq x < \min(1, 1 - \frac{\Lambda_1}{\Lambda_2}y)\}$,
- $D_{p+1} = \{p + 1 - \frac{\Lambda_2}{\Lambda_1}x \leq y \leq 1, p \frac{\Lambda_1}{\Lambda_2} \leq x \leq 1\}$.

Note that when $\Lambda_2 < \Lambda_1$ we have $p = 0$. Integrating along the characteristic lines, and using (7.32), we obtain by iteration $\forall k \in \llbracket 0, p + 1 \rrbracket, \forall (x, y) \in D_k, N^{-+}(x, y) = q_{22}^k N^{-+}(0, y - k + \frac{\Lambda_2}{\Lambda_1}x)$. In the same way, we can express kernel N^{+-} as a function of $N^{+-}(0, y)$. We have, for all $(x, y) \in \mathcal{S}$,

$$N^{+-}(x, y) = \mathbb{1}_{[0, \frac{\Lambda_2}{\Lambda_1}(1-y)]}(x) N^{+-}(0, y + \frac{\Lambda_1}{\Lambda_2}x).$$

This concludes the proof of LemmaB.1.1. ■

B.2 . Definition of the boundary terms as a solution of an integral equation (7.24)

Next, we rewrite $N^{-+}(0, y)$ and $N^{+-}(0, y)$ as the solutions of two integral equations. More precisely, we show that they satisfy

$$\begin{pmatrix} N_w(y) \\ N_z(y) \end{pmatrix} = \begin{pmatrix} \bar{N}^{-+}(0, y) \\ -N^{+-}(0, y) \end{pmatrix} - \int_0^1 \begin{pmatrix} -\mathcal{I}_{12}(\nu, y) & \mathcal{I}_{11}(\nu, y) \\ -\mathcal{I}_{22}(\nu, y) & \mathcal{I}_{21}(\nu, y) \end{pmatrix} \begin{pmatrix} \bar{N}^{-+}(0, \nu) \\ -N^{+-}(0, \nu) \end{pmatrix} d\nu, \quad (\text{B.1})$$

with \mathcal{I}_{ij} four bounded piecewise continuous coupling terms depending on N_w, N_z , defined by (B.4)-(B.6) and (B.9). Notice first that using the transport equation (7.29) in (7.31), we obtain $N^{++}(0, y) - q'_{22}N^{++}(1, y) = 0$ which simplifies (7.33). Then, we have $N^{-+}(0, y) = 0, \forall y \in [0, 1]$ and $N^{+-}(1, y) = 0, \forall y \in [\max(0, 1 - \frac{\Lambda_1}{\Lambda_2}), 1]$. We therefore have

$$\begin{aligned} N_z(y) - \int_0^1 N_w(\nu)N^{+-}(\nu, y) + N_z(\nu)N^{-+}(\nu, y)d\nu &= -N^{+-}(0, y) \\ &\quad + \mathbb{1}_{[0, 1 - \frac{\Lambda_1}{\Lambda_2}]}(y)q'_{22}N^{+-}(0, y + \frac{\Lambda_1}{\Lambda_2}), \\ N_w(y) - \int_0^1 N_w(\nu)N^{++}(\nu, y) + N_z(\nu)N^{-+}(\nu, y)d\nu &= N^{-+}(0, y). \end{aligned}$$

We decompose the integral terms into subdomains (depending on p) to express the kernels N^\cdot as functions of the boundary values $N^{+-}(0, \cdot)$ and $N^{-+}(0, \cdot)$. We obtain

$$N_w(y) = N^{-+}(0, y) - \int_0^1 I_{11}(\nu, y)(-N^{+-}(0, \nu)) - I_{12}(\nu, y)N^{-+}(0, \nu)d\nu, \quad (\text{B.2})$$

$$\begin{aligned} N_z(y) &= - \left(N^{+-}(0, y) - \mathbb{1}_{[0, 1 - \frac{\Lambda_1}{\Lambda_2}]}(y)q'_{22}N^{+-}(0, y + \frac{\Lambda_1}{\Lambda_2}) \right) \\ &\quad - \int_0^1 I_{21}(\nu, y)(-N^{+-}(0, \nu)) - I_{22}(\nu, y)N^{-+}(0, \nu)d\nu, \end{aligned} \quad (\text{B.3})$$

where

$$I_{11}(\nu, y) = \mathbb{1}_{[0, 1]}(\nu)(\mathbb{1}_{[0, \frac{\Lambda_1}{\Lambda_2}(1-y)]}(\nu)N_w(y + \frac{\Lambda_2}{\Lambda_1}\nu) + \mathbb{1}_{[\frac{\Lambda_1}{\Lambda_2}(1-y), \frac{\Lambda_1}{\Lambda_2}]}(\nu)q'_{22}N_w(y - 1 + \frac{\Lambda_2}{\Lambda_1}\nu)) \quad (\text{B.4})$$

$$\begin{aligned} I_{12}(\nu, y) &= \frac{\Lambda_1}{\Lambda_2} \left[\mathbb{1}_{[y, 1]}(\nu)N_z(\frac{\Lambda_1}{\Lambda_2}(\nu - y)) + \sum_{k=1}^p \mathbb{1}_{[0, \frac{\Lambda_2}{\Lambda_1} - k + y]}(\nu)q_{22}^k N_z(\frac{\Lambda_1}{\Lambda_2}(\nu - y + k)) \right. \\ &\quad \left. + \mathbb{1}_{[p+1 + \frac{\Lambda_1}{\Lambda_2}, 1]}(y)\mathbb{1}_{[0, \frac{\Lambda_2}{\Lambda_1} - (p+1) + y]}(\nu)q_{22}^{p+1} N_z(\frac{\Lambda_1}{\Lambda_2}(\nu - y + p + 1)) \right], \end{aligned} \quad (\text{B.5})$$

$$I_{21}(\nu, y) = \mathbb{1}_{[y, y + \frac{\Lambda_1}{\Lambda_2}]}(\nu)\mathbb{1}_{[0, 1]}(\nu)\frac{\Lambda_2}{\Lambda_1}N_w(\frac{\Lambda_2}{\Lambda_1}(\nu - y)),$$

$$I_{22}(\nu, y) = \sum_{k=0}^p \mathbb{1}_{[0, \frac{\Lambda_2}{\Lambda_1}(1-y) - k]}(\nu)q_{22}^k N_z(y + \frac{\Lambda_1}{\Lambda_2}(\nu + k)). \quad (\text{B.6})$$

The above computations the terms I_{ij} rely on Fubini's theorem. To rewrite the integral equations (B.2)-(B.3) using an integral operator of the form (7.24), we need to get rid of the term $\mathbb{1}_{[0,1-\frac{\Lambda_1}{\Lambda_2}]}(y)q'_{22}N^{+-}(0, y + \frac{\Lambda_1}{\Lambda_2})$ in (B.2). Let f be a bounded function, and define the function \bar{f} , such that for all $y \in [0, 1]$ we have

$$\bar{f}(y) = f(y) - \mathbb{1}_{[0,1-\frac{\Lambda_1}{\Lambda_2}]}(y)q'_{22}f(y + \frac{\Lambda_1}{\Lambda_2}). \quad (\text{B.7})$$

This yields the following lemma:

Lemma B.2.1: Change of variable

The operator $\bar{\cdot}$ defined by (B.7) is invertible. More precisely, the inverse change of variables is defined by

$$f(y) = \sum_{k=0}^p q_{22}^k \mathbb{1}_{[0,1-k\frac{\Lambda_1}{\Lambda_2}]}(y) \bar{f}(y + k\frac{\Lambda_1}{\Lambda_2}). \quad (\text{B.8})$$

Proof: Formula (B.8) is obtained by an iterative approach. Let us take $y \in [0, 1]$, and assume that $\Lambda_2 > \Lambda_1$ (else, the change of variables is equal to the identity and the proof is straightforward). We have

$$\left\{ \begin{array}{l} \bar{f}(y) = f(y), \quad \text{if } 1 - \frac{\Lambda_1}{\Lambda_2} < y \leq 1, \\ \bar{f}(y) = f(y) - \underbrace{q'_{22}f(y + \frac{\Lambda_1}{\Lambda_2})}_{\geq \frac{\Lambda_1}{\Lambda_2}}, \quad \text{if } 0 \leq y \leq 1 - \frac{\Lambda_1}{\Lambda_2}. \end{array} \right.$$

Then, if $1 - \frac{\Lambda_1}{\Lambda_2} \leq \frac{\Lambda_1}{\Lambda_2} \iff \frac{\Lambda_2}{\Lambda_1} < 2 \iff p = 1$, we directly have $f(y) = \bar{f}(y) + q'_{22}\bar{f}(y + \frac{\Lambda_1}{\Lambda_2})$. Else, we need to iterate $p - 1$ more times the operation, which successively add the terms $q_{22}^k \mathbb{1}_{[0,1-k\frac{\Lambda_1}{\Lambda_2}]}(y)\bar{f}(y + k\frac{\Lambda_1}{\Lambda_2})$. We finally obtain (B.8). ■

Defining, $\bar{N}^{+-}(y) = N^{+-}(0, y) - \mathbb{1}_{[0,1-\frac{\Lambda_1}{\Lambda_2}]}(y)q'_{22}N^{+-}(0, y + \frac{\Lambda_1}{\Lambda_2})$, we can rewrite (B.2)-(B.3) as

$$\begin{aligned} N_w(y) &= N^{-+}(0, y) - \int_0^1 \bar{I}_{11}(\nu, y)(-\bar{N}^{+-}(\nu)) - I_{12}(\nu, y)N^{-+}(0, \nu)d\nu, \\ N_z(y) &= -\bar{N}^{+-}(y) - \int_0^1 \bar{I}_{21}(\nu, y)(-\bar{N}^{+-}(\nu)) - I_{22}(\nu, y)N^{-+}(0, \nu)d\nu. \end{aligned}$$

Using the expression (B.8) in the integral terms, we can define the new coupling terms \bar{I}_{j1} , $j \in \{1, 2\}$ by

$$\bar{I}_{j1}(\nu, y) = \sum_{k=0}^p q_{22}^k \mathbb{1}_{[\frac{\Lambda_1}{\Lambda_2}k, 1]}(\nu) I_{j1}(\nu - \frac{\Lambda_1}{\Lambda_2}k, y). \quad (\text{B.9})$$

Note that in the case $\Lambda_2 \leq \Lambda_1$, the change of variables (B.8) is the identity. We can finally define on \mathcal{S} four bounded functions $\mathcal{I}_{11}, \mathcal{I}_{21}, \mathcal{I}_{12}, \mathcal{I}_{22}$ introduced in (B.10) by $\mathcal{I}_{j2} = I_{j2}$ and $\mathcal{I}_{j1} = \bar{I}_{j1}$ $j \in \{1, 2\}$ (B.5)-(B.6),(B.9).

B.3 . Invertibility of the integral operator

The last step of the proof consists in proving the invertibility of the above integral operator. From equation (B.1), we state

Theorem B.3.1: Invertibility of a Fredholm integral operator

The Fredholm integral operator \mathcal{Q} of form (7.24) defined by

$$\mathcal{Q} : \begin{pmatrix} u \\ v \end{pmatrix} \mapsto \begin{pmatrix} u \\ v \end{pmatrix} - \int_0^1 \begin{pmatrix} -\mathcal{I}_{12}(\nu, \cdot) & \mathcal{I}_{11}(\nu, \cdot) \\ -\mathcal{I}_{22}(\nu, \cdot) & \mathcal{I}_{21}(\nu, \cdot) \end{pmatrix} \begin{pmatrix} u(\nu) \\ v(\nu) \end{pmatrix} d\nu, \quad (\text{B.10})$$

is boundedly invertible.

Proof : We prove that conditions of Lemma 7.2.1 are satisfied. Indeed, the four functions \mathcal{I}_{ij} are bounded, such that the integral part of \mathcal{Q} is a compact operator. By [Bre10, Theorem 6.6] (Fredholm alternative), we have $\dim \ker(\mathcal{Q}) < \infty$. Let us show that conditions (a) – (d) are verified.

First, conditions (a), (b) are proved by evaluating the components of the kernel $R(x, y)$ in $y = 0$ and $y = 1$. We obtain

$$\begin{aligned} \mathcal{I}_{11}(0, \nu) &= \sum_{k=0}^p q_{22}^k \mathbb{1}_{[k \frac{\Lambda_1}{\Lambda_2}, 1]}(\nu) N_w \left(\frac{\Lambda_2}{\Lambda_1} \nu - k \right), \quad \mathcal{I}_{12}(0, \nu) = \frac{\Lambda_1}{\Lambda_2} \sum_{k=0}^p q_{22}^k \mathbb{1}_{[0, \frac{\Lambda_2}{\Lambda_1} - k]}(\nu) N_z \left(\frac{\Lambda_1}{\Lambda_2} (\nu + k) \right), \\ \mathcal{I}_{11}(1, \nu) &= q_{22}' \mathcal{I}_{11}(0, \nu), \quad \mathcal{I}_{12}(1, \nu) = q_{22}' \mathcal{I}_{12}(0, \nu), \quad \mathcal{I}_{21}(0, \nu) = \frac{\Lambda_2}{\Lambda_1} \mathcal{I}_{11}(0, \nu), \quad \mathcal{I}_{22}(0, \nu) = \frac{\Lambda_2}{\Lambda_1} \mathcal{I}_{12}(0, \nu). \end{aligned} \quad (\text{B.11})$$

Let us take $z = \begin{pmatrix} f \\ g \end{pmatrix} \in \ker(\mathcal{Q})$, such that, for all $x \in [0, 1]$, we have

$$\begin{pmatrix} f(x) \\ g(x) \end{pmatrix} = \begin{pmatrix} \int_0^1 -\mathcal{I}_{12}(\nu, x) f(\nu) + \mathcal{I}_{11}(\nu, x) g(\nu) d\nu \\ \int_0^1 -\mathcal{I}_{22}(\nu, x) f(\nu) + \mathcal{I}_{21}(\nu, x) g(\nu) d\nu \end{pmatrix}.$$

Due to the regularizing property of the integral, we have $\ker(\mathcal{Q}) \subset H^1([0, 1], \mathbb{R}^2)$. The boundary conditions (B.11) give $f(1) = q_{22}' f(0)$, and $f(0) = \frac{\Lambda_1}{\Lambda_2} g(0)$, such that $z \in D(A^*)$. Next, we evaluate the coupling terms $\mathcal{I}_{21}, \mathcal{I}_{22}$ in $y = 1$. We obtain $\mathcal{I}_{21}(1, \nu) = \mathcal{I}_{22}(1, \nu) = 0$. We then have $\Lambda_1 g(1) = 0$, such that $z \in \ker(B^*)$.

We now need to prove that $\ker(\mathcal{Q})$ is stable by A^* (condition (c)), i.e $\forall z \in \ker(\mathcal{Q}), \mathcal{Q}A^*z = \begin{pmatrix} 0 \\ 0 \end{pmatrix}$. We have

$$A^*z = \begin{pmatrix} \Lambda_2 f'(y) + \Lambda_2 f(0) N_w(y) \\ -\Lambda_1 g'(y) + \Lambda_2 f(0) N_z(y) \end{pmatrix}.$$

We compute the derivative of functions $(f, g) \in \ker(\mathcal{Q})$ on one side, and we integrate by parts in the integral terms on the other side. Some computations are given below. On the first component of $\mathcal{Q}A^*z$, we need to show that

$$\begin{aligned} \Lambda_2 f'(y) + \Lambda_2 f(0) N_w(y) + \int_0^1 \mathcal{I}_{12}(\nu, y) (\Lambda_2 f'(\nu) + \Lambda_2 f(0) N_w(\nu)) d\nu \\ - \int_0^1 \mathcal{I}_{11}(\nu, y) (-\Lambda_1 g'(\nu) + \Lambda_2 f(0) N_z(\nu)) d\nu = 0. \end{aligned} \quad (\text{B.12})$$

Let us check that the terms in $f(0)$ are compensated, that is to say,

$$f(0) \int_0^1 \mathcal{I}_{12}(y, \nu) \Lambda_2 N_u(\nu) - \mathcal{I}_{11}(y, \nu) \Lambda_2 N_v(\nu) d\nu = 0.$$

Due to the presence of characteristic functions, we obtain two sums of integral terms in $N_w(\cdot) \times N_z(\cdot)$. By a change of variables in the second term, we get the equality.

Next, we compute separately $\Lambda_1 \int_0^1 \mathcal{I}_{11}(y, \nu) g'(\nu) d\nu$ and $\Lambda_2 \int_0^1 \mathcal{I}_{12}(y, \nu) f'(\nu) d\nu$. Once again, we decompose the integral on different subdomains to eliminate the characteristic function. We integrate by parts and use the fact that $f(1) = q'_{22} f(0)$, $g(1) = 0$, $f(0) = \frac{\Lambda_2}{\Lambda_1} g(0)$ to simplify some terms. Finally, we compute the derivative of f . We have $f(y) = \int_0^1 \mathcal{I}_{11}(y, \nu) g(\nu) - \mathcal{I}_{12}(y, \nu) g(\nu) d\nu$, by definition of $z \in \ker(\mathcal{Q})$. We then verify that all the terms are compensated using several changes of variables in the integral terms and Fubini's theorem.

In a second time, we follow the same steps to show that the second component of $\mathcal{Q}A^*z$ vanishes, that is

$$-\Lambda_1 g'(y) + \Lambda_2 f(0) N_z(y) + \int_0^1 \mathcal{I}_{22}(\nu, y) (\Lambda_2 f'(\nu) + \Lambda_2 f(0) N_w(\nu)) d\nu \\ \int_0^1 \mathcal{I}_{21}(\nu, y) (-\Lambda_1 g'(\nu) + \Lambda_2 f(0) N_z(\nu)) d\nu = 0.$$

Once again, we show that $f(0) \int_0^1 \mathcal{I}_{22}(y, \nu) \Lambda_2 N_u(\nu) - \mathcal{I}_{21}(y, \nu) \Lambda_2 N_v(\nu) d\nu = 0$ using a change of variables ($\eta = \frac{\Lambda_2}{\Lambda_1}(\nu - y) - k$). Next, we compute separately the other integral terms and use integration by parts. The integral term $\int_0^1 \mathcal{I}_{22}(y, \nu) \Lambda_2 f'(\nu) d\nu$ rewrites

$$\sum_{k=0}^p \int_0^{\frac{\Lambda_2}{\Lambda_1}(1-y)-k} \mathbb{1}_{[0,1]}(\nu) q'_{22} N_z \left(\frac{\Lambda_1}{\Lambda_2}(\nu + k) + y \right) \Lambda_2 f'(\nu) d\nu.$$

We get rid of the characteristic function by decomposing it into different integration domains, as illustrated

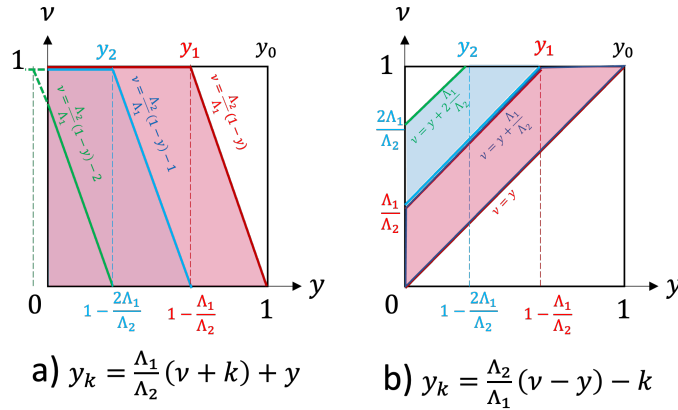


Figure B.3 – Representation of the integration domain for $2 < \frac{\Lambda_2}{\Lambda_1} < 3, p = 2$

in Figure B.3 a). Let us define the decreasing sequence $y_k = 1 - \frac{\Lambda_1}{\Lambda_2}(k + 1)$, $k \in \llbracket 0, p + 1 \rrbracket$. We decompose the integral term according to the value of y relative to y_k . We factorize all terms in $f(0)$ resulting from the integration by parts to obtain $-\Lambda_2 f(0) N_z(y)$. Integral term $\int_0^1 \mathcal{I}_{21}(y, \nu) \Lambda_1 g'(\nu) d\nu$ rewrites

$$-\Lambda_2 \sum_{k=0}^p q_{22}^k \int_{y+k \frac{\Lambda_1}{\Lambda_2}}^{y+(k+1) \frac{\Lambda_1}{\Lambda_2}} \mathbb{1}_{[0,1]}(\nu) N_w \left(\frac{\Lambda_2}{\Lambda_1}(\nu - y) - k \right) g'(\nu) d\nu.$$

Following the same procedure, we decompose the integration domain as illustrated in Figure B.3 b). Finally, we compute the derivative of g using condition (b) and the expression of $\ker(\mathcal{Q})$. It proves that $\forall z \in \ker(\mathcal{Q})$, $\mathcal{Q}A^*z = 0$. The condition (d) is given by Lemma 7.2.2 and derives from the spectral controllability of the system (Assumption 7.2.2). Using the arguments given in the proof of Lemma 7.2.1, we obtain that \mathcal{Q} is invertible. ■

By (B.1), we have $\mathcal{Q} \begin{pmatrix} N^{-+}(0, \cdot) \\ -N^{\bar{+}}(\cdot) \end{pmatrix} = \begin{pmatrix} N_w \\ N_z \end{pmatrix}$. The invertibility of the operator \mathcal{Q} given by

Theorem B.3.1 implies the existence and uniqueness of $N^{+-}(0, y), \bar{N}^{-+}(y)$ in $L^2([0, 1], \mathbb{R})$, and therefore the existence of $N^{+-}(0, y), N^{-+}(0, y)$. Since the kernels \mathcal{I}_{ij} are piecewise continuous, the integral operator \mathcal{Q}^{-1} has a regularizing effect. Since N_w and N_z are piecewise continuous, $\begin{pmatrix} N^{-+}(0, y) \\ -\bar{N}^{+-}(y) \end{pmatrix} = \mathcal{Q}^{-1} \begin{pmatrix} N_w(y) \\ N_z(y) \end{pmatrix}$ are in fact defined in $C_{pw}^0([0, 1], \mathbb{R}^2)$. According to Lemma B.1.1, the four kernels N^{ij} are then uniquely defined in $C_{pw}^0(\mathcal{S})$. This concludes the proof of 7.2.3.

C - Comments on target systems and kernels dof for a Timoshenko beam observer design

In the last section of Chapter 10, we designed a full-state feedback for a clamped Timoshenko beam. The Port-Hamiltonian framework showed its interest in selecting target systems with specific asymptotic properties. As for all backstepping-based controllers, boundary control input (10.25) required the knowledge of distributed values of the state. However, measurements are usually available in pointwise locations only for practical applications that can be modeled by such beams, such as fixed-wing aircraft or flexible endoscopes [WLG18]. Designing an adequate observer for the system from the available measurements is a crucial step to obtaining effective controllers. So far, the choice of the adequate target system for designing the observer gains has not been investigated. Similarly, fixing the boundary conditions of the kernels that can remain as degrees of freedom (dof) has not been investigated either. In this appendix, we present two backstepping-based observer designs for a clamped Timoshenko beam with in-domain damping and space-varying parameters that can be reformulated as a nonscalar hyperbolic PDE system (Chapter 10). We question their advantages and inconveniences and present some criteria for further quantitative analysis.

C.1 . System under consideration

C.1.1 . Damped Timoshenko beam

The damped Timoshenko beam model [Tim74] we consider in this test case corresponds to (10.15)-(10.16), in which, in addition to the axial forces, we take into account damping forces proportional to the velocity. From the balance equations on the momenta, we obtain the coupled governing equations

$$\begin{aligned} \rho(x) \frac{\partial^2 w}{\partial t^2}(t, x) + \eta_1(x) \frac{\partial w}{\partial t}(t, x) &= \frac{\partial}{\partial x} \left(K_s(x) \left(\frac{\partial w}{\partial x}(t, x) - \phi(t, x) \right) \right), \\ I_\rho(x) \frac{\partial^2 \phi}{\partial t^2}(t, x) + \eta_2(x) \frac{\partial \phi}{\partial t}(t, x) &= \frac{\partial}{\partial x} \left(E(x) I(x) \frac{\partial \phi}{\partial x}(t, x) \right) + K_s(x) \left(\frac{\partial w}{\partial x}(t, x) - \phi(t, x) \right). \end{aligned} \quad (\text{C.1})$$

Here, we assume that all physical parameters (ρ, I_ρ, E, I, K_s and the additional damping coefficients η_1, η_2) are strictly positive functions in $C^1([0, 1], \mathbb{R}^+)$. No movement is allowed at the clamped end $x = 0$, while the opposite end is free (unlike in Section 10.3, in which the opposite end was fully actuated). We have $K_s(1) \left(\frac{\partial w}{\partial x} \Big|_{x=1} - \phi(t, 1) \right) = 0$, $EI(1) \frac{\partial \phi}{\partial x} \Big|_{x=1} = 0$. We measure the momentum and angular momentum at this boundary $y_1(t) = \rho(1) \frac{\partial w}{\partial t} \Big|_{x=1}$ and $y_2(t) = I_\rho(1) \frac{\partial \phi}{\partial t} \Big|_{x=1}$. For practical application, we consider that the sensor size is sufficiently small compared to the length of the beam, such as we have access to a pointwise measurement. It is schematically illustrated in Figure C.1.

In the Port Hamiltonian framework, considering the energy states (10.17), the original

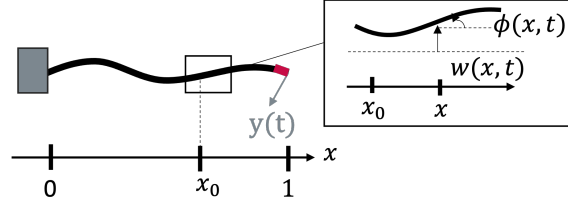


Figure C.1 – Schematic representation of the system

system (C.1) rewrites in the form (10.1), with

$$P_0(x) = \begin{pmatrix} 0 & 0 & 0 & -1 \\ 0 & 0 & 0 & 0 \\ 0 & 0 & -\eta_1 \rho(x) & 0 \\ 1 & 0 & 0 & -\eta_2 I_\rho(x) \end{pmatrix} \in \mathbb{R}^{4 \times 4}$$

and a space-varying Hamiltonian density $\mathcal{H}(x)$. The boundary conditions rewrite $X_2(t, 0) = 0_{\mathbb{R}^2}$, $X_1(t, 1) = 0_{\mathbb{R}^2}$, and the measurement $Y(t) = DX_2(t, 1)$, with $D = \text{diag}(\rho(1), I_\rho(1))^{-1}$. The initial conditions are set to $X(0, \cdot) = X_0 \in H^1([0, 1], \mathbb{R}^4)$, $\frac{\partial X}{\partial t}|_{t=0} = X_p \in H^1([0, 1], \mathbb{R}^4)$.

C.1.2 . Overall strategy

We aim to compare different observer designs from boundary measurement for the clamped Timoshenko beam model presented in the previous section. First, we apply the strategy presented in Section 10.1. We rewrite the energy states in Riemann coordinates using a first change of variables and apply a second exponential change of variables to suppress the diagonal coupling terms. Second, we propose two observer designs based on the backstepping methodology with different target systems. We show the convergence of the estimations to the real values in finite time. Finally, we compare the performances of the different designs in simulation and question their use in closed-loop feedback.

C.1.3 . Reformulation as an hyperbolic PDE system

Riemann coordinates

We first rewrite (10.1) in Riemann coordinates. For all $x \in [0, 1]$, the matrix $P_1 \mathcal{H}(x) \in \mathbb{R}^{4 \times 4}$ satisfies Assumption 10.9. Here, λ , μ , Λ and R , Q introduced in Section 10.3.2 are strictly positive space-dependent functions (of class C^1). For sake of simplicity, assume that for all $x \in [0, 1]$, $\mu(x) > \lambda(x)$. The state $\xi(t, x) = Q^{-1}(x)X(t, x)$ verifies the PDE system (9.1) with the boundary conditions

$$\xi^+(t, 0) = -R^{-1}(0)\xi^-(t, 0), \quad \xi^-(t, 1) = R(1)\xi^+(t, 1). \quad (\text{C.2})$$

Due to damping terms and the space dependence of the coefficients, the in-domain coupling matrix-valued functions differ. Their expression is given by (the space-dependence

of the physical parameters is omitted)

$$\begin{aligned}\Sigma^{++}(x) &= \frac{1}{2} \begin{pmatrix} \frac{\lambda}{2}(3\frac{\rho'}{\rho} - \frac{K'_s}{K_s}) - \eta_1 & \frac{K_s}{\lambda I_\rho} \\ -\lambda & -\frac{\mu}{2}(\frac{EI'}{EI} + \frac{I'_\rho}{I_\rho}) - \eta_2 \end{pmatrix}, \\ \Sigma^{+-}(x) &= \frac{1}{2} \begin{pmatrix} \frac{K_s}{\lambda}(\frac{\lambda}{2}(\frac{\rho'}{\rho} + \frac{K'_s}{K_s}) - \eta_1) & \frac{\mu K_s}{\lambda} \\ K_s & \mu I_\rho(\frac{\mu}{2}(\frac{EI'}{EI} + \frac{I'_\rho}{I_\rho}) - \eta_2) \end{pmatrix}, \\ \Sigma^{-+}(x) &= \frac{1}{2} \begin{pmatrix} -\frac{\lambda}{K_s}(\frac{\lambda}{2}(\frac{\rho'}{\rho} + \frac{K'_s}{K_s}) + \eta_1) & -\frac{1}{I_\rho} \\ -\frac{\lambda}{\mu I_\rho} & -\frac{1}{\mu I_\rho}(\frac{\mu}{2}(\frac{EI'}{EI} + \frac{I'_\rho}{I_\rho}) + \eta_2) \end{pmatrix}, \\ \Sigma^{--}(x) &= \frac{1}{2} \begin{pmatrix} \frac{\lambda}{2}(3\frac{K'_s}{K_s} - \frac{\rho'}{\rho}) - \eta_1 & -\mu \\ \frac{K_s}{\mu I_\rho} & \frac{\mu}{2}(3\frac{EI'}{EI} - \frac{I'_\rho}{I_\rho}) - \eta_2 \end{pmatrix}.\end{aligned}$$

The boundary measurement rewrites $Y(t) = \sqrt{2}D\xi^+(1)$.

Exponential change of variables

We then apply a second exponential change of variables to eliminate the diagonal coefficients of Σ^{++} , Σ^{--} . We define the following functions in $C^1([0, 1], \mathbb{R})$:

$$\begin{aligned}\alpha(x) &= \frac{1}{2}(\ln \frac{\rho(0)\lambda(x)}{\rho(x)\lambda(0)} + \int_0^x \frac{\eta_1(\nu)}{\lambda(\nu)} d\nu), & \beta(x) &= \frac{1}{2}(\ln \frac{\mu(x)I_\rho(x)}{\mu(0)I_\rho(0)} + \int_0^x \frac{\eta_2(\nu)}{\mu(\nu)} d\nu), \\ \gamma(x) &= -\frac{1}{2}(\ln \frac{K_s(x)\lambda(x)}{K_s(0)\lambda(0)} - \int_0^x \frac{\eta_1(\nu)}{\lambda(\nu)} d\nu), & \delta(x) &= -\frac{1}{2}(\ln \frac{\mu(x)EI(x)}{\mu(0)EI(0)} - \int_0^x \frac{\eta_2(\nu)}{\mu(\nu)} d\nu).\end{aligned}$$

and define the invertible matrices in $D_2^+([0, 1])$:

$$A(x) \doteq \text{diag}(e^{\alpha(x)}, e^{\beta(x)}), B(x) \doteq \text{diag}(e^{-\gamma(x)}, e^{-\delta(x)}).$$

From then, consider the state $z = [z^{+\top}, z^{-\top}]^\top \in H^1([0, 1], \mathbb{R}^4)$, defined by $\forall t > 0$, $x \in [0, 1]$,

$$z^+(t, x) = A(x)\xi^+(t, x), \quad z^-(t, x) = B(x)\xi^-(t, x).$$

It verifies the PDE system (9.1) with the boundary conditions

$$z^+(t, 0) = -R^{-1}(0)z^-(t, 0), \quad z^-(t, 1) = \bar{R}z^+(t, 1), \quad \text{with } \bar{R} \doteq B(1)R(1)A^{-1}(1), \quad (\text{C.3})$$

where the in-domain coupling terms are defined by

$$\begin{aligned}\Sigma_z^{++}(x) &= \frac{1}{2} \begin{pmatrix} 0 & \frac{K_s}{\lambda I_\rho} e^{\alpha(x)-\beta(x)} \\ -\lambda e^{\beta(x)-\alpha(x)} & 0 \end{pmatrix}, \quad \Sigma_z^{+-}(x) = A(x)\Sigma^{+-}(x)B^{-1}(x), \\ \Sigma_z^{-+}(x) &= B(x)\Sigma^{-+}(x)A^{-1}(x), \quad \Sigma_z^{--}(x) = \frac{1}{2} \begin{pmatrix} 0 & -\mu e^{-\gamma(x)+\delta(x)} \\ \frac{K_s}{\mu I_\rho} e^{-\delta(x)+\gamma(x)} & 0 \end{pmatrix}.\end{aligned}$$

The available measurement rewrites $Y(t) = \sqrt{2}DA^{-1}(1)z^+(t, 1) \doteq \hat{D}z^+(t, 1)$.

C.2 . Observer design

C.2.1 . Observer and error system

In this section, we design a Luenberger-type observer for state z [Krs08, AA19, HVDMK15]. Its state denoted \hat{z} satisfies a copy of the dynamics (9.1) with additional output injection gains

$$\begin{aligned}\frac{\partial}{\partial t}\hat{z}^+ + \Lambda(x)\frac{\partial}{\partial x}\hat{z}^+ &= \Sigma_z^{++}(x)\hat{z}^+(t, x) + \Sigma_z^{+-}(x)\hat{z}^-(t, x) + P^+(x)(\hat{D}^{-1}Y(t) - \hat{z}^+(t, 1)), \\ \frac{\partial}{\partial t}\hat{z}^- - \Lambda(x)\frac{\partial}{\partial x}\hat{z}^- &= \Sigma_z^{-+}(x)\hat{z}^+(t, x) + \Sigma_z^{--}(x)\hat{z}^-(t, x) + P^-(x)(\hat{D}^{-1}Y(t) - \hat{z}^+(t, 1)),\end{aligned}\tag{C.4}$$

with boundary conditions

$$\hat{z}^+(t, 0) = -R^{-1}(0)\hat{z}^-(t, 0), \quad \hat{z}^-(t, 1) = \bar{R}\hat{D}^{-1}Y(t).\tag{C.5}$$

Define the error state $\tilde{z}(t, x) \doteq z(t, x) - \hat{z}(t, x)$. Subtracting (C.4) from (9.1), we directly obtain the error system

$$\begin{aligned}\frac{\partial}{\partial t}\tilde{z}^+(t, x) + \Lambda(x)\frac{\partial}{\partial x}\tilde{z}^+(t, x) &= \Sigma_z^{++}(x)\tilde{z}^+(t, x) + \Sigma_z^{+-}(x)\tilde{z}^-(t, x) - P^+(x)\tilde{z}^+(t, 1), \\ \frac{\partial}{\partial t}\tilde{z}^-(t, x) - \Lambda(x)\frac{\partial}{\partial x}\tilde{z}^-(t, x) &= \Sigma_z^{-+}(x)\tilde{z}^+(t, x) + \Sigma_z^{--}(x)\tilde{z}^-(t, x) - P^-(x)\tilde{z}^+(t, 1),\end{aligned}\tag{C.6}$$

with boundary conditions

$$\tilde{z}^+(t, 0) = -R^{-1}(0)\tilde{z}^-(t, 0), \quad \tilde{z}^-(t, 1) = 0.\tag{C.7}$$

The objective reads as follows

Objective C.2.1: Observer design

Design adequate gain functions P^+ , P^- such that the error system (C.6)-(C.7) is exponentially stable. In other words, there exists $C, \nu > 0$, such that

$$\|z(t) - \hat{z}(t)\|_{L^2} \leq Ce^{-\nu t}\|z(0) - \hat{z}(0)\|_{L^2}.$$

To do so, we follow the backstepping methodology. Using an invertible transform, we map (C.6)-(C.7) to an exponentially stable system. Due to the invertibility of the transform, the two systems share equivalent stability properties. The values of the gains naturally derive from the methodology.

C.2.2 . First backstepping design

In the first naive design, we use a classical Volterra integral transform to move the destabilizing in-domain coupling terms in the error system (C.6)-(C.7) to the boundary $x = 0$. More precisely, we define the transform $\mathcal{L}_1 : H^1([0, 1], \mathbb{R}^4) \rightarrow H^1([0, 1], \mathbb{R}^4)$, using its inverse formulation, by

$$\tilde{z}(x) = \mathcal{L}_1(\gamma)(x) \doteq \gamma(x) - \int_x^1 L_1(x, y)\gamma(y)dy.\tag{C.8}$$

with kernels $L_1(x, y) = \begin{pmatrix} L_1^{++} & L_1^{+-} \\ L_1^{-+} & L_1^{--} \end{pmatrix} \in C_{pw}^0(\mathcal{T}^+, \mathbb{R}^{4 \times 4})$. With this invertible transform, we want the target PDE system satisfied by $\gamma = \mathcal{L}_1^{-1}(\tilde{z})$ to be given by

$$\frac{\partial}{\partial t} \gamma^+(t, x) + \Lambda(x) \frac{\partial}{\partial x} \gamma^+(t, x) = 0, \quad \frac{\partial}{\partial t} \gamma^-(t, x) - \Lambda(x) \frac{\partial}{\partial x} \gamma^-(t, x) = 0, \quad (\text{C.9})$$

with boundary conditions

$$\gamma^+(t, 0) = -R^{-1}(0) \gamma^-(t, 0) + \int_0^1 G^+(y) \gamma^+(t, y) + G^-(y) \gamma^-(t, y) dy, \quad \gamma^-(t, 1) = 0, \quad (\text{C.10})$$

with $G^+ = \begin{pmatrix} 0 & 0 \\ g^+(x) & 0 \end{pmatrix}$ a strictly lower triangular matrix. Define $\tau_\lambda = \int_0^1 \frac{d\nu}{\lambda(\nu)}$, $\tau_\mu = \int_0^1 \frac{d\nu}{\mu(\nu)}$. We have the following theorem:

Theorem C.2.1: Exponential stability of the target system

For any compatible initial conditions $(\gamma_0^+, \gamma_0^-) \in H^1([0, 1], \mathbb{R}^4)$, the solution of system (C.9)-(C.10) is exponentially stable. More precisely, it converges to zero in finite-time $t^ \doteq \tau_\lambda + \tau_\mu + \max(\tau_\lambda, \tau_\mu)$.*

Proof: We have a cascade structure from γ^- into γ^+ . First, for $t > \max(\tau_\lambda, \tau_\mu)$, the null-boundary condition in (C.10) has propagated in the entire domain such that the state $\gamma^-(t, x) = 0, \forall x \in [0, 1]$. Next, the boundary conditions for $t > \max(\tau_\lambda, \tau_\mu)$ rewrite $\gamma_1^+(t, 0) = 0, \gamma_2^+(t, 0) = \int_0^1 g^+(y) \gamma_1^+(t, y) dy$. Then, for $t > \max(\tau_\lambda, \tau_\mu) + \tau_\lambda$, state component $\gamma_1^+(t, x) \equiv 0$, and then similarly after τ_μ more time, state component $\gamma_2^+(t, x) = 0$. Similarly, the proof is given in [HDMVK16] for constant transport speeds. ■

Following the backstepping methodology, that is to say injecting (C.8) in (C.6), and integrating by parts, we show that kernels must satisfy the set of equations

$$\begin{aligned} \Lambda(x) \frac{\partial}{\partial x} L_1^{++} + \frac{\partial}{\partial y} (L_1^{++} \Lambda(y)) &= \Sigma_z^{++}(x) L_1^{++} + \Sigma_z^{+-}(x) L_1^{-+}, \\ \Lambda(x) \frac{\partial}{\partial x} L_1^{+-} - \frac{\partial}{\partial y} (L_1^{+-} \Lambda(y)) &= \Sigma_z^{++}(x) L_1^{+-} + \Sigma_z^{+-}(x) L_1^{-+}, \\ \Lambda(x) \frac{\partial}{\partial x} L_1^{-+} - \frac{\partial}{\partial y} (L_1^{-+} \Lambda(y)) &= -\Sigma_z^{-+}(x) L_1^{++} - \Sigma_z^{--}(x) L_1^{-+}, \\ \Lambda(x) \frac{\partial}{\partial x} L_1^{--} + \frac{\partial}{\partial y} (L_1^{--} \Lambda(y)) &= -\Sigma_z^{-+}(x) L_1^{+-} - \Sigma_z^{--}(x) L_1^{-+}. \end{aligned} \quad (\text{C.11})$$

as well as a set of boundary conditions in $x = y$

$$\begin{aligned} \Lambda(x) L_1^{++}(x, x) - L_1^{++}(x, x) \Lambda(x) &= \Sigma_z^{++}(x), \quad \Lambda(x) L_1^{-+}(x, x) + L_1^{-+}(x, x) \Lambda(x) = -\Sigma_z^{-+}(x), \\ \Lambda(x) L_1^{+-}(x, x) + L_1^{+-}(x, x) \Lambda(x) &= \Sigma_z^{+-}(x), \quad \Lambda(x) L_1^{--}(x, x) - L_1^{--}(x, x) \Lambda(x) = -\Sigma_z^{--}(x), \end{aligned} \quad (\text{C.12})$$

and the boundary conditions in $x = 0$,

$$(L_1^{++})_{ij}(0, y) = - (R^{-1}(0) L^{-+}(0, y))_{ij}, \quad i \leq j. \quad (\text{C.13})$$

This system is under-determined: we have 5 remaining degrees of freedom for the kernel

equations. In the considered case, they are given by

$$(L_1^{--})_{ij}(0, y) = l_1^{ij}(y), \quad i \leq j, \quad (L_1^{++})_{21}(x, 1) = l_1^+(x), \quad (L_1^{--})_{21}(x, 1) = l_1^-(x), \quad (\text{C.14})$$

with l_1^{ij} , $i \leq j$, l_1^\pm piecewise continuous functions defined on $[0, 1]$.

Once there are arbitrarily fixed, we have the following

Theorem C.2.2: Well-posedness of the kernel equations

The set of equations (C.11) with boundary conditions (C.12)-(C.14) admits a unique piecewise continuous solution on \mathcal{T}^+ .

Proof : This derives from [HDMVK16, HVDMK15]. ■

The observer gains are defined by

$$P^+(x) = -L_1^{++}(x, 1)\Lambda(1), \quad P^-(x) = -L_1^{--}(x, 1)\Lambda(1). \quad (\text{C.15})$$

Consequently, though we have introduced 5 degrees of freedom in the choice of the error target system and Volterra integral transform (C.8), only one of them (l_1^+) will have an impact on the convergence of the observer system. This questions their usefulness in the backstepping methodology. This aligns with the concerns presented in Chapter 10 in the context of control design. Though this inadequate choice does not directly impact the computation of the state estimation, implementing a resolution algorithm for the kernel equations (that are computed beforehand), will be more time-consuming, as shown in Section C.3.2.

To keep in mind

In the backstepping methodology, different target systems can be reached using an invertible transform. The simplest one is not always the most relevant choice for observer/controller design.

C.2.3 . Second backstepping design

We now compare this observer design with another obtained using a simpler Volterra integral transform [AA19, 19.3.2 P.362]. Here, we use the same form of Volterra integral transform

$$\tilde{z}(x) = \mathcal{L}_2(\gamma) \doteq \gamma(x) - \int_x^1 L_2(x, y)\gamma(y)dy. \quad (\text{C.16})$$

with a specific kernel of the form $L_2(x, y) = \begin{pmatrix} L_2^+ & 0 \\ L_2^- & 0 \end{pmatrix} \in C_{pw}^0(\mathcal{T}^+, \mathbb{R}^{4 \times 4})$. Indeed, we certified in the previous section that the two other kernel components have no impact on the observer system. With (C.16), we map the error system (C.6)-(C.7) to the following

exponentially stable system

$$\begin{aligned}\frac{\partial}{\partial t}\gamma^+(t, x) + \Lambda(x)\frac{\partial}{\partial x}\gamma^+(t, x) &= \Sigma_z^{+-}(x)\gamma^-(t, x) + \int_x^1 H^+(x, y)\gamma^-(t, y)dy, \\ \frac{\partial}{\partial t}\gamma^-(t, x) - \Lambda(x)\frac{\partial}{\partial x}\gamma^-(t, x) &= \Sigma_z^{-+}(x)\gamma^-(t, x) + \int_x^1 H^-(x, y)\gamma^-(t, y)dy,\end{aligned}\quad (\text{C.17})$$

with boundary conditions

$$\gamma^+(0) = -R^{-1}(0)\gamma^-(0) + \int_0^1 H_0(y)\gamma^+(y)dy, \quad \gamma^-(1) = 0. \quad (\text{C.18})$$

Note that this target system has a more complex structure than the one in Section C.2.2. Consequently, the design presented in Section C.2.2 is usually chosen by default (for instance, in the Coni toolbox presented in Section A.2.3). Since we simplified the Volterra integral transform, we suppressed some degrees of freedom such that some terms cannot be removed from the target system. Let us now consider the structure of matrices H^+ , H^- , H_0 . To ensure a cascaded structure, we need H_0 to be a strict triangular matrix. This imposes three boundary conditions $(L_2^+)_{ij}, i \leq j$ (for $\mu > \lambda$) given in (C.21). The functions are defined as the solution of

$$\begin{aligned}H^+(x, y) - \int_x^y L_2^+(x, \nu)H^+(x, \nu)d\nu &= L_2^+(x, y)\Sigma_z^{+-}(y), \\ H^-(x, y) &= L_2^-(x, y)\Sigma_z^{-+}(y) + \int_x^y L_2^-(x, \nu)H^+(x, \nu)d\nu, \\ H_0(y) &= L_2^+(0, y) + R^{-1}(0)L_2^-(0, y).\end{aligned}\quad (\text{C.19})$$

Equation (C.19) corresponds to a Volterra transform. More precisely, consider a fixed $x \in [0, 1]$, and function $h^+ : y \mapsto H^+(x, y)$ defined on $[x, 1]$. This function satisfies a Volterra integral equation of the second kind and is uniquely defined by [Yos60]. Then, the kernel $H^+(x, y)$ is uniquely defined on \mathcal{T}^+ . Consequently, the kernel H^- is uniquely defined on \mathcal{T}^+ . The matrices do not need to be strictly triangular to ensure the following

Theorem C.2.3: Exponential stability of the target system

For any compatible initial conditions $(\gamma_0^+, \gamma_0^-) \in H^1([0, 1], \mathbb{R}^4)$, the solution of system (C.17)-(C.18), for H_0 any strictly triangular matrix, is exponentially stable. More precisely, it converges to zero in finite-time t^ .*

Proof : Similarly to [HDMVK16] (in case of control design with constant transport speeds), or [AA19, Theorem 19.4], we can prove that system (C.6)-(C.7) converges to zero in finite time. First, it has a cascaded structure from z^- , which has zero input at the right boundary, into z^+ . Using the method of characteristics, we can prove that $\gamma^-(x, t) \equiv 0$, for $t \geq \tau_\lambda + \tau_\mu$. Due to the strictly lower triangular structure of H_0 , the state $\gamma^+(x, t)$ goes to zero. ■

Following the backstepping methodology, the kernels satisfy the set of equations

$$\begin{aligned}\frac{\partial}{\partial x}(\Lambda(x)L_2^+(x, y)) + \frac{\partial}{\partial y}(L_2^+(x, y)\Lambda(y)) &= \Sigma_z^{++}(x)L_2^+(x, y) + \Sigma_z^{+-}(x)L_2^-(x, y), \\ \frac{\partial}{\partial x}(\Lambda(x)L_2^-(x, y)) - \frac{\partial}{\partial y}(L_2^-(x, y)\Lambda(y)) &= -\Sigma_z^{-+}(x)L_2^+(x, y) - \Sigma_z^{--}(x)L_2^-(x, y),\end{aligned}\quad (\text{C.20})$$

with boundary conditions

$$\begin{aligned}\Lambda(x)L_2^+(x, x) - L_2^+(x, x)\Lambda(x) &= \Sigma_z^{++}(x), \quad \Lambda(x)L_2^-(x, x) + L_2^-(x, x)\Lambda(x) = -\Sigma_z^{-+}(x), \\ (L_2^+)_{ij}(0, y) &= (-R^{-1}(0)L_2^-(0, y))_{ij}, \quad i \leq j.\end{aligned}\tag{C.21}$$

Once again, as stated in [AA19], this system is under-determined. To ensure that this system is well-posed and guarantee the uniqueness of a piecewise continuous solution [HVDKM15], we impose the boundary condition

$$(L_2^+(x, 1))_{21} = l_2(x),\tag{C.22}$$

with $l_2 \in C_{pw}^1([0, 1], \mathbb{R})$. Note that the above equations define the same kernels as L_1^{++} , L_1^{-+} in (C.11)-(C.14) under the condition $l_2(x) = l_1^+(x)$, $\forall x \in [0, 1]$.

Theorem C.2.4: Well-posedness of the kernel equations

The set of equations (C.20) with boundary conditions (C.21)-(C.22) admits a unique piecewise continuous solution on \mathcal{T}^+ .

Proof : The proof is given in [HVDKM15, Theorem A.1]. ■

We now question the interest of defining l_2 in (C.22). In the case of constant coefficients, explicit expressions of the solution of (C.20)-(C.22) can be obtained using Bessel functions [VK14]. As in Section C.2.2, fixing l_2 has an impact on the gains defined by

$$P^+(x) = -L_2^+(x, 1)\Lambda(1), \quad P^-(x) = -L_2^-(x, 1)\Lambda(1).\tag{C.23}$$

Continuous kernels

A first natural choice could be to select l_2 to ensure the continuity of the kernels along the characteristic discontinuity line on \mathcal{T}^+ starting from $(1, 1)$. To do so, we impose

$$l_2(1) = \frac{\Sigma_z^{++}(1)}{\mu(1) - \lambda(1)}.\tag{C.24}$$

Arbitrary boundary conditions

In the case where we impose any other arbitrary (such as zero) boundary condition $l_2(x)$, not satisfying (C.24), the kernel is not continuous on its definition domain, as illustrated in Figure C.2. It could be interesting to quantify its impact on the numerical resolution of the coupled kernel equations.

In the case where we impose a zero boundary condition ($l_2(x) = 0$, $\forall x \in [0, 1]$), one of the components of P^+ equals zero. Considering only the observer system, we could not directly conclude its impact on the convergence time to the real state values. However, considering the equivalent error target systems (in both backstepping designs), it appears that it suppresses some re-circulation terms at the boundary $x = 0$. Therefore, we ought to obtain a faster convergence of the error system in this case. This is next illustrated in the simulation.

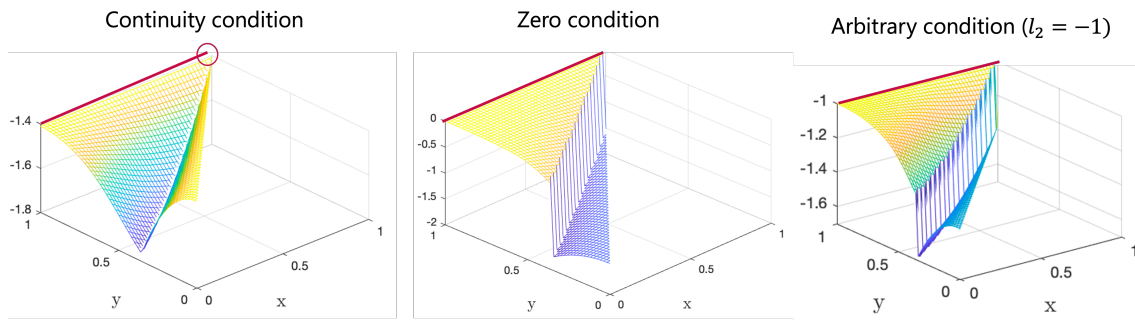


Figure C.2 – Representation of $(L_2^+)_{12}$ on its definition domain

To keep in mind

In the backstepping methodology, some degrees of freedom might remain in the kernels defined for the observer or controller design. They are usually arbitrarily set to zero. However, they might have an impact on some performance characteristics.

C.3 . Further analysis of the observer design

In this section, we illustrate the impact of boundary conditions for the second observer design with simulations. We propose some quantitative criteria to define the quality of the observer design.

C.3.1 . Simulation test case and first remarks

We use the physical parameters given in 10.1, and in-domain damping terms $c_3 = 0.5$, $c_4 = 0.8$. We follow the simulation procedure described in Sections 10.2.4 and 10.3.4. We represent the evolution of the L^2 -norm of the error energy states $\|\tilde{X}(t, \cdot)\|_{L^2}$, for the same constant observer initial states. We observe that the decay rate is higher when the structure of the error system is simplified at most.

When comparing the 2D projection of the error profile $|X(x, t) - \hat{X}(x, t)|$ for the four states, we observe that the amplitude of oscillation of the error state is higher when the continuous boundary condition is chosen (Figure C.5). This could be explained by higher values of the kernels, which amplify numerical discrepancies.

C.3.2 . Computation time

As mentioned in Chapter 11, one limitation of backstepping-based controllers proposed throughout this thesis is their numerical complexity. Indeed, they must be combined with an observer PDE system, solved at each time step using the available measurement. This currently limits their use on real systems with fast dynamics.

Kernel resolution is also time-consuming. For the same observer system, the two designs proposed in Section C.2 do not require the same computation time. For the first observer proposed in Section C.2.2, it takes 422s and 13 iterations to converge to the ker-

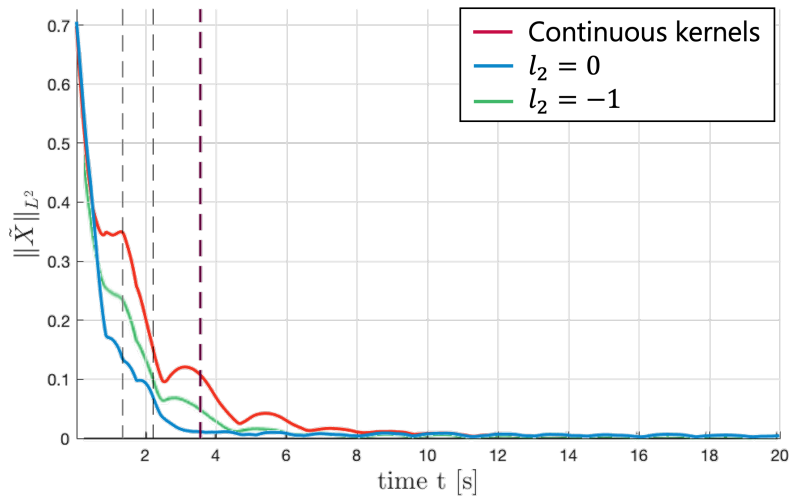


Figure C.3 – Evolution of the L^2 –norm of the error

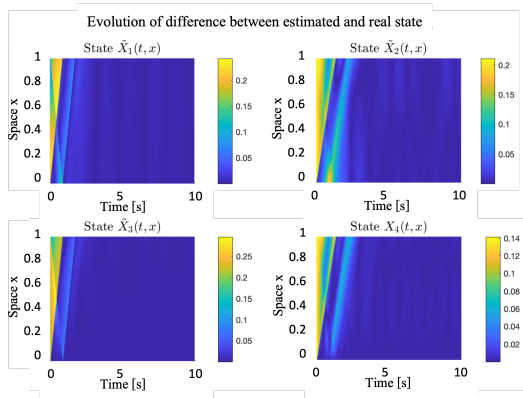


Figure C.4 – Case $l_2 = 0$)

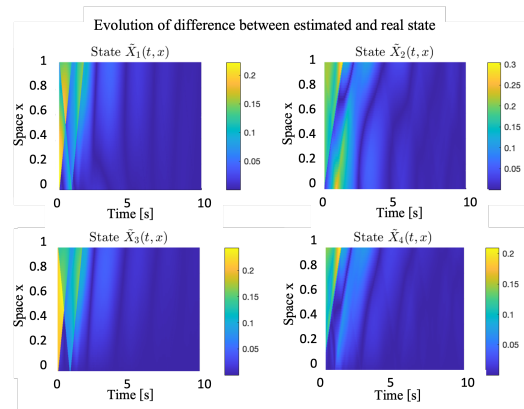


Figure C.5 – Case continuous kernel

nel values with an error $\epsilon_{\text{ps}} = 10^{-5}$, while for the observer proposed in Section C.2.3, computing the kernels only takes 146s. Though this operation can be done offline for constant physical parameters, this computation time must be considered for *adaptive observers*, since the kernel equations must then be solved at each time step.

C.3.3 . Quantitative criteria for *dof* selection

Finally, we propose some quantitative criteria, that could be used for selecting the remaining degrees of freedom (dof). As seen above, imposing values on the remaining boundary conditions seems to impact the convergence time of the implemented observer in this test case.

Convergence time with different l_2

A first evaluation criterion for an observer would be the time after which the given estimation is close to the real value (to a certain distance ϵ , that corresponds to $d\%$ of the real value). The L^2 –norm is generally considered to represent the distributed state.

Definition C.3.1: Convergence time

Define $t_{d\%}$ the $d\%$ -convergence time as

$$t_{d\%}(\hat{z}) \doteq \min_{t > \tau} \left\{ \frac{\|\hat{z}(t, \cdot) - z(t, \cdot)\|_{L^2}^2}{\|z(t, \cdot)\|_{L^2}^2} \right\} \leq d.$$

However, this time should be evaluated over a certain interval. As illustrated in Figure C.5, we could expect some oscillations of the norm of the error state, such that the threshold of a $d\%$ relative error could be reached for some t_0 , but not for some $t > t_0$. To quantify the quality of an observer, we propose the following definition

Definition C.3.2: Convergence time

Define $t_{\tau, d\%}$ the $\tau - d\%$ -convergence time as

$$t_{\tau, d\%}(\hat{z}) \doteq \min_{t > \tau} \left\{ \frac{\| \|\hat{z}(t, \cdot) - z(t, \cdot)\|_{L^2} \|D_\tau\|}{\| \|z(t, \cdot)\|_{L^2} \|D_\tau\|} \right\} \leq d.$$

It corresponds to the time when the D_τ -norm of the L^2 -norm of the error state is inferior to $d\%$ of the D_τ -norm of the L^2 -norm of the state to estimate.

Robustness to small delays

Next, another evaluation criterion could be the robustness of the estimation to small delays in the measurement. Indeed, we can expect that the measurement will be processed and available with some mechanical or numerical delays for real applications. This was illustrated in [KSo8] for scalar hyperbolic PDE system with sensor delay. The robustness could be quantified as the highest value of delay δ , such that the observer system

$$\begin{aligned} \frac{\partial}{\partial t} \hat{z}_\delta^+ + \Lambda(x) \frac{\partial}{\partial x} \hat{z}_\delta^+ &= \Sigma_z^{++}(x) \hat{z}_\delta^+(t, x) + \Sigma_z^{+-}(x) \hat{z}_\delta^-(t, x) + P^+(x) (\hat{D}^{-1} Y(t - \delta) - \hat{z}_\delta^+(t, 1)), \\ \frac{\partial}{\partial t} \hat{z}_\delta^- - \Lambda(x) \frac{\partial}{\partial x} \hat{z}_\delta^- &= \Sigma_z^{-+}(x) \hat{z}_\delta^+(t, x) + \Sigma_z^{--}(x) \hat{z}_\delta^-(t, x) + P^-(x) (\hat{D}^{-1} Y(t - \delta) - \hat{z}_\delta^+(t, 1)), \\ \hat{z}_\delta^+(t, 0) &= -R^{-1}(0) \hat{z}_\delta^-(t, 0), \quad \hat{z}_\delta^-(t, 1) = \bar{R} \hat{D}^{-1} Y(t - \delta). \end{aligned}$$

still converges to the real state.

Definition C.3.3: Delay-robustness margin

Define δ_r the measurement delay robustness margin of the observer by

$$\delta_r = \max \left\{ \delta > 0 \mid \forall \eta > 0, \exists T > 0, \forall t > T, \|\hat{z}_\delta(t, \cdot) - z(t, \cdot)\|_{L^2}^2 \leq \eta \right\}.$$

Robustness to parameter uncertainties

Finally, a last criterion could be the robustness of the estimation with regard to parameter uncertainties. Such uncertainties naturally arise when modeling physical systems. Some physical parameters (weight, length...) can be directly measured with a certain error inherent to the quality of the equipment. Other parameters (Young's modulus, shear modulus) are usually evaluated to minimize a discrepancy with an empirical model. In some cases, as in the drilling example of Chapter 11, some parameters are unknown. For

a system with n physical parameters of real value p_i , and known value \hat{p}_i ,

Definition C.3.4: Average relative model error

Define ϵ the average relative model error as

$$\epsilon \doteq \frac{1}{n} \left(\sum_{i=1}^n \left| \frac{\hat{p}_i - p_i}{p_i} \right| \right)$$

The robustness could be quantified as the highest value of error ϵ , such that the observer system

$$\begin{aligned} \frac{\partial}{\partial t} \hat{z}_\epsilon^+ + \hat{\Lambda}(x) \frac{\partial}{\partial x} \hat{z}_\epsilon^+ &= \hat{\Sigma}_z^{++}(x) \hat{z}_\epsilon^+(t, x) + \hat{\Sigma}_z^{+-}(x) \hat{z}_\epsilon^-(t, x) + P^+(x) (\hat{D}^{-1} Y(t) - \hat{z}_\epsilon^+(t, 1)), \\ \frac{\partial}{\partial t} \hat{z}_\epsilon^- - \hat{\Lambda}(x) \frac{\partial}{\partial x} \hat{z}_\epsilon^- &= \hat{\Sigma}_z^{-+}(x) \hat{z}_\epsilon^+(t, x) + \hat{\Sigma}_z^{--}(x) \hat{z}_\epsilon^-(t, x) + P^-(x) (\hat{D}^{-1} Y(t) - \hat{z}_\epsilon^+(t, 1)), \\ \hat{z}_\epsilon^+(t, 0) &= -\hat{R}^{-1}(0) \hat{z}_\epsilon^-(t, 0), \quad \hat{z}_\epsilon^-(t, 1) = \hat{R} \hat{D}^{-1} Y(t). \end{aligned}$$

still converges to the real state. Note that in the case of a Timoshenko beam, we have $n = 5$ physical parameters, which have different impacts on the transport speeds, in-domain, and boundary coupling terms.

Definition C.3.5: Parameter-robustness margin

Define ϵ_r the robustness margin of the observer with respect to parameters by

$$\epsilon_r = \max \left\{ \epsilon > 0 \mid \forall \eta > 0, \exists T > 0, \forall t > T, \|\hat{z}_\epsilon(t, \cdot) - z(t, \cdot)\|_{L^2}^2 \leq \eta \right\}.$$

Perspectives

In this Appendix, we aimed to raise concerns about one neglected aspect of the backstepping methodology so far: the choice of remaining degrees of freedom in the kernel equations. In a simple test case, we also showed that choosing the simplest target system is not always relevant in the observer design. A parallel can be drawn with the robustness concerns presented in Chapter 2 for controller design. Some criteria were proposed to represent different aspects to consider (robustness, convergence time...). They could be used to *optimize* the choice of degrees of freedom, in the eventuality where a o-boundary condition would not be optimal.

Titre: Contrôle robuste de systèmes linéaires d'équations aux dérivées partielles hyperboliques interconnectés en réseaux de chaîne.

Mots clés: EDPs hyperboliques, systèmes à retard de type neutre, contrôle par backstepping, systèmes interconnectés, robustesse.

Résumé: Cette thèse porte sur la synthèse de contrôleurs robustes par retour de sortie pour des systèmes d'équations aux dérivées partielles (EDP) hyperboliques interconnectés en une structure de chaîne. Nous proposons des solutions innovantes basées sur la méthode de backstepping et exploitant les liens entre systèmes d'EDP hyperboliques et systèmes à retard de type neutre présentés en Partie I. Nous étudions ici deux configurations d'actionnement de structures en chaîne. Tout d'abord, nous examinons le cas où l'actionnement est disponible à une extrémité (Partie II) pour deux différents réseaux (ODE-EDP-ODE et n EDPs-ODE). Ces structures peuvent modéliser des systèmes de forage. Ensuite, nous considérons une chaîne simple où l'actionnement est disponible au niveau de la jonction (Partie III). Sa stabilisation nécessite une transformation intégrale plus générale. Enfin, nous explorons les aspects négligés des contrôleurs basés sur la méthode de backstepping (Partie IV), tels que le choix d'un système cible atteignable avec des propriétés de stabilité spécifiques, ou la réduction du temps de calcul par des techniques d'apprentissage automatique.

Title: Robust control of linear hyperbolic partial differential equations systems interconnected in a chain network.

Keywords: hyperbolic PDEs, neutral time-delay systems, backstepping-based control, interconnected systems, robustness.

Abstract: This thesis focuses on designing robust output-feedback backstepping-based controllers for hyperbolic partial differential equation (PDE) systems interconnected in a chain structure. We take advantage of connections between the class of hyperbolic PDE systems under consideration and time-delay systems of the neutral type presented in Part I. Then, we focus on two classes of chain structures. First, we consider the case where the actuation is available at one end (Part II) for two different networks (ODE-PDE-ODE and arbitrarily many n PDEs-ODE). Such chain structures can be found in drilling applications. Next, we consider a simple chain of two hyperbolic PDE subsystems where the actuation is available at the junction (Part III). A more general integral transform is necessary for its stabilization. Finally, we explore controller design tuning and implementation limitations of backstepping-based controllers (Part IV). We question the choice of a reachable target system with specific stability properties. Additionally, we examine the potential of machine learning techniques to improve computation time in distributed state and parameter estimation.

